Contact Anatexis of Dalradian Metapelites from the Huntly-Knock Area, Aberdeenshire, NE Scotland

A thesis submitted to the University of Manchester for the Degree of doctor of philosophy in the Faculty of Science

1995

David J. Dalrymple
Department of Geology

ProQuest Number: 10758134

All rights reserved

INFORMATION TO ALL USERS
The quality of this reproduction is dependent upon the quality of the copy submitted.

In the unlikely event that the author did not send a complete manuscript
and there are missing pages, these will be noted. Also, if material had to be removed,
a note will indicate the deletion.

ProQuest 10758134

Published by ProQuest LLC (2018). Copyright of the Dissertation is held by the Author.

All rights reserved.
This work is protected against unauthorized copying under Title 17, United States Code
Microform Edition © ProQuest LLC.

ProQuest LLC.
789 East Eisenhower Parkway
P.O. Box 1346
Ann Arbor, MI 48106 – 1346

Th 19179
(DEUPH)

TABLE OF CONTENTS

CHAPTER 4

CHAPTER 5

CHAPTER 6

CHAPTER 7

CHAPTER 8

CHAPTER 9

CHAPTER 10

CHAPTER 11

APPENDICES

LIST OF FIGURES

CHAPTER 1

CHAPTER 3

CHAPTER 4

CHAPTER 6

CHAPTER 7

CHAPTER 8

CHAPTER 9

CHAPTER 10

LIST OF TABLES

CHAPTER 3

CHAPTER 5

CHAPTER 6

CHAPTER 8

CHAPTER 9

CHAPTER 10

LIST OF PLATES

CHAPTER 4

CHAPTER 5

CHAPTER 10

Declaration

No portion of the work referred to in the thesis has been submitted in support of an application for another degree or qualification at this or any other university or institute of learning

(1) Copyright in text of this thesis rests with the Author. Copies (by any process) either in full, or of extracts, may be made **only** in accordance with instructions given by the Author and lodged in the John Rylands University Library of Manchester. Details may be obtained from the Librarian. This page must form part of any such copies made. Further copies (by any process) of copies made in accordance with such instructions may not be made without the permission (in writing) of the Author.

(2) The ownership of any intellectual property rights which may be described in this thesis is vested in the University of Manchester, subject to any prior agreement to the contrary, and may not be made available for use by third parties without the written permission of the University, which will prescribe the terms and conditions of any such agreement.

Further information on the conditions under which disclosures and exploitation may take place is available from the Head of Department

ABSTRACT

Textural and geochemical evidence for *in-situ* fluid-absent partial melting of magnesian metapelites in the Huntly-Knock area of Aberdeenshire provides an insight into processes involved in crustal melting, granitic magma formation, and ~~crystal~~ crystal differentiation.

The intrusion of a sheet-like body of mafic magma, at a mid-crustal level, into Dalradian metasediments led to anatexis of pelitic lithologies from the inner-aureole, and of large xenoliths/rafts from the inner margins of the intrusion.

The three main rock types associated with partial melting are; (i) fine-grained, silica-poor aluminous hornfelses, (ii) igneous-textured cordierite norites, and (iii) garnet tonalites. The silica-poor hornfelses display a high degree of textural equilibrium, and the highest grade hornfelses contain the peak metamorphic paragenesis Grt + Opx + Crd + Pl ± Spl ± Kfs. Biotite, when present, occurs only as small relict plates and quartz is either absent, or only occurs in leucocratic coronas in and around garnets. The cordierite norites are mineralogically similar to the high grade hornfelses, but always contain quartz and biotite. They show well developed igneous textures, with large euhedral or subhedral plagioclase, orthopyroxene and cordierite; quartz is interstitial. Biotite forms late, either as large poikilitic plates, or replacing orthopyroxene in symplectic intergrowths with quartz. The garnet tonalites again display good igneous textures, but lack orthopyroxene, spinel and commonly cordierite. The garnets are large, whilst the matrix often consists of plagioclase, biotite and quartz. The hornfelses are interpreted as the anhydrous, restitic, depleted residues of partial melting. The cordierite norites represent poorly segregated melts with a high proportion of entrained restite, possibly formed from the final phase of melting, with the last dregs of partial melt being unable to separate from its host. The garnet tonalites are also restite-rich melts, though the melt fraction in these rocks is much greater than in the cordierite norites.

Geothermometry on the high grade orthopyroxene-cordierite hornfelses gives temperatures in the range 880 to 960°C, in excess of the temperatures required for extensive fluid-absent partial melting. Water activity calculations and low-total volatile contents in cordierites both indicate that the silica-poor hornfelses and cordierite norites crystallised in low aH_2O conditions.

Andalusite-mica schists and mica schists, exposed to the S of the Huntly Gabbro, are the non-melted protoliths of the silica-poor hornfelses and cordierite norites. Fluid-absent experiments, conducted at 900°C and 5 kbars, on two selected samples from these schists led to the formation of a large volume of quenched melt (melt volumes in excess of 50%). The melts are granitic in composition and peraluminous, making them analogous to 'S'-type granites. The solid residues of melting consisted of combinations of orthopyroxene, cordierite, relict biotite, spinel and ilmenite. These solid run products have compositions which match the compositions of these minerals in the orthopyroxene-cordierite hornfelses and cordierite norites. The experiments thus simulate the processes which led to the formation of the partially melted rocks and indicate that a large volume of melt has been

extracted from the restitic hornfelses.

These rocks therefore represent a snap-shot of the processes by which intrusion of larger mafic bodies, into the lower crust, could lead to extensive fluid-absent partial melting of pelitic rocks, and the formation of mobile 'S'-type granitoid magmas, leaving behind their complementary, depleted granulite residues.

ACKNOWLEDGEMENTS

I would firstly like to thank my supervisors, Dr. G.T.R. Droop and Prof. J.D. Clemens for guidance, advice and for proof reading most of this thesis and Dr. Droop for patient tuition on thermodynamics and phase diagrams.

During my time in the department I have used, or attempted to use various machines and much thanks must go to Dave Plant and Tim Hopkins for teaching me how to 'probe' and Steve Caldwell for setting up cold stages on the S.E.M. (also for the one time he played in our 5-a-side football team, when we beat the league leaders). Cath Davies was very patient with me when I annoyed her on the T.G. and Sue Maher was a star for helping me break the World Record for the fastest prepared poster for presentation at the M.S.G.

A lot of thanks must go to Dr. Gary Stevens, who ran the experiments for me, and welded the capsules (something which I had tried to do, but failed miserably). Gary also gave me some valuable advice and it was his idea to enter our 5-a-side footy team into the league.

Also I've enjoyed sharing an office with Quinny, Hardeep, Jenny (for constant attention), Obi, Mog, Anne-Marie, Rick, Andy Q and a few others. Eating curries has been an integral part of my social life in Manchester (I was thinner when I came here) and my main partner in the sampling of Indian cuisine over the last year or so has been Mog, without her I would have had to settle for take-outs. Graham is thanked for stimulating conversation during many of my long knights in the department (sorry about the pun!), whilst John Rowe has helped boost my moral at difficult times with early morning phone calls, and my holidays with Roly, Jez & Alex in Scotland were excellent, even if I did annoy them by 'Twitching' too much. The footballers also deserve a mention: Paul, Iain, Steve, James(s), Alison(s), Harry, John, Matt, Sam and of course Charlie plus others who have all witnessed my wizardry skills!

In putting this thesis together I have received help from several people, most notably Jason, who quite superbly proof read four chapters and Mog who helped to print out, check, put together and page number the thesis.

Newcastle United deserve much credit. When I started in Manchester they were languishing at the bottom of the second division (I will never forget the 3-0 hammering by Barnsley on a freezing December sunday afternoon), now as I submit they are top of the Premier League (I will also never forgot the 6-0 hammering of Barnsley one year later). How things change!

In Scotland, Joan Harvey was an excellent host for all my visits to Huntly, providing good sustenance and Pete Meads was an admiralble field assistant for a week as well as helping me carry my rocks back to England.

Lastly, and most importantly, none of this would have been possible without the support of my family. My parents and grandparents have helped to motivate me, as well as providing much love and financial support when it was most needed. Without them none of this work would have been possible. This thesis though, is dedicated to my Grandad who would have loved have seen me finish my PhD, but who unfortunately didn't quite make it.

CHAPTER 1 INTRODUCTION

1.1 Introduction to project

This project is a combined field and experimental study on the partial melting of Dalradian metasediments in contact with a mafic intrusion from the Huntly-Knock area of Aberdeenshire, NE Scotland.

In this chapter the problems which are still to be resolved in the studies on partial melting and granite genesis are described briefly. Then the problems which will be addressed in this project are highlighted, and the reasons for the choice of the Huntly-Knock area are discussed, together with the aims specific to this project. An outline of the thesis layout is then presented.

1.2 Major problems still to be resolved

It is generally accepted that peraluminous S-type granites are formed by melting of metapelites to metagreywackes at mid-low crustal levels (e.g. Clemens & Wall, 1981 ; Miller, 1985). Experimental and theoretical studies have shown that major fluid-absent melting of fertile metasedimentary rocks occurs in the temperature range of 850 to 950°C (e.g. Le Breton & Thompson, 1988 ; Vielzuef & Holloway, 1988) via biotite-consuming incongruent melting reactions, such as:

$$Bt + Als + Qtz + Pl = Grt/Crd + Kfs + M \qquad [1.1]$$

(Le Breton & Thompson, 1988)

and;

$$Bt + Qtz + Pl = Opx + Kfs + M \qquad [1.2]$$

(e.g. Vielzeuf & Clemens, 1992 ; Peterson & Newton, 1989).

The melts produced are peraluminous and compositionally analogous to S-type granites.

Field-studies and geothermobarometry conducted on regionally metamorphosed terrains have shown that the pressure-temperature conditions at which this partial melting occurs overlaps with those attained during granulite-facies metamorphism. Such studies have shown that many granulites have formed by fluid-absent partial melting (e.g. Phillips,

1980 ; Waters, 1990 ; Stevens & Van Reenen, 1992). Some granulitic terrains are restitic, indicating that a melt has been extracted from the protolith (e.g. the Ivrea Zone: Sighinolfi & Gorgoni, 1978), whilst others are migmatitic giving evidence of closed-system melting without any melt extraction (e.g. the Southern Marginal Zone of the Limpopo Belt: Stevens & Van Reenen, 1992).

By combining experimental and field-studies a link can be drawn between granulite-facies metamorphism and granite genesis. However, none of the published melting experiments have been undertaken using natural pelites or greywackes as starting products. In such natural systems the protoliths of partial melting can contain minor components which can effect both the melt composition, and the temperature range over which melting occurs (e.g. high contents of Ti and/or F in biotite can stabilise this mineral to temperatures in excess of 950°C (Koberski, 1995)). Although some studies have been made on the effects of these minor components on melting reactions individually, the starting products are still often synthetic. Additionally few field-studies on restitic-granulite terrains have been able to quantify the amount and composition of the extracted melt.

1.3 Problems to be tackled in this project

In this project both field and geochemical studies on natural granulite-facies rocks from a contact metamorphic setting will be made to ascertain whether they are restitic, or occur as anatectic migmatites from which the melt phase was not mobilised, or a combination of both. Field studies will also attempt to correlate the granulite-facies rocks with their unmelted protoliths, allowing calculations to be made, using geochemical data, to estimate the quantities and compositions of any extracted melts.

Experimental studies on natural rock samples from potential protoliths were made to confirm the quantity and compositions of melts and the solid (restitic) products from the melting reactions. Comparisons were then made with the granulite-facies rocks observed in the field and the experimental results.

1.4 Why NE Scotland was chosen?

The Huntly-Knock area of NE Scotland was chosen for this project (Figure 1.1). In

the this area a mafic igneous sheet intrudes medium-grade regionally metamorphosed metasediments of the Dalradian Supergroup. The inner-metamorphic aureole, and inner zone of the mafic sheet contains low-pressure granulite-facies cordierite-bearing hornfelses and closely associated igneous-textured cordierite norites (Read, 1923a). The study of such granulite-facies rocks, formed by contact metamorphism, as opposed to studies from regionally metamorphosed granulite terrains is advantageous for the purposes of this study for the following reasons:

(i) The study of regionally metamorphosed terrains is hampered by slow post-peak metamorphic cooling rates and often by subsequent retrograde metamorphic overprints. This leads to re-equilibration of minerals from their peak compositions, and makes estimation of peak pressure-temperature-fluid conditions from geothermobarometry problematic. Granulites formed by contact metamorphism, caused by the intrusion of medium-sized mafic bodies cool at geologically rapid rates, are less prone to retrograde metamorphism and therefore the mineral compositions from these rocks are more likely to represent those at peak temperature conditions.

(ii) By their very nature regionally metamorphosed granulite-facies terrains are large and often structurally complex. This invariably makes the accurate determination of their unmelted, lower-grade protoliths impossible. The protoliths of rocks formed by contact metamorphism, though, can often be traced by simply following the lithologies of non-metamorphosed rocks towards the contact aureole of the intrusion. Also the temperature gradients around an igneous intrusion will be much higher than in regionally metamorphosed terrains, allowing easier comparison of assemblages from different metamorphic grades in rocks of equivalent bulk composition.

The effects of intrusion of a medium-sized mafic igneous body can additionally be used as a small-scale analogue for the effects of intrusion of larger bodies of mafic magma into the lower crust; this is important as intraplating and underplating by large volumes of mafic magma into the middle to lower crust is suggested to be the major process by which extensive partial melting of fertile source rocks leads to melt extraction and the formation of mobile granitoid bodies (e.g. Clemens, 1990 ; Vielzeuf *et al.*, 1990 ; Stevens &

Clemens, 1994). This in turn is potentially one of the major processes by which crustal differentiation occurs.

1.5 Project aims

To meet the objectives outlined in 1.3 in this project, the following questions will be addressed:

(i) Do the aluminous, hornfelsic lithologies represent restitic granulites, from which a granitic melt has been extracted, or have they simply formed by static recrystallisation of pelitic hornfelses, without any bulk chemical alteration.?

(ii) Did the igneous-textured cordierite norites and garnet tonalites, which are closely associated with the hornfelses, form by partial melting of pelitic protoliths? If they did form by partial melting, then do the cordierite norites represent the sole melt fraction produced?

(iii) Did any melt segregation or mobilisation occur?

(iv) What the pressures and temperatures at which the regionally and thermally metamorphosed rocks formed were?

(v) What were the protoliths of the hornfelses and associated rocks?

(vi) What was the quantity and composition of melt formed (if any)?

These objectives will be tackled using a number of various techniques, which are summarised in the thesis plan which is presented below.

1.6 Plan of thesis

Chapter 2 is a short review of previous work on granite genesis and granulite facies metamorphism. The following chapter reviews the geology of NE Scotland; describing the stratigraphy, structure, and metamorphism of the Dalradian metasediments in the region, and the outcrop, age, petrology and tectonic settings of the Newer Gabbro intrusions, and other allied igneous rocks.

Field-observations from the rocks in and around the Huntly-Knock area are

described and discussed in Chapter 4. Particular attention is taken to the cordierite-bearing hornfelses and the associated igneous textured cordierite norites and garnet tonalites. Additionally the regionally metamorphosed rocks from outside the aureole of the Huntly Gabbro are described, with one of the main aims being to show which lithologies trend towards, and are truncated by the Gabbro.

Thin sections taken from all the rocks types studies are described in Chapter 5. Equilibrium mineral paragenesis from each rock type are given and combined with textural descriptions to give evidence on the metamorphic grade of the rocks, and the processes which may have led to their evolution.

In Chapter 6 the mineral chemical data acquired from analysis of selected samples on the electron microprobe are described . Also the methods, results and implications behind the determination of cordierite volatile contents are presented.

The metamorphism to which the rocks were subjected is described in this Chapter 7, in terms of their pressure-temperature evolution and the sequential mineral reactions with increasing metamorphic grade.

In Chapter 8 geothermobarometry using mineral chemical data from selected samples is used to constrain the pressure and temperature conditions over which the rocks of the Huntly-Knock area evolved.

Whole-rock chemistry from XRF analysis is used in Chapter 9 to provide evidence on the processes by which the cordierite-bearing hornfelses, cordierite norites and garnet tonalites evolved. The whole-rock data are also used for mixing calculations, estimating theoretical melt compositions of melts 'extracted' from the restitic cordierite-bearing hornfelses.

Chapter 10 describes the experiments conducted on the internally-heated pressure vessel. The choice of starting material and run conditions are outlined, the results from the experiments are presented, and the implications of these results for the rocks of the Huntly-Knock area and for the process of granite genesis as a whole are discussed.

Chapter 11 is a discussion of all the results from whole of the thesis, tying together the findings from all of the previous chapters. Implications are presented for the evolution of rocks from the Huntly-Knock area and for granite genesis and crustal differentiation as a whole.

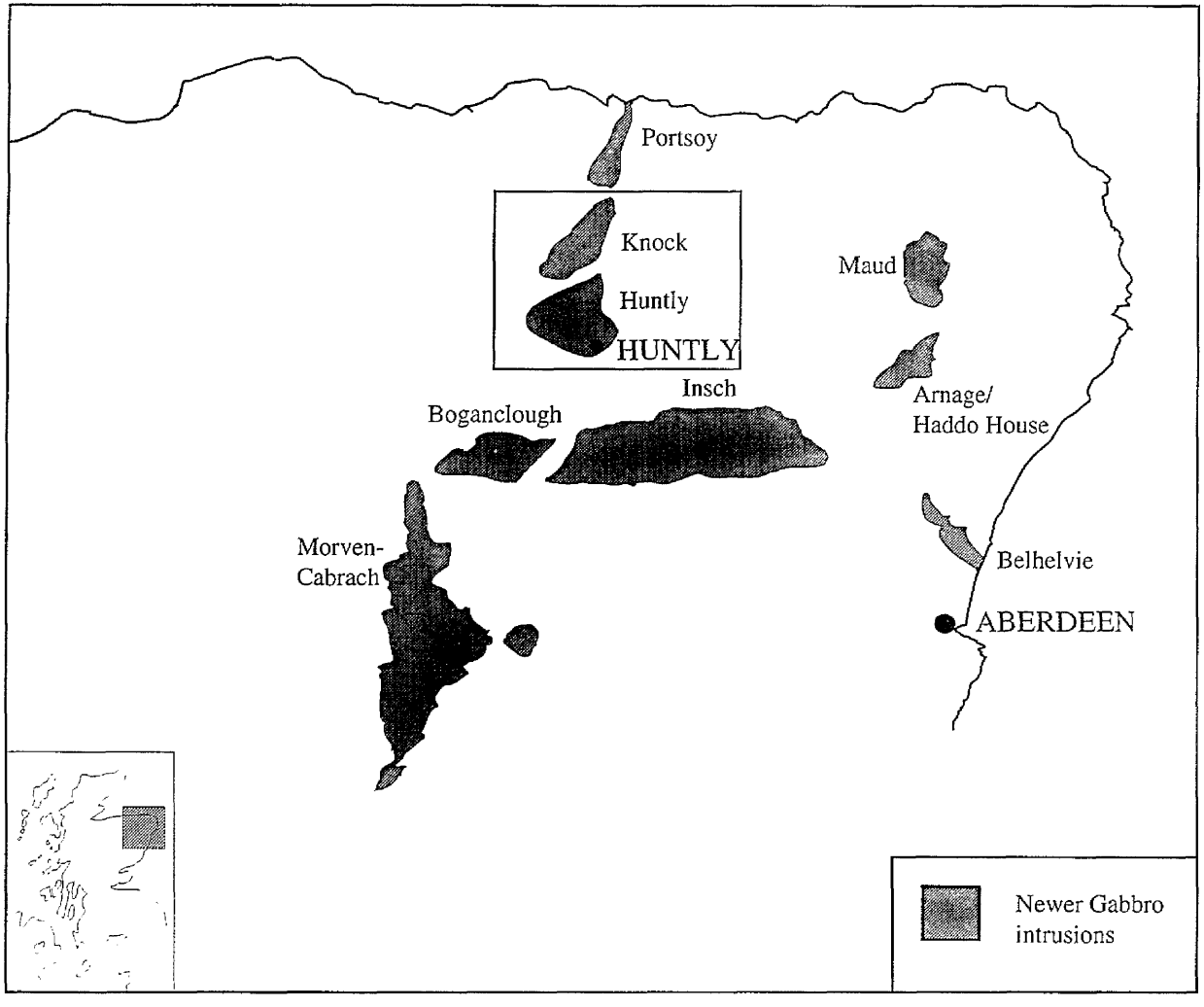

Figure 1.1 Location of the Huntly-Knock intrusions and the other Caledonian Newer Gabbro intrusions.

CHAPTER 2 PARTIAL MELTING AND GRANULITE FACIES METAMORPHISM

2.1 Introduction and Definition

The partial melting of a rock will be controlled by the following factors; P-T conditions, the presence (or absence) of fluids and the composition of the rock.

The temperature at which a rock will melt will be lowered by the presence of free H_2O fluid. The effect of other fluid components in the rock (especially CO_2) will also modify the P-T conditions under which a rock will partially melt. If the fluid is pervasive, that is the fluid acts as a continuous film over grain boundaries, then the reactions that occur are termed fluid-present (e.g. Clemens, 1990 ; Thompson, 1988).

If no fluid is present, or if there is no effective contact between fluid and grain boundaries, then the reactions can be termed fluid-absent (Clemens, 1990).

The terms 'vapour-absent melting' and 'dehydration melting' are not used here. Clemens (1990) observed that the term 'vapour-absent' melting is inaccurate simply because 'vapour' implies that a gaseous fluid is present which, in mid-lower crustal environments, is not the case. Clemens (1990) also criticised the term 'dehydration melting' as it can be misinterpreted as a process of dehydration of the rocks followed by partial melting in the presence of the liberated H_2O.

2.2 Fluid-Present Melting

For fluid present-melting to occur, a pervasive fluid phase must be present. However, both H_2O and CO_2-rich fluids may not be truly pervasive in crustal rocks. Watson & Brenan (1987) showed that CO_2-rich fluids formed isolated pockets in most isotropic rocks. H_2O-rich fluids may also not be truly pervasive (e.g. Rumble, 1988).

2.2.1 H_2O-Rich Fluids

Partial fusion of rocks containing quartz and feldspar will start at temperatures around 650°C at pressures in excess of two kilobars in the presence of an H_2O-rich fluid. (e.g. Le Breton & Thompson, 1988; Thompson, 1990; Clemens, 1990, 1992). A small amount

of free water is likely to be present in high-grade metamorphic rocks as some permeability and porosity (<1%) exists in these rocks due to the presence of microstrucures such as joints and faults (e.g. Rutter & Brodie, 1985).

Therefore, it seems likely that melting would begin in many rocks at the above conditions. However, all the H_2O present will be dissolved by the first melt produced, giving a water-undersaturated melt, unless there was a high influx of H_2O into the system. Only a small amount of melt could be produced, and the system will then become fluid-absent Clemens (1992).

If there were an adequate supply of H_2O, and an increase in temperature, larger volumes of melt could be created by the breakdown of hydrate minerals in the presence of fluid (Clemens, 1990). Experimental work by Vielzeuf & Holloway (1988, Figure 5) showed that incongruent melting involving the breakdown of micas in the presence of H_2O can occur at temperatures ranging from 730°C upwards. Examples of such reactions are:

$$Bt + Sil/Ky + Pl + Qtz + Fluid = Grt / Crd + M \qquad [2.1]$$

$$Bt \pm Grt + Pl + Qtz + Fluid = Opx \pm Hbl/Cpx + M. \qquad [2.2]$$

Reactions of this kind are believed to have formed some amphibolite-facies migmatites and some low pressure granulite-facies rocks. Vernon *et al.* (1990) quote an example of the later in the Mount Stafford area of Central Australia, with fluid-present melting having occurred at temperatures of 720°C-760°C at pressures of 2 to 3.5 kbars.

In most cases, the volume of melt produced by such fluid-present reactions is not deemed to be large, due to the limited supply of H_2O, which is removed by solution in the initial melts produced (Thompson, 1990).

Once all the available fluid has been removed by these melts no further melting will occur until the temperatures have been raised sufficiently for fluid-absent melting reactions to occur.

2.2.2 CO_2-Rich Fluids

The effect of CO_2-rich fluids is to buffer the aH_2O to lower levels (Newton *et al.*, 1980). The flushing of the crust with a CO_2-rich fluid will cause micas and amphiboles to

dehydrate by subsolidus reactions and no melt could be formed until the temperature reached at least 1000°C. The flushing of CO_2 is, however, unlikely to have occurred in most granulite-facies terrains, as such an event would result in:

(i) the precipitation of abundant graphite (Lamb & Valley, 1984),

(ii) the crystallisation of widespread assemblages typical of high aCO_2 conditions,

and (iii) the crystallisation of widespread high-variance externally buffered assemblages.

None of these phenomena are common in granulite-facies terrains.

Fitzsimons (1994) looking at isotopes from the CO_2 present in cordierites from granulites in E Antartica, noted that carbon isotopic signatures varied over a scale of hundreds of metres. This could only occur if the carbon had been locally derived, as pervasive flushing of CO_2 through the terrain would have left behind a single, widespread carbon isotopic signature.

2.3 Fluid-Absent Melting

For rocks in the mid-lower crust, prograde metamorphism, with a slow rate of temperature increase, will only lead to the release small volumes of volatiles from the breakdown of hydrous minerals. These volatiles can then escape by diffusion through grain boundaries, and the system will remain fluid-absent (Thompson, 1983). The exception to this may occur when a discontinuous reaction releases a large volume of volatiles over a small temperature interval. Therefore, fluid-absent metamorphism would be expected to be the rule in most tectonic regimes (Thompson, 1983).

Brown & Fyfe (1970) experimentally investigated the formation of melt fractions in fluid-absent systems using hydrous minerals as starting products. These experiments showed that melt fractions could be formed by the heating of muscovite, biotite and hornblende to progressively higher temperatures, with the solid residues from melting including pyroxenes and sillimanite, analogous to the minerals present in granulite facies rocks.

Experimental investigations showed that fluid absent melting of muscovite could

occur by the reaction;

$$Mu + Qtz = Kfs + Sil \text{ or } Ky + M \qquad \text{(Storre, 1977).} \qquad [2.3]$$

Such fluid-absent melting reactions have been further investigated by petrogenetic modelling, experimental work, and fieldwork studies. (e.g. Grant, 1985 ; Thompson, 1982 ; Le Breton & Thompson, 1988 ; Clemens & Vielzeuf, 1987 ; Waters, 1988 ; Vielzeuf & Holloway, 1988 ; Stevens & Van Reenen, 1992).

2.3.1 Fluid-absent melting of muscovite and biotite

The constraint of petrogenetic grids for the fluid-absent melting (e.g. Thompson, 1982 ; Grant, 1985) of micas to P-T space is difficult to achieve. This is due to the exchange of K-Na, Al_2-Mg-Si, Fe^{3+}-Al and Fe^{2+}-Mg in the micas which gives the conditions in which the reactions occur a high variance (Thompson, 1988).

The experimental work of Le Breton & Thompson (1988) addressed the conditions under which fluid-absent melting of muscovite and biotite occurred due to the reactions:

$$Mu + Pl + Qtz = Kfs + Als + M \qquad [2.4]$$

$$Bt + Pl + Als + Qtz = Kfs + Grt + M. \qquad [2.5]$$

The P-T grid (Le Breton & Thompson, 1988, Figure 3) shows that at high pressures of around 10 kilobars these two reactions converge to give a third, simultaneous melting reaction:

$$Bt + Mu + Plg + Qtz = Grt + Kfs + M. \qquad [2.6]$$

The amount of H_2O recovered from the micas in these reactions is small. Le Breton & Thompson calculate that a rock with 31wt% biotite will contain 1.2% H_2O. The melt will thus be rather water-undersaturated and the system will remain fluid-absent (Vielzeuf & Holloway, 1988).

The lower temperature fluid-absent melting of muscovite (reaction 2.3) will probably only produce a small amount of melt ≈6vol% at 5 kbars (Clemens & Vielzeuf, 1987). Such melts are water rich, will probably be unable to ascend and will freeze *in situ* forming veins,

pockets and small plutons (Clemens & Vielzeuf, 1987).

The biotite-consuming reaction 2.5 occurs over a large temperature range. In the experimental study of Le Breton & Thompson (1988) the melting reaction started at temperatures as low as 780°C. The melt proportion at this stage, however, was small. The experimental work of Vielzeuf & Hollaway (1988) and Le Breton & Thompson (1988) indicates that extensive melting will not occur until temperatures of around 850°C are reached. In quartz-saturated rocks at temperatures above 850°C, biotite may be consumed by melting reactions such as:

$$Bt + Pl + Qtz = Opx \pm Grt/Crd \pm Cpx/Hbl + Kfs + M \qquad \text{Clemens (1990)} \qquad [2.7]$$

This reaction will occur if:

(i) The aluminium silicate in the source rock is consumed before all the biotite in reaction 2.2.,

(ii) If aluminium silicate minerals were never present in the source rock (i.e. the source rock was not highly peraluminous).

Reactions 2.4, and 2.7, may be stabilised to higher temperatures due to the substitution of Ti and F in biotite (Le Breton & Thompson, 1988). This has the effect of increasing the variance of the above mentioned reactions (i.e. converting discontinuous reactions into continuous ones) and thus modifying the petrogenetic grids of Grant (1985) and Thompson (1982).

2.4 Melt Quantities and Melt Extraction

The volume of melt produced by fluid-absent melting is related to source rock composition and the pressure-temperature régime (Clemens & Vielzeuf, 1987).

The fertility of a potential source rock is a function of its hydrous mineral content. In a fluid-absent system all the available H_2O will be held in these hydrous minerals. Thus the melt volume which can be produced will also be a function of the H_2O content of the rock (Le Breton & Thompson, 1988). Estimates for the volume of melt produced as a product of temperature and wt% H_2O have been made by Clemens & Vielzeuf (1987, Figure 6); Le

Breton & Thompson (1988); and Johannes & Holtz (1990, Figure 4.6). These estimates show that at temperatures of around 800°C and a pressure of 5 kilobars a melt fraction of 20% can be generated from a source rock with a water content of only 0.8 wt%. (Johannes & Holtz, 1990). A pelitic rock containing 20% biotite would contain the 0.8% of water needed.

Pressure is an important factor in the amount of melt produced. This is due to the pressure dependence on the solubility of water in the silicate melt and at a given temperature the melt quantity produced will be greater at lower pressures (Clemens & Vielzeuf, 1987).

Therefore it can be seen that fluid-absent melting can potentially create reasonably large melt volumes. Less than 20 wt% melt may be enough for melt segregation to occur and for the formation of mobile granitoid magmas (Clemens & Vielzeuf, 1987 ; Clemens, 1992).

2.5 Rarity or Absence of K-feldspar in Leucosomes

The melts formed should, in theory, crystallise to compositions close to the "granite minimum" of Tuttle & Bowen (1958). The orthoclase content of the "granite minimum" should be around 20-30 wt% (Johannes, 1985, Figure 2.1). However, K-feldspar can be absent (as in some of the leucosomes in this study and those of (Ashworth, 1976) or scarce with the leucosomes containing essential quartz and plagioclase (Ashworth, 1985). Amit & Eyal (1976) argued that leucosomes of this type could not be formed by partial melting. However, Ashworth (1985) outlines several possibilities as to how melts could crystallise without K-feldspar. The most attractive of these arguments are:

(i) the K-feldspar may, in fact, crystallise from the melt. However, some melt mobilisation and extraction has removed the K-feldspar. The leucosomes will then crystallise without K-feldspar. For this to have happened the leucosomes should show a cumulate-type texture in thin section;

(ii) if the crystallisation of biotite from the melt is early then the K content of the melt may be consumed and no K-feldspar can therefore crystallise. This is a process termed 'trondhjemitic' melting and Ashworth (1976) uses this term to distinguish such rocks from K-feldspar bearing 'granitoid' migmatites.

2.6 Importance of Garnet Porphyroblasts in Leucosomes

In the biotite consuming melting reaction in the KFMASH system,

$$Bt + Sill + Qtz = Gt + Crd + Ksp + M. \qquad [2.8]$$

Garnet is one of the products of this reaction. Field studies show that garnets are common in the leucosomes of low-to medium-pressure migmatites. The reasons for the presence of, and preservation of, these garnet phenocrysts have been studied in detail by Powell & Downes (1990).

Powell & Downes (1990) firstly address the problems of the presence of such garnet porphyroblasts in leucosomes. These are:

(i) Why are garnets present in the leucosomes if segregation of leucosomes from restite is a physical process?

(ii) If all the reaction products are present in the melt (i.e. garnet + melt), cooling should lead to a retrogressive reaction in which the garnet is converted back into biotite.

(iii) Why are the mineral compositions (e.g. Fe/Mg ratios of garnet and biotite) in leucosomes and host the same, and not fractionated, as might be expected during to melt segregation?

(iv) Why do leucosome compositions differ from 'expected' melt compositions?

Problems i and ii can be answered if it is considered that instead of numerous small garnets being grown as products of reaction 2.5, nucleation around a few early formed garnets would continue instead. The other products of the reaction (i.e. melt and K-feldspar would then form around the garnets also). Diffusion from the host rock would give the garnet and melt the required components, thus explaining the similarities in the compositions of minerals in both leucosomes and hosts.

Once the reaction has completed and the system begun to cool, Powell & Downes (1990) point out that the garnet should be out of equilibrium with the leucosome. However, garnets seen in such leucosomes commonly show no evidence of break down. The simplest explanation for the preservation of these prograde garnets is that some melt was

lost from the system before the leucosomes crystallised. The effect of this would be to stabilise the garnets during retrogression. Another explanation for the preservation of garnets, is that a thin film of Mn-rich garnet develops during crystal growth. This remains in equilibrium with the melt and prevents the dissolution of the cores (by armouring).

The extraction of a small amount of melt can also explain the absence of K-feldspar in some leucosomes, as discussed in section 2.5.

2.7 Mafic Intrusions as a Heat Source for Partial Melting

For crustal rocks temperature normally increases with depth in accordance with an average geotherm of 20°C per km. This does not account for the temperatures required for fluid-absent melting of rocks (800-850°C) until depths of 40 km are reached. Geobarometry shows that many partially melted rocks were formed at depths of 15 km or less. One way in which such temperatures can be reached, in continental crust at low-medium depths, is by the intrusion of basic magmas. Huppert & Sparks (1988) investigated the effect of the intrusion of basic sills into the crust by using thermal modelling, and concluded that the temperatures required for extensive partial melting in the crust could be reached.

It can therefore be shown that a mechanism such as crustal underplating or intraplating by basic magma could provide the heat source needed for extensive partial melting and the creation of substantial volumes of granitic material.

CHAPTER 3. GEOLOGY OF NE SCOTLAND

3.1 Introduction

The following chapter comprises a literature review of previous work on the geology of the area in studied this project, namely the Huntly-Portsoy area of the Buchan District in Aberdeenshire, NE Scotland. The regional geology of the Buchan District is reviewed, bringing into context the geology of the Huntly-Portsoy area, which is described in more detail.

The regional metamorphic rocks of the Buchan District belong to the Dalradian Supergroup (Harris & Pitcher, 1975). The Dalradian Supergroup consists of metamorphosed marine sediments, with sub-ordinate meta-igneous rocks and crops out in a SW-NE trending belt from western Ireland, through to Islay, in the south-west Highlands, to the Banffshire coast and the Shetlands Islands to the NE (Figure 3.1.1).

The rocks of the Dalradian Supergroup underwent polyphase deformation, much crustal shortening and regional metamorphism from the Proterozoic to the early Ordovician, in an event termed the Grampian Orogeny (Lambert & McKerrow, 1976 ; Johnson, 1991 ; Tanner & Leslie, 1994). This orogenic activity is explained in plate tectonic theory, by northward subduction of oceanic crust, during closure of the ancient Iapetus Ocean (Lambert & McKerrow, 1976).

Intruded into the Dalradian of Aberdeenshire, NE Scotland are two suites of mafic-igneous rocks, the deformed and amphibolitised 'Older Gabbros' and the relatively undeformed post-tectonic 'Newer Gabbros' of Read (1919, 1923b). Post-tectonic granitic intrusions also occur, mainly in the southern parts of Aberdeenshire (Figure 3.1.2).

3.2 Regionally Metamorphosed Rocks

3.2.1 Introduction

The regionally metamorphosed rocks, which outcrop over the majority of NE Scotland, collectively belong to the Dalradian Supergroup. Harris & Pitcher (1975) divided the Dalradian Supergroup into three major groups; the Southern Highland Group, the Argyll (Middle) Group, and the Appin (Lower) Group. Figure 3.2.1 is a fold-out map, showing

the geology of NE Scotland, as mapped by the Geological Survey.

The base of the Dalradian Supergroup has traditionally been placed within the Upper Precambrian, with the succession passing through to the Cambrian, and possibly even up into the Ordovician (e.g. Harris & Pitcher, 1975 ; Downie *et al.*, 1971). However, Rogers *et al*. (1989) using U-Pb zircon data give a crystallisation age of 590 ± 2 Ma for the Ben Vuirich granite, which intrudes rocks of the Appin and Argyll Groups in the Central Highlands. Detailed structural study has shown that the Ben Vuirich granite was intruded post-D_1, but pre-D_2 as the granite is overprinted by the main S_2 fabric (Tanner & Leslie, 1994). Therefore all Dalradian sedimentation must have been Precambrian The fossiliferous, Lower Cambrian, Leny Limestone cannot be part of the Dalradian succession, and probably belongs to the Highland Border Complex (Rogers *et al.*, 1989).

3.2.2 Structural Evolution of the Dalradian

Geophysical studies of Scotland show the continental crust to be between 25-35km over the Dalradian, with the Dalradian Supergroup being 10-15km thick, and underlain by pre-Caledonian, Lewisian-type basement (Bamford *et al.*, 1977 ; Johnson, 1991). Phillips *et al.* (1976) believed that the Dalradian was deposited in a rifted basin, some distance away from the ancient Iapetus ocean to the south.

However, Anderton (1980) believed that the Iapetus Ocean had still not opened whilst much of the Dalradian was being deposited in a rifted basin. The evidence given for this is the supposed northwards movements of the ice sheets which deposited the Port Askaig Tillite and Anderton (1980) argues that this ice sheet must have grown and moved from continental crust to the south of the Dalradian. In Anderton's model the Iapetus Ocean began to open during Southern Highland Group times, with extensive rifting leading to rapid subsidence and to volcanic activity in the Dalradian.

The model of the evolution of the Dalradian as a rifted margin, with syndepositional faults trending NE-SW is challenged by Graham (1986) who recognised a number of important transverse NW-SE structures and presented a model in which the entire Dalradian was deposited in pull-apart basins, in a dextral transtensional regime. The Cruachan Lineament is suggested as being one such NW-SE trending structure which controlled Dalradian sedimentation (Graham, 1986).

3.2.3 Stratigraphy and Depositional History

The Dalradian of the Banffshire district was first mapped by Read (1923b, 1936) who used the well exposed coastal section to divide the Dalradian into two main divisions, the lower Keith Division and the upper Banff Division.

A summary of the stratigraphy of the Banffshire District is shown in Table 3.1. The Southern Highland Group is held to be equivalent to part of the Banff Group of Read (1923b), the Argyll Group to the lower parts of the Banff Division and the upper Keith Division, and the Appin Group to the lower and middle rocks of the Keith Division.

Much of the work on the depositional history of the Dalradian concentrates on the Dalradian of the SW Highlands. This is mainly due to the good exposure and preservation of original sedimentary structures in the relatively mildly metamorphosed rocks of the southwestern belt, compared to the poorly exposed and mainly higher grade rocks of the central and north-eastern Dalradian. However, Johnson (1991) argues that it is fair to suggest that the sedimentary environments of the SW Highlands are characteristic of the Dalradian elsewhere.

The base of the Lower Appin Group is characterised by quartzites (e.g. Eildhe Quartzite, and the Cullen Quartzite of Banffshire). The presence of cross-bedding with polymodal current directions, in the Glen Coe and Binnein Quartzites, shows these rocks were deposited in a shallow-water marine shelf environment (Hickman, 1975). The succession of these quartzites by finer-grained black shales and limestones over much of the Dalradian terrain suggests that the rocks of the mid to upper Appin Group were deposited in deeper water in an anoxic environment (Anderton, 1985).

The base of the Argyll Group is marked by the widespread occurrence of the glacially derived Port Askaig Tillite. The tillite crops out from the Dalradian of Ireland, to the Banffshire coast (Spencer & Pitcher, 1968 ; Johnson, 1991). Anderton (1980) presents evidence for the tillite having been deposited by a northwesterly moving ice sheet, probably moving off a large land mass to the south-east.

After the glacial episode, marine conditions returned, with the deposition of quartzites in a tidal shelf environment (Anderton, 1985). This was followed by a period of rapid subsidence, deepening of water and the deposition of turbidites and mudstones (e.g. Crinan

Grits, Lower Whitehills 'Group' of Banffshire) with eruption of the Tayvallich Volcanics (Anderton, 1985; Johnson, 1991).

The Southern Highland Group consists mainly of turbidites, with some volcanic rocks. Sutton & Watson (1955) describe a succession of greywackes and mudstones from NE Scotland, and show them to have been deposited by deep-water turbidity currents. This succession covers the whole of the Southern Highland Group in NE Scotland, consisting of the Upper Whitehills, Boydie Bay 'Groups', and the Macduff Slates, and is in excess of 2 km thick. Some glacial activity in Southern Highland Group times is inferred from the presence of a drop-stone horizon in the Macduff Slate (Sutton & Watson, 1954). Provenance studies of this group show that the clastic sediments contain granitic clasts and fragments of alkali feldspar (e.g. Sutton & Watson, 1955). The supply of these more immature sediments, compared to the mature sediments of the Appin and Argyll Groups, suggests uplift of an adjacent new landmass in Southern Highland times (Johnson, 1991).

3.2.4 Structural Geology of NE Scotland

The Dalradian rocks of the Buchan District lie mostly the right way up, in a large, shallow, north-south-trending syncline, termed the Boyndie Syncline, with a large, steeper anticline, the Buchan Anticline, to the east of the district (Sutton & Watson, 1956). Read & Farquhar (1956) interpreted the Buchan Anticline as being "a structure imposed on the great recumbent fold of a nappe"; they termed the latter structure the 'Banff nappe', and argued that the migmatitic core of the fold is separated from the Upper Dalradian by a major dislocation, the Boyne Line of Read (1923, 1955). Read (1923) suggested that the Boyne Line occurs as a folded thrust-plane, along which easterly members of the Keith Division, and westerly members of the Banff Division disappear.

Stewart and Johnson (1960) showed that the Newer Gabbros were all emplaced at similar structural levels, just before or during the D_3 deformation event, and their present-day distribution is due to the folding of the Boyndie Syncline. Stewart (1960) suggested that the Boyndie Syncline is a D_3 structure, which is superimposed on earlier D_1 and D_2 structures.

Treagus & Roberts (1981), however, re-examined the relationships of the Dalradian rocks of the Banffshire coast, stating that the geometry of D_1 minor folds supports the

contention that the Boyndie Syncline must be a D_1 structure. Previously workers believed the Boyndie Syncline to be a late D_3 structure (Johnson & Stewart, 1960 ; Johnson, 1962). D_2 structures are shown to be developed only locally to the west, being strongly developed in the Portsoy 'Group' and the Cowhythe gneiss and possibly related to thrusting. Late D_3 folding occurs as monoclinical folds, and a crenulation fabric on the steep limb of the Boyndie Syncline.

D_3 refolding of the Boyndie Syncline is a likely explanation for: (a) the shape of the metamorphic isotherms and isobars in the region (see 3.2.4), and (b) the present-day arrangement of the Newer Gabbros. Furthermore the need for the existence of a distinct Banff nappe is shown to be unnecessary, with the Dalradian of the Buchan District either occurring as (a) an uninverted limb of an extension of the Tay Nappe, or (b) (as preferred by Ashcroft *et al.* (1984)) that the Buchan Dalradian is autochthonous, to the extent that it is underlain by the basement on which it was deposited.

The existence of the 'Boyne Line' has also more recently been put into doubt, Ashworth (1975) suggested that the Boyne Line had little or no effect on the Dalradian stratigraphy in the region. The Portsoy lineament is suggested to be a more likely major tectonic break (Ramsay & Sturt, 1979 ; Treagus & Roberts, 1979). Thrusting along the Portsoy lineament, related to local D_2 deformation led to westward thrusting of the Buchan terrain, providing part of the tectonic thickening required for the surrounding, structurally lower Dalradian. Later movements along the Portsoy lineament led to its steepening to its present day position (Baker, 1987 ; Beddoe-Stephens, 1990).

Status of the Cowhythe Gneiss

The Cowhythe Gneiss is mainly a biotite-gneiss, outcropping on the eastern margins of the Huntly-Knock-Portsoy gabbros, and is stratigraphically correlated with the Donside, Ellon, and Queens Head Gneisses of Read (1923b, 1955). Read(1955) suggested that these gneisses were formed by migmatisation of pelitic rocks which are stratigraphically equivalent to the Ben Lui, Ben Lowes, and Sron Bheag Schists of Perthshire.

Read (1923b) considered the Cowhythe Gneiss to be part of the Dalradian succession in NE Scotland, overlying the Portsoy 'Group', and being succeeded by the Boyne Limestone. Ashworth (1972) suggested that there is a gradual transition from the fine, dark

schists of the Portsoy 'Group', to the migmatised muscovite-biotite schists of the western Cowhythe 'Group', and then to a muscovite-free Central Unit consisting mainly of biotite-gneiss.

However, Precambrian Rb/Sr ages for the Ellon and Inzie Head gneisses, and the presence of mylonitisation and shearing at the base of the gneisses led Sturt *et al.* (1977), and Ramsay & Sturt (1979) to believe that the Cowhythe and allied gneisses are slices of pre-Caledonian gneissic basement, thrust into their present positions during the Caledonian orogeny. This theory requires that the overlying Banff division rocks form an allochthonous assemblage, decoupled from the underlying basement during thrusting. Ashcroft *et al.* (1984), however, in supporting the idea that the Dalradian of NE Scotland is autochthonous, disagrees with the contention that Cowhythe and allied gneisses are pre-Caledonian. It is also important to note that, since the Dalradian succession has recently been shown to be entirely Precambrian, then the Precambrian ages for the given Ellon and Inzie Head gneisses (Sturt *et al.*, 1977) no longer constitute valid evidence for a pre-Dalradian age for these gneisses.

3.2.5 Regional Metamorphism

Pelitic rocks are best suited to a study in NE Scotland because: (a) they host a wide variety of mineral assemblages, which are controlled by the P-T-volatile conditions prevalent, and (b) pelitic rocks are common and widespread over NE Scotland.

Barrow (1893) showed that the different metamorphic assemblages in the pelitic rocks of the Central Highlands reflected different conditions of metamorphism. By mapping lines represented by the appearance of index minerals Barrow (1912). Elles & Tilley (1930) demonstrated that the metamorphic grade of the Dalradian rocks increases from the Highland Boundary Fault northwards, with the zones being defined, by the index minerals chlorite, biotite, garnet, staurolite, kyanite, and finally sillimanite.

However, Read (1923b, 1952), then Chinner (1966) and Harte & Hudson (1979) showed that the metamorphic sequences in the Buchan district of NE Scotland differed considerably from those of the Central Highlands, characterised by the index minerals ~~garnet~~ cordierite, andalusite, staurolite, then sillimanite-alkali feldspar, or kyanite. The rocks of this area are termed as belonging to a Buchan zonal sequence, distinguishing apart from the

Barrovian zone rocks of the Central Highlands.

Chinner (1966) used the Al_2SiO_5 polymorphs to map metamorphic isograds over NE. Scotland, defining 3 isograds; an andalusite isograd developed from hydrous assemblages, a kyanite isograd developed from hydrous assemblages, and an andalusite + kyanite isograd (Chinner, 1966. Figures 1 & 2).

The presence of sillimanite in the Buchan district is problematic. This is due to its often sporadic occurrence, usually as fibrolite, and the boundaries of regional sillimanite are complicated by the thermal metamorphism of the Newer Gabbros (Chinner, 1966 ; Harte & Hudson, 1979). This is highlighted by the presence of sillimanite in the Cowhythe Gneiss and the Buch of Cabrach where its presence is shown to be related to Newer Gabbro intrusions (Ashworth 1975 ; Fettes 1970). However, the presence of some regional sillimanite cannot be excluded, especially to the E. and SE. of the Buchan district where its presence does not appear to be solely related to gabbroic intrusions (Harte & Hudson, 1979; Baker & Droop, 1983).

Harte & Hudson (1979) presented an updated isograd map of NE Scotland, including zones defined by the first appearance of garnet and staurolite for lower-grade rocks. They also defined zonal sequences (facies series) for the area, highlighting the differences between higher-pressure Barrovian metamorphism, characterised by the presence of garnet and kyanite and structurally higher, lower-pressure Buchan metamorphism, characterised by the occurrence of andalusite and cordierite. Harte & Hudson (1979) also constructed a petrogenetic grid and attempted to quantify the peak pressure-temperature conditions, constructing maps of isotherms and isobars. These iso-lines are parallel to the limbs of the Boyndie-Turiff Syncline. This suggests that this D_1 structure (Treagus & Roberts, 1981) was refolded during M_3 (section 3.2.3), as the main metamorphic crystallisation event occurred just prior to, or during M_3 (Johnson, 1962 ; Fettes, 1970).

The occurrence of high-temperature minerals at low pressures in the Buchan district is indicative of a high geothermal gradient. A possible cause of this would be intrusion of mafic magma, at depth, possibly associated with the intrusion of the Newer Gabbros (Harte & Hudson, 1979).

More recently, geothermometry, and geobarometry has been carried out on rocks from the Buchan area, giving quantitative estimates of peak metamorphic temperatures, and of

overburden at the time of metamorphism. Hudson (1985), using garnet-hornblende and garnet-biotite calibrations, estimated temperatures ranging from 430 ± 15°C at the cordierite isograd, up to 550 ± 40°C in the upper staurolite zone. Pressure estimates, using Grt-Cpx-Pl-Qtz and Grt-Pl-Ep-Qtz-fluid calibrations yield pressures ranging from 2 kbars in the Turriff-Boyndie Syncline, to 4.5 kbars at the kyanite/andalusite isograd, at Portsoy. This implies overburdens, at the peak of metamorphism of 6km at the Turriff-Boyndie Syncline, up to 17 km at the Portsoy kyanite-andalusite locality. Droop & Charnley (1985) estimated pressures of between 4 and 5 kbars for the inner-aureoles of the Newer Gabbros, implying that the gabbros were all intruded at a similar crustal level. The kyanite-andalusite isograd lies structurally just below the Newer Gabbros, and the similar pressure estimate (4.5 kbars), for this isograd, suggests that very little, or no erosion had occurred between peak metamorphism, and the intrusion of the gabbros (Hudson, 1985).

Dempster *et al.* (1995) presented a model by which the overprint of kyanite after andalusite was linked to a pressure increase caused by intrusion of the Newer Gabbro intrusions, with this magmatic loading synchronous with the main tectonothermal event that generated the low-pressure metamorphism in NE Scotland (Illustrated in Figure 5 of this paper).

3.3 Igneous Rocks of NE Scotland

3.3.1 Introduction

Read (1919, 1923b) distinguished four main groups of intrusive igneous rocks in the Buchan District of NE Scotland. These are; (i) Older Basic rocks, pre-tectonic sill-like bodies of ultramafic and mafic rocks, (ii) less common Older acidic rocks, occurring mainly as narrow lenses of augen gneiss, (iii) Newer Basic rocks, and (iv) Newer Granites, forming large plutonic intrusions, mainly to the south of the area. The 'Older' igneous rocks were intruded prior to the main Caledonian deformation events, and are therefore distinguished from the undeformed, post-tectonic 'Newer' igneous rocks by the presence of a strong foliation, recrystallisation, and amphibolite-facies metamorphism (Read, 1919 ; 1923b).

3.3.2 Structural Status of the Newer Gabbros

Read (1923) showed that the Newer Gabbros were intruded after initial folding of the Dalradian, but prior to the deposition of the Old Red Sandstone.

Using the relative time scale of Johnson (1962), Fettes (1970) showed that a third-generation cleavage post-dates the Newer Gabbros. The semi-concordance of regional metamorphic isograds to the margins of the Insch Gabbro was interpreted as an effect of the gabbros being intruded during, or soon after the main M_3 metamorphic crystallisation event in the region.

3.3.3 The Newer Gabbros

(a) Outcrop, Age, and Occurrence

The Newer Gabbros, as described by Watt (1914) and Read (1919, 1923a, 1923b) are a suite of mafic igneous rocks, consisting of peridotites, picrites, and gabbros, with minor quantities of syenitic differentiates. These include intrusions at Huntly, Insch, Maud, Haddo House, Belhelvie, Arnage, Morven-Cabrach, and Boganclogh. Read's (1919) criterion for distinguishing the 'Newer' from the 'Older', gabbros, namely that the 'Older' gabbros can be distinguished by their foliation, and amphibolitisation, has since been challenged. The best example of this is the Morven Cabrach intrusion, which Allan (1970) showed to be entirely part of the 'Newer' suite. Robertson (1988) showed that 'Newer', or 'Younger' mafic rocks were in places strongly deformed in shear zones, making them indistinguishable from the 'Older' series.

Pankhurst (1970), dated the 'Newer' Gabbros, using the Rb-Sr whole-rock isochron technique. This gave a crystallisation age of 486 ± 17 Ma, placing the gabbros in the early Ordovician. As the Newer Gabbros are shown to have been intruded during, or soon after the main regional metamorphic crystallisation event (e.g. Fettes, 1970), this age is also taken as being the age of this event.

Positive Bouger gravity anomalies over much of NE Scotland, led McGregor & Wilson (1967) to conclude that the exposed gabbros form part of a single, continuous, mafic sheet, varying in thickness from 1-2 km near Huntly to 7km at Cabrach. Allan (1970), in a study of the Morven Cabrach intrusion suggested that this intrusion may have acted as a

feeder pipe to the other Newer gabbros. However, Droop & Charnley (1985), using geobarometry of the inner aureoles, showed that all off the Newer Gabbros were emplaced at similar structural levels, placing this observation in doubt.

Studies of other members of the Newer Gabbro suite (e.g. Wadsworth *et al.*, 1966 ; Clark & Wadsworth, 1970 ; Stewart, 1946 ; Ashcroft, 1970) have shown that there are considerable differences between the Huntly-Knock-Portsoy, Insch, and Belhelvie masses. One possible explanation for this could be that the bodies never formed a single sheet like intrusion but were, instead, intruded as separate bodies of magma with differing compositions (Munro 1970).

(b) Tectonic Setting

Synorogenic mafic igneous rocks in Connemara, Ireland have been correlated with the Newer Gabbros of NE Scotland. These intrusions have been dated at 510 ± 15 Ma (Pidgeon, 1969) compared to the younger Newer Gabbros age of 486 ± 17 Ma (Pankhurst, 1970). The absence of any additional contemporaneous mafic intrusions between Connemara, and NE Scotland makes construction of a plate-tectonic model for the origin of these intrusions difficult. Lambert & McKerrow (1976) hypothesised oblique-subduction of a spreading ridge, to explain the localised high heat-flow required for melting, and gabbro formation. However, Yardley & Senior (1982), pointed out the absence of any chemical evidence in the model of Lambert & McKerrow (1976), and using Pearce-Cann diagrams suggested that the mafic intrusions of Connemara, Tyrone, and NE Scotland represent the eroded roots of a volcanic arc.

(c) The Huntly-Knock-Portsoy Bodies

The earliest descriptions of the Huntly gabbro were made by Watt (1914), and later by Read (1923b). Read (1923b) mapped the mafic rocks between Huntly and Portsoy as a single continuous mass, recognising 5 distinct rock types; picrite-norite, diorite, monzonite/diorite, granite, and tourmaline pegmatite. He suggested that the intrusion was formed by successive intrusion of sill-like bodies from a continually differentiating, deeper, magmatic source.

At the Bin quarry, NW of Huntly, a fine example of layered cumulates can be seen.

Such cumulate rocks of the Huntly mass are mainly; olivine cumulates, with appreciable amounts of intercumulus plagioclase and pyroxene (mainly augite), olivine-plagioclase cumulates, with intercumulus augite, and generally gabbroic plagioclase-augite-olivine cumulates. Brown amphibole and biotite also occur, as overgrowths of earlier intercumulus ferromagnesian minerals (Munro, 1984).

Munro (1970), using a shallow drill-hole survey to compensate for the poor exposure over the area, showed that the 'Huntly mass' did not exist as a single body, but instead as three smaller bodies; centred at Huntly, Knock, and Portsoy. A re-examination of the Huntly mass by Weedon (1970) showed that an unbroken layered sequence from picrite and troctolite to olivine-gabbro does not occur, and a major break between ultrabasic rocks, and 'norites' suggests two phases of intrusion, from a differentiating magma chamber.

The cumulate rocks from the three masses between Huntly and Portsoy show differences in chemistry, texture, and mineralogy, from the other Newer Gabbro intrusions in NE Scotland (e.g. Wadsworth, 1982). The similarities between the three masses are sufficient to suggest that they originated by crystallisation of a single large mafic intrusion, with late-stage shearing and mylonitisation leading to fragmentation of the intrusion to its present day position (Munro, 1984).

(d) Post-Crystallisation Deformation of the Newer Gabbros

A palaeomagnetic survey by Blundell & Read (1958) gave uniform directions from all samples taken, and led these authors to conclude that no post-consolidation deformation of the Newer Gabbros had occurred (at least not after the rocks had cooled below their Curie point temperature). However, after a more detailed palaeomagnetic survey, McGregor & Wilson (1967) suggested that at least some post-consolidation deformation had occurred at the E end of the Insch intrusion. Good field evidence of this deformation is seen at the Bin quarry near Huntly, where rhythmic layering has been overturned (Shackleton, 1948). These cumulates appear to be nearly vertical over much of the Huntly area, although no folding is evident (Munro, 1970). Stewart & Johnson (1960), showed that the intrusions of Newer gabbros are exposed on the opposite flanks of the Boyndie Syncline, and concluded that post-intrusion, D_3 folding of this syncline (see also 3.3) explains the present day distribution of these bodies.

To address the problem of the poor exposure of the Newer Gabbros, over much of NE Scotland, a series of shallow borehole, trench, and geophysical surveys has been attempted over the last 15-20 years. This has led to the discovery of numerous shear zones, in and around the intrusions.

Late, post- emplacement, E-W-trending F_3 shears, in and around the Insch gabbro caused the removal of much of the southern contact of the intrusion, and much internal disruption (Ashcroft & Munro, 1978 ; Leslie, 1984). A second set of N-S-trending shear zones led to deformation of the Belhelvie and Huntly-Portsoy intrusions (Boyd & Munro, 1978 ; Munro & Gallagher, 1984). These zones lead to intense shearing, mylonitisation (Munro & Gallagher, 1984), and amphibolite-facies metamorphism (Kneller & Leslie, 1984).

(e) Contact Metamorphism

Intrusion of the Newer Gabbros led to thermal metamorphism of the surrounding Dalradian metasediments. This is well seen at Belhelvie, where the intrusion of the gabbro led to hornfelsing and recrystallisation of Highland schists, to a variety of both quartz-bearing and silica-undersaturated hornfelses (Stewart, 1942 ; Droop & Charnley, 1985). An example of the latter type, described by Stewart (1946) has the assemblage garnet - cordierite - plagioclase - biotite ± sillimanite - orthopyroxene - corundum - spinel (Stewart, 1946). Whole rock analyses of these hornfelses show them to be much more silica-poor, and aluminium-rich than the surrounding non-thermally metamorphosed schists (Stewart, 1942).

Gribble (1966) examined the thermal aureole of the Haddo House norites. From the edge of the aureole, inwards the following sequence of mineralogical changes was observed. The first visible effect of thermal metamorphism is the growth of sillimanite, as fibrolite. This is interpreted as replacement after andalusite, with biotite acting as a catalyst. The next effect is the replacement of regional cordierite by muscovite, possibly by a metasomatic reaction. Thirdly, biotite content decreases as the contact is approached, and K-feldspar appears. Gribble (1966) believes that potash metasomatism may have been an important process here, as insufficient K_2O is present in the local pelites (as a component in biotite) to account for the growth of K-feldspar. Closest to the contact with the norites, xenolith-bearing gneisses are found, and it is concluded that temperatures here may have

been high enough for mobilisation (or partial melting) of the country rocks (Gribble, 1966 ; 1968).

Intrusion of the Insch Gabbro at relatively high structural levels allowed the development of a ~~district~~ distinct thermal aureole around the intrusion. From the contact outwards, Sillimanite, then Andalusite Zones are mapped, (Fettes, 1970). The metamorphic sequences of these zones are analogous to the regional metamorphic sequences in the area, and Fettes (1970) suggests two possible causes for this phenomena on .

(1) Thermal metamorphism from the intrusion of the Insch sheet was responsible for the metamorphic pattern ('Buchan' type) over the whole of the region, leading to not only growth of sillimanite and andalusite around the intrusion, but also to growth of andalusite in the Boyndie Bay 'Group' further to the north.

(2) The Insch sheet was intruded during the peak regional metamorphic event, leading to modification ~~if~~ of the isograds.

The growth of sillimanite, late, after andalusite, over much of NE Scotland (Chinner, 1966), and the close correlation between the growth of sillimanite and the proximity of Newer Gabbros (Ashworth, 1975) supports explanation (2). Pankhurst (1970) also supports this explanation, and argues that in a wider context the Newer Gabbros are too local in occurrence to have led to the formation of the entire regional metamorphic pattern.

Ashworth (1975) mapped the thermal aureoles of the mafic masses between Huntly and Portsoy. He delimited two main metamorphic assemblages, comprising ~~of~~ a Sillimanite Zone and a higher-grade Sillimanite-potash feldspar Zone. These assemblages grew in unhornfelsed rocks, and the outer limit of the Sillimanite isograd is shown to follow the margins of the intrusions closely. This led Ashworth (1975) to conclude that intrusion of the mafic masses provided the heat source for this metamorphic overprint.

3.3.4 The 'Older' Gabbros

Read (1923b) ~~classified~~ defined the Older Gabbros as being a suite of igneous rocks that were intruded "prior to or during the earth-movements which caused the present character and disposition of the schistose rocks", meaning those igneous rocks which were foliated and

amphibolitised. These 'Older' Gabbros are then divided into two main suites; (i) Ultramafic rocks, consisting of rocks containing one or more of clinopyroxene, enstatite, olivine, hornblende, serpentine and tremolite, and (ii) Basic rocks, rocks such as amphibolites, and hornblende schists, that have been derived from gabbros and diorites.

As stated previously the effect of mylonitisation and amphibolitisation by numerous late-stage shear zones has led to great difficulty in distinguishing 'Older' from 'Newer' Gabbros. However, many amphibolites and serpentinites, that have undergone complete recrystallisation, can be reasonably classified as still being members of the 'Older' suite, whereas the origins of less deformed rocks, previously classified as being 'Older' Gabbros still remains problematic (Munro & Gallagher, 1984).

3.4 Partially Melted Rocks

Firstly Watt (1914), then Read (1923a, 1923b, 1935) described xenolith-bearing igneous rocks associated with the Newer Gabbros at Huntly, Haddo House, Arnage, and Insch. These igneous rocks have the typical assemblage: garnet - quartz - biotite - orthopyroxene or sillimanite - cordierite - plagioclase ± alkali feldspar, and the xenoliths contained in these 'cordierite-norites' mainly occur as fine-grained, silica-poor, alumina-rich rocks (Read, 1923a).

Read (e.g. 1923b) considered these cordierite norites, or 'contaminated rocks' to have formed by the digestion and assimilation of pelitic or psammitic country rocks, with SiO_2, CaO, Na_2O, and K_2O extracted into the basic magma, leaving behind a fine-grained, silica-poor, xenolithic residues enriched in alumina, FeO and MgO. The mafic rocks surrounding the cordierite norites commonly contain both quartz and orthopyroxene, and Read (1923a) considered these quartz norites to represent partly contaminated rocks, intermediate between the gabbros, and the cordierite-norites.

However, Gribble (1967) believed that the aluminous xenoliths were in fact pelitic residues formed after removal of a granitic liquid, with the residue then reacting with the mafic magma to produce orthopyroxene and anorthite.

Using whole-rock analyses both from quartz norites and the cordierite-bearing xenolithic rocks from Haddo House, Arnage, Insch and Huntly, Gribble & O'Hara (1967) and Gribble (1970) examined the phase relations of these two rock-types in the four-

component system CaO-MgO-Al_2O_3-SiO_2 (CMAS). By projecting the compositions of these rocks onto the 50% SiO_2 plane from the tridymite apex, the quartz norites and the cordierite norites plot as two separate groups. This confirmed the earlier work of Chinner & Shrairer (1962), who used experimentally derived phase equilibria to show that there is a thermal divide along the plane joining anorthite, enstatite and tridymite in CMAS. Liquid compositions to either side of this divide would evolve to compositions progressively further away from this plane as temperatures decrease and crystallisation takes place.

Pankhurst (1969) studied the initial $^{87}Sr/^{86}Sr$ (Sr_i) ratios of the mafic igneous rocks and the cordierite norites from Haddo House and Arnage. The mafic rocks have Sr_i ratios of 0.703 - 0.712, whilst the cordierite norites gave values of 0.720 - 0.730. The Sr_i ratios of Dalradian country rocks from the area are within the range of the Sr_i ratios of the cordierite-norites, and this therefore supports the hypothesis that these rocks formed by partial melting of metasediments adjacent to the mafic igneous sheets (Pankhurst, 1969).

Studies of the migmatites from the Huntly-Portsoy area were made by Ashworth (1976, 1979) who subdivided the migmatites according to their mineralogy. Three main groups of migmatite are described.

(i) Trondhjemitic migmatites, characterised by the presence of quartz, plagioclase, and biotite, with almandine garnet commonly present. Textural observations and the similarity of plagioclase compositions between leucosomes and melanosomes is interpreted as evidence for these migmatites having formed due to partial melting in small, closed systems.

(ii) Muscovite granitoid migmatites are classified as those containing quartz, plagioclase, K-feldspar, biotite, muscovite, and sillimanite. These rocks show advanced reaction textures, namely the replacement of fibrolite by muscovite, and replacement of K-feldspar by muscovite, quartz and myrmekite (Ashworth, 1972). These muscovite granitoids are interpreted as having been formed by the fluid-absent melting reactions:

$$\text{muscovite} + \text{quartz} = \text{K-feldspar} + Al_2SiO_5 + \text{melt.} \qquad [3.1]$$

A second, more advanced, melting reaction led to the production of most of the observed leucosomes:

$$\text{muscovite} + \text{quartz} + \text{plagioclase} = \text{K-feldspar} + Al_2SiO_5 + \text{melt.} \qquad [3.2]$$

The replacement reactions mentioned above ~~are~~ therefore could have occurred in the presence of a melt phase, due to retrogression of reaction 3.2.

(iii) Cordierite granitoids and noritoid migmatites. These rocks are the highest-grade migmatites in the area, and are closely associated with the Newer Gabbros. The cordierite granitoids have the assemblage quartz - plagioclase - K-feldspar - cordierite - garnet - sillimanite - biotite whilst the noritoid migmatites contain quartz - plagioclase - orthopyroxene - cordierite -biotite. Ashworth (1972, 1976) considered these rocks to have formed by biotite-consuming, partial-melting reactions.

Few attempts have been made to quantify the pressure-temperature conditions at which the partial melting migmatisation reactions occurred. However, in their preliminary study Droop & Charnley (1985) estimated pressures of bewteen 4 and 5 kbars (see also 3.2.4) and temperatures ranging from 700°C to 850°C from the inner-aureoles of the Morven-Cabrach, Knock, Huntly and Belhelvie intrusions.

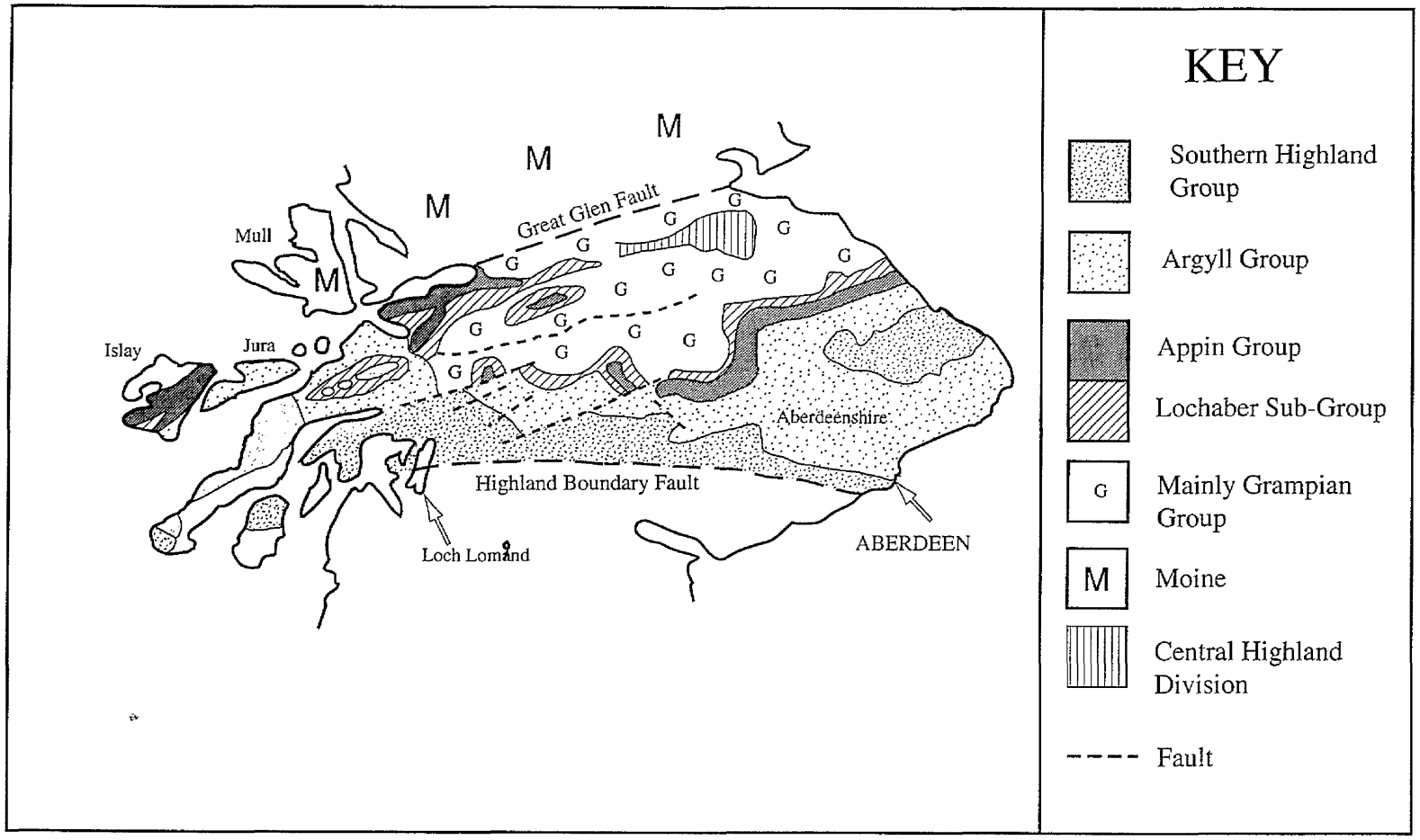

Figure 3.1.1 Map showing the distribution of the Dalradian Supergroup in mainland Scotland and its subdivisions after Harris & Pitcher (1975).

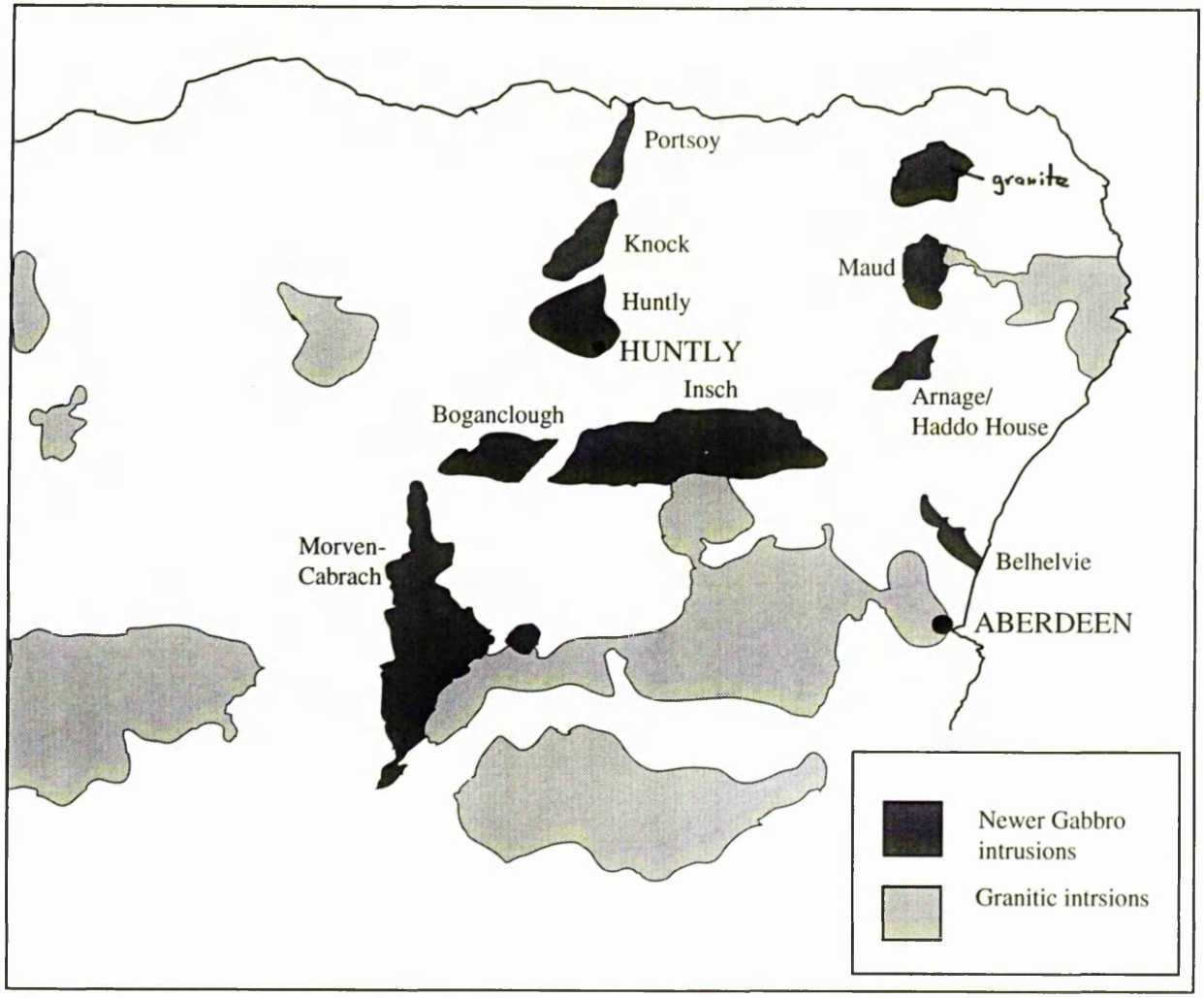

Figure 3.1.2 Location of the Newer Gabbros and granitic intrusions in NE Scotland (after Ashcroft *et al.*, 1984).

Table 3.1 Stratigraphy of the Dalradian in the Buchan District

SOUTHERN HIGHLAND GROUP	Macduff Slate	slate, greywacke and pebbly grit.
	Boyndie Bay 'Group'	andalusite-schist, and pebbly grit.
	Upper Whitehills 'Group'	pebbly grits, calcareous grits,
ARGYLL GROUP	Lower Whitehills 'Group'	flags, phyllites, limestones etc.
	Boyne Limestone	limestone with subordinate mica-shists.
	Cowhythe Gneiss-Basement Thrust	biotite gneiss.
	Portsoy Group	mica-shist, graphite-shist, limestones and quartzite.
	Durnhill Quartzite	quartzite and quartzose gneiss.
	Tillite.	
APPIN GROUP	Sandend Group	limestone, black shist, staurolite shist, mica-shist.
	Cairnfield Actinolite Flags or Garron point Group.	actinolite-shist, silvery mica-shists
	Findlater Flags	muscovite-biotite flags with scarce quartzite.
	West Sands Mica Shist	garnetiferous mica-shists
	Cullen Quartzite	granulitic quartzites, with subordinate dark garnetiferous mica-shists.

Taken from Sutton & Watson (1955) and Johnson (1983)

CHAPTER 4 FIELD-STUDY OF THE HUNTLY-KNOCK AREA

4.1 Introduction

4.1.1 Aims and objectives of the field-study

The main objectives of the field-study of the Huntly-Knock area were as follows:

(i) to locate and examine the field-relations of the metasedimentary rocks outcropping in the vicinity of the Huntly-Knock newer gabbro masses, in particular pelitic hornfelses and associated leucocratic rocks,

(ii) to ascertain whether or not these leucocratic rocks were formed by partial melting,

(iii) to examine the amount of melting (if any), to establish whether melting is lithologically controlled and to seek evidence for melt mobilisation and extraction,

(iv) to examine the field relationships between the partially melted rocks and the mafic igneous rocks,

(v) to examine the extent of the thermal aureole of the Huntly-Knock mafic bodies,

(vi) to study the regionally metamorphosed country rocks in the area, specifically trying to determine the lithologies which trend into the mafic-igneous bodies. This is important as it allows correlation between the various partially melted rocks and their probable parent rocks,

(vii) to make extensive sample collection from all the important rock types in the area for sectioning, whole rock analyses etc.

4.1.2 Description of the Huntly-Knock area

The area of study lies in the Huntly-Knock district in Aberdeenshire, north-east Scotland. Figure 3.1.2 shows the location of the separate Huntly and Knock mafic-igneous bodies as mapped by Munro (1970). Figure 3.2.1 shows the geology of the area, with the disposition of the Dalradian regionally metamorphosed rocks taken from sheet number 86 of the Scottish Geological Survey, and the location of partially melted

rocks from this study.

The landscape over the Huntly-Knock area is that of gently rolling pasture and heath land, with coniferous woodland covering some areas. The most prominent features in the area are Knock Hill (height 430 m) and Clashmach Hill (height 375 m).

Unfortunately rock exposure over the whole of the field area was found to be extremely poor, with fresh *in-situ* samples of both mafic-igneous and partially-melted rocks coming almost entirely from a few disused quarries and from a few scattered hilltop exposures. However, at certain localities samples from large loose blocks were taken, but only where it could be reasonably shown that the loose blocks were locally derived and had not been moved into their present positions by either glacial or slope processes.

4.2 Regionally Metamorphosed Rocks

4.2.1 Introduction

A field-study of the regionally metamorphosed rocks within a 5 to 7 mile radius of the Huntly Gabbro was conducted. The importance of this study was two-fold.

(i) To study rocks of different lithologies in the vicinity around their contact with the gabbro. The aim of this was to allow correlation between the partially melted rocks associated with the gabbro and their adjacent, probably non-thermally metamorphosed, protoliths. This was of great importance when making the choice of suitable rocks for experimental starting products.

(ii) To collect samples, for sectioning. These thin sections could then be used for detailed textural study and could be analysed on the electron micro-probe, allowing estimation of the temperature and pressure conditions of the local regional rocks. The field-work, coupled with petrographical and probe work, aimed to determine the local regional metamorphic conditions and to see whether or not intrusion of the gabbro led to modification of the regional metamorphic isograds in the Huntly-Knock area, as postulated by Fettes (1970) for the isograds around the Insch intrusion.

Read (1923b) mapped the rocks of the Banffshire District. The regionally

metamorphosed rocks of this district all belong to the Argyll and Southern Highland Groups of the Dalradian Supergroup. The main lithologies which transects the Huntly Gabbro are the Upper Whitehills 'Group', the Boyndie Bay 'Group', and the Portsoy 'Group', with some amphibolite (see Figure 3.2.1).

4.2.2 Mapping and Sample Collection

The majority of the mapped area lies to the S and W of the Huntly Gabbro. No mapping was possible to the east of the intrusion due to complete lack of exposure. The fold-out map Figure 4.1.1 shows the localities visited and the outline of the margins of the Huntly and Knock igneous masses.

Locality, 1a Cairnie Road Cutting, G.R. 4824463

The rocks are well exposed within a 40 m long road cutting, on the south side of the A96(T) trunk road. Here the rocks are banded, having light and dark coloured bands, varying in thickness from 2 to 8 cm. These bands strike NNE-SSW, and dip at 55-58° to the SSE. The light coloured bands are comprised of quartz and plagioclase; the dark bands consist mainly of biotite, foliated layer-parallel. Euhedral, red almandine garnet porphyroblasts, up to 1 cm in diameter, are present and sillimanite occurs as fine-grained fibrolite. The presence of light-dark mineral banding and foliation allows these rocks to be classified as garnet-quartz-biotite gneisses (Plate 4.2.1).

Locality 1b, Road Cutting W. of Cairnie, G.R. 48104485

Here the rocks are exposed along a 50 m long road cutting, on the north side of the A96(T), about 100 m further west from location 1a . The bulk of the rock consists of fine-medium grained quartz-poor, garnetiferous, mica-rich schist (e.g. DD.SIN107, DD.SIN105). The mineralogy of the rocks here differs from those at locality 1a by the presence of muscovite and the absence of sillimanite. The garnets are smaller than at the previous locality, never exceeding 5 to 6 mm in diameter. A good schistosity is present striking NE-SW and dipping 52° S. This schistosity is often strongly crenulated. Quartz segregations occur as medium-grained, lens shaped-boudins, forming schistosity-parallel layers. Similarly shaped pods containing garnet, quartz and mica also occur.

Locality 1c, Summit of Clashmach Hill, G.R. 49803850

No *in-situ* rocks could be found in the area on, and adjacent to, Clashmach Hill. However, the absence of any material derived by glacial, or slope-forming processes showed that the samples collected from loose blocks near the summit of Clashmach Hill must have been derived locally.

The samples collected can be classified as belonging to one of three main rock types; andalusite-mica schists, meta-siltstones, and arkosic grits.

The andalusite-mica schists (e.g. DD.BOG3, DD.CLAS5 and DD.CLAS112) are fine-grained dark grey coloured rocks. Both biotite and muscovite are present and are foliated to form a weak schistosity, with the biotite occasionally being coarser-grained than muscovite as seen in DD.CLAS5. Andalusite occurs as randomly oriented porphyroblasts varying in length from 4 to 8 mm and cross-cutting the main schistosity. Where present, the porphyroblasts vary in abundance from 30% down to 5% total rock volume. A secondary crenulation defined by folding of mica occurs in some samples.

The meta-siltstones are fine-grained, grey coloured rocks, often showing some original sedimentary banding (e.g. DD.CLAS2, DD.CLAS110). They contain small amounts (<20%) of foliated mica, but the dominant mineral is silt-sized quartz.

Arkosic sandstones or grits are massive, coarse-grained, pink coloured rocks. They are composed mainly of fragments of quartz and feldspar, and lack any visible metamorphic fabric.

Locality 1d, Western side of Clashmach Hill, G.R. 49143932

Samples were again collected from loose blocks. The rocks comprise andalusite-mica schists, mica schists and quartzites. The mica schists are dark coloured, mica-rich rocks. The micas are foliated, forming a good schistosity. Andalusite-mica schists differ from the mica schists only by the presence of andalusite porphyroblasts. The quartzites are grey, massive rocks with a fine-medium grain size, consisting entirely of quartz.

Locality 1e, Near Glen of Artloch Croft, G.R. 48013947

The rocks are exposed along the eastern flanks of a small stream, about 100 m from the Glen of Artloch Croft. They consist entirely of amphibolites which are dark green in colour, occasionally containing thin (2 to 4 mm) ~~of~~ light coloured bands. They are

composed mainly of amphibole, with some biotite. The rock displays a good foliation, defined by the amphibole and the biotite and striking NNE-SSW, with a dip of 58° to the E. The amphibole is also lineated.

The amphibolites form a prominent ridge which can be traced southwards for 1.5 km along the Burn of Craigentindy, as far as G.R. 47333750 where forestry inhibits any further mapping.

Locality 1f, Muckle Long Hill, G.R. 46343664

The rocks here occur as large, loose blocks of quartzites and psammite. Sample DD.MUCK1 is a dark grey fine-medium grained rock, composed mainly of quartz. The absence of any large amounts of mica and feldspar allows this rock to be classified as a psammite.

Locality 1g, Michael's Well, G.R. 51873588

Forming a small stream-side exposure, the rocks here consist of interbedded well-bedded meta-siltstones, and psammites. The rocks strike ENE-WSW and dip 82° N. The cleaved siltstones are dark coloured, fine-grained and are composed mainly of silt-sized quartz. The psammite is lighter coloured and more massive than the silty-mudstone, containing mainly quartz with some subordinate mica.

Locality 1h, Coynachie Farm, G.R. 49053440

These rocks outcrop in a small quarry (the above grid reference) and along a track side exposure G.R. 49223442. The rocks here are well bedded and comprise of uniformly dark-coloured silty-mudstones. These silty-mudstomes are fine-grained and are composed of fine mica, clay minerals and silt-sized quartz. The bedding strikes E-W and dips 88°N. A weak, discordant cleavage is present, striking NNW-SSW and dipping 52°E. Due to the weakness of the cleavage the rocks are classified as cleaved silty mudstones rather than as true slates.

4.2.3 Summary of findings

The trend of the regionally metamorphosed rocks on the southern and western margins of the Huntly Gabbro can be well constrained. The NNE-SSW trend of the

amphibolites near Glen of Artloch Croft and the ENE-WSW trend of the cleaved mud and siltstones to the south of Huntly prove that the Andalusite schists from on and around Clashmach Hill must trend towards, and be cut out by, the Huntly Gabbro (Figure 3.2.1).

Although no major or minor folds were seen in the area of study, two generations of deformation could be determined. The main deformation fabric is a foliation, which is defined by micas. This is clearly seen in the rocks from Cairnie and in the andalusite-schists from on and around Clashmach hill. This foliation is occasionally cut by a second generation crenulation cleavage, again defined by micas.

The highest grade rocks encountered away from the gabbro were the garnet-biotite gneisses at Cairnie Road Cutting (locality 1a), with lower grade garnet-mica schists immediately to the west of these (locality 1b). Andalusite schists outcrop close to the SW margin of the Huntly Gabbro. The andalusite is late, cross-cutting the main foliation. However, no sign of hornfelsing or recrystallisation is seen in these rocks. The lowest grade rocks occur to the south of these andalusite-schists and consist mainly of cleaved mudstones and cleaved siltstones. Deformation in these rocks is defined only by a single cleavage and no metamorphic porphyroblasts occur.

4.3 Mafic Igneous Rocks of the Newer Gabbro Intrusions

4.3.1 Introduction

A brief field-study coupled with sample collection was undertaken. ~~This~~ The aims of this study were to allow comparisons to be made between unaltered mafic rocks, such as at the Bin Quarry, and the altered mafic rocks, such as those at Battle Hill Quarry. These comparisons, together with chemical data obtained from samples collected, can then be used to study how the mafic rocks were locally affected by the hornfelses and partially melted rocks.

4.3.2 Mapping and sample collection

Locality 2a, Bin Quarry, G.R. 498431

The Bin Quarry contains a sequence of layered cumulates. The main rock types are

mixtures of olivine cumulates, and plagioclase cumulates. These cumulates are finely layered (2-10 cm near the quarry floor), with alternating dark, olivine-rich and lighter coloured, plagioclase-rich bands. This layering strikes approximately N-S and dips at 60-80° to the W. The cumulates at this quarry also show some grading, with the plagioclase-rich layers grading upwards into the dark olivine-rich rock, before a sharp contact marks the next plagioclase-rich layer. Shackleton (1948) argued that as this pattern was the reverse of that seen in other layered intrusions (e.g. the Rum layered complex in W. Scotland) then the rhythmic layering seen at the Bin Quarry must in fact be inverted.

Coarse-grained pegmatites are seen to cut through parts of the quarry face. Alteration of the cumulates occurs at the contact of the pegmatites and the altered rocks are characterised by friability and the presence of biotite. However, no xenoliths of country rock are seen at this quarry, and the majority of the rocks here are fresh and show no evidence of post magmatic alteration.

Locality 2b, Kinnoir Woods, G.R. 54224179

Samples were taken from a single track side exposure. The rock consists of uniform medium-coarse-grained norite. The rock is a norite, composed mainly of plagioclase and orthopyroxene, with a small amount of clinopyroxene. No evidence of any rhythmic layering was seen and the rock appears not to have suffered any post-magmatic alteration.

Locality 2c, Railway Bridge Road Cutting, G.R. 53233926

Mafic rocks are exposed on both sides of the A96(T) under the railway bridge. The rock is dark green-grey coloured with a medium grain size. The rock appears to consist of biotite, clinopyroxene, plagioclase and hornblende. Biotite occurs as large flakes, up to 5 mm in length. The rock is therefore classified as a biotite-hornblende dolerite. No xenoliths are found at this locality.

Locality 2d, Westerton, Bin Forest, G.R. 508423

Samples were collected from large loose blocks at the southern edge of the Bin Forest in the area immediately north of Westerton G.R. 508414. Sample W.TON1,

taken from a loose block at G.R. 50804219, is a medium-coarse-grained igneous textured rock. The rock contains abundant plagioclase, with some orthopyroxene, clinopyroxene, hornblende and biotite. The plagioclase grains are 1 to 3 mm long, whilst the darker minerals are slightly finer grained. The rock is homogenous, with no visible variation.

Slightly further north-west from this locality at G.R. 51704235 sample W.TON106 was taken from a loose block. The rock is coarse-medium grained and consists solely of plagioclase and olivine. The plagioclase is more abundant making up 60-70% of the rock. This rock is a plagioclase-olivine cumulate similar to the cumulates seen at the Bin Quarry, locality 2a.

4.3.3 Summary of findings

The mafic rocks exposed along the western edge of the Huntly igneous body comprising cumulates, mainly olivine-plagioclase cumulates. Rocks from the central area of the intrusion are orthopyroxene rich norites. Hydrated biotite-hornblende dolerites and biotite-hornblende gabbros occur near the S margin of the intrusion and at Westerton. The layered cumulates at the Bin Quarry may in fact be inverted.

4.4 Partially Melted Rocks, Hornfelses and Associated Rocks

4.4.1 Introduction

For the purposes of the present study partially melted rocks are classified as igneous rocks that appear not to be part of the mafic igneous masses and which appear to have been locally derived. This includes the cordierite-norites and the garnet-tonalites, encountered at various localities.

The aims of this study were to look at the field relationships between the partially melted rocks, the hornfelses and their relationships to the mafic igneous rocks, whilst making a representative sample collection of these rocks. It was hoped that observations of the field-relationships of these rocks would give an insight into the processes involved in the formation of the partially melted rocks. Evidence was also sought to determine whether partial melting took place in closed systems or had mobilised, leading to upward

movement and extraction.

4.4.2 Mapping and sample collection

Locality 3a, Battlehill Quarry, G.R. 539395

The rocks are exposed in a quarry at the south side of Battlehill Wood, about 500 m W from Huntly. Six main rock types are seen here. Field descriptions and classification of these rock types and their relative field relations are shown in Figure 4.4.1 and described below.

(i) Biotite dolerite. A dark green-black coloured rock, with a fine-medium grain size. These rocks display a good ophitic texture, with the intergrowth of both clinopyroxene and orthopyroxene, with plagioclase. Biotite occurs as large plates up to 5 mm in size.

(ii) Biotite-hornblende gabbro. These rocks again are dark green-black coloured and contain plagioclase, clinopyroxene, biotite, hornblende and orthopyroxene. These rocks are coarser-grained than biotite-hornblende dolerites and display good igneous textures. The biotite-hornblende gabbro is the most abundant rock type in the quarry, surrounding, and in sharp contact with, all other rock types bar the biotite-dolorite, with which there is a gradational contact, with an increase in grain size into the gabbro.

(iii) Micro norites. This rock is fine-medium grained, pale grey-brown in colour and contains orthopyroxene and plagioclase. The rock type occurs as either steeply inclined sheets or as large xenoliths or rafts sizing up to 3 to 5 m in length and in sharp contact with the biotite-hornblende dolerites/gabbros. One such body displays some banding, possibly some form of igneous layering, with the alignment trending approximately N-S and dipping 75°W.

(iv) Cordierite hornfels. The cordierite hornfels occurs as discordant bodies in sharp contact with biotite-hornblende dolerite or biotite-hornblende gabbro. These vary in size from 2 m by 1 m to a 6 m wide body which is exposed at the roof of the quarry. An example of one such xenolith is shown in Plate 4.4.1 and Figure 4.4.2. These hornfelses are fine-grained, dark blue-grey coloured rocks, containing cordierite.

Porphyroblasts of garnet up to 4 mm in diameter occur in many of the hornfelses. More rarely, some hornfelses contain porphyroblasts of plagioclase (seen in sample DD.BQ17) or cordierite (DD.CD3). Hornfelses near the quarry entrance are banded, with the bands being defined by variations in colour, as shown in Plate 4.4.2. The occurrence of garnet appears to be lithologically controlled with garnets concentrated in some bands and absent in others. Measurement of the angle of these bands gives varying results between near horizontal, and near vertical in different bodies.

The large xenolith shown in Plate 4.4.1 and Figure 4.4.2 mainly consists of fine-grained cordierite hornfels. However, fine bands (1 to 2 cm wide) of igneous-textured quartz, plagioclase-bearing rock occur as a film around blocks of hornfels and in sharp contact with the biotite-hornblende gabbro.

(v) Cordierite norites. These rocks occur as discordant bodies near the entrance to, and on the far side of, the quarry. They are medium-grained and display an igneous texture. The major minerals visible are cordierite, plagioclase, orthopyroxene, biotite and often garnet. Plate 4.4.3 shows a cordierite-norite taken from close to the quarry entrance. The biotite is often large (up 4 mm across) and poikilitic as in H.BHQ1. Cordierite also occurs as large blue xenocrysts up to 5 mm across, best seen in sample DD.BQ38.

(vi) Pegmatite. The pegmatites are coarse to very coarse-grained rocks, containing mainly quartz, plagioclase and biotite. However, locally the pegmatite displays a granophyric intergrowth of quartz and alkali feldspar. The pegmatites occur as veins, often sigmoidal in shape and up to 1 m in diameter, and cross cut all other rock types. Alteration halos occur around these veins defined by the growth of biotite in the host rocks.

Locality 3b, NW Side of Battlehill Woods, G.R. 51053979

The rocks here are exposed in a small quarry near the track. Two main rock types occur. The biotite-hornblende gabbro occurs over most of the quarry. This biotite gabbro is, however, cut by a discordant body of cordierite hornfels. The contact between the two rock types is sharp. The body of the hornfels is approximately 3 m across and is

exposed up to the quarry roof (2 m high).

The biotite-hornblende gabbro is medium-coarse-grained and contains plagioclase, clinopyroxene and flakes of biotite up to 2 mm in diameter. The cordierite-hornfels is very fine-grained, with the dark-blue colouration due to the presence of cordierite. Garnet and plagioclase occur as porphyroblasts, the garnets measuring up to 2 mm across and the plagioclase up to 3 mm.

Locality 3c, Castle Bridge, G.R. 53344085

Rocks are well exposed here along the river banks of the River Deveron. The majority of the rocks exposed are mafic igneous rocks, which are dark coloured, coarse-medium grained and belong to part of the Huntly Gabbro intrusion.

However, 100 to 200 m east of the bridge is a coarse-grained, lighter coloured xenolithic rock. The matrix rock here is undoubtedly igneous in origin containing euhedral orthopyroxene, plagioclase, cordierite, fine-grained quartz and large flakes of biotite. Some small, subhedral garnets occur, rarely larger than 2 to 3 mm in diameter and graphite commonly occurs as small, dark clots. Due to the igneous texture and the presence of orthopyroxene and cordierite together this rock is classified as a cordierite norite.

The xenoliths are small (mainly 2 to 10 cm in length) and occur as two types: fine-grained dark coloured rocks or light coloured rocks. The dark xenoliths are pelitic, containing cordierite, whilst the light coloured xenoliths are composed entirely of quartz and plagioclase.

Locality 3d, Dunbennan Woods, G.R. 499422

Samples were collected from large loose blocks on the eastern side of the River Deveron and from both loose blocks and an *in-situ* riverbank exposure on the western side.

Sample DD.DUN1 collected from a loose block at G.R. 50014222 is a fine-medium grained, dark blue-grey coloured rock containing garnet, cordierite, sillimanite, plagioclase, and biotite. Garnet occurs as euhedral porphyroblasts, 1 to 3 mm in diameter. Much of the sillimanite also occurs as porphyroblasts, forming elongate-bladed crystals, up to 5 mm in length.

On the E side of the river at G.R. 499422 the large blocks consist of light coloured, enclave-bearing rocks. The matrix in these rocks has an igneous texture, with plagioclase occurring as large (2 to 3 mm) crystals. Blue cordierite, orthopyroxene, garnet, biotite, and graphite are also present in these rocks. Garnets vary in size from 1 to 2 mm in diameter to 6 mm. Spinel can also be seen as small, dark clots inside cordierite crystals. These rocks are similar to those seen at Castle Bridge and can be classified as cordierite-norites. The enclaves are small (<2 cm), fine-grained and contain dark blue cordierite and orthopyroxene.

Sample DD.DUN12, taken from a large loose block, has a hornfelsic texture (rather than an igneous texture), and is finer-grained than the cordierite norites. The rock contains orthopyroxene, cordierite, plagioclase, garnet, biotite and spinel clots. Sample DD.DUN13 also has a hornfelsic texture, but lacks orthopyroxene and is composed mainly of garnet and large (2 to 3 mm long) cordierite crystals.

On the W side of the Deveron, veins of the garnetiferous cordierite-norite cut through fine-grained, meta-igneous mafic rock. This meta-igneous rock appears to contain biotite, clinopyroxene and possibly hornblende. The contact between these two rock types is sharp and no mixing between the two rock types is evident.

Locality 3e, Cormalet, G.R. 523448

All samples collected here came from large loose blocks in fields between Cormalet Farm G.R. 52794507 and Cumrie G.R. 51994453.

The lithologies seen here consist of mafic-igneous rocks and rocks containing varying proportions of hornfels and tonalitic leucosome.

The mafic igneous rocks occur mainly towards the top of the hill near Cumrie, around G.R. 51994453. They are mainly medium-coarse-grained, dark green coloured biotite-hornblende gabbros containing mainly plagioclase, orthopyroxene, biotite and hornblende, with occasionally some clinopyroxene.

The cordierite hornfelses widespread over the area, and are fine-grained, dark blue-grey to black, contain cordierite and often red almandine garnet porphyroblasts (e.g. H.COR10, DD.CUM2ii, DD.CUM7). An example of a cordierite-hornfels from Cormalet is shown in Plate 4.4.4 The garnets in cordierite hornfelses are relatively small,

ranging from 1 to 5 mm.

Many cordierite hornfelses contain igneous textured, coarse-grained leucocratic veins, containing quartz, plagioclase, and garnet. These veins appear to be lithologically controlled, forming parallel layers as shown in Plates 4.4.5, 4.4.6 and 4.4.7. Garnets also tend to occur only in leucocratic layers in many rocks, with haloes of leucosome around the garnets, as shown well in Plates 4.4.5–9 and 4.4.11. Garnets in these thin leucocratic bands tend to be larger than those in the cordierite hornfelses (Plate 4.4.11), sizes ranging from 2 to 4 mm up to 1 cm in diameter.

Plates 4.4.6, 4.4.7 and 4.4.10. show rocks in with numerous leucosome bands, with cross-cutting veinlets joining the bands and pods, or segregations of leucosomes occurring.

Plates 4.4.12–16 and Figures 4.4.3 and 4.4.4 show rocks with leucosome forming the bulk >70% of the rock, and with cordierite hornfels occurring as xenoliths. In these rocks the leucosome, or matrix rock, is mainly garnet tonalite, containing plagioclase, quartz, biotite, garnet and occasionally cordierite or alkali feldspar (Plates 4.4.17 and 4.4.18). Some leucosomes, as in the rock shown in Plate 4.4.14 lack garnet. Samples DD.CUM19 and DD.CUM22 are coarse-grained igneous-textured rocks, lacking xenoliths. Near the summit of Cumrie Hill (G.R. 51994453) the garnet tonalites often contain hornblende and/or orthopyroxene (Plate 4.4.19). These samples also contain hornblende, in addition to the assemblage listed above. Plate 4.4.16 is a close up of a contact between garnet tonalite and a xenolith. The garnets are large, up to 1 cm in diameter, occurring only in the tonalite, whilst the fine-grained xenolith lacks garnets.

Garnetiferous, leucocratic layers, similar to those seen in Plate 4.4.6 also occur in hornfelsic xenoliths as shown in Plate 4.4.15. Plate 4.4.13 shows garnet-bearing leucocratic bands which follow folded-lithological bands within a large xenolith.

Locality 3f, Barry Hill, G.R. 557543

The majority of the samples collected here were from large, loose blocks. However, some boulders here were *in-situ*. Here the rocks are all foliated, with the foliation trending NNE-SSW and dipping 77°W. The rocks here consist of banded garnet gneisses and mafic rocks. Two types of garnet gneiss occur: lighter coloured

garnet-tonalitic gneisses and darker coloured garnet-amphibole gneisses.

The garnet-tonalite gneisses are coarse-grained, banded rocks, with light bands composed mainly of quartz, plagioclase, small amounts of biotite and large (1 to 3 cm in diameter) garnet porphyroblasts. The darker bands have the same mineralogy as the lighter ones, except that biotite is much more abundant. Some enclaves of fine-grained, dark coloured material also occur. The foliation, defined by biotite, curves around both the large garnets and xenoliths.

The dark coloured garnet-amphibolite gneisses are medium to coarse-grained and contain garnet, amphibole and biotite. These rocks are again foliated, with the foliation curving around the garnet porphyroblasts. Foliation-parallel lens-shaped quartz segregations are seen in both types of gneiss.

Some bands of black-mafic rock are seen, these are medium-grained and appear to consist entirely of mafic minerals. These rocks have a strong foliation.

Locality 3g, Wether Hill, G.R. 570544

The rocks here are *in-situ*, forming small, hillside exposures near the summit of Wether Hill. Many of the rocks here are true migmatites, with darker coloured hornfelses containing veins of medium-grained biotite-rich, igneous-textured rock, such as DD.WET1. The hornfelses are fine-grained and commonly contain red, almandine garnet porphyroblasts (e.g. DD.WET 6,7). At one large exposure the hornfels shows original sedimentary type banding, which is tightly folded into a series of chevron folds. The exposure however, is insufficient to determine whether or not these folded rocks have remained in their original positions, or whether they occur as a large xenolith or raft.

The relative volume of igneous-textured rock and hornfels varies between exposures, from rocks where the igneous-textured rock forms only vein-like networks in the hornfels, to rocks where the hornfels occurs only as xenoliths. Unlike the rocks nearby at Barry Hill, the igneous textured rocks are not foliated and the crystals appear to be randomly oriented.

Locality 3h, Cuttle Hill, G.R. 510474

The rocks here are *in-situ*, forming small exposures along the slopes of Cuttle Hill. The rocks consist of a light coloured, medium-grained, biotite and plagioclase-bearing

matrix rock, in which there are numerous fine-grained xenoliths. Two main types of xenoliths can be distinguished: light-coloured xenoliths made entirely of quartz and darker coloured pelitic and calcareous xenoliths. The xenoliths are well rounded, with a modal size of 5 to 15 cm long and make up approximately 7-15% of total rock volume. A weak foliation, trending NE-SW and dipping NW can be seen in the matrix rocks, which curves around the xenoliths.

Locality 3i, Hill of Kinnoir, G.R. 555436

Here the rocks crop-out in small hillside exposures. As at Cuttle Hill, the rocks have rounded, fine-grained xenoliths lying in an igneous textured, biotite-plagioclase-rich matrix rock. However, the rocks are intensely weathered and no useful samples could be taken.

Locality 3j, Ternemny Quarry, G.R. 555528

Two main rock types can be distinguished at this quarry. The main rock type, occurring along the eastern, and parts of the northern, flanks of the quarry, is a dark coloured, medium-fine-grained altered dolerite, which appears to contain amphibole. Forming large vein like structures along the north-west side of the quarry is a banded rock, consisting of light coloured bands of tonalite, with vein-parallel biotite-rich darker coloured rock. The tonalite is medium grained and contains quartz, plagioclase and biotite, with occasional small red almandine garnets. The darker bands have the same mineralogy, differing only by the biotite being the most abundant mineral. Field relations show that the tonalite intrudes, and therefore post-dates, the altered dolerite.

Locality 3k, Barlatch Wood, G.R. 56294768

The rocks here occur along a small road-side exposure and consist of fine-grained cordierite hornfelses. The hornfelses contain medium-large garnets (up to 3 mm in diameter), with a fine-grained matrix consisting of cordierite, plagioclase, alkali feldspar and biotite.

4.5 Discussion and Conclusions

4.5.1 Regionally metamorphosed rocks

Structural data gained from the mapping of the regionally metamorphosed rocks from around the margins of the Huntly Gabbro shows that the rocks from the southern and south-eastern margins of the Gabbro are along strike from, and therefore cut out by, the intrusion (Figure 4.1.1). These rocks, which outcrop on and around the Clashmach Hill, consist mainly of andalusite schists, mica schists and arkosic sandstones which belong mainly to the Boyndie Bay 'Group' of Read (1923b). Some of these rocks, however, may belong to part of the overlying Upper Whitehills 'Group'.

The cleaved siltstones from Coynachie farm, belong to the Macduff 'Group' of Read (1923b) and strike approximately east-west and therefore are not truncated by the Gabbro.

The garnet-sillimanite gneisses and garnet-mica schists from the road cuttings at Cairnie belong to part of the Portsoy 'Group' and Read (1923b) showed that the strike of these rocks curves to east-west (from SW-NE), slightly to the north of Cairnie and these rocks are therefore truncated by the rocks at Cairnie-Cormalet.

The rocks exposed closest to the margins of the Huntly Gabbro are those at Cairnie (1 km from contact), and at Clashmach Hill (1.5 km. from contact). The rocks at neither of these two localities show any signs of hornfelsing, as might be expected if they had been subjected to thermal metamorphism cause by intrusion of the Gabbro. At Cairnie, however, the garnet-sillimanite gneisses are replaced by the lower grade muscovite bearing garnet-mica schists immediately to the west. A decrease in metamorphic grade also occurs progressively south from the intrusion, with andalusite only occurring in the rocks on, and close to, the Clashmach Hill The rocks further south around St Michael's Well and Coynachie lack even the schistose fabric seen in the rocks nearer the intrusion.

The observations above, are similar to those made by Fettes (1970), who noted that the regional andalusite isograd runs parallel to the edge of the Insch Newer Gabbro intrusion, in non-hornfelses rocks. Fettes (1970) interpreted this as evidence for the main metamorphic crystallisation event occurring just before, or whilst, the Newer Gabbros were being intruded and suggested that the intrusion of the Newer Gabbros led

to modification of the regionally isograd pattern prevalent at that time. This explanation is also valid for the regionally metamorphosed rocks around the Huntly Gabbro, and accounts for both the decrease in metamorphic grade away from the intrusion, and the lack of hornfelsing in any of the rocks any further than 1 km from the contact.

If the main metamorphic fabric is as suggested above, coeval with intrusion of the Newer Gabbros, then it is logical to assume that the crenulation fabric (best seen in the garnet-mica schists at Cairnie) must post-date the Gabbros, and was probably formed by the late regional D_3 event.

4.5.2 Mafic igneous rocks

Rocks from the central and western sides of the Huntly intrusion consist of norites and layered cumulates respectively. These rocks lack xenoliths. The mafic rocks from closest to the intrusions margins, and those closely associated with the cordierite-bearing xenolithic rocks are all biotite-hornblende dolerites and gabbros. This suggests that the biotite-hornblende-bearing rocks do not represent rocks crystallised from a primary mafic melt and have been subjected to some degree of hybridisation and/or post magmatic alteration. The petrographic and chemical aspects of these rocks are discussed in detail in Chapters 5 and 8.

4.5.3 Partially melted rocks

The relationships between leucosome and hornfels is clearly displayed by the large boulders around the hill above Cormalet (locality 3d). The leucosome is undoubtedly of igneous origin as shown by the igneous texture of the leucosome and by disturbance of hornfels-xenoliths in leucosome-rich rocks (Plate 4.4.14).

In the rocks with a low percentage of total leucosome, the leucosome is concentrated along lithologically garnet-rich bands. This suggests that either: (a) the leucosome (melt) only formed locally: from bands of rock with bulk-chemical compositions which allowed growth of garnet, or (b) the garnets grew during leucosome formation (melting). Observation (b) concurs with the conclusions of Powell & Downes (1991), who showed that the melt formed during partial melting of pelitic rocks preferentially migrated towards garnet, which formed as a solid product of the melting

reaction.

With increased quantities of leucosome, the parallel veins begin to interconnect and ellipsoidal pods of leucosome occur (Plates 4.4.6, 4.4.8, 4.4.10 and 4.4.11). This therefore represents the presence of melt in small pools and in interconnecting vein network.

In many of the boulders observed the leucosome predominates over the hornfels, with hornfels occurring as xenoliths, the leucosome therefore represents an extracted melt (Plates 4.4.12–16). The local disturbance of these xenoliths indicates that at least some melt disturbance occurred. The location of the origin of this 'extracted' melt is problematic as such a melt could either have been derived locally, by melting of local rocks, or from a deeper source and then intruded at their present level. Notably Plate 4.4.12 shows tonalitic host rock, with xenoliths of cordierite hornfels, one of which contains parallel bands of igneous-textured leucosome. Therefore, assuming that the rocks were subjected to only a single thermal event, leucocratic 'melt' bands must have formed in the cordierite-hornfelses before the hornfelses were broken-off as xenoliths in the tonalitic melt. This field evidence suggests that the garnet-tonalitic melt may have been soured from a lower structural level and migrated upwards, intruding the cordierite hornfelses. However, the mineralogical and textural similarity between the garnet tonalites and the leucocratic bands in the cordierite hornfelses suggests that the garnet tonalites and the cordierite hornfelses plus leucocratic veins formed from the same, or similar protoliths.

4.6 Summary

The regionally metamorphic rocks over 1 km over from the Huntly Gabbro show no obvious evidence of thermal metamorphism, except for the presence of sillimanite (as fibrolite) W from the intrusion at the Cairnie road cutting (locality 1a). However, the regional metamorphic grade decreases both westwards and southwards away from the intrusion, possibly representing modification of the regional metamorphic isograds by the intrusion.

Cordierite hornfelses, together with cordierite-norites and garnet-tonalites occur on the immediate edge of the Huntly Gabbro, and inside the gabbro as xenolithic bodies.

The cordierite norites and garnet tonalites are both igneous rocks. At Cormalet (locality 3e) the parallel, garnet-bearing leucocratic bands in the cordierite hornfelses formed by localised partial melting. Cross-cutting veins, and ellipsoidal leucosomes give evidence of some melt segregation. The garnet-tonalites represent an at least partially mobile, extracted melt which may have been soured from lower structural levels.

The andalusite schists, and allied rocks from on and around Clashmach Hill (localities 2c and 2d) trend towards, and are cut out by, the S and SW margins of the Huntly Gabbro, along strike from the Cordierite hornfelses and cordierite norites from Battle Hill (localities 1a and 1b), Castle Bridge (locality 3c) and Dunbennan Woods (locality 3d). The garnet-bearing gneisses and schists from Cairnie (localities 1a and 1b) trend towards the W margin of the Huntly Gabbro, along strike from the Cordierite hornfelses and garnet-tonalites at Cormalet (locality 3e).

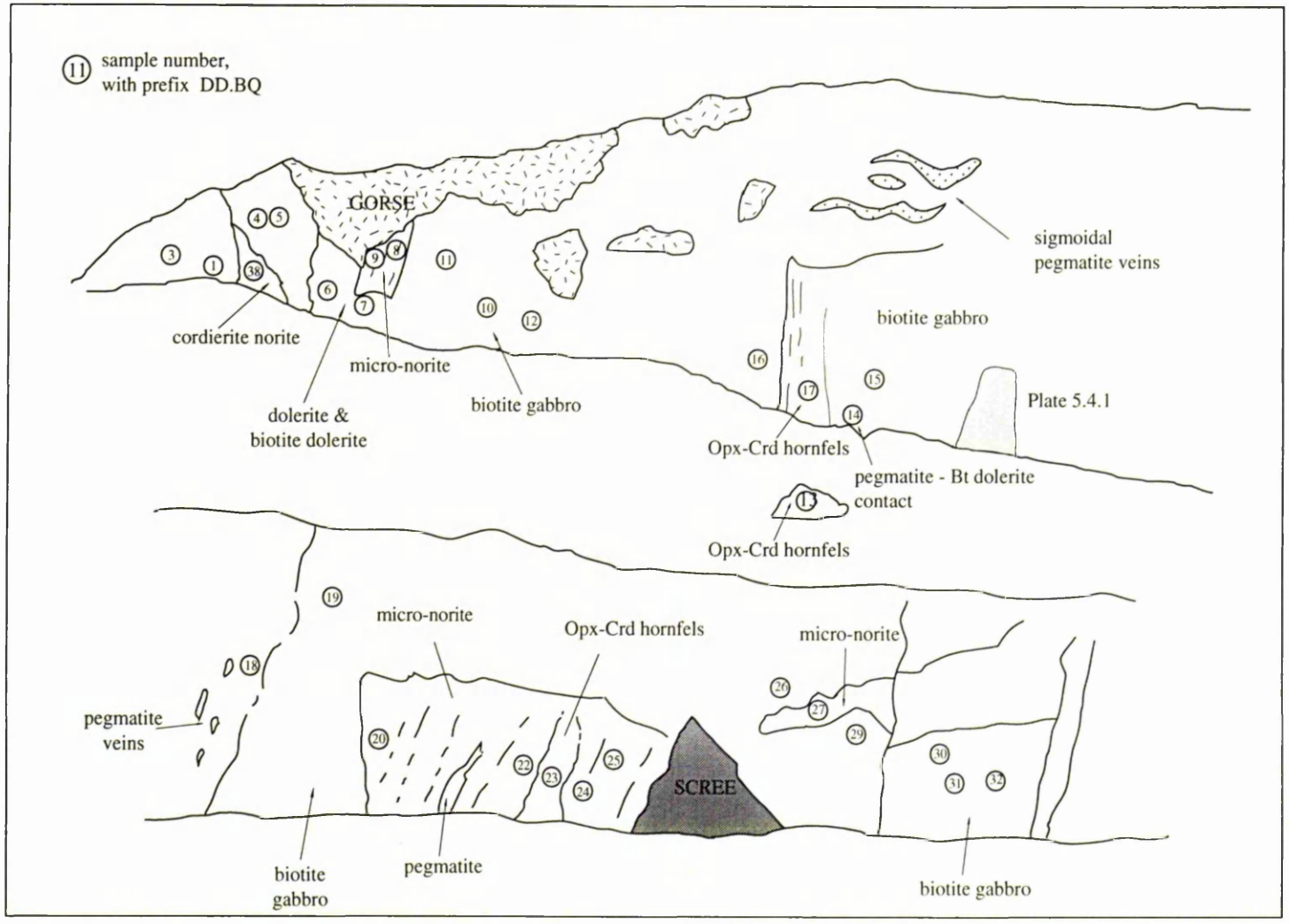

Figure 4.4.1 Profile across Battlehill Quarry (locality 3a) showing the field-relations and the location of the samples taken.

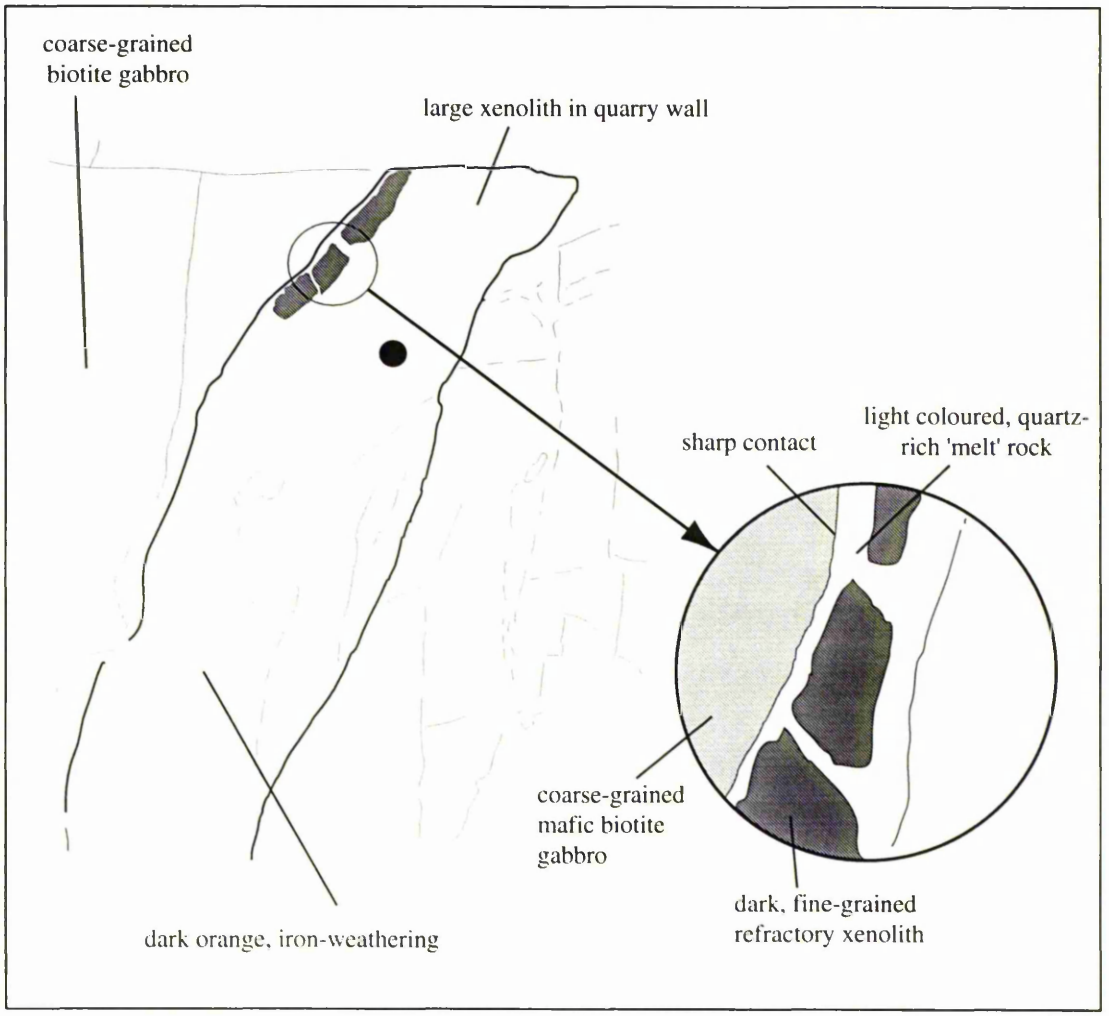

Figure 4.4.2 Sketch of Plate 4.4.1 (~~previous~~ next page). The large xenolith in the biotite gabbro itself contains a mixture of dark, fine-grained, cordierite-bearing hornfels, which locally forms 'xenoliths' inside a light-coloured, quartz-rich melt. This quartz-bearing melt is in sharp contact with the biotite gabbro.

Plate 4.4.1 Large xenolith in biotite gabbro at foot of quarry wall (Battlehill Quarry, locality 3a). The xenolith consists of dark, fine-grained cordierite-bearing hornfels, and an igneous-textured, coarser-grained, quartz-rich rock which displays a sharp contact with the gabbro (~~shown in the diagram overleaf~~).

diagram on page 75

Plate 4.2.1 Garnet-biotite gneiss from Cairnie road cutting (locality 1a). The rock is banded, with quartz-plagioclase-rich layers and biotite-rich layers. The biotite is foliated parallel to the banding (sample DD.SIN101).

Plate 4.4.2 Cordierite-norite from Battlehill Quarry (sample DD.BQ202, locality 1a). The rock displays a good igneous textured rock, with medium-grained, interlocking crystals of cordierite, plagioclase, orthopyroxene, biotite and garnet.

Plate 4.4.3 Banded hornfels from Battlehill Quarry (sample DD.BQ201, locality 1a). The hornfels is fine-grained and the blue-grey coloration is indicative of the presence of cordierite. The banding is defined by light-coloured plagioclase-rich layers and darker biotite-bearing layers. Large, red-almandine garnets are present, though are absent in the bottom layer.

Plate 4.4.4 Cordierite-K-feldspar hornfels from Cormalet (sample H.COR6, locality 3e). The rock is fine-grained, and contains blue cordierite. lighter-coloured K-feldspar-rich halos form around the garnets.

Plate 4.4.5 Cordierite-K-feldspar hornfels with leucocratic bands from Cormalet (sample H.COR11, locality 3e). The rock matrix consists of cordierite-rich (blue-grey), fine-grained hornfels. Parallel, lighter coloured, quartz-K-feldspar-bearing leucocratic layers run from the bottom-left to top-right of the sample. Large, red-almandine garnets are concentrated along the leucocratic bands.

Plate 4.4.6 Banded rock (Cormalet, locality 3e). Numerous parallel, light-coloured leucocratic bands cut across the fine-grained, blue-grey cordierite hornfels. Garnets are present only in the leucosome. Locally, cross-cutting veinlets connect the parallel bands.

Plate 4.4.7 Large boulder from Cormalet (locality 3e). Parallel bands of leucosome run along the length of the boulder, these bands are frequently connected by cross-cutting veins of leucosome. Medium-large red-almandine garnets are concentrated along the leucosomes.

Plate 4.4.8 Closer view of Plate 4.4.7 (above). Leucocratic (L) bands have locally coalesced (top left of plate), and the fine-grained hornfels forms small xenoliths (X).

Plate 4.4.9 Hornfels with leucocratic layers (Cormalet, locality 3e). Thin, parallel bands of garnetiferous leucosome run from left to right across the plate. The matrix consists of garnet-poor fine grained hornfels.

Plate 4.4.10 Large boulder from Cormalet (locality 3e). Banded rock with alternate bands of fine-grained blue-grey hornfels (H) and light coloured garnet-bearing leucosome (L).

Plate 4.4.11 Bands of leucosome (L) forming ellipsoidally shaped segregations in the fine-grained hornfels (H). Garnets are present throughout the rock, but are larger in the leucosomes.

Plate 4.4.12 Xenoliths of cordierite-bearing hornfels in garnet tonalite. The large xenolith contains parallel, garnetiferous leucocratic bands (Cormalet, locality 3e).

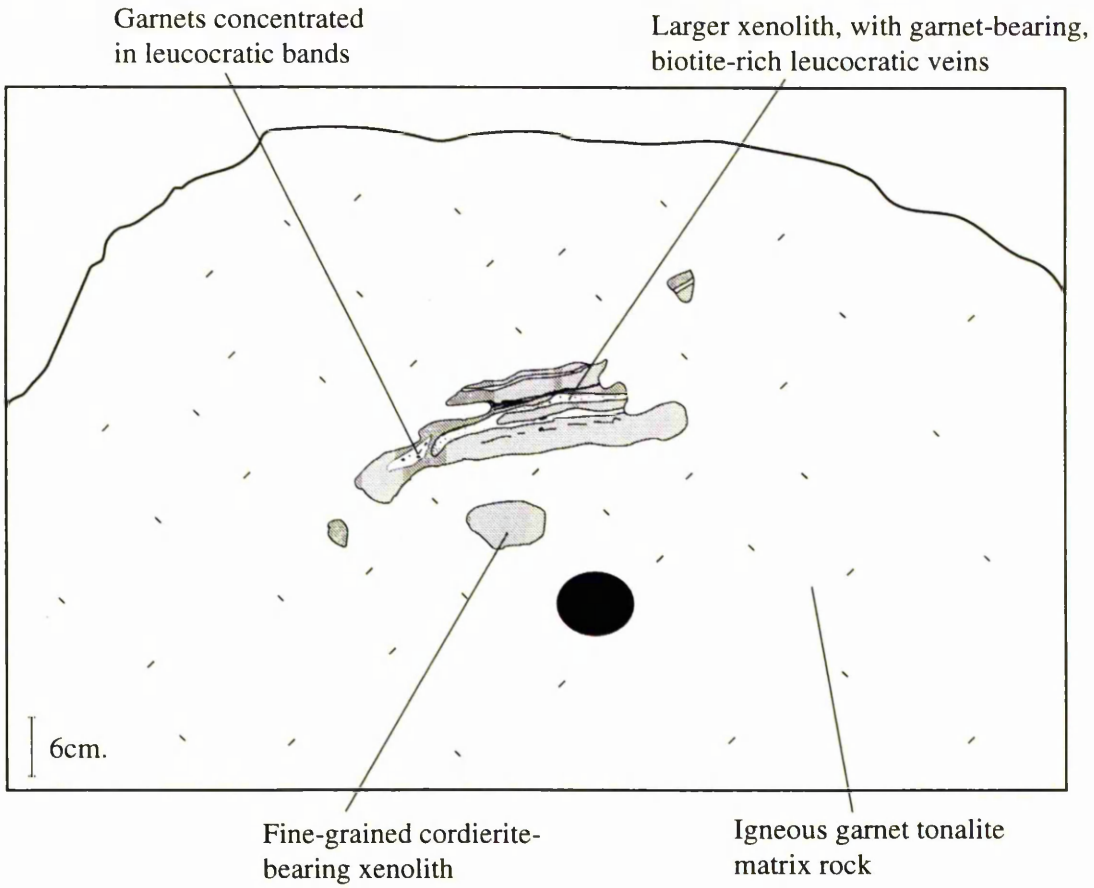

Figure 4.4.3 Sketch of Plate 4.4.12. The main matrix rock is an igneous garnet tonalite. The xenoliths within the tonalite are fine-grained cordierite-beating hornfelses. The large xenolith contains cross-cutting, garnet-bearing leucocratic bands. These bands display igneous textures and compositionally similar to the garnet tonalite host rock.

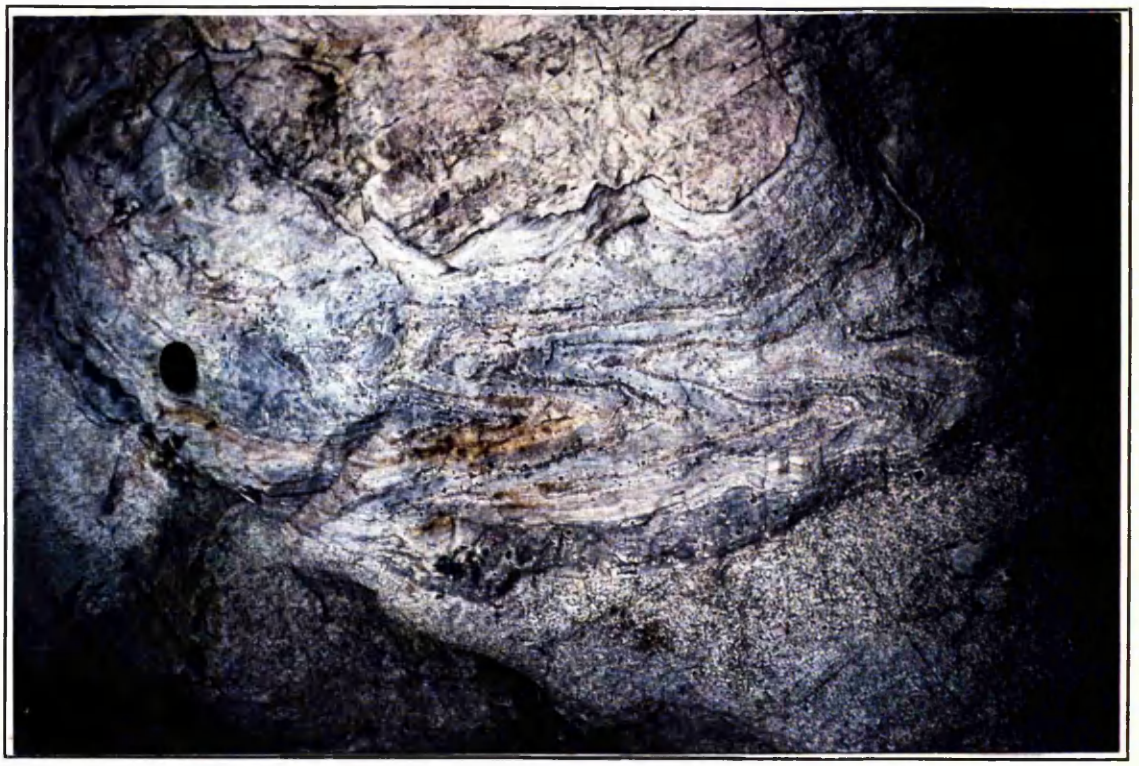

Plate 4.4.13 Large xenolith floating in a tonalite melt rock. The xenolith comprises of folded alernate bands of dark, fine-grained, blue-grey (cordierite-bearing) hornfels and light coloured garnet-rich leucososome (Cormalet, locality 3e).

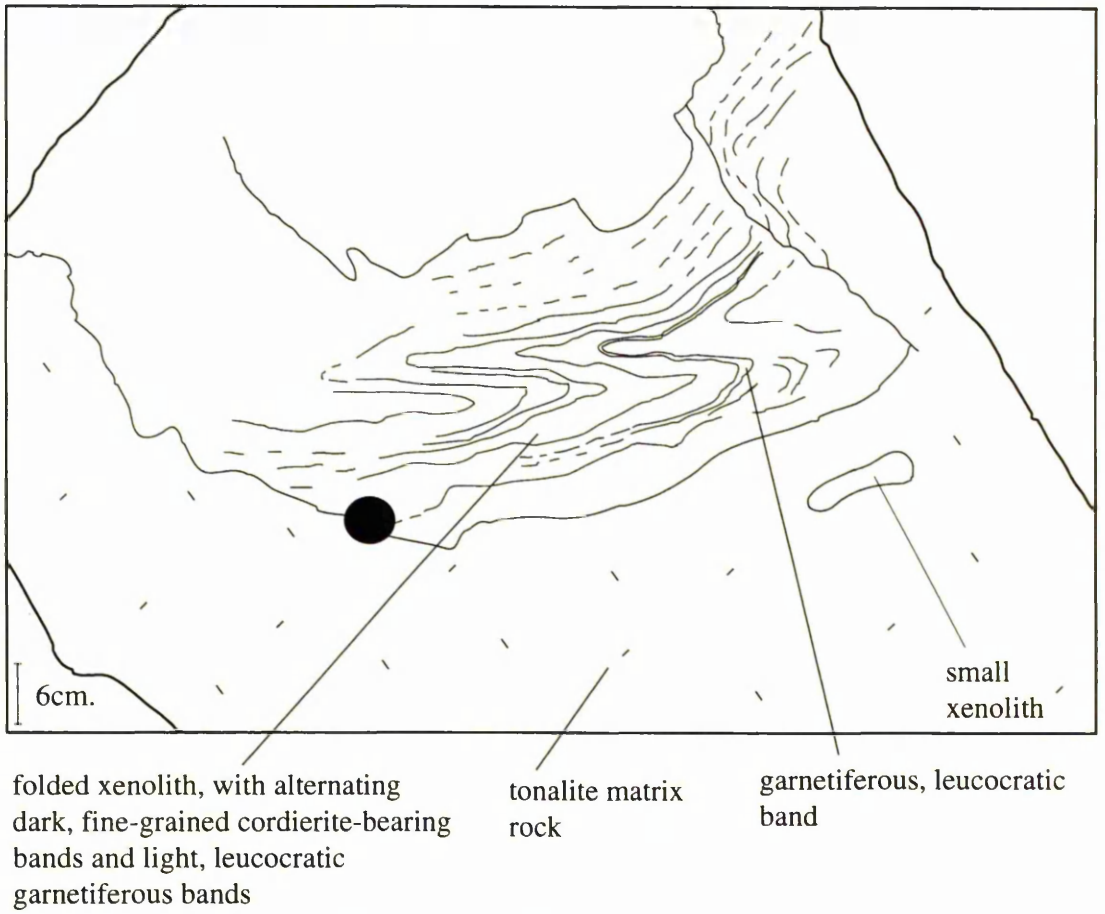

Figure 4.4.4 Sketch of Plate 4.4.13. Folded xenolith with alternating bands of dark, fine-grained, cordierite-bearing hornfels and light, garnet-bearing leucosome. The matrix rock is an igneous tonalite.

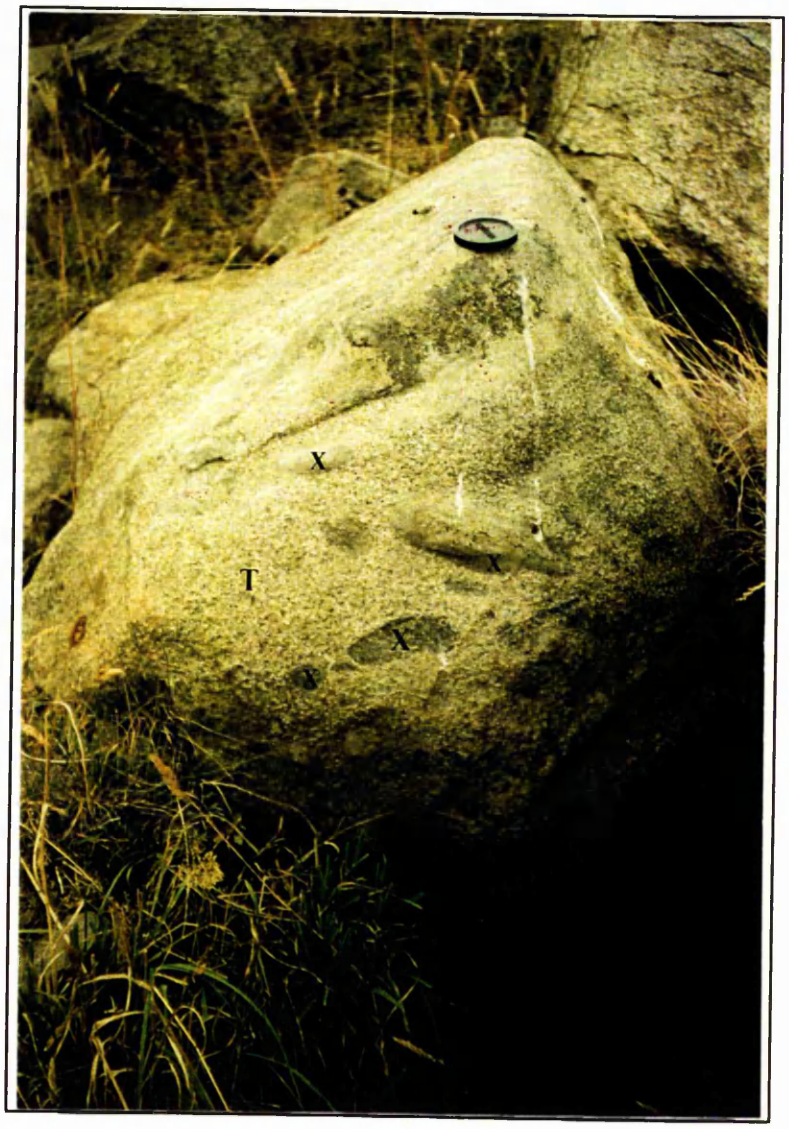

Plate 4.4.14 Large boulder from Cormalet (locality 3e). The rock is an igneous tonalite (T), with small, fine-grained, hornfelsic xenoliths (X). The igneous rock forms over 90% of total rock volume. The xenoliths are oriented randomly, possibly evidence of some melt mobilisation.

Plate 4.4.15 Fine-grained hornfelsic xenolith in tonalitic igneous rock. The garnets inside the xenolith are large and are surrounded by light leucocratic halos (Cormalet, locality 3e).

Plate 4.4.16 Contact between garnet tonalite and fine-grained xenolith. The garnets in the tonalite are large and surrounded by plagioclase-quartz halos. No garnets are present in the xenolith (Cormalet, locality 3e).

Plate 4.4.17 Garnet granitoid from Cormalet (sample DD.CUM22, locality 3e). The rock contains; medium-grained crystals of K-feldspar, plagioclase, biotite, quartz and large red-almandine garnets.

Plate 4.4.18 Garnet tonalite from Cormalet (sample H.COR7, locality 3e). The matrix consists of black biotite, light coloured plagioclase and quartz, with light blue cordierite crystals. The garnets are large and evenly distributed across the sample.

Plate 4.4.19 Garnet-hornblende tonalite from Cormalet (sample DD.CUM101, locality 3e). The rock contains dark-coloured hornblende and biotite, with plagioclase (white) and quartz (grey). Garnets occur in clusters, intergrown with plagioclase and quartz.

CHAPTER 5 PETROGRAPHY

5.1 Introduction

Samples from all relevant rock types were collected during the field-study of the Huntly-Knock area. 103 thin sections were made from these, and an additional 29 thin sections were donated by Dr. G.T.R. Droop.

Petrological studies have been used to first gain the full mineral assemblage present in each section and then to determine which of these minerals belong to the peak mineral paragenesis.

A mineral assemblage represents all the minerals present within a given compositionally distinct, volume of rock, including accessory minerals as well as prograde relict minerals and late retrogressive or secondary minerals.

The peak mineral paragenesis, though, represents the list of all minerals within a given compositionally distinct volume of rock, that appear, on texturally grounds to have coexisted together at the peak metamorphic conditions to which the rock was subjected.

Once determined, these peak metamorphic parageneses, coupled with other textural observations can be used to help determine the following:

(i) which parageneses have a low variance (i.e. a large number of mineral phases in equilibrium together) and are suitable for probe work to gain mineral chemical data to allow geothermobarometry to be undertaken,

(ii) to investigate the mode of origin of the cordierite-bearing rocks, looking for evidence of static recrystallisation, or of incipient partial melting in the cordierite hornfelses, and evidence on the crystallisation histories of all the igneous rocks,

(iii) to examine all the regionally metamorphosed rocks, noting changes in metamorphic assemblages, and look for any potential relationships between metamorphic assemblages and distance from the Huntly mafic intrusion.

5.2 Regionally Metamorphosed Rocks

5.2.1 Introduction

The full mineral assemblages present in the thin sections taken from regionally metamorphosed rock are given in Table 5.1. This table also includes the sample names and the localities (including grid references) from which they were taken. Figure 4.1.1 shows a map of the Huntly-Knock area, displaying the position of all of the localities visited.

As discussed in Chapter 4, the regionally metamorphosed rocks which crop-out around the margins of the Huntly Gabbro can be divided into those from the S and SW margins of the Gabbro (Whitehills and Boyndie Bay 'Group' rocks) and those which are exposed immediately to the W of the intrusion (rocks from the Portsoy 'Group'). The rocks from the S and SW margins consist of Andalusite-mica schists and mica schists, which are succeeded by lower-grade cleaved mudstones further to the S (Chapter 4.2). W of the intrusion the rocks form garnetiferous lithologies, unlike and unrelated to any of the metasediments to the S of the Huntly Gabbro. Therefore the petrography of the rocks from both of these areas are described separately below.

5.2.2 Rocks from S & SW margins of the Huntly Gabbro

(i) Andalusite-mica Schists and mica schists

The rocks closest to the S margin of the Huntly Gabbro consist of andalusite-mica schists, mica schists, with subordinate quartzites. The following mineral parageneses are displayed by the schists:

$$\text{And} + \text{Bt} + \text{Ms} + \text{Qtz} + \text{Ilm} \quad [5.1]$$

$$\text{And} + \text{Bt} + \text{St} + \text{Ms} + \text{Qtz} + \text{Ilm} \quad [5.2]$$

$$\text{Bt} + \text{Grt} + \text{Ms} + \text{Qtz} + \text{Ilm} \quad [5.3]$$

$$\text{Bt} + \text{Ms} + \text{Qtz} + \text{Ilm}. \quad [5.4]$$

Accessory tourmaline, zircon and rutile occur in many of these rocks.

In all of the sections a good foliation is displayed by the alignment of micas. Muscovite forms long, thin colourless crystals, on average 500 μm long and 40-60 μm wide. The biotite occurs as brown pleochroic flakes, which are more tabular in shape than

the muscovite, having similar lengths, but considerably wider, with widths measuring 100-400 μm. Some larger biotites are randomly oriented, often cutting the main foliation.

The andalusite occurs as large poikiloblasts (varying from 3 to 6 mm in diameter), rounded in cross section, and rectangular in profile. These poikiloblasts contain numerous small inclusions of quartz, with occasional larger muscovite or biotite (Plate 5.2.1). In section DD.CLAS111 large muscovite-quartz clots occur which are identical in shape and size to the andalusite poikiloblasts in for example DD.CLAS112, and therefore this muscovite almost certainly occurs as pseudomorphs after andalusite.

Quartz is evenly distributed across all of the sections, forming anhedral crystals varying in size from 80 to 250 μm in diameter and displaying strained extinction.

Staurolite only occurs in one sector of section DD.CLAS66, occurring as yellow pleochroic, subhedral crystals varying in length from 200 μm to 300 μm.

Scarce, small subhedral garnets are found in sections DD.CLAS6 and DD.CLAS111. These garnets form rounded, inclusion-free crystals, with average diameters of 150 μm.

Tourmaline occurs as an accessory phase in many of the samples and mainly occurs as small (80-200 μm in diameter) rounded crystals. The cores are frequently blue-green in colour and contain numerous small inclusions, whilst the rims of the crystals are green-brown and inclusion-free.

(ii) Cleaved siltstones

The cleaved siltstones which crop-out at St Michael's Well and Coynachie (localities 1g and 1h respectively) collectively contain the mineral paragenesis:

$$Bt + Ms + Chl + Qtz. \qquad [5.5]$$

Some accessory tourmaline occurs in sample DD.MIKE2.

These rocks are much finer-grained than the schists. The biotite, muscovite and chlorite are all aligned, with the biotite forming the largest flakes (up to 200 μm in length). The bedding in the cleaved siltstones is defined by fine compositional banding which is non-parallel to the cleavage in sample DD.MIKE2; with an angular discordance of Ca. 20° between the two planar structures in the section. A similar angular discordance between

cleavage and compositional banding occurs in the sections from Coynachie (DD.COY1 & 2). The quartz forms mainly sub-angular grains, mainly between 40 and 60 μm in diameter.

(iii) Amphibolites

A thin section was taken from an amphibolite exposed at Glen of Artloch Croft (locality 1e, G.R. 48013947). This section has the mineral paragenesis:

$$Hbl + Ep + Pl + Qtz. \qquad [5.6]$$

Accessory zircon is also present. The section displays some modal layering, with and plagioclase intergrown and forming hornblende-free layers, parallel to the main foliation.

Much of the hornblende is aligned, forming elongate crystals, with yellow-dark green pleochroism and with average lengths of 800 μm and average widths of 200 μm. Some hornblende, however, occurs as larger porphyroblasts up to 1 mm across, frequently cross cutting the earlier aligned hornblendes.

Epidotes mainly contact the hornblende crystals and form small rounded crystals with bright, anomalous interference colours.

(iv) Quartzites

Quartz-rich psammitic lithologies occur subordinate to the schists and siltstones across the whole of the area mapped. Some samples, such as DD.COL103, are quartzites, with 95% modal quartz. Such quartzites display some degree of textural equilibrium, with three grain contacts approaching 120°C and giving a weak granoblastic texture.

The sample from Muckle Long Hill (DD.MUCK1, locality 1f) contains sub-angular quartz and plagioclase grains. The rock is poorly sorted with quartz grains ranging from 1 to 4 mm in diameter.

5.2.3 Rocks from the W margin of the Huntly Gabbro

(i) Garnet-biotite gneisses

The garnet-biotite gneisses all originate from a road cutting near Cairnie (locality 1a), immediately to the W of the Huntly Gabbro. The samples from which sections were taken have the following mineral parageneses:

$$Grt + Pl + Bt + Qtz + Sil + Ilm \quad [5.7]$$

$$Grt + Pl + Bt + Qtz + St + Ilm. \quad [5.8]$$

Accessory zircon is present in all of the sections and secondary chlorite in sections DD.SIN101 and H.CaC1.

Some within-section modal layering occurs, with sequential biotite-rich and quartz-plagioclase-rich bands (as shown in Plate 5.2.2). The biotite and sillimanite, which occurs as fine fibrolite, are intergrown and foliated parallel to the modal layering. The biotite flakes are up to 3 mm long, display brown pleochroism and contain numerous inclusions of zircon, with dark brown pleochroic halos. Quartz grains also tend to have grown parallel to the foliated mica, forming anhedral crystals up to 3 mm in length.

Plagioclase occurs both as large (3 x 2 mm) subhedral crystals, as shown in sample H.CaC1, and as smaller (150 x 200 μm) crystals, which are interstitial to both quartz and the larger plagioclase crystals. Some larger plagioclase crystals display slight zonation, with albite-rich rims. Garnets vary in size from 0.5 to 4 mm in diameter and are mainly subhedral. Small quartz inclusions occur inside some garnets. Staurolite is found only in sample DD.SIN101 and forms elongate, subhedral crystals, which vary widely in length from 100 to 1500 μm.

Light-green chlorite is found in samples DD.SIN101 and HCaC1, often replacing biotite and also as larger segregations, parallel to the foliated biotite.

(ii) Garnet-mica schists

The garnet-mica schists are exposed approximately 100 m to the W of the garnet-biotite gneisses (locality 1b. One section (DD.SIN2) was made from a sample of garnet-mica schists and this contains the mineral paragenesis:

$$Grt + Bt + Ms + Pl + Qtz + Ru + Ilm. \quad [5.9]$$

Accessory zircon is also present.

This mineral paragenesis differs from 5.7 and 5.8 by the presence of muscovite and the absence of any fibrolite, staurolite or any secondary chlorite. Additionally, the minerals are generally finer grained than in any of the garnet-biotite gneisses, and no modal layering occurs (Plate 5.2.3).

The muscovite and biotite are both strongly aligned, forming a moderate schistosity and make up elongate crystals, with average lengths of 600 to 700 μm and widths of 50 to 150 μm. The quartz crystals show no obvious signs of preferential alignment and vary in size from 150 to 500 μm. Plagioclase is scarce and forms small anhedral crystals, up to 200 μm in length. The garnets are equally distributed across the section and form small (140 to 370 μm in diameter), pink, inclusion-free euhedral crystals. The zircon and rutile are both minor, with dark brown pleochroic halos forming around the zircons in biotite.

5.3 Mafic Igneous Rocks

The petrography of mafic igneous rocks of the Huntly Gabbro is only described briefly here, to allow comparisons with the thermally metamorphosed hornfelses and the associated igneous-textured rocks, and to look at any effects which these rocks have had on the mafic igneous rocks. More detailed petrographical descriptions of the mafic igneous rocks are given by Read (1923a,b), Weedon (1970) and Munro (1984).

Table 5.2 gives a list of the mineral assemblages present in the mafic igneous rocks sectioned from the Huntly igneous mass.

(i) Olivine gabbros

The olivine gabbro sectioned was taken from the Bin Quarry and has the mineral paragenesis:

$$Ol + Pl + Mag. \qquad [5.10]$$

Plate 5.3.1 is a photomicrograph of the olivine gabbro DD.BIN104. Plagioclase is the most abundant phase, forming large (average lengths of 1.5 mm) subhedral laths and is intergrown with smaller (0.2 to 0.5 mm in length) anhedral plagioclase crystals. The olivine forms semi-rounded, high relief crystals, which are heavily cracked and partially broken down to serpentine. The plagioclase crystals are preferentially aligned and display crystal lamination, indicating a high degree of textural equilibrium.

(ii) Olivine-augite gabbros

The olivine augite gabbros have the mineral paragenesis:

Ol + Pl + Aug + Mag. [5.11]

The olivine-augite gabbros are texturally similar to the olivine gabbros, but also contain augite. The augite forms large, colourless, often rectangular crystals, up to 2 mm in length and 1.5 mm wide. All of the olivine-augite gabbros encountered came from the W side of the Huntly mass, in and around the Bin Forest (located on the fold-out map Figure 4.2.1). Trace amounts of biotite are present in some sections, always contacting ilmenite grains.

(iii) Norite

The norite sample was taken from Kinnoir Woods (locality 2b), on the E side of the Huntly intrusion and has the mineral paragenesis:

Opx + Pl + Aug + Opaque. [5.12]

Some secondary biotite is also present.

Sample DD.KIN1 displays a good igneous texture, with large subhedral plagioclase crystals (up to 2.7 mm in length) intergrown with green-pink pleochroic orthopyroxene. A ophitic texture is displayed locally, with large orthopyroxenes partially enclosing smaller plagioclase laths. Other orthopyroxenes are late, occurring as small interstitial crystals. The augite is scarce and frequently interstitial.

(iii) Biotite dolerites and biotite gabbros

The biotite dolerites and biotite gabbros occur at several of the localities visited, all of which were, either near the margins of the intrusion, or exposed next to xenolithic rocks and/or cordierite norites or garnet tonalites. The full mineral parageneses given by the biotite dolerites/gabbros are:

Bt + Hbl + Pl + Opx + Aug + Qtz + Opaque [5.13]

Bt + Hbl + Pl + Opx + Qtz + Opaque [5.14]

Bt + Hbl + Pl + Aug + Qtz + Opaque. [5.15]

Accessory zircon occurs in many of the biotite-bearing mafic rocks.

The plagioclase and pyroxenes display good igneous textures, with the plagioclase forming randomly oriented subhedral laths, intergrown with the pyroxenes (Plates 5.3.2 and 5.3.3). A subophitic texture is shown in some of the samples, shown by orthopyroxene partially enclosing smaller plagioclase laths.

The hornblende is large and late, often overgrowing plagioclase and pyroxene, or occasionally replacing orthopyroxene (DD.WTON1). In most sections the hornblende displays brown-light brown pleochroism (e.g. DD.H2, Plate 5.3.2), though in DD.CUM14 and DD.CUM201 olive green-yellow green pleochroism is displayed. Biotite forms large (2-7 mm across in DD.H2), late, poikilitic flakes (Plate 5.3.4) and exhibits dark brown pleochroism. Quartz is fine-grained and interstitial to the plagioclase and pyroxenes.

(iv) Biotite-hornblende diorites

The biotite-hornblende diorites are similar to the biotite gabbros, but lack the presence of any augite. These rocks are always xenolithic and occur at Cuttle Hill and Wether Hill (localities 3d & 3h).

(v) Micro-norites

The micro-norites were only encountered at Battlehill Quarry (locality 3a) and have the mineral parageneses:

$$Opx + Pl + Aug + Ilm \quad [5.16]$$

$$Opx + Pl + Qtz + Ilm \quad [5.17]$$

$$Opx + Pl + Ilm. \quad [5.18]$$

Secondary biotite occurs in several of the sections.

In section H.BHQ4 a good igneous texture is displayed, the plagioclase forming randomly oriented laths, varying in length from 0.2 to 0.5 mm, intergrown with orthopyroxene (Plate 5.3.5). The orthopyroxene displays weak green-pink pleochroism and mainly forms small anhedral crystals, anhedral to the plagioclase laths. Quartz occurs as small interstitial crystals, whilst biotite is scarce, forming small crystals which often partially replace orthopyroxene.

Other micro-norites, such as DD.BQ22 have identical, or similar mineral parageneses to H.BHQ4; however, the textural relationship between the orthopyroxene and plagioclase differs from H.BHQ4, with the plagioclase and quartz forming anhedral, equant crystals with three grain contacts approaching 120°. The orthopyroxene forms small, rounded anhedral grains. Texturally therefore, DD.BQ22 resembles a hornfels, indicative of static recrystallisation due to heating.

In DD.BQ27 grain size layering occurs with a 3 mm wide band of relatively fine-grained material running across the section. The plagioclase and orthopyroxene crystals in the fine-grained band have sizes ranging from 20 to 50 μm in diameter, whilst in the fine-medium band the crystals have diameters of 5 to 150 μm.

5.4 Pelitic Hornfels Lithologies

The rocks described in this section represent all the types of pelitic hornfels that occur in the metamorphic aureole and inner zone of the Huntly and Knock igneous masses. A list of the full mineral assemblages present in the sections described in this section are given in Table 5.3.

5.4.1 Sillimanite-cordierite hornfelses

The sillimanite-cordierite hornfelses contain the mineral parageneses:

Grt + Sil + Bt + Crd + Pl + Qtz + Ilm [5.19]

Grt + Sil + Bt + Crd + Pl + Qtz + Kfs + Ilm [5.20]

Grt + Sil + Bt + Crd + Pl + Qtz + Kfs + Spl + Ilm. [5.21]

Accessory zircon and opaque phases other than ilmenite occur in all of the sections, secondary chlorite or muscovite in some sections and relict andalusite in DD.DUN1.

Paragenesis 5.19 occurs only in section DD.DUN1 and differs from the other sillimanite-bearing hornfelses by the occurrence of sillimanite as large rectangular bundles of long-prismatic needles (Plate 5.4.1). A small andalusite crystal occurs at the centre of one sillimanite bundle, distinguished from sillimanite by its large 2V angle. The presence of minor-andalusite and the similarity in shape of the sillimanite bundles to the andalusite porphyroblasts in the andalusite-mica schists (Plate 5.2.1) both imply that the sillimanite

grew as pseudomorphs after the andalusite. The garnets in section DD.DUN1 are large, subhedral and contain a few plagioclase and quartz inclusions. The remainder of the section contain abundant biotite and quartz, with some cordierite. The biotite contains numerous dark brown halos around zircon crystals.

The sillimanite in the sections which contain parageneses 5.20 and 5.21 does not occur in rectangular bundles, but instead occurs as: (a) randomly oriented needles, which surround garnets, or form small radial aggregates, intergrown with biotite (Section H.COR8, Plate 5.4.2) or (b) as small bundles of fibrolite (<0.5 mm across). The biotite and quartz are both scarce in these sections; the biotite forming small, thin crystals growing between cordierite, K-feldspar and subhedral to euhedral plagioclase porphyroblasts, which are zoned with albite-rich rims.

5.4.2 Cordierite-K-feldspar hornfelses

The cordierite-K-feldspar hornfelses are classed as those lithologies which lack both sillimanite and orthopyroxene, but contain cordierite and are found at most of the localities where hornfelses are found. The mineral parageneses present in the cordierite-K-feldspar hornfelses are:

Grt + Crd + Pl + Kfs + Bt + Spl + Ilm [5.22]

Grt + Crd + Pl + Kfs + Bt + Qtz + Spl + Ilm [5.23]

Grt + Crd + Pl + Kfs + Bt + Qtz + Ilm. [5.24]

Accessory zircon and other opaque minerals occur in all of the sections.

The cordierite, K-feldspar and plagioclase all occur as equant, anhedral crystals and are intergrown to form a good granoblastic polygonal texture (Matrix in Plate 5.4.3). Myrmekitic intergrowths are commonly present, partially replacing K-feldspar. Stringlet-type perthitic exsolution is also present in many K-feldspar crystals. Biotite forms small, thin crystals between cordierite, plagioclase and K-feldspar crystals. The spinel in the hornfelses from Cormalet (locality 3, H.COR10A) forms occasional rounded, dark brown crystals, though at Battlehill Quarry the spinel occurs more frequently and is dark green.

Garnet textures

Garnet occurs as three textural forms; (i) subhedral-euhedral, inclusion-free garnets, (ii) atoll type garnets and (iii) poikilitic garnets.

The atoll type garnets have hollow cores which are filled with K-feldspar and/or quartz. The garnets and their 'fillings' are much coarser-grained than the hornfelsic matrix as shown in sample H.COR4, Plate 5.4.3. The poikilitic garnets are found only in the cordierite hornfelses from Barlatch Wood (locality 3h, sections DD.RH1 & 2). The garnets are large (4 mm in diameter) and contain inclusions of cordierite and plagioclase (Plate 5.4.5). Biotite inclusions are scarce inside these garnets and biotite-free halos surround them (Plate 5.4.4).

Leucocratic veins

Some of the cordierite-K-feldspar hornfelses from Cormalet (locality 3e) are cut by veins of coarse-grained leucosome (Chapter 4.4.2). Sections through these leucocratic veins show them to contain the mineral parageneses:

$$\text{Grt} + \text{Kfs} + \text{Qtz} \qquad [5.25]$$

$$\text{Kfs} + \text{Qtz}. \qquad [5.26]$$

In section H.COR11 the leucosome vein contains paragenesis 5.25; the garnets being large (diameters greater than 6 mm) and atoll type, and the K-feldspar and quartz also coarse grained. A leucocratic vein from DD.CUM21 is shown in Plate 5.4.6, highlighting the contrast in grain size between the granoblastic hornfels matrix and the K-feldspar-quartz-bearing leucosome.

5.4.3 Orthopyroxene-cordierite hornfelses

The orthopyroxene hornfelses all came from Battlehill Quarry and Battle Hill Woods (localities 3a & b), bar one from Cormalet (locality 3e). These rocks contain the mineral parageneses:

Grt + Opx + Crd + Pl + Kfs + Bt + Qtz + Spl + Ilm [5.27]

Grt + Opx + Crd + Pl + Kfs + Bt + Qtz + Ilm [5.28]

Grt + Opx + Crd + Pl + Spl + Kfs + Ilm [5.29]

Grt + Opx + Crd + Pl + Bt + Spl + Ilm [5.30]

Grt + Opx + Crd + Pl + Kfs + Ilm [5.31]

Grt + Opx + Crd + Pl + Ilm [5.32]

Grt + Opx + Crd + Pl + Spl + Ilm [5.33]

Grt + Opx + Crd + Kfs + Ilm [5.34]

Opx + Crd + Pl + Spl + Ilm. [5.35]

Accessory zircon and pyrite are present in most sections.

The orthopyroxene-cordierite hornfelses are generally fine-grained rocks, displaying good hornfelsic textures, with cordierite, plagioclase and orthopyroxene intergrown, forming small, equant subhedral grains (Plates 5.4.7, 5.4.8 & 5.4.9). Locally, plagioclase and cordierite form good granoblastic polygonal textures, with three grain boundaries at, or approaching 120° This is well shown in sections DD.BQ201, H.BHQ5 and H.BHQ6. No metamorphic fabric is present in any of the hornfelses and all crystals are randomly oriented.

Matrix cordierite forms small, anhedral, equant crystals and is identified by its slightly 'dusty' appearance in plane polarised light, the presence of yellow pleochroic halos around zircons and by sector twinning. In some sections (e.g. DD.BQ17) the cordierite occurs as porphyroblasts, forming large subhedral crystals, up to 4 mm across and displaying good sector twinning. The cordierite in two sections from Battle Hill Woods (locality 3b, DD.BW1 & 2) forms large, monomineralic patches, which display good granoblastic polygonal textures (Plate 5.4.10).

As with the cordierite, the plagioclase usually occurs as small, anhedral crystals. However, in several sections the plagioclase forms large porphyroblasts. These

porphyroblasts frequently display normal zoning with albite-rich rims. In DD.BQ17 large patches of plagioclase occur, intergrown with K-feldspar (Plate 5.4.11).

Orthopyroxene crystals display good pink-green pleochroism, forming small, often rounded, crystals in the hornfels matrix (Plate 5.4.7). Large, subhedral, rectangular orthopyroxenes occur in some sections, and in sections DD.BQ13 and DD.BQ23 some orthopyroxene forms large, poikilitic crystals, growing around plagioclase and cordierite (Plate 5.3.12).

Spinel forms rounded, dark green, hercynitic crystals varying in diameter from 80 to 275 μm (Plate 5.4.13). Although spinel and quartz both occur in some sections, they are never seen in contact and the spinel is frequently shielded from the quartz as inclusions inside cordierite. Quartz, though, is scarce in most sections, normally forming small interstitial crystals, contacting garnet and/or K-feldspar or plagioclase.

Garnets vary in size and shape between sections, but generally can be classified as belonging to one of three types: medium-coarse grained subhedral garnets, large atoll-type garnets, or small ~~garnets~~ anhedral garnets.

The subhedral garnets vary in size from 600 to 3000 μm in diameter and usually display some good crystal faces. Inclusions of plagioclase, cordierite, opaque phase, or K-feldspar occur in some garnets.

In the atoll-type garnets the garnet cores are 'filled' by other minerals, giving the garnets a 'hollow' appearance. In section DD.BQ17 the garnet cores are filled solely by K-feldspar (Plate 5.4.14), whilst in section DD.BQ13 they are filled by both K-feldspar and quartz. The most spectacular atoll-type garnets, however, are displayed in section DD.BQ201, where large (4 to 7 mm in diameter) garnets are filled by coarse grained K-feldspar, biotite and interstitial quartz (Plate 5.4.15). The coarse grained nature of the garnet 'fillings' in DD.BQ201 is in sharp contrast with the fine grained granoblastic matrix, which is composed mainly of cordierite and plagioclase.

In sections DD.BQ17 and DD.CD3 garnet occurs as small (60 to 200 μm across), anhedral crystals, which have grown around ilmenite or pyrite grains.

Biotite usually occurs as small red-brown pleochroic crystals. In sections H.BHQ5, DD.BQ41 and DD.BQ23 the biotite forms small, ragged crystals which often grow around

ilmenites. Larger biotite flakes occur locally in section DD.BQ13, either forming poikilitic crystals, or growing around garnet or orthopyroxene.

Sections DD.BQ41 and DD.BQ101 are finely banded hornfelses. These bands are defined by layers of differing mineralogy and grain size. In DD.BQ41 these bands are displaced by a micro-fault running vertically through the section. Unusually, no plagioclase is present in these two sections, with alkali feldspar being a common mineral phase, identified by the presence of microperthitic intergrowths.

5.4.4 Orthopyroxene hornfels

Sample H.COR10B is a finely-banded hornfels, which contains orthopyroxene, but lacks cordierite. Two distinct mineral parageneses are present within the section, two main bands which contain the paragenesis:

$$Grt + Opx + Pl + Bt + Qtz + Ilm \qquad [5.36]$$

and an inner band with the paragenesis:

$$Aug + Opx + Pl + Qtz + Ilm. \qquad [5.37]$$

All of the minerals present are extremely fine grained with average crystal lengths of 90 to 140 μm. The plagioclase and orthopyroxene in paragenesis 5.36 are both intergrown to form a good hornfelsic texture. The quartz is interstitial between plagioclase and the pyroxenes or garnet.

5.5 Igneous Textured Rocks

The non-mafic igneous textured rocks that are associated with the Huntly Gabbro and which contain pelitic mineral assemblages are the cordierite norites and the garnet tonalites/granitoids. These rocks were all classified as igneous in the field by their textures and igneous structures (e.g. the presence of xenoliths in these rocks at Castle Bridge and Cormalet, localities 3c and 3e respectively). The mineral assemblages present in all of these rocks are given in Table 5.3.

5.5.1 Cordierite norites

The cordierite norites are igneous textured rocks and contain the following mineral assemblages (as opposed to mineral parageneses):

Grt + Opx + Crd + Pl + Bt + Qtz + Kfs + Spl + Ilm [5.38]

Grt + Opx + Crd + Pl + Bt + Qtz + Spl + Ilm [5.39]

Grt + Opx + Crd + Pl + Bt + Qtz + Ilm [5.40]

Opx + Crd + Pl + Bt + Qtz + Ilm. [5.41]

Accessory zircon and pyrite occur in all sections, and graphite occurs in the cordierite norites from Dunbennan Woods (locality 3d).

The sections all display good igneous textures, with plagioclase and orthopyroxene both forming large, sub-euhedral, randomly oriented laths and quartz forming small crystals, interstitial to the plagioclase and orthopyroxene (Plates 5.4.16). Plagioclase is zoned, with albite-rich rims. The orthopyroxene shows green-pink pleochroism (Plate 5.5.2) and forms long, rectangular crystals up to 1.5 mm long in section DD.BQ202. In sections DD.BQ38 and DD.BQ203 the orthopyroxenes often contain numerous 'rod-like' inclusions of biotite which trend at 90° to the length of the crystal.

Cordierite also forms fresh, large, euhedral, or subhedral crystals (Plate 5.5.3) and often displays good sector twinning. Zircon inclusions form yellow pleochroic halos inside cordierite crystals Plate 5.5.4). Rectangular-shaped clusters of dark green, hercynitic spinel occur in the centre of some cordierite crystals (Plate 5.5.5) in many samples. In section DD.CASB2i a small, relict sillimanite crystal occurs next to the spinel (Plate 5.5.6), and this together with the similarity in shape of these rectangular spinel-cordierite aggregates to the sillimanite bundles in DD.DUN1 (Plate 5.4.1) suggests that these minerals form pseudomorphs after earlier sillimanite. In all of the sections the spinel only occurs inside cordierite crystals, and is never in contact with quartz.

Biotite occurs in two generations. The main biotite generation consists of large, poikilitic, red-brown pleochroic plates, up to 5 mm long and overgrows plagioclase, garnet, orthopyroxene and cordierite (Plate 5.5.7, 5.5.8 & 5.5.9). A second generation of biotite occurs in symplectic intergrowths with quartz and replaces orthopyroxene (e.g. Sections

DD.BQ202, DD.DUN4). Both these textures show that the biotite grew late and suggest that it may not be a peak paragenesis mineral.

In sections DD.DUN4 and DD.DUN12 secondary anthophyllite replaces orthopyroxene, forming thin rims around these crystals.

5.5.2 Cordierite granitoids

The cordierite granitoids all come from the locality at Fowlwood, near Knock Hill (G.R. 534528). The sections contain the mineral assemblages:

Grt + Crd + Bt + Qtz + Spl + Kfs [5.42]

Grt + Crd + Bt + Qtz + Spl. [5.43]

Accessory zircon is present in FOW1ii and relict sillimanite in FOWi.

These rocks are texturally similar to the cordierite norites, with the plagioclase forming randomly oriented, subhedral laths and the cordierite also form subhedral and euhedral crystals, which locally exhibit spectacular sector twinning (Plate 5.5.10). The quartz is interstitial to cordierite, orthopyroxene and garnet, whilst K-feldspar is locally poikilitic in section FOWi. The garnets are of the atoll-type, described in section 5.5.1, and contain K-feldspar and quartz.

As with the cordierite norites, rectangular spinel aggregates occur inside cordierite crystals In FOW1 a sillimanite crystal is located in the centre of one such aggregate.

Biotite occurs as both large poikilitic plates, and as symplectic intergrowths with quartz, as is seen replacing orthopyroxene in the cordierite norites. This suggests that orthopyroxene may have been present in these rocks, but has been pseudomorphed by biotite + quartz.

5.5.3 Garnet tonalites and allied rock types

Garnet tonalites are igneous rocks, which are exposed at Cormalet (locality 3e) and Ternemny Quarry (locality 3j). These rocks can be further subdivided into the main garnet-biotite-plagioclase-quartz-bearing lithologies and the less common hornblende-bearing lithologies and these two rock types will be discussed separately here.

(i) Garnet tonalites

The garnet tonalites have the following mineral parageneses:

Grt + Pl + Bt + Qtz + Ilm [5.44]

Grt + Pl + Bt + Qtz + Crd + Ilm [5.45]

Grt + Pl + Bt + Qtz + Kfs + Ilm. [5.46]

Accessory zircon occurs in all the sections and apatite in some sections. Retrogressive fibrolite is present in section H.COR7.

A good igneous texture is displayed by these rocks (Plate 5.5.11), with plagioclase forming large, randomly oriented, subhedral laths, and quartz as interstitial crystals. Biotite forms large, brown-red, pleochroic, ragged flakes. Section H.COR7 contains cordierite, which forms large, inclusion-free euhedral crystals. Garnets are large in the tonalites from Cormalet (up to 2 cm in diameter), forming euhedral to subhedral crystals (Plate 5.5.11). In the garnet tonalites from Ternemny Quarry (locality 3j) the garnets are much smaller (less than 1 mm in diameter) and modally less common than in the rocks from Cormalet. Retrogressive fibrolite is present in H.COR7, forming fine needles, interstitial to plagioclase and biotite. K-feldspar is present in section DD.CUM22 and contains myrmekitic intergrowths.

(ii) Garnet-hornblende tonalites

The two garnet-hornblende tonalites sectioned both came from large boulders of igneous textured rock at Cormalet (locality 3e) and contain the following mineral assemblages:

Grt + Pl + Bt + Qtz + Opx + Hbl + Cum [5.47]

Grt + Pl + Bt + Qtz + Hbl. [5.48]

Accessory zircon occurs in section DD.CUM19.

Section DD.CUM19 is texturally complex. The garnets are large (2 cm in diameter) and subhedral. Plagioclase forms large, randomly oriented laths, which display normal zoning, with albite-rich rims. Biotite forms medium-large flakes and is evenly distributed across the section. The orthopyroxene often forms subhedral crystals, similar in shape to

those from the cordierite norites. However, locally the orthopyroxenes are partially replaced by hornblende (Plate 5.5.12). The hornblende displays olive green to light yellow-brown pleochroism, though some hornblende rims show blue-green pleochroism. Thin rims of cummingtonite grow around the rims of some hornblende crystals (Plate 5.5.13).

Section DD.CUM101i lacks orthopyroxene, but displays a similar igneous texture, as shown by DD.CUM19. The garnets are smaller in this section and occur together in clusters. The area around these garnet clusters lacks both hornblende and biotite.

5.5.4 Garnet anthophyllite gneisses

The garnet anthophyllite gneisses were only found on Barry Hill (locality 3f) and contain the mineral assemblage:

Grt + Ath + Crd + Bt + Qtz + Ilm + (accessory Zrn). [5.49]

The garnets are relatively large (1 to 2 mm in diameter) and are frequently rimmed by coarse-grained quartz. The anthophyllite is randomly oriented, forming large, weakly pleochroic crystals. The foliation is only defined by the alignment of brown-red, pleochroic biotite flakes. Yellow halos around zircons inside cordierite crystals occur commonly.

5.5.5 Garnet-K-feldspar-biotite gneisses

The garnet-K-feldspar-biotite gneisses were also only found on Barry Hill and contain the mineral assemblage:

Grt + Kfs + Crd + Bt + Pl + Qtz + Ilm + (accessory Zrn). [5.50]

The garnets in these gneisses are large, forming subhedral crystals, up to 6 mm in diameter, and are rimmed by K-feldspar and quartz. The rock matrix consists mainly of subhedral K-feldspar, plagioclase and cordierite, with interstitial quartz. The biotite forms thin, elongate flakes, aligned parallel to form a weak foliation. Myrmekitic intergrowths and perthitic exsolution are present in the K-feldspar.

5.6 Discussion

5.6.1 Regionally metamorphosed rocks

(i) Rocks from the S and SW Margins of the Huntly Gabbro

The cleaved siltstones from the most southerly mapped localities (Figure 4.1.1) contain mineral assemblages analogous to the Biotite Zone rocks described by Chinner (1966) and Hudson (1980). These are the lowest grade rocks found in NE Scotland.

To the N of the cleaved siltstones andalusite-mica schists are found on and around Clashmach Hill. The lack of any evidence of hornfelsing in the andalusite-bearing rocks suggests that the andalusite grew during a regional metamorphic event, as opposed to by thermal metamorphism by the Huntly Gabbro. This is supported by the similarity between these andalusite-mica schists and their stratigraphically equivalent counterparts on the Banffshire coast as described by Hudson (1980). The similarities can be compared between Plate 5.2.1 in this chapter and Plate 30 from Yardley *et al.* (1990, Plate 30), which shows a photomicrograph of an andalusite-staurolite schist from Whitehills, near Banff. In both plates the andalusite occurs as late poikiloblasts and only a weak schistosity is formed by the alignment of micas.

(ii) Rocks from the W margin of the Huntly Gabbro

The replacement of muscovite-bearing garnet schists by muscovite-absent fibrolite-bearing garnet-biotite gneisses over a short distance indicates a sharp increase in metamorphic grade occurred as the Huntly intrusion is approached. However, none of the rocks display any textural evidence of direct thermal metamorphism (i.e. hornfelsing, growth of late porphyroblasts), and both the gneisses and schists display a strong foliation. This correlation between distance away from the intrusion may simply be coincidental, or might be evidence for the gabbro being intruded synchronous to the main regional, foliation-forming metamorphic event. The latter observation supports the observations of Fettes (1970) who showed that the Insch intrusion was intruded during, or soon after, the main M_3 regional crystallisation event and led to modification of the pattern of regional isograds.

5.6.2 Mafic igneous rocks

The mafic igneous rocks, away from the margins of the Huntly intrusion, contain essentially anhydrous mineral assemblages, with only trace amounts of hydrous biotite present. The mafic rocks which are close to the margins of the intrusion, and which are often xenolithic, all contain biotite and/or hornblende, which forms late, often poikilitic crystals. The presence of these late, hydrous minerals suggests that these marginal igneous rocks are hybrids. Such hybridisation would have occurred due to either:

(i) the injection of hot hydrothermal fluids from xenolithic rocks and inner aureole metasediments,

or

(ii) from mixing with small fractions of granitic melt, formed from the partial melting of pelitic xenoliths and/or pelitic rocks from the inner aureole of the intrusion.

Some sections of micro-norite from Battlehill Quarry display good igneous textures and these rocks undoubtedly crystallised from a mafic melt. However, the micro-norites which have hornfelsic textures have undergone static recrystallisation in the presence of an external heat source. These 'hornfelsic' micro-norites also tend to be in contact with biotite dolerites. This evidence, coupled with the lack of any hornfelsing in the biotite-dolerites or gabbros, suggests that the micro-norites were intruded as a separate igneous sheet, prior to the intrusion of the biotite dolerites and gabbros.

5.6.3 Pelitic hornfels lithologies

All of the hornfelses, to some degree, display equilibrium textures (often displayed by a polygonal granoblastic texture, e.g. Plate 5.4.9) and lack and metamorphic foliation or lineation. These rocks all formed by static recrystallisation due to heating from the Huntly-Knock mafic bodies.

However, different lithologies of hornfels occur, sillimanite-cordierite hornfelses, cordierite-K-feldspar hornfelses and orthopyroxene-cordierite hornfelses. The metamorphism of these hornfelses will be discussed in Chapter 7, though textural and mineral paragenesis considerations suggest that the lowest-grade hornfelses are the

sillimanite-cordierite bearing rocks, as these still contain some quartz and biotite. Additionally, the highest grade hornfelses are likely to be the most-anhydrous, silica-poor orthopyroxene-cordierite hornfelses and sections from these rocks also display some of the best hornfelsic (granoblastic polygonal) textures (i.e. Plates 5.4.9 and 5.4.12).

Several textures shown by the pelitic hornfelses are indicative of incipient, or localised closed system, melting. These are the occurrence of atoll-type garnets, leucocratic veins and the presence of large, zoned plagioclase 'phenocrysts'.

Atoll-type garnets

The atoll-type garnets (Plates 5.4.3 , 5.4.4 & 5.4.15) are inferred to be evidence of localised incipient melting,. This is because:

(i) the garnet fillings are coarse-grained and sometimes form euhedral crystals (i.e. biotite in Plate 5.4.15), as opposed to the fine-grained, granoblastic hornfels matrix. If the garnet 'fillings' had formed by solid, static recrystallisation this would not be expected,

and

(ii) minerals present in the garnet fillings (combinations of K-feldspar, quartz and biotite, or all three in DD.BQ201) are all constituent minerals from the crystallisation of a granitic melt. Additionally, in sections which contain atoll-type garnets biotite and quartz, and often K-feldspar, are scarce or even absent in the surrounding hornfelsic matrix.

The presence of such small 'melt pools' around or inside garnets has been noted in other granulitic rocks (e.g. Powell & Downes, 1990). These melt pools form around garnets because the garnet itself is a solid product of biotite-consuming, fluid-absent incongruent melting reactions. The melt formed by such reactions will pool around the garnets which grow during the reaction (Powell & Downes, 1990).

Leucocratic veins

Lithologically controlled leucocratic bands run parallel across many hornfelsic rocks at Cormalet (Chapter 4.4.2, locality 3e). Thin sections through these leucocratic bands show them to contain K-feldspar, quartz and often large, atoll-type garnets (i.e. H.COR11). As with the 'fillings in the atoll-garnets, the minerals in the leucosomes are much coarser-

grained than in the hornfels (Plate 5.4.6) and contain 'granitic minerals' (K-feldspar and quartz) which are otherwise scarce in the hornfelsic domains. Together rhis evidence suggests that these leucosome bands represent thin layers of melt. The garnets in H.COR11 which are concentrated along leucocratic layers could represent the solid (restitic) products of incongruent melting, with the melt (leucosome) pooling around them.

Plagioclase porphyroblasts

Some sections (e.g. H.COR8, DD.BQ17) contain large euhedral to subhedral porphyroblasts. These plagioclases display 'normal' zoning with albite-rich rims and anorthite-rich cores. Such plagioclase crystals would not be expected if only static recrystallisation of solid plagioclase had occurred, which would lead to the formation of small equant, non-zoned crystals (Plate 5.4.9). Instead, large, subhedral or euhedral and zoned plagioclase crystals are typically formed by crystallisation from a melt, with the albite composition of the crystals increasing with decreasing temperature.

5.6.4 Igneous textured rocks

(i) Cordierite norites

The cordierite norites contain very similar mineral assemblages to the orthopyroxene-cordierite hornfelses, the exceptions being the presence of both quartz and biotite in all of the cordierite norites. The textures shown both in the field, and by closer petrographic study from thin sections, are igneous. Therefore, at least some portion of the cordierite norites must have crystallised from a melt. The question arises as to whether the garnet, cordierite, orthopyroxene and spinel (minerals present in the orthopyroxene-cordierite hornfelses): (a) all crystallised from the melt as phenocrysts, or (b) represent the solid (restitic) products of incongruous melting reactions.

That these crystals all grew as phenocrysts from a melt seems unlikely as melt compositions which crystallise abundant quantities of these minerals are unknown. Such a melt would have to be high in Al, Fe, Mg, but low in Si and Ca. The rectangular spinel-cordierite aggregates that occur in many of the cordierite norites appear to form pseudomorphs after andalusite or sillimanite, and therefore did not crystallise from a melt. Additionally cordierite, garnet and orthopyroxene are all commonly the solid restitic products

from biotite-consuming, incongruous, fluid-absent melting reactions (e.g. Thompson, 1982 ; Le Breton & Thomson, 1988 ; Vielzeuf & Clemens 1992). If, as suggested these crystals are restitic, then they would have grown in the presence of a melt phase and therefore would crystallise into some free-space and form subhedral or euhedral crystals.

The 'normal' compositional zoning in the plagioclase crystals in the cordierite norites suggests that this mineral may have crystallised from a melt. The biotite and quartz both grew late, respectively forming poikilitic and interstitial crystals, these minerals (both of which are consumed by incongruous melting reactions) may also have crystallised from a melt.

(ii) Garnet tonalites

The garnet tonalites display good igneous textures (Plate 5.5.10). These rocks also contain large subhedral or euhedral crystals of 'pelitic minerals', namely garnet and cordierite in section H.COR8. The arguments for their mode of formation are the same as those discussed above, and both the garnet and cordierite are likely to represent restitic crystals.

The two sections of garnet-hornblende tonalite both contain abundant hornblende and section DD.CUM19 contains additional orthopyroxene. The mineral assemblages present in these rocks are similar to those that can be produced by the partial melting of hornblende-bearing amphibolites (Rutter & Wyllie, 1988). Amphibolitic rocks, stratigraphically equivalent to DD.ART1 (described in section 5.2.2), trend towards, and are cut out by the rocks at Cormalet (as shown in Figure 3.2.1). Such horblende-plagioclase-quartz bearing amphibolites are therefore the likely protoliths of the garnet-hornblende tonalites.

(iii) Garnet-bearing gneisses

The anthophyllite in DD.BAR1 probably grew replacing earlier orthopyroxene (compositionally these two minerals only differ significantly by the presence of (OH) molecules in anthophyllite). Therefore, before the growth of the anthophyllite this rock may have contained a similar mineral assemblage to the cordierite norites. The garnet-K-feldspar-biotite gneisses contain the same mineral assemblage that might occur in a peraluminous 'S' type granite (Kfs +Pl + Qtz + Crd + Grt). Both types of gneiss contain higher quartz contents than either the cordierite norites or garnet tonalites. All the above observations

imply that these gneisses formed by partial melting of pelitic protoliths, and that the resultant melt crystallised *in-situ*, and that all the resultant rocks were mildly deformed, creating a weak foliation.

5.7 Conclusions

The metamorphic grade of the regionally metamorphosed rocks decreases with distance away from the intrusion. However, this is not a direct effect of contact metamorphism, though the intrusion of the Huntly Gabbro may have modified the regional isograds.

The cordierite-bearing hornfelses formed by static recrystallisation of metapelitic rocks. Locally these hornfelses display textures which are indicative of incipient melting. The cordierite norites and garnet tonalites are both igneous-textured rocks, which probably contain a high degree of entrained restite, with orthopyroxene, garnet, spinel and cordierite all representing the solid products of incongruent melting reactions. Textural observations suggest that the plagioclase, quartz and biotite may have crystallised from a melt.

A crystallisation sequence can be demonstrated, starting with the andalusite-mica schists (Plate 5.2.1). Thermal metamorphism of these schists lead to the formation of sillimanite-cordierite schists, with the andalusite being pseudomorphed by rectangular sillimanite bundles (Plate 5.4.1). Further heating lead to the crystallisation of cordierite-orthopyroxene hornfelses and cordierite norites, with rectangular spinel-cordierite aggregates forming pseudomorphs after the earlier sillimanite (Plates 5.4.20 & 5.4.21).

Table 5.1 Mineral assemblages of thin sections taken from regionally metamorphosed rocks from the Huntly area. Mineral abbreviations after Kretz (1979), with additionally, Op-opaque mineral(s). Modal percentages of the main minerals present are given where possible, with (m) denoting a minor (<1% modally) mineral. Also s = secondary mineral.

Location	G.R.	Slide no.	And	St	Pl	Bt	Grt	Sil	Qtz	Zrn	Ms	Chl	Hbl	Tur	Op	Other	Rock Type
Cairnie road cutting	4824463	DD.SIN1			10	15	10	5	55	m					5		Grt-Bt gneiss
		DD.SIN2			2	15	3		70	m	10				m		Grt-mica schist
		DD.SIN101		10	20	25	m		35	m		10s					Grt-Bt gneiss
		H.CaC1			5	27	5	m	60	m		3s					Grt-Bt gneiss
Clashmach Hill	49803850	DD.BOG1				15			34		50				m		And-mica schist
		DD.BOG3	10			30			40		19			m	1	Rt m	mica schist
		DD.CLAS6				35			45		20						mica schist
		DD.CLAS66	20	m		35	m		30		15				m		And-mica schist
		DD.CLAS112	10	m		32			35		23				m		And-mica schist
		DD.CLAS111	7			25	m		55		10			m	m		And-mica schist
W side of hill	49143932	DD.COLL103				2			95		3					Rt m	quartzite
		DD.COLL106	5			28			45		22			m	m	Rt 1	And-mica schist
Glen of Artloch Croft	48003950	DD.ART1			10	10			30	m			40			Ep 10	amphibolite
Muckle Long Hill	46303675	DD.MUCK1			5			5	90								quartzite
St Michaels Well near Bridgend	51923592	DD.MIKE1				X			X			X			X		cleaved siltstone
		DD.MIKE2			5			5	85								quarttzite
Coynachie Farm	490533440	DD.COY1				X			X			X			X		cleaved siltstone
		DD.COY2				X			X			X			X		cleaved siltstone

Table 5.2(i) Mineral assemblages in thin sections taken from mafic igneous rocks of the Huntly and Knock masses.
X = main paragenesis mineral, m = minor or accessory mineral, s = secondary mineral.

Location	G.R.	Slide no.	Pl	Bt	Opx	Qtz	Zrn	Aug	Ol	Hbl	Cum	Op	Other	Rock Type
Battlehill Quarry	539395	H.BHQ4	X	X	X			X				X		micro-norite
		DD.BQ7	X	m	X							X		micro-norite
		DD.BQ8 (a)	X		X	X								micro-norite
		DD.BQ22	X	X	X							X		micro-norite
		DD.BQ29	X	X		X		X		X				Bt gabbro
		DD.BQ31	X	m	X			X		X		X		gabbro
Cormalet	523448	DD.CUM14	X	X	X	X					X			Bt gabbro
		DD.CUM201	X	X	X	X	X	X		X				Bt gabbro
Dunbennan Woods	499422	DD.DUN5	X	X	X	X		X				X		gabbro
Wether Hill	570544	DD.WET13	X	X		X	X			X				Bt-Hbl diorite
Ternemny	555528	DD.TYQ8	X	X	X	X				X		X		Bt-Hbl diorite
Quarry		DD.TYQ10	X	X	X	X				s		X	Ap	Bt-Hbl diorite
		DD.TYQ11	X	X	X	X					X	X		Bt-Hbl diorite
Westerton,	508423	DD.W.TON1	X	X	X	X	X			X				Bt gabbro
Bin Forest		DD.W.TON4	X					X	X					gabbro

Table 5.2(ii) Mineral assemblages in thin sections taken from mafic igneous rocks of the Huntly and Knock masses.
X = main paragenesis mineral, m = minor or accessory mineral, s = secondary mineral.

Location	G.R.	Slide no.	Pl	Bt	Opx	Qtz	Zrn	Aug	Ol	Hbl	Cum	Op	Rock Type
Cuttle Hill	510474	DD.CUT1	X	X				X	X	X		X	weathered gabbro
		DD.CUT7	X	X		X		X		X			Bt gabbro
		DD.CUT12	X	X		X				X			Bt-Hbl diorite
		DD.CUT14	X	X	X						X	X	Bt norite
Bin Quarry	4984331	DD.BIN1	X					X	X			X	Ol-Aug gabbro
		DD.BIN2	X					X	X			X	Ol-Aug gabbro
		DD.BIN102	X					X	X				Ol-Aug gabbro
		DD.BIN104	X					X	X				Ol-Aug gabbro
		DD.BIN105	X					X	X			X	Ol-Aug gabbro
Hill of Kinnoir	5422419	DD.KIN102	X	s	X			X	s				norite
Ordiquahill,	508423	DD.ODQ6	X	s				X	X			X	Ol-Aug gabbro
Huntly Bridge,	53233926	DD.H2	X	X	X	X	X	X		X		X	Bt dolerite

Table 5.3(i) Mineral assemblages present in thin sections from the thermally metamorphosed (hornfelses) and associated igneous-textured rocks. X = peak metamorphic mineral, m = minor phase, s = secondary mineral and r = relict mineral phase.

Location	G.R.	Slide no.	Pl	Kfs	Crd	Bt	Grt	Opx	Sil	Qtz	Spl	Zrn	Op	Other	Rock Type
Battlehill Quarry	539395	H.BHQ1	X	X	X	X	X	X		X		X	X		Crd norite
Huntly		H.BHQ2	X	X	X	X	X	X		X	X	X	X		Gt-Cord hornfels
		H.BHQ3	X	X	X	X	X	X		?	m	X	X		Gt-Cord hornfels
		H.BHQ5 (a)	X		X		X	X				X	X		Gt-Cord hornfels
		(b)	X		X	m	X	X			X	X	X		Gt-Cord hornfels
		H.BHQ6	X		X	m	X	X			X	X	X		Gt-Cord hornfels
		L26A.M7	X	X	X	X		X			X	X	X		Opx-Crd hornfels
		L26 9994	X	X	X	X	X				X	X	X		Crd hornfels
		BHQ F2	X		X		X	X		?		X	X		Opx-Crd hornfels
		BHQ10035(a)	X		X	m	X	X			X	X	X		Opx-Crd hornfels
		(b)	X	X	X	m				?	X	X	X		Crd hornfels
		BHQ 9994	X		X	X	X	X			X	X	X	Ms(s)	Opx-Crd hornfels
		DD.BQ13	X	X	X	X	X	X		X		X	X		Opx-Crd hornfels
		DD.BQ17	X	X	X	X	X	X		X	X	X	X		Opx-Crd hornfels
		DD.BQ23	X		X	m	X	X		X		X	X		Opx-Crd hornfels
		DD.BQ27	X		X	s		X				X	X		Opx-Crd hornfels
		DD.BQ37	X		X			X				X	X	Ap	Opx-Crd hornfels
		DD.BQ38	X		X	X	X	X		X	X	X	X		Crd norite
		DD.BQ41		X	X	m	X	X				X	X		Opx-Crd hornfels

Table 5.3(ii) Mineral assemblages present in thin sections from the thermally metamorphosed (hornfelses) and associated igneous-textured rocks. X = peak metamorphic mineral, m = minor phase, s = secondary mineral and r = relict mineral phase.

Location	G.R.	Slide no.	Pl	Kfs	Crd	Bt	Grt	Opx	Sil	Qtz	Spl	Zrn	Op	Other	Rock Type
Battlehill Quarry	539395	DD.BQ101 (a)	X	X	X		m	X				X			Opx-Crd hornfels
Huntly		(b)			X	X							X		
		DD.BQ202	X		X	X	X	X		X		X	X		Crd norite
		DD.BQ203	X		X	s	X	X		X		X	X		Crd norite
		DD.HBQ CD	X	?	X		X	X			X		X		Opx-Crd hornfels
		DD.CD3	X		X			X			X		X		Opx-Crd hornfels
NW Side of	510533979	DD.BW1	X	X	X	X	X	X		X		X	X		Opx-Crd hornfels
Battle Hill		DD.BW2	X	X	X	X	X	X		X		X	X		Opx-Crd hornfels
Woods		DD.BW202	X	X	X	X	X	X		X		X	X		Opx-Crd hornfels
		DD.PIR1	X	X	X	s	X	X			X		X		Opx-Crd hornfels
		DD.PIR4	X		X		X	X		X			X		Opx-Crd hornfels
		DD.PIR101	X		X	s		X			X	X	X		Opx-Crd hornfels
Cormalet,	523448	H.COR2	X	X	X	X	X			X		X	X		Crd hornfels
Huntly		H.COR4	X	X	X	X	X						X	Ms(s)	Crd hornfels
		H.COR5	X	X	X	X	X		X	X			X		Sil- Crd hornfels
		H.COR6	X	X	X	X	X		X	X	X		X	Ms(s)	Sil-Crd hornfels
		H.COR7	X	?	X	X	X		X	X			X	Ms(s)	Grt tonalite
		H.COR8	X	X	X	X	X		X	X			X		Sil-Crd hornfels
		H.COR9	X	X	X	X	X		m			X			Crd hornfels
		H.COR10A	X	X	X	X	X	X		X	X	X			Opx-Cord hornfels

Table 5.3(iii) Mineral assemblages present in thin sections from the thermally metamorphosed (hornfelses) and associated igneous-textured rocks. X = peak metamorphic mineral, m = minor phase, s = secondary mineral and r = relict mineral phase.

Location	G.R.	Slide no.	Pl	Kfs	Crd	Bt	Grt	Opx	Sil	Qtz	Spl	Zrn	Op	Other	Rock Type
Cormalet,	523448	H.COR10B(a)	X					X		X			X	Aug	Opx hornfels
Huntly		(b)	X			X	X	X		X			X		Opx hornfels
		H.COR11(a)	X	X	X	m					X	X	X		Crd hornfels
		(b)	X	X	X	X	X			X		X	X		leucosome
		DD.CUM2(a)		X		X	X		X	X			X		Grt granitoid
		(b)	X	X	X	X							X		
		DD.CUM7	X	X	X	m	X		?	X	X	X	X	Ap	Crd hornfels
		DD.CUM8	X	X	X	X	X			X		X	X		Crd hornfels
		DD.CUM9	X		X	X	X			X		X	X		Crd hornfels
		DD.CUM11	X	X	X	X	X			X		X	X	Ap	Crd hornfels
		DD.CUM13	X	X	X	X	X		X	?	X	X	X		Sil-Crd hornfels
		DD.CUM16	X			X	X			X		X	X	Ms(s)	Grt tonalite
		DD.CUM17(a)	X			X	X			X		X	X	Ms(s)	Grt tonalite
		(b)	X			X	X			X		X	X		
		DD.CUM19	X			X	X	X		X		X	X	Hbl, Cum	Grt-Hbl tonalite
		DD.CUM21	X	X	X	X	X			X		X	X		Crd hornfels
		DD.CUM22	X	X		X	X			X		X	X	Ap	Grt tonalite
		DD.CUM101i	X			X	X			X			X	Hbl	Grt-Hbl tonalite
		DD.CUM101ii	X	X	X	X	X			X		X	X		Crd hornfels

Table 5.3(iv) Mineral assemblages present in thin sections from the thermally metamorphosed (hornfelses) and associated igneous-textured rocks. X = peak metamorphic mineral, m = minor phase, s = secondary mineral and r = relict mineral phase.

Location	G.R.	Slide no.	Pl	Kfs	Crd	Bt	Grt	Opx	Sil	Qtz	Spl	Zrn	Op	Other	Rock Type
Fowlwood,	534528	FOW1	X	X	X	X	X		r		X		X		Crd granitoid
Knock		FOW1 ii	X		X	X	X			X	X	X	X	Ms(s)	Crd granitoid
Dunbennan	499422	DD.DUN1	X		X	X	X		X	X		X	X	And, Gr	Sil-Crd hornfels
Woods		DD.DUN3(a)	X	X	X	X	X			X	X	X	X	Gr	Crd hornfels
		(b)	X		X						X		X		
		DD.DUN4	X		X	X	X	X	r	X	X	X	X	Ath, Gr	Crd norite
		DD.DUN7	X		X	X	X	X		X	X	X	X	Gr Ms(s)	Crd norite
		DD.DUN8	X	X	X	X	X	X		X	X	X	X		Crd norite
		DD.DUN9b	X		X	X	X	X		X	X	X		Gr Ms(s)	Crd norite
		DD.DUN10	X	X	X	X	X	X		X	X	X	X	Gr	Crd norite
		DD.DUN12	X		X	X	X	X		?	X	X	X	Ath(s), Gr	Crd norite
Wether Hill	570544	DD.WET3	X	X	X	X	X	X		X			X		Crd hornfels
nr. Knock		DD.WET4	X	X	X	X	X			X		X	X		Crd hornfels
		DD.WET5	X	X	X	X	X			X		X	X		Crd hornfels
		DD.WET6		X	X	X				X					Crd hornfels
Ternemny	555528	DD.TYQ3	X			X	X			X		X			Grt tonalite
Quarry		DD.TYQ5	X			X	X			X		m	X	Ap	Grt tonalite
		DD.TYQ10b	X			X	X			X		X	X		Grt tonalite

Table 5.3(v) Mineral assemblages present in thin sections from the thermally metamorphosed (hornfelses) and associated igneous-textured rocks. X = peak metamorphic mineral, m = minor phase, s = secondary mineral and r = relict mineral phase.

Location	G.R.	Slide no.	Pl	Kfs	Crd	Bt	Grt	Opx	Sil	Qtz	Spl	Zrn	Op	Other	Rock Type
Castle Bridge,	53344085	DD.CAS.B2i	X		X	X	X	X	r	X	X	X	X		Crd norite
		DD.CAS.B2ii	X		X	X		X		X		X	X		Crd norite
		DD.CAS.B5	X		X	X		X		X	X	X	X		Crd norite
		CB1P	X		X	X	X	X		X		X	X		Crd norite
Rivestone	55284636	DD.RIV2	X	X	X	X	X			X		X	X		Crd hornfels
Barlatch Wood	56294768	DD.RH2	X	X	X	X	X			X		X	X		Crd hornfels
		DD.RH3	X	X	X	X	X			X		X	X		Crd hornfels
Barry Hill	557543	DD.BAR22	X	X	X	X	X			X		X			Grantitc gneiss
		DD.BAR1			X	X	X			X		X	X	Ath	Grt-Ath gneiss

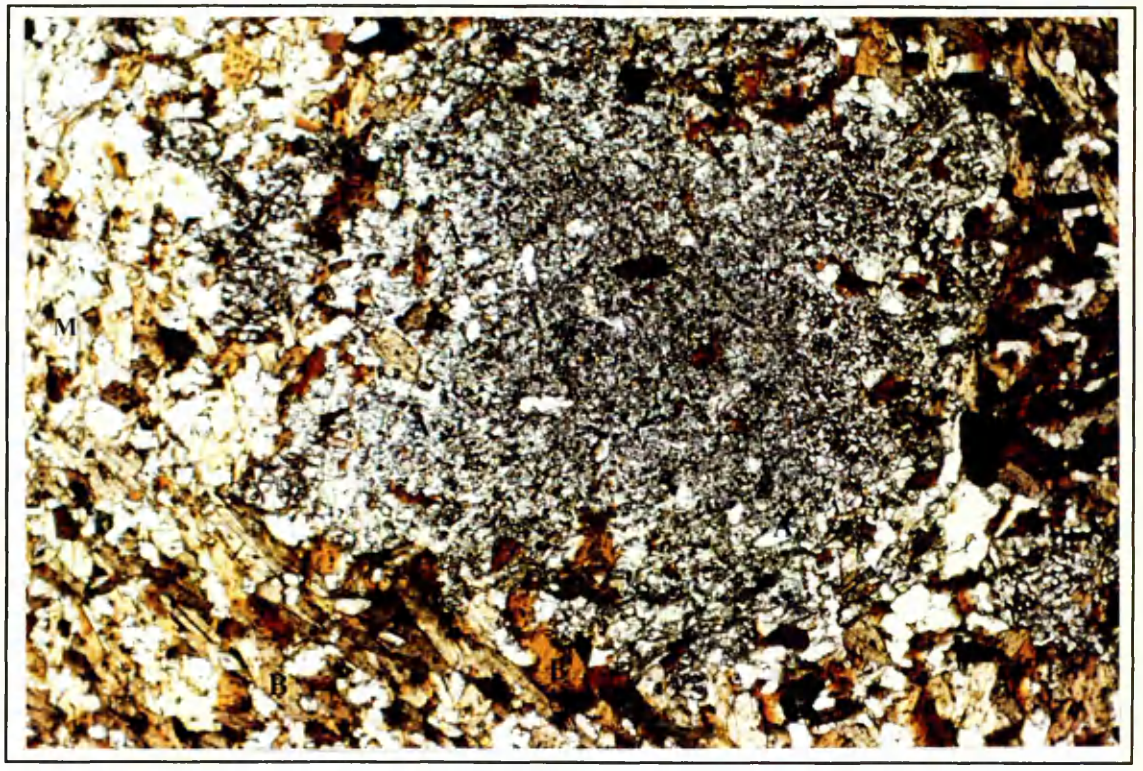

Plate 5.2.1 Photomicrograph of an andalusite-mica schist (DD.CLAS112). Andalusite (A) forms large poikiloblasts, with inclusions of quartz plus some mica. The remainder of the plate contains quartz and weakly foliated biotite (B) and muscovite (M). PPL, field of view 7.5 x 5 mm.

Plate 5.2.2 Photomicrograph of a garnet-biotite gneiss (DD.SIN101). The section is modally layered, with a biotite-rich layer running across the bottom half of the plate. Staurolite (S) is partly enclosed by the biotite and forms yellow, pleochroic crystals. PPL, field of view 7.5 x 5 mm.

Plate 5.2.3 Photomicrograph of a garnet-mica schist (DD.SIN2). The brown pleochroic biotite (B) and muscovite (M) are foliated, with small garnets (G) evenly distributed across the section. PPL, field of view 7.5 x 5 mm.

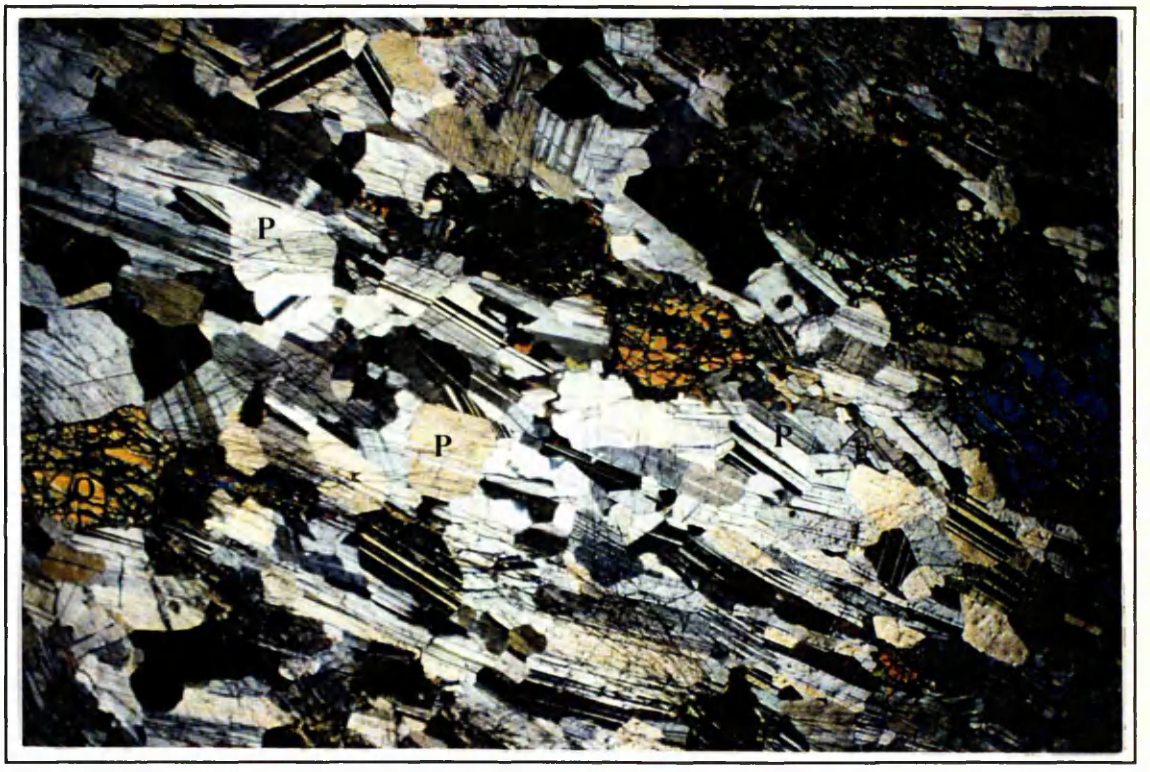

Plate 5.3.1 Photomicrograph of an olivine gabbro (DD.BIN104). The rock displays crystal lamination with the plagioclase (P) displaying a good equilibrium texture. The olivine (O) forms heavily cracked, high birefringence crystals. XPL, field of view 15 x 10 mm.

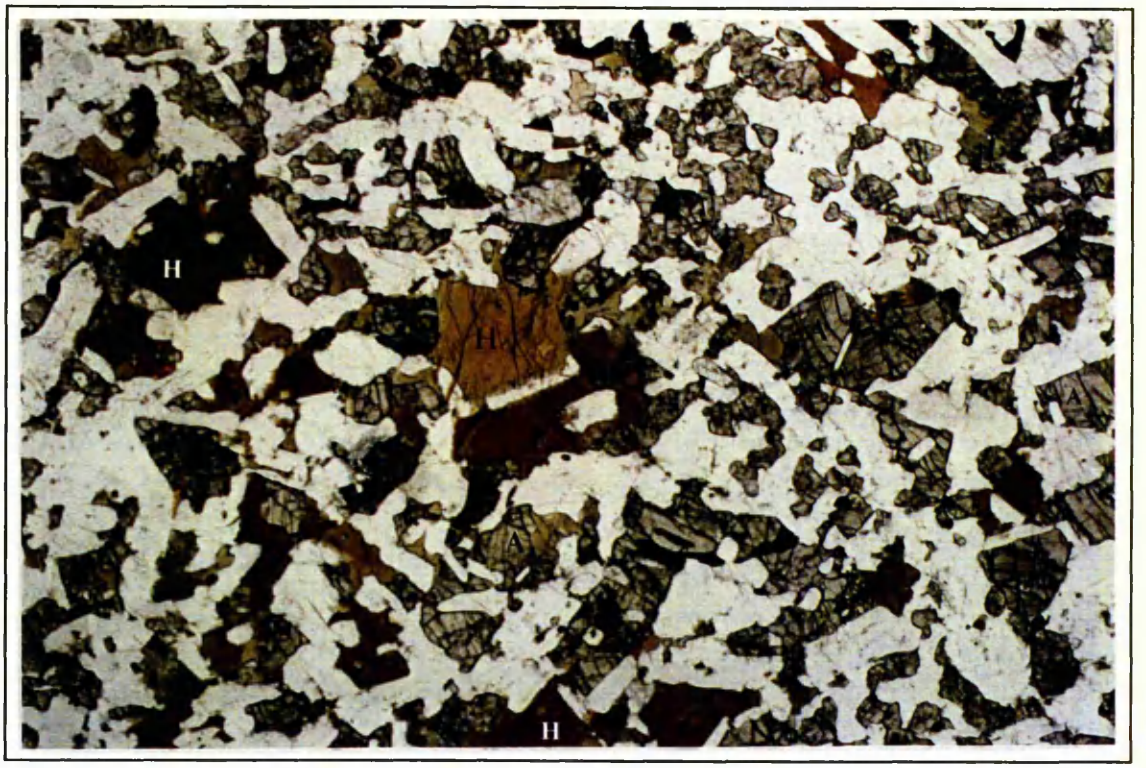

Plate 5.3.2 Photomicrograph of a biotite-hornblende dolerite (DD.H2). High relief, colourless augite (A), with brown pleochroic hornblende (H). PPL, field of view 7.5 x 5 mm.

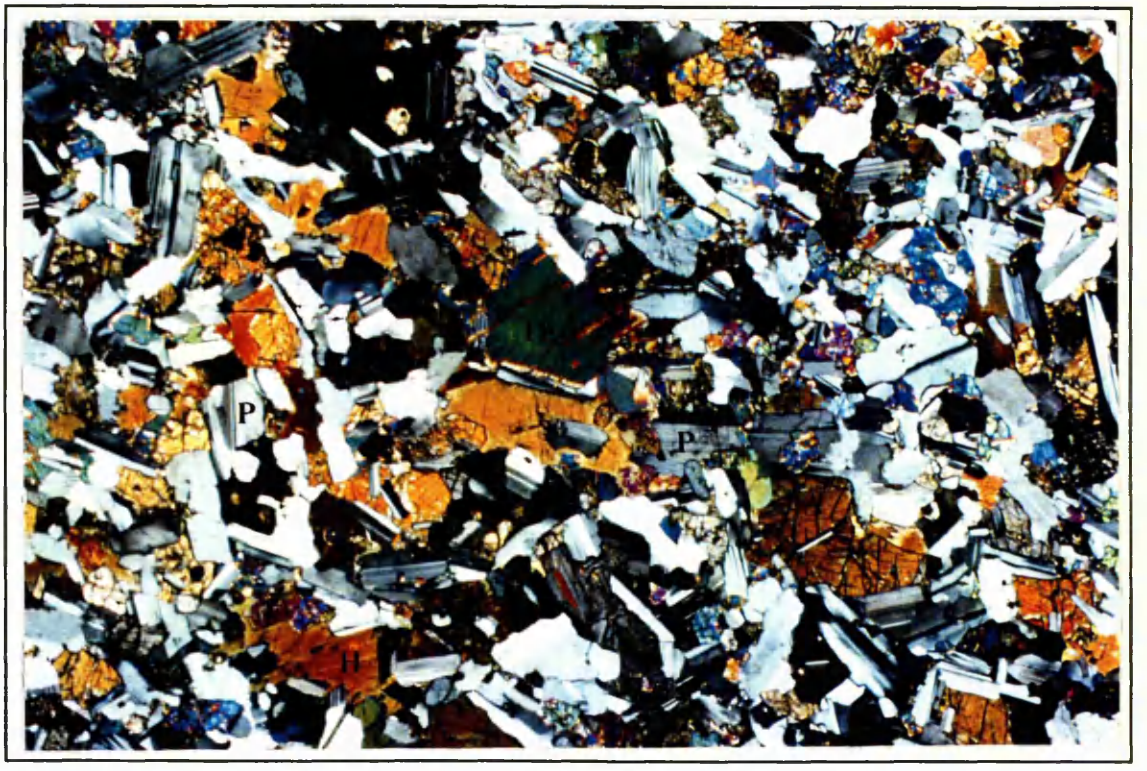

Plate 5.3.3 Photomicrograph of a biotite-hornblende dolerite (DD.H2). Plagioclase (P) forms randomly oriented, subhedral laths, with the high birefringence augite (A) mainly anhedral and interstitial. Hornblende (H) encloses smaller plagioclase laths. XPL, field of view 7.5 x 5 mm.

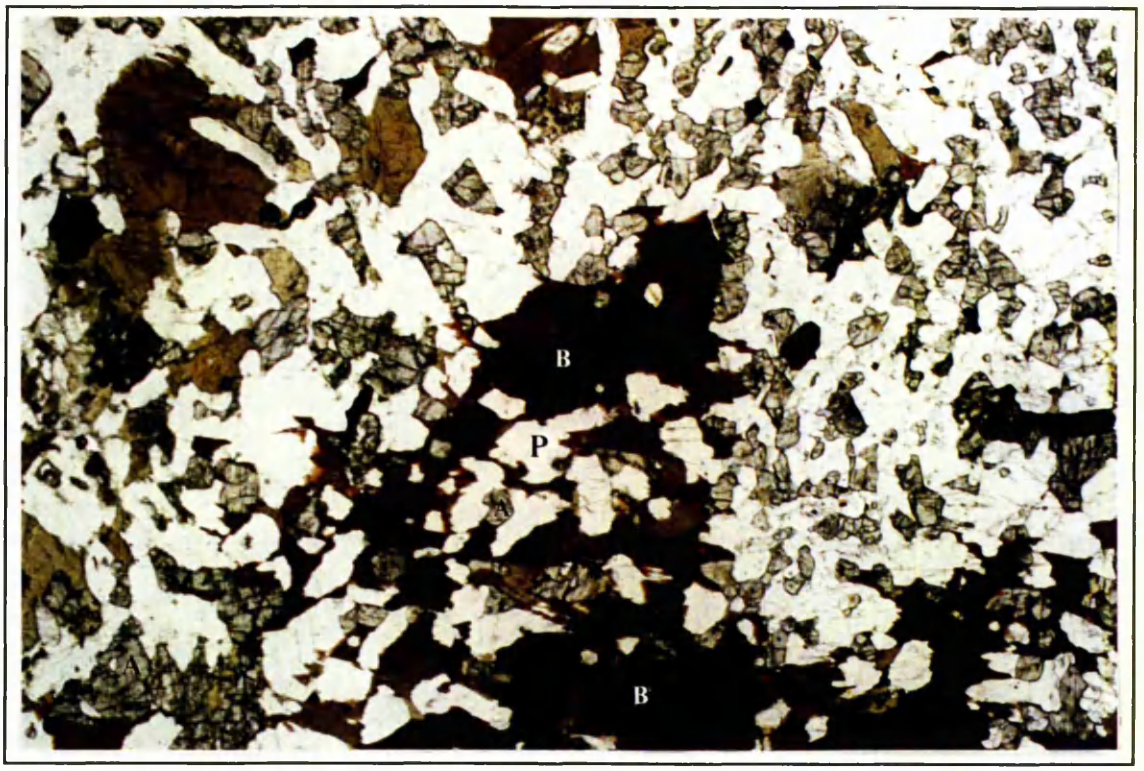

Plate 5.3.4 Photomicrograph of a biotite-hornblende dolerite (DD.H2). Part of a large, poikilitic biotite (B) covers the bottom half of the plate, containing inclusions of plagioclase and augite (A). Hornblende (H) forms lighter brown pleochroic crystals. PPL, field of view 7.7 x 5 mm.

Plate 5.3.5 Photomicrograph of a micro-norite (H.BHQ4). Plagioclase (P) forms randomly oriented laths, with anhedral, interstitial orthopyroxene (O). XPL, field of view 3.75 x 2.5 mm.

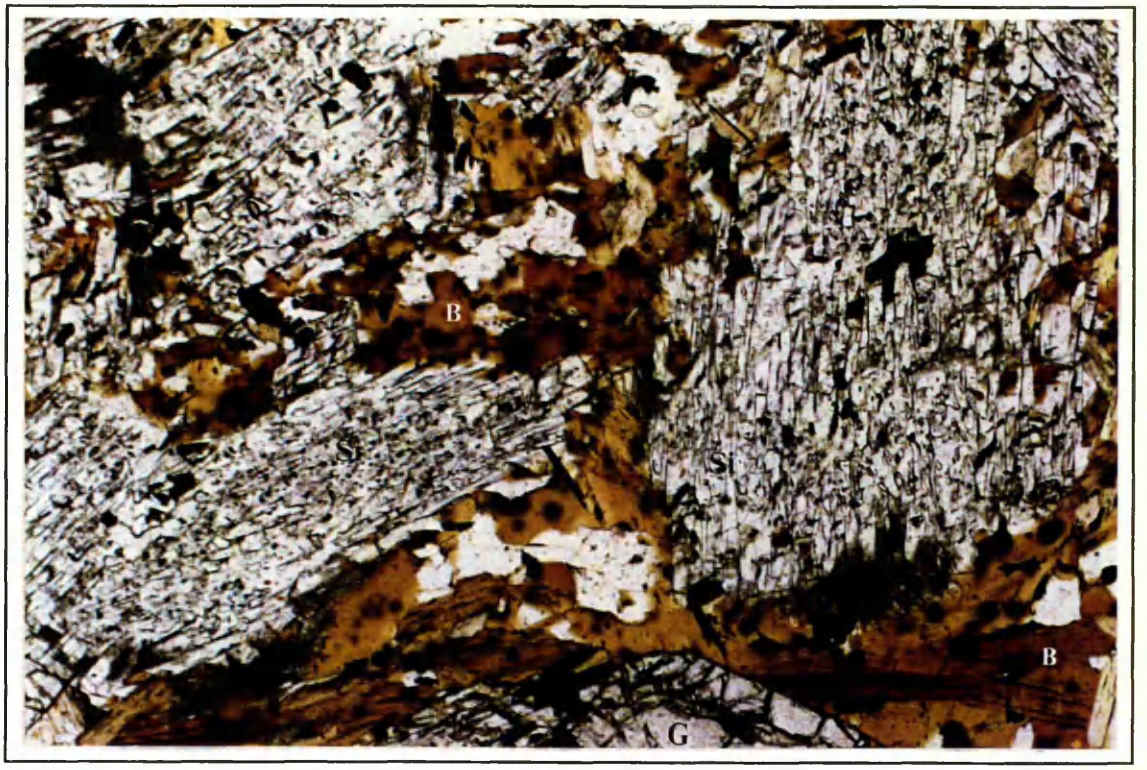

Plate 5.4.1 Photomicrograph of a cordierite-sillimanite schist (DD.DUN1). Sillimanite (Si) occurs as large rectangular bundles of prismatic crystals. Biotite (B) and quartz are present between these bundles, with numerous dark brown halos around zircons in the biotite. Part of a large garnet (G) is present at the base of the plate. PPL, field of view 7.5 x 5 mm.

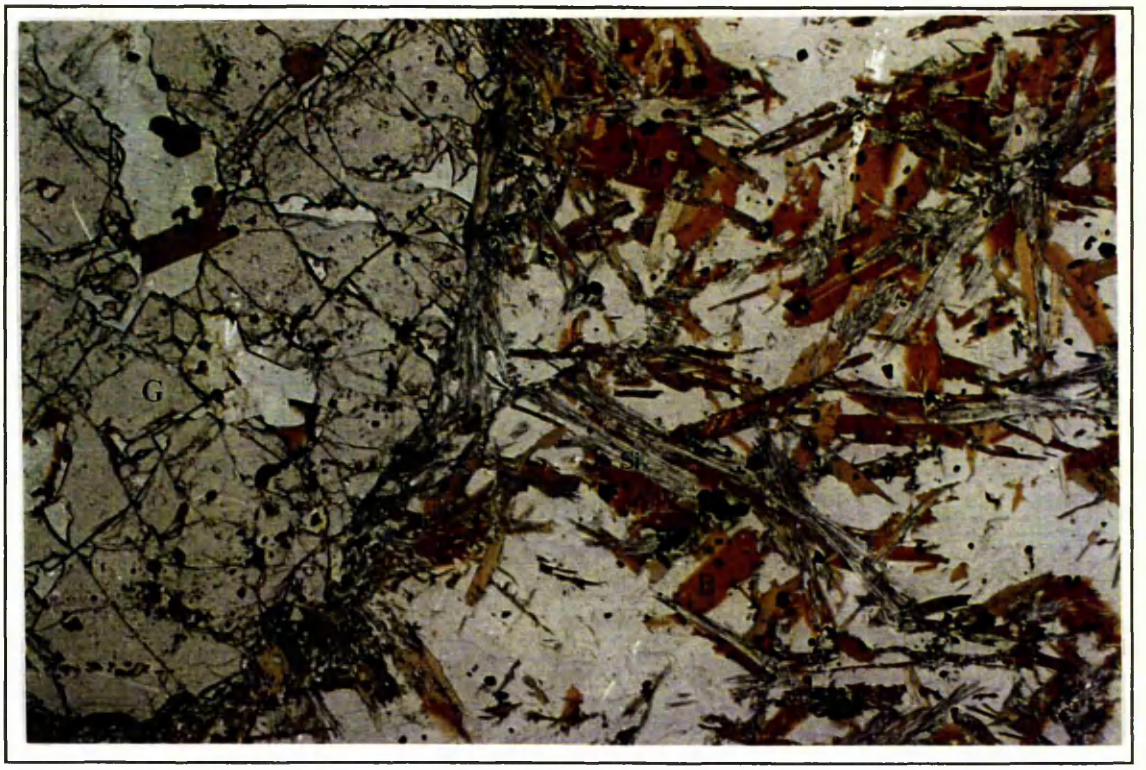

Plate 5.4.2 Photomicrograph of a sillimanite-cordierite hornfels (H.COR8). The sillimanite (Si) forms acicular needles, which form randomly oriented aggregates intergrown with biotite (B), and grow around the large garnet (G) on the left side of the plate. PPL, field of view 7.5 x 5 mm.

Plate 5.4.3 Photomicrograph of a cordierite-K-feldspar hornfels (H.COR4). Large atoll-type garnet (G), 'filled' with coarse grained K-feldspar (K)and quartz (Q). The matrix is composed mainly of fine-grained plagioclase and cordierite, which are intergrown to form a good granoblastic polygonal texture. XPL, field of view 7.5 x 5 mm.

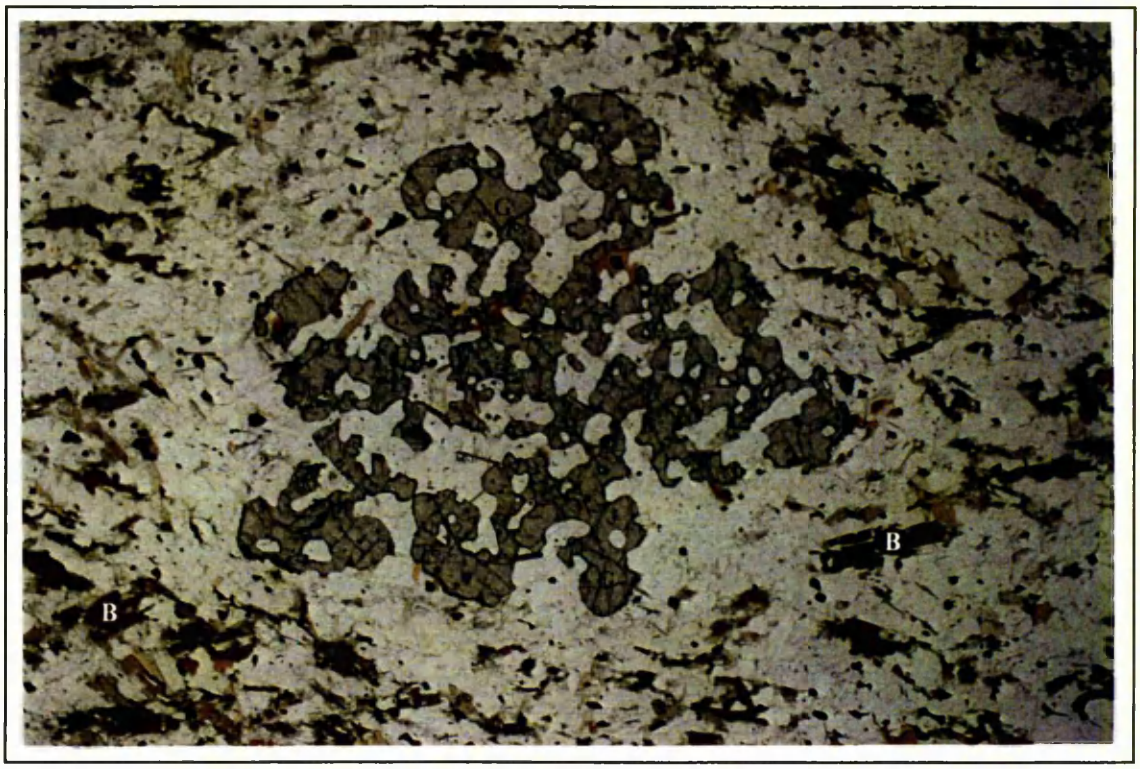

Plate 5.4.4 Photomicrograph of a cordierite-K-feldspar hornfels (DD.RH2). A large poikilitic garnet (G) covers the centre of the plate, and is surrounded by a biotite-free halo. PPL, field of view 7.4 x 5 mm.

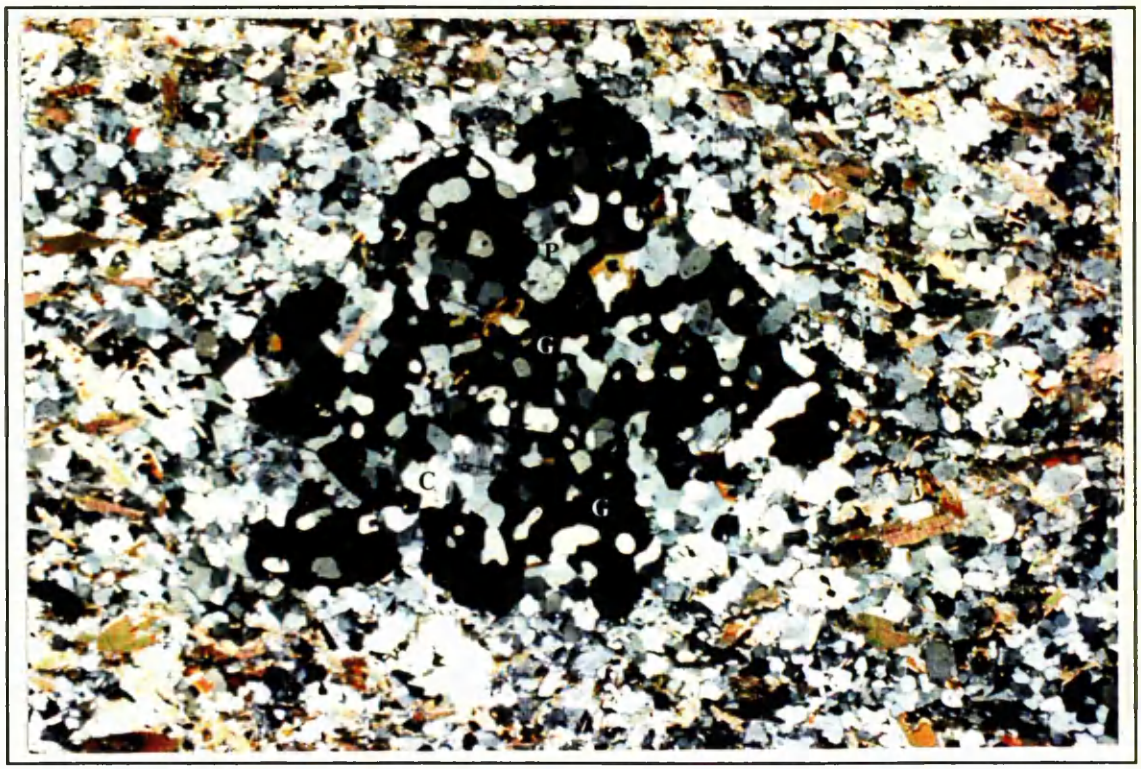

Plate 5.4.5 Photomicrograph of a cordierite-K-feldspar hornfels (DD.RH2). Same view as Plate 5.4.4 above, except in XPL. The poikilitic garnet (G) encloses cordierite (C) and plagioclase (P).

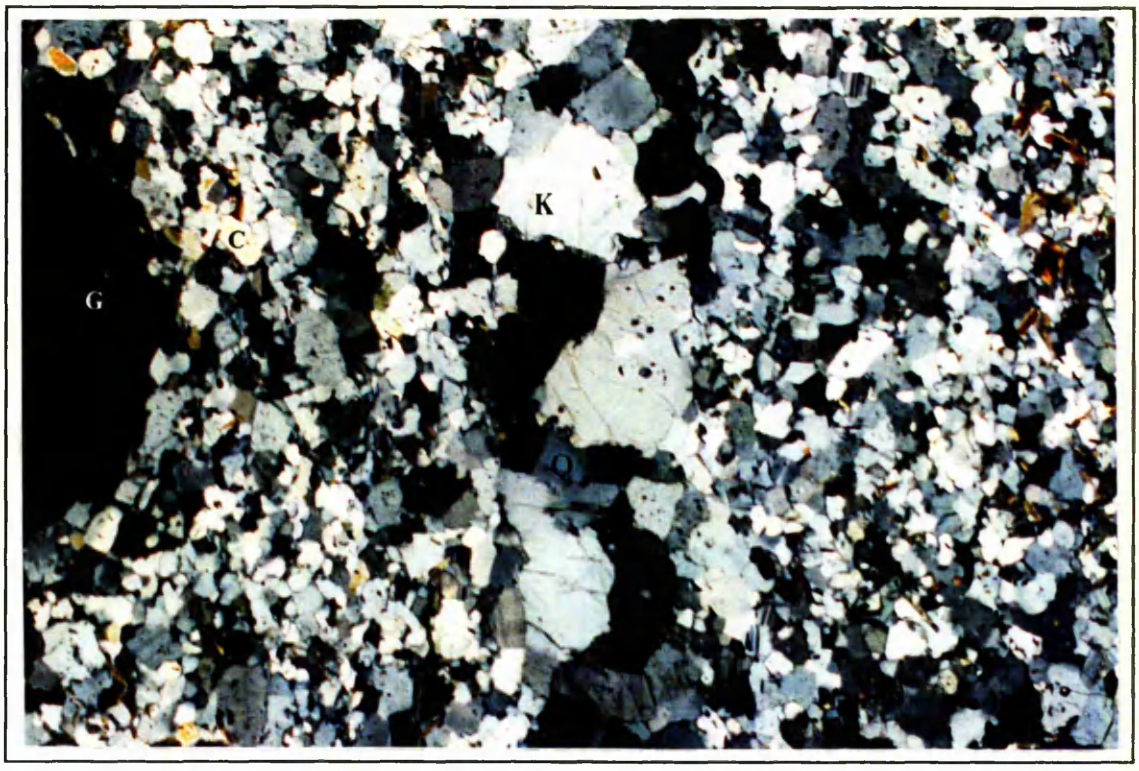

Plate 5.4.6 Photomicrograph of a cordierite-K-feldspar hornfels (DD.CUM21). The main rock matrix displays a good hornfelsic texture, with cordierite (C) and plagioclase (P) forming small, equant crystals. Running through the centre of the plate (top to bottom) is a leucocratic band, composed of coarse grained K-feldspar (K) and quartz (Q). XPL, field of view 7.5 x 5 mm.

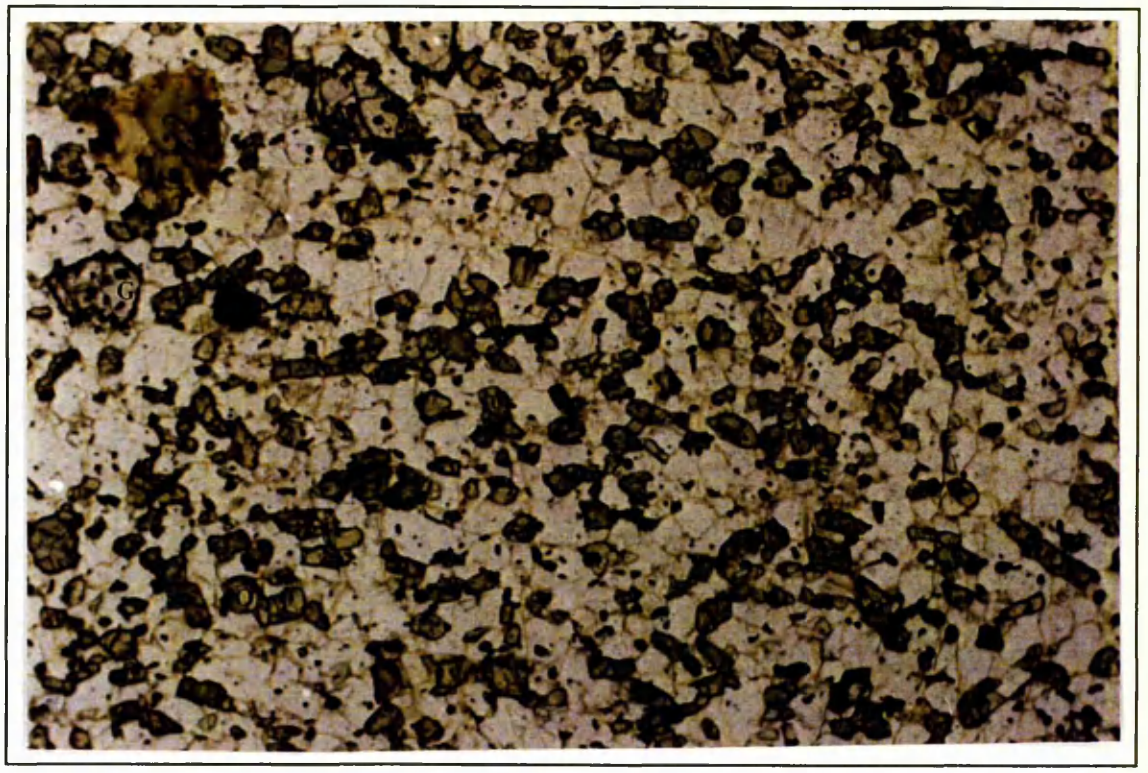

Plate 5.4.7 Photomicrograph of an orthopyroxene-cordierite hornfels (H.BHQ5). The rock is a fine grained hornfels. Orthopyroxene (O) forms small sub-rounded crystals which display green/pink pleochroism. Garnets (G) are present towards the top left of the plate. PPL, field of view 3.75 x 2.5 mm.

Plate 5.4.8 Photomicrograph of a orthopyroxene-cordierite hornfels (H.BHQ5). The rock is a fine grained hornfels, with interlocking, equant crystals of cordierite (C), plagioclase (P) and sub-rounded orthopyroxene (O). XPL, field of view 3.75 x 2.5 mm.

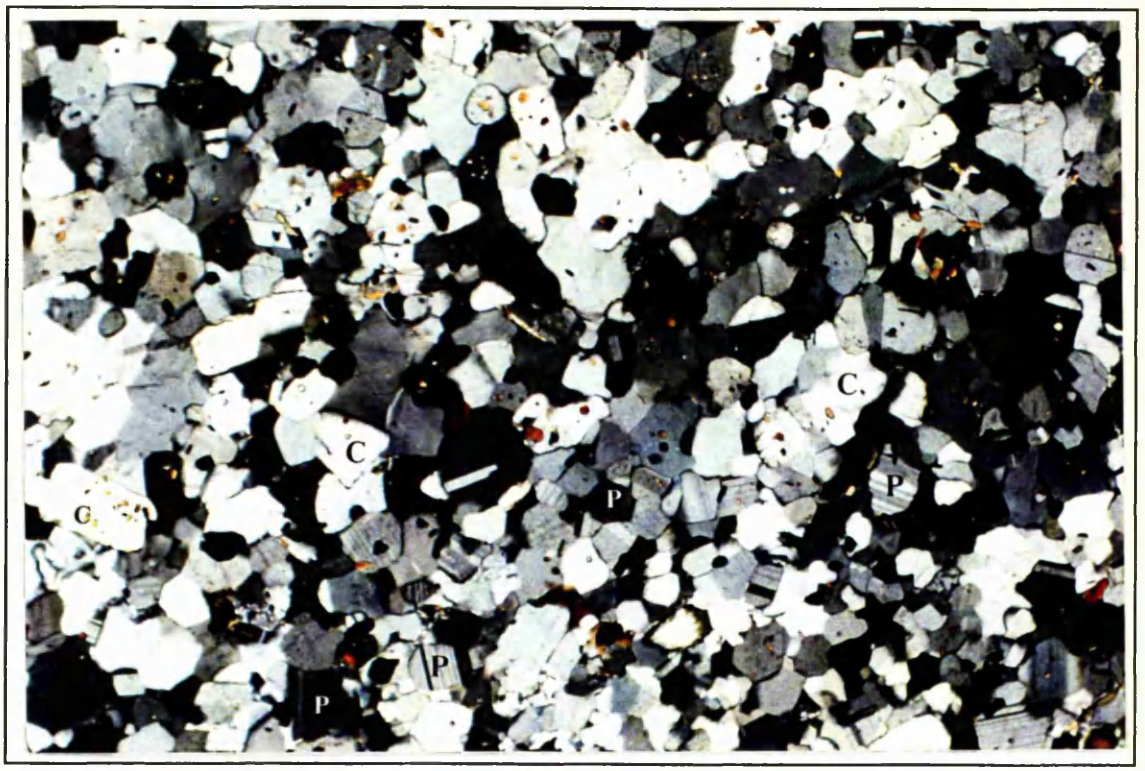

Plate 5.4.9 Photomicrograph of part of an orthopyroxene-cordierite hornfels (DD.BW1). Cordierite (C) and plagioclase (P) form interlocking crystals, displaying a granoblastic polygonal texture; indicative of a high degree of textural equilibrium. XPL, field of view 3.75 x 2.5 mm.

Plate 5.4.10 Photomicrograph of part of a orthopyroxene-cordierite hornfels (DD.BQ202). The central area of the plate is a monomineralic patch of granoblastic cordierite (C). The fringes of the plate contains plagioclase (P), additional cordierite and small opaque crystals. XPL, field of view 3.75 x 2.5 mm.

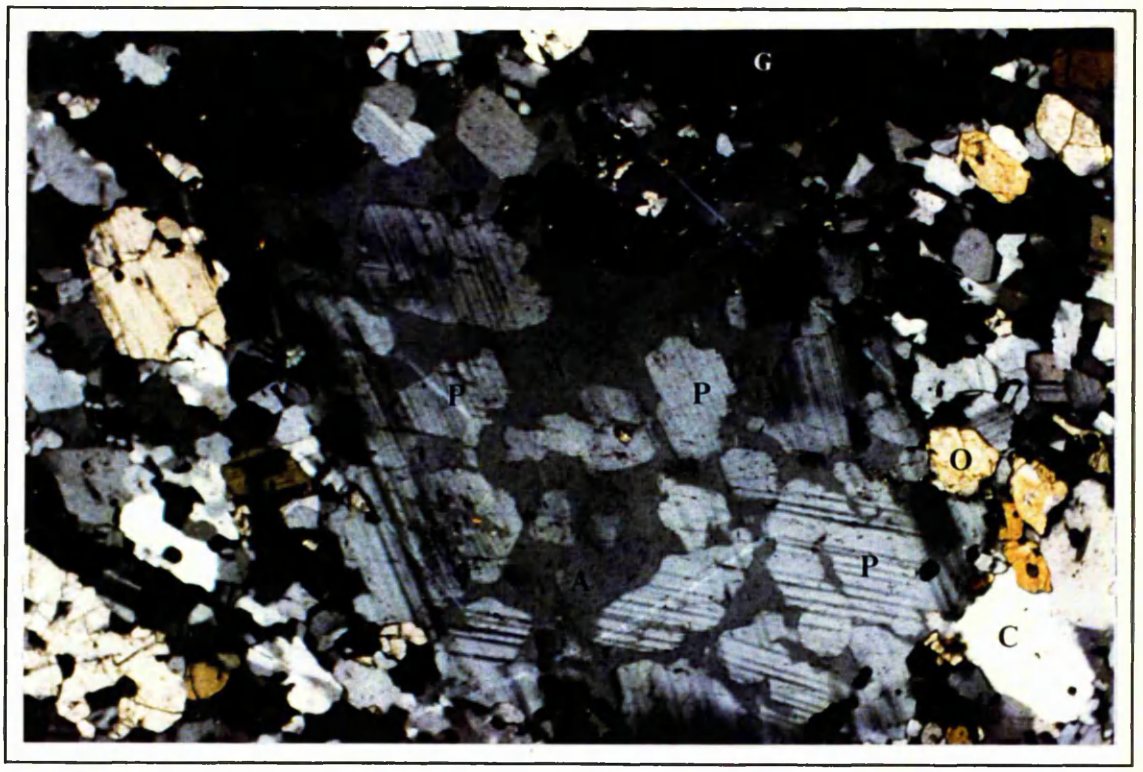

Plate 5.4.11 Photomicrograph of part of a orthopyroxene-cordierite hornfels (DD.BQ17), showing a large diamond shaped intergrowth of plagioclase (P) and K-feldspar (K). Other mineral phases present are garnet (G), orthopyroxene (O) and cordierite (C). XPL, field of view 3.74 x 2.5 mm.

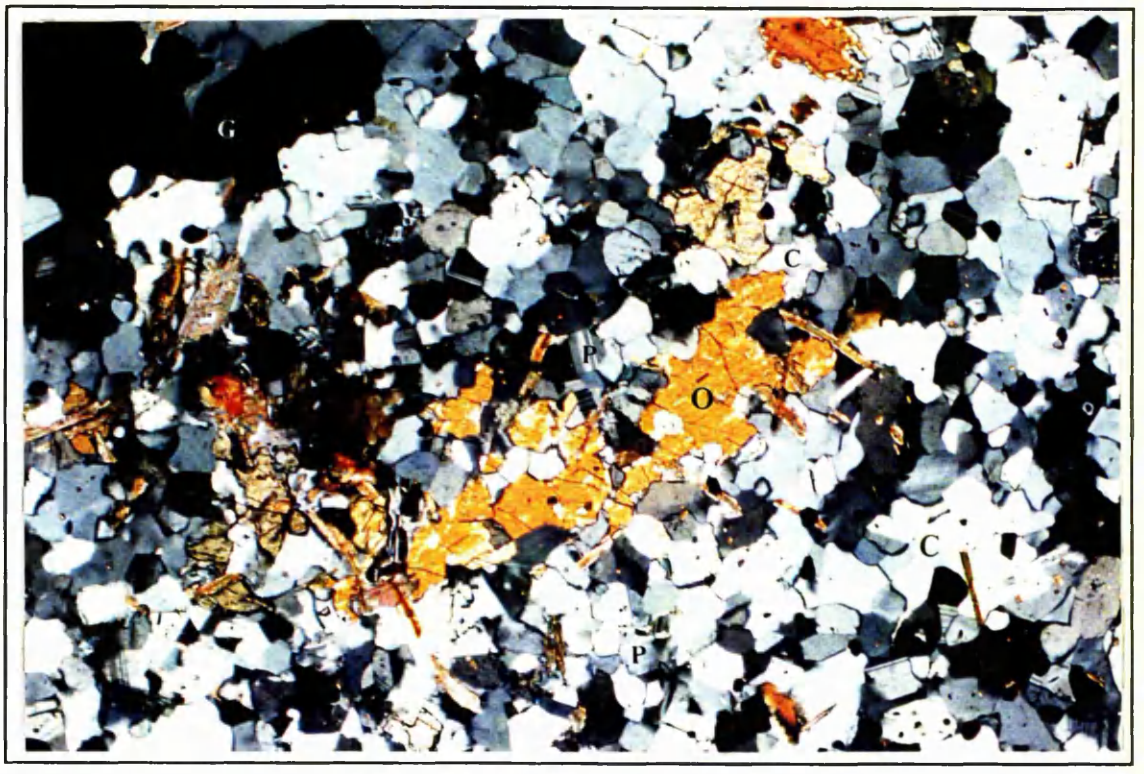

Plate 5.4.12 Photomicrograph of an orthopyroxene-cordierite hornfels (DD.BW1). A large, poikilitic orthopyroxene (O) overgrows plagioclase (P) and cordierite (C). The remainder of the plate displays a granoblastic polygonal texture formed by interlocking cordierite and plagioclase crystals. XPL, field of view 3.75 x 2.5 mm.

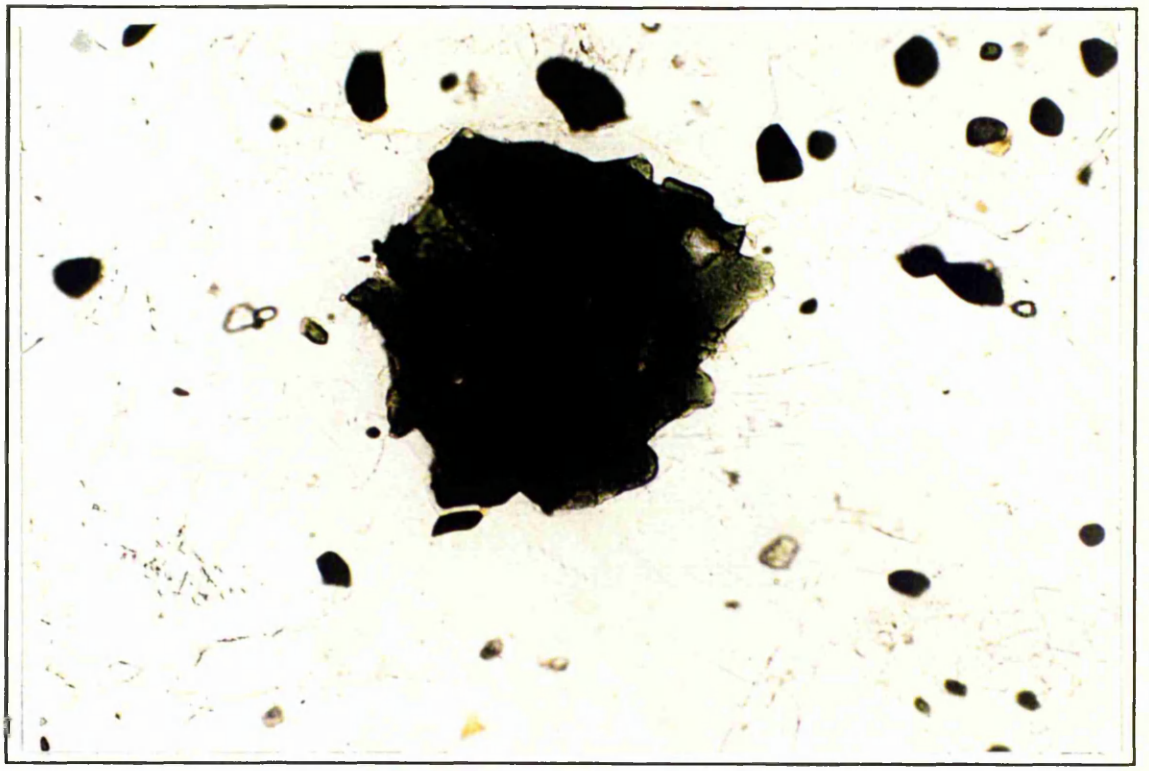

Plate 5.4.13 Photomicrograph of part of an orthopyroxene-cordierite hornfels (BQ10035). Rounded, dark green, hercynitic spinel. PPL, field of view 0.75 x 0.5 mm.

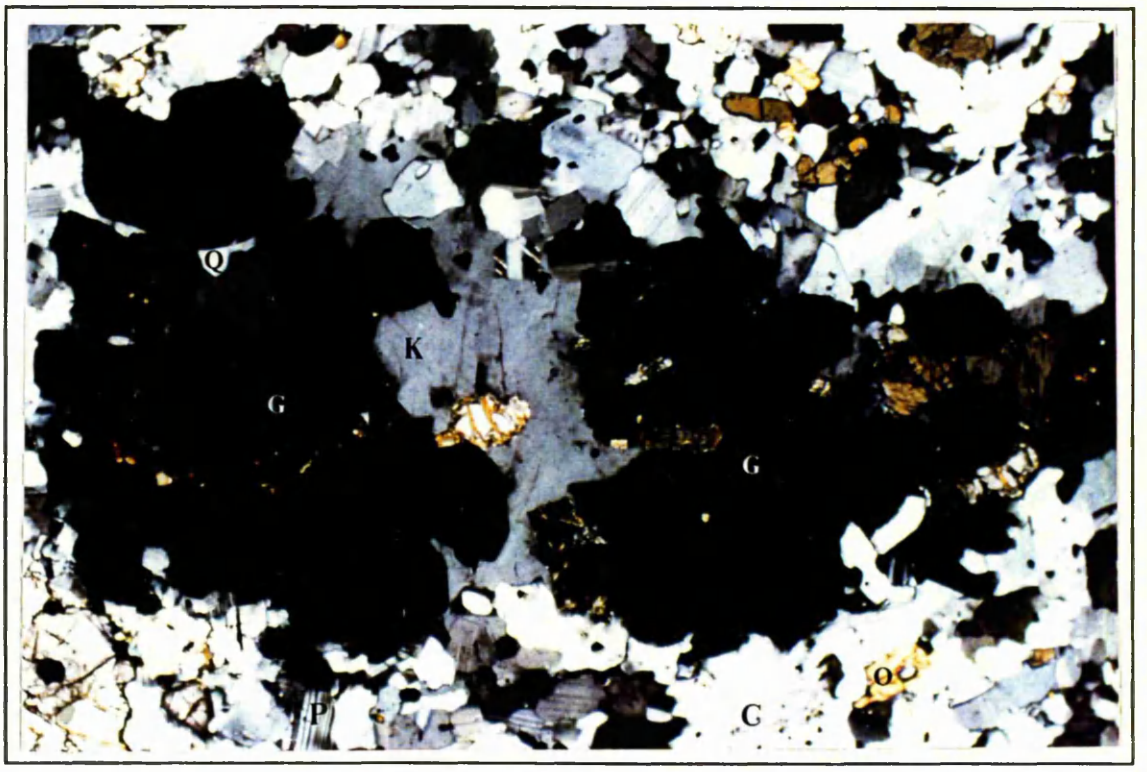

Plate 5.4.14 Photomicrograph of part of an orthopyroxene-cordierite hornfels (DD.BQ17). Atoll-type garnet (G), with 'filling' of coarse grained K-feldspar (K) and some fine grained quartz (Q). The remainder of the plate contains orthopyroxene (O), cordierite (C) and plagioclase (P). XPL, field of view 2.75 x 1.5 mm.

Plate 5.4.15 Photomicrograph of an orthopyroxene-cordierite hornfels (DDBQ201). A large atoll-type garnet (G) is 'filled' by coarse grained K-feldspar (K), quartz (Q) and biotite (B). The rock matrix is much finer grained and composed mainly of interlocking cordierite and plagioclase crystals, giving a good hornfelsic texture. XPL, field of view 7.5 x 5 mm.

Plate 5.5.1 Photomicrograph of a cordierite norite (DD.BQ38). A good igneous texture is displayed, with large euhedral and subhedral orthopyroxene (O) and plagioclase (P) forming randomly oriented crystals. The plagioclase is zoned, with albite rich rims. Quartz (Q) is interstitial. some biotite (B) is also present. XPL, field of view 7.5 x 5 mm,

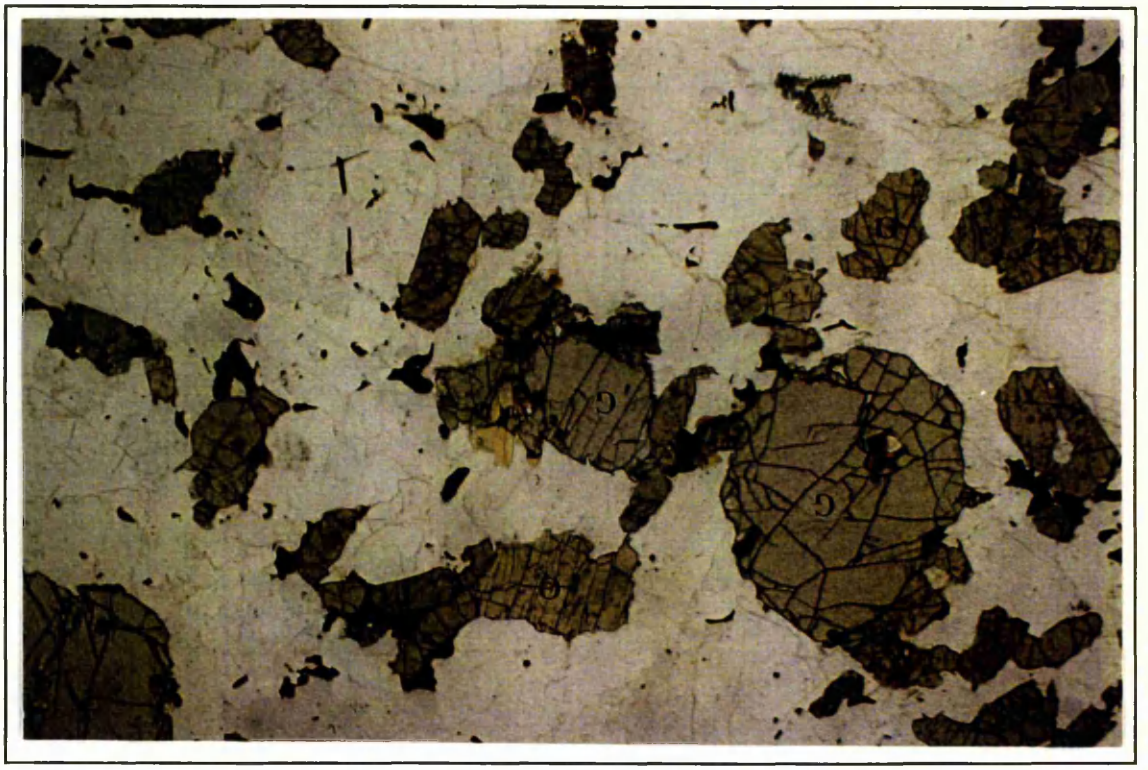

Plate 5.5.2 Photomicrograph of a cordierite norite (DD.BQ202ii). Large, rounded garnets (G) are present in this view, together with subhedral, green/pink pleochroic orthopyroxene (O) crystals. PPL, field of view 7.5 x 5 mm

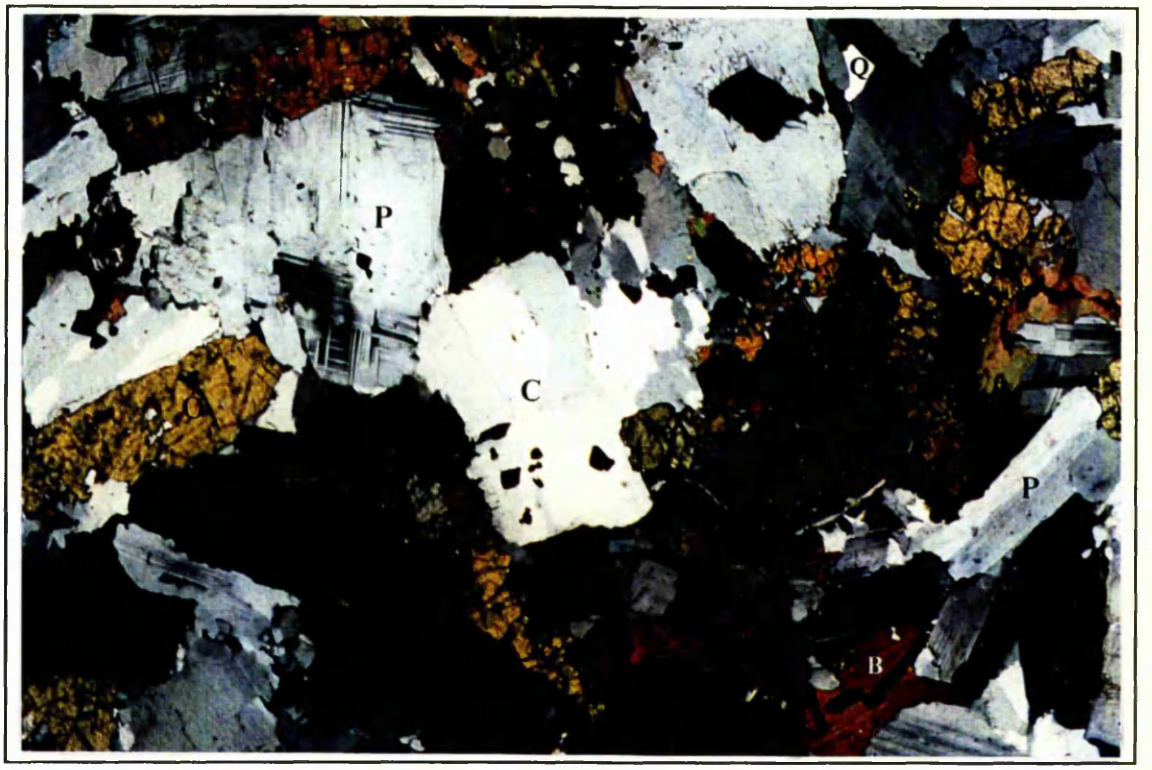

Plate 5.5.3 Photomicrograph of a cordierite norite (DD.BQ202ii). A good igneous texture is displayed, with orthopyroxene (O), plagioclase (P), and cordierite (C) all forming large, randomly oriented, subhedral crystals. A poikilitic biotite (B) is present on the lower right hand side of the plate and some interstitial quartz occurs. XPL, field of view 7.5 x 5 m.

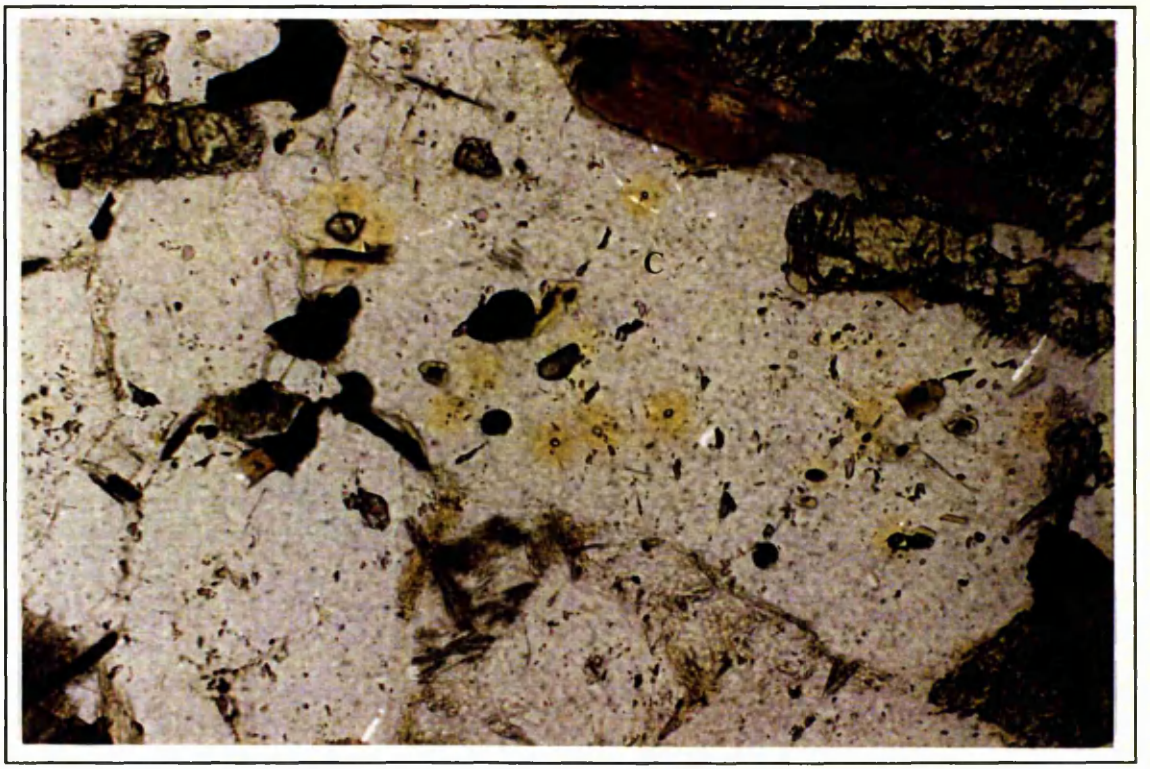

Plate 5.5.4 Photomicrograph from a cordierite norite (DD.CASB5). View of a large colourless cordierite (C), which contains yellow pleochroic halos around zircon crystals. PPL, field of view 1.5 x 1 mm.

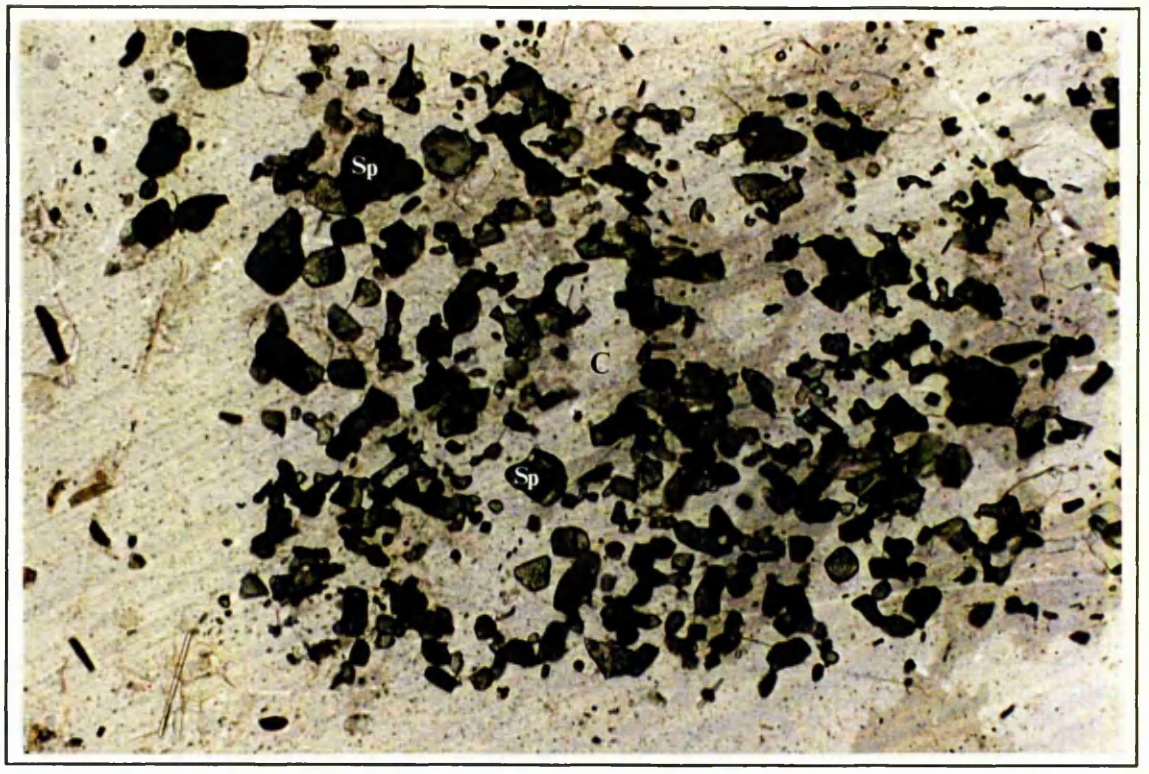

Plate 5.5.5 Photomicrograph from a cordierite norite (DD.DUN4). Large rectangular aggregate of green hercynitic spinel (Sp) inside a cordierite (C) crystal. PPL, field of view 1 x 1.5 mm.

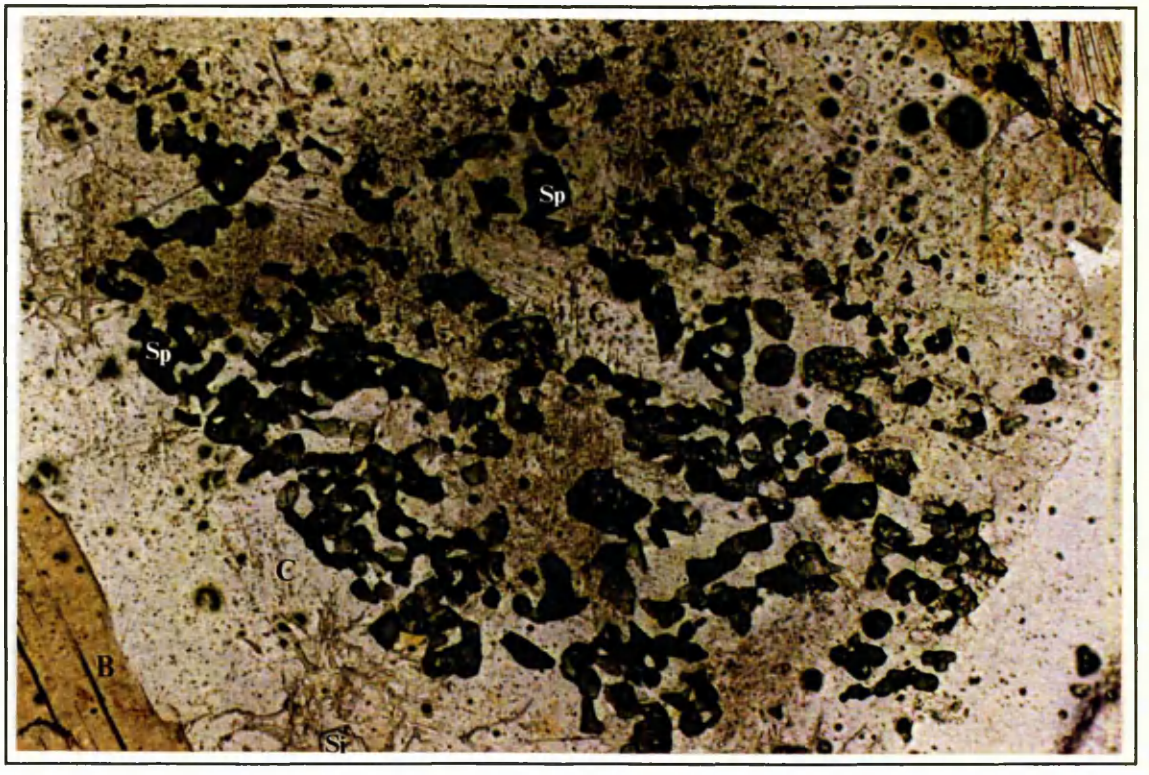

Plate 5.5.6 Photomicrograph from a cordierite norite (DD.CASB2i). Large rectangular aggregate of spinel crystals inside a large cordierite (C). At the bottom of the plate a small sillimanite crystal (Si) forms in inclusion inside the cordierite. Also present is part of a large biotite (B) flake. PPL, field of view 1.5 x 1 mm.

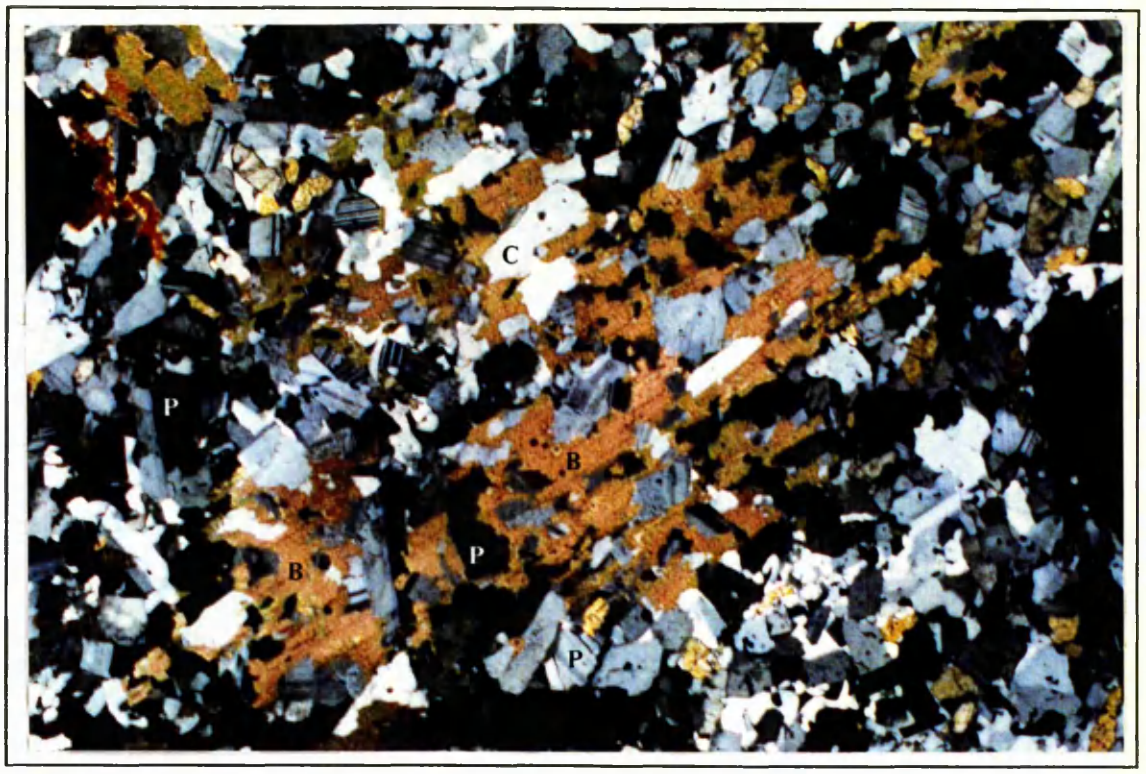

Plate 5.5.7 Photomicrograph from a cordierite norite (H.BHQ1). Large poikilitic biotite (B) enclosing plagioclase (P) and cordierite (C). XPL, field of view 7.5 x 5 mm.

Plate 5.5.8 Photomicrograph from a cordierite norite (DD.BQ202ii). Poikilitic biotite (B) partially enclosing plagioclase. Pleochroic orthopyroxene (O) is also present. PPL, field of view 7.5 x 5 mm.

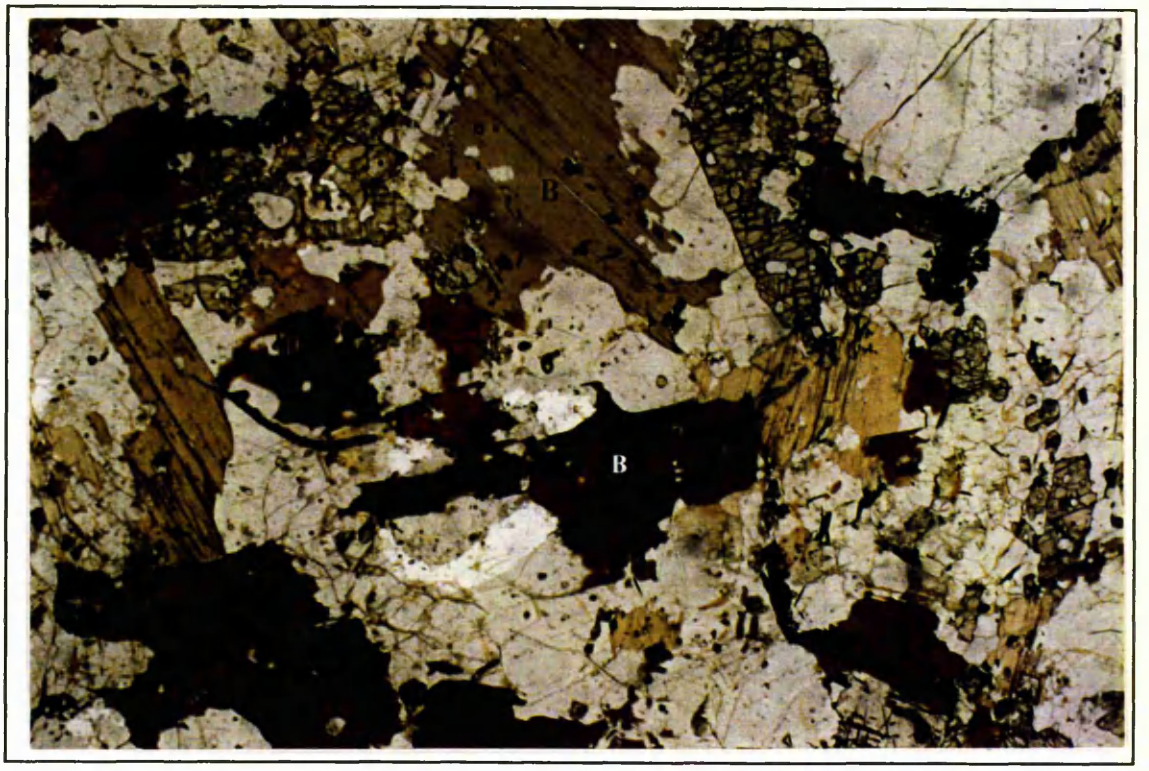

Plate 5.5.9 Photomicrograph of a cordierite norite (DD.CASB2i). Subhedral orthopyroxene (O) crystals, with large dark brown pleochroic biotite (B) flakes. PPL, field of view 7.5 x 5 mm.

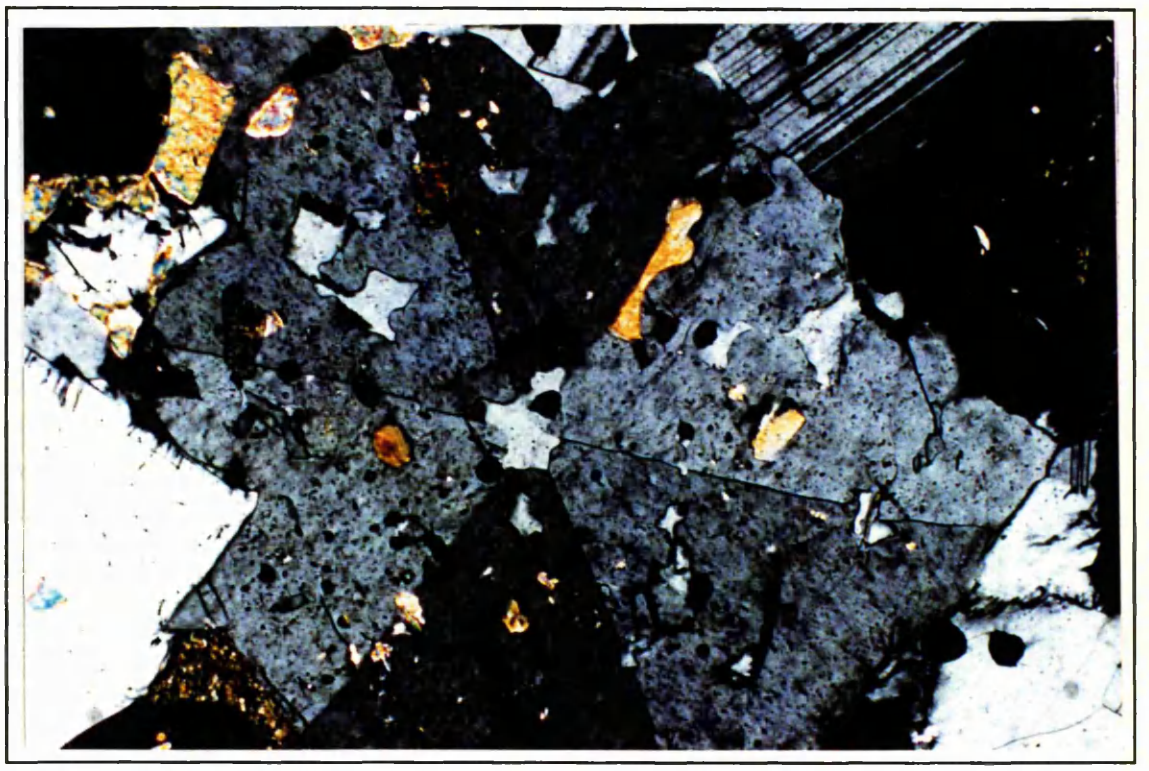

Plate 5.5.10 Photomicrograph from a cordierite granitoid (FOW1). Cordierite crystal displaying excellent sector twinning. XPL, field of view 3.75 x 2.5 mm.

Plate 5.5.11 Photomicrograph of a garnet tonalite (H.COR7). A good igneous texture is displayed; plagioclase (P) forms large randomly oriented, subhedral laths, biotite (B) forms large ragged flakes. Quartz is interstitial. The garnet (G) dwarfs all the other mineral phases, and contains inclusions of biotite, quartz and plagioclase. XPL, field of view 15 x 10 mm.

Plate 5.5.12 Photomicrograph from a garnet-hornblende tonalite (DD.CUM19). Weak-green pleochroic orthopyroxene (O), partially replaced by olive-green pleochroic hornblende (H). Red-brown biotite (B) is also present near the top of the plate. PPL, field of view 7.5 x 5 mm.

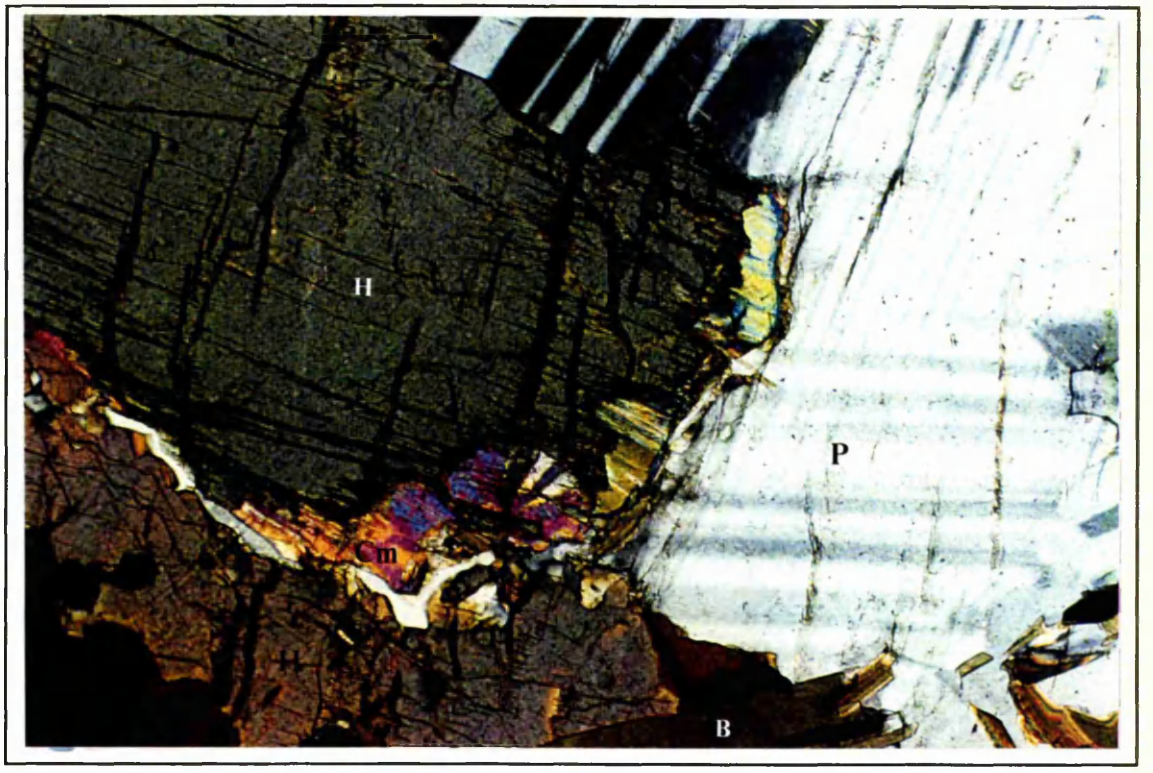

Plate 5.5.13 Photomicrograph from a garnet-hornblende tonalite (DD.CUM19). Large hornblende (H) crystal rimmed by brightly birefringent cummingtonite (Cm). Also present are plagioclase (P) and biotite (B).

CHAPTER 6 MINERAL CHEMISTRY

6.1 Introduction

6.1.1 Uses of mineral chemistry

Estimation of the metamorphic conditions which led to the formation of a suite of metamorphic rocks in a given area cannot be undertaken without first determining mineral chemistry. For the purposes of this study, mineral chemical data will be used in the calculation of the pressure-temperature-fluid conditions prevalent during the formation of the cordierite-bearing hornfelses, and the igneous-textured cordierite norites and garnet tonalites. The mineral chemistry from selected rocks from outside the aureole of the Huntly Gabbro was also used to allow estimation of the regional P-T conditions at the time of intrusion of the gabbro.

6.1.2 Machines used, sample preparation, data acquisition and processing

The chemical composition of the mineral phases present in selected sections of the rocks in study was determined by analysis of polished, uncovered thin sections on the Geoscan and Cameca electron microprobes. The Geoscan microprobe was used for the analysis of the major elements (Si, Ti, Al, Cr, Fe, Mn, Mg, Ca, Zn, Na, and K) present in the mineral phases from the majority of thin sections analysed. The Cameca microprobe was used for W.D. analysis of fluorine, barium and chlorine contents present in biotite.

A full description of the workings and specifications for the microprobes, the detection limits, and the software used to calculate oxide totals and the mineral stoichiometry of analyses is described in Appendix I.

Where cation totals were systematically greater than the expected number in anhydrous ferro-magnesian minerals the probe analyses were recalculated to determine Fe^{3+} and Fe_2O_3 contents using the equation of Droop (1987)

6.1.3 Sample selection and rationale behind data collection

Samples were selected in which the minerals present appeared to display an equilibrium texture (Chapter 5.4) and contained mineral assemblages which were

applicable to work for geothermobarometry (e.g., rocks containing mineral phases with Fe + Mg solid solution). The composition of minerals from samples which display these 'equilibrium' textures are inferred to represent the compositions of these minerals at peak pressure-temperature conditions during metamorphism. As many of the samples analysed were subjected to thermal metamorphism by a mafic-igneous intrusion and therefore presumably cooled relatively rapidly, it is reasonable to assume that little post-peak metamorphic retrogresive resetting of mineral compositions occurred (as might be the case in a slow cooling regional granulite terrain).

The analyses collected for thermobarometric work were taken from crystal cores, in areas of samples in which all the mineral phases of interest could be shown to be in equilibrium together. Ten or more analyses were taken from each mineral of interest, though between one and five analyses were taken from minerals which have no, or limited solid solution, or which were of limited thermodynamic interest (i.e. sillmanite, tourmalineand ilmenite). Mineral cores were used as their composition are inferred to represent peak metamorphic compositions, and are less likely to have undergone any post-peak metamorphic resetting by diffusion.

6.1.4 Criteria for accepting data

For probe analyses to represent the true composition of any given mineral the sum wt % of the oxides analysed and the stoichiometry of the calculated cation totals should match those expected in the mineral analysed. Therefore, a set of accuracy parameters were created for each mineral analysed, and probe analyses which failed any of these parameters were discarded. A full list of accepted oxide totals and stoichiometric tests is given in the Table 6.1.

6.2 Regionally Metamorphosed Rocks

6.2.1 Plagioclase

Plagioclase is present in the garnet-biotite gneisses and garnet mica schists from the Cairnie road cuttings (localities 2a & 2b), but not in any of the regionally metamorphosed rocks from the S & SW margins of the Huntly Gabbro. Selected electron

microprobe analyses of plagioclase crystals are shown in Table 6.2.1. The plagioclase in the garnet-biotite gneiss in DD.SIN101 is similar in composition to the plagioclase from the garnet-mica schist DD.SIN2, with the An values in the two sections varying from An_{17} to An_{23} (Figure 6.2.1). The orthoclase content in the plagioclase is very low, with the K content in most analyses below the detection limit of the microprobe. No zoning was present in any of the plagioclase crystals analysed, with rims and cores recording similar An values.

6.2.2 Garnet

Table 6.2.2 shows representative probe analyses of electron microprobe analyses taken from garnet cores. Figure 6.2.2 is a ternary plot displaying the compositions of garnet core analyses from the garnet-biotite gneisses DD.SIN1 and DD.SIN101, and the garnet-mica schist DD.SIN2. The garnets in the schist have higher Fe + Mn contents than those in the gneisses (which is partly due to the higher Mn content in DD.SIN2 of X_{Mn}^{Grt} 0.08-0.10, compared to X_{Mn}^{Grt} 0.04-0.07 for the garnet-biotite gneisses). The Ca content in the garnets from all three sections analysed from Cairnie is similar, with X_{Ca}^{Grt} varying from 0.02 to 0.05. Estimates of Fe_2O_3 contents gives between 0.59 and 1.84 wt% and the recalculated Fe^{2+} contents give increased accuracy in the stoichiometry of analyses, with the Fe^{2+}, Mn, Mg and Ca total being closer to the ideal 6 in the 24(O) formula unit.. Analyses from rims and cores of garnets show little variation, and Figures 6.2.3 and 6.2.4 are profiles across a single garnet crystals from DD.SIN2 and DD.SIN101, neither of which show evidence of any zonation.

The garnets present in the andalusite-mica schist DD.CLAS66 from Clashmach Hill (locality 2c) differ from those from Cairnie by their high Mn and low Mg contents, with X_{Mn}^{Grt} varying from 0.30 to 0.33 and X_{Mg}^{Grt} from 0.08 to 0.09. Figure 6.2.5 is a profile from a single garnet crystal, showing that no discernible zonation is present and displaying the high Mn content of the garnet.

6.2.3 Biotite

Representative analyses of biotite grains are given in Table 6.2.3. The compositions of analysed biotites, shown in Figure 6.2.6, in terms of the end-members

annite, phlogopite and siderophyllite, given by plotting Mg# (Mg# = Mg/(Fe^{2+} + Mg)) against the number of Al^{vi} atoms in the 22(O) formula unit (Al^{vi} calculated as sum (Si + Al)-8, assuming the total number of tetrahedral cation to equal eight). The analysed biotites in the schists from Clashmach Hill (DD.BOG1, DD.CLAS66 & DD.CLAS111) have lower Mg# (varying from 0.29 to 0.40) than those in the rocks from Cairnie (DD.SIN1, DD.SIN101, & DD.SIN101) with Mg# varying from 0.50 to 0.62, the highest Mg# being in the garnet-biotite gneiss (DD.SIN101). The Al^{vi} content in all of the sections analysed is closely grouped, with the number of Al^{vi} ions (in the 22(O) formula unit) mostly falling within the field 0.75-1.0. The Ti content present in the biotite analyses is displayed in Figure 6.2.7. The biotites in the sections from Clashmach Hill show slightly greater Ti contents (0.265 to 0.397 ions in the 22(O) formula unit) than in analyses from the biotites from the sections from Cairnie (0.168 to 0.245).

6.2.4 Muscovite

Table 6.2.3 gives representative analyses of muscovite from the three schists analysed from Clashmach Hill, and the garnet-mica schist (DD.SIN2) from Cairnie. The Clashmach Hill muscovites all contain appreciable amounts of Fe and Mg, with 1.00 to 2.71 wt% FeO (all Fe is quoted as FeO as ratios of FeO and Fe_2O_3 cannot be calculated from total Fe content in hydrous minerals from probe analyses) and 0.55 to 1.25 wt% MgO. The FeO and MgO contents in DD.SIN2 muscovites vary from 0.67 to 1.49 wt% and 0.59 to 1.00 wt% respectively. All the muscovite contain some Na in their alkali sites, with X_{Na}^{Mu} (X_{Na}^{Mu} = Na/(Ca + Na + K)) varying from 0.059-0.16 for the Clashmach Hill schists and from 0.189 to 0.261 in DD.SIN2.

6.2.5 Staurolite

Representative probe analyses of staurolite from section DD.SIN101 are given in Table 6.2.4. The Mg# of the analyses varies from 0.21 to 0.26 and between 0.48 to 0.89 wt% ZnO is present (0.104 to 0.193 ions Zn in 48(O) formula unit).

6.2.6 Tourmaline

Probe analyses for tourmaline were gained from sections DD.BOG1 and DD.CLAS111. Representative analyses are shown in Table 6.2.4. However, the B and F

contents are not given as the tourmaline results shown were all gained by E.D.S. analysis, which is unsuitable for calculating the contents of B and F.

6.3 Cordierite Hornfelses

The cordierite hornfelses are further subdivided into sillimanite-cordierite hornfelses and orthopyroxene-cordierite hornfelses and the mineral chemistry of the two rock types is described separately below.

6.3.1 Feldspars

Table 6.3.1 gives shows representative analyses of plagioclase and alkali feldspar analyses taken from sillimanite-cordierite and orthopyroxene-cordierite hornfelses.

(i) Sillimanite-cordierite hornfelses

Plagioclase and alkali feldspar compositions are displayed in Figure 6.3.1. Some normal zonation occurs in the plagioclase, as displayed in Figure 6.3.2, a zonation profile across a single plagioclase crystal. The plagioclase shows slightly Ab-rich, An-poor rims, with X_{An} varying from 0.34 at the rim to 0.46 near the crystal core.

The alkali feldspar in H.COR8 has X_{Or} contents of between 0.81 and 0.85.

(ii) Orthopyroxene-cordierite hornfelses

The compositions of plagioclase and alkali feldspar crystals from the orthopyroxene-cordierite hornfelses are displayed in the ternary plot Figure 6.3.3. The plagioclase compositions in the sections DD.PIR1 and DD.PIR4 (in which the plagioclase forms only small anhedral crystals) are closely clustered, with X_{An} varying from 0.341 to 0.381. However, in section DD.BQ17, large plagioclase porphyroblasts show some zoning as displayed in Figure 6.3.4.

The alkali feldspar in DD.BQ17 has X_{Or} contents varying between 0.87 and 0.90. The alkali feldspar in section DD.BQ41, however, has a high relatively An content, with X_{An} varying between 0.07 and 0.11 and the X_{Or} content varying widely between 0.12 and 0.53.

6.3.2 Garnet

Representative analyses of garnets from cordierite hornfelses are given in Table 6.3.2.

(i) Sillimanite-cordierite hornfelses

Garnet compositions are plotted in Figure 6.3.5 and zonation profiles from garnets in sections DD.DUN1 and H.COR8 are given in Figures 6.3.6 and 6.3.7. The garnet profile from H.COR8 (Figure 6.3.7) exhibits some zoning, with Fe-rich, Mg-poor rims possibly indicative of retrogressive Fe-Mg exchange between garnet and biotite. However, the Fe, Mn, Mg and Ca compositions remain constant across the centre of the garnet. The garnet profile from DD.DUN1 (Figure 6.3.6) shows slight zonation, also with Fe-rich, Mg-poor rims. The zonation in H.COR8 is, however, more pronounced than that shown in the garnet from DD.DUN1.

The cation totals of garnets from H.COR8 are all equal to, or slightly less than the ideal 16 (in the 24(O) formula unit), indicating the likely absence of significant Fe^{3+}. Recalculation of garnet analyses from DD.DUN1, though, gives estimated Fe_2O_3 contents of between 0.11 and 1.84 wt%.

(ii) Orthopyroxene-cordierite hornfelses

Figure 6.3.8 is a ternary plot of garnet compositions. The Mg content in the garnets from the orthopyroxene-cordierite hornfelses is higher (X_{Mg}^{Grt} ranging from 0.25 to 0.32 in the five orthopyroxene-bearing hornfelses analysed) than in the sillimanite-bearing hornfelses (X_{Mg}^{Grt} varying between 0.18 and 0.23). The Ca content in all of the cordierite hornfelses is similar, with X_{Ca}^{Grt} values mainly between 0.02 and 0.05. Zonation profiles across single garnet crystals from sections DD.BQ17 and DD.PIR1 are given in Figures 6.3.9 and 6.3.10. These profiles show that no zonation of Fe, Mg, Mn or Ca occurs in the garnets, with rims having identical compositions to crystal cores.

Recalculations for Fe^{3+} suggest that small amounts of Fe^{3+} are present in the garnets from many of the with between 0 and 1.66 wt% Fe_2O_3 present.

6.3.3 Cordierite

Table 6.3.3 gives representative microprobe analyses of cordierite crystals from cordierite hornfelses.

(i) Sillimanite-cordierite hornfelses

The Mg# values of cordierite from the two sillimanite-cordierite hornfelses analysed are similar, varying from 0.60 to 0.68 (H.COR8) and from 0.59 to 0.71 (DD.DUN1). Cation totals are equal to, or slightly less than 11 in the 18(O) formula unit indicative that no Fe^{3+} is present in the cordierites from both samples.

(ii) Orthopyroxene-cordierite hornfelses

The cordierites from the orthopyroxene bearing hornfelses have slightly higher Mg# than the cordierites from the sillimanite-cordierite hornfelses, with Mg# varying from 0.61 to 0.77 across the samples analysed. Cation totals systematically greater than 11 suggest the presence of some Fe^{3+} in three of the orthopyroxene-cordierite hornfelses. Recalculation of the probe analyses indicate between 0 and 2.18wt% Fe_2O_3 and Fe^{3+} cation contents of between 0 and 0.166.

6.3.4 Orthopyroxene

Representative orthopyroxene probe analyses from orthopyroxene-cordierite hornfelses are given in Table 6.3.4. The Mg# and X_{Al}^{M1} contents of the orthopyroxene from all of the orthopyroxene-cordierite hornfelses analysed are similar, with Mg# all falling between 0.4 and 0.5 and X_{Al}^{M1} varying between 0.075 and 0.61. Figures 6.3.11 and 6.3.12 are plots of Mg# and X_{Al}^{M1} against frequency, and highlight the similarities of Mg# and X_{Al}^{M1} between sections.

The orthopyroxene from the cordierite-absent section H.COR10 occurs in two separate domains, being present in an augite, anorthite-bearing (tuffaceous?) band, and in a garnet-bearing pelitic band. The Mg# and Al contents of orthopyroxene in the Cpx present band are lower (Mg# from 0.464 to 0.486 and X_{Al}^{M1} 0.009 to 0.011) than in the garnet present band (Mg# from 0.497 to 0.561 and X_{Al}^{M1} from 0.08 to 0.097), and the Ca content in the Cpx band is greater (0.68 to 1.04wt% CaO) than in the garnet-bearing band (<0.37wt% CaO)

6.3.5 Biotite

Representative biotite probe analyses from the four biotite-bearing hornfels sections analysed are given in Table 6.3.5.

(i) Sillimanite-cordierite hornfelses

Figure 6.3.13 plots the Al^{vi} content of biotite analyses against Mg#. The sillimanite-cordierite hornfelses have high Al^{vi} contents of between 0.668 and 1.46 atoms per 22(O). The Mg# varies between 0.44 and 0.51 in H.COR8 and between 0.54 and 0.55 in DD.DUN1. Figure 6.3.14 is a ternary plot, plotting Mg and Fe against Ti and displays the relatively low Ti content in the sillimanite-bearing hornfelses (1.45-3.48 wt % TiO_2, 0.159 to 0.541 cations), despite the presence of ilmenite in the rocks, which one would expect to result in Ti-saturation of biotite. Biotites close to, or contacting garnets generally have higher Mg# than biotites away from garnets. This complements the Fe-rich rims of the garntets and is likewise probably due to retrograde Fe-Mg exchange between these two minerals.

(ii) Orthopyroxene-cordierite hornfelses

The biotites from the orthopyroxene-cordierite hornfelses have lower Al^{vi} contents than those of the sillimanite-cordierite hornfelses, with 0.245 to 0.353 cations of Al^{vi} present. The Mg# in these hornfelses are overlap those in the sillimanite-bearing hornfelses, with Mg# values between 0.48 and 0.57. Ti contents of biotites in the orthopyroxene-cordierite hornfelses are high, with 5.14 to 6.24 wt% TiO_2 (0.567 to 0.699 cations Ti) in section H.COR10 and 5.53 to 6.63 wt% TiO_2 (0.609 to 0.752 cations Ti) in section H.BHQ5. As with the sillimanite-cordierite hornfelses, the biotites contacting or close to garnets generally have higher Mg# than biotites remote from garnets.

6.3.6 Spinel

Spinel occurs in two of the sections probed, H.BHQ5 and DD.BQ17, both of which are orthopyroxene-cordierite hornfelses. The Mg# values of the spinels from the two sections overlaps with Mg# varying from 0.18 to 0.32. Recalculation for Fe^{3+} contents indicates $X^{Spl}_{Fe^{3+}}$ ($X^{Spl}_{Fe^{3+}} = Fe^{3+} / 2$) contents of between 0.033 and 0.048 (3.11 to 4.47 wt% Fe_2O_3) for DD.BQ17 and between 0 and 0.051 (0 to 3.92 wt% Fe_2O_3) for H.BHQ5. Zn

occurs in the spinels from both sections, with X_{Zn}^{Spl} contents of between 0.044 and 0.058.

6.3.7 Sillimanite

Sillimanite analyses indicate that the sillimanite is essentially pure, with no Fe^{3+}, or Mn substitution.

6.3.8 Ilmenite

Ilmenite analyses indicate that the ilmenite lies close to its Fe^{2+} end member, with $X_{Fe^{2+}}^{Ilm}$ never less than 0.96. Some Mg occurs, but Mn contents are below the detection limits of the probes.

6.4 Igneous Rocks

6.4.1 Feldspars

Table 6.4.1 gives representative feldspar analyses from cordierite norites and garnet tonalites.

(i) Cordierite norites

The alkali feldspar in section H.BHQ1 contains X_{Or} contents varying from 0.82 to 0.88. Plagioclase, which occurs in all of the sections analysed, is frequently zoned with Ab-rich, An-poor rims, displayed in the zonation profiles Figures 6.4.1 and 6.4.2. This zonation leads to X_{An} contents varying greatly, such as in section DD.DUN12 with X_{An} values from 0.49 to 0.74. This zonation pattern is normally seen in plagioclase crystals from igneous rocks, and is interpreted as indicating crystallisation of the plagioclase over a decreasing temperature range. The orthoclase contents in the plagioclase are generally low with X_{Or} contents mainly lying between 0 and 0.04.

(ii) Garnet tonalites

The X_{Or} content of the alkali feldspars from DD.CUM22 varies from 0.820 to 0.876. The plagioclase crystals are again frequently zoned (Figure 6.4.3) such as in DD.CUM19 with X_{An} varying from 0.47 at a crystal rim to 0.60 in a crystal core.

6.4.2 Garnet

Representative garnet analyses from cordierite norites and garnet tonalites are given in Table 6.4.2.

(i) Cordierite norites

The relative proportions of Fe + Mn, Ca and Mg in garnet core analyses are represented in Figure 6.4.4. The Mg# values of garnet cores from the cordierite norites are generally in the range 0.26 to 0.3. Mn contents are low, with X_{Mn}^{Grt} never exceeding 0.042, and generally being in the range of 0.004 to 0.020. The Ca content varies across individual sections, but X_{Ca}^{Grt} values all lie between 0.027 and 0.068. Analyses from garnet rims show some enrichment of Fe^{2+} and Mg impoverishment relative to the cores. This is displayed in the profile diagram for H.BHQ1 in Figure 6.4.5.

Cation totals systematically exceed 16 per 24(O) in garnet analyses from samples DD.CAB2i, DD.DUN4, 12 and DD.BQ38 indicating the presence of Fe^{3+}. Recalculation for Fe_2O_3 and Fe^{3+} contents indicate up to 1.74 wt% Fe_2O_3 (up to 0.203 cations Fe^{3+}).

(ii) Garnet tonalite

The Fe + Mn, Ca and Mg content of garnet analyses from garnet tonalites are represented in Figure 6.4.6. These garnets are more Fe-rich than those in the cordierite norites, with low Mg# (e.g., 0.17 to 0.14 for DD.CUM22). Figure 6.4.7 is zonation profile from the rim to core of a large garnet from section DD.CUM19. The profile shows two distinct chemical domains across the garnet, with an outer Ca-rich, Fe-poor zone and an inner Ca-poor, Fe-rich core. The outer 1300 μm of the garnet has X_{Ca}^{Grt} contents from 0.172 to 0.181, whilst the inner 2200 μm has X_{Ca}^{Grt} of 0.12.

Some Fe^{3+} occurs in the garnets, with 0 to 2.41 wt% Fe_2O_3 (0 to 0.260 cations Fe^{3+} per formula unit).

6.4.3 Cordierite

Representative cordierite analyses from cordierite norites are given in Table 6.4.4. The Mg# from analyses of crystal rims do not differ significantly from the Mg# of core analyses. Fe^{3+} recalculation indicate up to 1.60 wt% Fe_2O_3 in some cordierites (up to 0.121 cations Fe^{3+} per 18(O)).

6.4.4 Orthopyroxene

Selected orthopyroxene analyses from cordierite norites and garnet tonalites are given in table 6.4.4.

(i) Cordierite norites

Figures 6.4.8 and 6.4.9 are two sets of graphs, plotting Mg# and X_{Al}^{M1} against frequency. The Mg# varies between 0.45 to 0.523 in the most of the sections analysed, the exception being the orthopyroxene from section DD.CASB2i which has an Mg# varying from 0.50 to 0.58. Orthopyroxenes from all section have X_{Al}^{M1} greater than 0.05, and in section DD.BQ38 as high as 0.175. The Ca content in the orthopyroxenes from all of the cordierite norites is low, with X_{Ca}^{M2} rarely greater than 0.01. Analyses from crystal cores are chemically similar to analyses from crystal rims, with no zonation evident.

(ii) Garnet tonalites

The Mg# and X_{Al}^{M1} contents of orthopyroxene from section DD.CUM19 are represented in Figures 6.4.8 and 6.4.9. Both the Mg# (0.23 to 0.30) and the X_{Al}^{M1} (0.016 to 0.025) are lower than in the cordierite norites, whilst the Ca content is higher X_{Ca}^{M2} 0.029 to 0.045).

6.4.5 Biotite

Representative biotite analyses from cordierite norites and garnet tonalites are given in Table 6.4.5.

(i) Cordierite norites

Figure 6.4.10 plots the Al^{vi} content of biotite probe analyses against Mg#. The biotites have slightly higher Al^{vi} contents than in biotites from the mineralogically similar orthopyroxene-cordierite hornfelses and similar Mg# values. The amount of Ti present varies between sections (displayed in Figure 6.4.11), being relatively low in DD.DUN4 (3.06 to 4.13 wt % TiO_2) to high in H.BHQ1 (5.32 to 5.65 wt%). As with the cordierite hornfelses, biotites contacting, or adjacent to garnet crystals display higher Mg# than biotites distal (at least 1000 μm away) from nearest garnet crystal.

Biotite from samples DD.BHQ1 and DD.BQ38 were analysed on the Cameca

microprobe using W.D. analysis to determine their F and Ba contents. The biotites from H.BHQ1 contained F contents from X_F^{Bt} 0.017 to 0.061 X_F^{Bt} calculated as F/4). Sample DD.BQ38 contained X_F^{Bt} values from 0.014 to 0.052. The Ba contents from both samples were generally less than 0.50 wt%.

(ii) Garnet tonalites

The biotites from the garnet tonalites have lower Mg# (higher Fe^{2+} contents) than the cordierite norites as displayed in Figure 6.4.10 and 6.3.12. The lowest Mg# are displayed by biotites from sections DD.CUM19 and DD.CUM22, with Mg# from 0.24 to 0.29. The Al^{vi} contents in H.COR7 and DD.CUM22 vary from 0.494 to 0.651, whilst DD.CUM19 contains less Al^{vi} than all other igneous rocks (Al^{vi} 0.068 to 0.236). Ti contents overlap (Figure 6.4.12) varying from 0.462 to 0.605 cations (3.85 to 5.45 wt% TiO_2)

6.4.6 Spinel

Representative probe analyses of spinel crystals from cordierite norites are given in Table 6.4.6. Figure 6.4.13 is a ternary diagram, plotting the Zn, Fe and Mg contents of spinel analyses. The spinels are all hercynitic, with low high Fe^{2+} and low Mg# (all spinel analyses have Mg# within the range 0.214 to 0.292). X_{Zn}^{Spl} values fall between 0.034 to 0.067 (1.34 to 3.26 wt% ZnO). Cation totals systematically over 3 (in 4(O) formula unit) indicate the presence of Fe^{3+} in all cordierite norite sections except H.BHQ1. Recalculation of probe analyses to estimate the Fe^{3+} contents indicates varying magnetite contents between sections, with up to $X_{Fe^{3+}}^{Spl}$ 0.061 (2.97 wt% Fe_2O_3).

6.4.7 Hornblende

Hornblende occurs only in section DD.CUM17. The hornblende probe analyses are plotted in Figure 6.4.14, with compositions expressed as total Na + K in A sites against number of Si atoms in a 23(O) formula unit; all analyses lie within the pargasite field. Some zonation occurs, with crystal rims being Fe-rich (Mg# 0.16 to 0.22) and cores being more Mg-rich (Mg# up to 0.28).

6.4.8 Ilmenite

All of the ilmenite analysed is Fe^{2+}-rich (0.96 to 0.99 cations in 3(O) formula unit) with small amounts of Mg, and no detectable Mn.

6.5 Cordierite Volatile Contents

6.5.1 Introduction

It is well known that structural channels in cordierite incorporate amounts of volatile species (Figure 6.6.1) within the crystal framework (e.g. Smith & Schreyer, 1962 ; Goldman *et al.*, 1977). The volatile species consist mainly of H_2O and CO_2 (e.g. Armbruster & Bloss, 1980 ; Wood & Nassau, 1967), with charge deficiencies caused by the H_2O ions being balanced by the incorporation of alkali cations such as Na, Ca and K (e.g. Armbruster, 1986 ; Gordillo *et al.*, 1985). Johannes & Schreyer (1977), using lattice space considerations, showed that up to 1 mole of gas per formula unit could by incorporated into pure Mg-cordierite (equal to 2.99 wt% H_2O or 6.99 wt% CO_2).

Being able to determine the volatile content of natural cordierites is important to the petrologist as the amount and composition of volatiles species in cordierites gives evidence on the fluid conditions that were prevalent during the minerals growth and therefore, in the case of granulitic rocks, the fluid conditions that were prevalent during granulite facies metamorphism. In addition the activity of cordierite in rock systems is affected by it s volatile content. This is most important when cordierite activities are used in geobarometry, with activities taking into account $X_{H_2O}^{Crd}$ contents leading to the calculation of higher pressures than would be given by using activities of anhydrous cordierite (Lonker, 1981 ; Bhattacharya, 1986). Vry *et al.* (1990) analysed the volatile contents of natural cordierites from high-grade metamorphic rocks. Their results showed that cordierites from granulite-facies rocks were characterised by low total volatile contents, with high but variable $X_{CO_2}^{Crd}$ ($X_{CO_2}^{Crd} \geq 0.3$).

6.5.2 Experimental methods

Two rock samples were chosen, both of which contained large, fresh, inclusion-free cordierite porphyroblasts . One samples chosen was a cordierite norite (sample DD.BQ38)

and the other an anhydrous (mica-free) cordierite hornfels (sample 10035). The rock samples were then ground, using a Tema, and sieved until only sand sized grains remained. Inclusion-free cordierite grains were hand picked from the ground sand-sized fraction. A grain mount from the extracted cordierite fraction was made, and this was analysed under the electron microprobe to ensure that only cordierite grains had been selected.

Fractions of cordierite grains weighing approximately 15 milligrams were placed in a platinum crucible, then heated using a thermogravimetric balance to allow calculation of the total volatile content by weight loss during heating. Argon gas was passed through the samples during heating to prevent any weight gain due to oxidation. Samples were heated to at least 900°C and the maximum temperature was held for at least 30 minutes. Baselines were run by heating the platinum crucible alone at the identical conditions to the experimental runs, and this baseline was subtracted from the experimental runs to eliminate errors from crucible buoyancy etc. Printouts from the experimental runs, after subtraction of the base lines and the run conditions are given in Appendix III.

6.5.3 Results

Heating of the cordierite fraction from the cordierite norite DD.BQ38 caused a weight loss of 1.07% from the sample. The cordierite from the cordierite hornfels 10035 gave a weight loss of 0.65 wt% when heated. As mentioned above, the volatile species present in cordierites have been shown to consist essentially of only H_2O and CO_2, with maximum contents of 2.99 wt% H_2O or 6.99 wt% CO_2 incorporated into the Mg-Cordierite lattice in fluid saturated conditions (Johannes & Schreyer, 1977 ; Vry *et al.*, 1990). Therefore maximum possible $X_{H_2O}^{Crd}$ and $X_{CO_2}^{Crd}$ contents can be calculated for both rocks.

For the cordierite norite DD.BQ38 a total volatile content of 1.07 wt% indicates a maximum $X_{H_2O}^{Crd}$ value of 0.36 and a maximum $X_{CO_2}^{Crd}$ value of 0.15. A total volatile content of 0.65 wt% for the cordierite hornfels 10035 indicates a maximum $X_{H_2O}^{Crd}$ value of 0.22 and a maximum $X_{CO_2}^{Crd}$ value of 0.092. This indicates a maximum possible volatile content of only 36% of the experimental values determined by Johannes & Schreyer (1981).

One major source of error in determining X_{fluid}^{Crd} contents by using the volatile

contents from natural cordierites stems from the effects of post-metamorphic leakage (Vry *et al.*, 1990). However, the relatively short retrogressive cooling paths for the rocks in this study (i.e. the rocks formed by contact metamorphism) supports the contention that any fluid loss during retrogression was probably minor (this is again supported by the 'fresh' appearance of the cordierite, and the lack of any major pinitisation).

6.6 Discussion of Results

6.6.1 Mineral data

The chemical data for individual minerals from the regionally metamorphic rocks are relatively closely clustered. However, some minor retrogressive Fe-Mg exchange occurs between garnet and biotite, where the minerals have grown adjacently. Retrogressive Fe-Mg exchange between garnet and biotite also occurs in the sillimanite-cordierite hornfelses, displayed by the zoned garnets with Fe-rich rims from H.COR8 (Figure 6.3.7). All the minerals in the orthopyroxene-cordierite hornfelses display a tight clustering of compositions, with no zonation occurring in any minerals, bar the plagioclase in DD.BQ17 (Figure 6.3.4). This lack of any zonation, and uniformity of mineral compositions suggests that the metamorphic rocks analysed, especially the orthopyroxene-cordierite hornfelses, have achieved a high degree of chemical equilibrium.

The orthopyroxenes and cordierites from the cordierite norites display closely clustered compositions, though some Fe-Mg retrogressive exchange between garnet and biotite is displayed. The plagioclase crystals though are frequently zoned, with Ab-rich An-poor rims, indicative of crystallisation of the plagioclase from an igneous melt, with A_N^b content increasing with decreasing temperature. This chemical evidence suggests that the cordierite norites have not attained equilibrium between all minerals. The plagioclase core compositions may have grown in equilibrium with the other mineral phases, if all these minerals attained chemical equilibrium at the peak temperatures attained by the rocks.

The plagioclase zonation profile from the garnet tonalite DD.CUM19 suggests that the mineral crystallised from a melt. The garnet zonation profile from sample DD.CUM19 is unusual, with the outer 1000 μm having high-Ca, low-Fe contents. One possible

explanation for this phenomena could be that mixing with a Ca-rich melt occurred late in the cooling history of this rock. This late growth of hornblende, replacing orthopyroxene also supports this explanation.

6.6.2 Cordierite volatile contents

Cordierite volatile contents are determined by the availability of volatiles during the growth of this mineral (e.g. Fitzsimons, 1994). The low total volatile content given by the igneous-textured cordierite norite DD.BQ38 ~~infers~~ implies that the cordierite grew in the presence of a volatile-undersaturated melt. The even lower total volatile contents given by the anhydrous cordierite hornfels 10035 indicates that the cordierite crystallised in low aH_2O and aCO_2 conditions. If the hornfels is restitic then this shows that the cordierite was probably not in prolonged contact with even a volatile undersaturated melt.

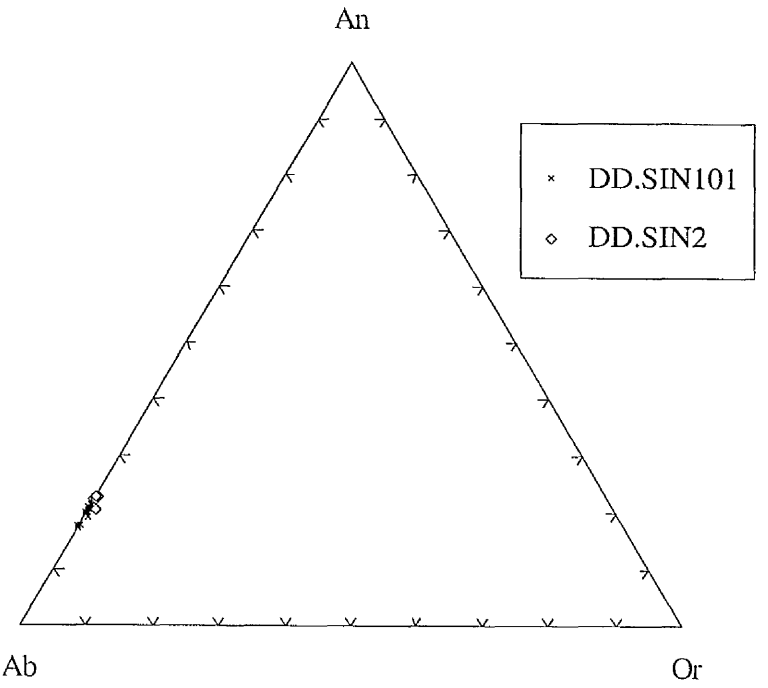

Figure 6.2.1 Feldspar composition diagram, plotting mol% An, Ab and Or for plagioclase analyses from regionally metamorphosed rocks.

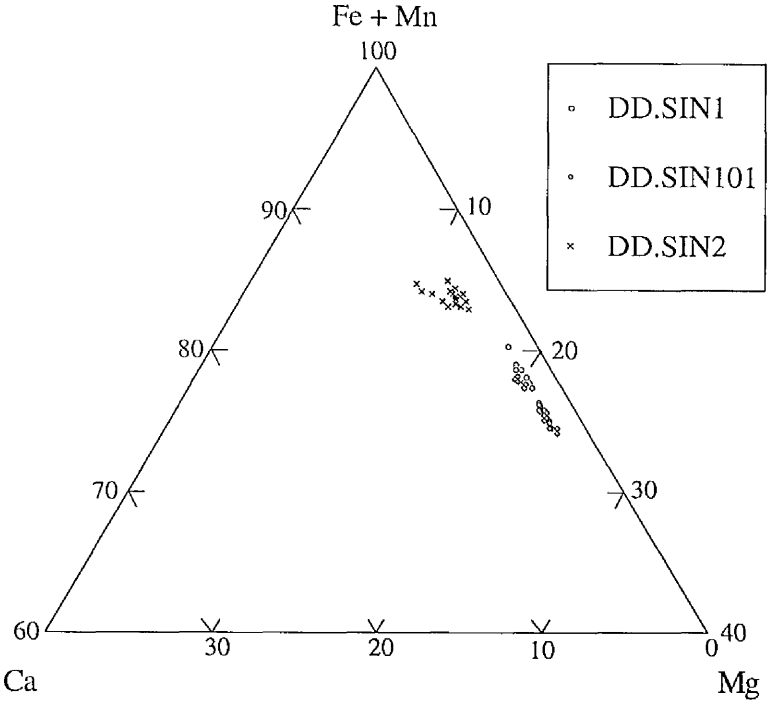

Figure 6.2.2 Ternary plot for compositions of garnet analyses from regionally metamorphosed rocks, plotting mol% Fe^{2+} + Mn, Ca and Mg. Analyses taken from garnet cores.

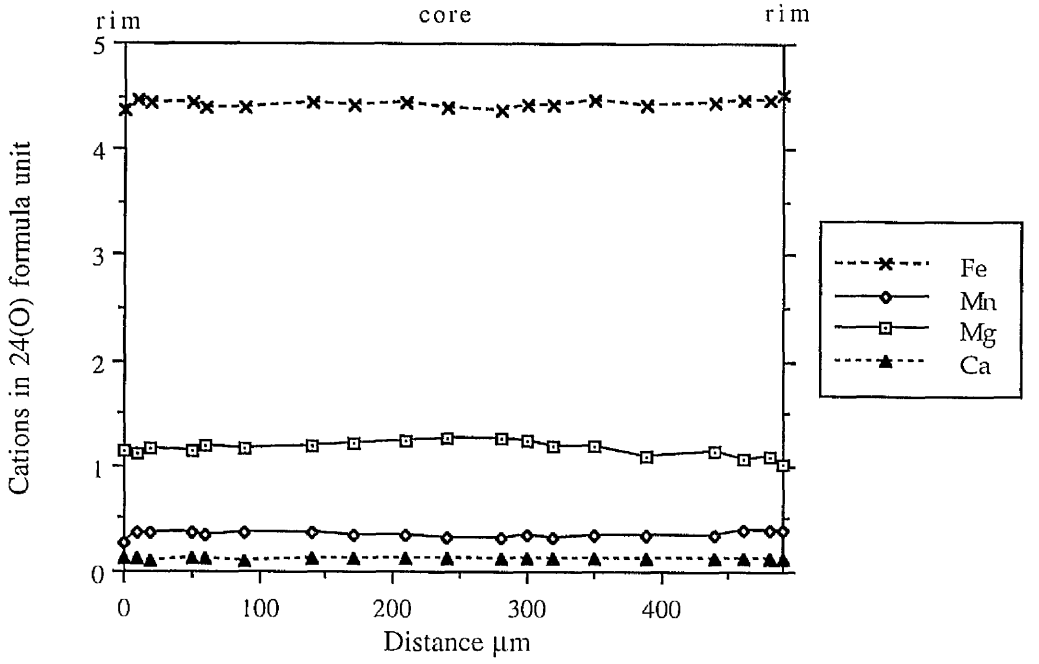

Figure 6.2.3 Zonation profile across a garnet from sample DD.SIN1. Some slight enrichment of Fe^{2+} and depletion of Mg occurs towards the crystal rims.

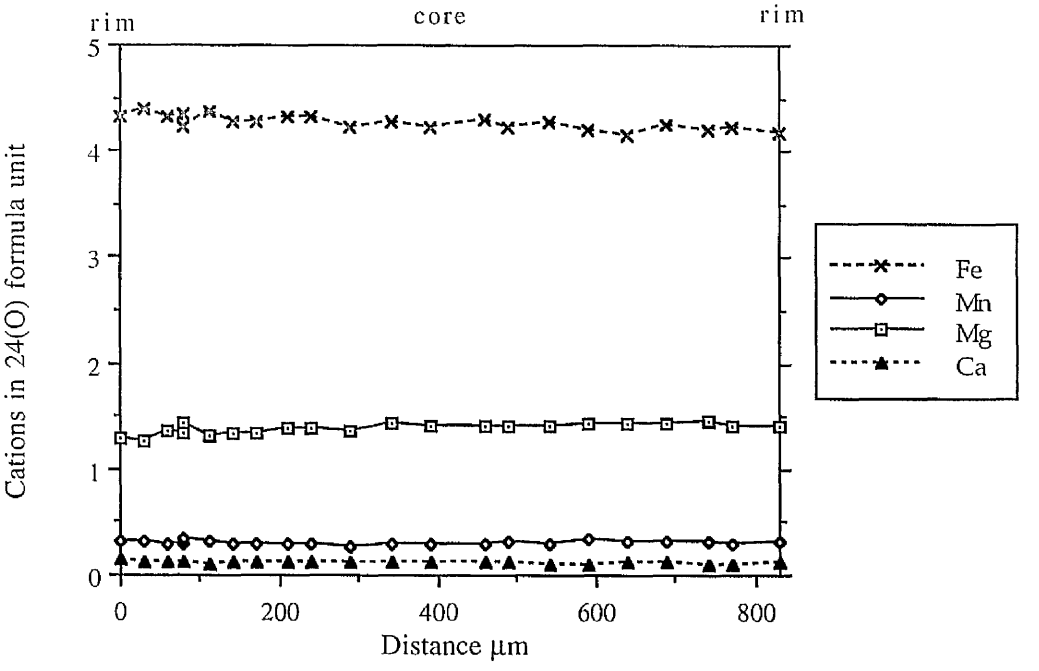

Figure 6.2.4 Zonation profile across a garnet from section DD.SIN101. No visable chemical varitaion occurs across the crystal.

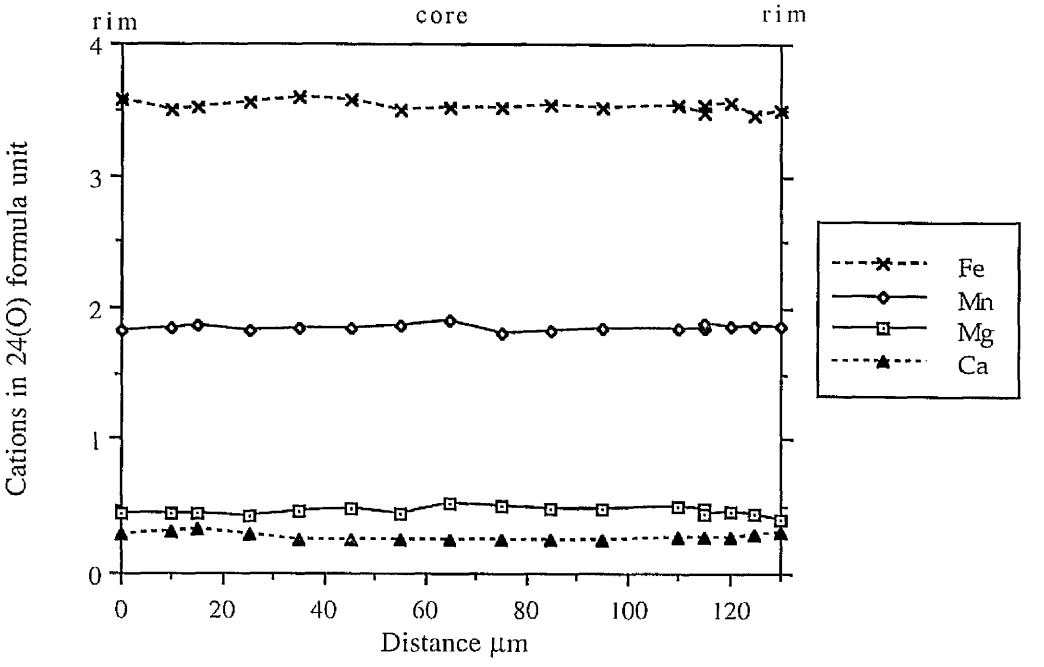

Figure 6.2.5 Zonation profile across a garnet from sample DD.CLAS66. The garnet has relatively high Mn, low Mg contents, but shows no major chemical variation trends across the profile.

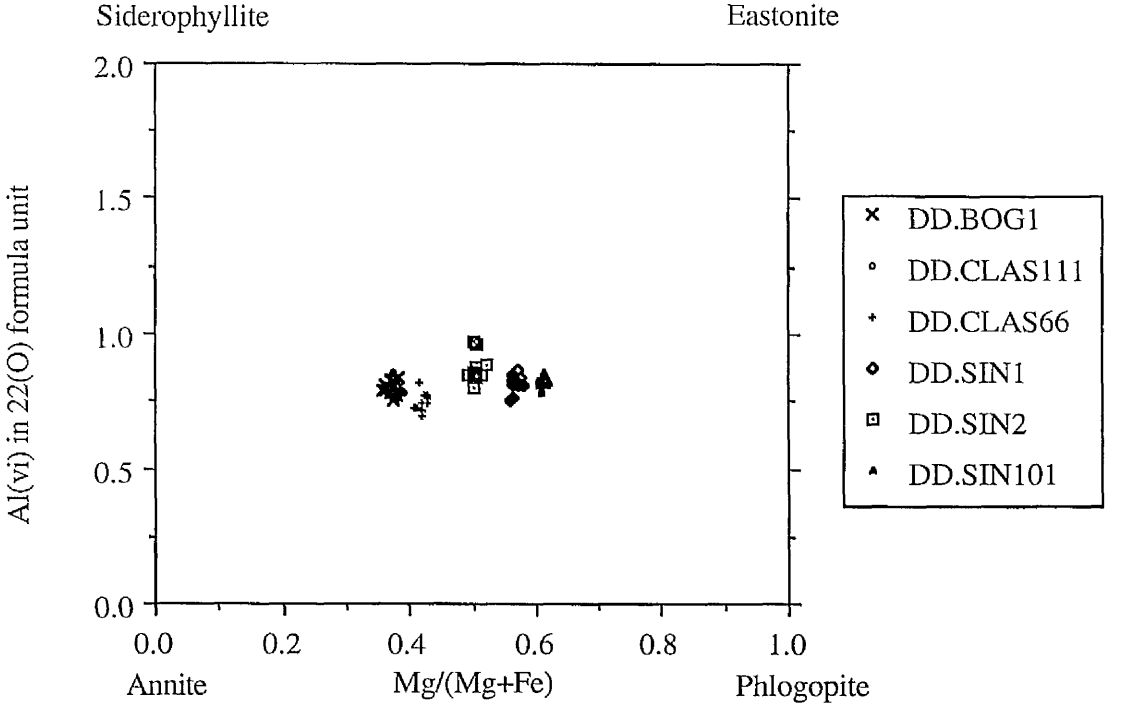

Figure 6.2.6 Composition of biotites from regionally metamorphosed rocks, with analyses plotted within the field of the four end members annite ($K_2Fe_6[Si_6Al_2O_{20}](OH_4)$), phlogopite ($K_2Mg_6[Si_6Al_2O_{20}](OH_4)$), siderophyllite ($K_2Fe_4Al_2[Si_4Al_4O_{20}](OH_4)$), and eastonite ($K_2Mg_4Al_2[Si_4Al_4O_{20}](OH_4)$).

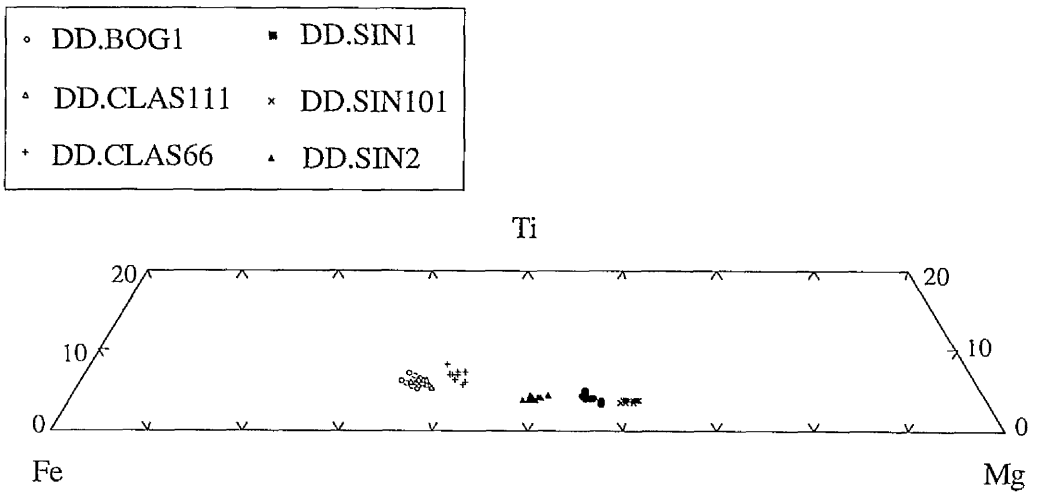

Figure 6.2.7 Composition plot for biotites from regionally metamorphosed rocks. The biotites in rocks from Clashmach Hill (localities 2c & 2d, samples DD.BOG1, CLAS66, 111) are relatively Fe^{2+} rich compared to the biotites from Cairnie (localities 2a & 2b, SIN1, 2, 101) and have slightly higher Ti contents.

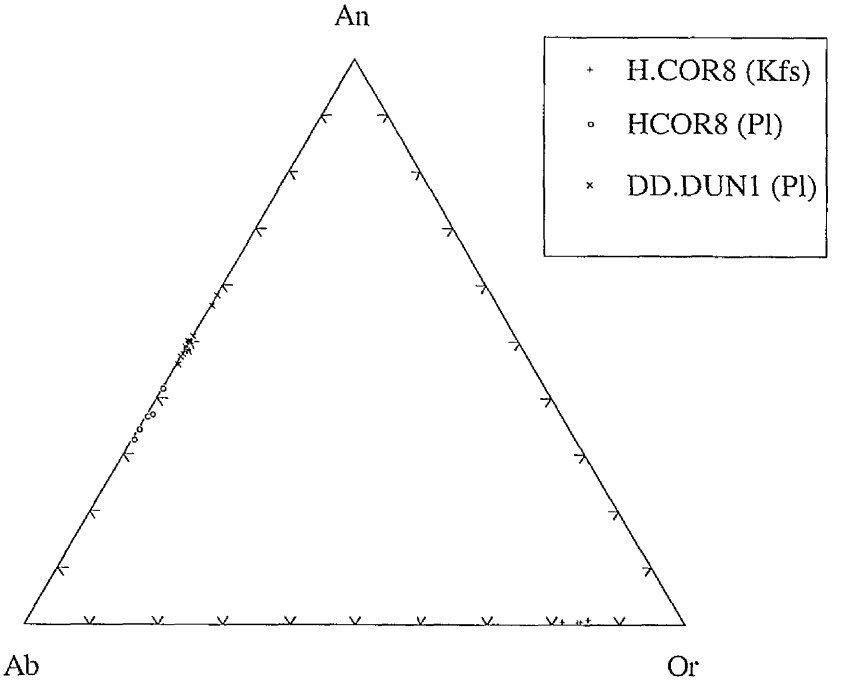

Figure 6.3.1 Feldspar composition diagram, plotting mol% An, Ab and Or for plagioclase and alkali feldspar analyses from sillimanite-cordierite hornfelses.

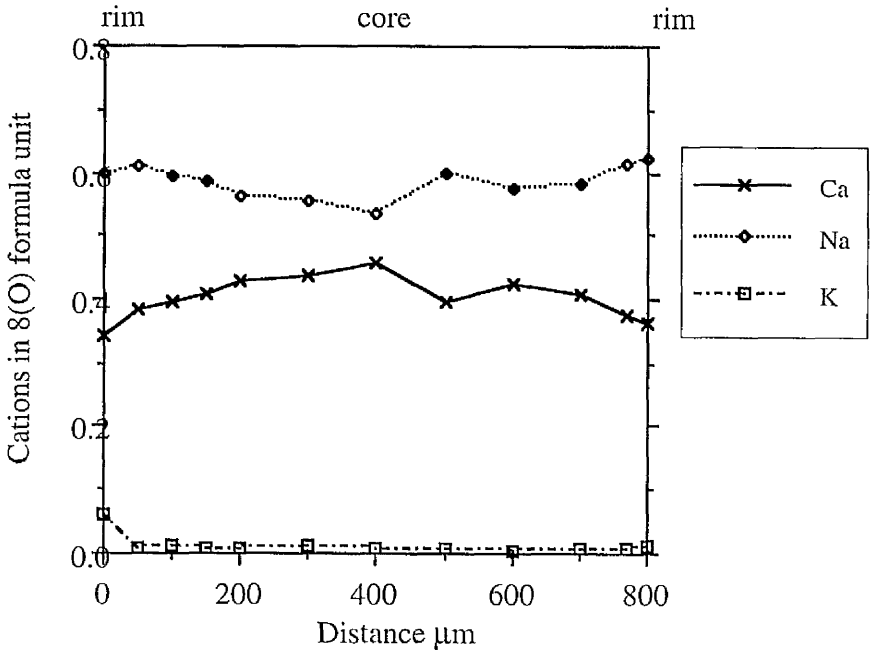

Figure 6.3.2 Zonation profile across a plagioclase crystal from sample H.COR8. The crystal displays some 'normal' zonation, with Na-rich, Ca-poor rims.

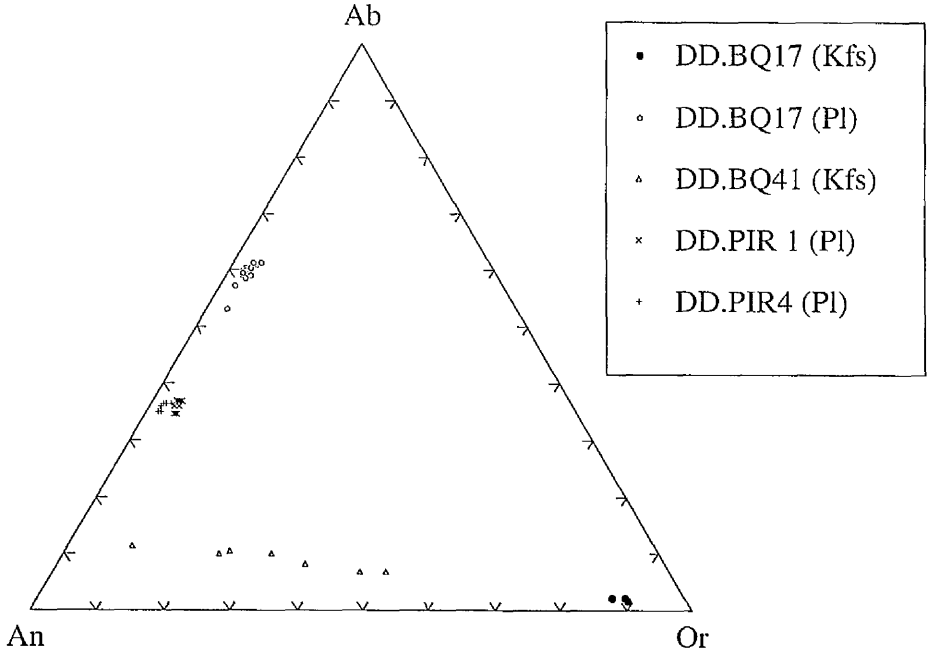

Figure 6.3.3 Feldspar composition diagram, plotting mol% An, Ab and Or for plagioclase and alkali feldspar analyses from orthopyroxene-cordierite hornfelses.

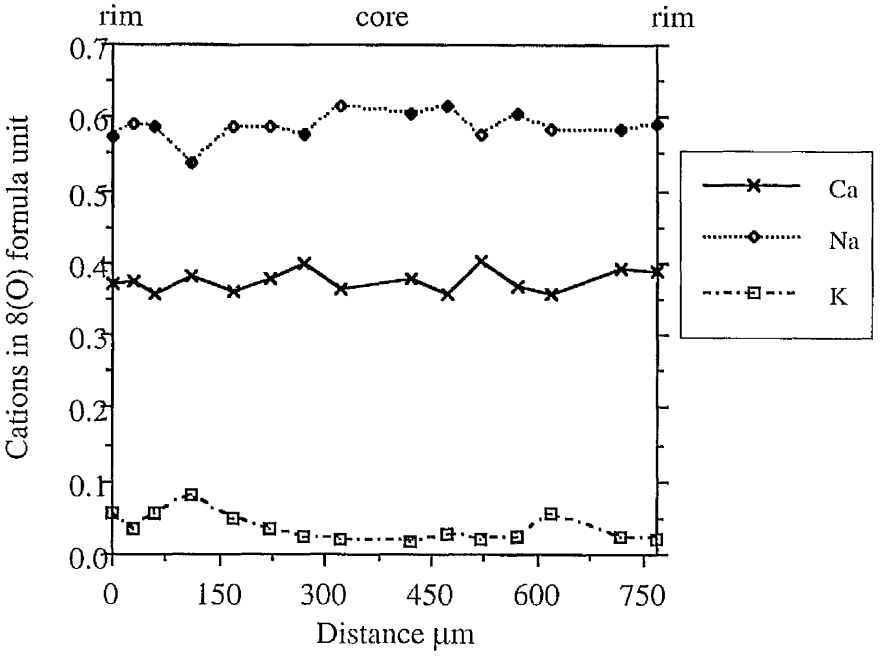

Figure 6.3.4 Zonation profile across a plagioclase crystal from sample DD.BQ17. The Ca and Na proportions vary across the profile, possibly indicating minor oscillatory zoning.

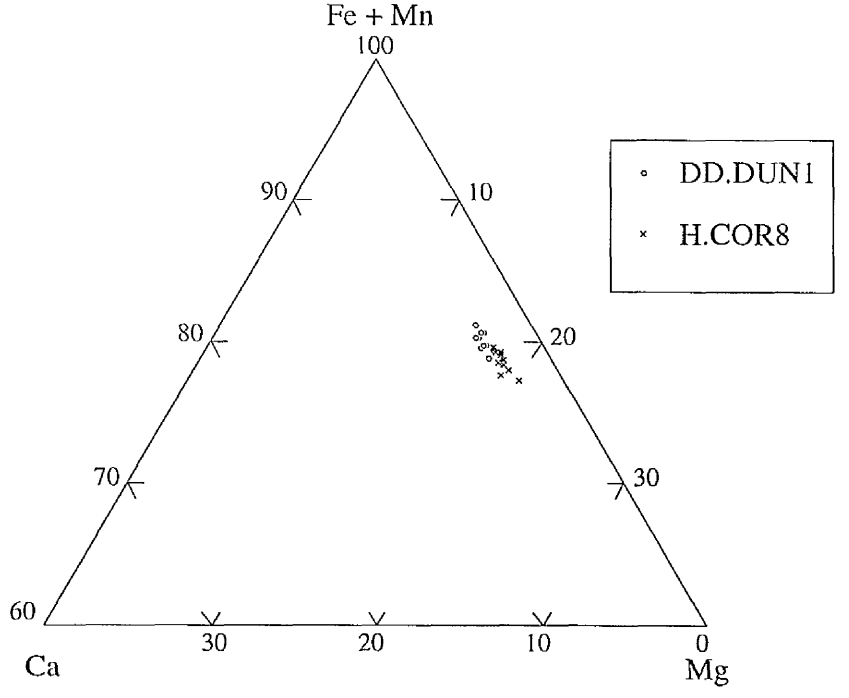

Figure 6.3.5 Ternary plot for compositions of garnet analyses from sillimanite-cordierite hornfelses, plotting mol% Fe^{2+} + Mn, Ca and Mg. Analyses taken from garnet cores.

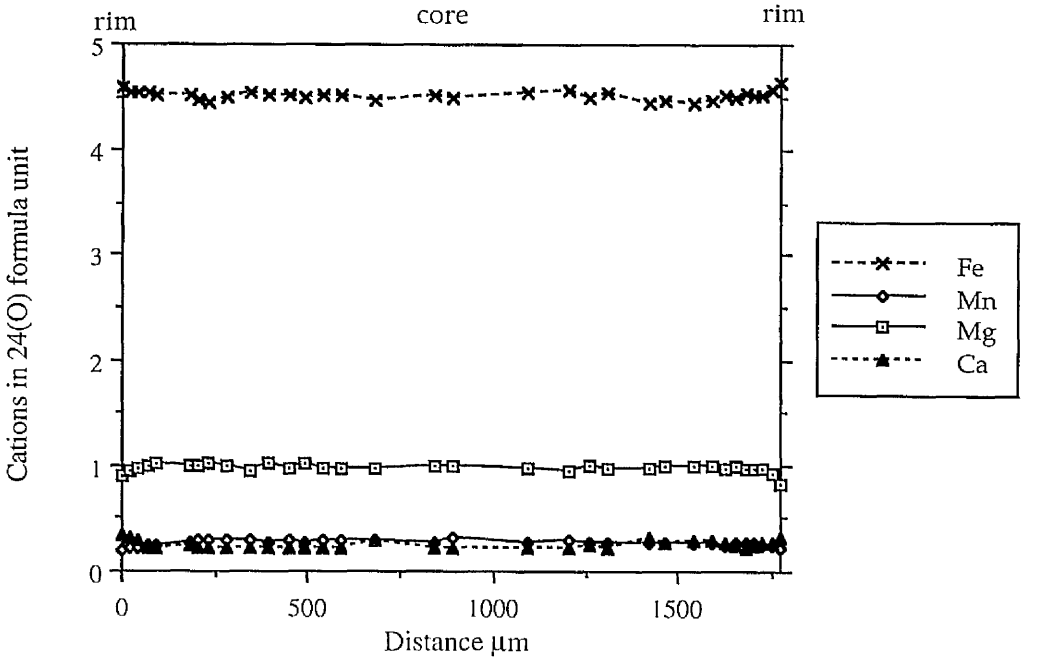

Figure 6.3.6 Zonation profile across a garnet from sample DD.DUN1. The crystal rims are slightly Fe^{2+}-rich, Mg-poor relative to the core.

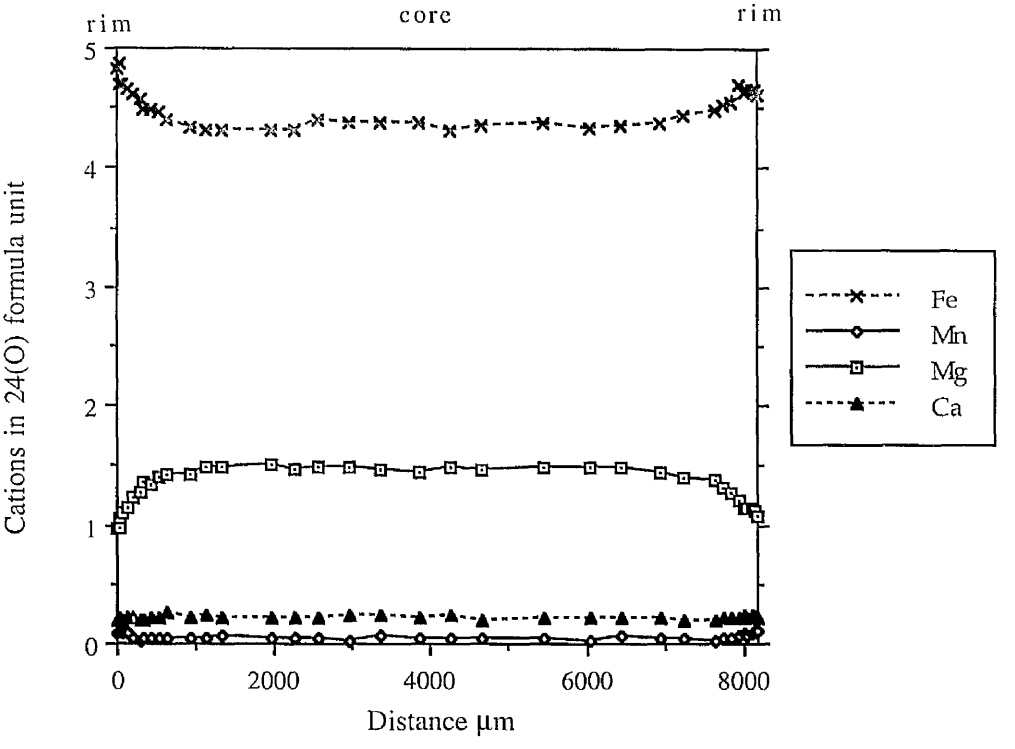

Figure 6.3.7 Zonation profile across a garnet from sample H.COR8. The outer 1000 µm of the crystal displays progressive enrichment of Fe^{2+} and depletion of Mg. Some Ca enrichment also occurs across the outer 200 µm.

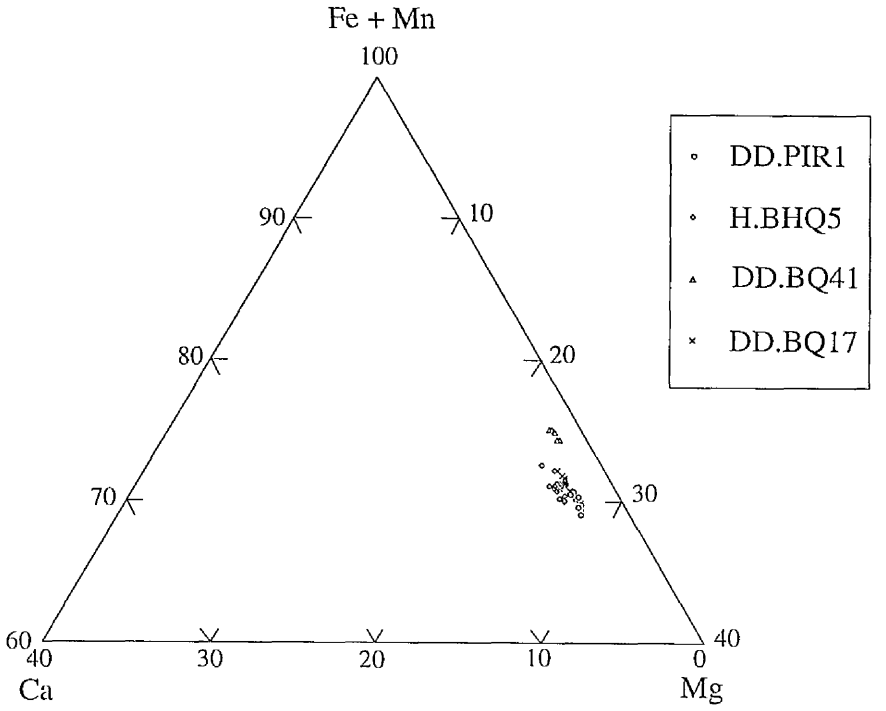

Figure 6.3.8 Ternary plot for compositions of garnet analyses from orthopyroxene-cordierite hornfelses, plotting mol% Fe^{2+} + Mn, Ca and Mg. Analyses taken from garnet cores.

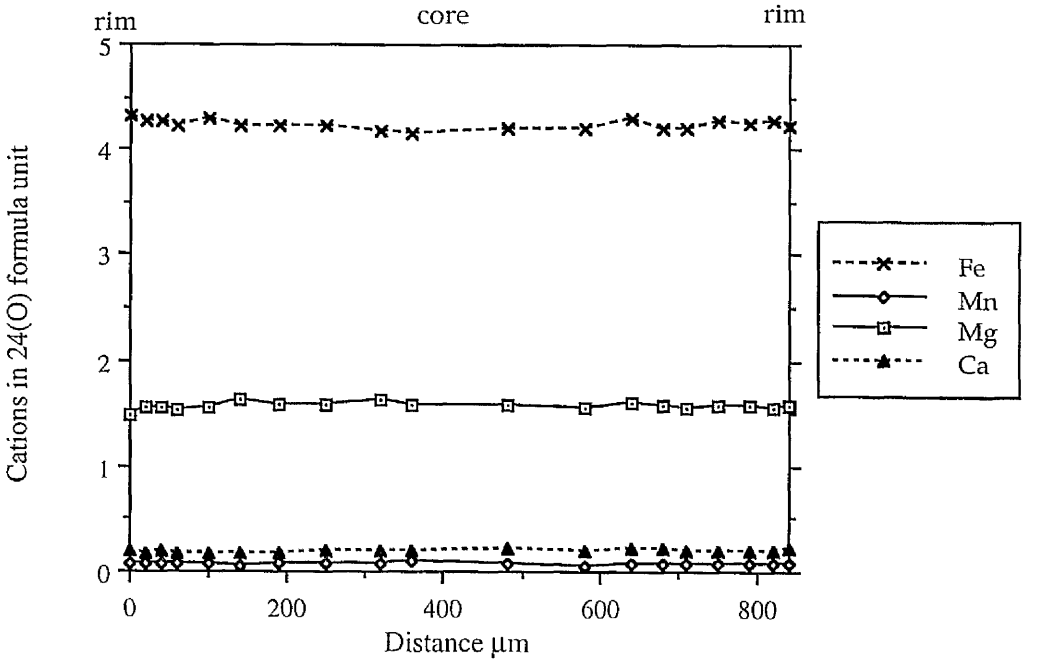

Figure 6.3.9 Zonation profile across a garnet from sample DD.BQ17. Little chemical variation occurs from the crystal rims to core.

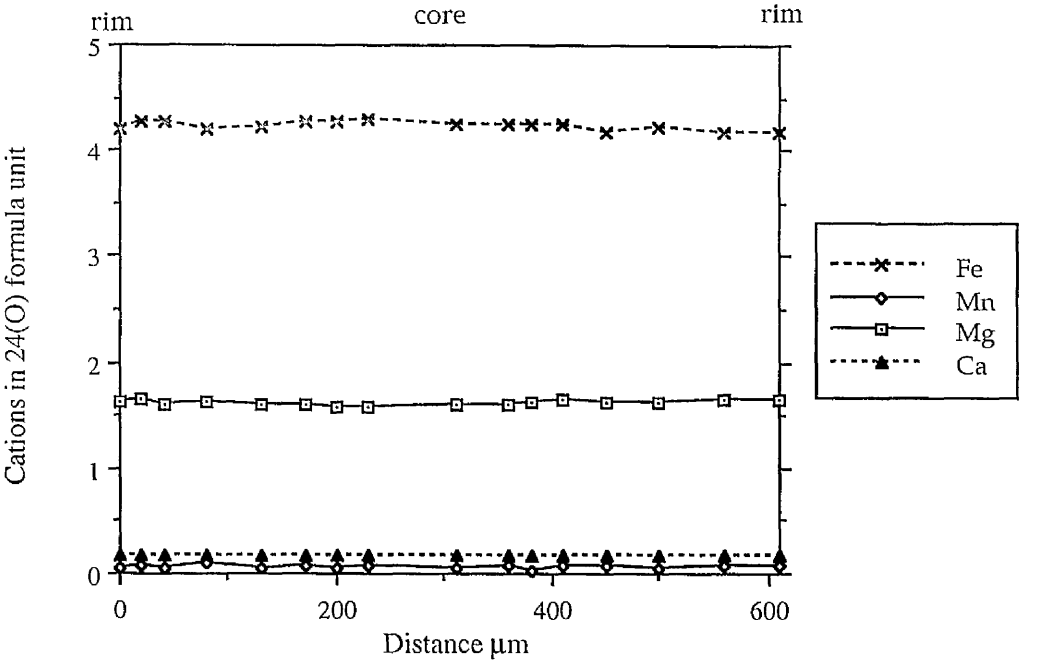

Figure 6.3.10 Zonation profile across a garnet from sample DD.PIR1. As with the garnet from Figure 6.3.9 the crystal rims and cores are chemically equivalent.

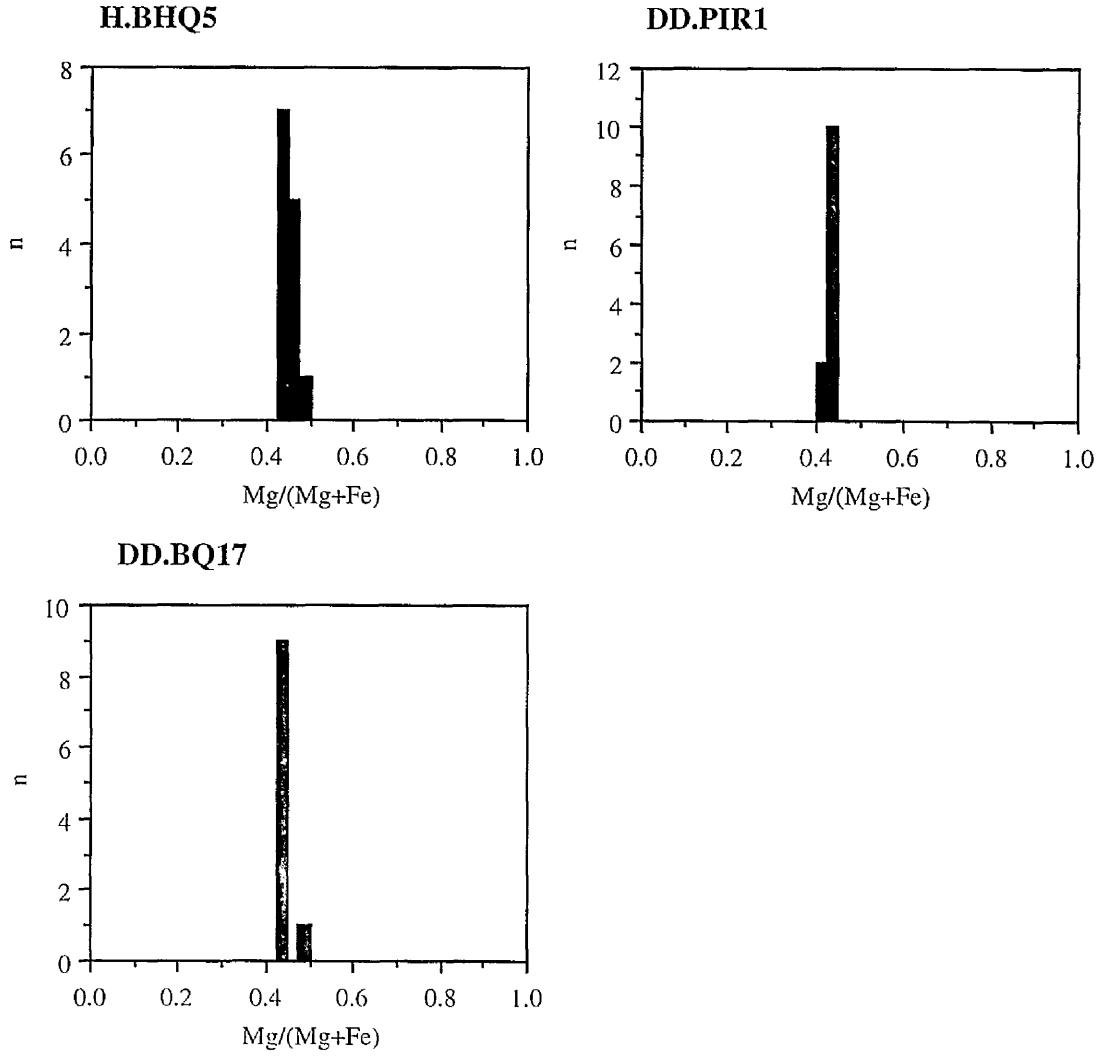

Figure 6.3.11 Frequency-Mg# plots for orthopyroxene analyses from orthopyroxene-cordierite hornfelses. The Mg# values of all analyses fall between 0.4 and 0.5.

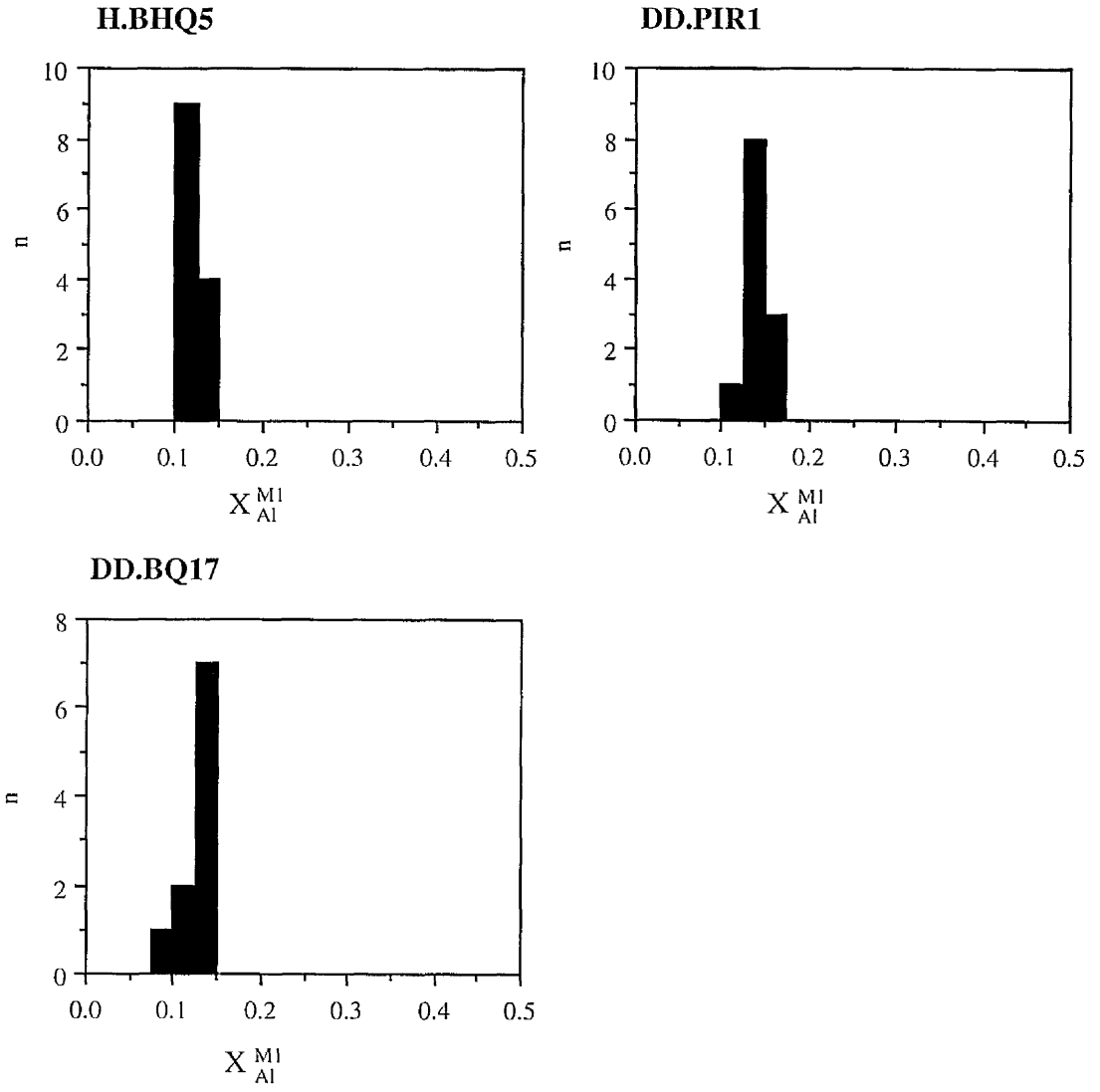

Figure 6.3.12 Frequency-X_{Al}^{MI} plot for orthopyroxene analyses from orthopyroxene-cordierite hornfelses. X_{Al}^{MI} varies between 0.075 and 0.175 across the three samples.

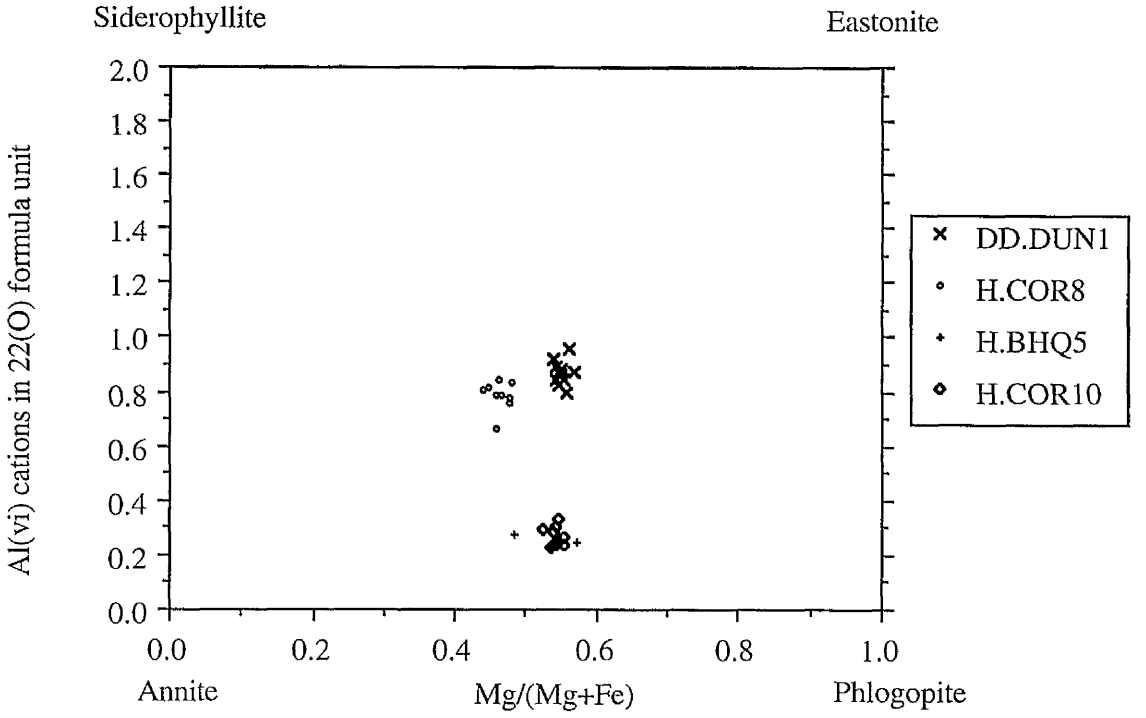

Figure 6.3.13 Composition of biotites from cordierite hornfelses, with analyses plotted within the field of the four end members annite ($K_2Fe_6[Si_6Al_2O_{20}](OH_4)$, phlogopite ($K_2Mg_6[Si_6Al_2O_{20}](OH_4)$, siderophyllite ($K_2Fe_4Al_2[Si_4Al_4O_{20}](OH_4)$, and eastonite ($K_2Mg_4Al_2[Si_4Al_4O_{20}](OH_4)$.

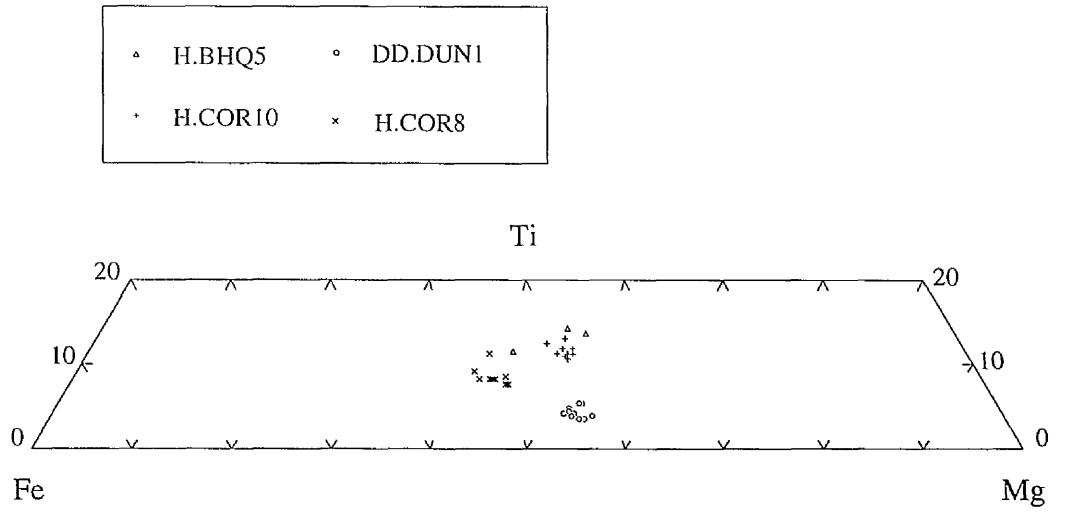

Figure 6.3.14 Composition plot for biotites from cordierite-bearing hornfelses. The orthopyroxene-cordierite hornfelses have higher Ti values (Ti /(Ti+Fe+Mg)*100) than the sillimanite-cordierite hornfelses.

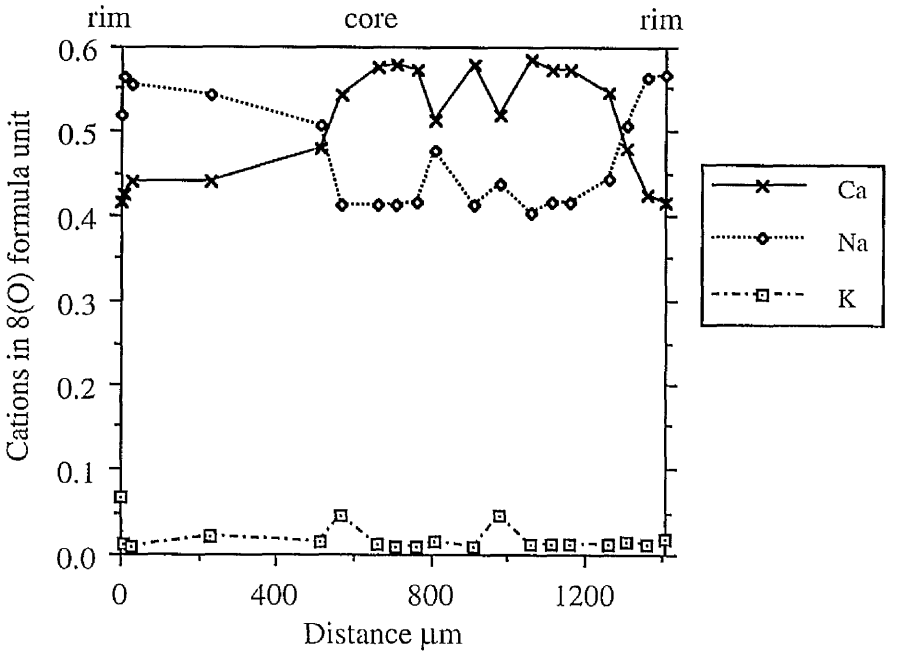

Figure 6.4.1 Zonation profile across a plagioclase crystal from sample DD.BQ38, displaying Na-rich, Ca-poor rims.

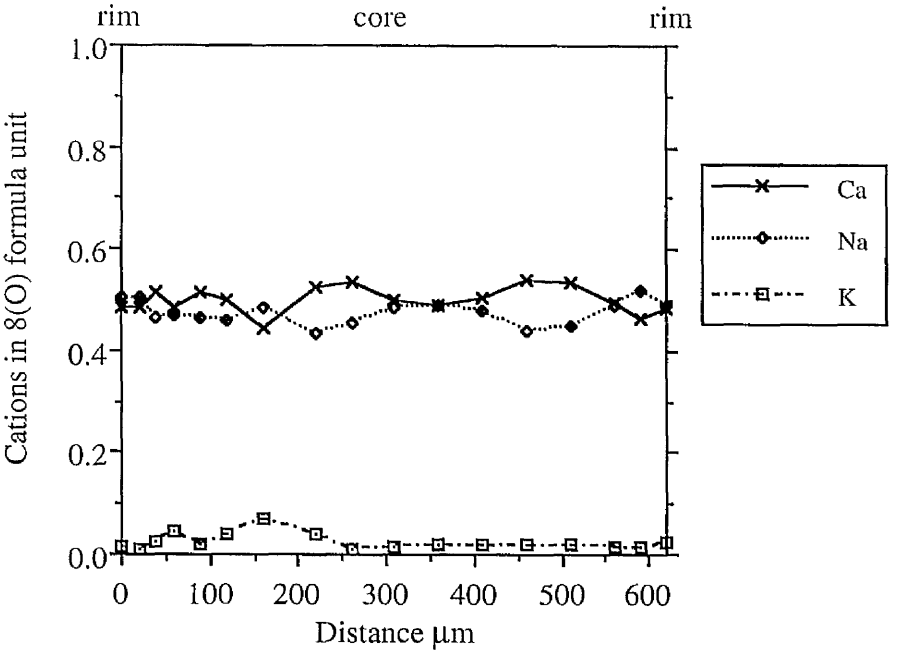

Figure 6.4.2 Zonation profile across a plagioclase crystal from sample DD.DUN4, displaying somr Na enrichment near the crystal rims.

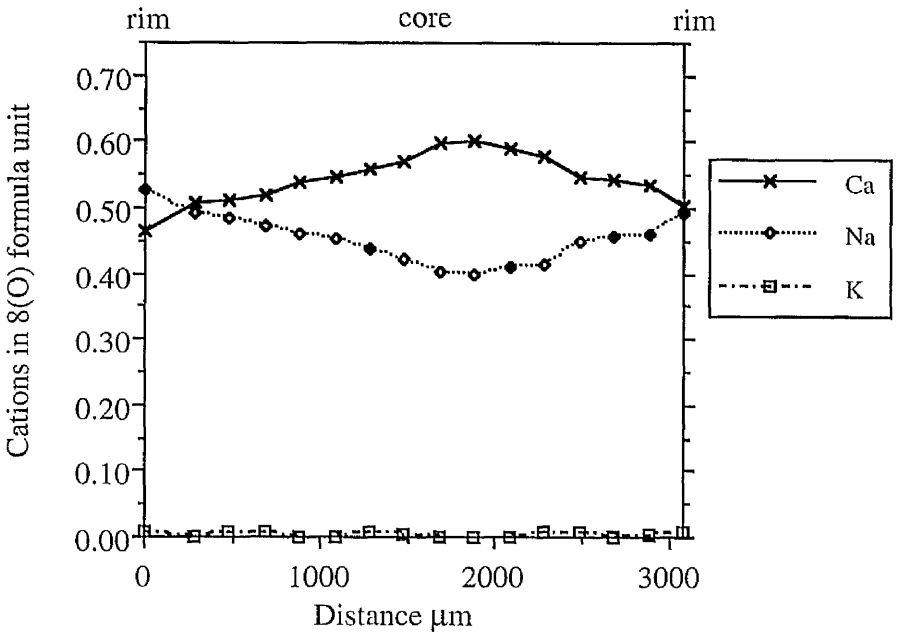

Figure 6.4.3 Zonation profile across a plagioclase crystal from sample DD.CUM19. Their is a gradational increase in Na (decrease in Ca) from the crystal core to the rims

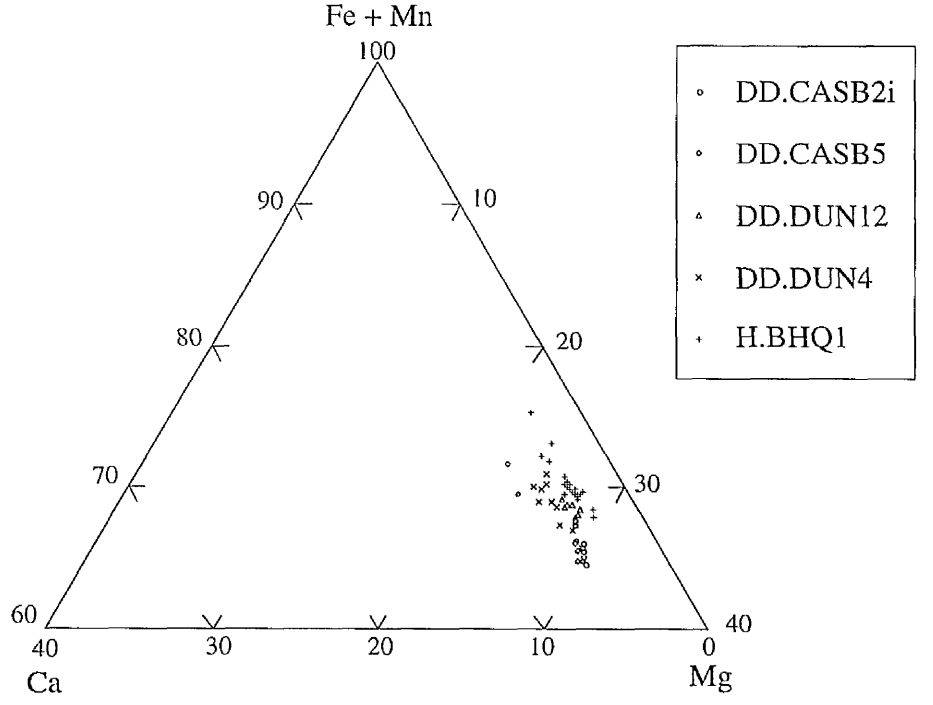

Figure 6.4.4 Ternary plot for compositions of garnet analyses from cordierite norites, plotting mol% Fe^{2+} + Mn, Ca and Mg. Analyses taken from garnet cores.

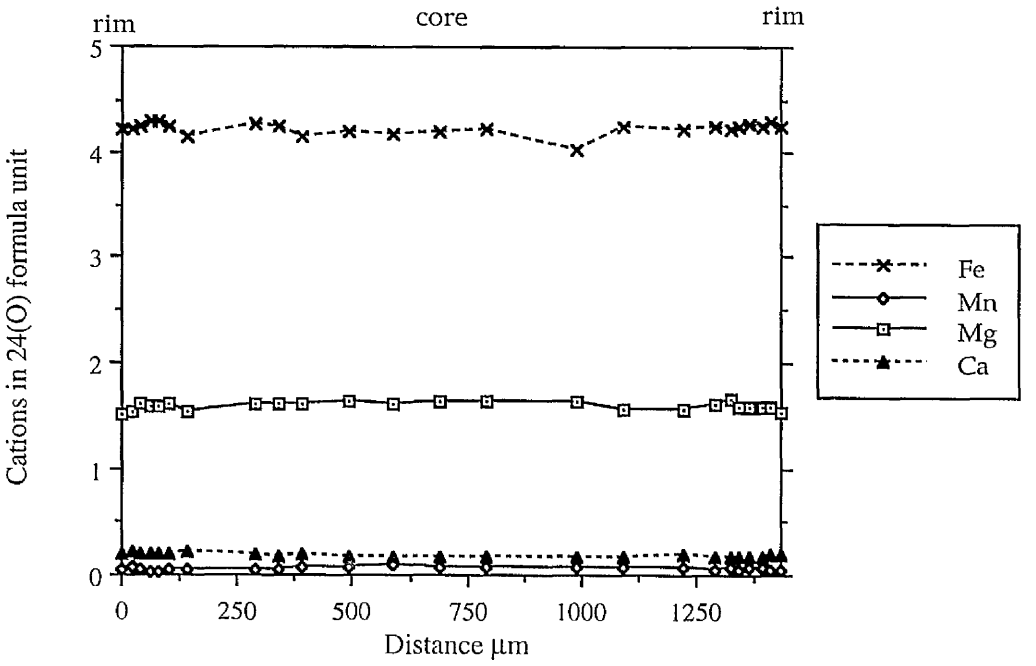

Figure 6.4.5 Zonation profile across a garnet from sample H.BHQ1. There is some Fe enrichment and Mg impoverishment near the crystal rims.

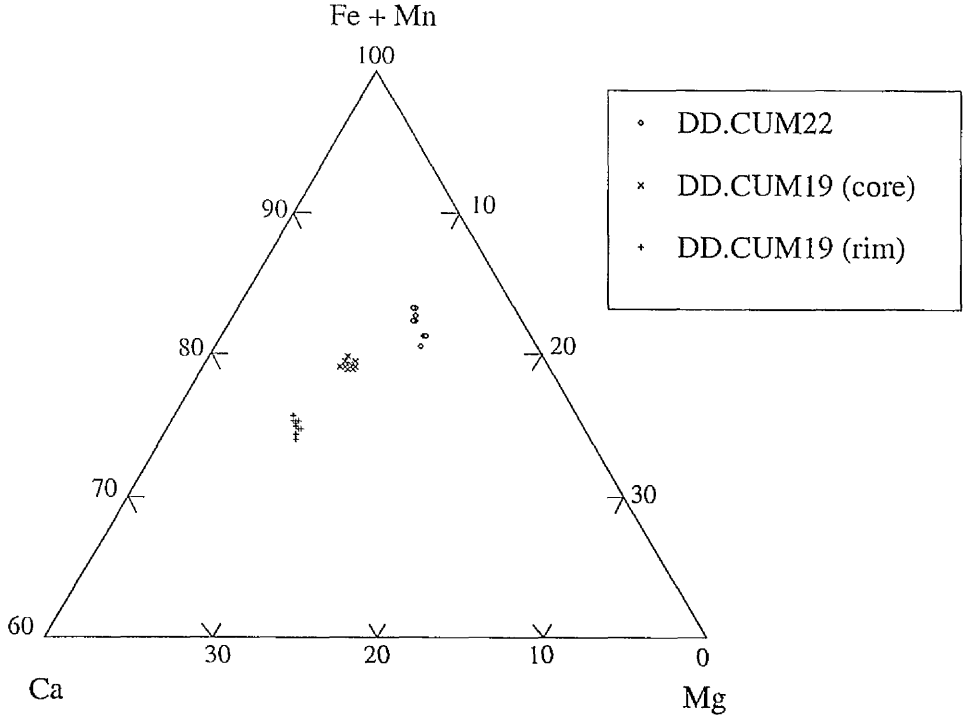

Figure 6.4.6 Ternary plot for compositions of garnet analyses from garnet tonalites, plotting mol% Fe^{2+} + Mn, Ca and Mg.

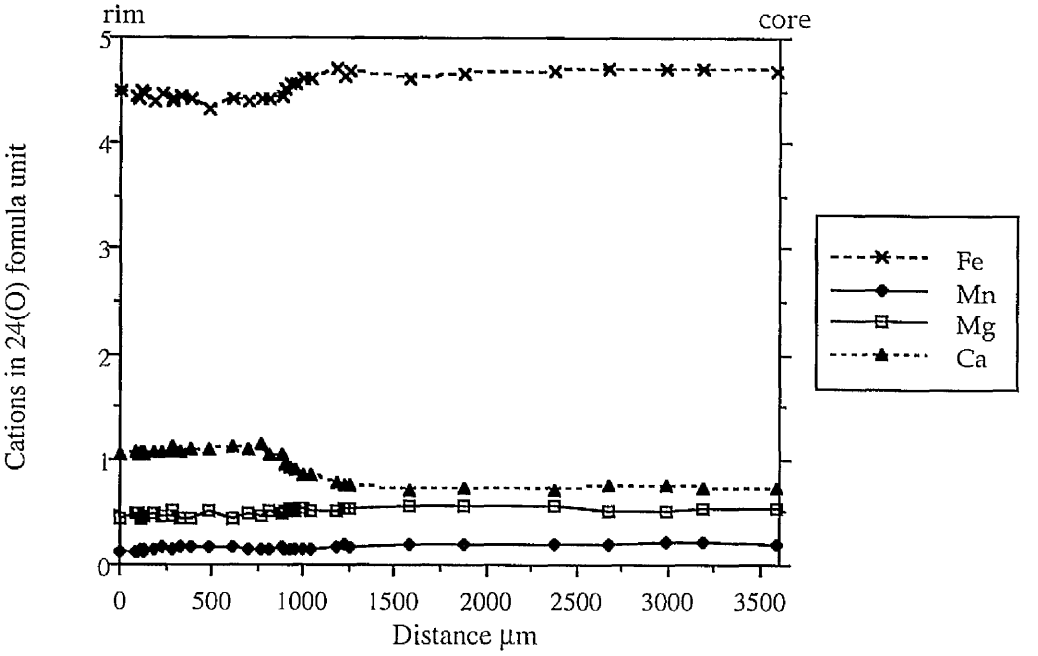

Figure 6.4.7 Zonation profile across half a garnet crystal from sample DD.CUM19. The outer 1000 µm of the garnet have less Fe and higher amounts of Ca than the inner 2500 µm. The Mg and Mn contents remain relatively constant across the garnet.

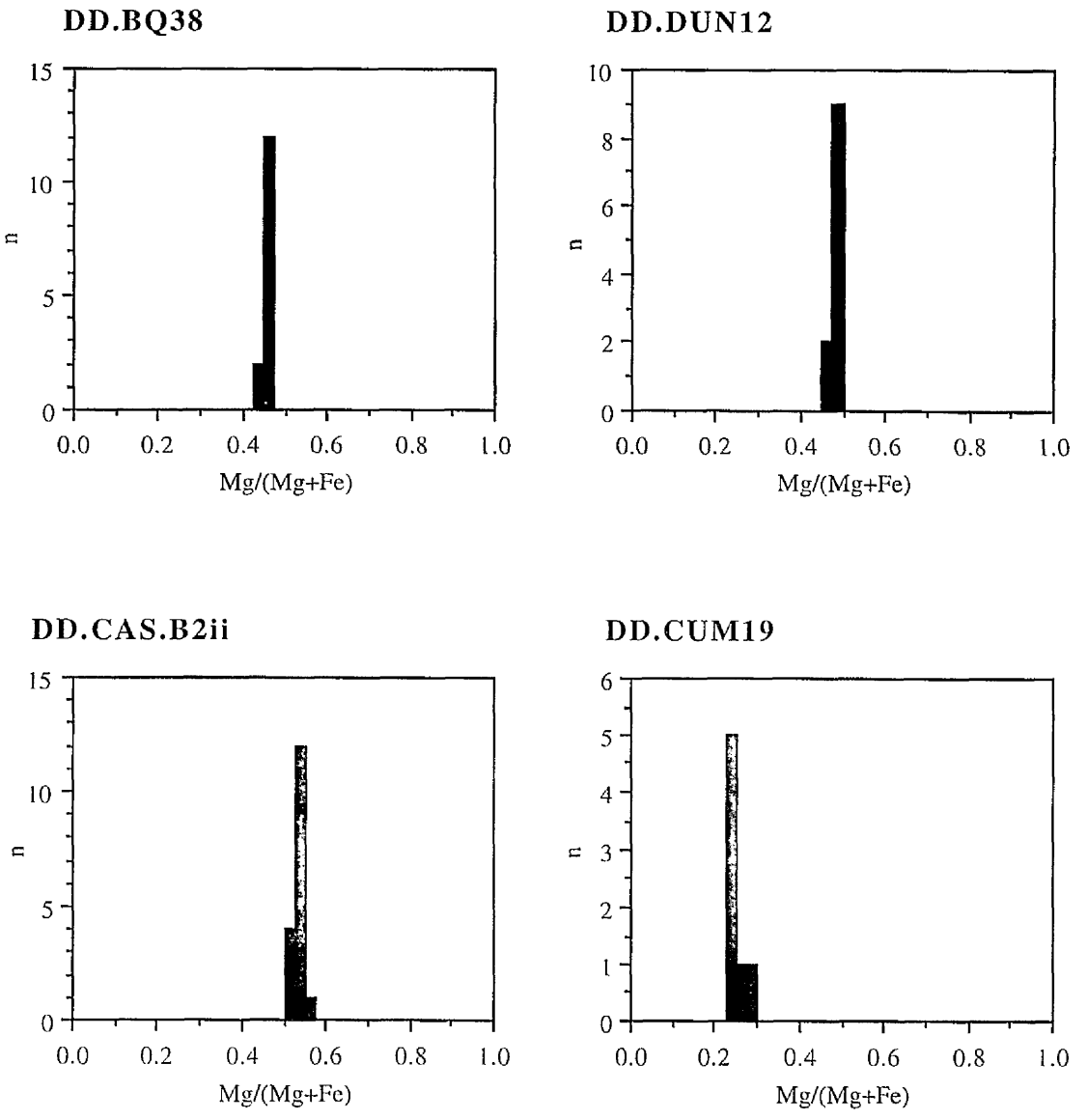

Figure 6.4.8 Frequency-Mg# plots for orthopyroxene analyses from cordierite norites and a garnet tonalite (DD.CUM19). The orthopyroxenes from the garnet tonalite have lower Mg# values (0.225 to 0.3) than the cordierite norites (>0.425 up to 0.575 in DD.CASB2i).

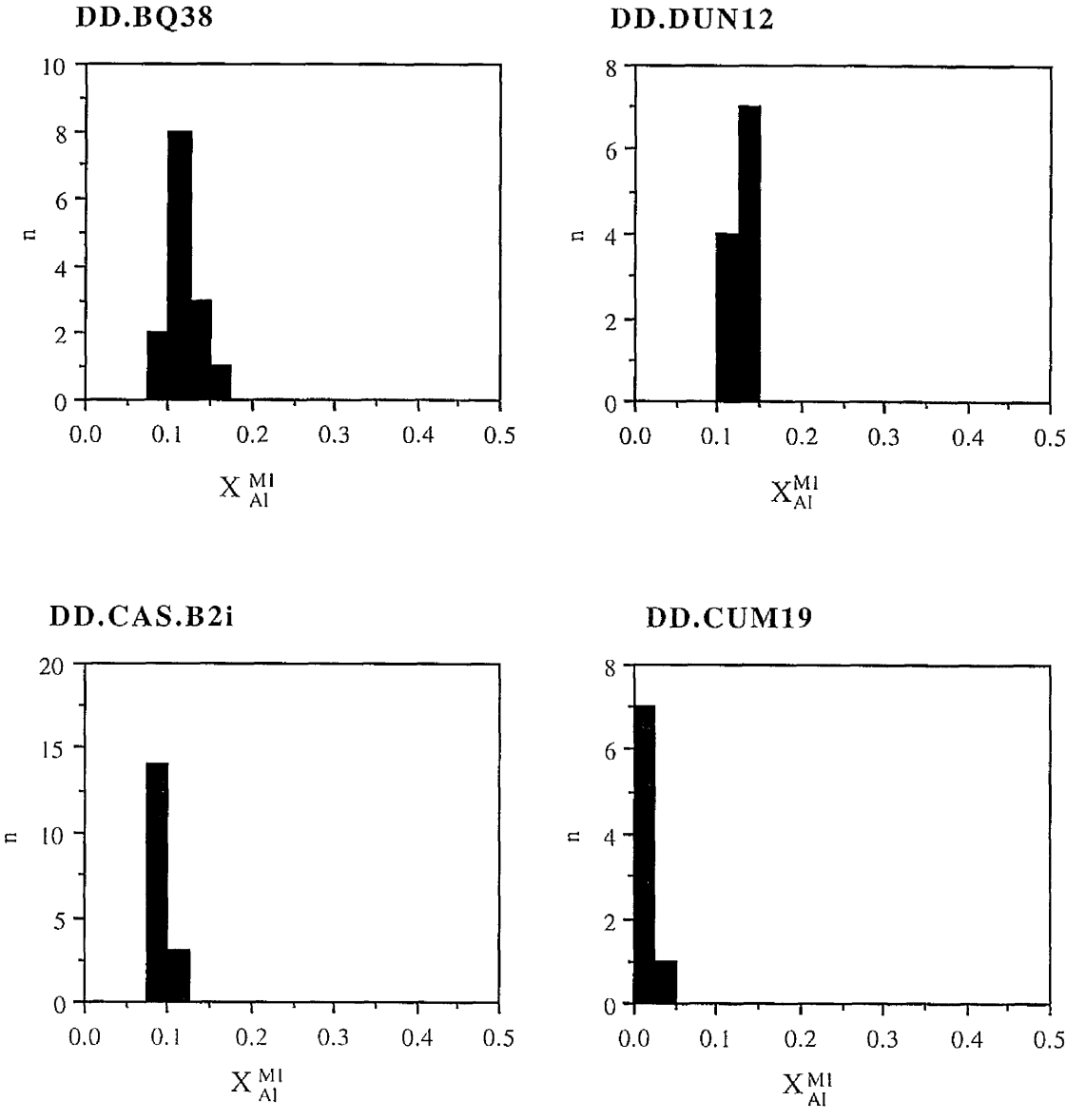

Figure 6.4.9 Frequency-X_{Al}^{M1} plot for orthopyroxene analyses from cordierite norites and a garnet tonalite (DD.CUM19). The cordierite norites have much higher X_{Al}^{M1} values (>0.075) than the garnet tonalite.

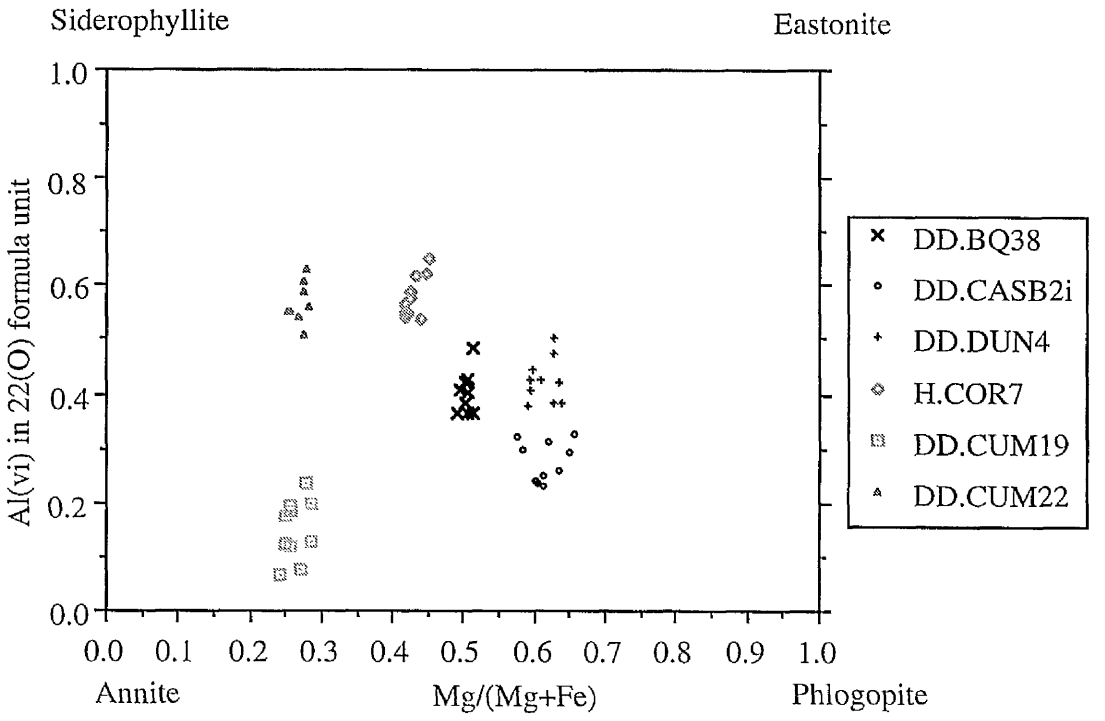

Figure 6.4.10 Composition of biotites from cordierite norites and garnet tonalites, with analyses plotted within the field of the four end members annite ($K_2Fe_6[Si_6Al_2O_{20}](OH_4)$), phlogopite ($K_2Mg_6[Si_6Al_2O_{20}](OH_4)$), siderophyllite ($K_2Fe_4Al_2[Si_4Al_4O_{20}](OH_4)$), and eastonite ($K_2Mg_4Al_2[Si_4Al_4O_{20}](OH_4)$)

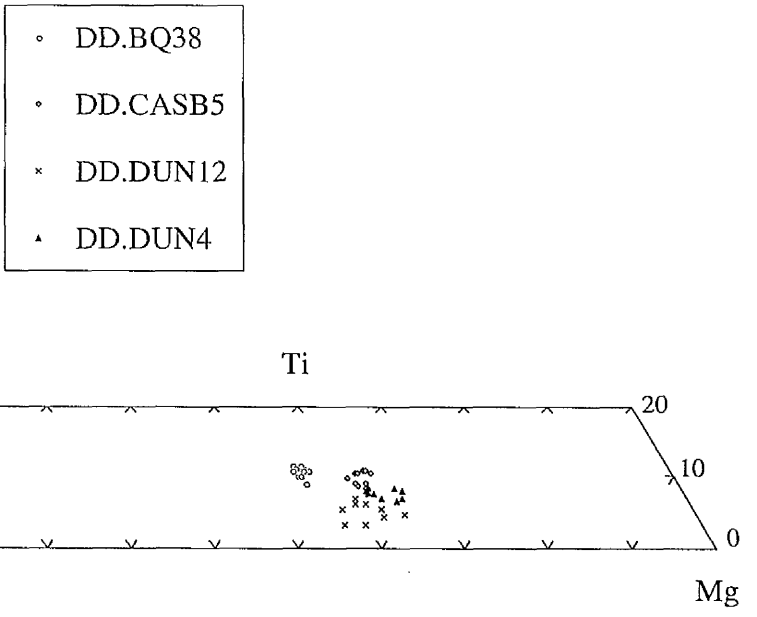

Figure 6.4.11 Compositional plot for biotites from cordierite norites.

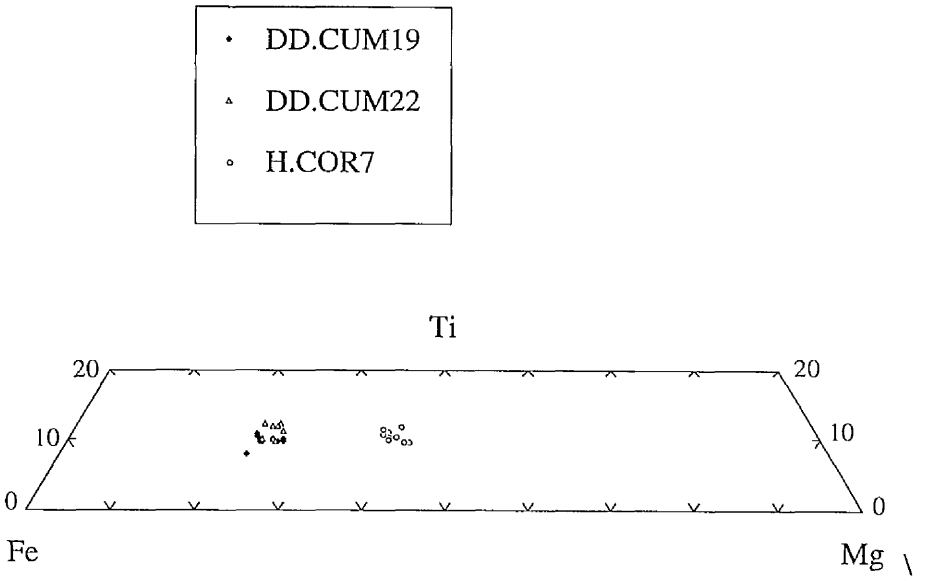

Figure 6.4.12 Compositional plot for biotites from garnet tonalites.

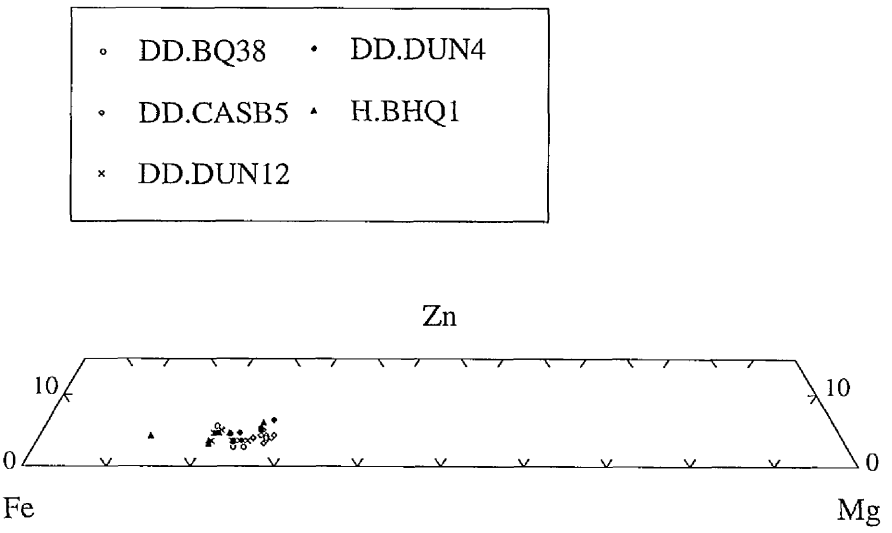

Figure 6.4.13 Compositional plot for spinel analyses from cordierite norites, plotting the ralative Fe, Mg and Zn compositions.

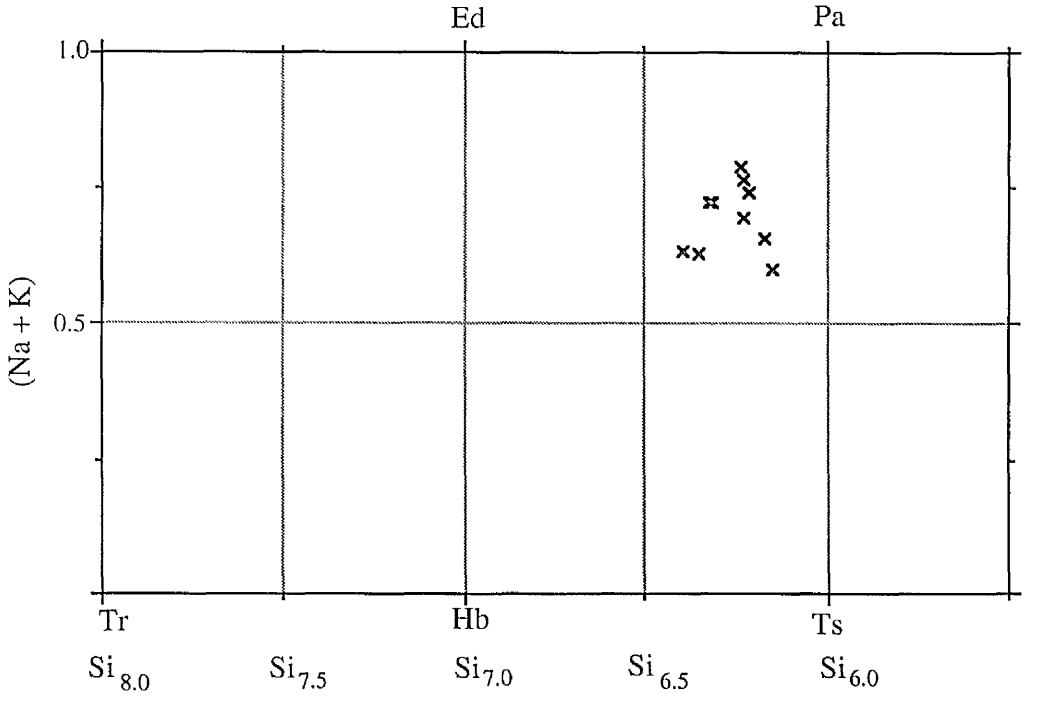

Figure 6.4.14 Calcic amphibole composition diagram for probe analyses from DD.CUM19, plotting A (alkali) Na + K atoms against no of Si atoms per 23(O) formula unit. End member abreviations: Tr, tremolite; Hb, hornblende; Ed, edenite; Pa, pargasite; Ts, tschermakite. All of the analyses fall within the pargasite field.

Table 6.1 Criteria for acceptance of probe data

Mineral	Oxide(wt%)	No. O in formula	Cation Total	Stoichiometric Criteria	
Plagioclase	98-102	8	4.90-5.10	(Si, Al)	3.96-4.04
				(Na,Ca, K)	0.98-1.02*
Alkali feldspar	98-102	8	4.90-5.10	(Si, Al)	3.96-4.04
				(Na,Ca, K)	0.98-1.02*
Garnet	98-102	24	15.70-16.00*2	(Si, Al, Ti, Cr, Fe^{3+})	9.80-10.2(
				(Fe^{2+}, Mn, Mg, Ca)	5.90-6.10
Cordierite	96-101	18	10.80-11.00*2	(Si, Al, Ti, Cr, Fe^{3+})	8.8-9.2
				(Fe^{2+}, Mn, Mg)	1.96-2.04
Orthopyroxene	98-102	6	3.96-4.00*2		
Biotite	93-98	22		(K, Na, Ba, Ca)	1.70-2.00
Muscovite	93-98	22		(K, Na, Ca)	1.70-2.00
Spinel	98-102	4	2.94-3.00*2	(Al, Ti, Cr, Fe^{3+})	1.96-2.04
				(Fe^{2+}, Mn, Mg, Zn)	0.98-1.02
Sillimanite	98-102	5	2.97-3.03	(Si)	0.98-1.02
				(Al)	1.96-2.04
Hornblende	95-99	23			
Staurolite	95-99	48			

*1 Does not include Ba which was not analysed for on the Geoscan microprobe.

*2 Cation totals systematically greater than these are taken to indicate the presence Fe^{3+} and were recalculated to the ideal cation total.

Table 6.2.1 Representative plagioclase and muscovite analyses from regionally metamorphosed rocks.

Wt% Oxide	Grt-Bt gneiss Plagioclase DD.SIN101	Grt-mica schist Plagioclase DD.SIN2
SiO_2	63.42	62.79
Al_2O_3	23.07	23.68
CaO	4.16	4.84
Na_2O	9.38	9.02
K_2O	0.00	0.03
TOTAL	**100.02**	**100.37**
Cations		
Si	2.800	2.769
Al	1.201	1.231
Ca	0.197	0.229
Na	0.803	0.772
K	0.000	0.002
(O)	8	8
TOTAL	**5.001**	**5.003**
X_{An}	**0.197**	**0.229**
X_{Ab}	**0.803**	**0.772**
X_{Or}	**0.000**	**0.002**

Wt% Oxide	Grt-mica schist Muscovite DD.SIN2	And-mica schist Muscovite DD.CLAS66	And-mica schist Muscovite DD.CLAS111
SiO_2	45.75	44.98	44.87
TiO_2	0.66	0.83	0.82
Al_2O_3	35.54	34.01	34.88
Cr_2O_3	0.07	0.10	0.12
FeO	1.49	1.91	1.41
MnO	0.00	0.00	0.00
MgO	0.84	0.99	0.77
CaO	0.07	0.00	0.14
Na_2O	1.72	0.47	0.97
K_2O	8.76	9.81	9.64
TOTAL	**94.90**	**93.11**	**93.61**
Cations			
Si	6.091	6.137	6.081
Ti	0.066	0.085	0.084
Al	5.577	5.470	5.573
Cr	0.007	0.010	0.013
Fe^{2+}	0.166	0.218	0.159
Mn	0.000	0.000	0.000
Mg	0.167	0.202	0.155
Ca	0.011	0.000	0.017
Na	0.445	0.125	0.255
K	1.487	1.708	1.666
(O)	22	22	22
TOTAL	**14.017**	**13.955**	**14.003**

Figure 6.2.2 Representative garnet analyses from regionally metamorphosed rocks.

Wt% Oxide	And-mica schist DD.CLAS66	Grt-Bt gneiss DD.SIN1	Grt-Bt gneiss DD.SIN101	Grt-mica schist DD.SIN2
SiO_2	36.89	38.08	37.96	37.41
TiO_2	0.00	0.05	0.00	0.00
Al_2O_3	20.59	21.30	21.15	20.92
Cr_2O_3	0.00	0.02	0.00	0.00
Fe_2O_3	0.59	0.33	0.53	0.00
FeO	25.18	32.80	32.11	34.27
MnO	13.57	2.40	2.05	3.65
MgO	1.87	5.30	5.81	3.02
CaO	1.45	0.67	0.68	1.09
TOTAL	**100.13**	**100.98**	**100.28**	**100.36**
Cations				
Si	5.992	5.998	5.998	6.016
Ti	0.000	0.006	0.000	0.000
Al	3.941	3.952	3.939	3.966
Cr	0.000	0.002	0.000	0.000
Fe^{3+}	0.072	0.039	0.063	0.000
Fe^{2+}	3.421	4.324	4.243	4.609
Mn	1.867	0.322	0.275	0.497
Mg	0.454	1.244	1.367	0.724
Ca	0.253	0.113	0.115	0.188
(O)	24	24	24	24
TOTAL	**16.000**	**16.000**	**16.000**	**16.000**
Mg#	**0.117**	**0.223**	**0.244**	**0.136**

Table 6.2.3 Representative biotite analyses from regionally metamorphosed rocks.

Wt %Oxide	And-mica schist DD.CLAS111	Mica schist DD.BOG1	And-mica schist DD.CLAS66	Grt-Bt gneiss DD.SIN1	Grt-Bt gneiss DD.SIN101	Grt-mica schist DD.SIN2
SiO_2	34.31	34.50	34.80	35.97	36.50	35.65
TiO_2	2.36	2.45	3.11	1.87	1.65	1.69
Al_2O_3	18.90	19.03	18.19	19.33	19.02	19.38
Cr_2O_3	0.00	0.00	0.00	0.17	0.00	0.10
FeO	21.65	22.45	20.43	16.28	15.08	18.44
MnO	0.00	0.00	0.13	0.00	0.00	0.00
MgO	7.66	7.42	8.28	11.79	13.23	10.59
CaO	0.06	0.12	0.11	0.15	0.00	0.03
Na_2O	0.39	0.50	0.45	0.73	0.71	0.79
K_2O	8.71	8.76	8.97	8.15	8.63	8.42
TOTAL	**94.05**	**95.22**	**94.49**	**94.44**	**94.82**	**95.09**
Cations						
Si	5.349	5.332	5.382	5.406	5.439	5.386
Ti	0.277	0.284	0.362	0.211	0.185	0.192
Al(iv)	2.651	2.668	2.618	2.594	2.561	2.614
Al(vi)	0.822	0.798	0.697	0.831	0.780	0.837
Cr	0.000	0.000	0.000	0.020	0.000	0.011
Fe^{2+}	2.823	2.902	2.642	2.046	1.879	2.331
Mn	0.000	0.000	0.018	0.000	0.000	0.000
Mg	1.779	1.708	1.908	2.642	2.938	2.386
Ca	0.010	0.019	0.019	0.024	0.000	0.005
Na	0.119	0.151	0.136	0.213	0.205	0.231
K	1.733	1.726	1.770	1.563	1.641	1.623
(O)	22	22	22	22	22	22
TOTAL	**15.562**	**15.588**	**15.552**	**15.550**	**15.628**	**15.616**
Mg#	**0.387**	**0.370**	**0.419**	**0.564**	**0.564**	**0.506**

Figure 6.2.4 Representative tourmaline and staurolite analyses from regionally metamorphosed rocks

Wt% Oxide	And-mica schist Tourmaline **DD.BOG1**	And-mica schist Tourmaline **DD.CLAS111**
SiO_2	35.31	35.24
TiO_2	1.27	1.02
Al_2O_3	32.75	34.00
Cr_2O_3	0.00	0.10
FeO	8.22	7.18
MnO	0.00	0.00
MgO	5.53	5.27
CaO	0.49	0.58
Na_2O	2.06	1.84
K_2O	0.07	0.00
TOTAL	**85.69**	**85.23**
Cations		
Si	7.391	7.356
Ti	0.200	0.159
Al	8.079	8.366
Cr	0.000	0.016
Fe2+	1.438	1.253
Mn	0.000	0.000
Mg	1.724	1.641
Ca	0.109	0.130
Na	0.836	0.745
K	0.019	0.000
(O)	31	31
TOTAL	**19.796**	**19.666**

Wt% Oxide	Grt-Bt gneiss Staurolite **DD.SIN101**
SiO_2	27.24
TiO_2	0.82
Al_2O_3	52.81
FeO	13.29
MnO	0.00
MgO	2.41
CaO	0.00
ZnO	0.73
TOTAL	**97.30**
Cations	
Si	7.956
Ti	0.180
Al	18.183
Fe2+	3.248
Mn	0.000
Mg	1.049
Ca	0.000
Zn	0.157
(O)	48
TOTAL	**30.773**
Mg#	**0.244**

Table 6.3.1 Representative feldspar analyses from cordierite hornfelses.

	Sil-Crd hornfels	Sil-Crd hornfels	Opx-Crd Hornfels	Opx-Crd Hornfels	Opx-Crd Hornfels	Opx-Crd Hornfels	Opx-Crd Hornfels
	Plagioclase	Plagioclase	Plagioclase	Plagioclase	Plagioclase	Anorthoclase	K-feldspar
Wt% Oxide	**DD.DUN1**	**H.COR8**	**H.BHQ5**	**DD.PIR4**	**DD.BQ17**	**DD.BQ41**	**DD.BQ17**
SiO_2	55.35	58.16	57.42	59.64	57.95	64.74	64.62
Al_2O_3	27.97	26.02	27.25	25.73	26.46	21.11	19.56
CaO	10.04	7.67	9.09	7.38	8.44	2.12	0.42
Na_2O	5.79	7.08	6.37	7.36	6.58	7.65	0.99
K_2O	0.07	0.12	0.32	0.31	0.40	4.11	14.83
TOTAL	**99.22**	**99.04**	**100.45**	**100.41**	**99.82**	**99.73**	**100.42**
Cations							
Si	2.508	2.632	2.564	2.651	2.599	2.892	2.959
Al	1.494	1.382	1.434	1.348	1.399	1.111	1.056
Ca	0.488	0.371	0.435	0.351	0.406	0.102	0.021
Na	0.509	0.619	0.552	0.634	0.572	0.662	0.088
K	0.004	0.007	0.018	0.017	0.023	0.234	0.867
(O)	8	8	8	8	8	8	8
TOTAL	**5.003**	**5.011**	**5.003**	**5.001**	**4.999**	**5.001**	**4.991**
X_{An}	**0.488**	**0.372**	**0.433**	**0.350**	**0.406**	**0.102**	**0.022**
X_{Ab}	**0.508**	**0.621**	**0.549**	**0.633**	**0.571**	**0.663**	**0.090**
X_{Or}	**0.004**	**0.007**	**0.018**	**0.017**	**0.023**	**0.234**	**0.888**

Table 6.3.2 Representative garnet analyses from cordierite hornfelses.

Wt% Oxide	Sil-Crd hornfels **DD.DUN1**	Sil-Crd hornfels **H.COR8**	Opx-Crd hornfels **DD.BQ17**	Opx-Crd hornfels **DD.BQ41**	Opx-Crd hornfels **DD.PIR1**	Opx-Crd hornfels **H.BHQ5**
SiO_2	37.52	37.36	37.85	37.55	38.66	38.38
TiO_2	0.00	0.00	0.12	0.15	0.17	0.03
Al_2O_3	21.12	21.07	21.45	21.46	21.78	21.42
Cr_2O_3	0.03	0.19	0.16	0.09	0.00	0.09
Fe_2O_3	0.25	0.00	0.08	0.00	0.33	0.23
FeO	32.99	35.32	32.12	32.68	32.39	32.18
MnO	2.31	0.35	0.44	0.17	0.33	0.84
MgO	4.16	4.08	6.57	6.40	6.90	6.22
CaO	1.64	1.22	0.97	0.57	1.07	1.40
TOTAL	**100.02**	**99.58**	**99.75**	**99.05**	**101.64**	**100.77**
Cations						
Si	5.995	6.001	5.968	5.968	5.975	6.004
Ti	0.000	0.000	0.014	0.018	0.019	0.004
Al	3.978	3.988	3.988	4.020	3.969	3.949
Cr	0.004	0.025	0.019	0.011	0.000	0.011
Fe^{3+}	0.030	0.000	0.010	0.000	0.039	0.027
Fe^{2+}	4.408	4.745	4.215	4.344	4.188	4.211
Mn	0.312	0.047	0.058	0.023	0.043	0.111
Mg	0.991	0.978	1.545	1.516	1.590	1.450
Ca	0.282	0.210	0.163	0.097	0.178	0.234
(O)	24	24	24	24	24	24
TOTAL	**16.000**	**15.994**	**16.000**	**15.997**	**16.000**	**16.000**
Mg#	**0.184**	**0.171**	**0.268**	**0.259**	**0.275**	**0.256**

Table 6.3.3 Representative cordierite analyses from cordierite hornfelses.

Wt% Oxide	Sil-Crd hornfels **DD.DUN1**	Sil-Crd hornfels **H.COR8**	Opx-Crd hornfels **DD.BQ41**	Opx-Crd hornfels **DD.PIR1**	Opx-Crd hornfels **H.BHQ5**	Opx-Crd hornfels **DD.BQ17**
SiO_2	49.17	49.22	48.86	48.95	48.97	48.64
TiO_2	0.00	0.04	0.00	0.00	0.02	0.00
Al_2O_3	33.36	34.40	32.96	32.95	33.04	32.57
Cr_2O_3	0.05	0.04	0.00	0.00	0.03	0.03
Fe_2O_3	0.00	0.00	0.00	0.00	0.68	0.37
FeO	9.77	7.55	8.68	9.23	8.46	8.11
MnO	0.00	0.16	0.00	0.00	0.00	0.00
MgO	7.82	9.02	8.26	8.14	8.36	8.53
TOTAL	**100.17**	**100.43**	**98.76**	**99.27**	**99.56**	**98.25**
Cations						
Si	4.994	4.932	5.009	5.006	4.988	5.009
Ti	0.000	0.003	0.000	0.000	0.001	0.000
Al	3.994	4.063	3.983	3.972	3.967	3.953
Cr	0.004	0.003	0.000	0.000	0.002	0.002
Fe^{3+}	0.000	0.000	0.000	0.000	0.052	0.029
Fe^{2+}	0.830	0.633	0.744	0.789	0.721	0.698
Mn	0.000	0.014	0.000	0.000	0.000	0.000
Mg	1.184	1.347	1.263	1.241	1.269	1.309
(O)	18	18	18	18	18	18
TOTAL	**11.006**	**10.995**	**10.999**	**11.008**	**11.000**	**11.000**
Mg#	**0.588**	**0.680**	**0.629**	**0.611**	**0.638**	**0.652**

Table 6.3.4 Representative orthopyroxene analyses from cordierite hornfelses.

Wt% Oxide	Opx-Crd Hornfels **DD.BQ17**	Opx-Crd Hornfels **DD.BQ41**	Opx-Crd Hornfels **DD.PIR1**	Opx-Crd Hornfels **H.BHQ5**	Opx-Crd Hornfels **H.COR10***	Opx-Crd Hornfels **H.COR10****
SiO_2	47.85	47.63	47.40	47.21	50.66	50.56
TiO_2	0.10	0.25	0.29	0.30	0.41	0.14
Al_2O_3	4.59	5.51	6.45	6.17	0.73	4.38
Cr_2O_3	0.21	0.17	0.00	0.10	0.24	0.19
Fe_2O_3	1.74	0.00	0.00	0.00	0.00	0.00
FeO	30.59	33.27	32.36	31.63	29.83	27.60
MnO	0.00	0.00	0.00	0.00	2.04	0.36
MgO	14.18	13.46	13.62	14.16	15.55	17.81
CaO	0.07	0.07	0.00	0.23	1.04	0.12
TOTAL	**99.31**	**100.37**	**100.12**	**99.80**	**100.50**	**101.15**
Cations						
Si	1.884	1.861	1.847	1.843	1.968	1.904
Ti	0.003	0.007	0.009	0.009	0.012	0.004
Al	0.214	0.254	0.296	0.284	0.033	0.194
Cr	0.006	0.005	0.000	0.003	0.007	0.006
Fe^{3+}	0.052	0.000	0.000	0.000	0.000	0.000
Fe^{2+}	1.007	1.087	1.055	1.033	0.969	0.869
Mn	0.000	0.000	0.000	0.000	0.067	0.012
Mg	0.832	0.784	0.791	0.824	0.900	0.999
Ca	0.003	0.003	0.000	0.009	0.043	0.005
(O)	6	6	6	6	6	6
TOTAL	**4.000**	**4.001**	**3.998**	**4.005**	**3.999**	**3.993**
Mg#	**0.452**	**0.419**	**0.428**	**0.444**	**0.482**	**0.535**
X_{Al}^{M1}	**0.116**	**0.139**	**0.153**	**0.157**	**0.032**	**0.096**

Table 6.3.5 Representative biotite analyses from cordierite hornfelses.

Wt% Oxide	Sil-Crd hornfels **DD.DUN1**	Sil-Crd hornfels **H.COR8**	Opx-Crd hornfels **H.BHQ5**	Opx-Crd hornfels **H.COR10**
SiO_2	35.85	34.98	36.10	36.02
TiO_2	1.74	3.22	6.63	6.15
Al_2O_3	19.71	19.38	15.77	15.75
Cr_2O_3	0.02	0.00	0.09	0.07
FeO	17.41	18.44	15.99	16.47
MnO	0.00	0.00	0.09	0.00
MgO	11.11	9.35	10.87	10.97
CaO	0.07	0.13	0.01	0.06
Na_2O	0.63	0.48	0.22	0.32
K_2O	8.99	9.16	9.18	9.14
TOTAL	**95.53**	**95.14**	**94.95**	**94.94**
Cations				
Si	5.375	5.312	5.444	5.444
Ti	0.196	0.368	0.752	0.699
Al(iv)	2.625	2.688	2.556	2.556
Al(vi)	0.859	0.780	0.247	0.250
Cr	0.002	0.000	0.011	0.008
Fe^{2+}	2.184	2.341	2.016	2.082
Mn	0.000	0.000	0.012	0.000
Mg	2.483	2.117	2.444	2.472
Ca	0.011	0.022	0.001	0.009
Na	0.184	0.142	0.065	0.094
K	1.720	1.775	1.765	1.762
(O)	22	22	22	22
TOTAL	**15.639**	**15.545**	**15.313**	**15.376**
Mg#	**0.532**	**0.475**	**0.548**	**0.543**

Table 6.3.6 Representative spinel and sillimanite analyses from cordierite hornfelses.

Wt% Oxide	Opx-Crd hornfels Spinel H.BHQ5	Opx-Crd hornfels Spinel DD.BQ17
SiO_2	0.03	0.10
TiO_2	0.09	0.12
Al_2O_3	57.89	57.57
Cr_2O_3	0.96	0.54
Fe_2O_3	3.92	3.62
FeO	28.06	29.63
MnO	0.00	0.00
MgO	7.35	5.93
ZnO	2.39	2.73
CuO	0.00	-
TOTAL	**100.68**	**100.24**
Cations		
Si	0.001	0.003
Ti	0.002	0.003
Al	1.891	1.905
Cr	0.021	0.012
Fe^{3+}	0.082	0.077
Fe^{2+}	0.651	0.696
Mn	0.000	0.000
Mg	0.304	0.249
Zn	0.048	0.056
Cu	0.000	-
(O)	4	4
TOTAL	**3.000**	**3.000**
Mg#	**0.318**	**0.263**

Wt% Oxide	Sil-Crd hornfels Sillimanite DD.DUN1	Sil-Crd hornfels Sillimanite H.COR8
SiO_2	36.58	38.21
Al_2O_3	62.64	60.00
FeO	0.45	0.22
MnO	0.00	0.00
TOTAL	**99.66**	**98.42**
Cations		
Si	0.992	1.046
Al	2.003	1.936
Fe	0.010	0.005
Mn	0.000	0.000
(O)	5	5
TOTAL	**3.005**	**2.987**

Table 6.4.1 Representative feldspar analyses from cordierite norites and garnet tonalites.

Wt% Oxide	Crd norite Plagioclase **DD.BQ38**	Crd norite Plagioclase **DD.CASB2i**	Crd norite Plagioclase **DD.DUN4**	Crd norite K-feldspar **H.BHQ1**	Grt tonalite Plagioclase **DD.CUM22**	Grt tonalite Plagioclase **DD.TYQ5**	Grt tonalite K-feldspar **DD.CUM22**
SiO_2	57.95	49.86	54.03	63.58	59.88	58.20	64.04
Al_2O_3	26.86	32.10	29.73	18.77	25.39	26.50	19.24
CaO	8.63	15.13	11.56	0.00	6.93	8.33	0.20
Na_2O	6.35	3.09	5.03	1.00	7.63	6.76	1.87
K_2O	0.49	0.00	0.00	14.89	0.16	0.32	13.71
TOTAL	**100.27**	**100.18**	**100.34**	**98.25**	**99.99**	**100.11**	**99.06**
Cations							
Si	2.588	2.269	2.430	2.961	2.667	2.602	2.944
Al	1.414	1.722	1.576	1.031	1.333	1.396	1.043
Ca	0.413	0.738	0.557	0.000	0.331	0.399	0.010
Na	0.550	0.272	0.439	0.090	0.659	0.586	0.166
K	0.028	0.000	0.000	0.885	0.009	0.018	0.804
(O)	8	8	8	8	8	8	8
TOTAL	**4.993**	**5.001**	**5.002**	**4.967**	**4.999**	**5.001**	**4.967**
X_{An}	**0.417**	**0.731**	**0.559**	**0.000**	**0.331**	**0.398**	**0.010**
X_{Ab}	**0.555**	**0.269**	**0.441**	**0.092**	**0.660**	**0.584**	**0.169**
X_{Or}	**0.028**	**0.000**	**0.000**	**0.908**	**0.009**	**0.018**	**0.820**

Table 6.4.2 Representative garnet analyses from cordierite norites and garnet tonalites.

Wt% Oxide	Crd norite **CASB2i**	Crd norite **DD.DUN4**	Crd norite **DD.DUN12**	Crd norite **H.BHQ1**	Grt tonalite **DD.CUM22**	Grt tonalite **DD.CUM19**	Grt tonalite **DD.TYQ5**
SiO_2	38.40	38.14	38.19	38.55	37.17	36.82	37.63
TiO_2	0.00	0.15	0.04	0.22	0.07	0.00	0.02
Al_2O_3	21.23	21.35	21.34	21.92	20.77	20.66	21.01
Cr_2O_3	0.00	0.01	0.07	0.17	0.07	0.00	0.06
Fe_2O_3	0.00	0.58	0.25	0.00	0.30	1.179	1.13
FeO	28.46	32.19	30.17	30.90	36.44	32.04	31.26
MnO	1.82	0.30	0.83	0.64	0.19	0.69	2.56
MgO	7.57	5.98	7.19	6.64	2.74	1.91	4.40
CaO	1.66	2.00	1.44	1.16	2.33	6.14	2.60
TOTAL	**99.14**	**100.70**	**99.52**	**100.80**	**100.08**	**99.44**	**100.67**
Cations							
Si	6.034	5.976	6.001	5.959	5.995	5.958	5.963
Ti	0.000	0.018	0.004	0.009	0.009	0.000	0.002
Al	3.931	3.943	3.953	4.102	3.949	3.941	3.925
Cr	0.000	0.001	0.008	0.002	0.008	0.000	0.006
Fe^{3+}	0.000	0.069	0.030	0.000	0.036	0.144	0.135
Fe^{2+}	3.740	4.219	3.966	3.960	4.915	4.337	4.143
Mn	0.243	0.040	0.111	0.128	0.026	0.095	0.343
Mg	1.773	1.398	1.685	1.584	0.660	0.461	1.040
Ca	0.279	0.336	0.243	0.185	0.403	1.065	0.441
(O)	24	24	24	24	24	24	24
TOTAL	**16.000**	**16.000**	**16.000**	**15.929**	**16.000**	**16.000**	**16.000**
Mg#	**0.322**	**0.249**	**0.298**	**0.290**	**0.118**	**0.096**	**0.201**

Table 6.4.3 Representative cordierite analyses from cordierite norites.

Wt% Oxide	Crd norite **DD.CASB2i**	Crd norite **DD.BQ38**	Crd norite **H.BHQ1**	Crd norite **DD.DUN4**	Crd norite **DD.DUN12**
SiO_2	49.07	49.14	48.25	49.35	48.58
TiO_2	0.00	0.00	0.00	0.00	0.02
Al_2O_3	32.99	32.98	33.79	33.34	32.84
Cr_2O_3	0.00	0.00	0.00	0.00	0.05
Fe_2O_3	0.55	0.60	0.00	0.47	0.59
FeO	6.11	7.89	7.96	6.95	6.93
MnO	0.00	0.00	0.34	0.00	0.01
MgO	9.74	8.77	8.16	9.30	9.11
TOTAL	**98.46**	**99.37**	**98.51**	**99.41**	**98.13**
Cations					
Si	4.998	4.999	4.953	4.995	4.987
Ti	0.000	0.000	0.000	0.000	0.002
Al	3.960	3.954	4.088	3.977	3.973
Cr	0.000	0.000	0.000	0.000	0.004
Fe^{3+}	0.042	0.046	0.000	0.036	0.046
Fe^{2+}	0.521	0.671	0.683	0.588	0.594
Mn	0.000	0.000	0.030	0.000	0.001
Mg	1.478	1.330	1.249	1.404	1.393
(O)	18	18	18	18	18
TOTAL	**11.000**	**11.000**	**11.003**	**11.000**	**11.000**
Mg#	**0.739**	**0.665**	**0.646**	**0.705**	**0.701**

Table 6.4.4 Representative orthopyroxene analyses from cordierite norites and garnet tonalites.

Wt% Oxide	Crd norite **DD.BQ38**	Crd norite **DD.CASB5**	Crd norite **DD.DUN4**	Crd norite **DD.DUN12**	Grt tonalite **DD.CUM19**
SiO_2	48.11	49.67	48.69	48.12	48.34
TiO_2	0.25	0.00	0.21	0.37	0.00
Al_2O_3	5.86	4.20	4.03	5.25	0.70
Cr_2O_3	0.18	0.00	0.13	0.09	0.00
FeO	30.88	27.31	30.27	30.14	40.84
MnO	0.00	0.41	0.00	0.00	0.00
MgO	15.23	17.54	15.73	15.34	8.94
CaO	0.17	0.17	0.19	0.14	0.94
TOTAL	**100.67**	**99.31**	**99.24**	**99.45**	**99.77**
Cations					
Si	1.852	1.907	1.898	1.870	1.981
Ti	0.007	0.000	0.006	0.011	0.000
Al	0.266	0.190	0.185	0.241	0.034
Cr	0.005	0.000	0.004	0.003	0.000
Fe^{2+}	0.994	0.877	0.987	0.979	1.400
Mn	0.000	0.013	0.000	0.000	0.000
Mg	0.874	1.004	0.914	0.888	0.546
Ca	0.007	0.007	0.008	0.006	0.041
(O)	6	6	6	6	6
TOTAL	**4.005**	**3.998**	**4.002**	**3.992**	**4.002**
Mg#	**0.468**	**0.534**	**0.481**	**0.476**	**0.281**
X_{Al}^{M1}	**0.133**	**0.095**	**0.093**	**0.121**	**0.017**

Table 6.4.5 Representative biotite analyses from cordierite norites and garnet tonalites.

Wt% Oxide	Crd norite DD.BQ38	Crd norite H.BHQ1	Crd norite CASB2i	Crd norite DD.DUN4	Grt tonalite DD.CUM19	Grt tonalite DD.CUM22
SiO_2	36.37	35.80	36.35	36.21	34.50	34.24
TiO_2	5.33	5.32	4.23	3.68	4.60	4.22
Al_2O_3	17.32	16.82	16.23	16.69	14.92	18.04
Cr_2O_3	0.19	0.00	0.10	0.05	0.00	0.00
FeO	18.45	17.45	16.64	14.34	27.91	25.24
MnO	0.07	0.00	0.00	0.00	0.00	0.00
MgO	10.13	10.51	12.57	14.06	5.40	5.39
CaO	0.00	0.06	0.08	0.13	0.21	0.10
Na_2O	0.27	0.05	0.47	0.50	0.42	0.47
K_2O	9.06	9.24	8.79	8.65	8.68	8.96
Cl	0.73	0.14	-	-	-	-
F	0.18	0.31	-	-	-	-
BaO	0.98	0.48	-	-	-	-
TOTAL	**99.06**	**96.18**	**95.46**	**94.31**	**96.63**	**96.66**
Numer of ions on the basis of 22(O) formula unit						
Si	5.384	5.391	5.452	5.433	5.427	5.299
Ti	0.593	0.603	0.477	0.416	0.544	0.491
Al(iv)	2.616	2.610	2.548	2.567	2.573	2.761
Al(vi)	0.406	0.375	0.322	0.384	0.193	0.530
Cr	0.022	0.000	0.012	0.006	0.000	0.000
Fe^{2+}	2.284	2.197	2.087	1.799	3.672	3.267
Mn	0.008	0.000	0.000	0.000	0.000	0.000
Mg	2.235	2.360	2.810	3.146	1.266	1.243
Ca	0.000	0.010	0.013	0.021	0.036	0.017
Na	0.077	0.014	0.137	0.145	0.127	0.142
K	1.711	1.775	1.683	1.656	1.742	1.769
Cl	0.018	0.037	-	-	-	-
F	0.086	0.147	-	-	-	-
Ba	0.057	0.028	-	-	-	-
(O)	22	22	22	22	22	22
TOTAL	**15.497**	**15.547**	**15.541**	**15.573**	**15.580**	**15.519**
Mg#	**0.495**	**0.518**	**0.574**	**0.636**	**0.256**	**0.276**

Table 6.4.6 Representative spinel analyses from cordierite norites.

Wt% Oxide	Crd norite **DD.BQ38**	Crd norite **H.BHQ1**	Crd norite **DD.CASB5**	Crd norite **DD.DUN12**
SiO_2	0.00	0.18	0.00	0.00
TiO_2	0.00	0.00	0.00	0.04
Al_2O_3	54.11	60.56	59.04	59.32
Cr_2O_3	1.96	1.34	0.00	0.14
Fe_2O_3	5.97	0.00	2.53	2.66
FeO	30.66	32.81	29.46	31.08
MnO	0.00	0.00	0.00	0.00
MgO	5.42	4.98	6.47	5.86
CaO	0.00	1.62	0.00	0.00
ZnO	1.66	0.00	1.93	1.70
TOTAL	**99.77**	**101.49**	**99.43**	**100.80**
Cations				
Si	0.000	0.005	0.000	0.000
Ti	0.000	0.000	0.000	0.001
Al	1.826	1.968	1.947	1.941
Cr	0.044	0.029	0.000	0.003
Fe^{3+}	0.129	0.000	0.053	0.056
Fe^{2+}	0.734	0.756	0.690	0.722
Mn	0.000	0.000	0.000	0.000
Mg	0.231	0.205	0.270	0.242
Ca	0.000	0.033	0.000	0.000
Zn	0.035	0.000	0.040	0.035
(O)	4	4	4	4
TOTAL	**3.000**	**2.996**	**3.000**	**3.000**
Mg#	**0.239**	**0.213**	**0.281**	**0.251**
X_{Hc}	**0.686**	**0.756**	**0.671**	**0.701**
X_{Mag}	**0.065**	**0.000**	**0.027**	**0.028**

Table 6.4.7 Representative amphibole analyses from garnet tonalites.

Wt% Oxide	Green Hbl DD.CUM19	Blue Hbl DD.CUM19	Cummingtonite DD.CUM19
SiO_2	41.11	39.49	50.76
TiO_2	1.30	0.00	0.00
Al_2O_3	12.81	16.22	0.47
FeO	24.73	27.06	38.24
MnO	0.00	0.00	0.00
MgO	5.48	2.94	7.27
CaO	10.87	10.32	0.33
Na_2O	1.83	1.36	0.41
K_2O	0.90	0.95	0.00
TOTAL	**99.03**	**98.33**	**97.48**
Cations			
Si	6.317	6.152	8.001
Ti	0.151	0.000	0.000
Al	2.321	2.978	0.087
Fe^{2+}	3.179	3.526	5.041
Mn	0.000	0.000	0.000
Mg	1.254	0.682	1.708
Ca	1.789	1.722	0.056
Na	0.545	0.411	0.126
K	0.177	0.189	0.000
(O)	23	23	23
TOTAL	**15.733**	**15.660**	**15.019**
Mg#	**0.283**	**0.162**	**0.253**

CHAPTER 7 METAMORPHISM

7.1 Introduction

In this chapter the metamorphism of the rocks from the Huntly-Knock area is discussed. Petrogenetic grids and AFM projections are used to illustrate the broad pressure-temperature limits for the rocks belonging to each metamorphic grade and the mineral reactions which led to the formation of each metamorphic assemblage. This includes the reactions which lead to partial melting by the breakdown of hydrous minerals. The pressure-temperature trends described here are essentially qualitative, and detailed quantitative temperature and pressure calculations are given in Chapter 8.

The first section of this chapter discusses the metamorphism of the regionally metamorphosed rocks. The remainder of the chapter deals with the hornfelsic and associated igneous-textured rocks. The sillimanite-cordierite hornfelses are discussed first, then the cordierite-K-feldspar hornfelses, and finally the higher-grade and mineralogically similar cordierite-orthopyroxene hornfelses and cordierite norites are discussed together.

7.2 Regionally Metamorphosed Rocks

7.2.1 Introduction

The regionally metamorphosed rocks which surround the Huntly Gabbro belong to the Dalradian Supergroup, with rocks of the Whitehills and Boyndie Bay 'Groups' outcropping to the S and SW of the intrusion and members of the Portsoy 'Group' trending towards the W margin of the intrusion (Figure 3.2.1) in the vicinity of Cormalet (locality 3e).

The Whitehills / Boyndie Bay 'Group' rocks contain andalusite-mica schists and mica schists and are succeeded by biotite-chlorite phyllites to the S (Chapter 4.2). The Portsoy Group rocks consist of garnet-mica schists replaced by garnet-biotite gneisses as the contact of the Huntly Gabbro is approached. These rocks therefore contain two distinct metamorphic sequences which will be dealt with separately.

7.2.2 Rocks from S and SW of the Huntly Gabbro (Whitehills / Boyndie Bay 'Groups')

The Dalradian metasediments which crop-out to the S and SW of the Huntly Gabbro display assemblages ~~which~~ belong to the classic Buchan sequence described by Harte & Hudson (1979). These are indicative of high-temperature low-pressure regional metamorphism described in Chapter 3.2.5.

(i) Biotite-chlorite meta-siltstones

The chlorite-biotite-bearing meta-siltstones are the lowest grade rocks in the area mapped and belong to the lowest grade hydrous assemblages of Chinner (1966), re-classified as the Biotite Zone by Harte & Hudson (1979). They are characterised by the assemblage;

chlorite + biotite + muscovite + quartz. [7.1]

This is the typical Biotite Zone assemblage over much of the Buchan region, and indicates that the rocks have moderate Al contents, as typical of Dalradian pelites as a whole.

(ii) Andalusite-mica schists

The low grade chlorite-bearing rocks are succeeded northwards by andalusite-mica schists and mica schists, though due to poor exposure there is a large gap in the succession between these two rock types.

Stable K_2O-FeO-MgO-Al_2O_3-SiO_2-H_2O (KFMASH) mineral parageneses are:

andalusite + biotite + muscovite + quartz, [7.2]

and;

andalusite + staurolite + muscovite + quartz. [7.3]

Garnet is present in some of the andalusite-bearing schists, though, where present both is minor, and the high Mn contents from the garnets in DD.CLAS66 suggests that this mineral is metastable in the KFMASH system.

The presence of regional andalusite indicates that these rocks belong to a relatively

low pressure facies series, and that the creation of andalusite-bearing assemblages from lower grade biotite-zone assemblages is typical of Buchan series metamorphism (Harte & Hudson, 1979). Additionally, the presence of staurolite in DD.CLAS112 indicates that the rocks must lie at pressures above the staurolite stability reaction in the KFMASH system from the petrogenetic grid of Harte & Hudson (1979);

staurolite = andalusite + cordierite [7.4]

As both staurolite and andalusite are present in these rocks, then, following the petrogenetic grid of Harte & Hudson (1979) the cordierite, staurolite and andalusite isograds must all have been crossed in the area from the Biotite Zone rocks to the S. The absence of any rocks which contain the mineral assemblages which correspond to the Cordierite or ~~Staurolite~~ Andalusite Zones (cordierite + chlorite + biotite and andalusite + cordierite + biotite respectively) therefore is probably due to the lack of exposure between the biotite-chlorite metasiltstones and the andalusite-mica schists.

The andalusite-in isograd in the Buchan Series Zones (D) and (E) from Harte & Hudson (1979) is heralded by the AFM continuous reaction:

Crd (+ Qtz + Ms) = And + Bt (+ H_2O). [7.5]

This reaction moves towards increasingly Mg-rich compositions with increased temperature.

Andalusite can also be formed by the staurolite-consuming reaction:

St (+ Qtz + Ms) = And + Bt (+ H_2O) [7.6]

This reaction is continuous and moves towards increasing Fe-rich compositions.

As reactions 7.5 and 7.6 move apart with increased temperature, the field in which only andalusite and biotite are stable together, therefore increases in size (Figure 7.2.1) ~~until the following discontinuous reaction is reached~~ These two reactions are preceeded by the reaction:

St + Crd (+ Ms + Qtz) = And + Bt (+ H_2O). [7.7]

Therefore the rocks from the S and SW margins of the Huntly Gabbro are characteristic of Buchan type low-pressure metamorphism, and the presence of medium

grade rocks (andalusite-mica schists) at low pressures is indicative of a high geothermal gradient during the main metamorphic event.

7.2.3 Rocks from the W margin of the Huntly Gabbro (Portsoy 'Group')

Muscovite-bearing garnet-mica schists are replaced by fibrolite-bearing garnet-biotite gneisses over the space of 100 m as the W margin of the Huntly Gabbro is approached. The gneisses are banded, with leucocratic and biotite-rich bands, indicative of their formation by localised closed-system partial melting, without any major melt extraction (Chapter 5.2).

The absence of K-feldspar in either the muscovite-bearing schists, or the muscovite-absent gneisses suggests that the gneisses may have formed via a muscovite consuming melting reaction such as:

$$\text{muscovite} + \text{biotite} + \text{quartz} + H_2O = \text{sillimanite} + \text{melt.} \qquad [7.8]$$

This shows that the K-feldspar-absent solidus was crossed by these rocks, as displayed in the petrogenetic grid of Grant (1985) shown in Figure 7.1. Any such melting reaction would be restricted by the availability of a pervasive H_2O-rich fluid, and unless unusually large quantities of H_2O were available, all of the available H_2O would be partitioned into the initial melt. The melt would also be H_2O saturated, at the low temperature needed for reaction 7.8 (Clemens & Wall, 1981), and would crystallise biotite, explaining the absence of any K-feldspar in these rocks.

The lack of any evidence for melt extraction and the absence of K-feldspar from the garnet-biotite gneisses implies that the fluid-absent melting did not occur

7.3 Cordierite-sillimanite hornfelses

Sample DD.DUN1 contains rectangular sillimanite bundles, which have psuedomorphed earlier andalusite crystals (Plate 5.4.1). This, and the close proximity of the andalusite-mica schists from Clashmach Hill (Figure 4.1.1) suggests that the sillimanite-cordierite hornfelses formed by recrystallisation of such andalusite schists, due to contact metamorphism by the Huntly Gabbro. Muscovite is absent from the sillimanite-bearing hornfelses, whilst biotite remains an abundant mineral phase, little quartz is

present (though modally less than in the andalusite-bearing schists). Therefore, these rocks attained the temperatures required for muscovite breakdown (650 to 700°C at pressures below 5 kbars), but insufficient for the major breakdown of biotite. In sample DD.DUN1 no K-feldspar is present and a likely muscovite consuming reaction would be:

$$\text{muscovite} + \text{biotite} + \text{quartz} + H_2O = \text{sillimanite} + \text{melt.} \qquad [7.8]$$

with the remainder of the sillimanite forming pseudomorphs after andalusite by the reaction;

$$\text{andalusite} = \text{sillimanite.} \qquad [7.9]$$

Other sillimanite-bearing hornfelses contain additional K-feldspar, and the sillimanite forms randomly-oriented acicular crystals, and does not pseudomorph any earlier andalusite. The presence of large zoned plagioclase crystals in H.COR8 is indicative of the presence of some melt, and such a rock would have formed by the muscovite-consuming fluid-absent melting reaction:

$$\text{muscovite} + \text{quartz} = \text{K-feldspar} + \text{sillimanite} + \text{melt.} \qquad [7.10]$$

This reaction has been experimentally calibrated (e.g. Storre, 1977) and the position of the sillimanite-cordierite hornfelses, in P-T space, relative to the andalusite schists and orthopyroxene-bearing rocks is displayed in the petrogenetic grid Figure 7.3.1. AFM projections from K-feldspar representing the compositions of the various rock types in the system KFMASH are shown in Figure 7.3.2. The sillimanite-cordierite hornfelses would therefore have initially crystallised in field [S] in this diagram. However, the biotite consuming reaction (described in section 7.4) which borders the upper temperature limit of field [S] is continuous, and most of the sillimanite-bearing rocks will have crossed into field [C].

The non-migmatitic appearance of the sillimanite-K-feldsapar cordierite hornfelses indicates that any melt formed by reaction 7.10 has at least been partially extracted from these rocks.

7.4 Cordierite-K-feldspar hornfelses

The cordierite-K-feldspar hornfelses are quartz-biotite-poor, garnet-cordierite-rich rocks. The increase in the modal quantity of cordierite in these rocks and the decline in biotite is due to the continuous reaction after Le Breton & Thompson (1988):

biotite + aluminosilicate + quartz + plagioclase = garnet/cordierite + K-feldspar + melt. [7.11]

The occurrence of this reaction is supported by textural evidence from these rocks, with atoll-type garnets contain 'fillings' of quartz and K-feldspar (Plate 5.4.3), which represent localised partial melting (Chapter 5.6).

Reaction 7.11 is continuous and its position in pressure-temperature space is included in Figure 7.3.1. The presence of Ti and/or F in biotite though, will stabilise the reaction to higher temperatures. The cordierite-K-feldspar hornfelses therefore lie in field [C] in Figure 7.3.1, although if all the ~~reactants of~~ biotite in reaction 7.8 became exhausted then further heating would not lead to any further melting until liquidus temperatures were met (>1200°C).

7.5 Cordierite-orthopyroxene hornfelses and cordierite norites

The cordierite-orthopyroxene hornfelses and the cordierite norites are mineralogically similar, the only major differences being textural and the absence of quartz in many of the hornfelses (Chapter 5.6).

Orthopyroxene and sillimanite never occur together as peak paragenesis minerals in any of the rocks from the Huntly-Knock area. Some sillimanite though, occurs as small-relict crystals, shielded by cordierite inside rectangular-shaped spinel-cordierite clots in two of the cordierite norites (Plate 5.5.6). These spinel-cordierite clots form as pseudomorphs after sillimanite, and the likely reaction by which they grew is displayed in Figure 7.4.1, with the sillimanite being consumed in the fluid-absent melting reaction:

biotite + sillimanite + quartz = cordierite + spinel + melt. [7.12]

This reaction is similar to reaction 7.13, calibrated by Le Breton & Thompson (1988).

Orthopyroxene occurs abundantly in both the high-grade hornfelses and the cordierite norites, and can be formed, once all the sillimanite has been exhausted from reactions 7.8 and 7.9, as the solid product of the higher-temperature incongruent melting reaction:

$$\text{biotite} + \text{quartz} = \text{orthopyroxene} \pm \text{K-feldspar} + \text{melt.} \qquad [7.13]$$

This reaction has been experimentally investigated by several workers (e.g. Bohlen *et al.* 1983 ; Grant, 1986 ; Vielzeuf & Clemens, 1992; Koberski, 1995) and the experimental equilibria of Vielzeuf & Clemens (1992) is plotted in Figure 7.3.1. As shown in Figure 7.3.1 the Mg-end member of this reaction can begin at temperatures in the region of 750°C at mid-crustal pressures. All of the orthopyroxene-bearing hornfelses and cordierite norites would therefore have initially crystallised in field [O] in Figure7.3.1. However, reaction 7.10 is continuous and Ti can stabilise the biotite up to temperatures of around 900°C (Koberski, 1995), and the absence of any biotite in some of the high grade orthopyroxene hornfelses from Battle Hill Woods (e.g. sample DD.PIR1 & DD.PIR4) indicates that temperatures in excess of these may have been achieved.

The anhydrous, non-migmatitic nature of many of the orthopyroxene-bearing hornfelses indicate that any melt formed by reactions 7.8–10 must have been efficiently extracted. However, the cordierite norites, by contrast, have igneous textures and consequently crystallised in the presence of a melt (Chapter 5.5). The presence of biotite-quartz simpletic overgrowths, replacing orthopyroxene, implies a reversal of reaction 7.10, with orthopyroxene reacting with melt. This is good evidence for biotite not being a peak paragenesis mineral in these rocks, as biotite crystallisation must have occurred at temperatures below those required for reaction 7.10.

7.6 Conclusions

The intrusion of the Huntly mafic mass led to contact metamorphism of andalusite-mica schists and mica schists. A metamorphic sequence can be determined, by which isobaric heating led to the formation of increasingly higher-grade thermally metamorphosed rocks. The first effect of heating was for muscovite to break down, via the fluid-absent melting reactions 7.5 and 7.7, leading to the formation of sillimanite-bearing

hornfelses (field [S] in Figure 7.3.1). As the temperature increased both the biotite and sillimanite were consumed by reactions 7.11 and 7.12, with cordierite becoming more abundant as temperature increased (field [C]). The highest-grade rocks were formed by the biotite plus quartz consuming reaction 7.13, leading to the formation of both anhydrous, silica-poor orthopyroxene hornfelses and of igneous textured cordierite norites.

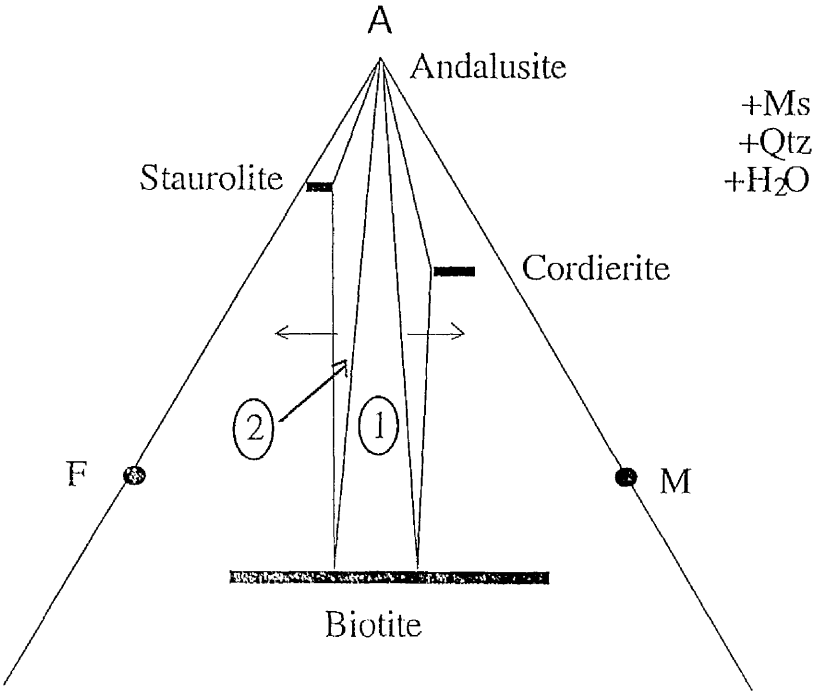

Figure 7.2.1 AFM projection from muscovite showing the fields in which the andalusite-mica schists (1) and andalusite-staurolite-mica schists plot (2). The field in which andalusite-biotite alone exists increases with increasing temperature.

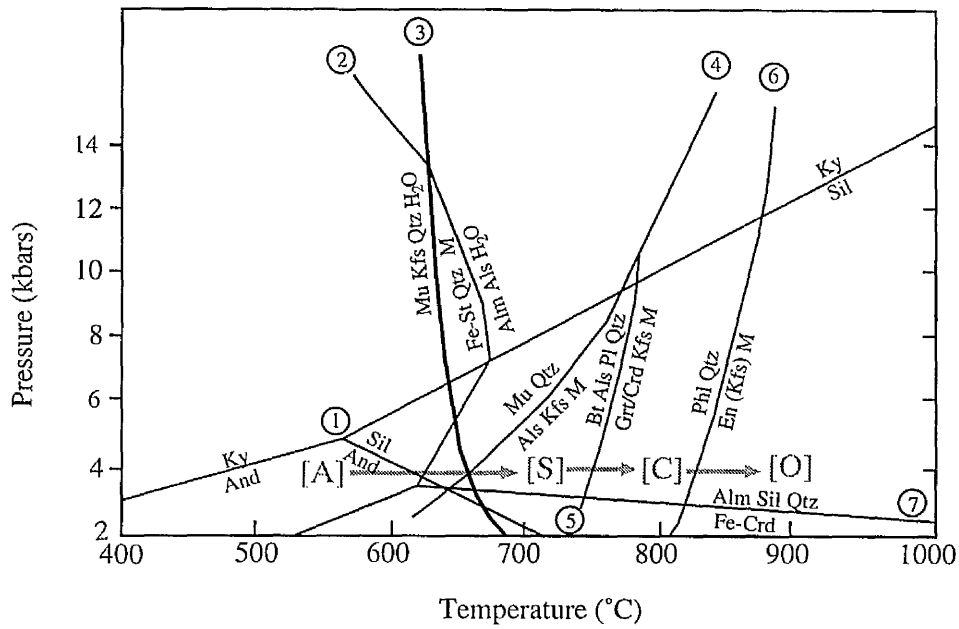

Figure 7.3.1 Petrogenetic grid for pelitic rocks in the system KFMASH. The dark-grey lines represent the isobaric heating path to which the regionally metamorphosed rocks in the aureole of the Huntly Gabbro were subjected; on heating, assemblage [A]-regionally metamorphosed andalusite schists, progressively recrystallised to form [S]-sillimanite-bearing assemblages, then [C]-cordierite-K-feldspar-bearing assemblages and the highest grade [O]-orthopyroxene-bearing assemblages. Melt is produced by all the fluid-absent, mica-consuming reactions crossed that led to the formation these assemblages. Sources for reactions: (1) Holland & Powell (1990), (2) Richardson (1968), (3) Luth *et al.* (1964), (4) & (5) Thompson (1982), (6) Vielzeuf & Clemens (1992), (7) Holdaway & Lee (1977).

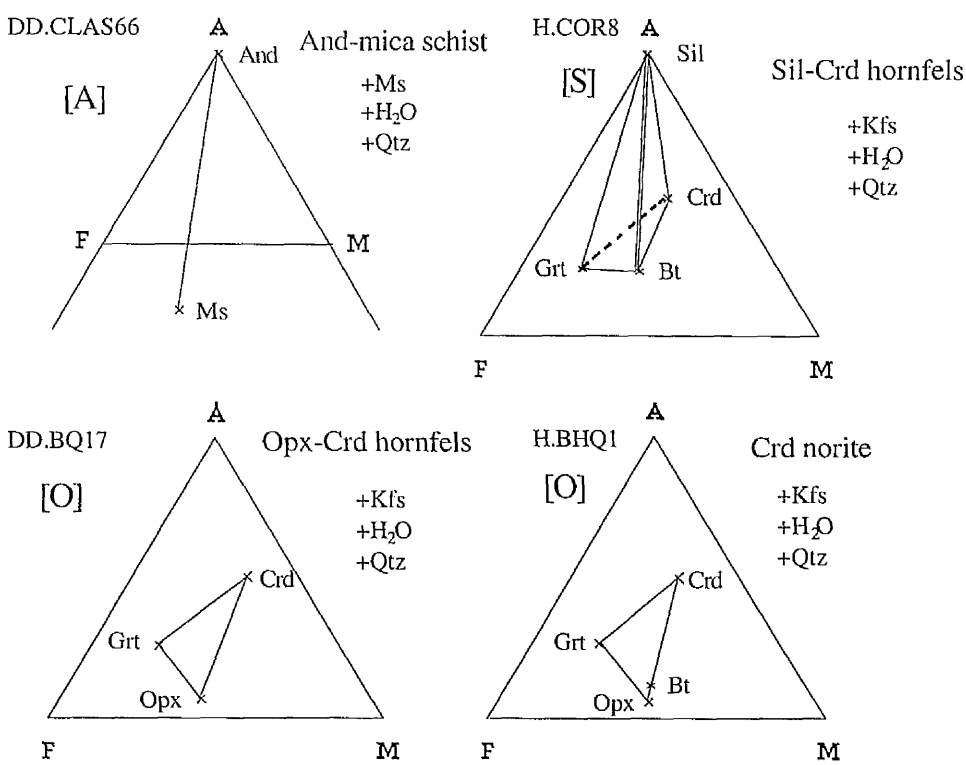

Figure 7.3.2 AFM projections for an andalusite schist, sillimanite-cordierite hornfels, orthopyroxene-cordierite hornfels and a cordierite norite, displaying the progressive change in AFM mineral parageneses during isobaric heating from intrusion of the Huntly mafic igneous body.

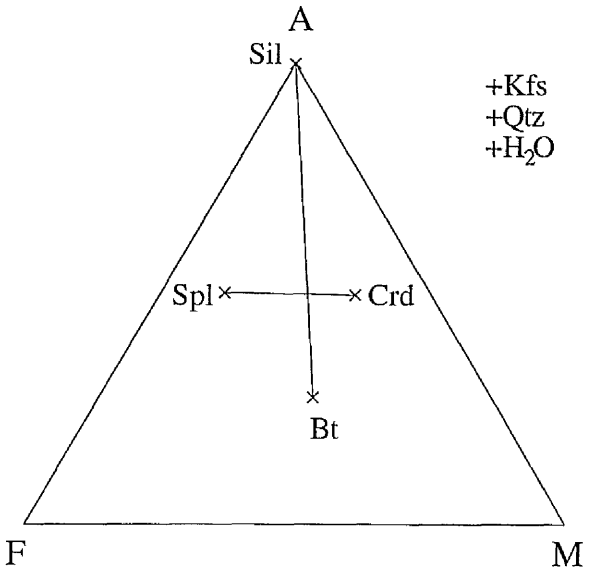

Figure 7.4.1 AFM projection, plotting sillimanite and biotite compositions from DD.DUN1, with cordierite and spinel from DD.DUN4. The projection displays the reaction by which the cordierite and spinel clots (Plate 5.5.6) form pseudomorphs after sillimanite:

sillimanite + biotite + quartz = cordierite + spinel + melt. [7.9]

CHAPTER 8 GEOTHERMOBAROMETRY

8.1 Introduction

In this study geothermobarometry is used to give temperature and pressure estimates which represent the peak conditions at which the partially melted rocks and the surrounding regionally metamorphic rocks crystallised. The acquisition of well-constrained pressure-temperature estimates is important as it helps allow the following to be determined:

(i) The temperature and pressures at which partial melting and the formation of the resultant melts and restitic hornfelses occurred.

(ii) Whether or not the temperatures gained were sufficiently high to allow extensive partial melting (major fluid-absent melting by biotite consuming reactions will only occur at temperatures in excess of 850°C).

(iii) The depth at which the Huntly Gabbro was intruded.

(iv) The regional P-T conditions prevalent at the time of intrusion of the Huntly mass, and metamorphic effects (if any) on the surrounding regionally metamorphosed rocks by the gabbro.

For any given rock with a number of mineral phases present together at equilibrium a series of reactions may be written between the end-members of the minerals present if enough minerals coexist. The varying concentrations (or, more strictly, activities) of the end-members in their respective solid solutions is a function of both pressure and temperature. Reactions which are more sensitive to temperature change than pressure (e.g. Fe-Mg exchange reactions) make good potential geothermometers, whilst reactions with a large ΔV (volume change) are of use in geobarometry. The mineral reactions which are of greatest use to the petrologist are those which have been calibrated, by accurate thermodynamic data of mineral end-members, and by carefully reversed experiments over the pressure-temperature range at which the reaction occurs.

8.2 Thermodynamic Basis for Geothermobarometry

The thermodynamic basis for geothermobarometry is well established (see e.g. Wood & Fraser, 1977 ; Fraser, 1977 ; Essene, 1989). Briefly, once an equilibrium reaction has been identified for a set of end-members presented in an equilibrium assemblage, it is possible, in principle, to calculate an isopleth (a line on a P-T diagram corresponding to a particular value of K, the equilibrium constant) for that assemblage. If the reaction is

$$\underset{\text{phase p}}{dA} + \underset{\text{phase q}}{eB} = \underset{\text{phase r}}{fC} \qquad [8.1]$$

where d, e and f are the molecular coefficients of each end-member components A, B and C, respectively, K is defined as

$$K = \left[\frac{(a_C^r)^f}{(a_A^p)^d . (a_B^q)^e} \right] \qquad [8.2]$$

where a_i^j is the activity (or effective concentration) of component i in phase j. For any given reaction, K is a function of pressure and temperature only. For any given reaction the pressure-temperature plane may therefore be contoured with a set of isopleths, provided that the necessary thermodynamic data are available for all the end-members involved. Chemical analysis of coexisting minerals yields concentration data, from which activities can be estimated (see below). Once this is done, K is fixed, and the pressure-temperature conditions of equilibration are constrained to lie somewhere on that isopleth. Application of a second equilibrium (one with a dP/dT slope different from the first) to the same assemblage from the same locality, provides a second isopleth that intersects the first, thus providing a "fix" on the pressure-temperature conditions of equilibrium.

For a balanced chemical reaction at equilibrium the equilibrium constant is related to pressure and temperature by the equation:

$$\Delta G^{\circ}_{(r)P,T} = -RTLnK \qquad [8.3]$$

where $\Delta G^{\circ}_{(r)P,T}$ is the free energy change of the reaction at the pressure and temperature of interest and R is the gas constant. ΔG° at one bar pressure and the temperature of intersect may be given by the equation;

$$\Delta G^{\circ}_{(r)1,T} = \Delta H^{\circ}_{(r)1,298} + \int_{298}^{T} \Delta Cp dT - T(\Delta S^{\circ}_{(r)1,298} + \int_{298}^{T} \frac{\Delta Cp}{T} dT) \qquad [8.4]$$

where $\Delta H^{\circ}_{(r)1,298}$, $\Delta G^{\circ}_{(r)1,298}$ and ΔC_p are the standard state enthalpy change, entropy change and heat capacity change of reaction, respectively.

In each case, the Δ quantity is the difference between the value for the product assemblage and that of the reactant assemblage for a balanced reaction. For an individual end-member, heat capacity and C_p, can be expressed in polynomial form:

$$C_p = a + bT + cT^{-2} + dT^{-0.5} + eT^2 \qquad [8.5]$$

where a, b, c, d and e are coefficients that depend on the end-member in question. Extrapolating $\Delta G^{\circ}_{(r)1,T}$ from 1 bar to the pressure of interest yields:

$$\Delta G^{\circ}_{(r)P,T} = \Delta G^{\circ}_{(r)1,T} + (P-1)(\Delta Vs + \Delta(\alpha V)(T-298) - \Delta(\beta V)P/2) + n_i RT\ln f_i \qquad [8.6]$$

where ΔVs is the volume change for solids, f_i is the fugacity of any gas species present in the reaction, n_i the molecular coefficient of the gas, α is the coefficient of isobaric volume expansion, and β the coefficient of isothermal volume compressibility.

Combining equations 8.3 and 8.6 gives the "master equation":

$$0 = \Delta G^{\circ}_{(r)1,T} (P-1)(\Delta Vs + \Delta(\alpha V)(T-298) - \Delta(\beta V)P/2) + n_i RT\ln f_i + RT\ln K \qquad [8.7]$$

where $\Delta G^{\circ}_{(r)1,T}$ is given by equation 8.4. Provided that $\Delta H^{\circ}_{(r)1,298}$, $S^{\circ}_{1,298}$, $V^{\circ}_{1,298}$, α, β, a, b, c, d and e quantities are known for all end-member components in a reaction, and f_i is known as a function of pressure and temperature for the gas phase(s), then equation 8.7 can be solved iteratively for pressure at any given value of temperature, or vice versa.

8.3 Calculation of Mineral Activities From Mineral Probe Data

8.3.1 Introduction and Theory

The activity of a component i represents the probability of i being present in a defined space at any one time. In minerals which exhibit solid solution, the defined space is the mixing site (j), on which two or more components can occur in varying quantities. The activity of component i in the mixing site j can then be calculated using the equation:

$$a_i^j = (X_i^j)^n \qquad [8.8]$$

Where $(X_i^j)^n$ equals the number of moles of i in j, and n equals the number of cations needed to fill site j in one formula unit. This equation is only valid if simple ionic mixing is assumed, with complete cation disorder and the cations of i being randomly distributed on the site j.

Ideal-mixing in natural systems rarely (if ever) occurs as solid solutions in silicate systems deviate from ideality because H_{mix} (enthalpy of mixing) is never exactly equal to zero. This occurs because any two elements mixing on a site will have different chemical and physical properties (e.g. atomic charges). Activity models can then be made, based on the association or avoidance of an element on a mixing site and the equation for activity on a given site is re-written as:

$$a_i^j = (X_i^j \cdot \gamma_i^j) \qquad [8.9]$$

γ is the activity coefficient, and defines the probability of atomic association or avoidance and, for a binary mixing site with mixing of atoms of A and B, is given by the equation:

$$RT\ln\gamma_A = W_G(1-X_A)^2 \qquad [8.10]$$

The term W_G is the interaction parameter and represents the difference in energy, or strength of bonding between A-B and the average of the A-A and B-B bonds. The above equation applies to symmetrical or regular solution mixing, which occurs when the strength of the A-B bond when X_A is close to zero is assumed to be equal to the A-B bond when X_B

is close to zero. When they are unequal an asymmetrical or sub-regular mixing model is required and two W parameters are needed.

Minerals which have no solid solution and have fixed compositions are considered to be pure and therefore for these end members a = 1. In this study this applies to quartz, sillimanite, rutile, and when no Mn or Mg is present, ilmenite.

For many minerals which do have solid solution, W_G values are assumed to be near or equal to zero and the ideal mixing equation 8.1 is used to calculate the activity of mixing cations on individual mixing sites. Experimental data on WG are available for a few minerals (e.g. garnets, feldspars, some pyroxenes), but are lacking for most rock-forming minerals, and for these it must be assumed that $W_G = 0$.

8.3.2 Cordierite activities

Cordierite has the general formula $(Fe,Mg)_2[Al_4Si_5O_{18}].nH_2O$ where n can be any value between 0 and 1.2 (Johannes & Schreyer, 1981). For the calculation of activities, mixing is assumed to occur only between Fe^{2+} and Mg on a single octahedral site. Analyses from samples where the cation total is systematically greater than 11 were recalculated for Fe^{3+}, and therefore the activities are calculated as follows:

$$a^{Crd}_{Fe\text{-}Crd} = (X^{Crd}_{Fe^{2+}})^2 \cdot (X^{Crd}_{Al})^4 \cdot (1-X^{Crd}_{H_2O}) \qquad [8.11]$$

$$a^{Crd}_{Mg\text{-}Crd} = (X^{Crd}_{Mg})^2 \cdot (X^{Crd}_{Al})^4 \cdot (1-X^{Crd}_{H_2O}) \qquad [8.12]$$

8.3.3 Orthopyroxene activities

In orthopyroxene, mixing occurs on three site, two M1 and M2 octahedral sites and a single T tetrahedral site. However, mixing on the M1 and T sites is not independent, with coupled substitution of $Al^{M1}Al^{T}$ for $Mg^{M1}Si^{T}$ occurring ('Tschermak' substitution). The implication of this is that, provided that mixing on the M2 and M1 sites is accounted for, no extra entropy is introduced by Al·Si mixing on the T sites, since that is coupled to mixing on the M1 site. No T-site terms therefore appear in the a-X equations. Ca, Na, and Mn are assumed to only occur in M2 sites and Ti, Al^{vi} and Fe^{3+} in M1. Mixing between Fe^{2+} and

Mg is assumed to occur equally on both sites (e.g. Perkins *et al.*, 1985). The ideal, two-site model of Wood & Banno (1973) is then used for calculating the activities of the three end members, enstatite, ferrosilite and Mg-Tschermak component:

$$a_{En}^{Opx} = X_{Mg}^{M1} \cdot X_{Mg}^{M2} \quad [8.13]$$

$$a_{En}^{Opx} = X_{Fe^{2+}}^{M1} \cdot X_{Fe^{2+}}^{M2} \quad [8.14]$$

$$a_{Mg\text{-}Tsch}^{Opx} = X_{Al}^{M1} \cdot X_{Mg}^{M2}. \quad [8.15]$$

8.3.4 Biotite and muscovite activities

Difficulties in obtaining reliable experimental data on the mixing properties in biotite mean that ideal mixing is assumed when calculating biotite activities. Holland & Powell (1990) and Hoisch (1991) presented biotite activity models which assumed ideal-mixing on all sites. However, the models used in this study are those presented by Patiño Douce *et al.* (1993), based on experimental work from a natural metapelitic rock. The models presented take into account partial decoupling of Al^{vi} and Al^{iv} and excess octahedral mixing properties. Octahedral Ti and Al are attributed to the M2 sites, whilst the Fe/Mg ratios are assumed to be equal on both M1 and M2. The ideal-activity models presented are:

$$a_{phlogopite}^{biotite} = \frac{256}{27} \cdot (X_{Mg}^{M2})^2 \cdot (X_{Mg}^{M1}) \cdot (X_{Al}^{T}) \cdot (X_{Si}^{T})^3 \cdot (X_{K}^{A}) \cdot (X_{OH}^{H})^2 \quad [8.16]$$

$$a_{eastonite}^{biotite} = 64 \cdot (X_{Mg}^{M2}) \cdot (X_{Al}^{M1}) \cdot (X_{Al}^{M1}) \cdot (X_{Al}^{T})^2 \cdot (X_{Si}^{T})^2 \cdot (X_{K}^{A}) \cdot (X_{OH}^{H})^2 \quad [8.17]$$

Activities for annite and siderophyllite can be calculated by substituting Fe for Mg in these two equations.

The muscovite activity model given by Patiño Douce *et al.* (1993) is also used in this study, and is given as:

$$a^{muscovite} = 64 \cdot (X_{Al}^{M2})^2 \cdot (X_{Al}^{M2}) \cdot (X_{V}^{T}) \cdot (X_{Si}^{T})^3 \cdot (X_{K}^{A}) \cdot (X_{OH}^{H})^2 \quad [8.18]$$

8.3.5 Feldspar activities

As with orthopyroxene and biotite, feldspars display coupled substitution, with Ca, Na and K substituting on an A site and Al with Si on a T site. That mixing in feldspars is non-ideal is without doubt (i.e. there is only limited solid solution between Na and K until

extreme metamorphic temperatures are reached (Deer *et al.*, 1992)). Newton *et al.* (1980), presented a model for anorthite activity in plagioclase, which was further refined by Newton (1983). This model was widely used in geothermobarometry (e.g. Perkins & Chipera, 1985), but is limited as it ignores the effects of Al-Si ordering and of small K contents in plagioclase. The model of Elkins & Grove (1990), which is used in this study, gives interaction parameters for anorthite, albite and orthoclase, calculated from data from experiments on natural feldspars, and from thermodynamic data.

Application of the model of Elkins & Grove (1990) in geothermobarometry gives P-T results which agree well with stabilities of the aluminosilicates as calculated by Applegate & Hodges (1993). Activities for anorthite and alkali feldspar are calculated for use in this study, and the equations and interaction parameters given by Elkins & Grove (1990) are shown in Appendix III.

8.3.6 Garnet activities

The non-ideal nature of mixing between Fe, Mg, Ca and Mn in garnets is well known. Earlier attempts to determine garnet activities neglected the effect of Mn in garnet (e.g. Haselton & Newton, 1980), and were only applicable to garnets with a very low spessartine content. More recently several attempts have been made to model quaternary mixing in garnet (Hodges & Spear, 1982 ; Ganguly & Saxena, 1984 ; Berman, 1990). These activity models all give differing results which in turn will lead to a divergence in pressure-temperature estimates.

The model of Berman (1990) is chosen in this study. This model was developed by mathematical programming of reversed phase-equilibrium and thermodynamic data from the internally consistent data set of Berman (1988). Application of the Berman (1990) model to geothermobarometry gives a good convergence when various equilibria are applied to a single P-T granulitic terrain, and P-T estimates from aluminosilicate-bearing assemblages plot within, or close to the stability fields of andalusite, sillimanite and kyanite (Berman, 1990, Figure 13).

The equations used to calculate the activity coefficients, and the W_H values given for there use are shown in Appendix III. Once calculated these activity coefficients are used to calculate garnet activities as follows:

$$a_{Alm}^{Grt} = (X_{Fe}^{Grt} \cdot \gamma_{Fe})^3 \cdot (X_{Al}^{Grt})^2 \quad [8.19]$$

$$a_{Py}^{Grt} = (X_{Mg}^{Grt} \cdot \gamma_{Mg})^3 \cdot (X_{Al}^{Grt})^2 \quad [8.20]$$

$$a_{Gr}^{Grt} = (X_{Ca}^{Grt} \cdot \gamma_{Ca})^3 \cdot (X_{Al}^{Grt})^2 \quad [8.21]$$

8.4 Use of the Computer Program THERMOCALC

8.4.1 Introduction

The computer program THERMOCALC allows the calculation of pressures and temperatures from the mineral end-member activities for a given rock. The program can be used to give average pressures and/or temperatures for a single rock, or for calculation of the pressures or temperatures of reactions between selected end-members.

The first version of THERMOCALC was created by Powell & Holland (1988), and was developed from the internally-consistent dataset of Powell & Holland (1985) and Holland & Powell (1985), which contained thermodynamic data for 43 mineral and fluid end-members. An enlarged and updated dataset, which included thermodynamic data for 123 end-members was given by Holland & Powell (1990). The most recently updated version, THERMOCALCv2.3 is used in this study, and this program uses the thermodynamic dataset produced on 11th June, 1994.

8.4.2 Theory behind THERMOCALC

The theory behind the creation and application of THERMOCALC is mentioned only briefly here, but a full description of THERMOCALC and the methods used to create of the self-consistent independent dataset is given in the papers mentioned above.

The thermodynamic data used in THERMOCALC are fully self-consistent, i.e. they have been optimised *simultaneously* with respect to a large dataset of experimental reversals on various equilibria, rather than *sequentially* as with earlier datasets such as that of Helgeson *et al.* (1978). In extracting thermodynamic data from experiments, Holland & Powell (1985) took, for each end-member, best published values of the following quantities "as read": $V^\circ_{1,298}$, $S^\circ_{1,298}$, a, b, c, d, e, α, β. Existing fugacity data for H_2O and CO_2 were fitted to complete polynomal equations. Standard state enthalpies of formation from the elements ($\Delta H_f H^\circ_{1,298}$) for all the end members were then optimised simultaneously

using a least-squared approach; each resultant enthalpy value has an uncertainty associated with it.

The computer program THERMOCALC works by selecting a pressure value, and then varying values of temperature iteratively until the right hand side of equation 8.7 equals zero.

8.4.3 Calculation of errors by THERMOCALC

One of the main advantages of THERMOCALC, over pressure-temperature estimates from independent calibrations, is that the program generates realistic errors for it's pressure and temperature estimates. This is because the program allows the propagation of errors from uncertainties on the enthalpies of end-members, together with errors from activity composition data through thermobarometric calculations, to give overall errors on pressures and temperatures quoted as 1σ. The program requires the user to input errors generated from chemical variation in the form of the standard deviation of mean calculated activities. However, any overconfidence on the accuracy of activities is avoided, as the program has default values for the minimum standard deviations for each end-member, which account for errors caused by small mole fractions and uncertainties in the activity models used.

8.5 Error Estimation from Geothermobarometry

The estimation of many of the errors involved in geothermobarometry is problematic simply because there is no possible method available for direct measurement of pressures and temperatures from metamorphic terrains, and the calculations which are used contain a large number of uncertainties from both the thermodynamic data and the chemical measurements used. These errors can be both random and systematic.

8.5.1 Errors from data collection

Random errors come mainly from the collection of the chemical data from which mineral activities and distribution coefficients are calculated. These errors result from both random error from the electron microprobe measurements and from within-sample chemical variation. Within-sample variation can result from mineral zoning, and from retrogressive diffusion between minerals. Random errors can lead to large uncertainties in pressure and/or

temperature when low mole fractions of a particular element are being measured, as the standard deviations are frequently large and additionally, uncertainties in end-member activity models at low molar quantities can lead to large errors.

The random errors from chemical variation can be limited by using microprobe analyses from mineral cores, and by careful selection of analyses which meet stoichiometric tests for the mineral in question. In addition, increasing the number of analyses made for each mineral is more likely to give representative mean compositions, and smaller standard deviations of the data.

8.5.2 Errors from thermodynamic data

Errors from the thermodynamic data used in geothermobarometry are mainly systematic, and are constant in the application of each individual activity model, or calibrated geothermometer or geobarometer. These errors are slowly being reduced by additional experimental work on mineral end-members.

8.6 Results from Geothermometry

8.6.1 Garnet-biotite geothermometry

(a) Background and theory

The partitioning of Fe and Mg between coexisting garnet and biotite is strongly temperature-dependent, and relatively insensitive to pressure. The exchange reaction between garnet and biotite is written as:

$$Fe_3Al_2Si_3O_{12} + KMg_3AlSi_3O_{10}(OH)_2 = Mg_3Al_2Si_3O_{12} + KFe_3AlSi_3O_{10}(OH)_2 \quad [8.22]$$

garnet biotite garnet biotite.

The corresponding equilibrium constant for this reaction is written as the distribution coefficient $K_D = (Fe/Mg)_{Bt}/(Fe/Mg)_{Grt}$. Numerous attempts have been made to calibrate this reaction, the earliest of which were empirical calibrations (e.g. Frost, 1962 ; Saxena, 1969; Thompson, 1976 ; Goldman & Albee, 1977) of which the widely used equation from Thompson (1976), based on temperature estimates from natural assemblages, is used in this study.

Ferry & Spear (1978) presented the first calibration to be based on experimental work on pure biotite and garnet end-members. Their calibration is applicable for use on many garnet-biotite-bearing rocks. However, as the calibration ignores the effects of minor components in garnet or biotite, then the presence of significant concentrations of Mn and Ca in garnet is shown to lead to significant departures from the relationships of the calibration (Indares & Martignole, 1985). Therefore, the effects of Ca and/or Mn in garnet-biotite geothermometry has been widely studied, with new calibrations (many of which still rely on the experimental data of Ferry & Spear (1978) presented by, for example, Hodges & Spear (1982), Pigage & Greenwood, (1982), Ganguly & Saxena (1984) and Bhattacharya *et al.* (1992).

Indares & Martignole (1985) showed that the high Ti content in biotites from upper amphibolite and granulite facies rocks lead to inconsistencies in garnet-biotite geothermometry, with the calibrations of Thompson (1976), Goldman & Albee (1977) and Ferry & Spear (1978) all giving abnormally high temperatures (gained from garnet-clinopyroxene geothermometry) in granulitic rocks. Indares and Martignole (1985) then presented two new calibrations, using the original experimental data of Ferry & Spear (1978), with thermodynamic and empirical data to determine the effects of Ca and Mn in garnet and Ti and Al^{vi} in biotite.

Additional problems in garnet-biotite geothermometry in high-grade rocks result from post-peak metamorphic re-equilibration of the Fe and Mg and leading to temperature under-estimates. This down-temperature re-equilibration tends to have a much greater effect on biotite crystals, than in garnets, due to the open structure of biotite compared to the closed structure in cubic garnets (e.g. Loomis, 1975 ; Tracy *et al.*, 1976). The effects of this re-equilibration can be limited by using biotite samples with modally abundant biotite relative to garnet, and by only using analyses from matrix biotites (biotites close to, and contacting, garnets have higher Mg# than matrix biotites due retrogressive re-equilibration; Chapter 6.3.5).

(b) Strategy for garnet-biotite geothermometry

Ten or more analyses were taken from garnet cores which had not undergone any retrogressive re-equilibration (see zonation profile diagrams in Chapter 6). Upwards of ten

biotite analyses were taken from the cores of matrix biotite crystals, at least 500 μm away from the nearest garnet. From the rock samples analysed, the following meet the criteria for biotite having a greater modal abundance than garnet; DD.SIN1, DD.SIN101, H.COR8, DD.BQ38, DD.CASB2i,5, and DD.TYQ5.

Temperature estimates were made from the calibrations of Thompson (1976), Ferry & Spear (1978), Indares & Martignole (1985), Bhattacharya (1992) and from the computer package THERMOCALC. The calibrations of Bhattacharya (1992) are based on earlier calibrations from Ganguly & Saxena (1984) and Hackler & Wood (1988), but with improved mixing data for the effects of Mn and Ca in garnet activities. For temperature estimates using the THERMOCALC program, activities for pyrope and almandine in garnet were calculated using the non-ideal mixing model of Berman (1990) and the ideal mixing model of Patiño Douce (1994) for phlogopite and annite.

(c) Choice of preferred calibration(s)

All the temperature estimates from the calibrations used are given in Table 8.6.1. For all of the samples analysed, bar the regionally metamorphosed rocks, there is a large divergence in the temperatures given by the various calibrations. The temperature estimates from THERMOCALC, Thompson (1976) and Ferry & Spear (1978), which do not take into account the effect of minor components in garnet and biotite, all give generally much higher temperatures for the hornfelses and igneous-textured rocks than the other calibrations. Indares & Martignole (1985) showed that these high temperature estimates were an artefact of the high Ti contents in biotites from high-grade rocks. This is best highlighted by the estimates given by THERMOCALC, which gives temperatures in excess of 950°C (up to 1200°C for sample H.BHQ1!) for the majority of the igneous-textured rocks. These temperatures are well in excess of the maximum temperatures at which even Ti saturated biotite can remain stable, and therefore can not represent the true temperatures at which the biotite crystallised. Therefore the calibrations of Ferry & Spear (1978), Thompson (1976) and THERMOCALC are not applicable for the orthopyroxene hornfels or igneous-textured rocks.

Temperatures given by the calibrations of Indares & Martignole (1985) are systematically lower than those given by all the other calibrations. The low temperatures are

due to the introduction of interaction parameters for Ti and Al^{vi} in biotite and Mn and Ca in garnet, into the original calibration of Ferry & Spear (1978). However, the temperatures given for the sillimanite-cordierite hornfelses are 90 to 100°C lower than the minimum temperatures given by garnet-cordierite geothermometry (Table 8.6.2), suggesting that these calibrations possibly over-correct for the effects of the minor components.

The calibrations of Bhattacharya *et al.* (1992), which include improved garnet Ca-Mn mixing data, give temperatures intermediate to those of Indares & Martignole (1985) and Ferry & Spear (1978). The temperatures given by the two Bhattacharya *et al.* (1992) calibrations are in close agreement with the garnet-cordierite temperatures of Nichols *et al.* (1992) for the sillimanite-cordierite hornfelses. Therefore the calibrations of Bhattacharya *et al.* (1992) are taken to best represent the temperatures at which the Fe and Mg contents of biotite and garnet equilibrated together.

(d) Results from garnet-biotite geothermometry

All temperatures quoted in this section are taken from the calibrations of Bhattacharya *et al.* (1992), and are given to the nearest 10°C.

(i) Regionally Metamorphosed Rocks

The garnet-biotite gneisses from locality 2a (DD.SIN1 and DD.SIN101) give temperatures of 620 and 630°C. However, sample DD.SIN2 from locality 2b (150 metres west from locality 2a) gives temperatures of 560 and 570°C.

(ii) Sillimanite or orthopyroxene-bearing hornfelses

Of the sillimanite-cordierite hornfels, DD.DUN1 gives a temperature of 600°C, whilst the alkali-feldspar bearing H.COR8 gives a temperate of 680°C. The orthopyroxene-bearing hornfels H.COR10 records a temperature of 740°C.

(iii) Cordierite norites

The cordierite norites from Battlehill Quarry (locality 3a ; samples H.BHQ1, DD.BQ38) give the record the highest temperatures, varying from 750 to 760°C. The samples from Castle Bridge (locality 3c; DD.CASB2i,5) give a slightly lower temperature of

720°C. The widest spread in temperatures is shown to the samples from Dunbennan Woods (locality 3d ; DD.DUN4,9b,12), with recorded temperatures varying from 660 to 750°C.

(iv) Garnet tonalites

The two samples from Hill of Cormalet (locality 3e) give differing temperatures, with orthopyroxene-bearing DD.CUM19 recording temperatures of 690 and 710°C and DD.CUM22 recording temperatures of 780 and 790°C. The garnet tonalite from Ternemny Quarry (locality 3j ; sample DD.TYQ5) gives a temperature of 730°C.

(v) Garnet-anthophyllite gneiss

The garnet-anthophyllite gneiss from Barry Hill (locality 3f; sample DD.BAR1) gives garnet-biotite temperatures of 680°C and 690°C.

8.6.2 Garnet-cordierite geothermometry

(a) Background and theory

The Fe-Mg exchange reaction between garnet and cordierite is written as:

$$2Fe_3Al_2Si_3O_{12} + 3Mg_2Al_4Si_5O_{18} = 2Mg_3Al_2Si_3O_{12} + 3Fe_2Al_4Si_5O_{18} \qquad [8.23]$$

garnet cordierite garnet cordierite

As with garnet-biotite geothermometry, early attempts to calibrate the garnet-cordierite equilibrium used empirical methods, based on natural samples (i.e. Thompson, 1976 ; Holdaway & Lee, 1977). However, these early calibrations assumed ideal mixing of Fe and Mg in both garnet and cordierite. The calibration model of Bhattacharya *et al.* (1988) incorporates non-ideal mixing models for both garnet and cordierite, derived from the garnet mixing data of Ganguly and Saxena (1984), and data from natural coexisting cordierites. Nichols *et al.* (1992) using experiments in the spinel-cordierite-quartz-sillimanite field, combined with earlier garnet-cordierite data, presented a new calibration. This calibration assumes ideal solid solution in cordierite, but requires the user to incorporate the garnet activity models of Berman (1990) to give improved K_D values for the equilibrium.

(b) Strategy for garnet-cordierite geothermometry

Upwards of ten analyses were taken from the cores of garnet and cordierite crystals. Analyses were not taken from cordierites which contacted garnets, or which were heavily pinitised. For the calibration of Nichol *et al.* (1992) activities were calculated from the garnet data using the models of Berman (1990).

(c) Choice of preferred calibration(s)

Temperature estimates for garnet-cordierite geothermometry from the calibrations of Thompson (1976), Holdaway & Lee (1977), Bhattacharya *et al.* (1988), Nichols *et al.* (1992), and THERMOCALC are given in Table 8.6.2. Apart from THERMOCALC, all of the calibrations used give temperatures substantially lower than the temperatures recorded from garnet-orthopyroxene geothermometry (Table 8.6.3), with the temperatures recorded for the orthopyroxene-cordierite hornfelses being up to 192°C lower. The temperatures given by THERMOCALC are consistently higher than those given by all other garnet-cordierite calibrations, with the temperatures recorded by the many of the cordierite-norites being anomalously high (e.g. sample H.BHQ1 gives a garnet-cordierite temperature of 1150°C, compared to a garnet-orthopyroxene temperature of 860°C, also using THERMOCALC). The choice of a suitable garnet-cordierite thermometer is therefore problematic, due to uncertainties in cordierite activity-relations caused by the presence of varying amounts of H_2O and CO_2 in the mineral, and for the purposes of comparisons of temperatures between various rock types the calibration of Nichols *et al.* (1992) is used as it was formulated using updated experimental data and non-ideality in garnet is accounted for.

The temperature errors given by the THERMOCALC, although large, are taken to also apply to the other calibrations. This is because these errors not only take into account within-sample chemical variation, but also inherent errors from uncertainties in the activity models used and the thermodynamic data for garnet and cordierite end members.

(d) Results from garnet-cordierite geothermometry

(i) Sillimanite or orthopyroxene-cordierite hornfelses

The sillimanite-cordierite hornfelses record lower temperatures than the orthopyroxene-cordierite hornfelses, with temperatures of 600 and 720°C, compared to 760 to 880°C for the orthopyroxene-bearing rocks. Errors given by THERMOCALC are in excess of 111°C, up to 218°C for sample DD.PIR1.

The temperatures given for the sillimanite-cordierite hornfelses are in reasonably close agreement with the garnet-biotite temperatures given for these rocks.

(ii) Cordierite norites

As with the garnet-biotite temperatures, the highest temperatures recorded by the cordierite norites for garnet-cordierite geothermometry are given by the samples from Battlehill Quarry (DD.BQ38 and H.BHQ1), with both samples recording a temperature of 820°C. The two samples from Castle Bridge give divergent temperatures, with DD.CASB5 recording 700°C and DD.CASB2i a higher temperature of 790°C. Temperatures of 680 and 720°C are given by the samples from Dunbennan Woods.

Errors given by THERMOCALC are large for estimates from the cordierite norites, with average errors in the order of ±180°C.

(iii) Garnet-anthophyllite gneiss

The garnet-anthophyllite gneiss from Barry Hill (DD.BAR1) records a garnet-cordierite temperature of 690°C, which is in good agreement with the garnet-biotite temperature estimate.

8.6.3 Garnet-orthopyroxene Fe-Mg exchange geothermometry

(a) Background and theory

The Fe-Mg exchange reaction between garnet and orthopyroxene is written as:

$$2Fe_3Al_2Si_3O_{12} + 3Mg_2Si_2O_6 = 2Mg_3Al_2Si_3O_{12} + 3Fe_2Si_2O_6 \qquad [8.24]$$

garnet orthopyroxene garnet orthopyroxene

Calibrations for this equilibrium have been made by Harley (1984a), Sen & Bhattacharya (1984), Lee & Ganguly (1988) and Bhattacharya *et al.* (1991). The early thermometer of Harley (1984a) was formulated from experimental work in the FMAS (FeO-MgO-Al_2O_3-SiO_2) and CFMAS (CaO-FeO-MgO-Al_2O_3-SiO_2) systems, and includes an interaction term for non-ideal Ca-Mg interactions. Sen & Bhattacharya (1984) presented an alternative garnet-orthopyroxene thermometer, with thermodynamic data for their calibration taken from earlier published data (e.g. O'Neill & Wood, 1979 ; Hasleton & Newton, 1980), and their equation also includes an interactive term for Ca-Mg mixing. The calibration presented by Lee & Ganguly (1988) was formulated from experimental work, and includes terms for Ca and Mn interaction in garnet from Ganguly & Saxena (1984). The most recent calibration, presented by Bhattacharya *et al.* (1991) uses updated interaction terms for Fe-Mg-Ca interaction in garnet, and claims to produce more consistent results than the calibrations of Harley (1984a) and Lee & Ganguly (1985).

(b) Strategy for garnet-orthopyroxene geothermometry

Ten or more analyses were taken from garnet and orthopyroxene mineral cores. Only analyses of orthopyroxenes which were not contacting garnets were used.

(c) Choice of preferred calibration and errors

Table 8.6.3 gives garnet-orthopyroxene Fe-Mg exchange temperatures from the calibrations of Harley (1984a), Sen & Bhattacharya (1984), Lee & Ganguly (1988), Bhattacharya *et al.* (1991) and from THERMOCALC.

Choice of a preferred calibration is problematic. However, the calibration of Harley (1984a) gives systematically low temperatures, whilst the calibration of Sen & Bhattacharya (1984) gives abnormally high temperatures. The most consistent temperatures (for rocks of the same rock type, from the same locality) are given by the calibration of Bhattacharya *et al.* (1991) and these temperatures are used below, with temperatures quoted to the nearest 10°C.

The errors given by THERMOCALC are large (173°C up to 334°C for sample DD.PIR4) and these errors are probably a result of uncertainties in garnet-orthopyroxene thermodynamic properties at higher temperatures, which is reflected by the positive

correlation between estimated temperature and calculated error (the exception to this being the large error given for DD.CUM19, which is probably a product of uncertainties from the high grossular content in the garnet).

(d) Results from garnet-orthopyroxene geothermometry

(i) Orthopyroxene-bearing hornfelses

The highest temperatures are recorded by the hornfelses from the northern end of Battle Hill Woods (locality 3b ; samples DD.PIR1,4), with temperatures of 960°C. However, THERMOCALC records a large error margin of 330°C. The hornfelses from Battlehill Quarry (300 m south from locality 3b, and nearer the southern margin of the gabbro body) give lower (yet still high) temperatures of 880 to 920°C. The orthopyroxene hornfels from Cormalet (H.COR10) gives a temperature of 800°C.

(ii) Cordierite norites

The cordierite norites give closely clustered temperatures with all recording between 810°C (DD.DUN4) and 880°C (DD.DUN12).

(iii) Garnet tonalite

The garnet tonalite DD.CUM19 gives a garnet-orthopyroxene temperature of 770°C.

8.6.4 Garnet-orthopyroxene Mg-Tschermak geothermometry

(a) Background and theory

A reaction between pyrope in garnet and enstatite in orthopyroxene buffers the alumina content in orthopyroxene, and is written as:

$$Mg_2Si_2O_6 \quad + \quad MgAl_2SiO_6 \quad = \quad Mg_3Al_2Si_3O_{12} \qquad [8.25]$$

orthopyroxene garnet

This reaction occurs due to coupled substitution of Mg·Si for Al·Al and is strongly sensitive to both temperature and pressure. Earlier attempts to use this equilibrium as a geobarometer were made by Wood (1974) and O'Hara & Yarwood (1978). Harley & Green (1982) presented a geobarometer, calibrated by experiments in the CMAS (CaO-

$MgOAl_2O_3SiO_2$) system. However, this 'geobarometer' is strongly temperature dependent (ΔT=20-30°C per kbar) and for low pressure terrains is of greater use as a geothermometer, especially if the pressures for the terrain have already been tightly constrained. Harley (1984b) produced a new garnet-orthopyroxene geobarometer. However, this geobarometer is much more pressure dependant (ΔT>100°C per kbar) than the Harley & Green (1982) calibration, and is mainly suited to studies in high-pressure terrains (i.e. pressures greater than 20 kbars) and is not used in this study.

(b) Strategy for garnet-orthopyroxene Mg-Tschermak geothermometry

As with garnet-orthopyroxene Fe-Mg exchange geothermometry, all analyses were taken from garnet and orthopyroxene cores.

Temperature estimates were made at reference pressures of 3.5, 4.5 and 5.5 kbars, which span the range of likely pressure values (see Droop & Charnley (1985) and geobarometric work presented below), using the calibration of Harley & Green (1982).

(c) Error estimation

Errors were calculated to 2σ from probe data. At any single pressure the calculated temperature errors were in the order of ±60°C. Errors inherent in the calibration itself are not given, though an error of ±2 kbar is quoted for the Harley (1984b) geobarometer, and if similar errors are assumed for the Harley & Green (1982) calibration then the temperature uncertainties for the calibration are probably in the scale of ±40 to 60°C (assuming ΔT values of 20 to 30°C per kbar).

(d) Results from garnet-orthopyroxene Mg-Tschermak geothermometry

Table 8.6.4 shows the temperature estimates from the calibration of Harley & Green (1982), with temperatures calculated for 3.5, 4.5 and 5.5 kbars.

(i) Orthopyroxene-bearing hornfelses

The orthopyroxene-cordierite hornfelses from Battlehill Quarry and the NW of Battle Hill Woods (DD.BQ17,41, H.BHQ1, DD.PIR1,4) record consistently close temperatures at 4.5 kbars, with temperatures varying from 880 to 920°C. These temperatures are in

reasonable agreement with those from the garnet-orthopyroxene Fe-Mg exchange thermometer of Bhattacharya *et al.* (1991), but higher than those given by the garnet-cordierite thermometer of Nichols (1992).

The orthopyroxene hornfels (H.COR10) gives a temperature of 790°C, in good agreement with temperatures from garnet-orthopyroxene Fe-Mg exchange geothermometry (800°C) and garnet biotite geothermometry (740°C).

(ii) Cordierite norites

The cordierite norites give temperatures from 800 to 880°C, with the highest temperatures being recorded by the rocks from Battlehill Quarry (DD.BQ38, H.BHQ1, and the lowest from Castle Bridge (DD.CASB2i, DD.CASB5). These temperatures agree reasonably with the temperatures from garnet-orthopyroxene Fe-Mg exchange geothermometry (820 to 880°C from calibration of Bhattacharya *at al.,* 1991), but are higher than the temperatures given by garnet-cordierite geothermometry (680 to 820°C, Nichols *et al.* (1992)).

(iii) Garnet tonalite

The garnet tonalite gives a temperature of 690°C, in close agreement to the garnet-biotite temperatures for this rocks (680 and 720°C, using calibration of Bhattacharya *et al.* (1992)), but lower than the temperature gained from garnet-orthopyroxene Fe-Mg exchange geothermometry (770°C, Bhattacharya *et al.*, 1992).

8.6.5 Other geothermometers

8.6.5.1 Biotite-orthopyroxene geothermometry

An Fe-Mg exchange reaction can be written between biotite and orthopyroxene:

$$3Fe_2Si_2O_6 + 2KMg_3AlSi_3O_{10}(OH)_2 = 3Mg_2Si_2O_6 + 2KFe_3AlSi_3O_{10}(OH)_2 \quad [8.26]$$

orthopyroxene biotite orthopyroxene biotite.

Sengupta *et al.* (1990) calibrated this reaction, and their calibration was used. The calculated temperatures are given in Table 8.6.5. The results give a wide scatter of temperatures, up to 100°C either side of garnet-biotite temperatures (Table 8.6.1).

8.6.5.2 Garnet-hornblende geothermometry

Graham & Powell (1984) calibrated a geothermometer for the garnet-hornblende Fe-Mg exchange reaction:

$$Fe_2Al_2Si_3O_{12} + Ca_2Mg_3Si_6Al_4O_{22}(OH)_2 = Mg_2Al_2Si_3O_{12} + Ca_2Fe_3Si_6Al_4O_{22}(OH)_2$$

garnet hornblende garnet hornblende. [8.27]

The accuracy and effectiveness of garnet-hornblende geothermometry is restricted due to uncertainties in amphibole solution models. The application of this geothermometer gives a temperature of 700°C, in good agreement with the garnet-biotite temperatures, but 110°C lower than the biotite-orthopyroxene temperature.

8.7 Geobarometry

8.7.1 Garnet-plagioclase-orthopyroxene-quartz geobarometry

(a) Background and theory

A geobarometer which can be applied on the majority of the orthopyroxene-bearing rocks in this study is used by the calibration of the reaction:

$$Ca_3Al_2Si_3O_{12} + 2Mg_3Al_2Si_3O_{12} = 3SiO_2 + 3Mg_2Si_2O_6 + 3CaAl_2Si_2O_8 \quad [8.28]$$

garnet garnet quartz orthopyroxene plagioclase.

This reaction was first used by Wood (1975), then by Perkins & Newton (1981) and Newton & Perkins (1982). An Fe equivalent for this reaction can also be written as:

$$Ca_3Al_2Si_3O_{12} + 2Fe_3Al_2Si_3O_{12} = 3SiO_2 + 3Fe_2Si_2O_6 + 3CaAl_2Si_2O_8 \quad [8.29]$$

garnet garnet quartz orthopyroxene plagioclase.

This Fe-reaction has been calibrated by Bohlen *et al.* (1983) and both the Fe and Mg reactions by Perkins & Chipera (1985), Essene (1989) and Bhattacharya *et al.* (1991).

(b) Strategy for Garnet-orthopyroxene-plagioclase-quartz geobarometry.

The plagioclase crystals present in the cordierite norites and garnet tonalites are zoned (Chapter 6.4.1 and 6.5.1) with Ab-rich, An-poor rims. For the purposes of pressure

estimates it is assumed that the plagioclase cores crystallised in equilibrium with garnet and orthopyroxene, as smaller non-zoned plagioclase crystals have similar compositions to the cores. Therefore only analyses from small plagioclase crystals and crystal cores are used. The orthopyroxene-cordierite hornfels samples DD.PIR1,4, H.BHQ5 and DD.BQ41 were not used for pressure estimates as all of these samples lack quartz, which is necessary to balance the two reactions.

End-member activities were calculated using the garnet models of Berman (1990), the anorthite model of Elkins & Grove (1990), and orthopyroxene using the two-site mixing model of Wood & Banno (1973). In addition, for the calibrations of Newton & Perkins (1982) and Bhattacharya *et al.* (1991) the activity models suggested by the authors were used to allow comparison with results from the preferred activity models. Orthopyroxene activities were calculated using the two-site mixing model of Wood & Banno (1972), except for the calibrations of Bhattacharya *et al.* (1991), which require the use of their own orthopyroxene activity model.

Pressure estimates were calculated at the temperatures given by garnet-orthopyroxene Fe-Mg geothermometry from the preferred calibration of Bhattacharya *et al.* (1991).

(c) Choice of preferred calibration

Table 8.7.1 gives the pressure estimates from garnet-orthopyroxene-plagioclase-quartz geobarometry given by the calibrations of Newton & Perkins (1982), Perkins & Chipera (1985), Essene (1990), Bhattacharya *et al.* (1991) and using THERMOCALC.

A large source of error in garnet-orthopyroxene-plagioclase-quartz geobarometry comes from the low grossular content in garnet, with uncertainties arising from both probe data and from activity relations. The calculation of reliable activities for the grossular component in garnet is therefore important, as shown by the fact that the activity models of Ganguly & Saxena (1984) and Newton (1983) give pressures up to 2 kbar lower than the preferred models of Berman (1990) and Elkins & Grove (1990) on the same calibration.

The calibrations of Perkins & Chipera (1985) show large discrepancies between the Fe and Mg end members irrespective of which activity models are used (a mean difference of 0.84 kbars between the Fe and Mg calibrations). These authors suggest that such discrepancies occur as a result of uncertainties in enstatite activities in Mg-poor

orthopyroxenes and suggest that the Mg-reaction should be ignored when Mg / (Mg + Fe) in orthopyroxenes is greater than 0.5. However, in their calibration Bhattacharya *et al.* (1991) present a new model for orthopyroxene activities, and the use of these, in addition to the models of Berman (1990) and Elkins & Grove (1990), leads to a good agreement between the pressures given by the Fe and Mg-end member reactions (differences between the Fe and Mg pressures are ≥0.5 kbar for all but two samples). In addition, there is no relation between low Mg content in orthopyroxene and large pressure discrepancies between the Fe and Mg reactions when the calibrations of Bhattacharya *et al.* (1991) are used (e.g. Fe and Mg pressure estimates vary by 0.5 kbar for sample DD.CUM19, with X_{Mg}^{Opx} 0.25, and vary by 1.4 kbar in sample DD.CASB2i, with X_{Mg}^{Opx}0.53). Therefore the calibrations of Bhattacharya *et al.* (1991) are preferred here.

(d) Results from garnet-orthopyroxene-plagioclase-quartz geobarometry

(i) Orthopyroxene-bearing hornfelses

The orthopyroxene-cordierite hornfels from Battlehill Quarry (DD.BQ17) yields pressures of 4.4±1.5 kbar (Fe) and 4.7±1.6 kbar (Mg). Higher pressures are given by the orthopyroxene hornfels from Cormalet (H.COR10 ; locality 3e), which records pressures of 5.9±0.8 kbar (Fe) and 6.0±1.5 kbar (Mg).

(ii) Cordierite norites

A slightly greater variation is shown by the pressures given by the Fe calibration, which yields pressures of 3.8 to 5.2 kbars for the cordierite norites. The Mg calibration gives more closely clustered pressures from 4.4 to 5.7 kbars. The pressures recorded by the samples from different localities overlap. Errors vary from ±0.9 up to ±2.2 kbars.

(iii) Garnet tonalite

The garnet tonalite DD.CUM19 gives pressures of 5.9±0.8 kbar (Fe) and 5.4±1.5 kbar (Mg), consistent with the pressures given by the orthopyroxene hornfels (H.COR10) from the same locality.

8.7.2 Garnet-plagioclase-sillimanite-quartz geobarometry

(a) Background and theory

A Ca end-member reaction can be written between garnet, plagioclase, sillimanite and quartz:

$$3CaAl_2Si_2O_8 = Ca_3Al_2Si_3O_{12} + 2Al_2SiO_5 + SiO_2 \qquad [8.30]$$

plagioclase garnet sillimanite quartz.

The first attempts to calibrate this reaction was made by Ghent (1976). Newton & Haselton (1981), using the experimental data of Goldsmith (1980), presented a calibration which included improved considerations for non-ideality in grossular and anorthite. However, Powell & Holland (1990) noted that the geobarometer of Newton & Haselton (1981) had been calibrated by experiments performed at temperatures in excess of 1100°C and required a considerable amount of extrapolation back to the temperatures for which the geobarometer is commonly used (500-800°C). The calibration used in THERMOCALC, though, uses thermodynamic data extracted from a large number of reactions over a large temperature range (400-1300°C) and therefore Powell & Holland (1990) believe the entropy and volume relations of their calibration to be correct.

(b) Strategy for garnet-plagioclase-sillimanite-quartz geobarometry

Analyses were taken from garnet and plagioclase cores (garnets from HCOR8 display retrogressive Fe-rich rims; Chapter 6.3.2, Figure 6.3.7). Grossular and anorthite activities were calculated using the models of Berman (1990) and Elkins & Grove (1990) respectively. Activity models given by Ghent & Stout (1981) and Newton & Hasleton (1981) were also used to allow comparison.

The garnet-plagioclase-sillimanite-quartz geobarometer is also relatively temperature-sensitive (with a positive dP/dT slope of 1.0 to 2.6 kbar per 100°C) and therefore the acquisition of accurate temperature estimates is important. Two sets of pressures are then calculated, one at the temperatures given from the garnet-biotite geothermometer of

Bhattacharya *et al.* (1992), and another using the slightly higher garnet-cordierite temperatures from THERMOCALC.

(c) Choice of preferred calibration

Table 8.7.2 gives the calculated pressures from the calibrations of Ghent (1976), Newton & Haselton (1981), and THERMOCALC.

The use of the preferred activity models (Berman, 1990 ; Elkins & Grove, 1990) leads to the calculation of higher pressures (1.0 to 2.4 kbars), than if the original activity models are used. The pressures given by Newton & Haselton (1981) agree closely with those from THERMOCALC. However, temperatures given by THERMOCALC are preferred here, as the thermodynamic data Holland & Powell (1990) has been extracted from temperatures overlapping those at which pressures have been calculated in this study.

(d) Results from garnet-plagioclase-sillimanite-quartz geobarometry

Pressure of 4.9 and 5.5±1.1 kbars, calculated at 600°C (Grt-Bt) and 650°C (Grt-Crd) respectively are given for sample DD.DUN1. Sample H.COR8 yields higher pressures of 6.5 and 7.6 ±1.5 kbars at 680 and 780°C respectively.

8.7.3 Garnet-cordierite-sillimanite-quartz geobarometry

(a) Background and theory

A reaction can be written between almandine, Fe-cordierite, sillimanite and quartz:

$$2Fe_3Al_2Si_3O_{12} + 4Al_2SiO_5 + 5SiO_2 = 3Fe_2Al_4Si_5O_{18} \qquad [8.31]$$

garnet sillimanite quartz cordierite.

A similar Mg-end member reaction can also be written as:

$$2Mg_3Al_2Si_3O_{12} + 4Al_2SiO_5 + 5SiO_2 = 3Mg_2Al_4Si_5O_{18} \qquad [8.32]$$

garnet sillimanite quartz cordierite.

The use of these two equilibria in geobarometry is potentially very good, as both involve relatively large volume changes, and are less temperature dependent than the garnet-

plagioclase-sillimanite-quartz equilibrium. These two reactions yield the garnet-cordierite Fe-Mg-exchange reaction 8.23 when added together to eliminate quartz; any two of these reactions may be treated as independent.

Early calibrations of the Fe end-member equilibrium were made by Thompson (1976) and Holdaway & Lee (1978). However, neither of these calibrations takes into account the effects of the H_2O content in cordierite. Lonker (1981), then Bhattacharya (1986) both introduced XH_2O terms into their calibrations, and temperature estimates from both of these indicate that cordierite-bearing equilibria are stabilised to higher pressures by increased H_2O content. Nichols *et al.* (1992) presented calibrations for the Fe and Mg end members of the reaction, but omitted to account for the effect of XH_2O in cordierite.

(b) Strategy for garnet-cordierite-sillimanite-quartz geobarometry

Upwards of ten analyses were taken from garnet and cordierite cores. Garnet activities were calculated using the models of Berman (1990).

For application of the calibrations which require XH_2O to be specified, three different values of XH_2O were used, XH_2O=0, 0.25 and 0.5. The low modal abundance of cordierite in the sillimanite-bearing hornfelses made the extraction of this mineral to allow determination of the total volatile mass impossible. However, the high abundance of (hydrous) biotite in the sillimanite-cordierite hornfelses rocks, compared to the relative absence of this mineral in the orthopyroxene-cordierite hornfelses, suggests that the sillimanite-bearing rocks equilibrated at higher aH_2O conditions than the anhydrous orthopyroxene-bearing rocks. However, it is suggested that the cordierite in the sillimanite-bearing hornfelses may have had similar cordierite volatile contents as the (biotite-bearing) cordierite norites. The total volatile content from the cordierites from the cordierite norite sample DD.BQ38 infer a maximum $X_{H_2O}^{Crd}$ value of approximately 0.3-0.35. Taking into account that the sillimanite-bearing hornfelses could contain slightly different $X_{H_2O}^{Crd}$ contents to the cordierite norites, preferred $X_{H_2O}^{Crd}$ values of 0.25 and 0.5 are used here.

(c) Choice of preferred calibration(s)

Pressure estimates from the calibrations of Lonker (1981), Bhattacharya (1986) and from THERMOCALC are given in Table 8.7.3. All of the pressures given from the Fe end-

member calibrations give similar pressures. However, pressures for the Mg end-member equilibrium from THERMOCALC give pressures up to 1.6 kbar higher than the Fe version. The calibrations of Bhattacharya (1986) and of THERMOCALC are chosen here as both give similar pressures for the Fe-version, and THERMOCALC allows comparison with the Mg-equilibrium, and gives credible error margins.

(d) Results from garnet-cordierite-sillimanite-quartz geobarometry

Pressures from the Fe end-member calibrations of Bhattacharya (1986) and THERMOCALC yield pressures from 4.2 to 4.4 kbar at $XH_2O = 0.25$, whilst pressures from 4.6 to 5.0 kbars are given at $XH_2O = 0.5$. The errors calculated by THERMOCALC are ±0.41 kbar for DD.DUN1 and ±0.45 kbar for H.COR8.

Pressures given by THERMOCALC for the Mg end-member reaction are similar to those given by the Fe-reaction for DD.DUN1 (4.1±0.62 and 4.7±0.62 kbar at XH_2O=0.25 and 0.5 respectively), though pressures up to 1.6 kbar higher are given by sample H.COR8 (5.7±0.67 and 6.3±0.67 kbar at XH_2O=0.25 and 0.5 respectively.

8.7.4 Other Geobarometers

8.7.4.1 Garnet-rutile-ilmenite-plagioclase-quartz geobarometry

Bohlen & Liotta (1986) presented a geobarometer based on the equilibrium:

$$CaFe_2Al_2Si_3O_{12} + 2TiO_2 = 2FeTiO_3 + CaAlSi_3O_8 + SiO_2 \qquad [8.33]$$

garnet rutile ilmenite plagioclase quartz.

The calibration of Bohlen & Liotta yields pressures of 5.8 kbars for the two regionally metamorphosed rocks from Cairnie (localities 1a and 1b), DD.SIN2 and DD.SIN101. However, using updated experimental data, the calibration of Essene (1990) yields pressures of 4.8 (DD.SIN2) and 5.6 kbar (DD.SIN101).

8.7.4.2 Garnet-muscovite-plagioclase-biotite geobarometry

Two equilibria involving garnet, biotite, plagioclase and muscovite can be written as:

$$\underset{\text{garnet}}{Mg_3Al_2Si_3O_{12}} + \underset{\text{garnet}}{Ca_3Al_2Si_3O_{12}} + \underset{\text{muscovite}}{KAl_3Si_3O_{10}(OH)_2} = \underset{\text{plagioclase}}{3CaAl_2Si_2O_8} + \underset{\text{biotite}}{KMg_3AlSi_3O_{10}(OH)_2} \quad [8.34]$$

and;

$$\underset{\text{garnet}}{Fe_3Al_2Si_3O_{12}} + \underset{\text{garnet}}{Ca_3Al_2Si_3O_{12}} + \underset{\text{muscovite}}{KAl_3Si_3O_{10}(OH)_2} = \underset{\text{plagioclase}}{3CaAl_2Si_2O_8} + \underset{\text{biotite.}}{KFe_3AlSi_3O_{10}(OH)_2} \quad [8.35]$$

These two equilibria were calibrated by Ghent & Stout (1982), using the experimental data of Ferry & Spear (1978). The Fe version of the geobarometer is more temperature-dependent than the Mg version, and when both are plotted together will give a fix on temperature as well as pressure, with the resultant temperature equalling the temperature of the garnet-biotite geothermometer of Ferry & Spear (1978).

Application of these calibrations on the garnet-mica schist DD.SIN2 (Cairnie; locality 1b) yields a pressure of 4.8 kbar at 610°C.

8.8 Use of THERMOCALC for Average P-T Calculations

8.8.1 Strategy for use of THERMOCALC

Samples which contained a large number of peak-paragenesis minerals were chosen for average pressure-temperature calculations using the THERMOCALC program. End-member activities and their standard deviations were calculated using the preferred models described in Section 8.3.

(i) Regionally metamorphosed rocks

The samples DD.SIN2 and DD.SIN101 were chosen for average pressure temperature calculations as both contained a large number of mineral phases which appeared to coexist at equilibrium. An H_2O-bearing fluid is assumed to exist in both samples, and results were then calculated at varying aH_2O values from 0.1 to 1.0.

(ii) Sillimanite-cordierite hornfelses

Activities from the end-members of all the major phases in the sillimanite-cordierite hornfelses DD.DUN1 and H.COR8 were used. The computer program THERMOCALC allows calculations to be made at varying values of aCO_2 and aH_2O. The total volatile content in cordierites from the sillimanite-bearing hornfelses was not determined, and therefore average pressure-temperatures were calculated at aH_2O values varying from 0.0 to 1.0. Variation of aCO_2 has only a small effect on the results given, aCO_2 was considered to equal 0 for all the calculations.

(iii) Cordierite norites

The total volatile content of 1.0 wt% for sample DD.BQ38 (Chapter 6.4) indicates a maximum possible $X_{H_2O}^{Crd}$ value of 0.33 for this sample (assuming a maximum of 2.99 wt% H_2O can be accommodated in the cordierite structure Johannes & Schreyer (1981)). Assuming that rocks with low $X_{H_2O}^{Crd}$ crystallised at low aH_2O values, the average pressures and temperatures were then calculated at aH_2O values of 0 and 0.33.

Hercynitic spinel occurs in most of the cordierite norites. However, the spinel always occurs as inclusions inside cordierite and is never in contact with quartz, and is therefore not considered to be a peak paragenesis mineral and is omitted from the end-members used for the calculations.

Biotite forms late-poikilitic flakes in the cordierite norites (Chapter 5.4) and this, together with the large discrepancies in the temperatures estimated from garnet-biotite geothermometry compared to the temperatures from garnet-orthopyroxene and garnet-cordierite geothermometry, suggests that biotite also may not represent a peak-paragenesis mineral. Average pressure-temperature calculations were made both with and without biotite end-members included to allow comparisons to be made.

8.8.2 Results from THERMOCALC

(i) Regionally metamorphosed rocks

Table 8.8.1 gives the average pressure-temperature results from the regionally metamorphosed rocks, with calculations made at varying values of aH_2O. The garnet-mica schist DD.SIN2 records a temperature of 548±148°C at a pressure of 5.9±1.6 kbars.

Variation of aH_2O has no effect on the results, as none of the independent equilibria written by the program either consume or produce H_2O. The garnet-biotite gneiss at $aH_2O = 1.0$ gives a temperature of 734±66°C at 7.8±1.8 kbars, with pressures and temperatures decreasing for reduced aH_2O, with T = 643±52°C and P = 5.9±1.1 kbars at $aH_2O = 0.25$. Calculations made for aH_2O values <0.25 give fit values greater than 1.61, indicating an uncertaincy in the averaging of the pressures and temperatures given by the independent equilibria used (for 95% confidence in the averaging of three reactions the fit index should be less than 1.61).

(ii) Sillimanite-cordierite hornfelses

Average pressure-temperature results for the sillimanite-cordierite hornfelses using THERMOCALC are given in Table 8.8.2. Increased aH_2O values lead to higher estimates of both pressure and temperature. Low aH_2O values lead to fit index values greater than 1.61 (see above), whilst high aH_2O values give lower f values, indicating a closer fit from the averaging of the reactions. Pressures vary from 4.3 kbar at the lowest aH_2O value with f <1.61, up to 5.8 kbar at $aH_2O = 1.0$. Sample H.COR8 gives the highest temperatures, 768±168°C, compared to 603°C for DD.DUN1.

(iii) Orthopyroxene-cordierite hornfels

Sample DD.BQ17 gives a temperature of 1000±102°C and a pressure of 5.1±0.5 kbars at $aH_2O = 0.213$. A slightly lower pressure and temperature is given if aH_2O is taken to be zero (Table 8.8.2).

(iv) Cordierite norites

Table 8.8.3 gives the average pressure-temperature results from cordierite norites. Temperatures vary from 850 to 1031°C when $aH_2O = 0.33$, and from 850 to 1015°C for anhydrous cordierite. Errors in temperature vary from 97 to 148°C. The pressures recorded are closely grouped, varying from 4.8 to 5.3 kbars at $aH_2O = 0.33$, and from 4.5 to 4.9 kbars for anhydrous cordierite. Errors in pressure fall between 0.7 and 1.0 kbars. When biotite end members are included, slightly higher temperatures and pressures are recorded. However, these temperatures are mainly in excess of 950°C and are in excess of the

maximum stability temperatures of even Ti-saturated biotite, and these results are therefore not used.

8.8.3 Use of THERMOCALC to calculate water activities

(i) Introduction

Using mineral end-member activity data from selected samples, lines of equal aH_2O in P-T space can be calculated for dehydration reactions using THERMOCALC. Average pressures and temperatures for the various rock types have already been calculated in section 8.8.2. aH_2O values for individual samples can therefore be estimated from the aH_2O iso-line which plots next to the average pressure-temperature for a given sample.

The two dehydration reactions used to calculate aH_2O, which are applicable to high-grade pelitic hornfelses are:

$$\text{biotite} + \text{sillimanite} + \text{quartz} = \text{K-feldspar} + \text{garnet} + H_2O \qquad [8.36]$$

and;

$$\text{biotite} + \text{quartz} = \text{K-feldspar} + \text{orthopyroxene} + H_2O. \qquad [8.37]$$

aH_2O can be calculated using both the Fe and Mg end-members from these reactions.

(ii) Strategy for calculating aH_2O

The cordierite-sillimanite hornfels H.COR8 is chosen here as this sample contains suitable paragenesis minerals for the application of equation 8.36 (garnet, sillimanite, biotite and quartz). For reaction 8.37 the cordiete norite H.BHQ1 was selected as this is the only sample which contains K-feldspar, in addition to biotite, quartz and orthopyroxene. Mineral activities from both these samples were then used to calculate the pressures and temperatures for the Fe and Mg end-member reactions of equations 8.36 and 8.37, at aH_2O values of 0.1, 0.2, 0.4, 0.6, 0.8 and 1.0. These lines of equal aH_2O can then be plotted against the average pressures and temperatures calculated for these two samples using THERMOCALC (section 8.8.2), allowing the aH_2O values at which the two samples crystallised to be estimated.

(iii) Results from aH_2O calculations

Figures 8.8.1 and 8.8.2 plot varying aH_2O for reaction 8.36 using mineral activities from H.COR8. Calculated temperatures decrease with lower aH_2O values. The average pressures-temperatures calculated for H.COR8 (709 to 768°C at 4.0 to 4.8 kbars for aH_2O values from 0 to 1.0) are lower even than those for the calculated $aH_2O = 0.1$ line for the Mg reaction, though plot next to the $aH_2O = 0.2$ line for the Fe end-member reaction.

The varying aH_2O values plotted using mineral activities from H.BHQ1 for reaction 8.37 are shown in Figures 8.8.3 and 8.8.4. The plot for the Mg end-member reaction shows that the average pressure-temperature given for H.BHQ1 plots next to the $aH_2O = 0.4$ line, whilst in Figure 8.8.4 for the Fe end-member reaction the average pressure-temperature calculated for H.BHQ1 plots in between the $aH_2O = 0.4$ and 0.6 lines.

Errors on these calculations are in the order of ±100 to 200°C, and when combined with the large errors given for temperatures from average pressure-temperature calculations for the two samples (±170°C for H.COR8 and ±140°C for H.BHQ1) mean that overall errors on the calculation of aH_2O for these two samples must be large. However, low aH_2O are infered for the sillimanite-cordierite hornfels H.COR8 ($aH_2O < 0.2$) and low-medium aH_2O for the cordierite norite H.BHQ1 ($aH_2O = 0.2$ to 0.55).

The temperatures plotted for $aH_2O = 1.0$ for all the reactions are unreasonably large (greater than 1100°C at pressures over 3 kbars), implying that neither of these two samples could have crystallised in high aH_2O fluid-present conditions.

8.9 Summary of Pressure-Temperature Results

Figures 8.9.1-3 displays the pressures and temperatures given by independent calibrations for the regionally metamorphosed rocks, sillimanite-bearing hornfelses, and orthopyroxene-bearing rocks respectively. Average pressures and temperatures given from the computer program THERMOCALC are given in Figure 8.9.4.

(i) Regionally metamorphosed rocks

The garnet-mica schist DD.SIN2 gives mean temperatures in the range of 550 to 610°C, compared to temperatures of 650 to 710°C for the garnet-biotite gneiss DD.SIN101.

This indicates a rapid drop in temperature away from the contact with the Huntly Gabbro (100°C over 200 m). Pressures from independent calibrations fall between 4.5 and 5.8 kbars. THERMOCALC gives a pressure of 5.9 kbars from both samples if $aH_2O = 0.25$.

(ii) Sillimanite-cordierite hornfelses

Geothermometry indicates mean temperatures in the range of 580 to 720°C (errors of ±139 to 171°C from THERMOCALC) for the sillimanite-cordierite hornfelses, with the alkali feldspar-bearing sample H.COR8 recording the higher temperatures. Independent calibrations give a wide range of pressures for the two samples, varying from 4.2 to 7.6 kbars (errors of ±1.2 kbars for both samples). However, average pressures using THERMOCALC give similar pressures for the two samples, with pressures ranging from 4.3 to 5.8 kbars calculated at values of $aH_2O = 0.4$ to 1.0.

(iii) Orthopyroxene-bearing hornfelses

Garnet-orthopyroxene geothermometry gives temperatures from 880 to 960°C for the orthopyroxene-bearing hornfelses. THERMOCALC gives an average temperature of 1000±102°C (at $aH_2O = 0.213$) for sample DD.BQ17. The pyrope-enstatite-Mg Tschermak geothermometer yields similar temperatures at the expected pressures for these rocks. Garnet-orthopyroxene-plagioclase-quartz geobarometry gives pressures of 4.4 (Fe) and 4.7 (Mg) kbars for DD.BQ17, and higher pressures of 5.9 (Fe) and 6.0 (Mg) kbars for H.COR8. Errors in these pressures a large (1.5 to 2.6 kbars), mainly due to errors generated from the low grossular contents in garnets. THERMOCALC gives a well constrained average pressure of 5.1±0.5 kbars for DD.BQ17.

(iv) Cordierite norites

Temperatures from 820 to 880°C are given by garnet-orthopyroxene geothermometry for the cordierite norites. THERMOCALC gives average temperatures which are higher, varying from 870 to 1030°C. A wide spread of pressures between 3.8 and 5.7 kbars are given from garnet-orthopyroxene-plagioclase-quartz geobarometry, with the low grossular contents in garnet again contributing towards large error margins (up to 2.1 kbars). However, average pressures given by THERMOCALC are more tightly constrained, with

pressures from 4.5 to 4.9 kbars at $aH_2O = 0.0$ and 4.8 to 5.3 kbars at $aH_2O = 0.33$. The errors given by THERMOCALC vary from ±0.7 to 1.0 kbars.

8.10 Discussion

8.10.1 Temperature calculations

(i) Reliability of temperature estimates

Temperatures from garnet-biotite geothermometry are only applicable for the regionally metamorphosed rocks, and sillimanite-bearing hornfelses. The high Ti and Al^{vi} contents in biotites from the cordierite norites, lead to inaccurate temperatures being given by calibrations for garnet-biotite geothermometry (e.g. Patiño Douce *et al.*, 1993). In addition, the late growth of biotite in the cordierite norites suggests that any temperatures given by garnet-biotite geothermometry do not represent the peak temperatures at which the other minerals from these rocks equilibrated. Garnet-orthopyroxene, and pyrope-enstatite-Mg Tschermak geothermometry give the highest, and most consistent (for rocks from the same locality) temperatures for the cordierite norites and orthopyroxene-bearing hornfelses.

Average temperatures using THERMOCALC are similar to those from independent calibrations, except for the orthopyroxene-bearing rocks, for which THERMOCALC gives higher temperatures (850 to 1030°C). Temperatures in excess of 1000°C are not unreasonable as the orthopyroxene-bearing rocks mainly occur inside the margins of the Huntly Gabbro, often as large xenoliths, and the initial temperature of an intruding mafic magma would be in the region of 1000 to 1200°C.

(ii) Implications for partial melting

The temperatures given for the hornfelses confirm that the orthopyroxene-cordierite hornfelses are higher grade rocks than the sillimanite-bearing rocks. The temperatures given for the sillimanite-cordierite hornfelses (600 to 770°C) are below those required for major biotite-consuming fluid-absent partial melting reactions to take place, and any melting in the temperature range 600 to 800°C would probably be due to muscovite-consuming reactions, and would be minor unless the protolith contained large quantities of muscovite.

The temperatures given for the orthopyroxene-cordierite hornfelses and cordierite norites (850 to 1030°C) are well in excess of those required for extensive fluid-absent

partial-melting by biotite-consuming reactions. Therefore, the silica-poor orthopyroxene-cordierite hornfelses could represent the restitic residues of partial melting reactions.

The temperatures given for the igneous-textured cordierite norites are similar to those given by the mineralogically similar orthopyroxene-cordierite hornfelses. This shows that the orthopyroxene, cordierite, garnet, and plagioclase in these rocks crystallised at temperatures above the maximum stability temperatures for biotite and therefore these rocks could have formed by crystallisation in the presence of a melt formed from biotite-consuming partial melting reactions.

aH_2O estimates using THERMOCALC give low aH_2O values for a sillimanite-cordierite hornfels and low-medium aH_2O for a cordierite norite. These values are indicative of the formation of these rocks in fluid-undersaturated conditions.

8.10.2 Pressure calculations

(i) Reliability of pressure estimates

Average pressure estimations using THERMOCALC give closely grouped pressures for all the hornfelses and cordierite norites from the Huntly Gabbro (4.8 to 5.3 kbars), compared to the wide spread of pressures given by various independent calibrations (3.9 to 7.6 kbars), with different samples from the same locality giving pressures up to 1.4 kbars apart. Pressures from garnet-orthopyroxene-plagioclase-quartz geobarometry are handicapped by the low grossular contents in many of the garnets, which leads to large errors on the calibration, due to probe detection limits, and to large uncertainties in the grossular activity models. Therefore the pressures given by THERMOCALC are taken to be the most reliable.

(ii) Relationships with regionally metamorphosed rocks

Average pressures given by THERMOCALC the rocks from the garnet-bearing regionally metamorphosed rocks from the western (structurally lower) side of the Huntly Gabbro (Cairnie, localities 1a and 1b) are slightly higher than those given by the hornfelses and cordierite norites. This would be compatible with simultaneous crystallisation of the two groups of rocks, the former at slightly lower structural levels. The decrease in temperature away from the intrusion supports the time sequence proposed by workers such

as Fettes (1970), who suggested that regional metamorphism was synchronous with intrusion of the Newer Gabbros.

Similar pressure estimates are given for the andalusite schists (maximum pressure of 4.7 kbars), sillimanite-bearing hornfelses, cordierite-bearing hornfelses and cordierite norites. This suggests that all of these rocks could have formed on an isobaric heating path. This is supported by petrographical observations, with the sillimanite in the sillimanite-cordierite hornfelses forming rectangular aggregates pseudomorphing earlier andalusite (Plate 5.5.6). In addition large rectangular cordierite-spinel clots in the cordierite norites contain occasional relict sillimanite crystals (Plate 5.5.6), and in turn form pseudomorphs after sillimanite. Therefore, with increasing temperature, at constant pressure, the andalusite schists form sillimanite-cordierite hornfelses, and then the higher grade cordierite norites.

(iii) Overburden estimates

Assuming average density for the metamorphic and igneous rocks in NE Scotland a depth/pressure ratio of 0.27 kbars/km can be inferred. The pressures given from the cordierite norites and hornfelses by THERMOCALC (4.8 to 5.3 kbars) imply an overburden between 18 and 20 km, in excellent agreement with the overburden estimates of Droop & Charnley (1985). Pressures in the region of 6 kbars given by the regionally metamorphosed rocks from the base of the Huntly Gabbro imply overburden depths of approximately 22 km.

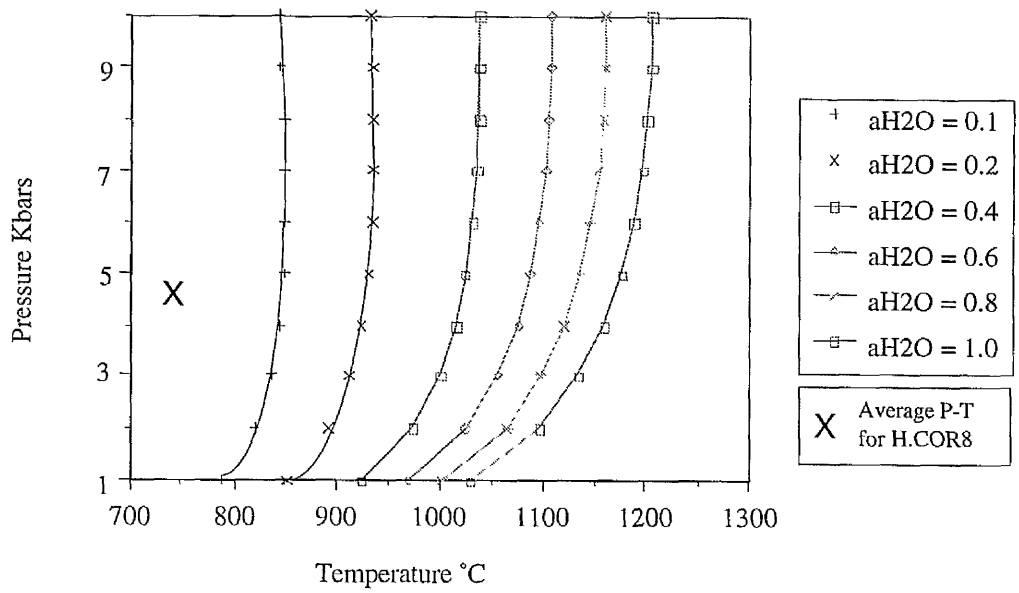

Figure 8.8.1 P-T plot for the Mg end-member reaction Phl + Sil + Qtz = Kfs + ~~Alm~~ Py + H_2O calculated at varying aH_2O values using the computer program THERMOCALC for the mineral end-member activities from the sillimanite-cordierite hornfels H.COR8. Decreased aH_2O reduces the calculated temperatures. However, the average P-T value calculated for sample H.COR8 (738°C at 4.8 Kbars for aH_2O = 0.5) lies below the calculated temperatures for all aH_2O values.

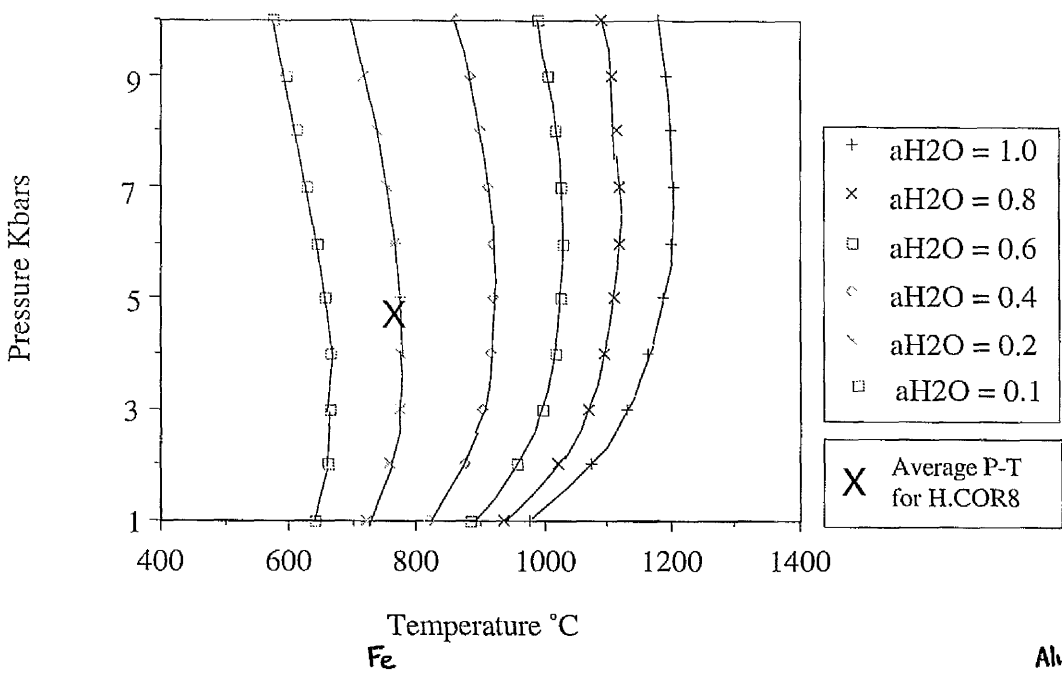

Figure 8.8.2 P-T plot for the ~~Mg~~ Fe end-member reaction Ann + Sil + Qtz = Kfs + ~~Py~~ Alm + H_2O, calculated at varying aH_2O values using the computer program THERMOCALC for the mineral end-member activities from the sillimanite-cordierite hornfels H.COR8. Decreasing aH_2O reduces the calculated temperatures, and the average P-T for H.COR8 given using THERMOCALC corresponds close to aH_2O = 0.2 for this reaction.

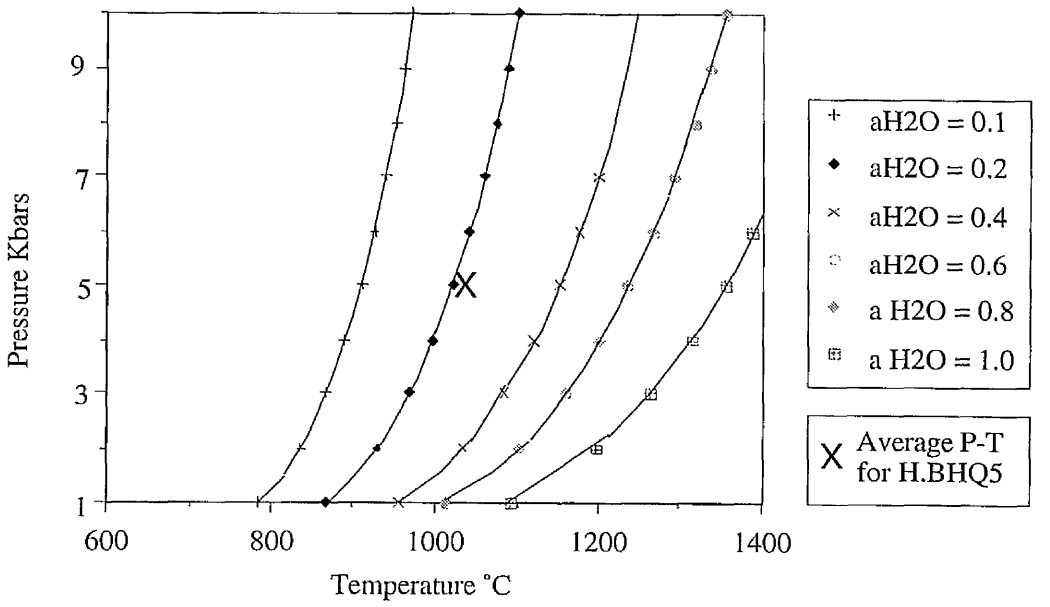

Figure 8.8.3 P-T plot for the Mg end-member reaction Phl + Qtz = Kfs + En + H_2O, calculated at varying aH_2O values using the computer program THERMOCALC for mineral end-members from the cordierite norite H.BHQ1. The average P-T calculation for H.BHQ1 (Table 8.8.3) of 1031°C at 5.0 kbars plots next to the aH_2O = 0.2 line for this reaction.

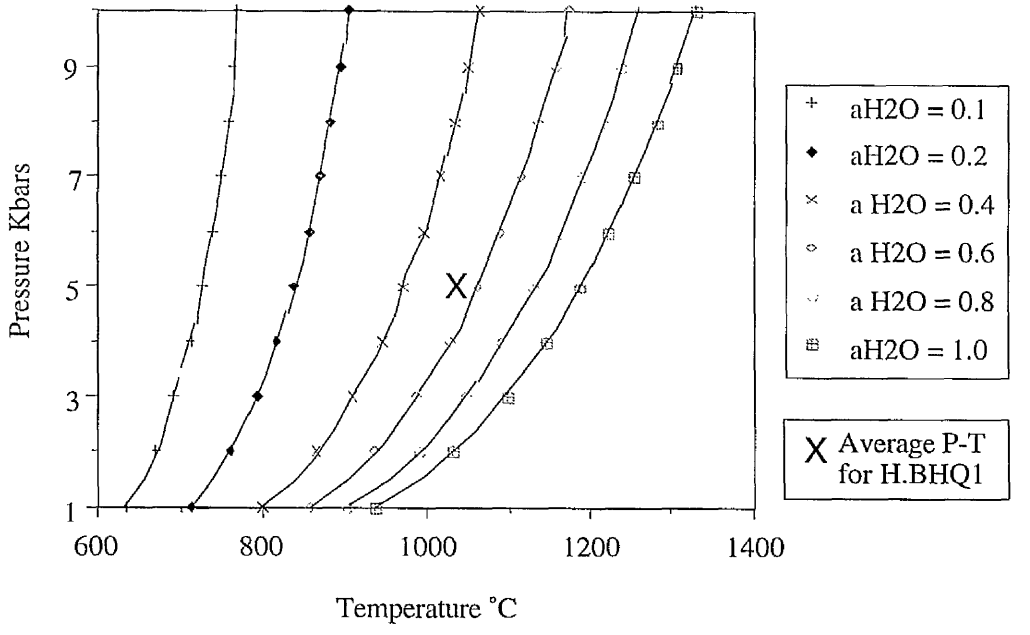

Figure 8.8.4 P-T plot for the Fe end-member reaction Ann + Qtz = Kfs + Fs + H_2O, calculated at varying aH_2O values using the computer program THERMOCALC for mineral end-members from the cordierite norite H.BHQ1. The average P-T calculation for H.BHQ1 (Table 8.8.3) of 1031°C at 5.0 kbars plots in-between the lines plotted for aH_2O = 0.4 & 0.6.

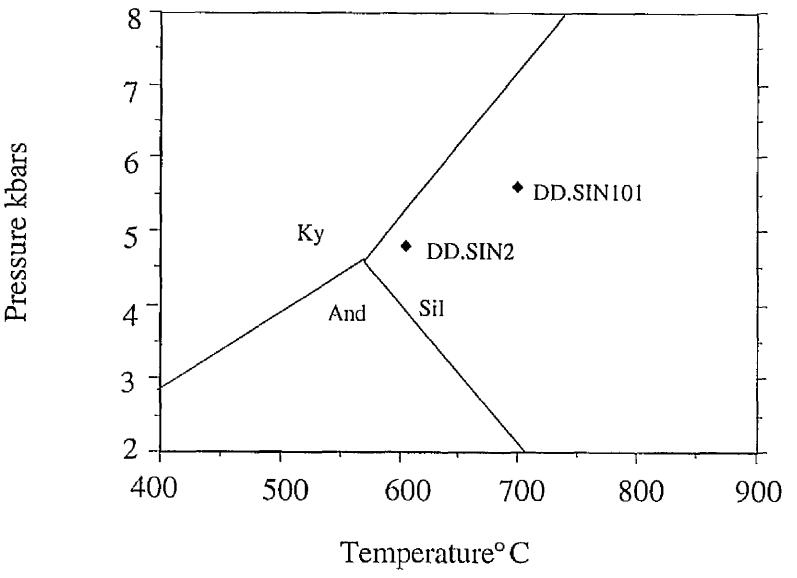

Figure 8.9.1 Pressure-temperature estimates from regionally metamorphosed rocks. Temperatures are from garnet-biotite geothermometry (Ferry & Spear, 1978), and pressures from garnet-rutile-ilmenite-plagioclase geobarometry (Essene, 1990). The pressure estimated from garnet-plagioclase-muscovite-biotite geobarometry for DD.SIN2 matches the Grt-Rt-Ilm-Pl pressure.

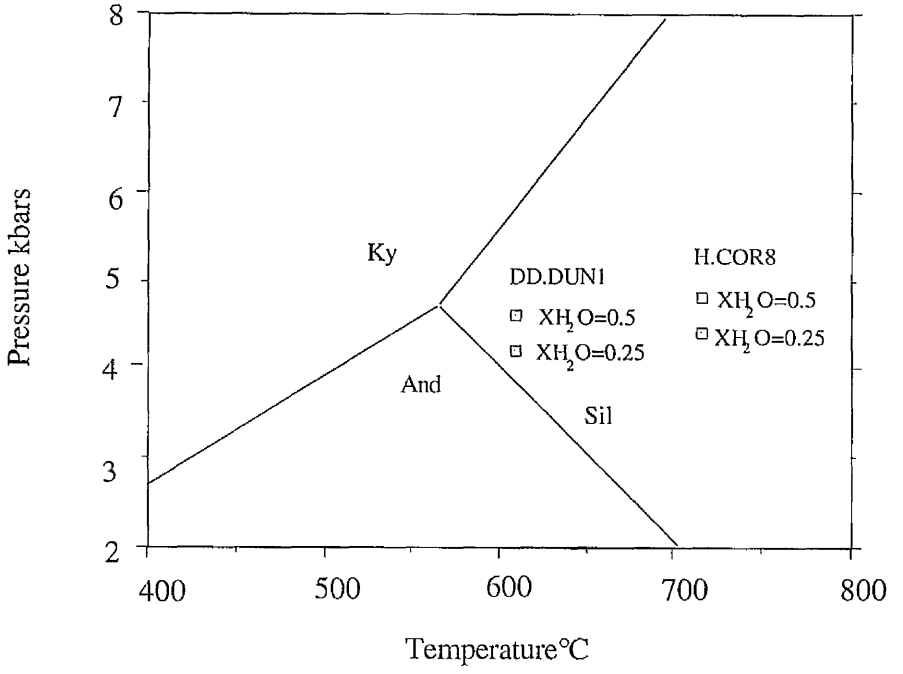

Figure 8.9.2 Pressure temperature estimates for sillimanite-cordierite hornfelses. Temperatures plotted from the garnet-cordierite calibration of Nichols et al. (1992), and pressures from the garnet-cordierite-sillimanite-quartz calibration of Bhattacharya (1986), with pressures calculated at $XH_2O=0.25$ and $XH_2O=0.5$. Pressures calculated for DD.DUN1 are below the maximum stability limit of andalusite (Holland & Powell, 1990), which shows that (a) the nearby regionally metamorphosed andalusite schists (see Figure 4.2) could have crystallised at similar pressures as the hornfelses, and (b) that an isobaric heating path for DD.DUN1 is possible, as suggested by the occurrence of sillimanite aggregates ?pseudomorphing earlier andalusite (see Plate 5.4.21)

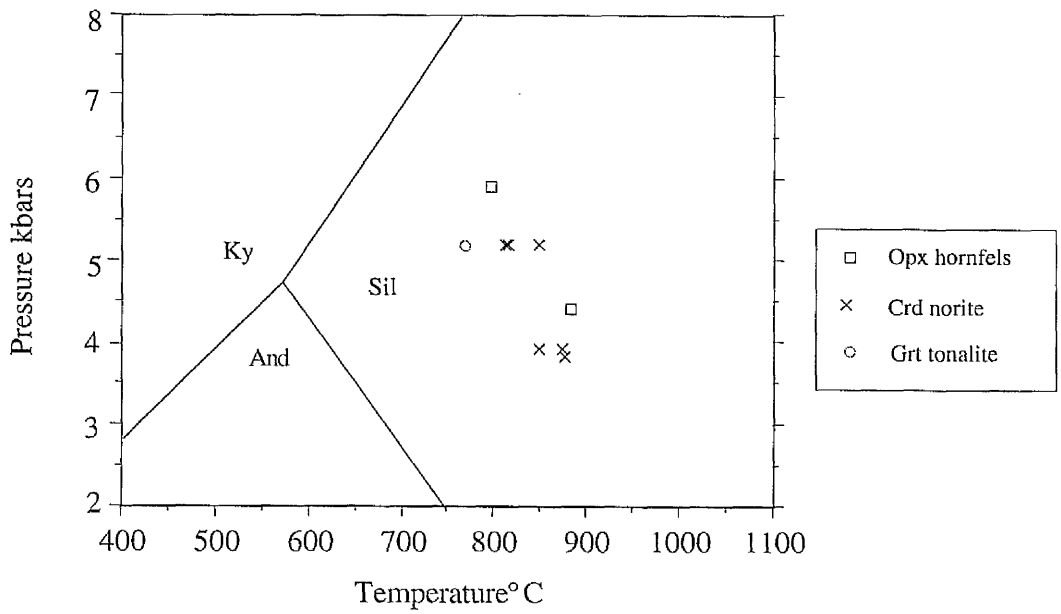

Fugure 8.9.3 Pressure-temperature estimates from garnet-orthopyroxene-bearing rocks. Temperatures from garnet-orthopyroxene geothermometry, and pressures from almandine-grossular-anorthite-ferrosilite-quartz geobarometry, with both calibrations from Bhattacharya *et al.* (1991).

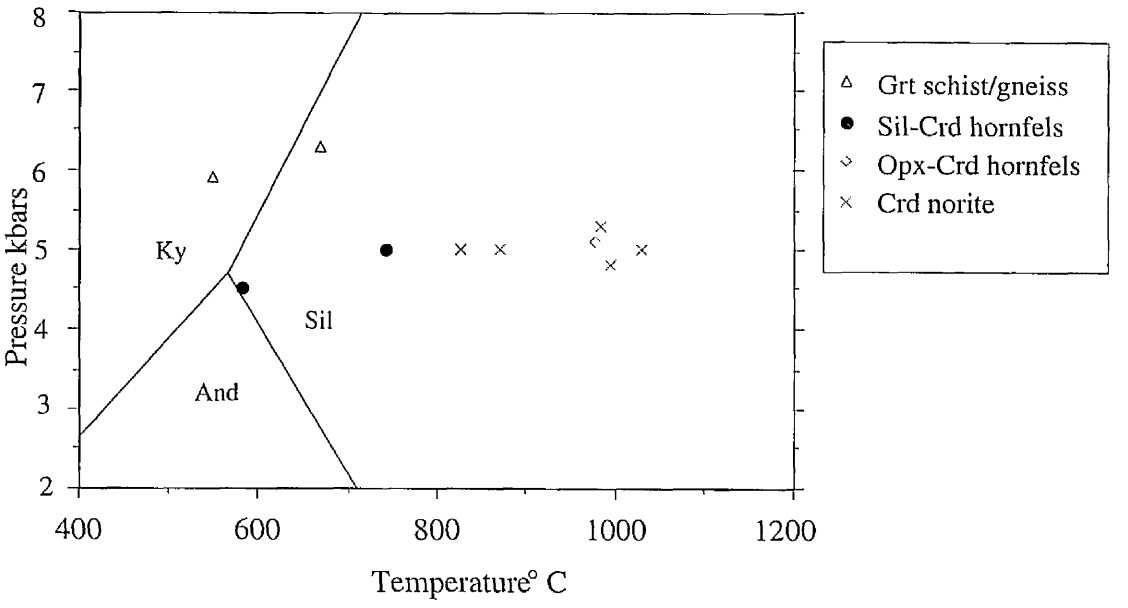

Figure 8.9.4 Plot of average pressures and temperaures calculated by THERMOCALCv2.3. For the regionally metamorphosed rocks results are plotted for calculations at $aH_2O = 0.5$. The sillimanite-cordierite hornfelses are plotted at calculations of $aH_2O = 0.5$, the orthopyroxene-cordierite ~~corlorites~~ hornfelses at $aH_2O = 0.213$ and the cordierite norites at $aH_2O = 0.33$. Error margins are given in Tables 8.5.1-3. The regionally metamorphosed rocks from Clashmach Hill (localities 1c and 1d) contain andalusite, and therefore must plot in the andalusite field (i.e. P <4.7 kbars, T <700°C).

Table 8.6.1 Garnet-biotite thermometry, with temperature estimates from (T-Thompson (1976), F&S-Ferry & Spear (1978), I&M1 and I&M2-Indares & Martingnole (1985), G&S* and H&W*-Ganguly & Saxena(1984) and Hackler & Wood (1988) with garnet mixing data from Bhattacharya (1992), and the THERMOCALCv2.3 computer package of Holland & Powell (1994). All temperatures given in °C.

Sample No.	Rock type	T(76)	F&S(78)	I&M1	I&M2	G&S*	H&W*	THERMOCALC
DD.SIN1	GBG	646	705	588	590	629	622	711±160
DD.SIN101	GBG	639	698	587	581	625	618	701±151
DD.SIN2	GMS	570	606	504	523	567	564	626±138
H.COR8	SCH	712	734	617	584	684	676	849±219
DD.DUN1	SCH	593	577	528	514	605	592	598±131
H.COR10	OH	811	882	688	688	741	738	1037±270
H.BHQ1	CN	834	917	769	746	754	753	1204±364
DD.BQ38	CN	836	920	750	738	760	758	1086±300
DD.CASB2i	CN	782	837	697	713	724	719	992±245
DD.CASB5	CN	777	831	696	707	724	718	980±245
DD.DUN4	CN	681	694	604	587	660	655	778±171
DD.DUN12	CN	760	807	739	725	706	705	926±224
DD.DUN9b	CN	828	907	723	718	753	751	1068±284
DD.CUM19	GT	749	790	703	750	686	710	1183±390
DD.CUM22	GT	853	946	771	747	794	783	1255±443
DD.TYQ5	GT	782	839	689	722	726	725	1045±291
DD.BAR1	GAG	742	780	691	660	681	685	859±202

Rock types: GBG-garnet-biotite gneiss, GMS-garnet-mica schists, AS-andalusite schist, SCH-sillimanite-cordierite hornfels, OH-orthopyroxene hornfels, CN-cordierite norite, GT-garnet tonalite and GAG-garnet-anthophyllite gneiss.

Table 8.6.2 Garnet-cordierite Fe-Mg exchange geothermometry. Temperature estimates from the independent calibrations of Th-Thompson (1976), H&L-Holdaway & Lee (1977), Bh(88)-Bhattacharya *et al.*. (1988), Nich(92)-Nichols *et al.*. (1992) and the THERMOCALCv2.3 computer package of Holland & Powell (1994). All temperatures given in °C.

Sample	Rock type	Th(76)	H&L(77)	Bh(88)	Nich(92)	THERMOCALC
DD.DUN1	SCH	643	667	694	601	651±111
H.COR8	SCH	700	722	721	715	776±141
DD.PIR1	OCH	918	903	836	879	1087±218
DD.BQ17	OCH	803	807	783	760	1003±191
H.BHQ5	OCH	889	879	828	859	978±188
DD.BQ41	OCH	839	837	790	789	987±189
H.BHQ1	CN	859	855	813	819	1154±232
DD.BQ38	CN	847	844	810	816	950±181
DD.CASB2i	CN	819	820	806	788	986±190
DD.CASB5	CN	724	739	755	693	832±150
DD.DUN4	CN	713	729	741	682	851±149
DD.DUN12	CN	762	772	766	724	937±171
DD.BAR1	GAG	746	758	743	687	760±133

Rock types: SCH-sillimanite-cordierite hornfels, OCH-orthopyroxene-cordierite hornfels, CN-cordierite norite, and GAG-garnet-anthophyllite gneiss.

Figure 8.6.3 Garnet-orthopyroxene Fe-Mg exchange thermometry. Temperatures calculated from the independent calibrations of Harley (1984a), S&B(84)-Sen & Bhattacharya (1984), L & G(88)-Lee & Ganguly (1988), B-Bhattacharya et al. (1991) and from the computer program THERMOCALCv2.3 (Holland & Powell, 1994). All temperatures given in °C.

Sample	Rock type	Harley(84a)	S & B(84)	L & G (88)	B(91)	THERMOCALC
DD.BQ17	OCH	831	981	945	883±100	947+267
DD.BQ41	OCH	862	1037	968	915±67	889±250
H.BHQ5	OCH	822	965	941	880±109	888±173
DD.PIR1	OCH	918	1130	1037	960±58	1071±332
DD.PIR4	OCH	918	1128	1041	957±113	1068±334
H.COR10	OH	729	815	849	795±90	725±167
H.BHQ1	CN	799	926	917	848±111	859±217
DD.BQ38	CN	822	964	945	873±86	891±246
DD.CASB2i	CN	804	925	945	849±71	859±216
DD.CASB5	CN	757	853	894	815±146	788±219
DD.DUN4	CN	747	844	855	814±147	773±185
DD.DUN12	CN	826	867	971	877±78	898±244
DD.CUM19	GT	689	780	857	768±135	914±344

Rock types: OCH-orthopyroxene-cordierite hornfels, OH-orthopyroxene hornfels, CN-cordierite norite, and GT-garnet tonalite.

Table 8.6.4 Temperature estimates from pyrope-enstatite-Mg-Tschermak geothermometer of Harley & Green (1982). All temperatures in °C.

Sample	Rock Type	T°C at 3.5 kbars	T°C at 4.5 kbars	T°C at 5.5 kbars
DD.BQ17	OCH	871	900	929
DD.BQ41	OCH	882	911	940
H.BHQ5	OCH	853	882	910
DD.PIR1	OCH	888	918	947
DD.PIR4	OCH	889	919	948
H.COR10	OH	761	787	812
DD.BQ38	CN	850	878	906
H.BHQ1	CN	831	859	886
DD.CASB2i	CN	779	805	831
DD.CASB5	CN	770	797	823
DD.DUN4	CN	801	828	855
DD.DUN12	CN	851	880	909
DD.CUM19	GT	665	685	705

Rock types: OCH-orthopyroxene-cordierite hornfels, OH-orthopyroxene hornfels, CN-cordierite norite and GT-garnet tonalite.

Table 8.6.5 Temperture estimates from biotite-orthopyroxene geothermometry. All temperatures in °C from the calibration of Sengupta *et al.* (1990).

Sample	Rock Type	T°C
H.COR10	OH	762
H.BHQ1	CN	827
DD.BQ38	CN	682
DD.CASB2i	CN	667
DD.CASB5	CN	712
DD.DUN4	CN	592
DD.DUN12	CN	621
DD.CUM19	CN	810

Rock types: OH-orthopyroxene hornfels, CN-cordierite norite, GT-garnet tonalite.

Table 8.7.1 Pressure estimates from garnet-plagioclase-orthopyroxene-plagioclase-quartz barometry, using calibrations of N&P - Newton & Perkins (1982), P&Ch - Perkins & Chipera (1985), TCALC - THERMOCALCv2.3, Ess(90) - Essene (1990), and Bh(91) - Bhattacharya *et al.* (1991).
All pressures given in kbars, and calculated at the preferred Grt-Opx temperatures of Bhattacharya *et al.* (1991).
The errors given are calculated from 2σ of probe analyses.

Sample	Rock Type	T°(C) B(91)	N&P (Mg)*1	N&P (Mg)*3	P&Ch (Mg)*3	P&Ch (Fe)*3	TCALC (Mg)*3	Ess(90) (Mg)*3	Bh(91) (Fe)*2	Bh(91) (Mg)*2	Bh(91) (Fe)*3	Bh(91) (Mg)*3
DD.BQ17	OCH	883	4.6	6.7	5.6	6.5	5.6	6.0	3.5	4.9	4.4±1.5	4.7±1.6
H.COR10	OH	795	4.5	7.3	7.6	7.9	4.1	6.8	4.7	5.7	5.9±2.3	6.0±2.6
DD.DUN12	CN	877	4.0	6.3	5.2	6.1	4.9	4.8	3.5	4.9	3.8±1.4	5.1±1.6
DD.CASB2i	CN	849	3.6	4.1	5.5	6.4	5.5	6.0	4.6	4.9	3.9±0.9	5.2±0.9
DD.CASB5	CN	815	4.7	5.7	5.2	6.4	5.3	5.2	5.6	4.8	5.2±1.3	5.7±2.1
H.BHQ1	CN	848	3.5	5.5	5.3	6.3	3.8	4.8	3.4	4.8	5.2±1.6	5.5±2.2
DD.BQ38	CN	873	4.1	6.4	5.3	6.1	5.2	5.6	3.2	4.6	3.9±0.9	4.4±1.0
DD.DUN4	CN	814	4.5	6.9	5.7	7.0	4.8	5.8	4.2	5.2	5.2±2.1	5.3±2.1
DD.CUM19	GT	768	5.4	8.1	7.6	7.9	6.1	7.2	5.8	5.8	5.9±0.8	5.4±1.5

Rock types as Table 6.3.1.

*1 Garnet activities calculated from models of Ganguly &Saxena (1984), anorthite from Newton (1983).

*2 Garnet activities after Ganguly & Saxena (1984), orthopyroxene and anorthite activities after Bhattacharya *et al.* (1991).

*3 Garnet activities after Berman (1990), anorthite activities after Elkins & Grove (1990).

Table 8.7.2 Garnet-plagioclase-sillimanite-quartz geobarometry. Pressures calculated at the temperatures given from garnet-biotite (Bhattacharya *et al.*, 1992) and garnet-cordietite (THERMOCALCv2.3) geothermometry. The calibrations used are from G&S - Ghent & Stout (1976), N&H - Newton & Haselton (1981) and TCALC - THERMOCALCv2.3.

		T°C	G&S	G&S*1	N&H	N&H*1	TCALC*1
DD.DUN1	Grt-Bt	600	1.8	4.1	3.6	4.6	4.9±1.04
DD.DUN1	Grt-Crd	650	2.4	4.9	4.2	5.3	5.5±1.04
H.COR8	Grt-Bt	680	3.8	5.8	5.5	6.4	6.5±1.54
H.COR8	Grt-Crd	780	5.1	7.5	6.8	7.7	7.6±1.54

*1 Activities calculated using models of Berman (1990) for grossular, and Elkins & Grove (1990) for anorthite.

Table 8.7.3 Pressure estimates from garnet-cordierite-sillimanite-quartz geobarometry. Pressures calculated at $X^{Crd}_{H_2O}$ values of 0.0, 0.25 and 0.5. All pressures calculated from the Fe-end member reaction unless otherwise stated.

	XH_2O=0.0	XH_2O=0.25	XH_2O=0.5
Lonker (1981)			
DD.DUN1	4.5	4.9	5.5
H.COR8	4.5	4.9	5.5
Bhattacharya (1986)			
DD.DUN1	4.1	4.4	5.0±0.55
H.COR8	4.0	4.4	5.0±0.46
THERMOCALcv2.3			
DD.DUN1	4.1	4.2	4.6±0.41
H.COR8	4.0	4.4	4.8±0.45
THERMOCALv2.3 (Mg-end member reaction)			
DD.DUN1	3.6	4.1	4.7±0.67
H.COR8	5.0	5.7	6.3±0.62

Table 8.8.1 Average pressure-temperature calculations for regionally metamorphosed rocks using the computer progamme THERMOCALCv2.3., with calculations made at decreasing values of aH_2O. aH_2O values below 0.25 for DD.SIN101 and 0.5 for DD.SIN2 lead to f (fit index) values which fail the 95% confidence limit from the averaging of reactions.

Sample	Rock Type	aH_2O	T°C	sd	P kbars	sd	cor	f
SIN101	GBGn	1.0	734	66	7.8	1.8	0.673	0.12
		0.75	686	47	6.5	0.9	0.292	0.65
		0.5	670	45	6.3	0.9	0.282	0.85
		0.25	643	52	5.9	1.1	0.265	1.21
DD.SIN2	GMSch	1.0	548	148	5.9	1.6	0.817	1.33
		0.5	548	148	5.9	1.6	0.817	1.33

Rock Types: GBGn - garnet-biotite gneiss; GMSch - garnet-mica schist

Table 8.8.2 Average pressure-temperature calculations for sillimanite-cordierite hornfelses and an orthopyroxene cordierite hornfels using the computer progamme THERMOCALCv2.3,. For the sillimanite-bearing hornfelses, calculations were made at increasing values of aH_2O. Only aH_2O values exceeding 0.3 for DD.DUN1 and 0.2 for H.COR8 result in f <1.61 (fit index), indicating 95% confidence on the averaging of reactions. For the orthopyroxene-bearing hornfels calculations made at aH_2O equals 0.0 and 0.213 are shown.

Sample	aH_2O	T°C	sd	P kbars	sd	cor	f
DD.DUN1	0.0	547	158	3.2	1.2	0.901	1.88*
	0.4	576	145	4.3	1.2	0.928	1.6
	0.5	581	143	4.5	1.2	0.931	1.56
	0.75	593	140	4.9	1.2	0.939	1.48
	1.0	603	139	5.2	1.2	0.944	1.43
H.COR8	0.0	709	193	4.0	1.2	0.899	1.66*
	0.25	728	183	4.5	1.2	0.916	1.51
	0.5	743	176	5.0	1.2	0.927	1.41
	0.75	757	171	5.5	1.2	0.935	1.33
	1.0	768	168	5.8	1.3	0.941	1.27
DD.BQ17	0.0	979	105	4.8	0.5	0.181	1.06
	0.213	1000	102	5.1	0.5	0.240	1.00

Table 8.8.3 Average pressure-temperature results for cordierite norites using the computer progamme THERMOCALCv2.3, with calculations made for aH_2O values of 0.0 and 0.33.

Sample	aH_2O	T°C	sd	P kbars	sd	cor	f
DD.BQ38	0.0	979	97	4.5	0.7	0.281	0.86
	0.33	995	99	4.8	0.7	0.325	0.75
H.BHQ1	0.0	1015	148	4.6	1.0	0.444	1.25
	0.33	1031	139	5.0	0.9	0.484	1.15
DD.DUN4	0.0	850	113	4.6	0.8	0.205	1.35
	0.33	871	102	5.0	0.7	0.263	1.18
DD.DUN12	0.0	964	99	4.9	0.7	0.249	1.03
	0.33	983	98	5.3	0.7	0.299	0.90
DD.CASB2	0.0	906	108	4.5	0.8	0.135	1.17
	0.33	925	97	5.0	0.7	0.189	1.03

CHAPTER 9 WHOLE ROCK CHEMISTRY

9.1 Introduction

9.1.1 Aims of whole rock analysis

The main aims of this Chapter are:

(i) To give chemical evidence for which processes could have led to the formation of the cordierite norites, garnet tonalites and cordierite hornfelses. These data can then be used to support or invalidate the models presented here for the formation of these rocks,

(ii) To aid the choice of suitable starting products for experimental work,

(iii) To allow comparison between the partially melted rocks (i.e. cordierite norites, and garnet tonalites) and cordierite hornfelses, and the compositions of the crystals and melts (if any) generated by experimental work.

Aims (ii) and (iii) are dealt with in Chapter 10.

9.1.2 Evolutionary Models

Four models are presented here, all of which can describe the models which could have led to the formation of the cordierite norites, garnet tonalites and the cordierite hornfelses which are associated with the Huntly Gabbro. Models 1 and 2 have been previously presented in the literature and a fuller description of these is given in Chapter 3.4. Figures 9.1.1–4 are flow chart diagrams which show graphical representations of the processes suggested by these 4 models.

Model 1. (Figure 9.1.1). Read (1923a ; 1923b ; 1935) believed that the xenolith-bearing cordierite norites associated with the Newer Gabbros of NE. Scotland were formed by digestion and assimilation of the pelitic schists which surround the intrusions, leading to the formation of "contaminated" or "mixed" rocks, with the un-melted residue of the schists forming xenoliths in the 'contaminated' rock. This model requires that the mixing of quantities of pelitic schist with mafic igneous rock can be chemicaly shown to form rocks chemically identical to the cordierite hornfelses and cordierite norites. Therefore, data which

supports this model must show that the cordierite norites (or garnet tonalites) and cordierite hornfelses have elemental concentrations which lie in-between the pelitic schists and mafic igneous rocks, as shown in Figure 9.1.5.

Model 2. (Figure 9.1.2). Gribble & O'Hara (1966), then Gribble(1967, 1970) and Ashworth (1972) all presented a second model for the formation of these rocks (described more fully in Chapter 3.4). They argued that the cordierite norites and their complementary xenoliths formed due to partial melting of the country rock in closed systems, without any chemical input from the mafic-igneous rocks. In this model the melt generated does not mobilise and therefore crystallises *in-situ*. Chemical evidence which supports this model must therefore show that the pelitic schists along strike from the 'partially melted' rocks can form both the igneous textured cordierite norites and the residual cordierite hornfelses without the need of any external chemical input. This evidence would be shown by relative enrichment of mobile elements in the cordierite norites, with depletion in the cordierite hornfelses, and by the same argument, enrichment of immobile elements in the cordierite hornfelses, and depletion of them in the cordierite norites; this is highlighted in Figure 9.1.6.

Model 3, (Figure 9.1.3) is similar to model 2, in that partial melting of a pelitic protolith forms both the restitic xenolithic cordierite hornfelses, and the igneous-textured cordierite norites. However, the abundance of minerals in the cordierite norites, which are common to the cordierite hornfels xenoliths (i.e. cordierite, orthopyroxene, garnet, spinel) suggests that the cordierite norites may not be 'true melts', instead representing a late stage, immobile melt, rich in entrained restite. In this model most of the melt generated from heating of the pelitic protolith is able to segregate and migrate upwards. For this model to be validated, the cordierite norites must show chemical trends which show that they cannot represent the sole melt produced. This would be the case if both the cordierite hornfelses and cordierite norites are either depleted or enriched in the same element relative to the pelitic schists and is highlighted in Figure 9.1.7.

In **Model 4** (Figure 9.1.4) the mafic igneous rocks, cordierite norites, and garnet tonalites represent separate bodies of igneous rock, intruded adjacently. The cordierite hornfelses are formed by thermal metamorphism, and recrystallisation without chemical

alteration of xenoliths and/or rafts of the pelitic schists broken off from the contact with these igneous rocks. No common source magma body for the various igneous rocks is necessarily inferred. Evidence to support this model must show that the cordierite hornfelses have the same bulk rock compositions as the surrounding pelitic schists (Figure 9.1.8), and that no genetic links between the cordierite norites/garnet tonalites and the cordierite hornfelses or pelitic schists are displayed.

9.2 Sample Classification and Methods of Data Analysis

To allow easy comparison of the whole rock chemistry between different rock types a similar scheme of classification as used in Chapters 4 to 6 is used here. The only divergence from this classification scheme is the grouping of the regionally metamorphosed rocks into a single category. The schists, siltstones and slates are grouped together under the term pelitic schists.

Approximately 70 rocks were analysed for their major and trace element contents. This was achieved by X-Ray fluorescence analysis of powdered rock capsules, encased in boric acid pellets. A full description of sample preparation, machine set up and data derivation is given in Appendix III of this thesis. The major elements analysed were Si, Al, Fe, Mg, Ca, Na, K, Ti, Mn and P, with the trace elements are Nb, Zr, Y, Sr, Rb, Zn, Cu, Ni, Cr, Ce, Nb, V, La, Ba, Sc. A full listing of the major element chemistry of the samples analysed is shown in table 9.2.1 and the trace elements in table 9.2.2. Major elements are quoted as weight percent oxide and trace elements in parts per million.

To test the data against the possible models of rock formation, a series of Harker type plots are presented, plotting the various elements against SiO_2 wt%. Plots of SiO_2 against Mg# (molar Mg/(Mg+Fe)) are also presented.

Two sets of graphs are plotted here; one set representing rocks from the S and SW margins of the Huntly Gabbro and a set for rocks from the W margin of the Gabbro.

The rocks from the S and SW margin are all those rocks which are shown in Chapter 4 to be along strike from the metasediments of the Boyndie Bay and Whitehills 'Groups' (undivided). This incudes rocks from Battle Hill Quarry and Woods, Castle Bridge, and Dunbennan Woods.

Rocks from the W margins of the Huntly Gabbro are those rocks which were shown by Read (1923b) to be along strike from the garnet-bearing pelites of the Portsoy 'Group'. These rocks are those from the localities around Cormalet, and the road cuttings near Cairnie.

The analyses taken from the xenolith-free mafic igneous rocks from Bin Quarry and from other localities in the central area of the Huntly Gabbro are taken to represent the mean composition of the mafic igneous rocks of the intrusion and these data are plotted in both the above sets of graphs.

9.3 Analysis of Results

9.3.1 Samples from S and SW of the intrusion, major elements

Figures 9.3.1–7 are scatter plots, representing elements in wt% against SiO_2 wt%. Figure 9.3.8 is a plot of Mg# plotted against SiO_2 wt%. The MnO and P_2O_5 contents of all the samples analysed were uniformly below detection limits.

(i) SiO_2

The SiO_2 content of the pelitic schists varies from 55-65 wt%. It is of importance to note that the SiO_2 contents of both the cordierite hornfelses and the cordierite norites are mainly lower than those of the pelitic schists. The SiO_2 contents of the mafic igneous rocks, biotite gabbros and micro-norites are quite closely grouped, varying from 45-55 wt%

(ii) Al_2O_3 Figure 9.3.1

The Al_2O_3 contents of all rock types varies greatly and overlap with values from 15 to 27 wt%. However, it can be shown that the mafic igneous rocks and biotite gabbros are well clustered. Also the Al_2O_3 contents of most cordierite hornfelses and of two of the cordierite norites are higher than all of the mafic rocks and all but one of the pelitic schists analysed.

(iii) Fe_2O_3 Figure 9.3.2

The mafic igneous rocks and the biotite gabbros are again well clustered. The pelitic schists, cordierite norites and cordierite hornfelses appear to show a linear trend with the Fe_2O_3 content increasing with decreasing SiO_2.

(iv) MgO Figure 9.3.3

The mafic igneous rocks and biotite gabbros have considerably higher MgO contents than most other rock types, the exception being a few cordierite hornfelses and cordierite norites which have MgO values comparable with the lower MgO values of the mafic rocks. The MgO contents of the pelitic schists are lower than those of the other rock types, varying little from 2 to 2.7 wt%. The micro-norites also have much lower MgO contents than the other mafic rocks.

(v) CaO Figure 9.3.4

The mafic igneous rocks and biotite gabbros are well grouped, having higher CaO values than all other rock types. The micro-norites also have a greater CaO content than the pelitic schists and the cordierite bearing rocks. There is an overlap in the CaO content between the pelitic schists, cordierite hornfelses and cordierite norites, but the cordierite bearing rocks tend to be slightly richer in CaO than the pelitic schists.

(vi) Na_2O Figure 9.3.5

Na_2O varies widely, with a great deal of overlap between all rock types. However, the highest Na_2O values are displayed by hornfelses and the micro-norites.

(vii) K_2O Figure 9.3.6

The mafic igneous rocks, biotite gabbros and micro-norites are all well clustered with low K_2O contents relative to the other rock types. The highest K_2O values are those of the pelitic schists and of a single cordierite norite (sample BQ102 from Battlehill Quarry). The cordierite norites and hornfelses mainly have K_2O contents intermediate between the pelitic schists and the mafic rocks.

(viii) TiO_2 Figure 9.3.7

The mafic igneous rocks have considerably lower TiO_2 values than all the other rock types. The biotite gabbros have varying TiO_2 contents, varying from 1.1 to 2.7 wt%. A roughly linear trend can be seen between the pelitic schists and the cordierite norites and hornfelses, with TiO_2 increasing with decreasing SiO_2. The micro-norites also have relatively high TiO_2 contents.

(ix) Mg# Figure 9.3.8

The mafic igneous rocks all have higher Mg# than all other rock types, all with Mg# values between 0.60 to 0.85. The Mg# values of the biotite gabbros varies from 0.62 to 0.38. The lowest Mg# are displayed by the pelitic schists, most having values around 0.3 to 0.4. The cordierite norites and hornfelses have Mg# overlapping with the pelitic schists, but increasing up to about 0.6. The micro-norites both have significantly lower Mg# than the other mafic rocks, with values around 0.35.

9.3.2 Samples from S and SW of the intrusion, trace elements

Figures 9.3.9-9.3.23 are all scatter plots of trace elements in parts per million plotted against SiO_2 wt%.

(i) Nb Figure 9.3.9

The mafic igneous rocks have low Nb contents, with all having less than 7 ppm. The biotite gabbros and micro-norites, however, have higher Nb contents, varying from 12 to 49 ppm. The pelitic schists, cordierite hornfelses and cordierite norites have overlapping amounts of Nb, with the pelitic schists tending to have lower amounts than the cordierite norites and hornfelses.

(ii) Zr Figure 9.3.10

Mafic igneous rocks again have a considerably lower contents of the trace element Zr than the other rock types, being the only rock type to have Zr contents lower than 50 ppm. The rocks with the next lowest contents are the biotite gabbros, with Zr contents from 100 to 470 ppm . The pelitic schists and cordierite bearing rocks mainly have Zr contents in excess of 300 ppm.

(iii) Y Figure 9.3.11

The rocks with the lowest Y totals are the mafic-igneous rocks, with 23 to 36 ppm of this element. Again the biotite gabbros are relatively more enriched in the element, with between 45 to 74 ppm Y. The country rocks and the cordierite norites and hornfelses have a wide scatter of Y values, varying from 33 to 193 ppm.

(iv) Sr Figure 9.3.12

A considerable spread in Sr content is shown in all the major rock types. However, the pelitic schists have lower Sr contents than the cordierite norites and the highest Sr values occur in the micro-norites, and two of the cordierite hornfelses analysed.

(v) Rb. Figure 9.3.13

The mafic igneous rocks, biotite gabbros and micro-norites all have low Rb contents relative to the other rock types, with mafic igneous rocks, biotite gabbros from Battlehill Quarry and micro-norites all having less than 10 ppm, and the biotite gabbros from Westerton 21 and 48 ppm Rb. The cordierite norites and hornfelses all have Rb contents from 17 ppm to 104 ppm. The pelitic schists have the highest Rb contents, with all but one of the samples collected having greater than 100 ppm.

(vi) Zn Figure 9.3.14

The rocks with the lowest Zn content are mainly mafic igneous rocks, with most such rocks having less than 50 ppm. The pelitic schists also have relatively low contents, with 55 to 145 ppm of Zn present. The cordierite hornfelses and cordierite norites have the highest values, with 84 to 220 ppm Zn.

(vii) Cu Figure 9.3.15

The Cu content of all the rock types overlaps to some extent, but, a few patterns can be determined. The pelitic schists in general have lower Cu contents than the other rock types, with concentrations of between 1 and 59 ppm. The rocks with the highest Cu content are mafic igneous rocks, two of which have over 200 ppm Cu.

(viii) Ni Figure 9.3.16

Six of the mafic igneous rocks have very high nickel contents of over 1000 ppm. Also three pelitic schists, a cordierite hornfels, and a cordierite norite have Ni contents in excess of 500 ppm. The other rocks have varying Ni contents mainly between 0 to 250 ppm.

(ix) Cr Figure 9.3.17

Six of the mafic-igneous rocks analysed have Cr contents well in excess of the other rocks, with Cr contents between 762 and 1504 ppm. The Cr contents of all other rock types

lie between 41 to 459 ppm, and no obvious patterns of the distribution of this element between the rock types are visible.

(x) Ce Figure 9.3.18

The Ce contents of all the mafic igneous rocks, and all but one (W.TON4 from Westerton, Bin Forest) of the biotite gabbros lie between 0 and 24 ppm. All of the pelitic-schists, cordierite-bearing rocks and micro-norites have higher Ce contents than this. The cordierite norites and hornfelses have on average higher Ce content than the pelitic schists, with a mean content of 103 ppm (11 rocks) for the cordierite-bearing rocks, compared to a mean of 84 ppm (11 rocks) for the pelitic schists.

(xi) Nd Figure 9.3.19

Only one sample from the mafic igneous rocks contained any detectable amount of Nd, with sample BIN103 containing 13 ppm Nd. The biotite gabbros contain some Nd, with one sample containing 47 ppm. However, the cordierite-bearing rocks and the pelitic schists mainly have Nd contents from 16 to 60 ppm.

(xii) V Figure 9.3.20

The rocks with the lowest V content are the mafic igneous rocks, with all samples having less than 200 ppm V. The biotite gabbros are slightly more enriched in V than the mafic igneous rocks with up to 265 ppm. The pelitic schists have intermediate V contents, with a range between 93 and 189 ppm. The highest V values are recorded solely by the cordierite norites and hornfelses, with all of the hornfelses and all but one of the cordierite norites having V contents between 271 to 412 ppm.

(xiii) La Figure 9.3.21

The mafic igneous rocks, biotite gabbros and micro-norites have lower La content than all but a few of the pelitic schists and cordierite hornfelses. The pelitic schists have La contents varying from 27 to 45 ppm. The highest La contents occur in the cordierite norites and hornfelses, with all but two of the hornfelses lying within the range 35 to 64 ppm.

(xiv) Ba Figure 9.3.22

The mafic igneous rocks and the biotite gabbros from Battlehill Quarry have either no detectable Ba, or extremely low Ba contents, with only four of these rocks registering the presence of this element. However, the two biotite gabbros analysed from Westerton, Bin Forest have much higher Ba contents of 431 and 785 ppm. The pelitic schists have a wide range of Ba contents, varying from 111 to 1172 ppm. The cordierite hornfelses and norites again have varying Ba contents, with most having between 400 to 1000 ppm.

(xv) Sc Figure 9.3.23

The Sc content of the mafic igneous rocks and biotite gabbros varies continuously from 9 to 50 ppm. The pelitic schists have generally low Sc contents, with between 7 to 20 ppm. The cordierite hornfelses and cordierite norites have higher Sc contents than the pelitic schists, varying from 23 to 53 ppm.

9.3.3 Samples from W margin of the intrusion, major elements

Figures 9.3.24 to 9.3.30 are scatter plots, representing elements in wt% against SiO_2 wt% Figure 9.3.31 is a plot of Mg# (molar Mg/(Mg+Fe)) plotted against SiO_2 wt%. The MnO and P_2O_5 contents of all the samples analysed were again too low to warrant any discussion. The analyses given for mafic igneous rocks for rocks from the S and SW margins of the Huntly Gabbro are taken to represent the average composition of the Gabbro as a whole, and are again used here.

(i) SiO_2

The cordierite hornfelses again have lower SiO_2 contents than the pelitic schists, the sole exception to this is sample SIN107, (a garnet-mica schist from Cairnie, which is composed virtually entirely of mica, with subordinate garnet) which has a lower SiO_2 content than all the hornfelses. The garnet tonalites, as with the cordierite norites from the S and SW margins of the Gabbro, have generally less SiO_2 than the pelitic schists. The mafic igneous rocks and biotite gabbros have less SiO_2 than all other rock types.

(ii) Al_2O_3 Figure 9.3.24

The Al_2O_3 contents of all rock types overlap, though the lowest quantities of Al_2O_3 are generally found in the pelitic schists. However, when plotted against SiO_2 a linear trend can be seen between the pelitic schists, garnet tonalites, and to a lesser extent the cordierite hornfelses, with the mafic-igneous rocks and biotite gabbros well grouped together.

(iii) Fe_2O_3 Figure 9.3.25

The garnet tonalite Fe_2O_3 totals are slightly higher than most of the pelitic schists, whilst the cordierite hornfelses have higher Fe_2O_3 contents again, up to nearly 15 wt%. The amount of Fe_2O_3 in the mafic igneous rocks overlaps with the other rock types.

(iv) MgO Figure 9.3.26

The MgO contents of the mafic igneous rocks and biotite gabbros are generally greater than those of the other rock types. The cordierite hornfelses and garnet tonalites both have on average slightly less MgO than the pelitic schists, with means of 2.61 and 3.91 wt% MgO respectively, compared to a mean of 4.76 wt% for the pelitic schists.

(v) CaO Figure 9.3.27

As with the rocks from the S and SW margins of the Gabbro the mafic-igneous rocks and biotite gabbros contain considerably more CaO than the other rock types. The CaO contents of cordierite hornfelses and garnet tonalites are greater than those of the pelitic schists, which have a mean CaO content of 0.67 wt%. The hornfelses have on average slightly more CaO than the garnet tonalites.

(vi) Na_2O Figure 9.3.28

The Na_2O contents of the pelitic schists ranges from 0.25 to 2.82 wt%. The garnet tonalites contain slightly more Na_2O, with a mean of 3.23 wt% and the cordierite hornfelses have higher Na_2O contents again, up to 4.77 wt%. The spread of Na_2O contents in the mafic igneous rocks and biotite gabbros cuts across the Na_2O contents of all the other rock types.

(vii) K_2O Figure 9.3.29

The cordierite hornfelses, garnet tonalites and pelitic schists have amounts of K_2O varying from 1.70 to 5.21 wt%. These rocks therefore all have higher K_2O contents than all of the mafic-igneous rocks, and biotite gabbros, with the maximum amount of K_2O recorded in the mafic igneous rock, pelitic schists and biotite gabbros being 1.39 wt%.

(vii) TiO_2 Figure 9.3.30

The cordierite hornfelses and garnet tonalites have slightly higher mean TiO_2 totals than the pelitic schists, the hornfelses and tonalites having mean TiO_2 totals of 1.72 and 1.52 wt% respectively, compared to a mean total of 0.89 wt% for the pelitic schists. All bar one of the mafic igneous rocks analysed have lower TiO_2 totals than the other rock types, and the three biotite gabbros from Westerton, Bin Forest all have in excess of 2 wt% TiO_2.

(viii) Mg# Figure 9.3.31

Again, as with the rocks from the S and SW margins, the mafic igneous rocks all have higher Mg# values than all the other rocks and the biotite gabbros have Mg# values which overlap with the remaining rock types. The pelitic schists have higher Mg# values than the cordierite hornfelses and garnet tonalites.

9.3.4. Samples from W margin of the intrusion, trace elements

Figures 9.3.32-9.3.23 are all scatter plots of trace elements in ppm. plotted against SiO_2 wt%.

(i) Nb Figure 9.3.32

The cordierite hornfelses, garnet tonalites and biotite gabbros are all preferentially enriched in Nb relative to the pelitic schists. The pelitic schists in turn have uniformly greater concentrations of Nb than the mafic igneous rocks.

(ii) Zr Figure 9.3.33

Again, all rock types have higher amounts of Zr than the mafic igneous rocks, with the greatest concentrations in garnet tonalites and cordierite hornfelses, with maximum Zr contents of over 1500 ppm.

(iii) Y Figure 9.3.34

Except for a single analysis of a garnet tonalite all of the garnet tonalites and cordierite hornfelses have greater amounts of Y than all the other rock types. The graph shows that the pelitic-schists, garnet tonalites and cordierite hornfelses form a linear trend, with increase in Y with decrease in SiO_2, with the mafic igneous rocks and biotite gabbros forming a separate cluster.

(iv) Sr Figure 9.3.35

All of the cordierite hornfelses and garnet tonalites have greater Sr concentrations than the peltic schists and have concentrations of Sr which overlap with the mafic igneous rocks and biotite gabbros.

(v) Rb Figure 9.3.36

The pelitic schists, cordierite hornfelses and garnet tonalites have Rb concentrations greater than the mafic igneous rocks and all but one of the biotite gabbros analysed, varying between 40 to 176 ppm.

(vi) Zn Figure 9.3.37

There is a linear trend with decreasing SiO_2 with progressively greater concentrations of Zn in the pelitic schists, garnet tonalites, then cordierite hornfelses. These three rock types are well seperated from the mafic igneous rock and biotite gabbros, which all have low SiO_2 and Zn values.

(vii) Cu Figure 9.3.38

The Cu concentration in the pelitic schists, cordierite hornfelses and garnet tonalites varies between 0 to 104 ppm, overlapping with most of the mafic igneous rocks.

(viii) Ni Figure 9.3.39

No pattern can be seen between the Ni contents of the five rocks types.

(ix) Cr Figure 9.3.40

There is a slight increase in Cr with increasing SiO_2 from the cordierite hornfelses and garnet tonalites to the pelitic schists. The hornfelses and tonalites mainly have lower Cr concentrations than the mafic igneous rocks and biotite gabbros.

(x) Ce Figure 9.3.41

A linear trend can be seen here with increasing Ce with decreasing SiO_2, with the pelitic schists, garnet tonalites and cordierite hornfelses having progressively higher Ce concentrations.

(xi) Nd Figure 9.3.42

A similar trend to that shown for Ce in Figure 9.3.41 is shown here with the pelitic schists having less of the trace element than the cordierite hornfelses and garnet tonalites. However, for Nd the concentration in the cordierite hornfelses and garnet tonalites occurs over the same range (49 to 73 ppm).

(xii) V Figure 9.3.43

The V contents of all the rock types overlap, and no patterns or trends are apparent here.

(xiii) La Figure 9.3.44

The pelitic schists, mafic igneous rocks, biotite gabbros and one of the garnet tonalites analysed all have La contents over the range 16 to 32 ppm. The remainder of the garnet tonalites and all the cordierite hornfelses have, however, greater concentrations of La, with between 44 and 63 ppm.

(xiv) Ba Figure 9.3.45

The cordierite-hoenfelses, garnet tonalites and pelitic schists have much higher Ba concentrations than all the mafic igneous rocks, which all have less than 25 ppm Ba. The cordierite hornfelses have mainly a higher Ba content than the pelitic schists, and the garnet tonalites have higher Ba contents again, up to 1157 ppm.

(xv) Sc Figure 9.3.46

A spread in Sc content is shown in most of the rock types, the exception being the pelitic schists with between 9 and 19 ppm. The cordierite hornfelses and garnet tonalites have generally slightly higher Sc concentrations than the pelitic schists, whilst the Sc contents of all three rock types overlaps with the mafic igneous rocks and biotite gabbros .

9.3.5 Rocks from other localities

(i) Ternemny Quarry G.R. 555528

Analyses of three garnet tonalites were made. The garnet tonalites here have both major and trace element chemistry very similar to the garnet tonalites from Cormalet.

(ii) Wether Hill G.R. 570544

Three cordierite hornfelses from this locality were analysed. The major and trace element chemistry of these cordierite hornfelses is essentially the same as the chemistry of the cordierite hornfelses from the S and SW and the W margins of the Huntly Gabbro.

A biotite gabbro from this locality was also analysed, and exvept for a slightly lower Al_2O_3 total, this rock has a similar major element chemistry to the biotite gabbros from Westerton and Battlehill Quarry.

9.4 Discussion of Results

An attempt is made here to bring together the chemical distribution patterns which are outlined above in section 9.3 and to test these patterns against the four models presented in 9.1. Figure 9.4 summarises the chemical distribution patterns which are seen between the various rock types, and shows which of the four models these patterns either support, or invalidate. A brief discussion is now made of the validity of each of these four models as a possible model for the formation of the cordierite norites, cordierite hornfelses, and garnet tonalites of the Huntly District.

Model 1 Mixing of Pelitic Country Rocks and Mafic Magma

This model, proposed by Read (e.g. 1923b) for the formation of the cordierite norites and the cordierite hornfelses of the Huntly district relies on the 'assimilation of country rocks' by mafic magma at and near the margins of the Huntly Gabbro. Therefore, the chemical patterns which support such a model require that the concentrations of elements in some additive combination of cordierite norites and cordierite hornfelses can be achieved by mixing of positive quantities of mafic igneous rock and of pelitic schist (Figure 9.1.5).

The cordierite norites and hornfelses do have concentrations of K_2O, SiO_2, CaO, MgO, Rb, Cu, and Rb that lie in-between the concentrations of these elements in the mafic igneous rocks and the pelitic schists. However, the Fe_2O_3, TiO_2, Zn and V contents in the cordierite-bearing rocks are higher than in both the pelitic schists and the mafic igneous rocks (Figures 9.3.2,7,14,20). Mixing together positive amounts of these pelitic rocks and mafic igneous rocks cannot therefore have resulted in the cordierite-bearing rocks acquiring the observed concentrations of the elements Fe_2O_3 , TiO_2, Zn and V, no matter which proportions of the two starting rock types are used. The trace elements Nb, Zr, Ba, Y, Ce, and Nd are distributed approximately equally between the cordierite-bearing rocks and the pelitic schists, but occur in lower concentrations in the mafic igneous rocks. This again invalidates any mixing model for the formation of these rocks.

The set of graphs plotted for chemical data for rocks from Cormalet, and the W margins of the Huntly Gabbro show the same patterns as seen in the graphs presented for the rocks from the S and SW margins of the Gabbro; concentrations of the major elements Fe_2O_3, and TiO_2 and the trace elements Nb, Zr, Y, Zn, Nd, Ba are all higher in the garnet tonalites and the cordierite hornfelses than in the pelitic schists and the mafic igneous rocks. This disproves the hypothesis that the garnet tonalites were formed by mixing of the pelitic and mafic igneous rocks.

Model 2 Partial Melting of Pelitic Schists in Closed Systems

Gribble (e.g. 1970), then Ashworth (1972) believed that the cordierite norites were formed by partial melting of pelitic country rocks close to the contact with and broken off into the Huntly Gabbro. Ashworth (1972) believed that this melting was of limited extent,

with none of the melt produced being extracted. Therefore the cordierite norites were seen to represent the sole melt fraction, and the cordierite hornfelses the depleted residue of this melting. Chemical data in support of this model must show that any elements enriched in the cordierite norites relative to their implied protoliths (i.e. Pelitic schists from outside the aureole of the gabbro) must subsequently be depleted in such elements in the cordierite hornfelses, and vice versa. Therefore this model requires that concentrations of elements in the pelitic schists should be intermediate, relative to the cordierite norites and the cordierite hornfelses (Figure 9.1.6).

Examination of the graphs presented in 9.3 shows that for none of the elements analysed does the concentration of the element in the pelitic schists lie in-between the concentration of the element in the cordierite norites/garnet tonalites and the cordierite hornfelses. Chemical concentrations of elements in the pelitic schists commonly trend towards the cordierite norites, and then towards the cordierite hornfelses (e.g. for K_2O, Rb, Zn). The cordierite norites, as with the cordierite hornfelses, are relatively depleted in mobile elements such as SiO_2, and K_2O and enriched in immobile elements such as MgO, CaO and Zn; this would not be the case if these rocks represented the sole melt fraction of a partial melting reaction.

It can therefore be concluded that the cordierite norites, and garnet tonalites cannot represent the only melt fraction formed by the partial melting of rocks equivalent to the pelitic rocks which trend towards the Huntly intrusion.

Model 3 Partial Melting of Pelitic Schists, with Melt Extraction

With this model, as in model 2, the pelitic schists are believed to have partially melted. With this model, however, most of the melt formed is extracted from the system. The cordierite hornfelses are therefore seen to represent the restitic residue of partial melting and the cordierite norites or garnet tonalites to represent a late melt fraction which contains a large percentage of entrained restite. Chemical patterns that support this model are those that show linear trends from the pelitic schists through the cordierite norites, towards the cordierite hornfelses (Figure 9.1.7).

As mentioned in the discussion on the validity of model 2, the cordierite norites and cordierite hornfelses are both relatively enriched in immobile elements, and depleted in

mobile elements compared to the pelitic schists. Also the cordierite norites have concentrations of many elements which lie in-between the concentrations of these elements in the pelitic schists and the cordierite hornfelses, and the chemical distribution patterns seen in many of the graphs (e.g. 9.3.2, 9.3.3, 9.3.8) resemble the suggested elementary distribution pattern for this model (Figure 9.1.7). In addition for none of the elements analysed do the concentrations in the cordierite norites/garnet tonalites and cordierite hornfelses lie opposite each other, relative to the pelitic schists (as shown in Figure 9.1.6). Such patterns, if present would represent evidence against the possibility of this model occurring.

The evidence above is all in support of model 3 as being the process which led to the formation of the cordierite-bearing rocks and the garnet tonalites. One problem in being able to prove the validity of this model is the lack of any other igneous rocks in the Huntly area which can be proved to represent this 'extracted' melt, making the plotting of the compositions of the 'extracted' melts against the other rock types impossible. However, by qualitative observations, it can be assumed that any of the 'extracted' melt must be enriched in the elements which are depleted in the cordierite hornfelses/norites relative to the pelitic schist protoliths, and vice versa. Therefore, any such 'extracted' melt would be relatively enriched in the major elements such as SiO_2 and K_2O, and depleted in elements such as Al_2O_3, Fe_2O_3, MgO, CaO, and TiO_2 relative to the pelitic schists .

Model 4 Multiple Intrusion of Mafic Igneous Rock, Cordierite norites, and Garnet tonalites

With model 4 the mafic igneous rocks, cordierite norites, and garnet tonalites are all igneous rocks that are intruded adjacently, and originated from one or more deeper source magma bodies. The cordierite hornfelses subsequently represent recrystallised pelitic country rocks, which have not undergone any partial melting. This model therefore requires that the cordierite hornfelses are chemically identical to the adjacent non-thermally metamorphosed pelitic schists (Figure 9.1.8).

The cordierite hornfelses are, however, enriched in immobile major elements (e.g. Al_2O_3, MgO, Fe_2O_3, CaO, TiO_2) and greatly depleted in SiO_2 and K_2O relative to the pelitic schists from the margins of the Huntly Gabbro. If these pelitic schists represent the true

protoliths of the cordierite hornfelses then they have must have undergone extensive chemical alteration. Many of the graphs plotted also appear to show linear trends between the pelitic schists, the cordierite hornfelses and the cordierite norites/garnet tonalites. These observations, coupled with the mineralogical similarities between the cordierite hornfelses and cordierite norites are evidence against the validity of this model.

Biotite gabbros

As highlighted in Figure 9.4 the biotite gabbros are relatively enriched in a number of elements relative to the mafic igneous rocks from the Bin Quarry and other localities. The biotite gabbros are enriched in the major elements K_2O and TiO_2 , notably the two additional components required to form biotite that occur in only low concentrations in the other mafic igneous rocks. As biotite is a hydrous mineral, the biotite gabbros must also by such an argument contain more H_2O than present in the mafic igneous rocks, which contain only the anhydrous minerals olivine, clino and ortho-pyroxenes, plagioclase and magnetite. Concentrations of the trace elements Nb, Zr, Y, Zn, Rb, Ce, and Nb are all much higher in the biotite gabbros than in the mafic igneous rocks. The concentrations of these trace elements in the biotite gabbros are similar to their concentration in the pelitic schists, and occasionally (as for Zr), as high as the concentration of the trace elements in the cordierite norites and cordierite hornfelses.

The close proximity of the biotite gabbros to either the xenolithic cordierite-bearing rocks, and/or to the edge of the Huntly intrusion, tied in with their enrichment in the elements mentioned above suggests that these rocks have undergone some form of metasomatic alteration, possibly by fluids sourced from adjacent pelitic rocks and the cordierite norites.

Micro-norites

Although only two analyses of micro-norites from Battlehill Quarry are presented, they show sufficient chemical differences from the mafic igneous rocks and biotite gabbros to suggest that they originate from a separate source magma. The similarity in the trace element composition of the micro-norites with the cordierite norites/hornfelses also suggests that the

micro-norites may have undergone some form of alteration similar to that seen in the biotite gabbros.

9.5 Theoretical Melt Compositions

The whole rock chemistry data from both the W, and S and SW margins of the Huntly Gabbro all support model 3. In this model the cordierite hornfelses represent the restitic residues of partial melting, and the pelitic schists their non-melted protolith. As the bulk compositions of this 'protolith' and the complementary restite are known it is therefore possible to model the compositon of the 'extracted' melt via simple mixing calculations.

The cordierite hornfels and pelitic schist analyses used in the two sets of graphs from section 9.3 were used for the mixing calulations, and were averaged to give two mean hornfels and two mean pelitic schist compositions (one set from the rocks from the W margin of the gabbro, theother from the S and SW margins). Positive quantities of theoretical melt were then mixed with quantities of mean cordierite hornfels so that the sum composition was equal to that of the mean pelitic schist.

The theoretical melt compositions calculated from the mean hornfels and pelitic schist data are given in Table 9.5.1.

(i) Rocks from S and SW margins, theoretical melt composition

The minimum mixing melt/cordierite hornfels ratio which uses only positive quantaties of all elements, to give the mean pelitic schist composition, requires the mixing of three parts melt with two parts of cordierite hornfels. Any mixing with greater ratios of cordierite-hornfels requires negative amounts of CaO, then MgO to be used from the melt composition. The melt compositions given in Table 9.5.1 show that the 'extracted' melts are relatively enriched in SiO_2 and K_2O compared to the pelitic shist, but depleted in Fe_2O_3, MgO, CaO, and TiO_2.

The CIPW norm calculations (Table 9.5.2) show that the melts are peraluminous (corundum normative), and plot within the granite field in the QAP diagram (Figure 9.5.1).

(ii) Rocks from W margin of Huntly Gabbro

Any theoretical melts calculated with melt/cordierite hornfels ratios of less than 4:1 require negative quantaties of CaO to be used (Table 9.5.1). Such a ratio could suggest that

unusually large amounts of melt must have been extracted from the pelitic schists from the W margins of the Gabbro. However, as the number of cordierite hornfels analyses used to calculate the mean hornfels composition is relatively small (three), this suggests that their mean CaO value could be an overestimate, and therefore cause the negative CaO quantaties required to give pelitic schist compositions (Table 9.5.1).

The theoretical 'extracted' melt, (WM5), is again peraluminous (Table 9.5.2), and plots within the granite field on the QAP diagram (Figure 9.5.1). The norm calculation for this melt also contains more plagioclase than the 'extracted' melts from the S and SW margins.

9.6 Conclusions

Chemical distribution patterns shown between the cordierite hornfelses, cordierite norites/garnet tonalites, pelitic schists, mafic igneous rocks, and biotite gabbros show that the cordierite hornfelses and the cordierite norites/garnet tonalites could not have been formed by either, mixing of mafic magma with pelitic schist, or by limited partial melting of pelitic schists in closed systems. The chemical evidence instead points towards a model by which these rocks formed by extensive partial melting of pelitic schists, with the cordierite hornfelses left behind as the restitic residue of this melting, and the cordierite norites and garnet tonalites containing a large proportion of entrained restite crystallising *in-situ*. Mixing calculations suggest that silica-potassium-rich, calcium-iron-magnesium-poor granitic melts may have been extracted from pelitic schist protoliths. These calculations also suggest that a large quantity of melt may have been extracted from the pelitic schist protoliths.

The biotite gabbros from near the intrusions edge and from those associated with the cordierite-bearing rocks show chemical evidence of being contaminated, possibly by hydrothermal fluids derived from the country rocks, or even from the now absent 'extracted' melt.

These conclusions highlight the need for experimental work to determine whether or not subjecting representative samples of the suggested pelitic-protolith rocks to the estimated inner-aureole pressure and temperature conditions can lead to such extensive partial melting. Such experiments would attempt to recreate the same restitic mineral assemblages as seen in

the cordierite hornfelses, and could also allow the compositions and quantities of the 'extracted' melt to be determined.

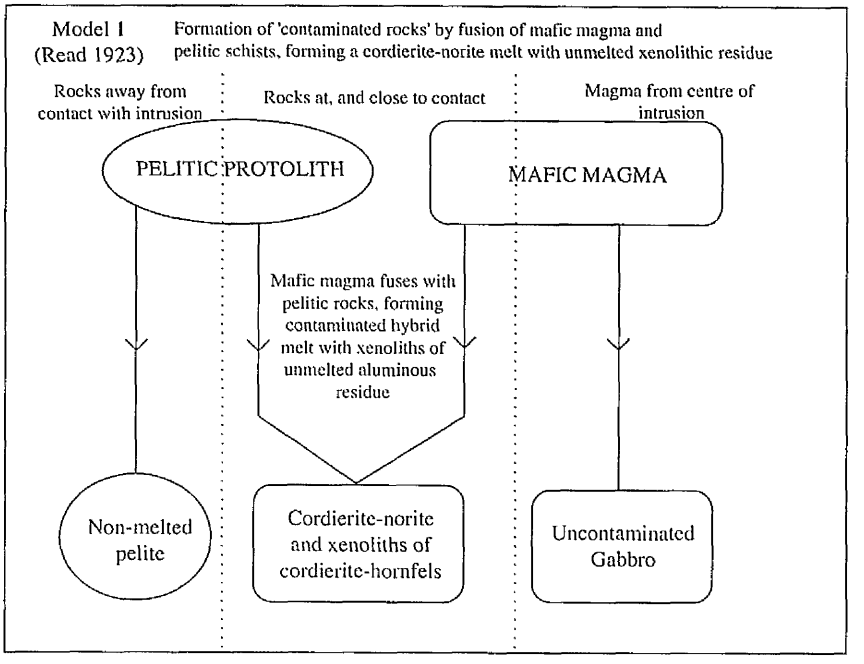

Figure 9.1.1

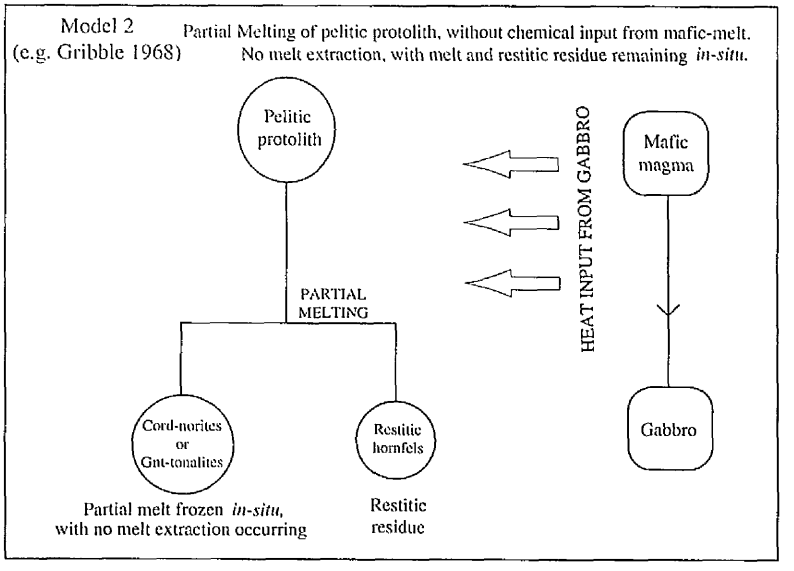

Figure 9.1.2

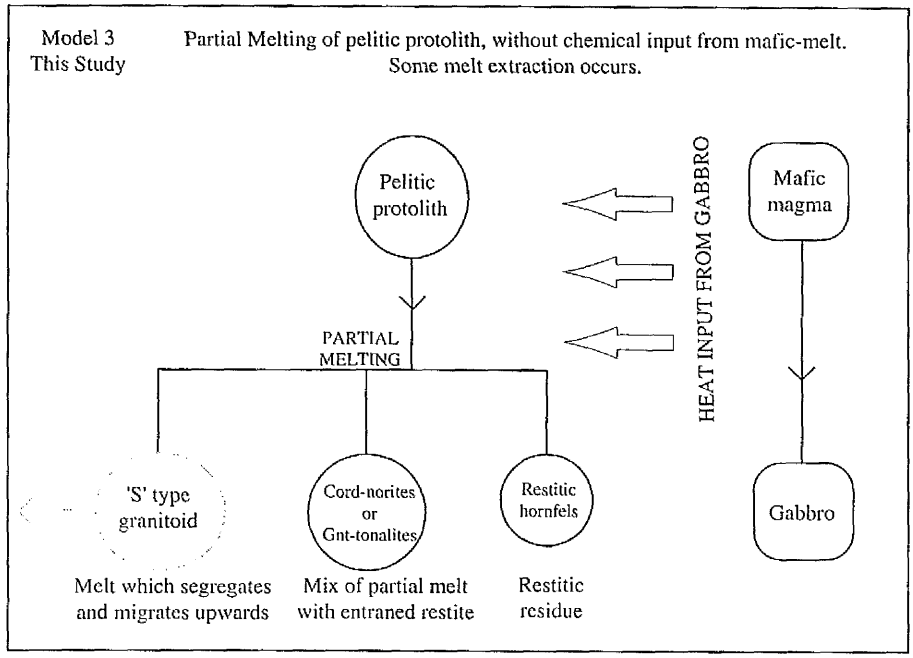

Figure 9.1.3

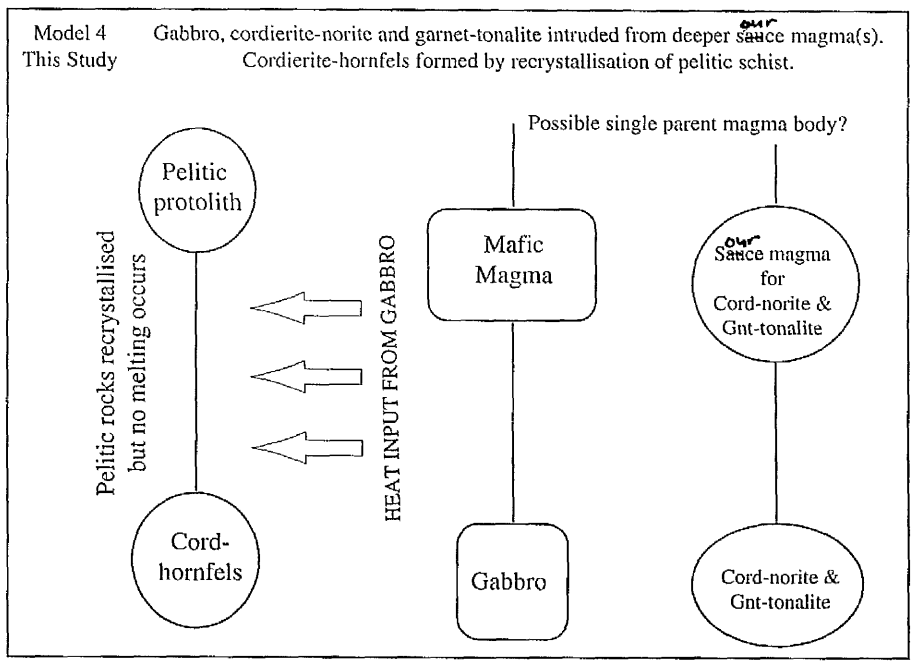

Figure 9.1.4

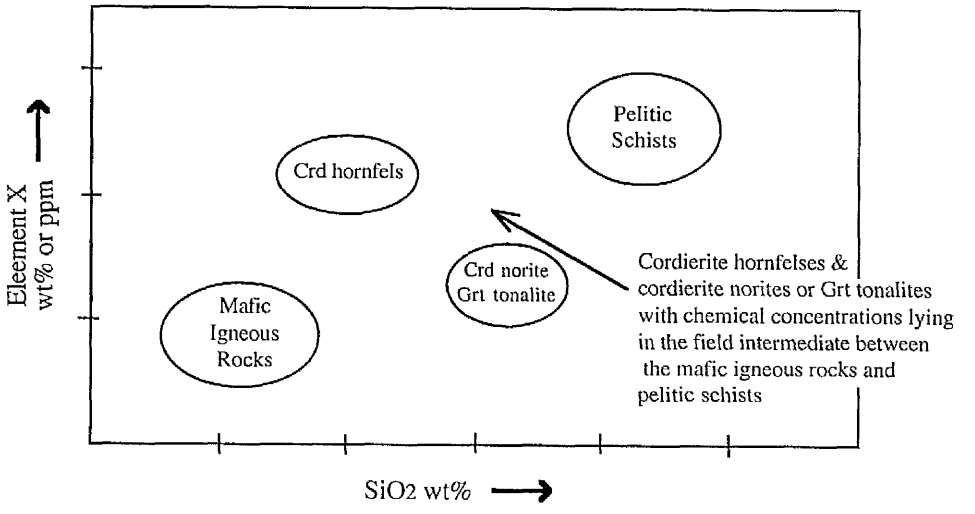

Figure 9.5.1

Representative Diagram, showing chemical distribution pattern which might be expected for Model 1 (Assimilation of Pelitic schist by Mafic magma)

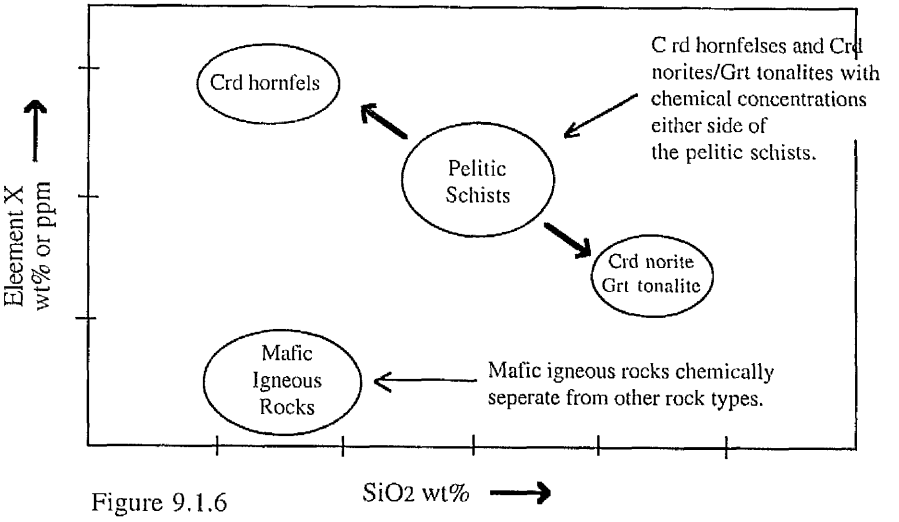

Figure 9.1.6

Diagram, showing chemical distribution patterns which might be expected for Model 2 (Partial melting of pelitic rocks in closed systems).

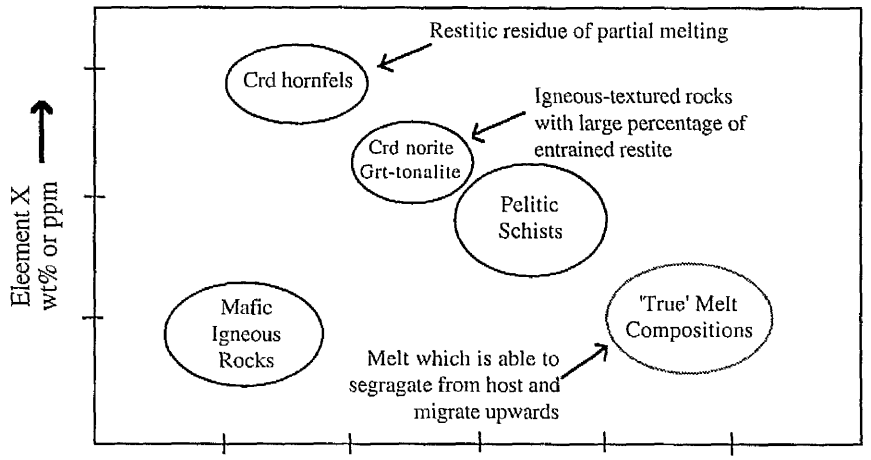

Figure 9.1.7

Diagram, showing chemical distribution pattern which might be expected for Mechanism 3 (Partial melting of pelitic rocks, with some degree of melt extraction).

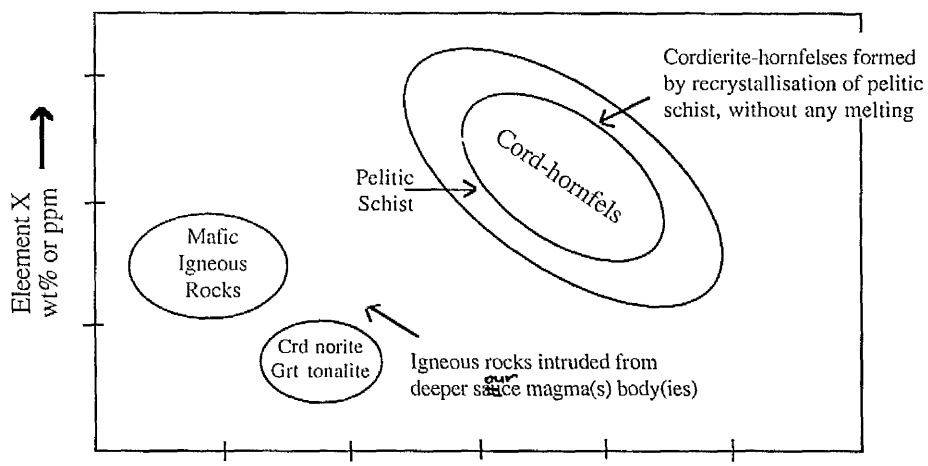

Figure 9.1.8

Diagram represeting the chemical patterns which might be expected for Mechanism 4. (Intrusion of Mafic igneous rocks, cordierite-norites and garnet-tonalites intruded separately).

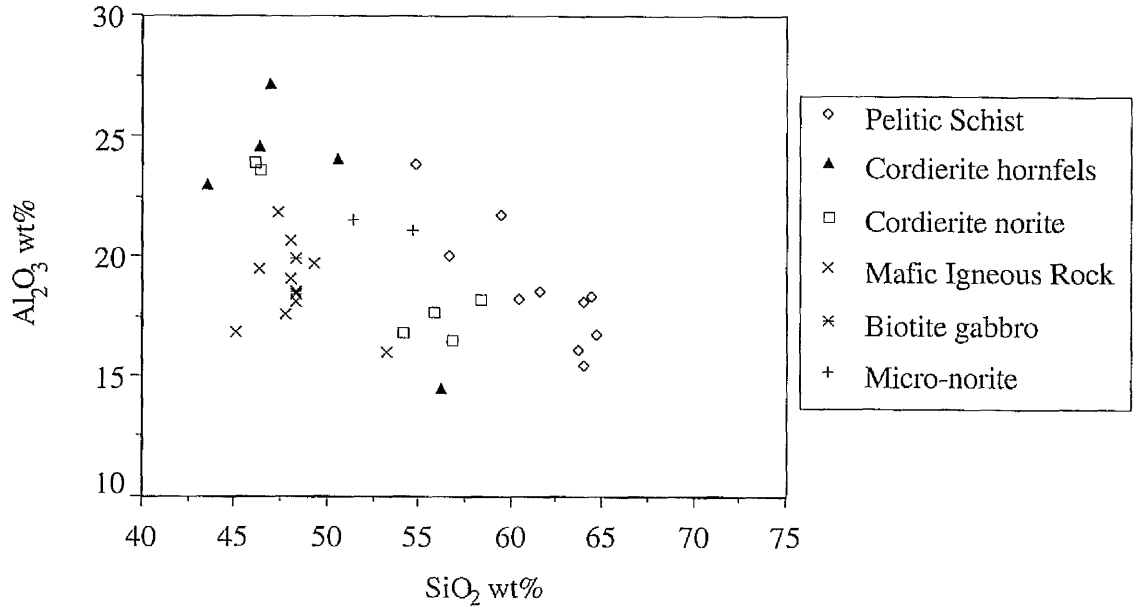

Figure 9.3.1 SiO_2-Al_2O_3 plot for rocks from the S and SW margins of the Huntly Gabbro.

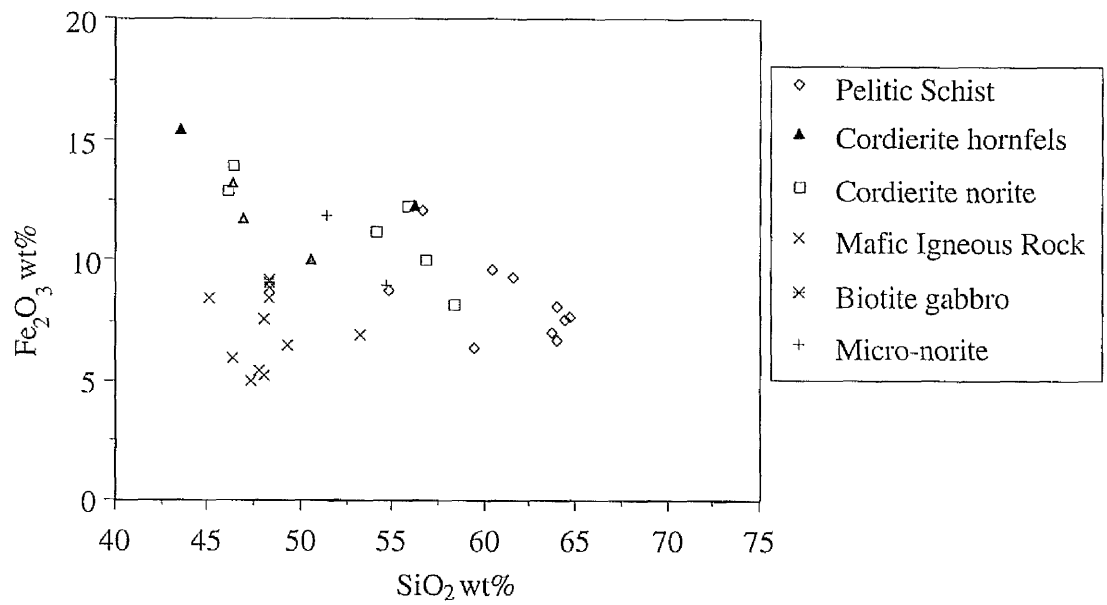

Figure 9.3.2 SiO_2-Fe_2O_3 plot for rocks from the S and SW margins of the Huntly Gabbro.

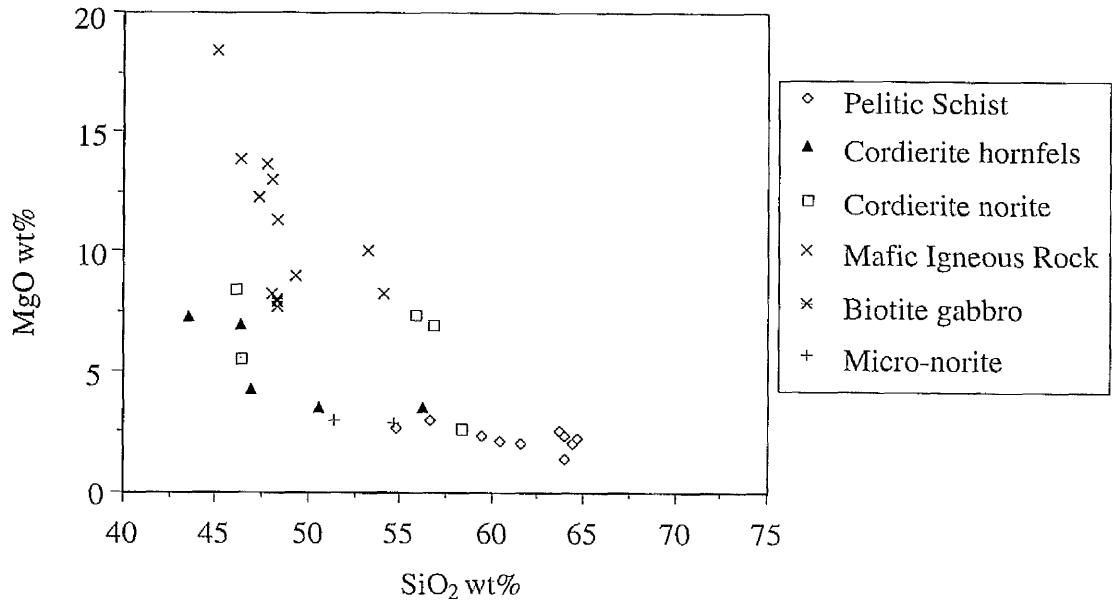

Figure 9.3.3 SiO_2-MgO plot for rocks from the S and SW margins of the Huntly Gabbro.

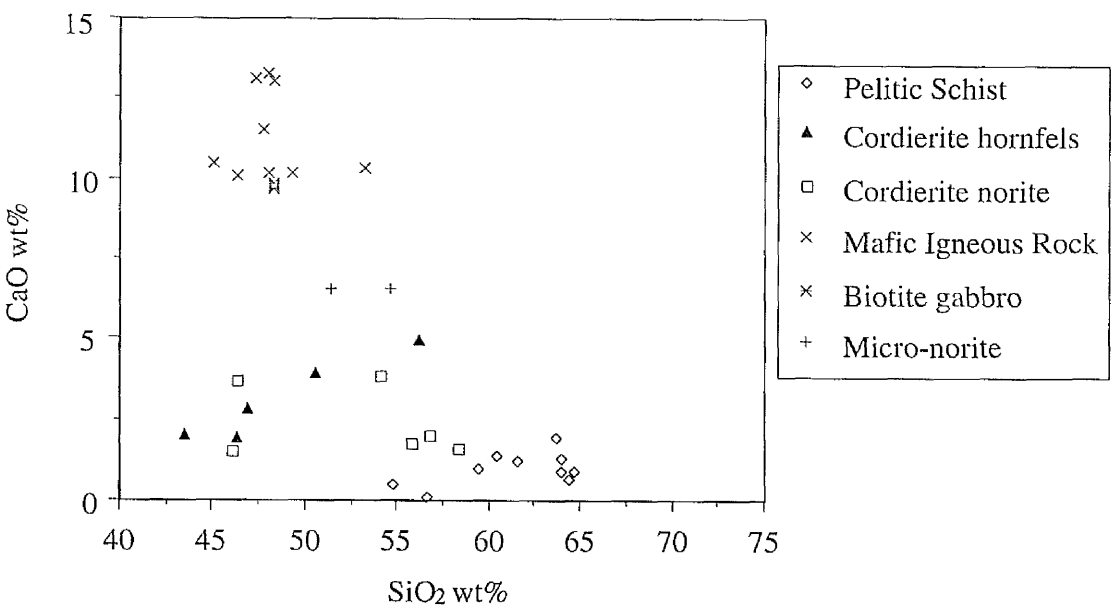

Figure 9.3.4 SiO_2-CaO plot for rocks from the S and SW margins of the Huntly Gabbro.

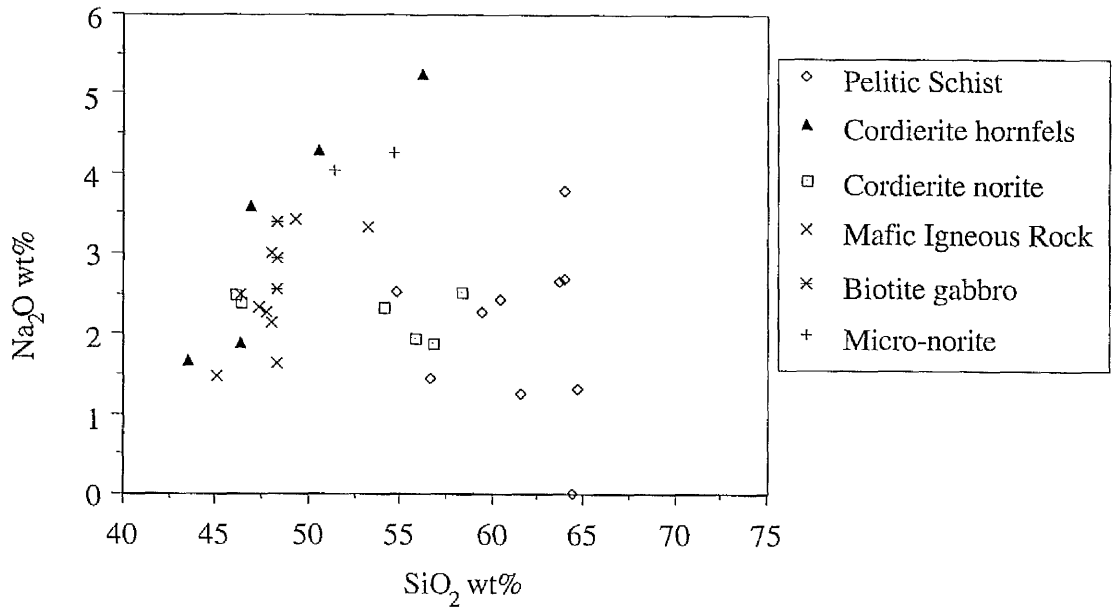

Figure 9.3.5 SiO_2-Na_2O plot for rocks from the S and SW margins of the Huntly Gabbro.

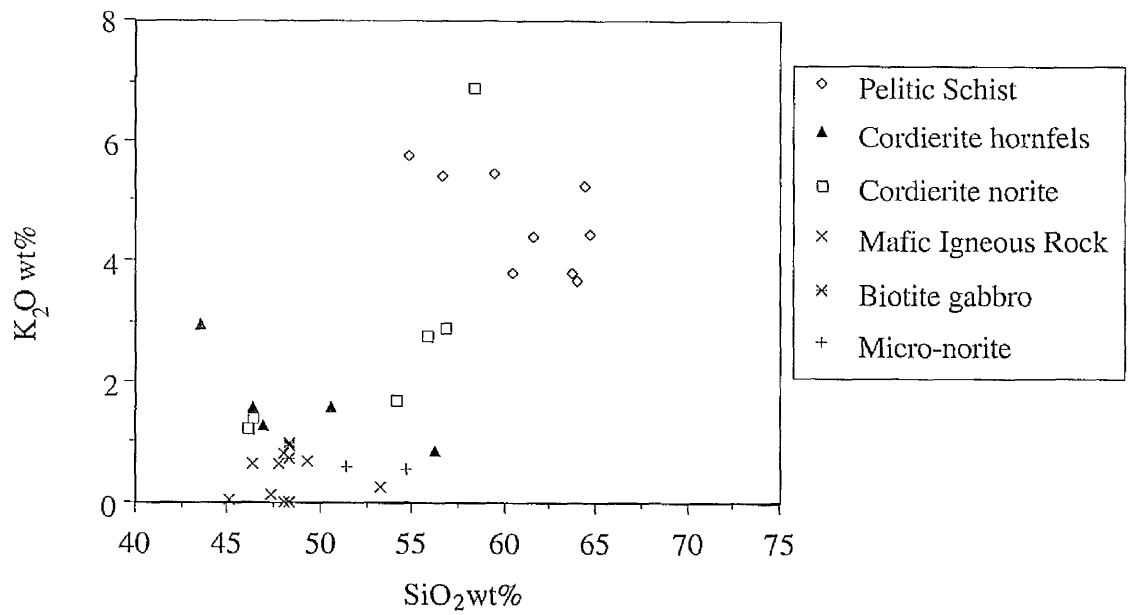

Figure 9.3.6 SiO_2-K_2O plot for rocks from the S and SW margins of the Huntly Gabbro.

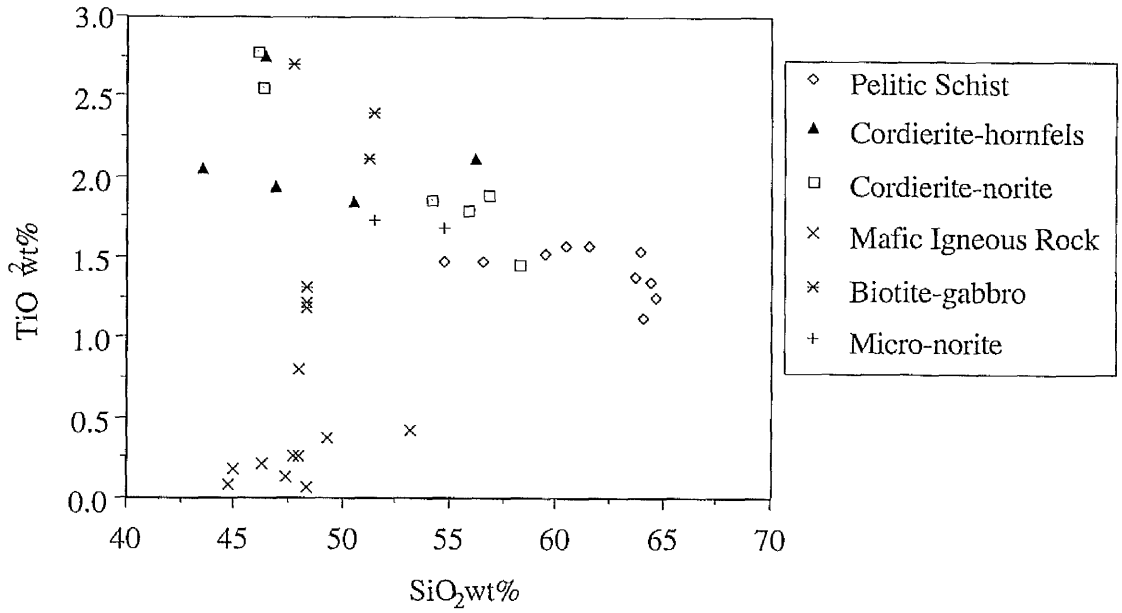

Figure 9.3.7 SiO_2-TiO_2 plot for rocks from the S and SW margins of the Huntly Gabbro.

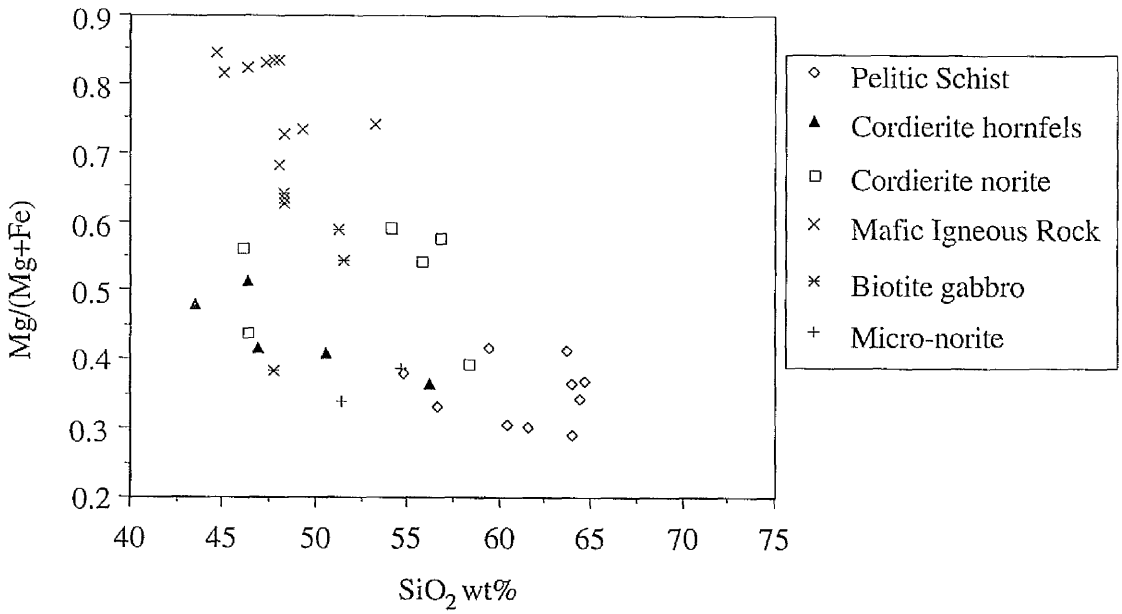

Figure 9.3.8 SiO_2-Mg# plot for rocks from the S and SW margins of the Huntly Gabbro.

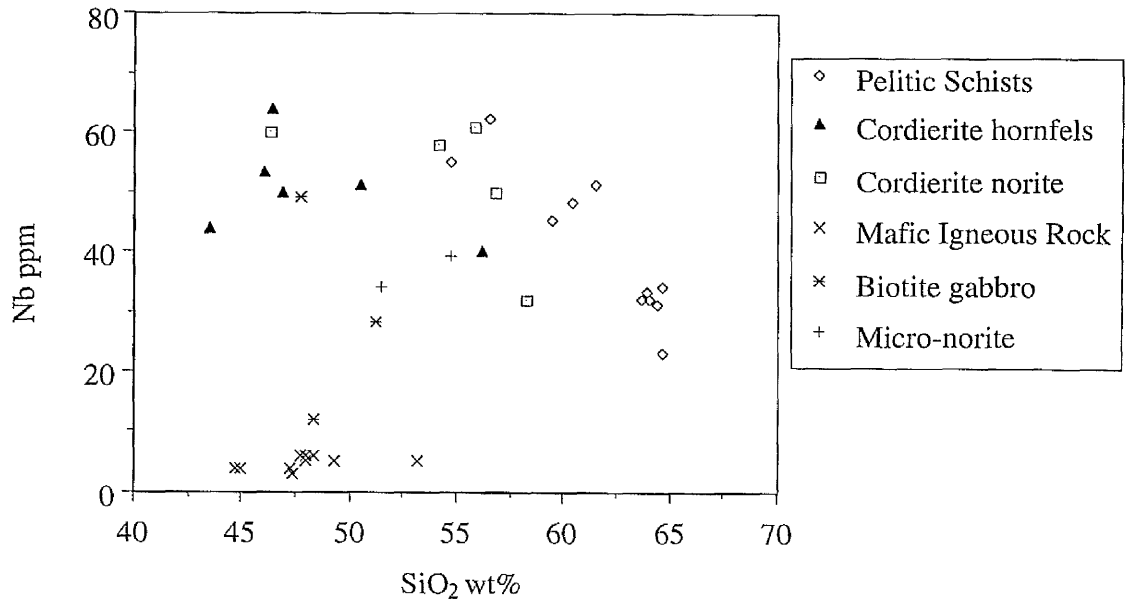

Figure 9.3.9 SiO_2-Nb plot for rocks from the S and SW margins of the Huntly Gabbro.

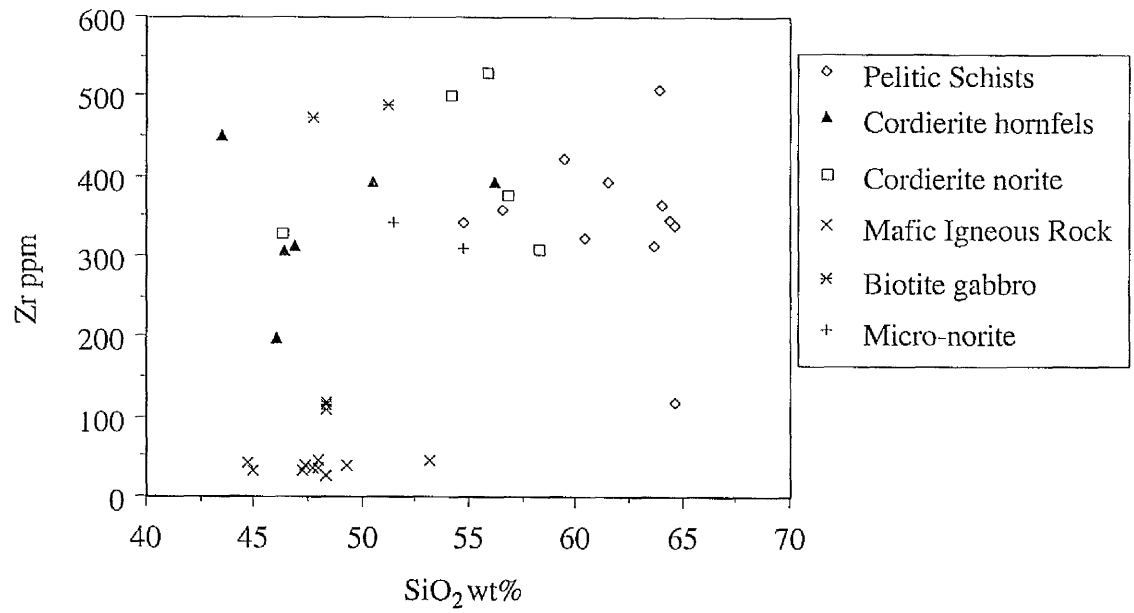

Figure 9.3.10 SiO_2-Zr plot for rocks from the S and SW margins of the Huntly Gabbro.

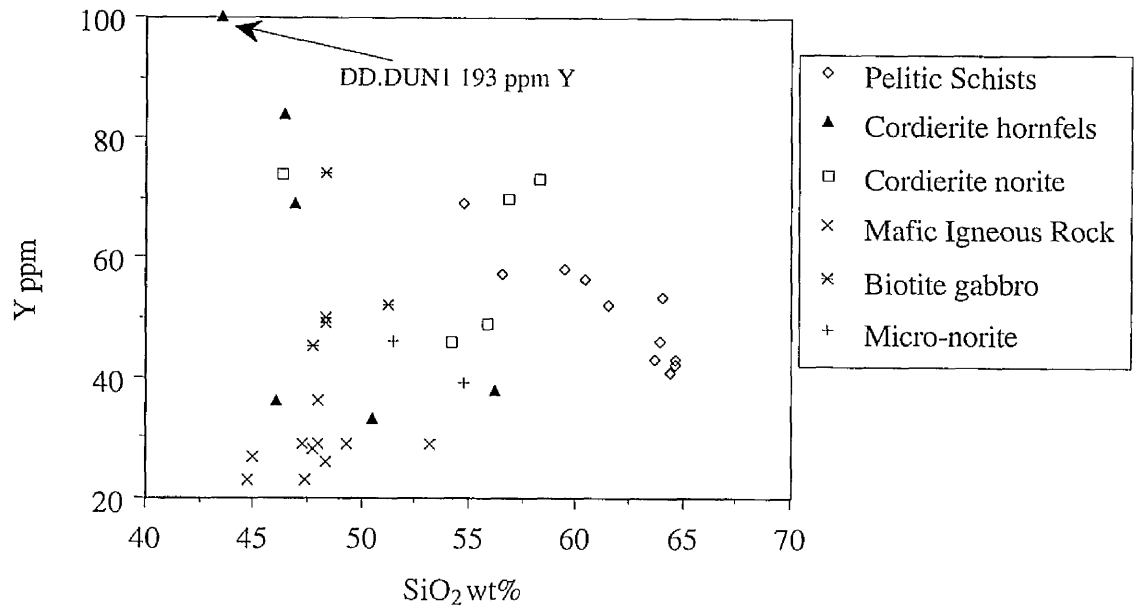

Figure 9.3.11 SiO_2-Y plot for rocks from the S and SW margins of the Huntly Gabbro.

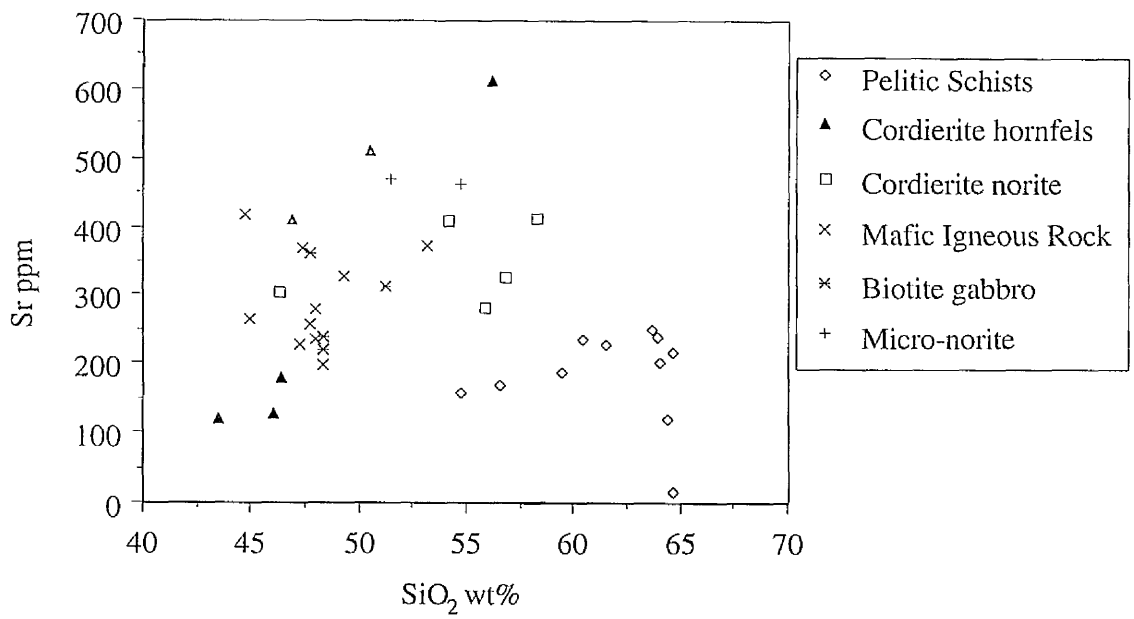

Figure 9.3.12 SiO_2-Sr plot for rocks from the S and SW margins of the Huntly Gabbro.

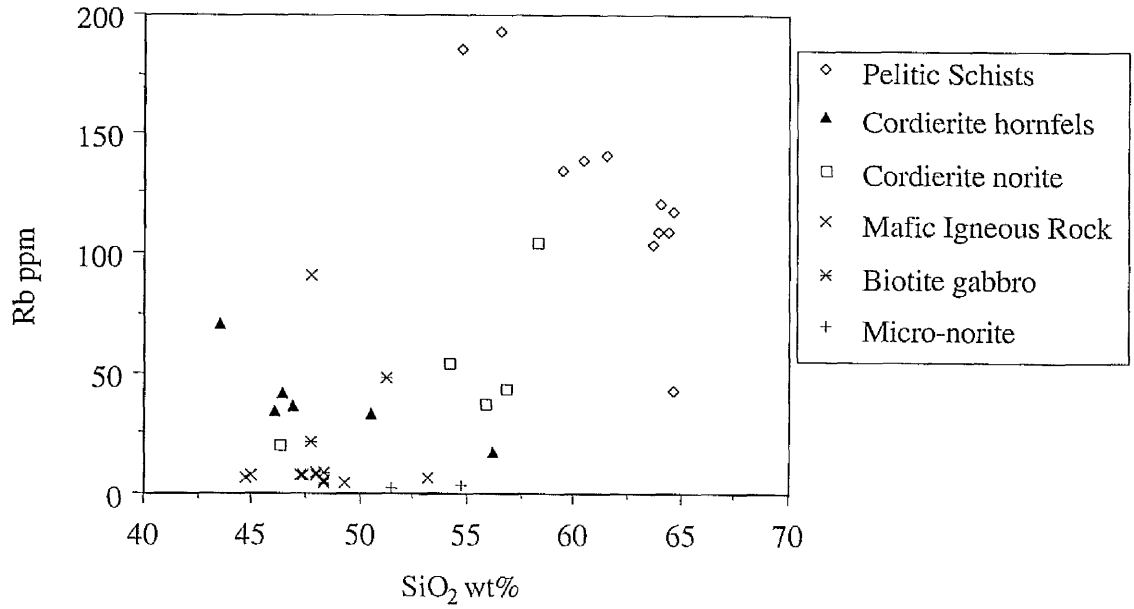

Figure 9.3.13 SiO_2-Rb plot for rocks from the S and SW margins of the Huntly Gabbro.

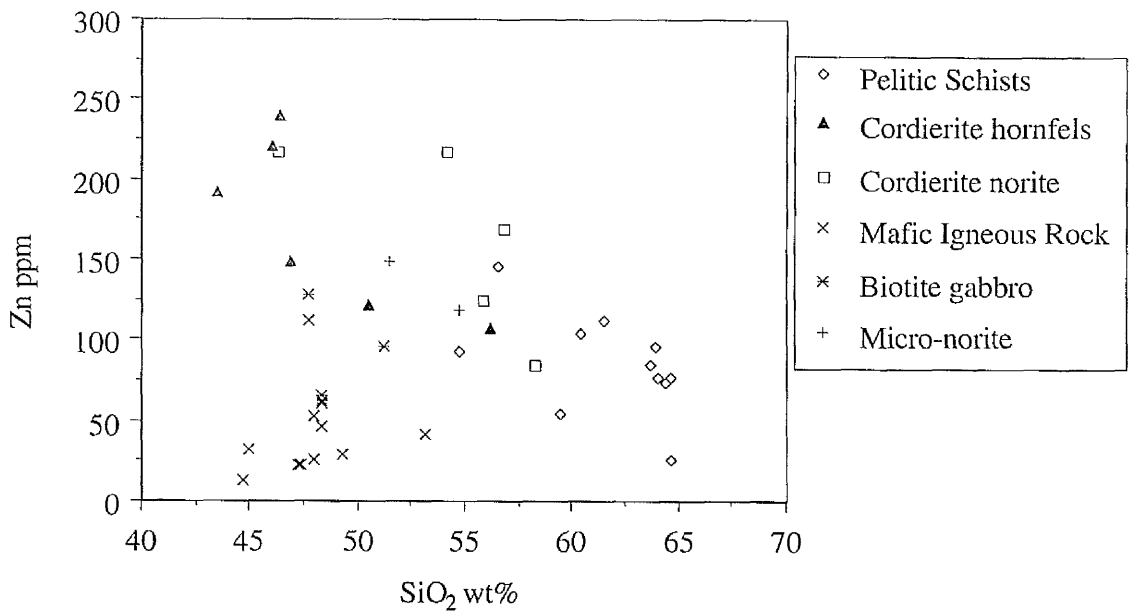

Figure 9.3.14 SiO_2-Zn plot for rocks from the S and SW margins of the Huntly Gabbro.

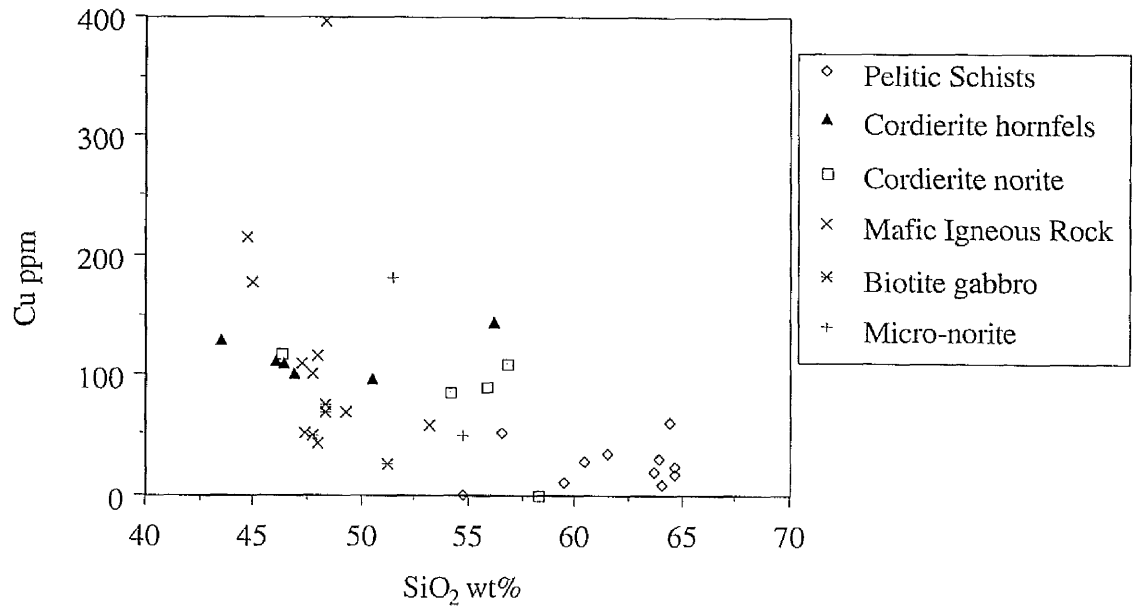

Figure 9.3.15 SiO_2-Cu plot for rocks from the S and SW margins of the Huntly Gabbro.

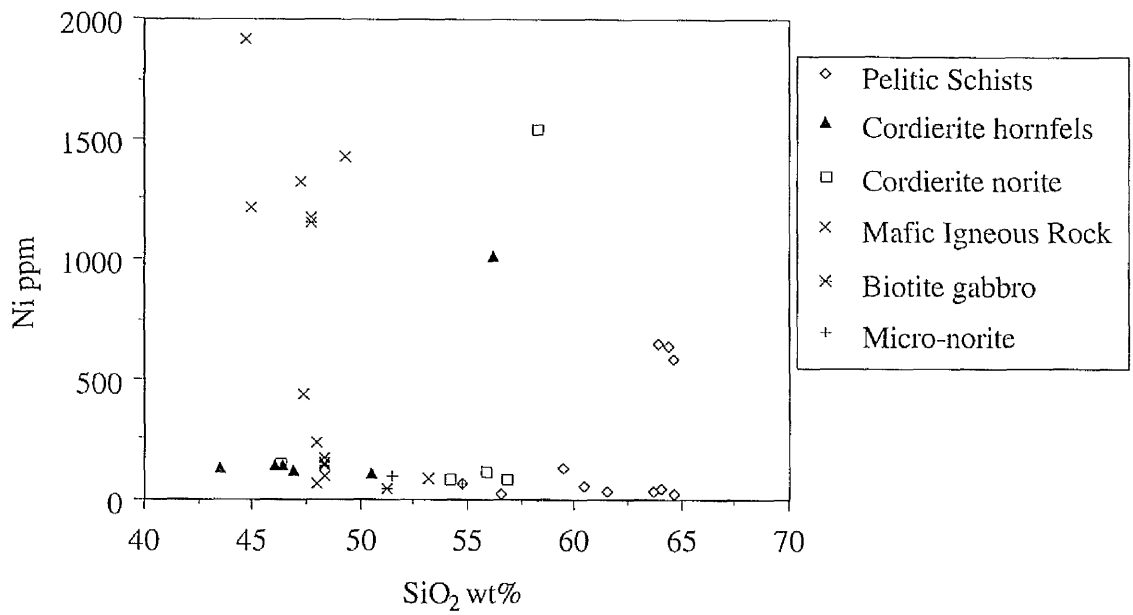

Figure 9.3.16 SiO_2-Ni plot for rocks from the S and SW margins of the Huntly Gabbro.

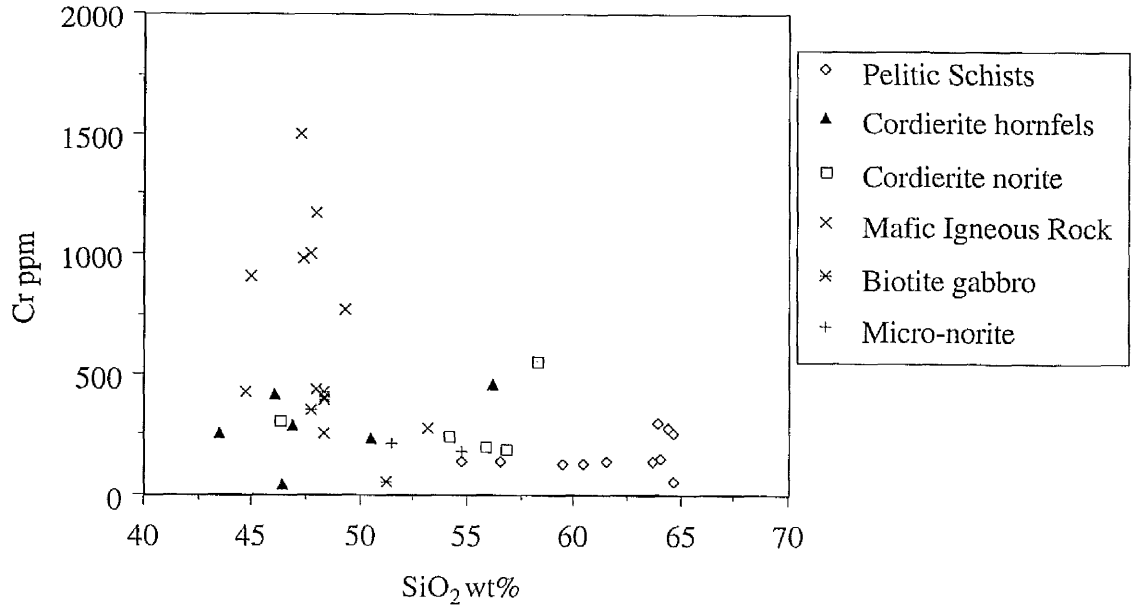

Figure 9.3.17 SiO_2-Cr plot for rocks from the S and SW margins of the Huntly Gabbro.

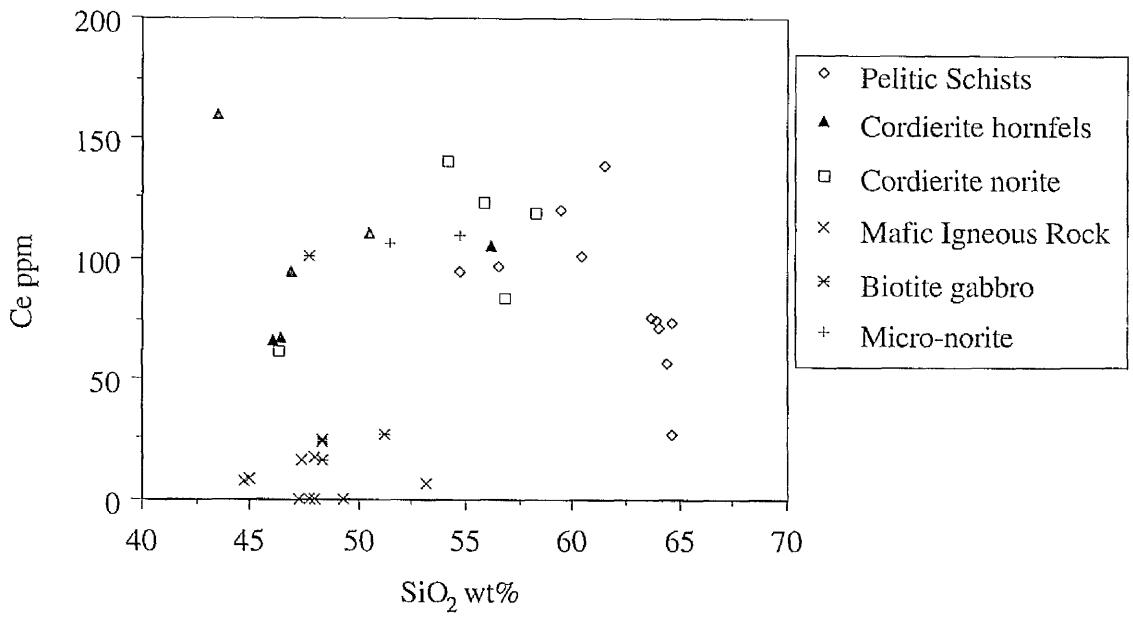

Figure 9.3.18 SiO_2-Ce plot for rocks from the S and SW margins of the Huntly Gabbro.

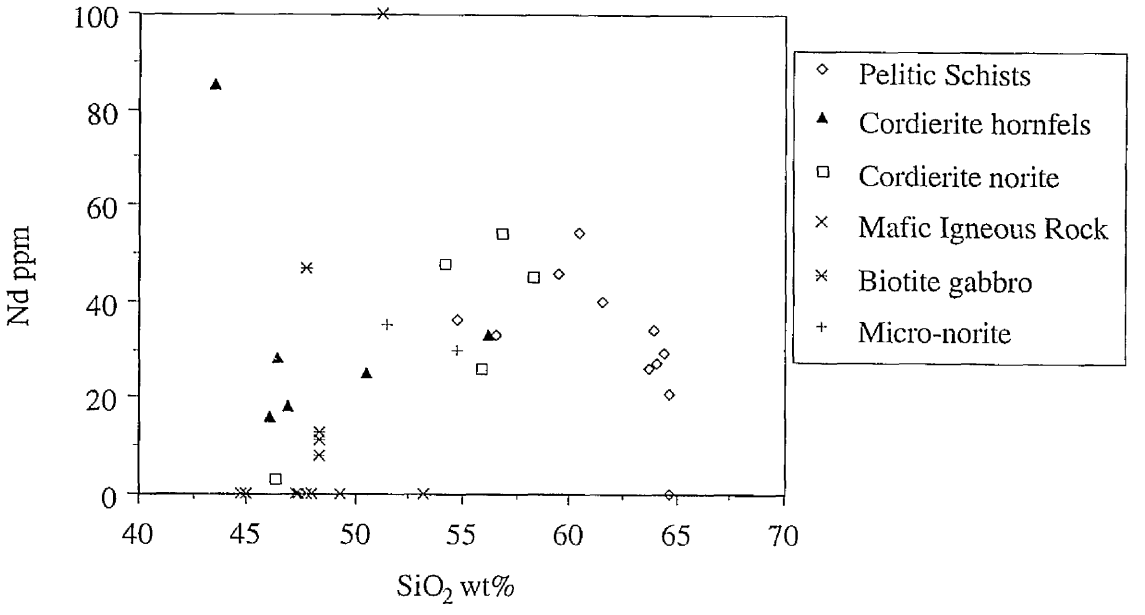

Figure 9.3.19 SiO_2-Nd plot for rocks from the S and SW margins of the Huntly Gabbro.

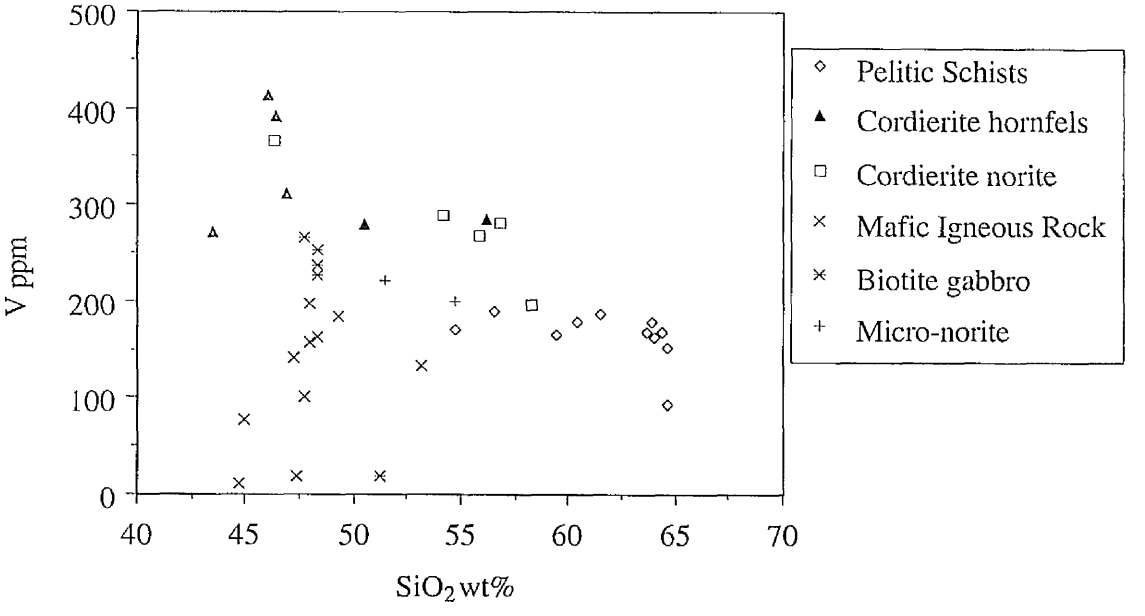

Figure 9.3.20 SiO_2-V plot for rocks from the S and SW margins of the Huntly Gabbro.

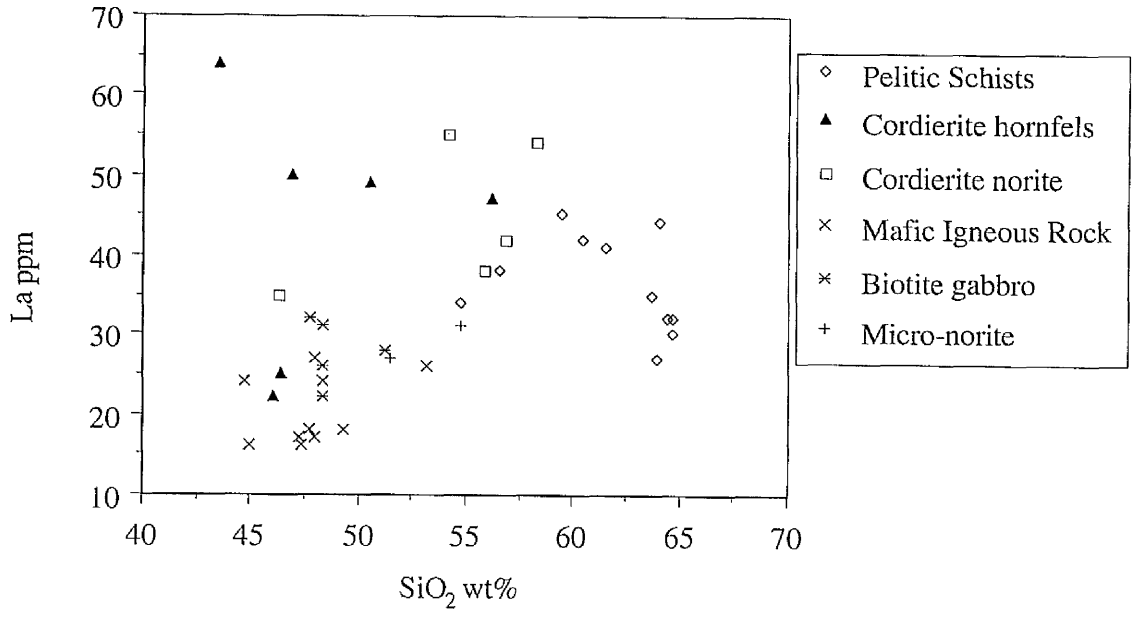

Figure 9.3.20 SiO_2-La plot for rocks from the S and SW margins of the Huntly Gabbro.

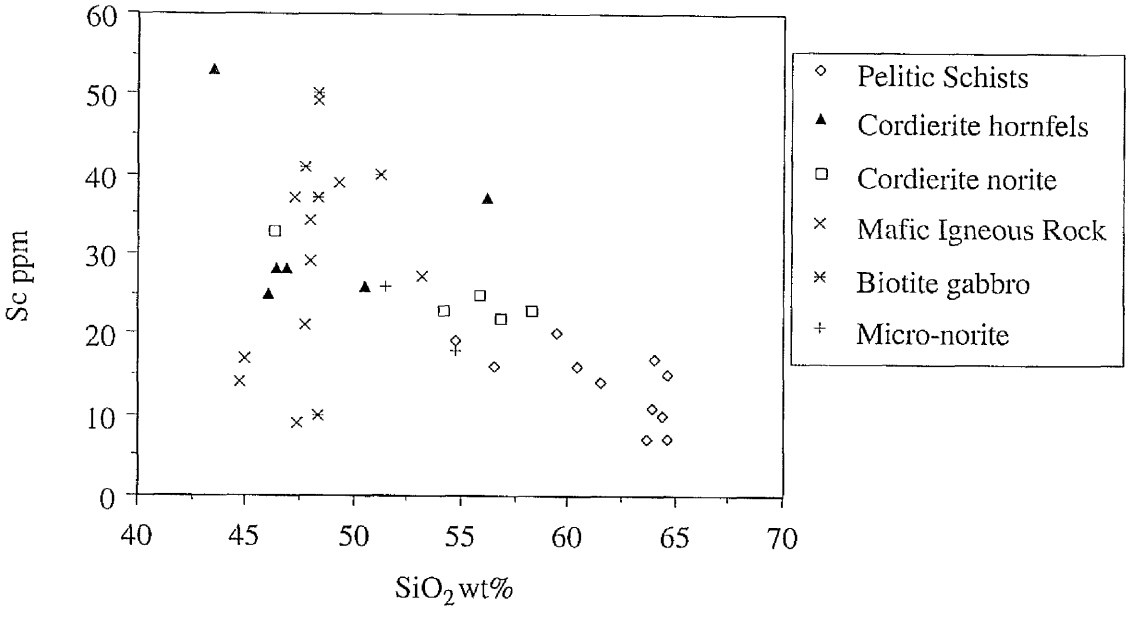

Figure 9.3.22 SiO_2-Sc plot for rocks from the S and SW margins of the Huntly Gabbro.

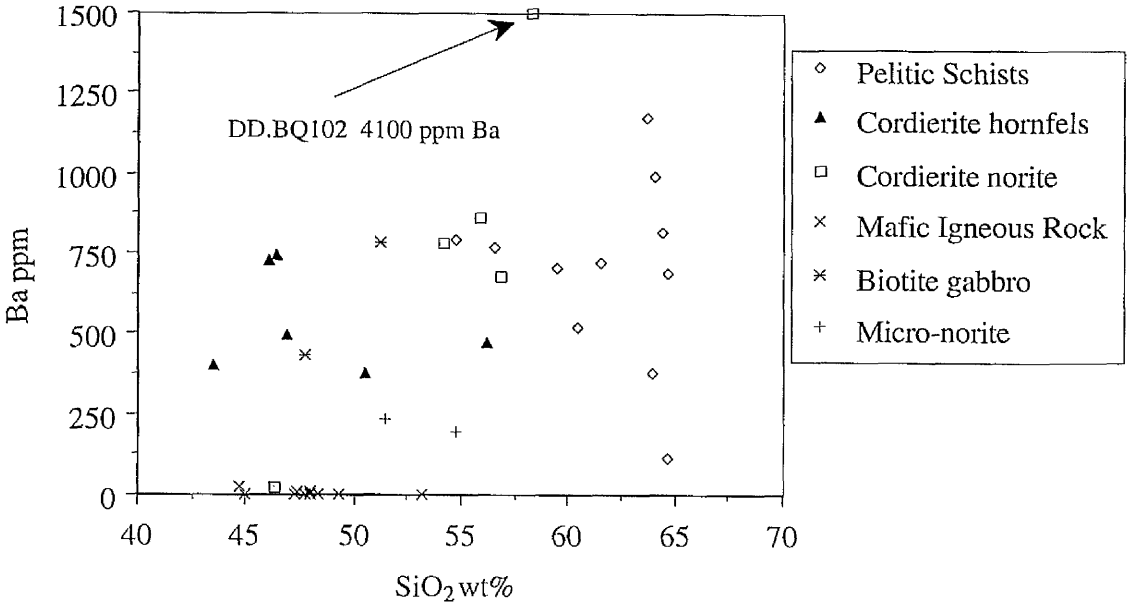

Figure 9.3.23 SiO_2-Ba plot for rocks from the S and SW margins of the Huntly Gabbro.

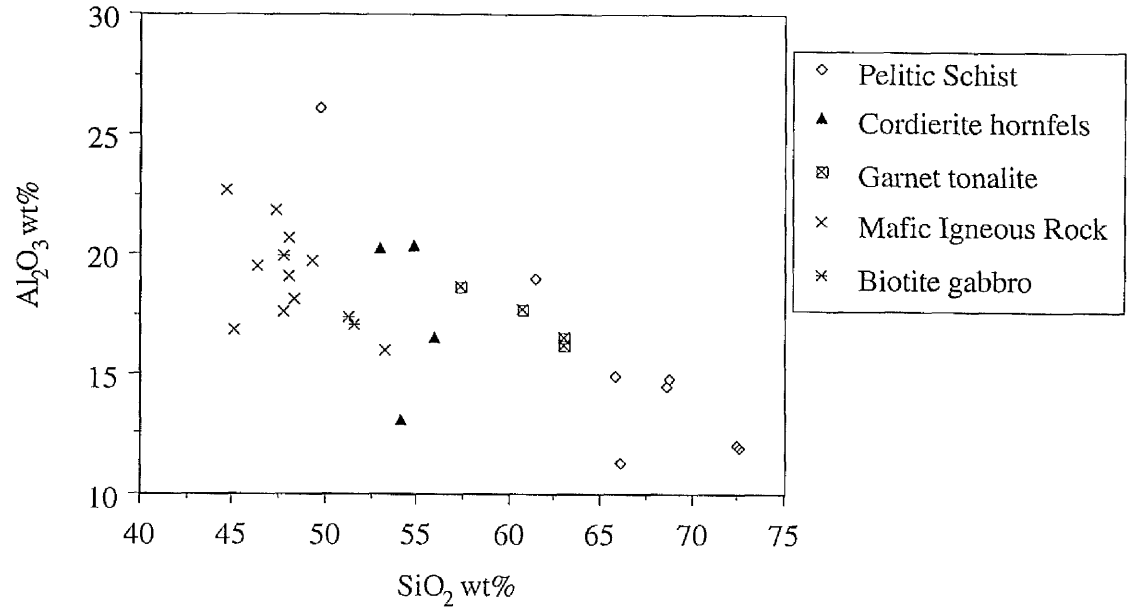

Figure 9.3.24 SiO_2-Al_2O_3 plot for rocks from the W margin of the Huntly Gabbro.

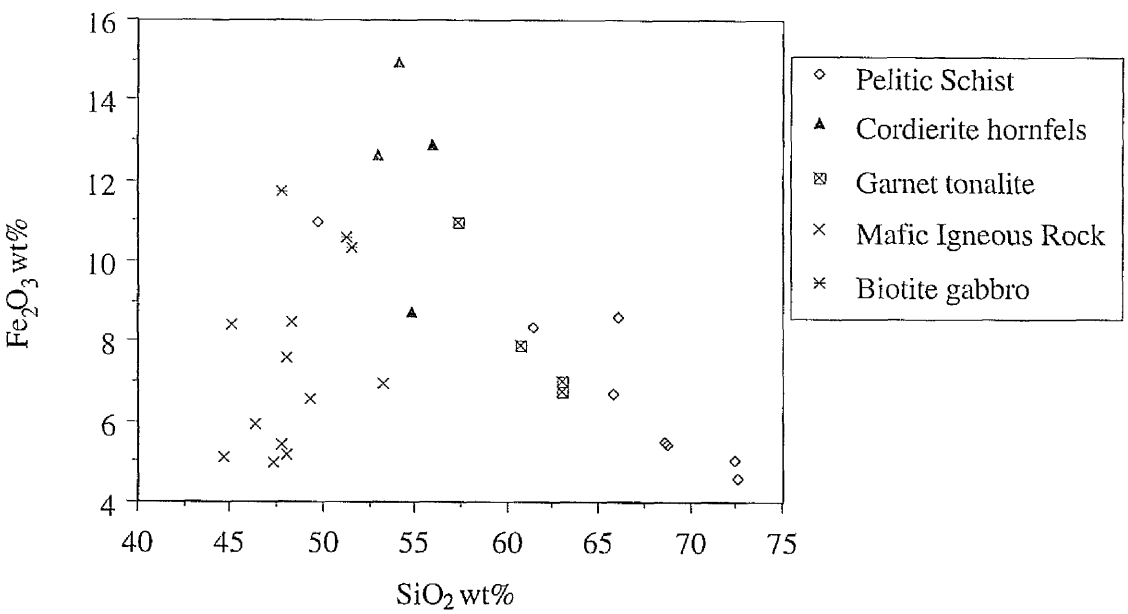

Figure 9.3.25 SiO_2-Fe_2O_3 plot for rocks from the W margin of the Huntly Gabbro.

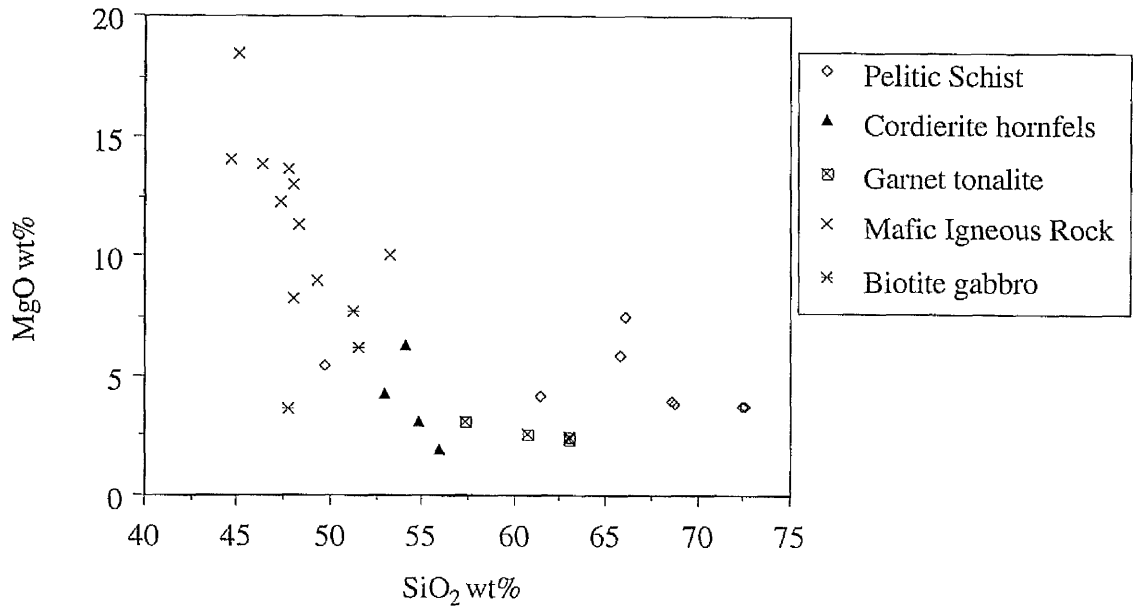

Figure 9.3.26 SiO_2-MgO plot for rocks from the W margin of the Huntly Gabbro.

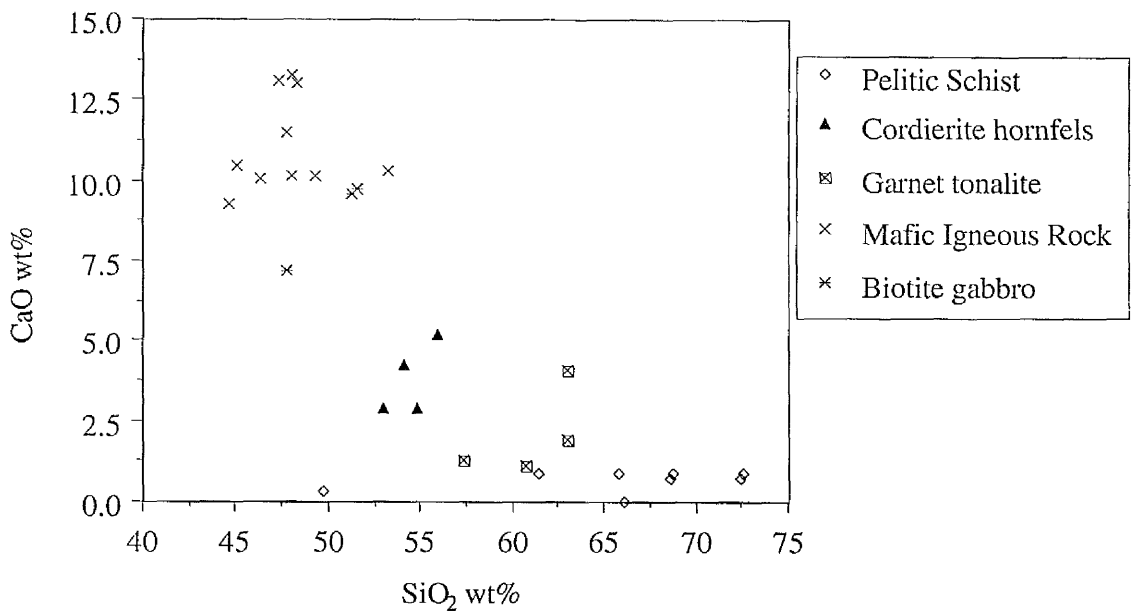

Figure 9.3.27 SiO_2-CaO plot for rocks from the W margin of the Huntly Gabbro.

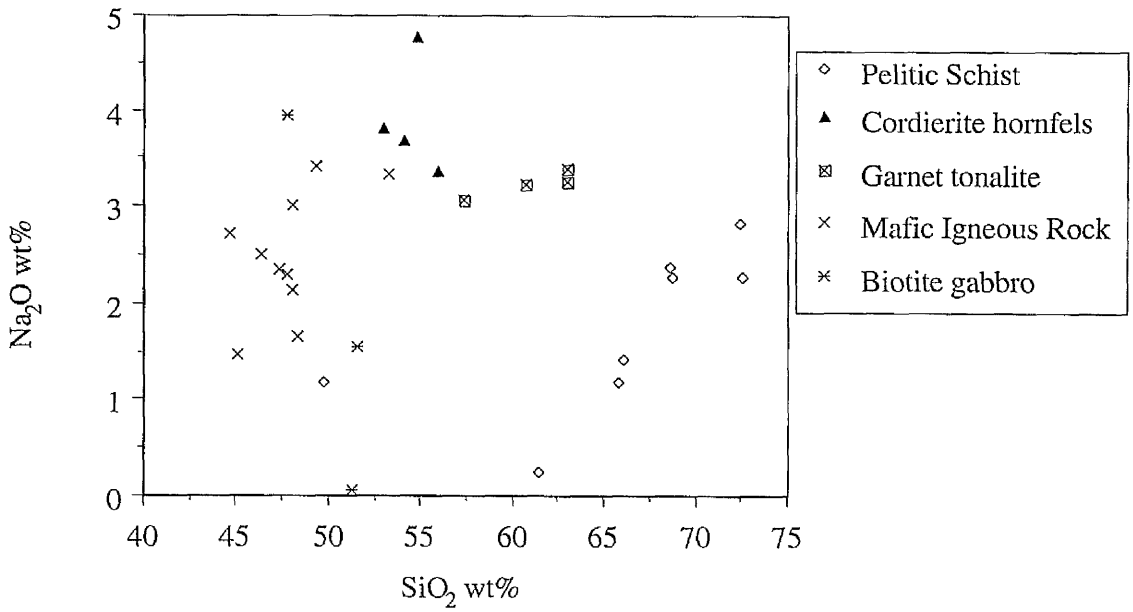

Figure 9.3.28 SiO_2-Na_2O plot for rocks from the W margin of the Huntly Gabbro.

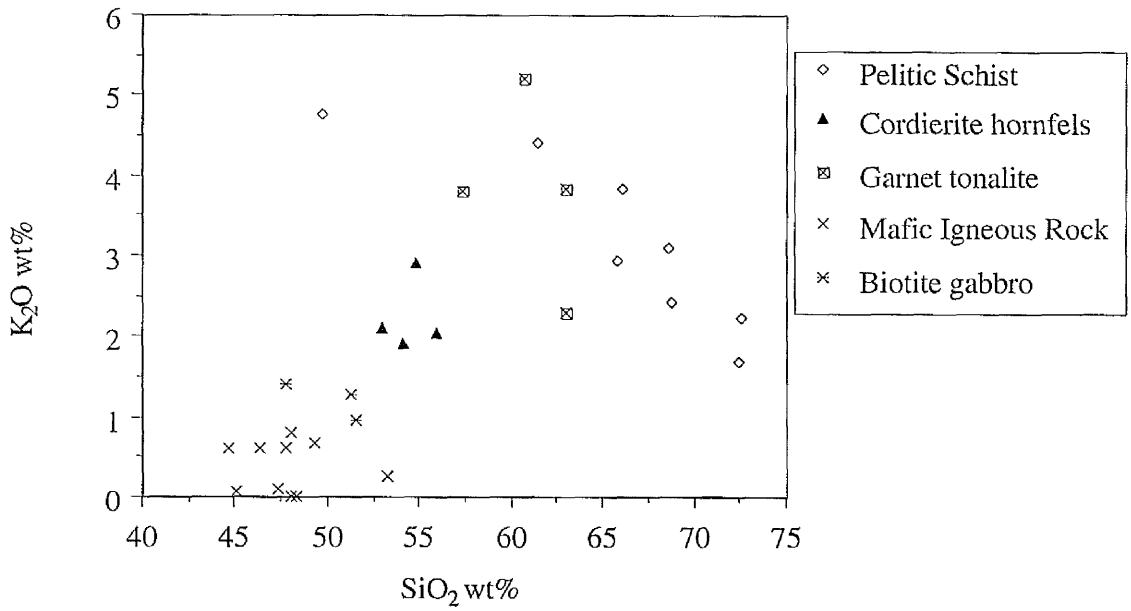

Figure 9.3.29 SiO_2-K_2O plot for rocks from the W margin of the Huntly Gabbro.

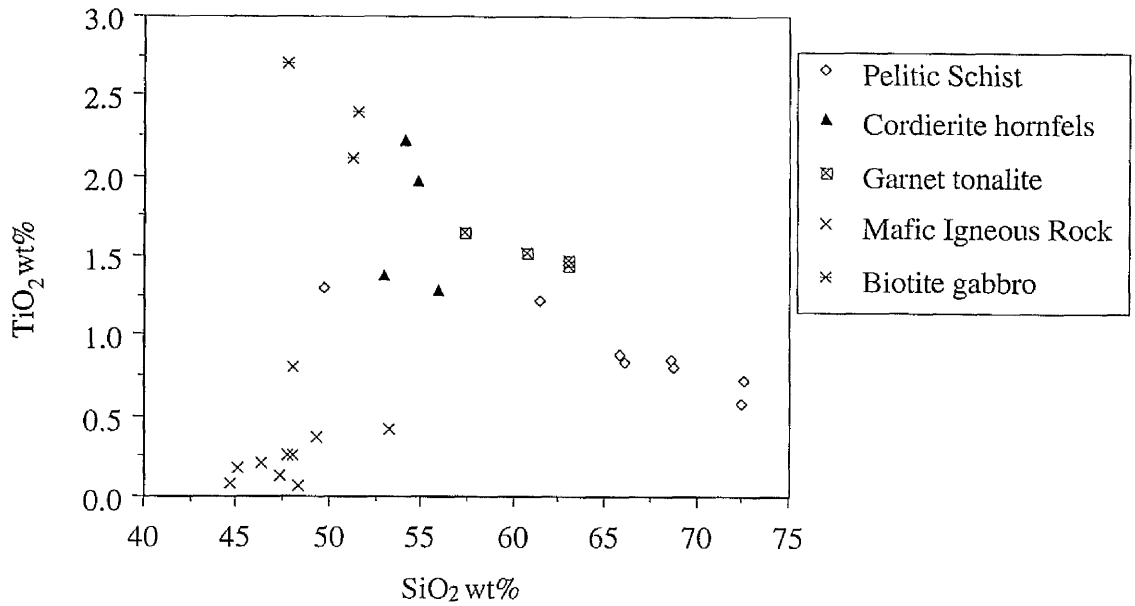

Figure 9.3.30 SiO_2-TiO_2 plot for rocks from the W margin of the Huntly Gabbro.

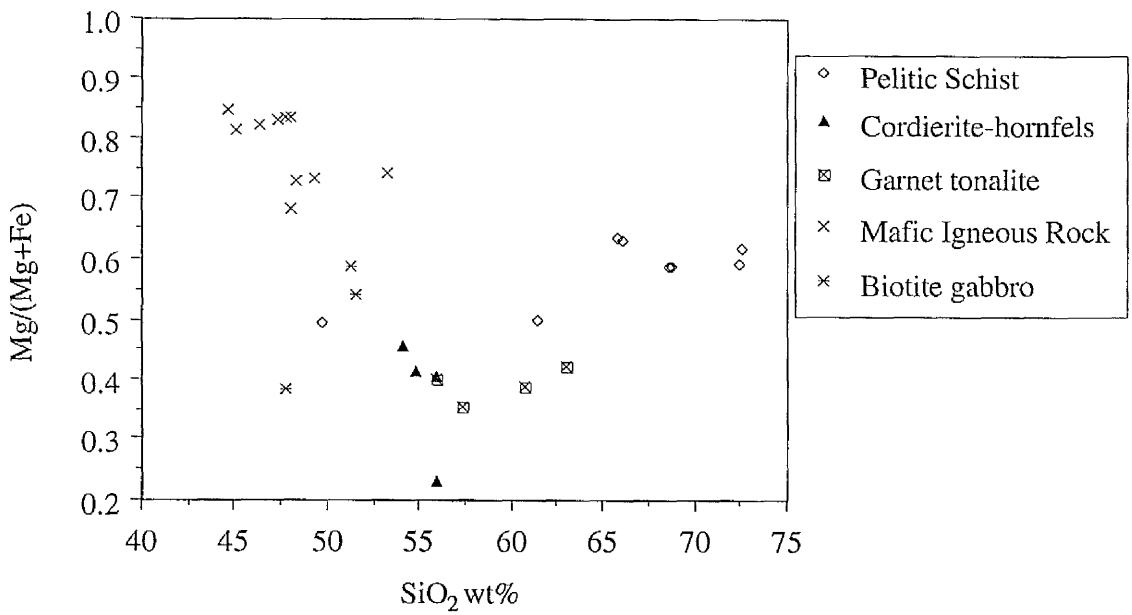

Figure 9.3.31 SiO_2-Mg# plot for rocks from the W margin of the Huntly Gabbro.

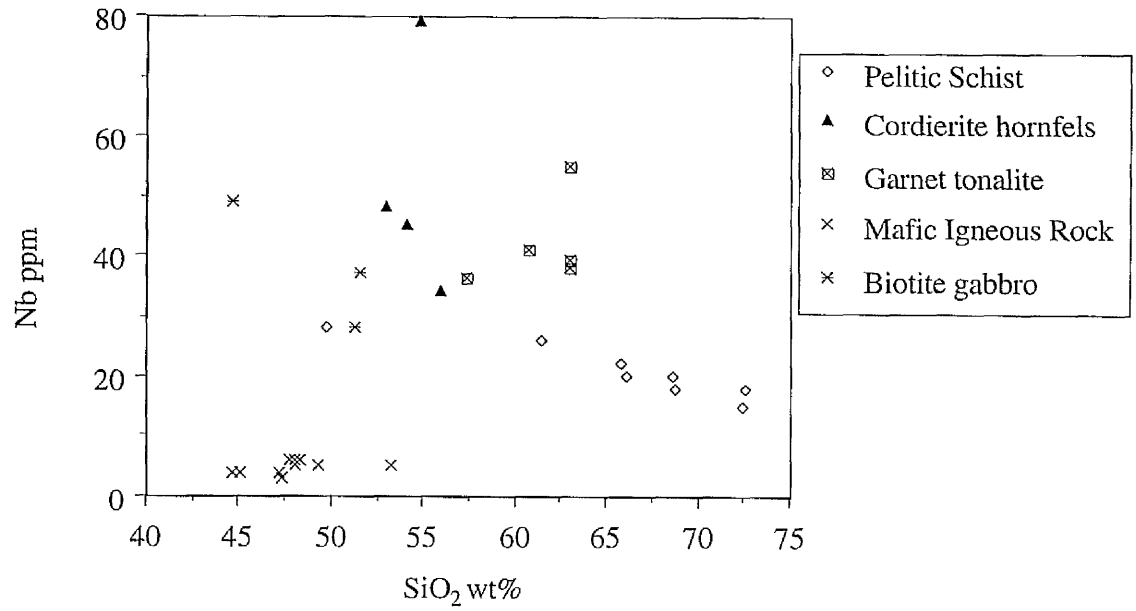

Figure 9.3.32 SiO_2-Nb plot for rocks from the W margin of the Huntly Gabbro.

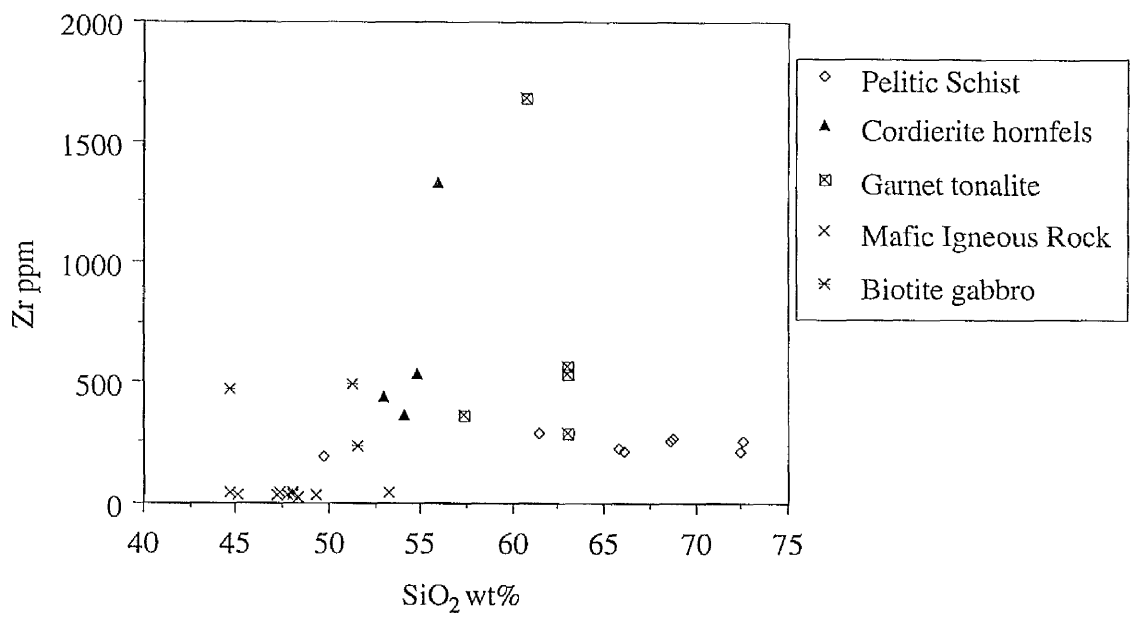

Figure 9.3.33 SiO_2-Zr plot for rocks from the W margin of the Huntly Gabbro.

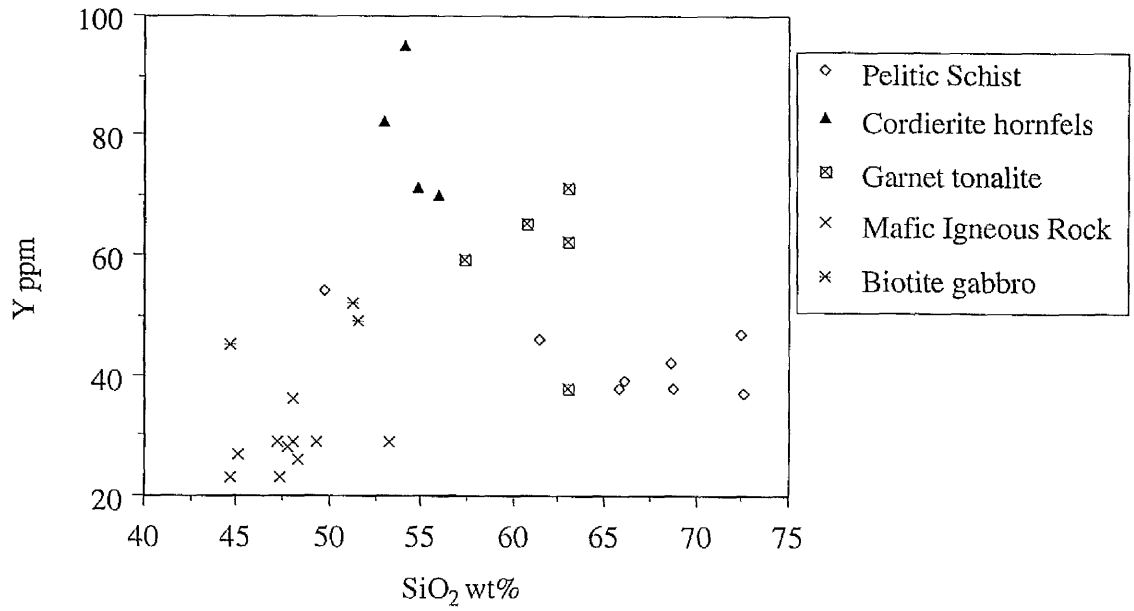

Figure 9.3.34 SiO_2-Y plot for rocks from the W margin of the Huntly Gabbro.

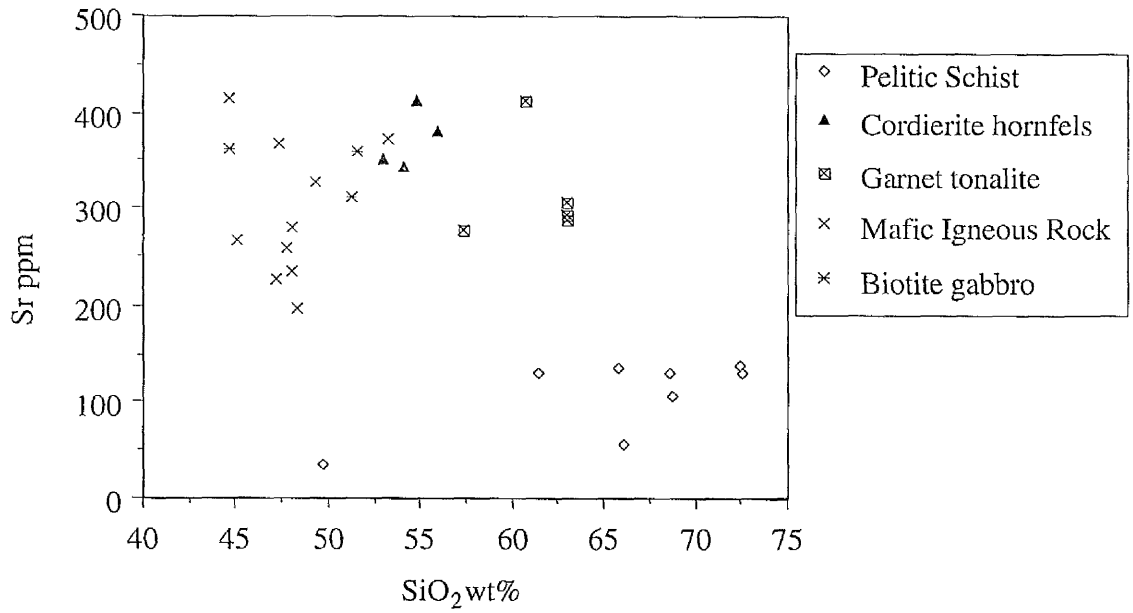

Figure 9.3.35 SiO_2-Sr plot for rocks from the W margin of the Huntly Gabbro.

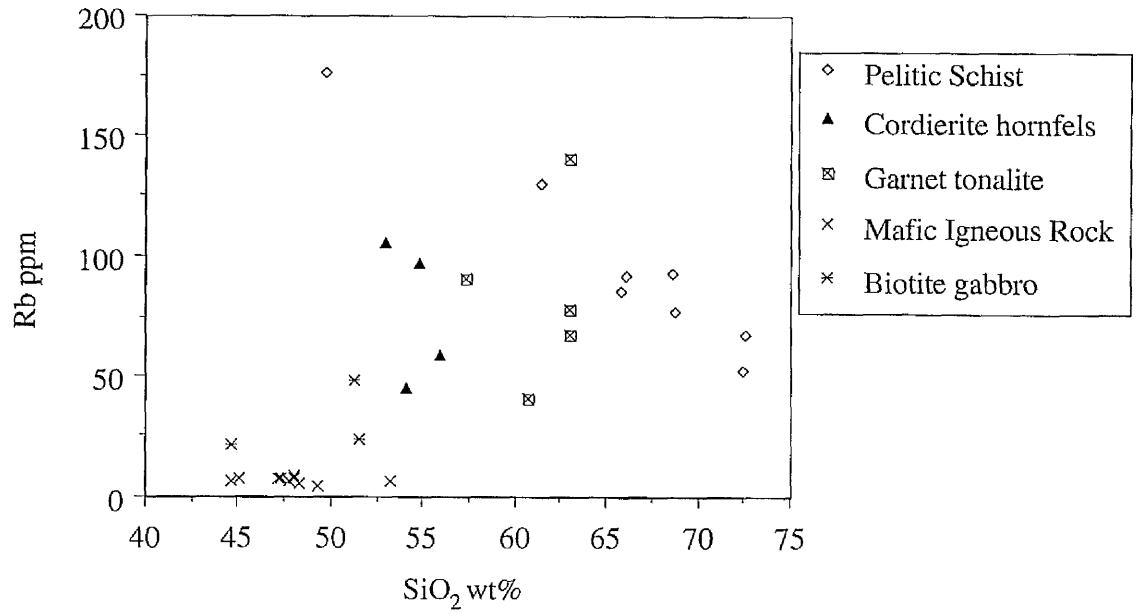

Figure 9.3.36 SiO_2-Rb plot for rocks from the W margin of the Huntly Gabbro.

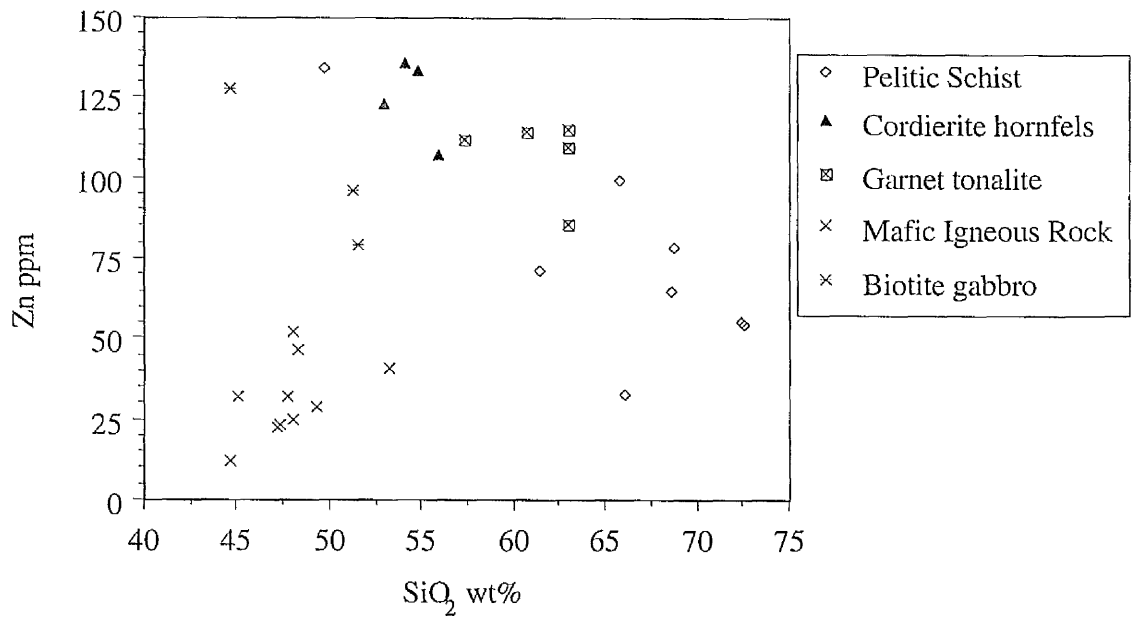

Figure 9.3.37 SiO_2-Zn plot for rocks from the W margin of the Huntly Gabbro.

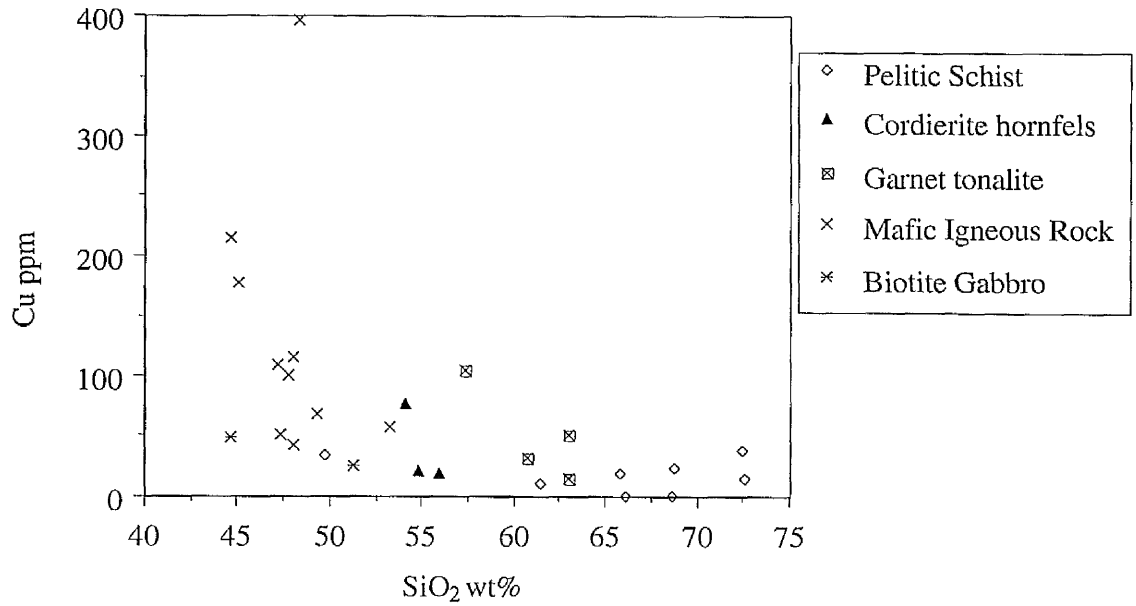

Figure 9.3.38 SiO_2-Cu plot for rocks from the W margin of the Huntly Gabbro.

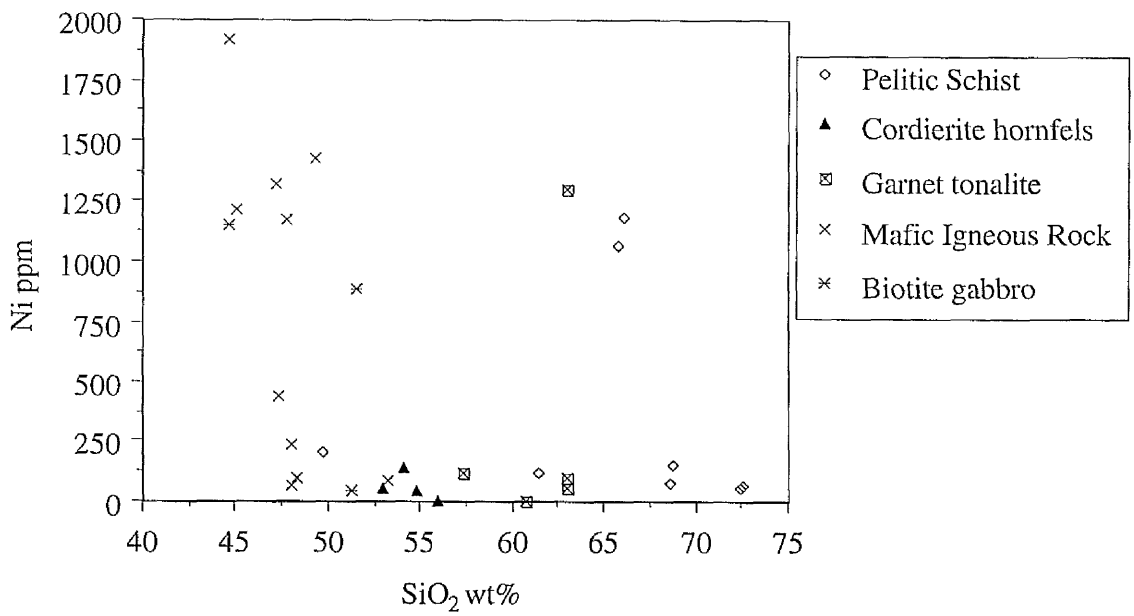

Figure 9.3.39 SiO_2-Ni plot for rocks from the W margin of the Huntly Gabbro.

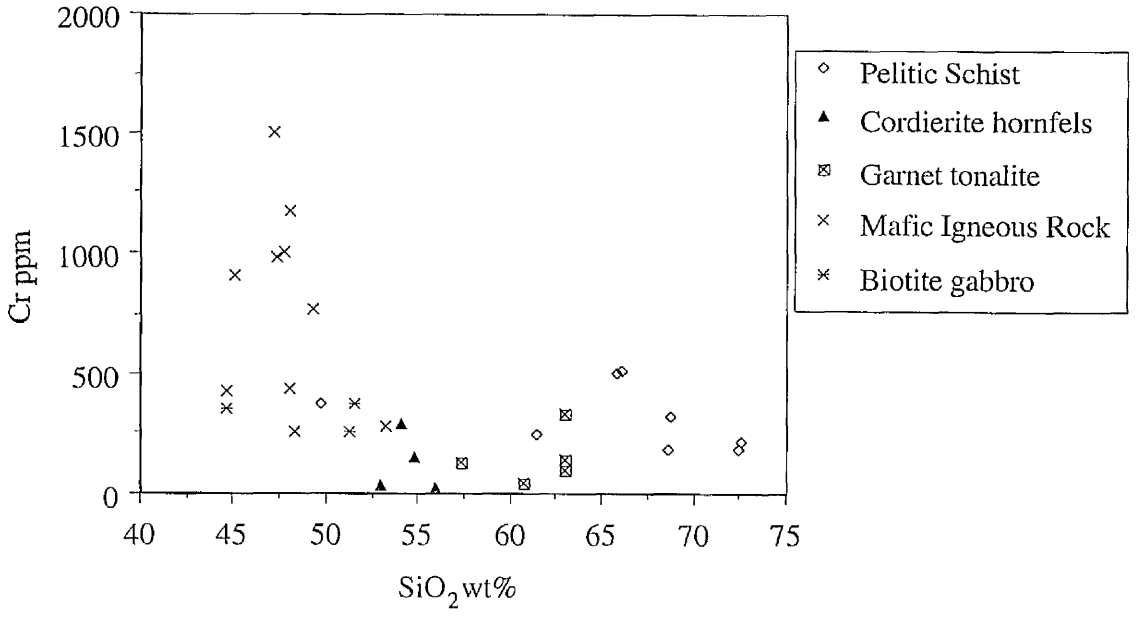

Figure 9.3.40 SiO_2-Cr plot for rocks from the W margin of the Huntly Gabbro.

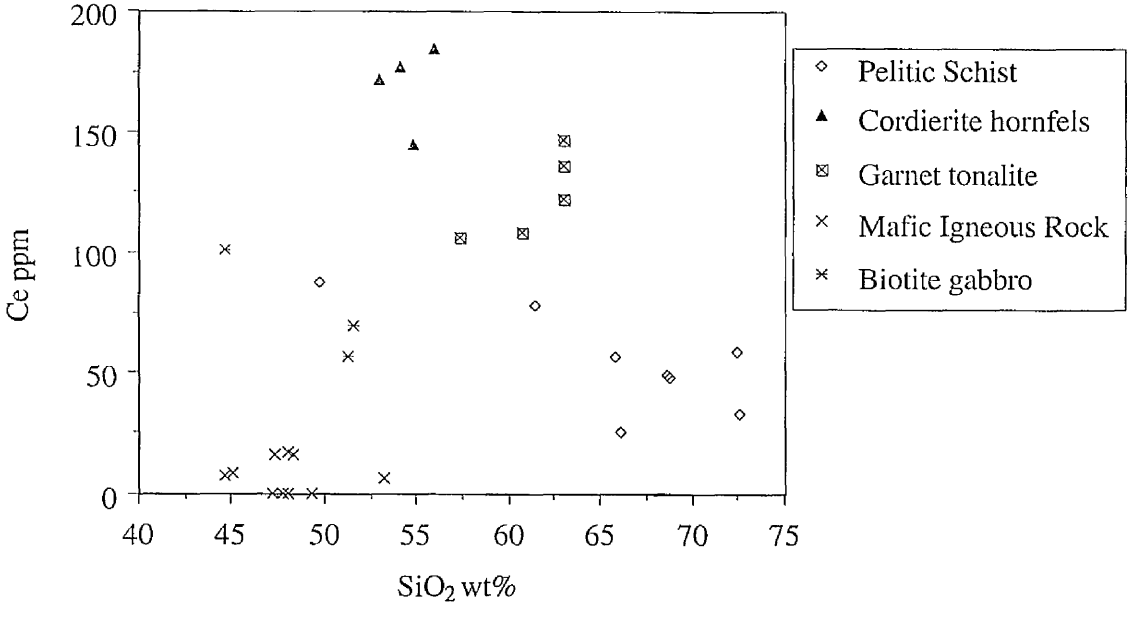

Figure 9.3.41 SiO_2-Ce plot for rocks from the W margin of the Huntly Gabbro.

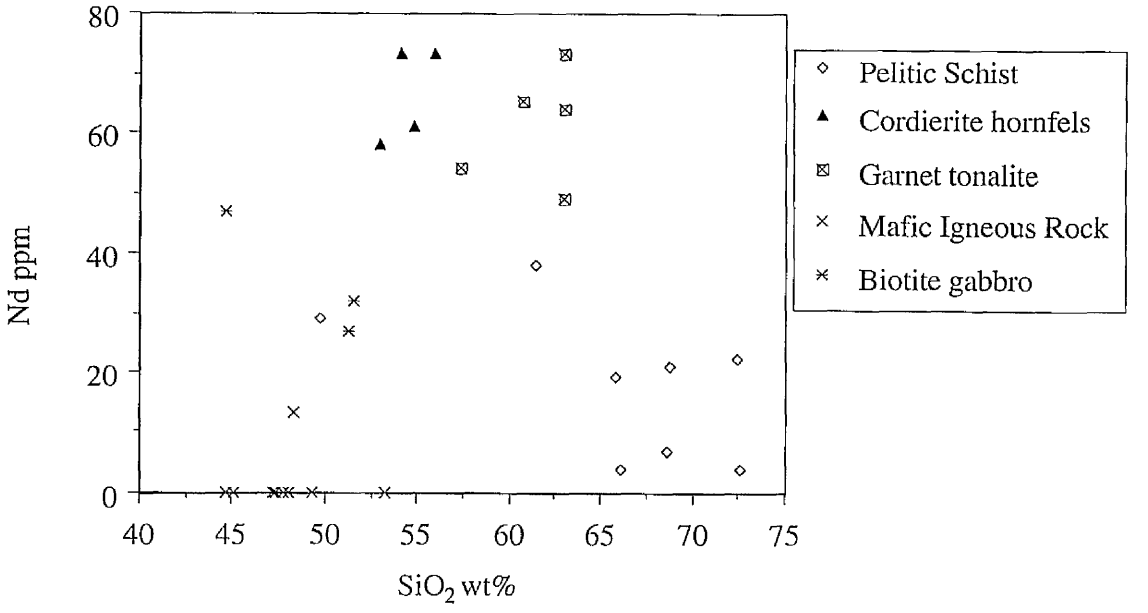

Figure 9.3.42 SiO_2-Nd plot for rocks from the W margin of the Huntly Gabbro.

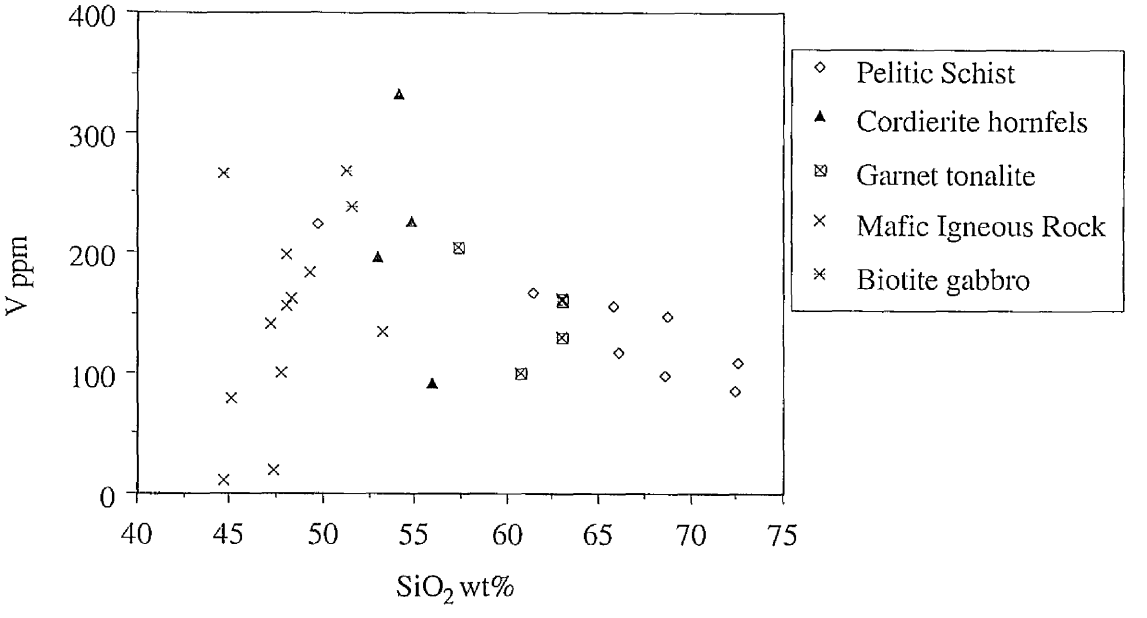

Figure 9.3.43 SiO_2-V plot for rocks from the W margin of the Huntly Gabbro.

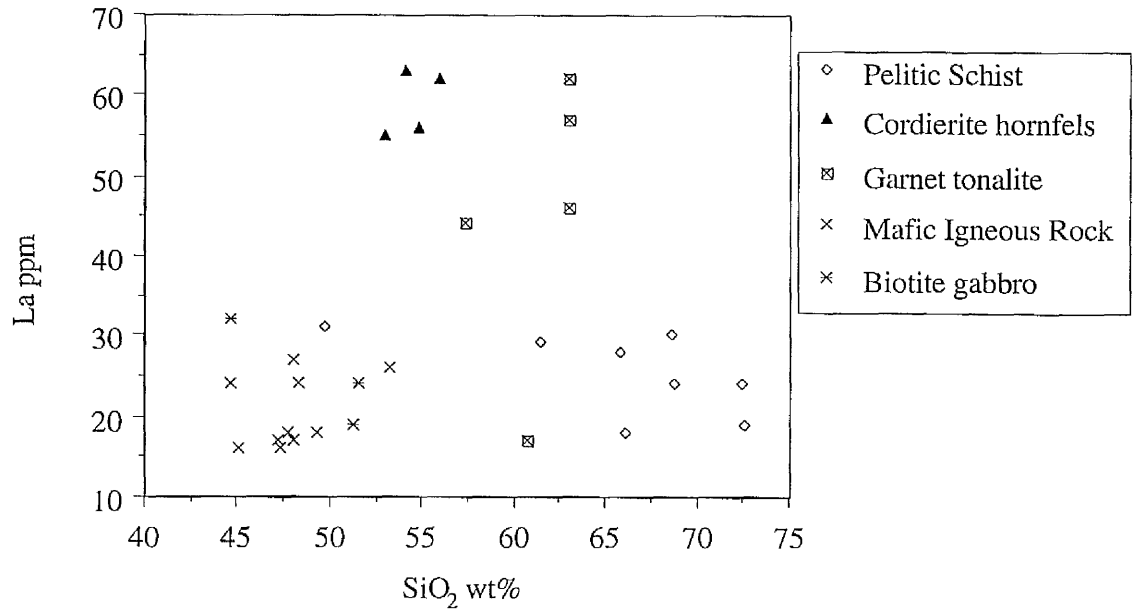

Figure 9.3.44 SiO_2-La plot for rocks from the W margin of the Huntly Gabbro.

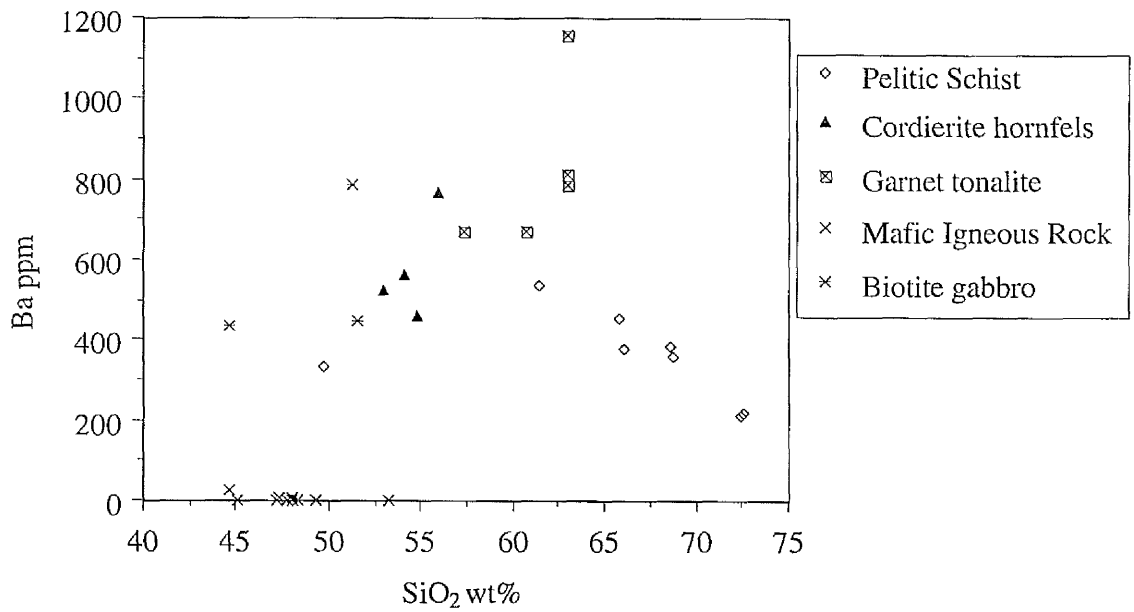

Figure 9.3.45 SiO_2-Ba plot for rocks from the W margin of the Huntly Gabbro.

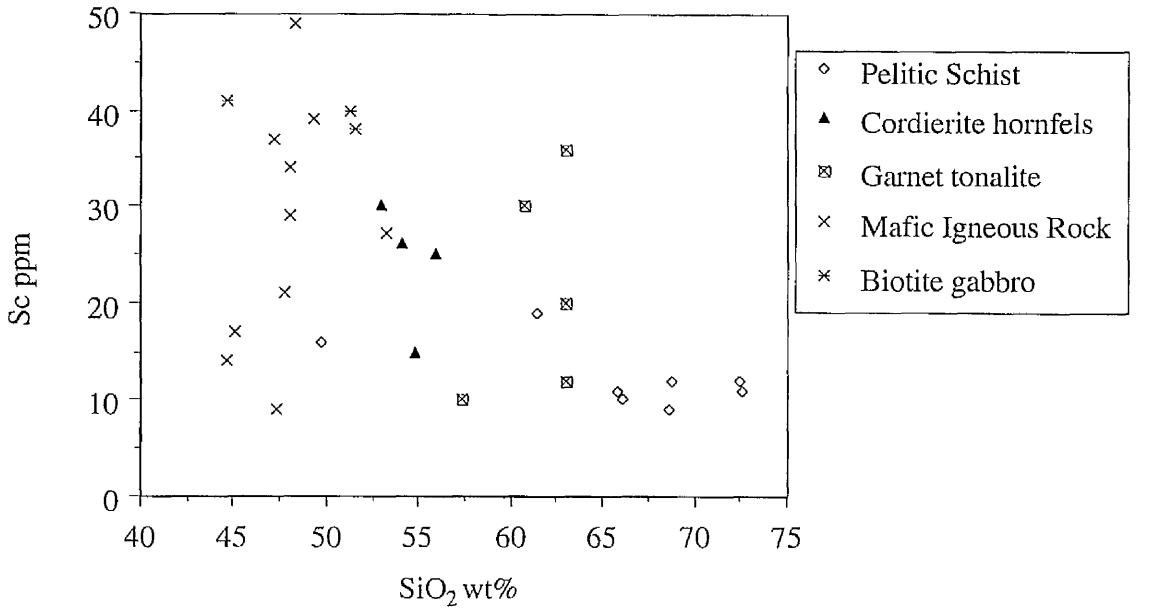

Figure 9.3.45 SiO_2-Ba plot for rocks from the W margin of the Huntly Gabbro.

Table 9.2.1(i) Major element whole-rock chemistry of rock samples from the Huntly-Knock area.

	Schist	Schist	Quartzite	Schist	Arkose	Schist	Schist	Schist	Schist	Pelite	Quartzite	Quartzite
Wt% Oxide	**BOG1**	**BOG3**	**MUCK1**	**CLAS110**	**CLAS113**	**CLAS102**	**COLL102**	**CLAS112**	**COLL101**	**MIKE2**	**MUCK2**	**NEWT1**
SiO_2	59.43	54.76	76.80	64.39	73.62	61.54	60.42	56.63	71.09	64.04	78.54	83.97
Al_2O_3	21.68	23.83	13.41	18.34	10.55	18.51	18.20	19.98	13.18	18.07	8.89	5.21
Fe_2O_3	6.39	8.74	2.82	7.60	3.56	9.21	9.56	12.06	7.77	6.73	3.73	3.66
MgO	2.29	2.67	0.58	1.98	1.69	1.98	2.12	2.98	1.65	1.38	1.14	1.29
CaO	0.97	0.49	0.00	0.61	6.62	1.16	1.34	0.06	0.45	0.88	0.57	0.10
Na_2O	2.28	2.52	1.95	0.00	1.12	1.23	2.41	1.45	0.17	3.76	2.89	3.67
K_2O	5.43	5.75	3.04	5.22	0.85	4.39	3.79	5.40	3.91	3.68	3.89	2.15
TiO_2	1.51	1.47	0.58	1.34	0.46	1.57	1.56	1.47	1.37	1.11	0.81	0.53
MnO	0.16	0.00	0.16	0.16	0.33	0.19	0.23	0.18	0.17	0.18	0.20	0.17
P_2O_5	0.25	0.06	0.08	0.11	0.35	0.17	0.39	0.32	0.12	0.17	0.10	0.06
TOTAL	**100.39**	**100.29**	**99.42**	**99.75**	**99.15**	**99.95**	**100.02**	**100.53**	**99.88**	**100.00**	**100.76**	**100.81**

	Schist	Schist	Schist	Schist	Schist	Schist	Schist	Schist	Schist	Schist	Schist	Crd hfls
Wt% Oxide	**CLAS1**	**CLAS6**	**CLAS111**	**SIN105**	**SIN104**	**SIN103a**	**SIN103b**	**SIN101**	**SIN1**	**SIN2**	**SIN107**	**CUM1**
SiO_2	63.95	63.70	64.69	66.13	68.73	72.59	61.39	65.81	72.53	68.71	49.77	54.13
Al_2O_3	15.44	16.07	16.65	11.29	14.83	11.92	18.98	14.85	12.05	14.47	26.06	13.13
Fe_2O_3	8.11	7.01	7.61	8.58	5.41	4.60	8.33	6.69	5.03	5.47	10.96	14.92
MgO	2.35	2.50	2.25	7.40	3.87	3.76	4.18	5.86	3.69	3.90	5.38	6.29
CaO	1.31	1.90	0.91	0.00	0.91	0.88	0.89	0.91	0.72	0.74	0.32	4.21
Na_2O	2.69	2.64	1.31	1.41	2.27	2.27	0.25	1.17	2.82	2.36	1.17	3.67
K_2O	3.64	3.77	4.41	3.83	2.44	2.25	4.40	2.95	1.70	3.08	4.75	1.93
TiO_2	1.53	1.38	1.25	0.83	0.80	0.72	1.21	0.88	0.57	0.84	1.29	2.22
MnO	0.19	0.23	0.18	0.17	0.18	0.13	0.20	0.15	0.07	0.00	0.18	0.29
P_2O_5	0.19	0.19	0.17	0.13	0.12	0.08	0.12	0.06	0.09	0.09	0.15	0.10
TOTAL	**99.40**	**99.39**	**99.43**	**99.77**	**99.56**	**99.20**	**99.95**	**99.33**	**99.27**	**99.66**	**100.03**	**100.89**

Table 9.2.1(ii) Major element whole-rock chemistry of rock samples from the Huntly-Knock area.

Rock Type	Crd hfls.	Crd hfls	Crd hfls	Crd hfls	Crd hfls	Crd hfls	Crd hfls	Crd hfls	Crd hfls	Crd hfls	Crd hfls	Crd norite
Wt% Oxide	**CUM2ii**	**CUM101**	**CUM7**	**DUN3**	**DUN1**	**WET14**	**WET6**	**WET10**	**BQ17**	**PIR4**	**PIR101**	**BAR1**
SiO_2	54.84	55.94	53.04	46.42	43.50	51.48	52.81	50.11	50.53	46.94	56.22	61.46
Al_2O_3	20.33	16.44	20.25	24.58	23.03	18.41	24.46	20.13	24.02	27.14	14.47	13.31
Fe_2O_3	8.73	12.87	12.62	13.15	15.47	11.46	9.42	11.08	10.02	11.72	12.23	13.04
MgO	3.09	1.96	4.29	6.95	7.24	4.55	3.22	3.63	3.48	4.21	3.51	8.81
CaO	2.91	5.15	2.87	1.93	2.00	4.25	1.03	5.16	3.89	2.82	4.94	0.00
Na_2O	4.77	3.34	3.79	1.89	1.66	3.96	3.00	4.25	4.29	3.57	5.25	1.04
K_2O	2.91	2.04	2.12	1.57	2.94	2.96	4.36	2.23	1.56	1.26	0.87	1.75
TiO_2	1.97	1.28	1.38	2.75	2.04	2.15	1.55	2.55	1.84	1.93	2.11	0.67
MnO	0.17	0.23	0.21	0.18	0.86	0.25	0.17	0.23	0.16	0.20	0.21	0.15
P_2O_5	0.18	0.75	0.03	0.10	0.47	0.03	0.08	0.15	0.05	0.04	0.06	0.06
TOTAL	**99.90**	**100.00**	**100.60**	**99.52**	**99.21**	**99.50**	**100.10**	**99.52**	**99.84**	**99.83**	**99.87**	**100.29**

Wt% Oxide	Crd norite	Crd norite	Crd norite	Crd norite	Crd norite	Crd norite	Garnet tonalite	Garnet tonalite	Garnet tonalite	Garnet tonalite	Garnet tonalite	Garnet tonalite
	DUN4	**DUN9B**	**DUN 10**	**CAS.B2**	**CAS.B5**	**BQ102**	**CUM8**	**CUM19A**	**CUM102**	**TYQ5**	**TYQ3**	**CUM16**
SiO_2	54.11	46.30	46.10	55.80	56.81	58.29	57.33	60.72	62.95	60.09	66.24	63.00
Al_2O_3	16.77	23.59	23.89	17.63	16.54	18.17	18.58	17.62	16.50	17.97	15.37	16.22
Fe_2O_3	11.19	13.89	12.90	12.21	10.04	8.14	10.97	7.91	7.03	6.54	4.57	6.72
MgO	8.16	5.48	8.38	7.30	6.87	2.68	3.04	2.54	2.38	2.97	2.01	2.46
CaO	3.84	3.64	1.49	1.74	2.03	1.61	1.27	1.15	1.94	4.36	4.23	4.05
Na_2O	2.34	2.40	2.48	1.95	1.87	2.53	3.06	3.23	3.37	3.49	4.26	3.25
K_2O	1.72	1.39	1.25	2.78	2.89	6.90	3.79	5.21	3.84	2.83	2.35	2.29
TiO_2	1.85	2.55	2.78	1.78	1.89	1.46	1.65	1.51	1.44	1.43	1.05	1.47
MnO	0.07	0.21	0.14	0.16	0.32	0.21	0.17	0.18	0.16	0.16	0.18	0.17
P_2O_5	0.39	0.07	0.03	0.03	0.08	0.09	0.11	0.10	0.03	0.04	0.06	0.32
TOTAL	**100.44**	**99.52**	**99.44**	**101.39**	**99.34**	**100.08**	**99.97**	**100.17**	**99.64**	**99.88**	**100.32**	**99.95**

Figure 9.2.1(iii) Major element whole-rock chemistry of rock samples from the Huntly-Knock area.

	Grt tonalite	Mafic rock	Mafic rock	Mafic rock	Mafic rock	Mafic rock	Mafic rock	Mafic rock	Mafic rock	Mafic rock	Mafic rock	Bt-gabbro
Wt% Oxide	**TYQ10**	**BIN104**	**KIN102**	**BIN1**	**BIN2**	**BIN102**	**BIN107**	**BIN101**	**DUN5**	**W.TON104**	**RIV3**	**W.TON4**
SiO_2	56.57	47.38	53.23	47.73	46.30	48.03	48.35	45.02	48.01	44.67	49.32	47.80
Al_2O_3	16.79	21.80	15.93	17.55	19.45	19.00	18.05	16.79	20.69	22.68	19.71	19.92
Fe_2O_3	10.49	4.98	6.94	5.39	5.93	5.17	8.45	8.42	7.58	5.08	6.54	11.72
MgO	4.48	12.21	9.97	13.62	13.85	13.00	11.29	18.42	8.16	13.99	8.98	3.66
CaO	3.36	13.12	10.32	11.46	10.07	13.23	13.04	10.48	10.10	9.29	10.17	7.16
Na_2O	2.12	2.33	3.33	2.28	2.50	2.13	1.64	1.47	3.00	2.71	3.40	3.94
K_2O	3.58	0.11	0.25	0.62	0.62	0.00	0.00	0.05	0.81	0.60	0.67	1.39
TiO_2	2.13	0.12	0.42	0.25	0.20	0.26	0.06	0.18	0.80	0.08	0.36	2.70
MnO	0.21	0.17	0.22	0.19	0.19	0.19	0.22	0.15	0.20	0.15	0.21	0.22
P_2O_5	0.10	0.02	0.03	0.02	0.02	0.01	0.00	0.02	0.03	0.02	0.02	0.81
TOTAL	**99.83**	**102.24**	**100.64**	**99.11**	**99.13**	**101.02**	**101.10**	**101.00**	**99.38**	**99.27**	**99.38**	**99.32**

	Bt gabbro	Bt gabbro	Bt gabbro	Bt gabbro	Bt gabbro	Bt gabbro	Bt gabbro	Bt gabbro	Bt gabbro	Bt gabbro	Micro-norite	Micro-norite
Wt% Oxide	**W.TON5**	**W.TON106**	**BQ26**	**BQ29**	**BQ30**	**BAR2**	**CUT1**	**WET13**	**CUT7**	**CUT18**	**BQ27**	**BQ4**
SiO_2	51.53	51.25	48.36	48.30	48.35	49.52	52.62	50.41	49.45	57.10	54.73	51.46
Al_2O_3	16.99	17.39	18.53	18.43	19.85	15.85	16.53	14.54	19.33	15.25	21.09	21.47
Fe_2O_3	10.34	10.60	8.78	9.16	9.06	9.49	8.36	10.55	8.77	9.26	8.95	11.85
MgO	6.15	7.61	7.85	7.97	7.61	9.97	7.41	7.91	7.08	6.24	2.83	3.03
CaO	9.74	9.61	9.85	9.77	9.65	10.22	8.07	8.82	8.79	4.79	6.58	6.52
Na_2O	1.55	0.05	3.39	2.94	2.56	2.36	3.08	3.30	3.49	2.78	4.23	4.01
K_2O	0.95	1.27	0.93	0.99	0.72	1.66	1.71	1.37	0.91	2.43	0.54	0.61
TiO_2	2.40	2.11	1.22	1.31	1.18	1.24	1.27	1.65	1.19	1.47	1.67	1.72
MnO	0.25	0.23	0.21	0.22	0.20	0.25	0.20	0.22	0.19	0.21	0.08	0.11
P_2O_5	0.76	0.50	0.12	0.14	0.17	0.18	0.16	0.30	0.18	0.13	0.04	0.22
TOTAL	**100.66**	**100.62**	**99.24**	**99.23**	**99.35**	**100.74**	**99.41**	**99.07**	**99.38**	**99.66**	**100.74**	**101.00**

Figure 9.2.2 (i) Trace element abundance in rock samples from the Huntly-Knock area.

	Schist	Schist	Schist	Schist	Schist	Schist	Schist	Schist	Pelite 1	Quartzite	Quartzite	Pelite 1	Pelite 1	Pelite 1	Quartzite	Schist
ppm	**BOG1**	**BOG3**	**CLAS111**	**CLAS1**	**CLAS107**	**COLL102**	**CLAS112**	**COLL101**	**MIKE2**	**MUCK2**	**NEWT1**	**CLAS111**	**CLAS110**	**KIN102**	**MUCK1**	**CLAS66**
Nb	45	55	34	33	51	48	62	32	32	16	18	23	31	5	17	32
Zr	421	343	337	509	392	323	357	482	365	369	230	118	345	44	354	314
Y	58	69	43	46	52	56	57	44	53	32	33	42	41	29	35	43
Sr	188	155	16	237	227	233	166	101	201	104	114	217	120	372	52	248
Rb	134	185	117	108	140	138	193	125	120	79	36	43	109	6	74	103
Zn	55	93	77	96	111	103	145	95	77	24	47	25	74	41	28	85
Cu	10	1	23	30	33	28	50	12	9	5	18	18	59	58	1	20
Ni	130	62	588	645	28	54	18	512	44	1828	3	24	636	82	1328	37
Cr	130	138	258	299	137	130	135	246	149	483	44	57	278	273	388	134
Ce	120	95	73	74	138	101	97	80	71	57	42	27	56	6	60	76
Nd	46	36	21	34	40	54	33	28	27	23	16	0	29	0	23	26
V	165	171	151	177	187	178	189	169	161	62	44	93	167	133	62	168
La	45	34	30	27	41	42	38	29	44	39	29	32	32	26	22	35
Ba	702	789	685	375	720	517	766	488	986	562	300	111	810	0	282	1172
Sc	20	19	7	11	14	16	16	12	17	9	4	15	10	27	7	7

	Schist	Schist	Schist	Schist	Schist	Schist	Schist	Schist	Crd hfls	Crd hfls	Crd hfls	Crd hfls	Crd hfls	Crd hfls	Crd hfls	Crd hfls
ppm	**SIN104**	**SIN101**	**SIN107**	**SIN103**	**SIN103b**	**SIN1**	**SIN2**	**SIN105**	**WET14**	**DUN 10**	**BQ17**	**DUN1**	**PIR4**	**CUM2ii**	**CUM8**	**CUM101**
Nb	18	22	28	18	26	15	20	20	49	53	51	44	50	79	36	34
Zr	264	224	192	258	292	213	260	218	685	197	393	449	314	528	359	1332
Y	38	38	54	37	46	47	42	39	78	36	33	193	69	71	59	70
Sr	107	135	34	129	131	138	129	56	380	128	509	119	408	413	277	380
Rb	77	85	176	67	130	52	93	92	86	34	33	70	36	97	90	59
Zn	78	99	134	54	71	55	65	33	120	220	122	191	148	133	112	107
Cu	23	19	33	14	10	39	0	0	70	110	95	127	101	22	104	19
Ni	144	1059	204	67	122	53	74	1176	64	138	109	128	114	43	115	0
Cr	317	497	375	208	246	179	186	507	199	417	234	259	283	151	129	25
Ce	48	56	87	33	78	58	49	25	97	66	111	160	95	145	106	184
Nd	21	19	29	4	38	22	7	4	39	16	25	85	18	61	54	73
V	147	156	224	109	165	85	98	118	257	412	278	271	312	225	204	92
La	24	28	31	19	29	24	30	18	43	22	49	64	50	56	44	62
Ba	356	454	335	218	536	213	380	377	699	0	377	396	495	461	671	767
Sc	12	11	16	11	19	12	9	10	35	25	26	53	28	15	10	25

Table 9.2.2 (ii) Trace element abundance in rock samples from the Huntly-Knock area.

	Crd hfls	Crd hfls	Crd hfls	Crd hfls	Crd hfls	Crd hfls	Crd hfls	Crd hfls	Crd norite	Crd norite	Crd norite	Crd norite	Crd norite	Crd norite	Grt tonalite	Grt tonalite
ppm	**WET6**	**WET10**	**BQ102**	**PIR101**	**CUM1**	**DUN3**	**CAS.B2**	**CAS.B5**	**DUN4**	**DUN4**	**DUN5**	**DUN9b**	**DUN9B**	**BAR2**	**CUM7**	**CUM19**
Nb	44	66	32	40	45	64	61	50	58	57	6	56	60	15	55	41
Zr	388	786	310	394	357	307	531	378	500	541	45	317	330	122	565	1676
Y	73	47	73	38	95	84	49	70	46	45	36	71	74	49	62	65
Sr	262	427	413	609	344	179	282	329	410	420	280	297	307	243	292	412
Rb	95	42	104	17	45	41	37	44	54	58	9	20	20	59	140	40
Zn	120	116	84	107	136	239	125	169	217	232	52	214	217	63	115	114
Cu	72	78	1	143	77	108	90	108	85	101	43	112	117	69	50	32
Ni	96	4	1539	1011	133	143	116	88	86	95	63	124	147	114	50	0
Cr	207	73	548	459	291	41	206	191	245	248	432	301	313	372	135	42
Ce	138	107	119	105	177	67	123	84	140	133	17	96	62	26	122	108
Nd	58	31	45	33	73	28	26	54	48	47	0	31	3	5	49	65
V	257	233	198	284	331	390	269	282	290	315	198	333	367	234	162	100
La	54	33	54	47	63	25	38	42	55	52	17	22	35	21	46	17
Ba	1687	514	4100	472	562	0	864	677	785	763	5	97	26	99	1157	669
Sc	24	37	23	37	26	28	25	22	23	21	29	37	33	34	12	30

	Grt tonalite	Grt tonalite	Grt tonalite	Grt tonalite	Mafic rock	Mafic rock	Mafic rock	Mafic rock	Mafic rock	Mafic rock	Mafic rock	Mafic rock	Mafic rock	Mafic rock	Bt gabbro	Bt gabbro
ppm	**CUM102**	**CUM16**	**TYQ3**	**TYQ5**	**W.TON104**	**BIN102**	**BIN103**	**BIN1**	**BIN2**	**RIV3**	**BIN101**	**BIN104**	**KIN102**	**DUN5**	**W.TON106**	**W.TON4**
Nb	36	38	14	19	4	5	6	4	6	5	4	3	5	6	28	49
Zr	359	291	391	509	43	35	24	33	34	37	32	38	44	45	487	471
Y	59	38	85	62	23	29	26	29	28	29	27	23	29	36	52	45
Sr	277	307	324	373	416	234	196	227	258	327	266	368	372	280	312	362
Rb	90	67	53	87	6	7	5	7	90	4	7	7	6	9	48	21
Zn	112	85	32	57	12	25	46	22	112	29	32	23	41	52	96	128
Cu	104	15	3	0	215	114	396	108	101	69	176	52	58	43	26	48
Ni	115	1294	8	1848	1918	239	91	1320	1174	1422	1215	438	82	63	42	1148
Cr	129	331	38	510	428	1172	255	1504	1003	762	903	976	273	432	56	356
Ce	106	147	193	169	7	0	16	0	0	0	8	16	6	17	27	101
Nd	54	73	78	73	0	0	13	0	0	0	0	0	0	0	269	47
V	204	129	74	144	10	156	161	140	101	183	78	19	133	198	19	265
La	44	57	61	60	24	27	24	17	18	18	16	16	26	17	785	32
Ba	671	788	591	916	23	0	0	0	1	0	0	8	0	5	785	431
Sc	10	20	15	16	14	34	49	37	21	39	17	9	27	29	40	41

Table 9.2.2 (iii) Trace element abundance in rock samples from the Huntly-Knock area.

	Bt gabbro	Bt gabbro	Bt gabbro	Bt gabbro	Bt-gabbro	Bt-gabbro	Bt-gabbro	Bt-gabbro	Micro-norite	Micro-norite
ppm	**W.TON5**	**BQ29**	**BQ26**	**BQ30**	**WET13**	**CUT1**	**CUT7**	**BAR1**	**BQ27**	**BQ4**
Nb	37	12	12	12	21	20	15	18	39	34
Zr	234	117	110	114	206	144	119	114	310	343
Y	49	49	74	50	56	53	45	48	39	46
Sr	360	237	220	239	300	270	259	17	463	469
Rb	23	4	9	9	22	42	9	58	3	2
Zn	79	65	60	63	84	70	75	43	118	148
Cu	18	68	75	68	42	44	60	0	48	180
Ni	883	133	165	144	771	51	54	2119	67	99
Cr	376	421	394	400	506	406	511	601	186	212
Ce	69	24	16	23	61	48	35	55	110	106
Nd	32	11	8	13	29	14	16	16	30	35
V	238	252	226	237	281	221	228	110	200	220
La	24	26	31	22	31	29	26	36	31	27
Ba	449	0	0	0	183	193	31	125	192	228
Sc	38	10	37	50	40	35	34	10	18	26

Table 9.4 Summary of findings of chemical trends from XRF data, with applicability to models for formation of the cordierite norites, garnet tonalites, and cordierite hornfelses of the Huntly area.

DESCRIPTION OF CHEMICAL TRENDS	S and SW Margins Major Elements	S and SW Margins Trace Elements	W Margin Major Elements	W Margin Trace Elements	SUPPORTS MODEL No.	INVALIDATES MODEL No.
Crd norites / Grt tonalites & Crd hornfelses have higher concs of the following element(s) than the pelitic schists & mafic igneous rocks.	Fe_2O_3, TiO_2	Zn, V	Fe_2O_3, TiO_2	Nb, Zr, Y, Zn, Nd, Ba	**3**	**1, 2 & 4**
Crd norites / Grt tonalites & Cord hornfelses have higher concs of the following element(s) than the mafic igneous rocks, but equal to the pelitic schists.	NONE	Nb, Zr, Ba, Y, Ce, Nd	K_2O	Rb	**3**	**1**
Crd norites / Grt tonalites and Crd hornfelses have higher concs of the following element(s) than the mafic ign. rocks, but lower conc. than pelitic schists.	K_2O, SiO_2	Rb	SiO_2	NONE	**1 & 3**	**2 & 4**
Crd norites / Grt-tonalites and Crd hornfelses have higher conc. of the following element(s) than the pelitic schists, but lower conc. than mafic igneous. rocks.	CaO, MgO	Cu	CaO	Sr, Cu, Sc	**1 & 3**	**2**
Conc. of these element(s) in Crd norites / Grt tonalites greater than in the pelitic schists, but conc. in the cord-hornfelses lower than in the pelitic schists.	NONE	NONE	NONE	NONE	*2*	*1,3 & 4*
Conc. of these element(s) in Crd norites or Grt tonalites lower than in the pelitic schists, but conc. in Crd hornfelses greater than in the pelitic schists.	NONE	NONE	NONE	NONE	*2*	*1,3 & 4*
Biotite gabbros enriched in the following element(s) relative to the mafic igneous rocks.	K_2O, TiO_2	Zr, Y, Rb, Zn, Ce, Nd, Ba	K_2O, TiO_2	Nb, Zr, Y, Zn, Rb, Ce, Nb, Ba		

Table 9.5.1 Theoretical 'extracted' melt compositions. When added together, the composition given by mixing positive quantities of melt with mean cordierite hornfels is equal to the mean composition of pelitic schist. For the rocks from the S and SW margins of the Huntly Gabbro the minimum mixing ratio, which uses only positive quantities of all elements from the melt, is 3 parts of melt to 2 parts hornfels. For rocks from the W margins of the Huntly Gabbro a minimum ratio of 4 parts melt to 1 part hornfels is required if only positive amounts of CaO are used from the melt composition.

Rocks from S and SW margins of Huntly Gabbro

	Mean schist	Mean hornfels	SM 1 3M + 2H	SM 2 7M + 4H	SM 3 2M + 1H	SM 4 3M + 1H
SiO_2	63.18	49.29	72.44	71.12	70.12	67.81
Al_2O_3	17.54	22.16	14.46	14.90	15.23	16.00
Fe_2O_3	7.86	12.37	4.86	5.29	5.61	6.36
MgO	2.15	4.61	0.51	0.75	0.92	1.33
CaO	1.39	3.41	0.04	0.24	0.38	0.72
Na_2O	1.80	3.69	0.53	0.71	0.85	1.16
K_2O	4.19	1.66	5.87	5.64	5.45	5.03
TiO_2	1.34	1.99	0.91	0.97	1.02	1.12
MnO	0.18	0.36	0.06	0.08	0.09	0.12
P_2O_5	0.21	0.16	0.24	0.24	0.23	0.23

Rocks from W margin of Huntly Gabbro

	Mean schist	Mean hornfels	WM 1 3M + 2H	WM 2 7M + 4H	WM 3 2 M + 1H	WM 4 3 M + 1H	WM 5 4 M + 1H
SiO_2	65.69	54.97	72.44	70.38	69.79	68.43	67.74
Al_2O_3	15.56	16.63	16.17	16.08	16.02	15.87	15.79
Fe_2O_3	6.89	12.19	4.00	4.42	4.72	5.45	5.81
MgO	4.76	3.78	3.67	3.83	3.94	4.21	4.35
CaO	0.68	4.09	-1.13	-0.87	-0.68	-0.22	0.00
Na_2O	1.72	3.92	0.30	0.50	0.66	1.01	1.19
K_2O	3.18	2.29	4.44	4.26	4.13	3.81	3.65
TiO_2	0.89	1.83	0.57	0.61	0.65	0.73	0.77
MnO	0.14	0.23	0.11	0.11	0.11	0.12	0.13
P_2O_5	0.11	0.35	0.02	0.03	0.04	0.06	0.07

M - one part melt compostition, H - one part mean hornfels, with for example; 3M + 2H representing three parts melt mixed with two parts hornfels.

Table 9.5.2 CIPW norm calculations from theoretical melt compositions. Melt compositions given in Table 9.5.1. All Fe recalculated to FeO.

	SM1	SM3	WM5
quartz	43.49	39.02	37.07
corundum	7.24	7.30	10.01
orthoclase	34.99	32.54	21.86
albite	44.80	7.30	10.17
anorthite	0.20	1.90	0.00
hypersthene	7.85	9.97	19.41
ilmenite	1.75	1.97	1.48
TOTAL	99.99	100.00	100.00

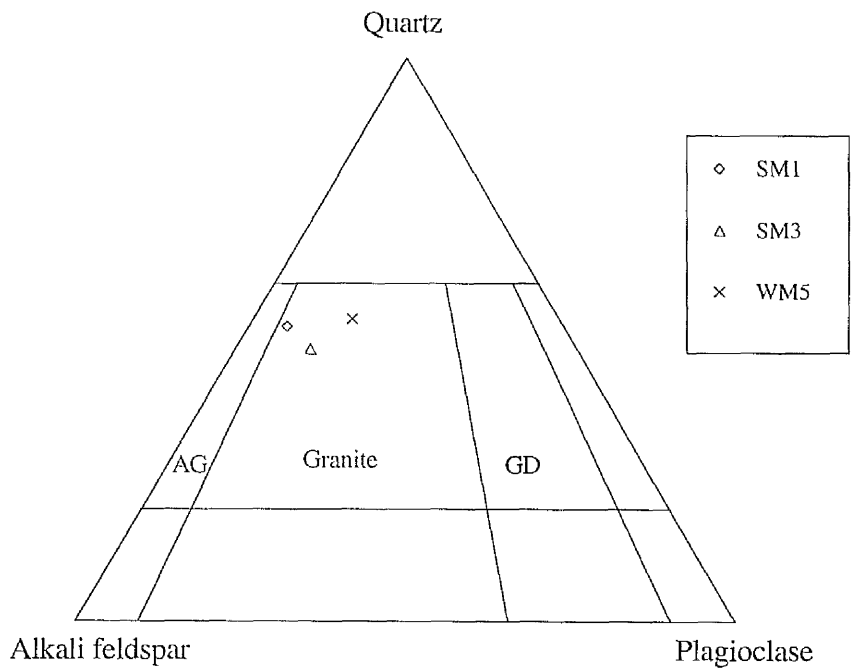

Figure 9.5.1 QAP diagram, plotting quartz, alkali feldspar and plagioclase from CIPW norm calculations (Table 9.5.2, above) using theoretical 'extracted' melt compositions. All of the melts plot within the granite field. Melts SM1 and SM3 from calculations on rocks from S and SW margins of Huntly Gabbro, WM5 from W margin of Huntly Gabbro. Other fields labelled are AG - alkali-feldspar granite, and GD - granodiorite.

CHAPTER 10 EXPERIMENTAL WORK

10.1 Introduction

Field-studies (Chapter 4) have shown which pelitic rocks are the likely protoliths of the cordierite-bearing hornfelses and associated igneous-textured rocks from the inner aureole and margins of the Huntly Gabbro. Petrological (Chapter 5) and whole-rock chemical (Chapter 9) data have demonstrated that the cordierite-bearing hornfelses have the chemical and textural characteristics of melt-depleted restitic rocks. Such studies also suggest that the cordierite norites and garnet tonalites both represent melts that contain a high percentage of entrained restite. Mixing calculations, using the whole-rock chemical data from the pelitic schists and the cordierite-bearing hornfelses, have been used to give theoretical 'extracted' melt compositions.

By selecting suitable starting materials that represent the likely protoliths of the cordierite hornfelses, cordierite norites and garnet tonalites, and subjecting them experimentally to the conditions under which the hornfelses were metamorphosed, the resultant run products can be used to determine the following:

(i) Whether the pelitic schists from outside the aureole of the Huntly Gabbro are the true protoliths of the cordierite hornfelses, cordierite norites and garnet tonalites. This can be achieved by comparing and contrasting the experimental solid-phase run products with the mineral assemblages of the natural rocks. Additionally, for the pelitic schists to be the true protoliths of the cordierite hornfelses, the experimentally derived melts should be similar in composition to the theoretical melts calculated from mixing data (Chapter 9.5).

(ii) The volumes and compositions of melt formed. These data can be used to determine whether or not the melting was sufficient for melt segregation and mobilisation to occur. Also the relative fertility of various kinds of pelite used can be compared and contrasted, to determine which rocks types are most likely to represent fertile source rocks for granite production.

(iii) Which mineral phases in the cordierite norites represent entrained restite, and which are likely to have crystallised from a melt.

10.2 Choice of Experimental Starting Products and Run Conditions

10.2.1 Choice of starting products

The starting materials for the experimental work were chosen from rock units that are believed to represent the protoliths of the cordierite-bearing hornfelses. Therefore, samples were chosen from the regionally metamorphosed rocks that trend towards, and are cross-cut by Huntly Gabbro. The occurrence of cordierite, orthopyroxene and almandine in the hornfelses indicates that their protoliths were unquestionably pelitic, or semi-pelitic in composition. The chosen starting products were accordingly chosen from representative pelitic or semi-pelitic rock units, that display no evidence of late hydrothermal alteration (which could have altered the primary compositions of the rocks).

Three samples were chosen for experimental work, two pelitic schists (DD.CLAS112 and DD.BOG1) from Clashmach Hill (locality 1c) and one semi-pelitic schist (DD.SIN2) from the Cairnie road cutting (locality 1b). The whole-rock chemistry and modal mineralogy of the three samples is given in Table 10.2.1.

The two samples from Clashmach Hill represent examples of the two main pelitic rock types from this locality, one an andalusite schist (DD.CLAS112) and the other a mica schist (DD.BOG1). Both contain high modal quantities of mica (55 and 65% respectively). However, the mica in sample DD.BOG1 is predominately muscovite (77% of total mica content), whereas biotite forms 68% of the mica in DD.CLAS112.

Sample DD.SIN2 from Cairnie is a semi-pelitic garnet-mica schist. The sample has modally less total mica (35%) than the two samples from Clashmach Hill, and is relatively quartz-rich.

The water contents for the three starting materials were measured using the thermogravimetric balance and are also given in Table 10.2.1.

10.2.2 Choice of run conditions

The temperatures and pressures at which the experiments were run were designed to mimic those to which the melt-depleted orthopyroxene-cordierite hornfelses were subjected. Therefore, accurate temperature and pressure estimates from geothermobarometry are required to determine the run conditions.

The most reliable temperature estimates for the orthopyroxene-cordierite hornfelses are given by garnet-orthopyroxene geothermometry (Chapter 8.8), which yields temperatures from 880 to 960°C for these rocks. The most consistent and accurate pressure estimates are given by THERMOCALC, which gives mean pressures of between 4.8 and 5.3 kbars for the cordierite norites and a pressure of 5.1±0.5 kbars for the orthopyroxene-cordierite hornfels DD.BQ17.

The temperature at which the experiments were to be run was chosen as 900°C, as all the orthopyroxene-cordierite hornfelses recorded temperatures close to this value, and none more than 20°C less. A pressure of 5.0 kbars was chosen, as this represents the mean pressure given by the cordierite norites, and the orthopyroxene-cordierite hornfels.

The total volatile deficiency displayed by the cordierites from the cordierite norite DD.BQ38 and the cordierite hornfels 10035 is inferred to indicate that the cordierites crystallised in fluid-absent conditions (e.g. Fitzsimons, 1994). Therefore, the experiments were conducted in fluid-absent conditions (i.e. without addition of H_2O).

10.3 Experimental Methods and Analytical Techniques

Two experiments were run, one with the starting material alone, and one with garnet seeds (from sample H.COR7) added to the starting material. Both experiments were run at temperatures of 900°C and pressures of 5 kbars.

10.3.1 Preparation of run charges

Portions of the three chosen samples were powdered using a tema, then an agate ball mill, so that a grain size of approximately 1 μm was obtained. Garnet seeds were added to one set of the ground samples, and these were ground again using the ball mill to ensure good uniform mixing of the grain size between the rock powder and garnet. The powder was then stored in a oven dryer at 100°C to prevent the absorbance of any surface moisture.

Gold tubing, 3 mm in diameter and with a wall thickness of 0.15 mm, was used to form the casings of the charges. 1.5 cm lengths of Au tubing were cut and then annealed in a flame. One end of the tubing was crimped flat, then welded using a carbon arc welder. A small quantity of the powdered starting material was added into the open end of the

tubing and pressed down, ensuring that no powder contaminated the upper lip of the tubing. The top of the capsule was then crimped and welded shut.

10.3.2 Experimental vessel used

Experiments were conducted using an internally heated gas vessel. Detailed desriptions of this equipment are given by Ulmer (1971), Edgar (1973) and Wood & Holloway (1988).

The internal arrangement of the components in the internally heated gas vessel are shown in Figure 10.3.1. Up to three capsules per run were placed in a high temperature glass tube. Thermocouples were placed either side of the run capsules to allow the thermal gradient to be measured and minimised. One of these thermocouples was connected to the furnace temperature controller and the other to a monitor. These temperatures are believed to be accurate to within ±5°C. The pressure medium used was high purity argon and pressure was measured using a manganin resistant cell and are accurate to ±10 MPa.

10.3.3 Control of fO_2

Stevens (1995) showed that during experimental runs at 5 kbars H_2 was lost through the run capsules into the surrounding argon medium. This had the effect of reducing the amount of melt present in the run products and of stabilising Fe-rich biotite to higher temperatures. The technique used to counter the loss of H_2 involves use of a H_2 diffusion membrane (Figure 10.3.1). This membrane was used to impose a log $fH_2 = -1$ relative to the fayalite-magnetite-quartz buffer, at a nominal $aH_2O = 0.35$. The aH2O = 0.35 was chosen as this seems a reasonable estimation of water activity from the maximum $X_{H_2O}^{Crd}$ values given for the cordierite norite DD.BQ38 and cordierite hornfels 10035 (Chapter 6).

10.3.4 Post experiment sample treatment

On completion of the experiments the gold capsules were cut open, and grain mounts were made from the run products. These grain mounts were then carbon-coated, viewed and analysed under the S.E.M. The major minerals and melts were analysed for major elements using electron beam spot analysis (using the same method of analysis and

data processing as the electron microprobe).

10.3.5 Analysis of mineral phases

Mineral phases were both observed and analysed under the JEOL JSM 6400 scanning electron microscope. Analysis of mineral compositions was undertaken using the same technique as used with the electron microprobe. A full list of the oparating variables and analytical run conditions is given in Appendix V.

10.3.6 Melt analysis

Melt compositions were obtained by cold stage analyses on the S.E.M.. Cold-stage analysis was necessary as room temperature (20°C) work gave low totals for sodium and potassium. This occurs because when the quenched melt is hit by the electron beam, the alkalis either diffuse away from the point of beam incidence, or volatilise into the vacuum. Cold-stage analysis minimises these effects as the alkali atoms are considerably less mobile at very low temperatures.

Cold-stage analysis is achieved by cooling of the specimen stage with oxygen-free liquid nitrogen. Analyses were made at temperatures between -191 and -193°C, with a beam current of 1.5nA and a lifetime of 40 seconds. The need for cold-stage analysis is highlighted in Table 10.3.1, which gives the mean melt compositions from CLAS112(900), taken using both cold stage and room temperature analysis. The room temperature analyses have lower mean Ca, Na and K totals than the cold stage analyses, with 8% greater Ca and Na, and 40 % K contents given by cold-stage analysis.

10.4 Results From Mineral Phases

To avoid confusion with the samples used as starting materials the run charges are renamed, with the starting materials DD.CLAS112, DD.BOG1 and DD.SIN2 renamed as the run charges CLAS112(900), BOG1(900) and SIN2(900) respectively.

10.4.1 CLAS112(900)

(i) General observations

The sample CLAS112(900) contains the mineral phases; orthopyroxene, cordierite, hercynite, ilmenite, and small amounts of biotite (Plate 10.4.1). All of these crystals are suspended in a matrix of quenched melt. The charge from the garnet seeded experiment contains identical phases to the garnet-absent charge, with garnet again not present . No quartz was present in either run sample. Representative analyses from the mineral phases are given in Table 10.4.1.

(ii) Orthopyroxene

The orthopyroxene occurs mainly as euhedral crystals, up to 50 μm in length and 15 μm in across (Plate 10.4.2). Inclusions of small ilmenite and/or hercynite crystals occur abundantly. The Mg# (Mg# = Mg/(Mg + Fe)) vary from 0.50 to 0.53, values within the range of the cordierite norites and orthopyroxene-cordierite hornfelses. The X_{Al}^{MI} (X_{Al}^{MI} = Al/2) contents are higher than those given by the cordierite norites and hornfelses, varying from 0.18 to 0.25.

(iii) Cordierite

Cordierite forms euhedral crystals, hexagonal in cross section, with average diameters of 10 μm (Plates 10.4.1 and 10.4.2). Cross sections of crystal are rectangular, with average lengths of 15 μm. The Mg# vary from 0.63 to 0.74, and fall within the Mg# range of both the cordierite norites and orthopyroxene-cordierite hornfelses (Tables 6.3.3 and 6.4.3).

(iv) Biotite

The biotite occurs uncommonly, forming small, usually ragged flakes (Plate 10.4.1), up to 8 μm long. The Ti content in the biotite is high, and in the same range as the Ti contents from the orthopyroxene-bearing hornfelses H.BHQ5 and H.COR10 (Table 6.3.5), varying from 0.631 to 0.742 in the 22(O) formula unit. However, the Mg# values are slightly lower than those given by the hornfelses, and range from 0.41 to 0.46.

(v) Hercynite

The hercynite occurs as small octahedral crystals (Plate 10.4.3), that are bright in B.S.E. (back scattered electron) images due to their high atomic number contrast (i.e. abundant Fe). The majority of the crystals have diameters of between 1 and 2 μm, making the acquisition of accurate analyses difficult, as the electron beam has a diameter of 2 μm. Two analyses gained from larger crystals show with low Mg# values (approximately 0.20). The two analyses have cation totals greater than 6 in the 8(O) formula unit, and recalculation for Fe^{3+} gives X_{Mag}^{Spl} contents of around 0.13.

(vi) Ilmenite

Ilmenite is also common, forming bright crystals (due to the high average atomic number) in B.S.E. image, and can be distinguished from hercynite by it's 'rounded' appearance (Plate 10.4.2). The crystals are small, with diameters mainly less than 1 to 2 μm, making quantitative analysis impossible.

10.4.2 BOG1(900)

(i) General observations

The garnet-absent and garnet-seeded run products BOG1(900) both contained the mineral phases, cordierite, ilmenite and hercynite. No garnet, biotite or quartz occurs in either run product. Representative analyses of cordierite and ilmenite are given in Table 10.4.2.

(ii) Cordierite

Blocky cordierite crystals appear hexagonal in cross-section and rectangular in longitudinal section (Plates 10.4.4 and 10.4.5), with mean diameters and lengths of 10 μm. The Mg# vary from 0.64 to 0.73, within the range of Mg# from the cordierite norites.

(iii) Hercynite

Hercynite forms small, bright crystals with diameters less than 1 μm, making them unsuitable for quantitative analysis.

(iv) Ilmenite

Forming abundant, rounded crystals, the ilmenite is slightly larger than the

hercynite, with a few crystals large enough for analysis. These analyses are not stoichiometrically accurate, though do indicate the presence of some Mg and recalculation for Fe^{3+} indicates that up to 5.11 wt% Fe_2O_3 may be present.

10.4.3 SIN2(900)

(i) General observations

Both the garnet-seeded, and un-seeded run products contain the same solid phases, with garnet, orthopyroxene, cordierite, plagioclase, ilmenite and quartz present. Representative orthopyroxene, cordierite, garnet and plagioclase analyses are given in Table 10.4.3.

(ii) Orthopyroxene

The orthopyroxene occurs as light coloured, thin, elongate crystals, with lengths from 1 to 12 μm and widths from 0.1 to 2 μm (Plate 10.4.6). The orthopyroxenes have Mg# values from 0.53 to 0.58 and X_{Al}^{MI} contents of between 0.23 and 0.31.

(iii) Cordierite

Cordierite forms blocky crystals that are hexagonal in cross-section (Plates 10.4.6 and 10.4.7), with diameters mainly between 2 and 10 μm and similar lengths. The Mg# values given by the cordierites range from 0.68 to 0.76.

(iv) Garnet

The garnet forms bright, sub-rounded crystals, up to 15 μm in diameter (Plates 10.4.6 and 10.4.7). Plate 10.4.7 shows a garnet, with a bright white core, with slightly greyer rims. Figure 10.4.5 is a compositional profile of this crystal, showing the distribution of XMg. The light coloured garnet rims have higher Mg# values (0.34 to 0.37) than the crystal cores (0.17 to 0.21). The crystal cores also have higher Mn contents than the rims, and have similar compositions to the garnets from the starting product sample DD.SIN2 (see analysis in Table 6.2.2). This suggests that the core represents a relict garnet crystal, and the Mg-rich, Mn-poor rims overgrew the crystal during the experimental run.

(v) Plagioclase

The recognition of plagioclase from the S.E.M. image was not possible, due to the low atomic contrast between the plagioclase, quartz, and the quenched melt. However, random spot analysis revealed the presence of this mineral. The two analyses gained both have X_{An} values of 0.20, lower than the X_{An} values of 0.30 for the plagioclase present in the starting product.

(vi) Quartz

The quartz forms dark crystals in B.S.E. and is difficult to distinguish from the quenched melt.

10.5 Melt Compositions

Cold stage analysis under the S.E.M. was used to provide ten or more analyses of the quenched melts from each of the three run products. The means of these analyses and CIPW norms are given in Table 10.5.1. The CIPW norms were calculated using the Apple Macintosh computer package CIPWnorm 3.1 Mason (1990). All Fe is calculated as FeO for use in the program.

10.5.1 Estimation of Melt Quantities

Attempts to estimate the volume of melt present in run samples CLAS112(900) and BOG(900) were made by tracing the areas of melt from B.S.E. images onto graph paper, and then counting the percentage of squares in which the melt occurred. This method assumes that the area of visible melt shown on the two dimensional image is proportional to the total melt volume. This might not be the case if any crystal settling had occurred, though no evidence of this was seen. Errors from this method are large, and can stem from crystal clustering, with some areas of the run product being more crystal-rich. Other errors occur due to difficulties in differentiating the melt phase from other mineral phases with similar atomic-number contrasts (i.e. quartz and plagioclase). To minimise the former problem, relatively low magnification images were used, and the melt volumes were estimated from three images from each sample. No attempt was made to estimate the

melt volume from run sample SIN2(900), as the presence of both plagioclase and quartz made the accurate identification of the melt phase difficult. Quartz and plagioclase are absent from both CLAS112(900) and BOG1(900), allowing areas of melt to be easily distinguished from crystals.

(i) CLAS112(900)

Analysis of images from CLAS112(900) indicate that between 55 and 65% volume of melt occurs throughout the run sample. For example, approximately 60% melt volume is present in Plate 10.4.1.

(ii) BOG1(900)

A minimum approximate melt volume of 55% is given by analysis of the crystal-rich image Plate 10.4.4. However, the majority of images contain melt volumes of approximately 70% (e.g. Plate 10.4.5) and the overall melt volume is probably in the region of at least 65%.

10.5.2 Correlation of experimental melts with natural rock data

Since the starting materials for the experiments are inferred to represent protoliths of the melt-depleted cordierite hornfelses, cordierite norites and garnet tonalites, the melts produced from the experiments should represent the compositions of the melts extracted from these rocks. Theoretical 'extracted' melts were derived from mixing calculations, using mean pelitic schist and cordierite hornfels whole-rock analytical data (Chapter 9.5.1 and Table 9.5.1). If the pelitic schists from the margins of the Huntly Gabbro, used in the experiments, are the true protoliths of the cordierite hornfelses, and their associated igneous textured rocks, then chemical (Harker) plots of the experimental melts should plot opposite to the hornfelses, relative to the pelitic schists. That is, they should be chemically similar to the theoretically modelled 'extracted' melts.

The starting products DD.CLAS112 and DD.BOG1 both come from samples from Clashmach Hill (locality 1c) to the S of the Huntly Gabbro and sample DD.SIN2 from the W margins. Accordingly two sets of graphs are presented, the first plotting data from the mean melt analyses of CLAS112(900) and BOG1(900), the theoretical 'extracted' melt SM1 (Table 9.5.1), and the cordierite hornfelses and cordierite norites from the S and SW

margins of the Gabbro. The second set shows data from the SIN2(900) mean melt composition, 'extracted' melt WM4 (Table 9.5.1), and the cordierite hornfelses and garnet tonalites from the W margins of the Gabbro.

10.5.3 S and SW margins of the Huntly Gabbro (CLAS112(900), BOG1(900))

Chemical data from the rocks from the S and SW margins of the Huntly Gabbro, and the relevant experimental, and theoretical melt compositions are plotted in Figures 10.5.1-7, with SiO_2 plotted against the other major elements.

The experimental melts match rather closely with the modelled theoretical melt for their SiO_2, Al_2O_3, Fe_2O_3, MgO and K_2O contents, though have slightly higher Na_2O and CaO contents, and slightly less TiO_2. The higher CaO and Na_2O values from the experimental melts, relative to those from the estimated theoretical melts, result from the absence of plagioclase in the experimental run products, compared to the common presence of this mineral in the cordierite hornfelses. This leads to the lower Ca and Na contents calculated for the theoretical melts.

The experimental melts plot opposite the cordierite hornfelses, relative to the pelitic schists (protoliths) for all elements, and are relatively enriched in SiO_2 and K_2O, but depleted in Al_2O_3, Fe_2O_3, MgO, CaO, Na_2O, and TiO_2 relative to the hornfelses.

CIPW norm calculation on the melt analyses (Table 10.5.1) yield normative corundum for both CLAS112(900) and BOG1(900), indicating that both melts are strongly peraluminous. When plotted on a QAP diagram (Figure 10.5.8) the melts both plot in the granite field, though have less quartz, and greater plagioclase contents than the theoretical melts SM1 and SM3 (see Table 9.5.1).

10.5.4 W margin of the Huntly Gabbro (SIN2(900))

The mean composition from cold stage analysis of the melt phase in run SIN2(900) is given in Table 10.5.1. The melt composition differs from the estimated theoretical melt WM5 (Table 9.5.1) for most elements, with SiO_2, TiO_2, Fe_2O_3, and MgO all being considerably lower and CaO, Na_2O and K_2O contents all much higher in the experimental melts. Some of these discrepancies could result from the large quantities of melt required in the mixing calculations (Chapter 8.5), if only positive CaO quantities are used.

Figures 10.5.8-15 are graphs plotting the whole-rock chemistry data from the garnet tonalites, cordierite hornfelses and pelitic schists from the W margins of the Huntly Gabbro against the mean melt compositions from SIN2(900) and the calculated theoretical 'extracted' melt WM5. The melt from SIN2(900) plots opposite to the hornfelses, relative to the pelitic schists, for Al_2O_3, Fe_2O_3, K_2O and TiO_2. However, the MgO contents of both the cordierite hornfelses and of the experimental melt are lower than the pelitic schist; this could not be the case if the schists represent the protolith of the hornfelses and their extracted melt. Additionally the CaO and Na_2O contents of the cordierite hornfelses and of the melt are higher than in the pelitic schists, again showing that they may not represent the protolith of the hornfelses and their extracted melt.

The CIPW norm of the SIN2(900) mean melt composition is shown in Table 10.5.1. Plotting the quartz, alkali feldspar and plagioclase components onto a QAP diagram (Figure 10.5.8) shows the melt to be granitic, though with lower quartz and higher plagioclase contents than the calculated theoretical melt WM5. The calculated melt also yields higher plagioclase contents than the experimental melts CLAS112(900) and BOG1(900).

10.6 Discussion

10.6.1 CLAS112(900) from S margin of Huntly Gabbro)

When heated to 900°C at 5 kbars in fluid-absent conditions the resultant run product CLAS112(900) contains a large volume (55-65%) of quenched, peraluminous granitic melt, coexisting with cordierite, orthopyroxene, hercynite, ilmenite and some biotite. This resultant restitic mineral paragenesis is mineralogically similar to the parageneses given by the orthopyroxene-cordierite hornfelses and cordierite norites, the exceptions being the absence of plagioclase or garnet in the run products, and the absence of any quartz in relation to the cordierite norites. The minerals are compositionally similar to those in both the cordierite norites and hornfelses. The lack of quartz, plagioclase and major biotite in CLAS112(900) suggests that in the cordierite norites these minerals must have crystallised from a melt, with the orthopyroxene, cordierite, ilmenite and hercynite occurring as entrained restite.

Graphs plotting whole-rock chemical data from the cordierite hornfelses, cordierite norites and pelitic schists from the S and SW margins of the Huntly Gabbro against the theoretical 'extracted' melt and the mean experimental melt composition all support the field and petrological evidence that shows that the pelitic schists are the protoliths of the cordierite hornfelses and cordierite norites. The experimental melt is compositionally similar to the theoretical melt WM1 (Table 9.5.1). The volume of the experimental melt (55-65%) and the volume of melt used in the mixing calculations (a minimum of three parts melt mixing with two parts hornfels, giving a minimum melt volume of 50%) are similar.

The biotite in CLAS112(900) is Ti-rich and is compositionally similar to the relict biotite in H.BHQ5 (Table 6.3.5). This biotite is modally minor in CLAS112(900) (< 5%) compared to the starting sample DD.CLAS112 (32%). Most of the biotite and all of the muscovite have therefore been consumed by melting reactions. Such reactions also consumed all of the quartz and andalusite. Thus melting could have occurred by reactions such as:

muscovite + quartz = aluminosilicate + K-feldspar + melt [10.1]

biotite + aluminosilicate + quartz = K-feldspar + cordierite + hercynite+ melt [10.2]

biotite + quartz = orthopyroxene + melt. [10.3]

Textural evidence for the replacement of prismatic sillimanite by aggregates rich in hercynite in the cordierite norites (e.g. Plate 5.5.6), supports the occurrence of melt forming reaction 10.2.

The H_2O produced from these melting reactions will be partitioned between the coexisting melt and the cordierite, and the low H_2O content in the starting material (2.62 wt%) indicates that both the melt and the cordierite will be H_2O-undersaturated.

10.6.2 BOG1(900) from S margin of Huntly Gabbro

The run product BOG1(900) contains a large volume (approximately 65%) of quenched, peraluminous granitic melt, coexistsing with cordierite, hercynite and ilmenite.

The occurrence of a limited restitic paragenesis of modally abundant cordierite, with some ilmenite and hercynite resembles some of the cordierite-rich hornfelses from Battlehill Quarry (locality 3b), some of which contain modally 90% or more cordierite, and lack both orthopyroxene and garnet (e.g. DD.CD3). As with the mean melt composition from CLAS112(900), the melt in BOG1(900) is peraluminous and granitic in composition.

Graphs plotting whole-rock chemical data for the natural rocks against the theoretical and experimental melt compositions, again demonstrate that the pelitic schists from the S and SW of the Huntly Gabbro are the likely protoliths of the cordierite hornfelses and cordierite norites.

No mica or quartz is present in BOG1(900), and therefore these minerals have been completely consumed by melting reactions. Muscovite is the most abundant mica in DD.BOG1 (modally 50%) and the bulk of the melt would have been formed by muscovite-consuming reactions. Such fluid-absent melting reactions occur in temperatures as low as 740°C (Clemens 1984), and a likely such reaction would be 10.1. Biotite would react with the resultant aluminosilicate and with quartz to form additional melt by the reaction 10.2. The K-feldspar formed in reactions 10.1 and 10.2 would later be dissolved at higher temperature, hence its absnece in the run product.

10.6.3 SIN2(900) from W margin of Huntly Gabbro

The run product SIN2(900) probably contains only a small volume of melt, coexisting with garnet, plagioclase, orthopyroxene, cordierite, quartz and ilmenite. The restitic mineral paragenesis does not correlate with any of the hornfelses from the W margins of the Gabbro (i.e. Cormalet, locality 3e), none of which contain abundant quartz, or both orthopyroxene and cordierite together. Additionally, graphs plotting the MgO, CaO, and Na_2O contents from the whole rock chemical data of the pelitic schists, cordierite hornfelses and garnet tonalites against the experimental melt composition show that the analysed pelitic schists are probably not the protoliths of the cordierite hornfelses and garnet tonalites from the W margins of the Huntly Gabbro.

The melt volume present in SIN2(900) is restricted by the low modal mica content in the starting material DD.SIN2, with only 25% total mica. This also accounts for the continued presence of quartz in the run product, as the mica would be consumed in the

melting reactions before the quartz, which has a modal abundance of 60% in the starting material.

10.7 Conclusions

Data from the run products CLAS112(900) and BOG1(900) shows that the andalusite-mica schists and mica schists which crop-out to the S and SW of the Huntly Gabbro are undoubtedly the protoliths of the cordierite-bearing hornfelses and cordierite norites. The pelitic schists that crop out to the W of the Huntly Gabbro probably do not represent the protoliths of the cordierite hornfelses and garnet tonalites from Cormalet (locality 3e).

Melting would have occurred via mica-consuming, fluid-absent melting reactions (such as reactions 10.1, 10.2 and 10.3). The volume of melt produced from the run products CLAS112(900) and BOG1(900) is in excess of 50%, and would be able to segregate from its host and mobilise, if produced in a natural system. This illustrates that the Whitehills-Boyndie Bay 'Group' pelitic schists, from which the starting materials were taken, and that crop out to the S and SW of the Huntly Gabbro, represent fertile source rocks.

The cordierite-orthopyroxene hornfelses and cordierite hornfelses are analogous to the solid, restitic products from CLAS112(900) and BOG(900) respectively and consequently these rocks represent the restitic residues of fluid-absent partial melting, from which large volumes of peraluminous granitic melt must have been extracted.

The cordierite norites are igneous-textured rocks that contain a high proportion of entrained restite; the cordierite, orthopyroxene and hercynite representing restitic crystals that grew in the presence of a melt. The plagioclase and quartz both crystallised from the melt, and the last H_2O-saturated portion of melt would have crystallised biotite (which forms late poikilitic flakes in the cordierite norites). The small volume of melt inferred to have been present in the cordierite norites (i.e. restitic orthopyroxene and cordierite are modally abundant) suggests that these rocks may have crystallised in the presence of the last fraction of melt produced, which was unable to efficiently segregate from its restitic host , and hence froze *in-situ.*

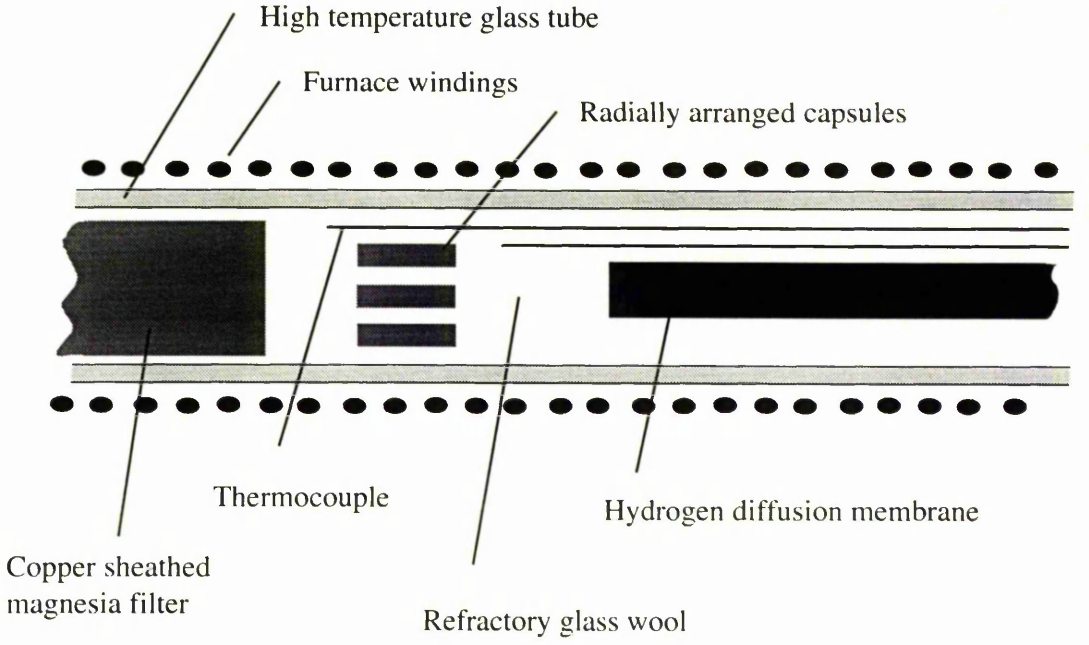

Figure 10.3.1 The internal arrangement of the components in the internally heated gas vessel, after Stevens (1995).

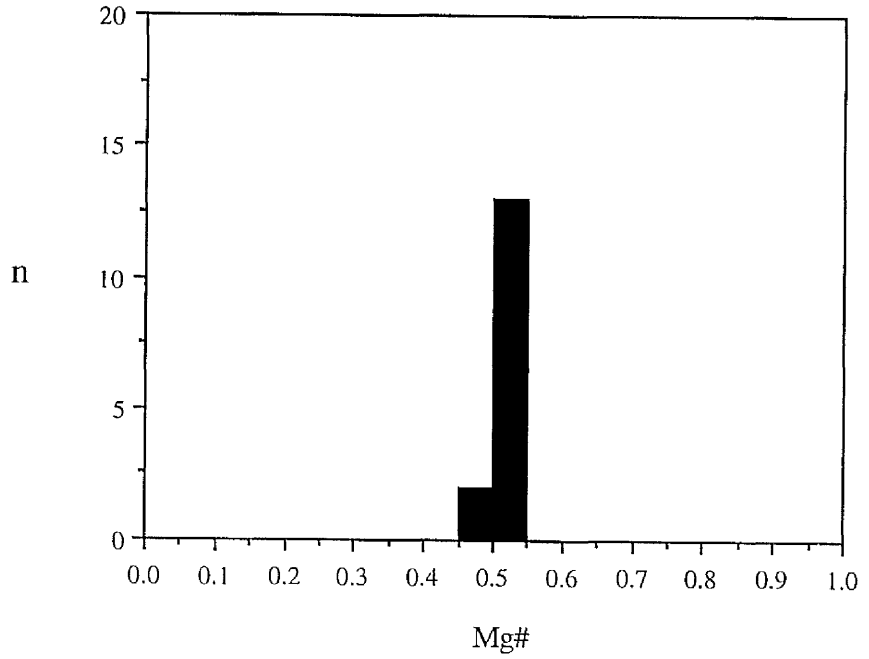

Figure 10.4.1 Mg# frequency plot for orthopyroxene analyses from CLAS112(900).

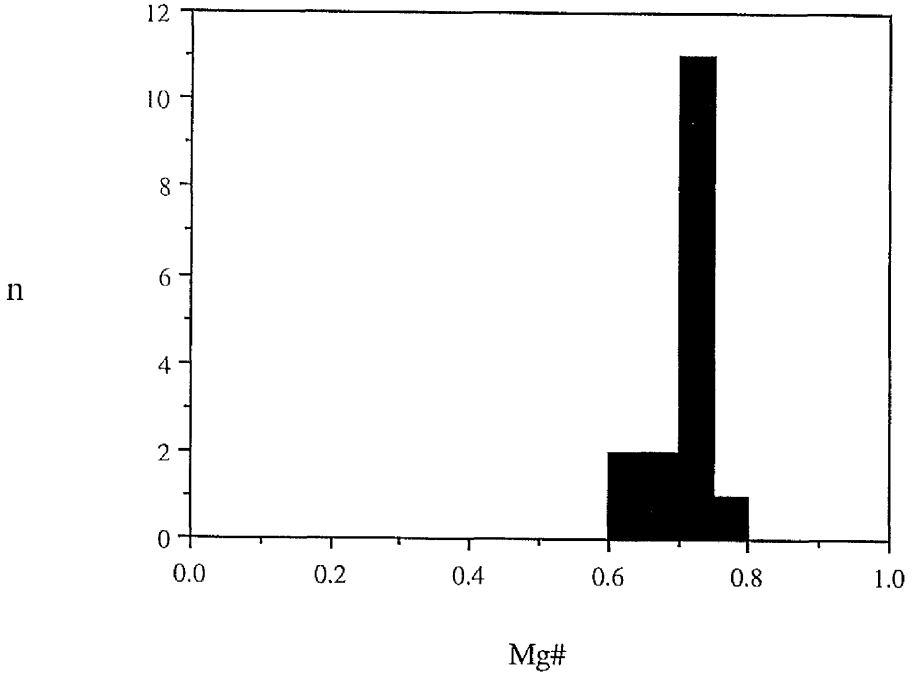

Figure 10.4.2 Mg/(Mg+Fe) frequency plot for cordierite analyses from CLAS112(900).

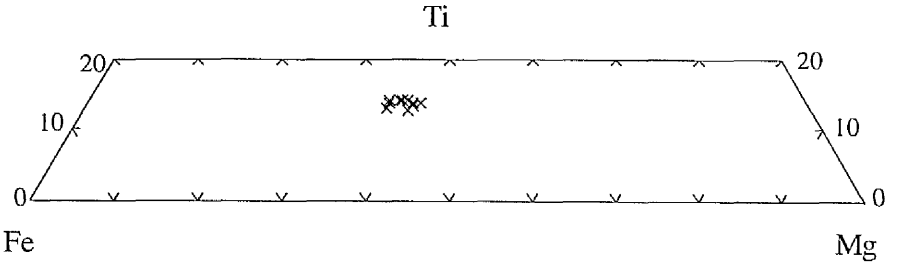

Figure 10.4.3 Compositional plot of biotite analyses from CLAS112(900).

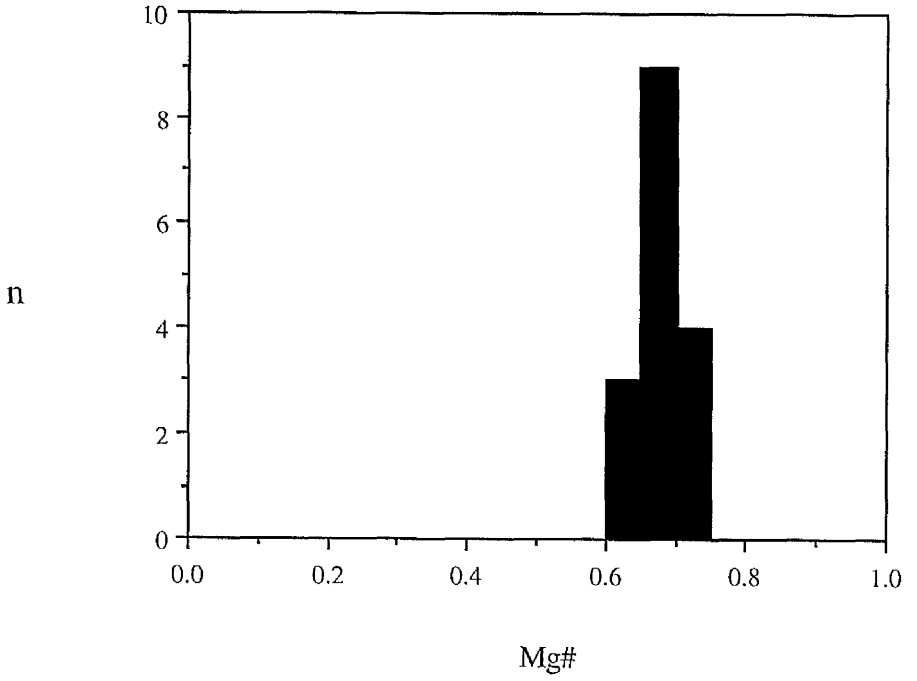

Figure 10.4.4 Mg# frequency plot for cordierite analyses from BOG1(900).

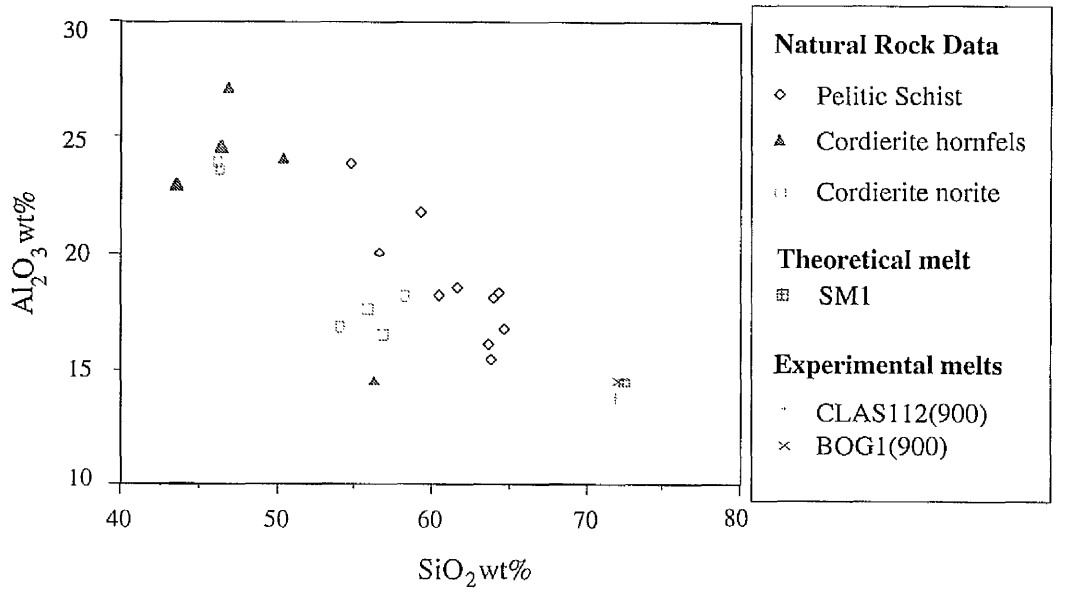

Figure 10.5.1 Graph plotting SiO_2-Al_2O_3 contents of theoretical melt (Table 9.5.1) and experimentally derived melts (Table 10.6.1) against natural rock compositions from the pelitic schists, cordierite hornfelses and cordierite norites from the S and SW margins of the Huntly Gabbro.

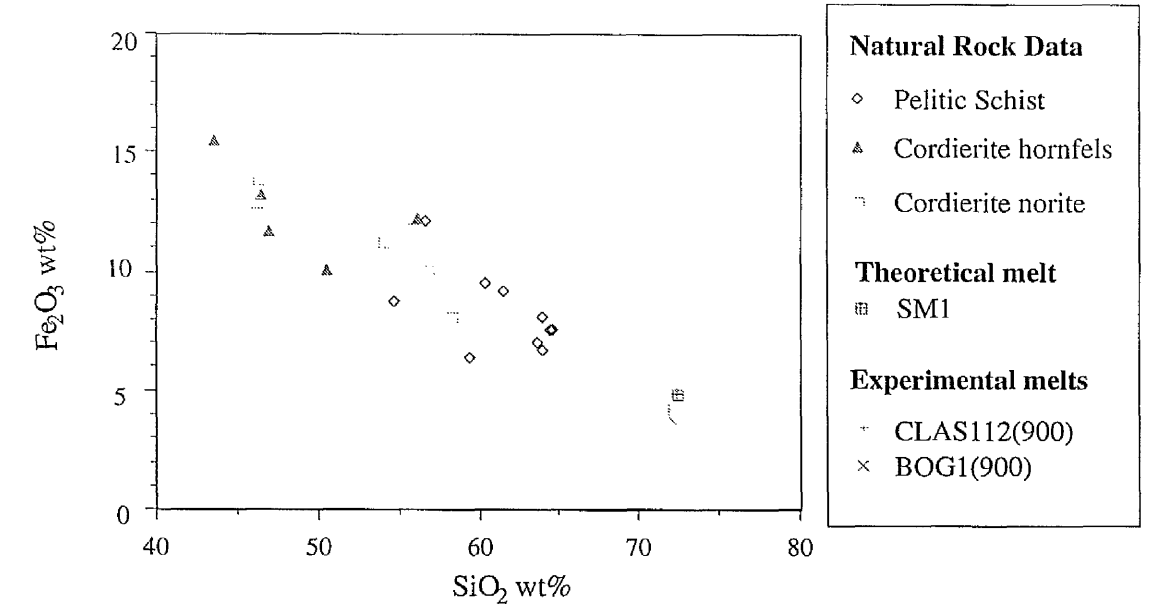

Figure 10.5.2 Graph plotting SiO_2-Fe_2O_3 contents of theoretical melt (Table 9.5.1) and experimentally derived melts (Table 10.6.1) against natural rock compositions from the pelitic schists, cordierite hornfelses and cordierite norites from the S and SW margins of the Huntly Gabbro.

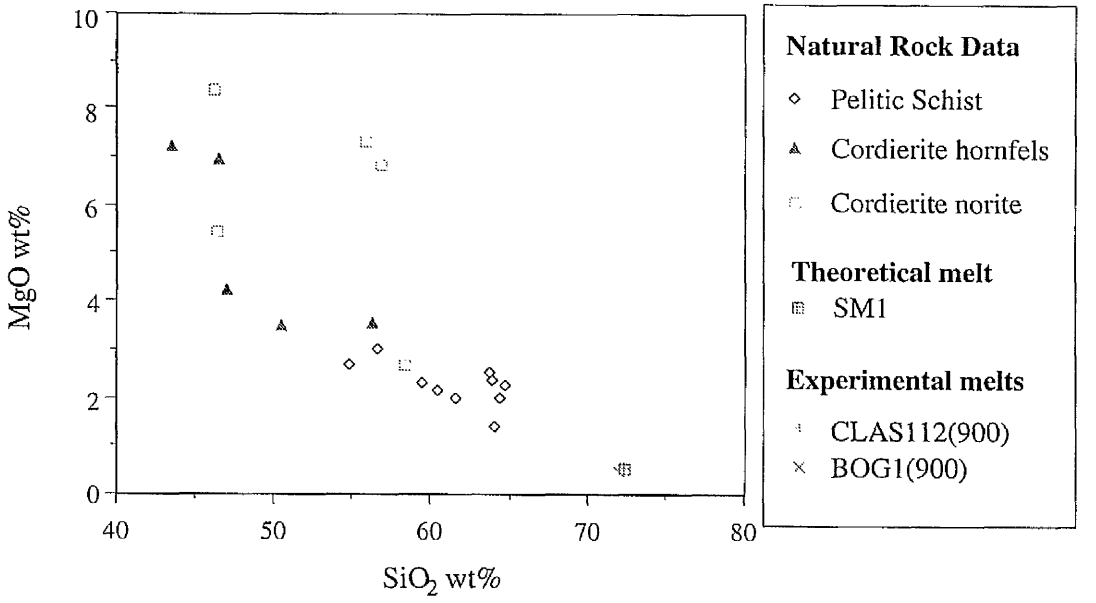

Figure 10.5.3 Graph plotting SiO_2-MgO contents of theoretical melt (Table 9.5.1) and experimentally derived melts (Table 10.6.1) against natural rock compositions from the pelitic schists, cordierite hornfelses and cordierite norites from the S and SW margins of the Huntly Gabbro.

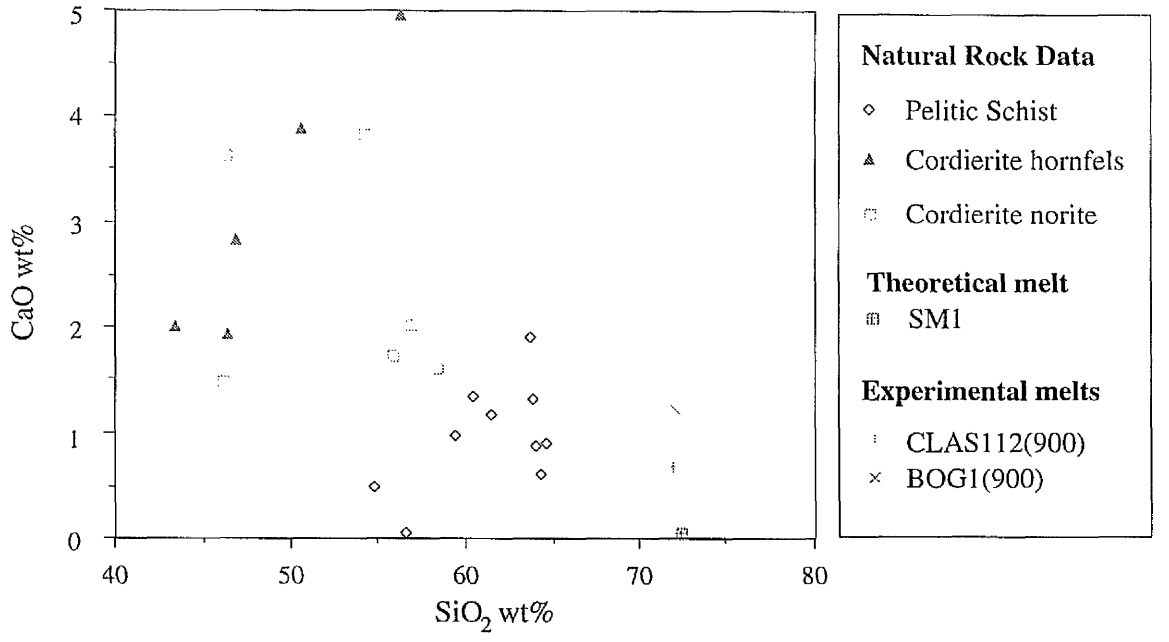

Figure 10.5.4 Graph plotting SiO_2-CaO contents of theoretical melt (Table 9.5.1) and experimentally derived melts (Table 10.6.1) against natural rock compositions from the pelitic schists, cordierite hornfelses and cordierite norites from the S and SW margins of the Huntly Gabbro.

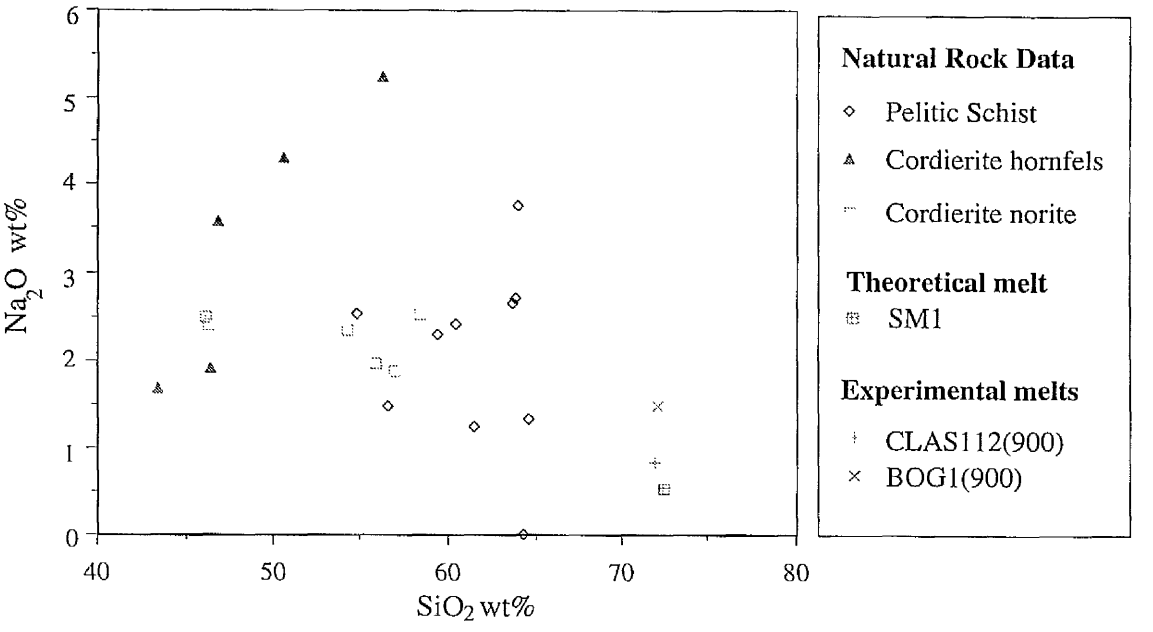

Figure 10.5.5 Graph plotting SiO_2-Na_2O contents of theoretical melt (Table 9.5.1) and experimentally derived melts (Table 10.6.1) against natural rock compositions from the pelitic schists, cordierite hornfelses and cordierite norites from the S and SW margins of the Huntly Gabbro.

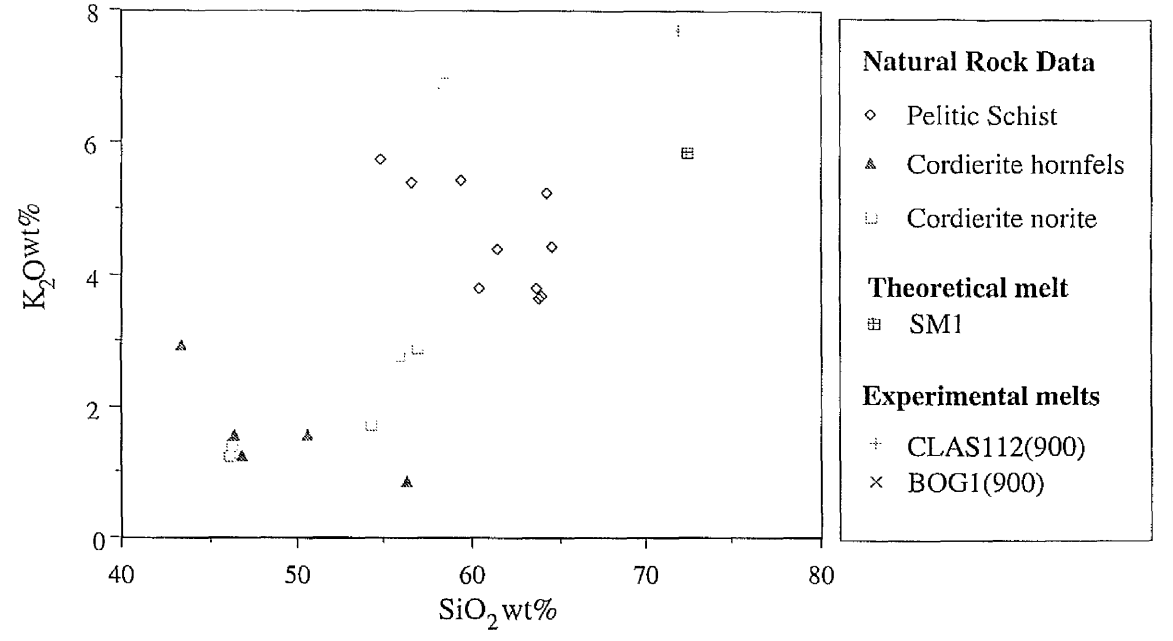

Figure 10.5.6 Graph plotting SiO_2-K_2O contents of theoretical melt (Table 9.5.1) and experimentally derived melts (Table 10.6.1) against natural rock compositions from the pelitic schists, cordierite hornfelses and cordierite norites from the S and SW margins of the Huntly Gabbro.

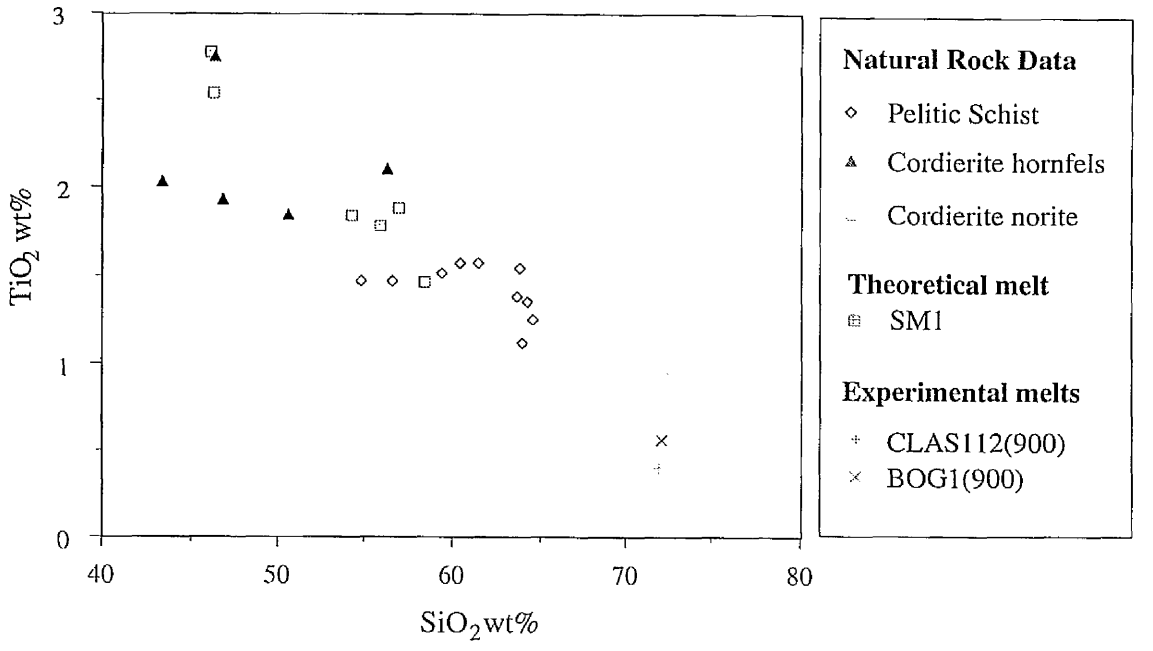

Figure 10.5.7 Graph plotting SiO_2-TiO_2 contents of theoretical melt (Table 9.5.1) and experimentally derived melts (Table 10.6.1) against natural rock compositions from the pelitic schists, cordierite hornfelses and cordierite norites from the S and SW margins of the Huntly Gabbro.

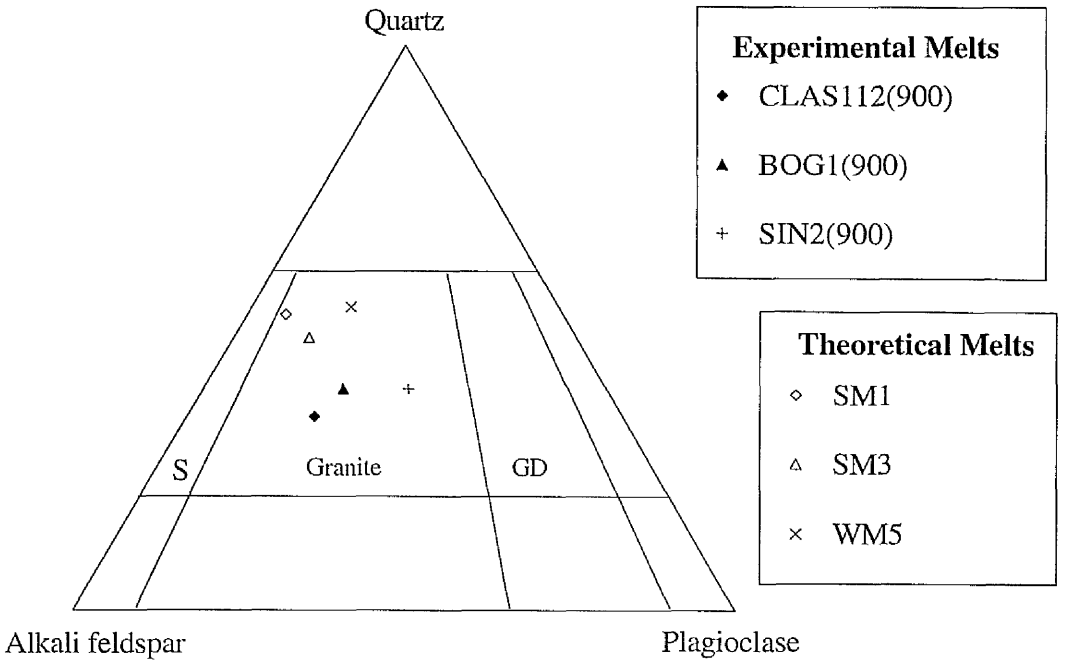

Figure 10.5.8 QAP diagram, plotting quartz, alkali feldspar and plagioclase from CIPW norm calculations from experimental and theoretical melt compositions (Table 9.5.2). Melts SM1 and SM2 calculated from mean pelitic schist analyses (from the S and SW margins of the Huntly Gabbro) including DD.CLAS112 and DD.BOG1, and WM3 from analyses (from W margin of the Huntly Gabbro) including DD.SIN2. All melts, plot within the granite field, though the experimentally derived melts contain less quartz, and more plagioclase than the theoretical melts. Other fields labelled are; S - syeno-granite, and GD - granodiorite.

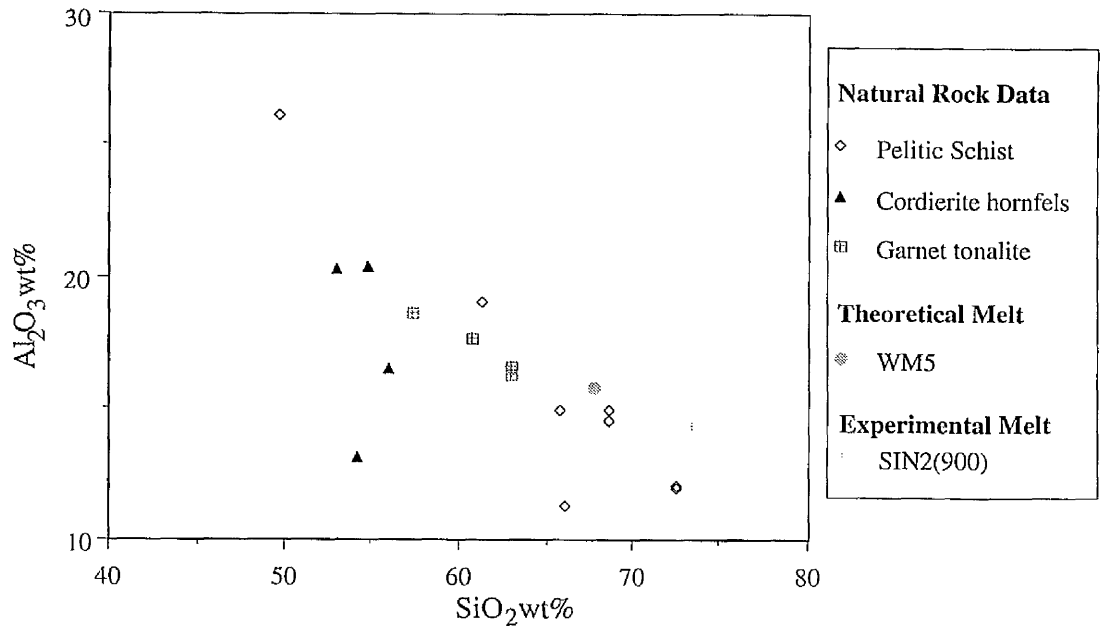

Figure 10.5.9 Graph plotting SiO_2-Al_2O_3 contents of theoretical melt (Table 9.5.1) and experimentally derived melt (Table 10.6.1) against natural rock compositions from the pelitic schists, cordierite hornfelses and garnet tonalite from W margin of the Huntly Gabbro.

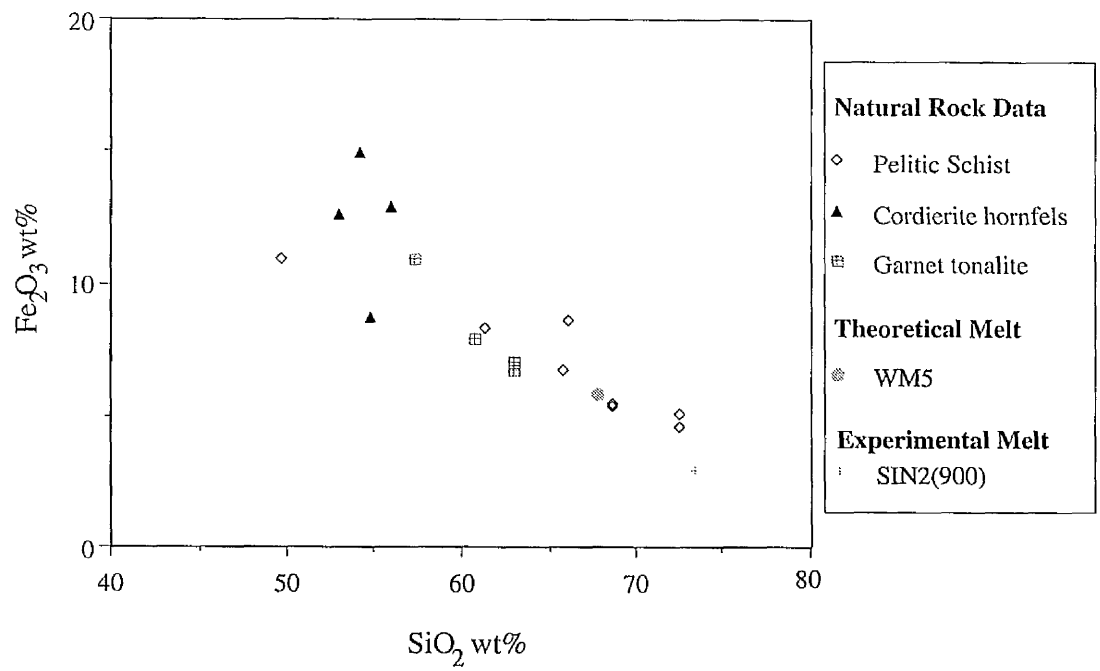

Figure 10.5.10 Graph plotting SiO_2-Fe_2O_3 contents of theoretical melt (Table 9.5.1) and experimentally derived melt (Table 10.6.1) against natural rock compositions from the pelitic schists, cordierite hornfelses and garnet tonalite from W margin of the Huntly Gabbro.

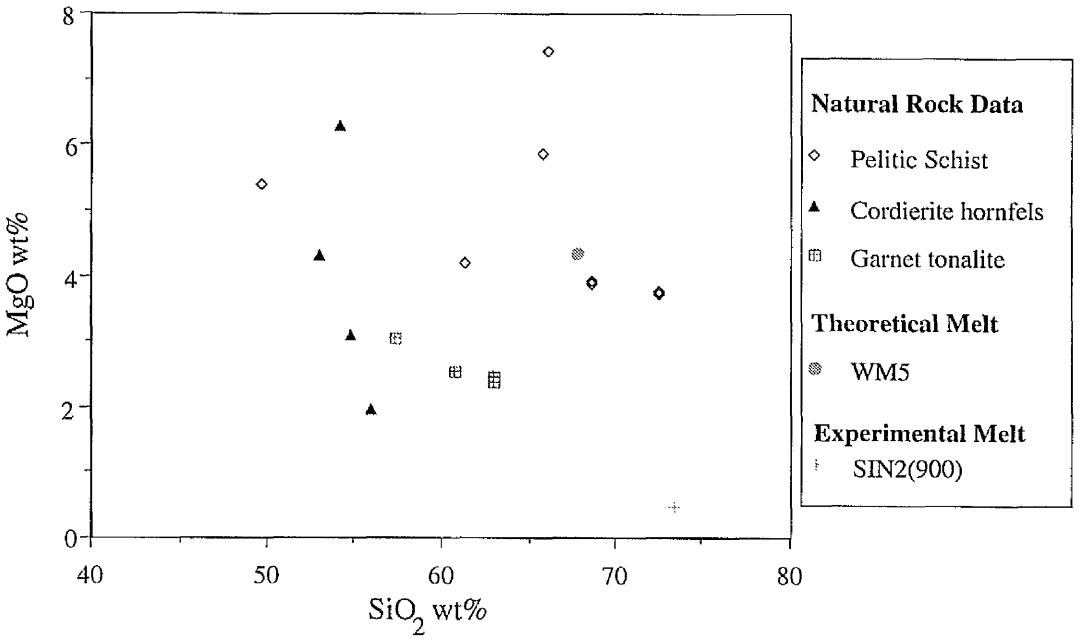

Figure 10.5.11 Graph plotting SiO_2-MgO contents of theoretical melt (Table 9.5.1) and experimentally derived melt (Table 10.6.1) against natural rock compositions from the pelitic schists, cordierite hornfelses and garnet tonalite from W margin of the Huntly Gabbro.

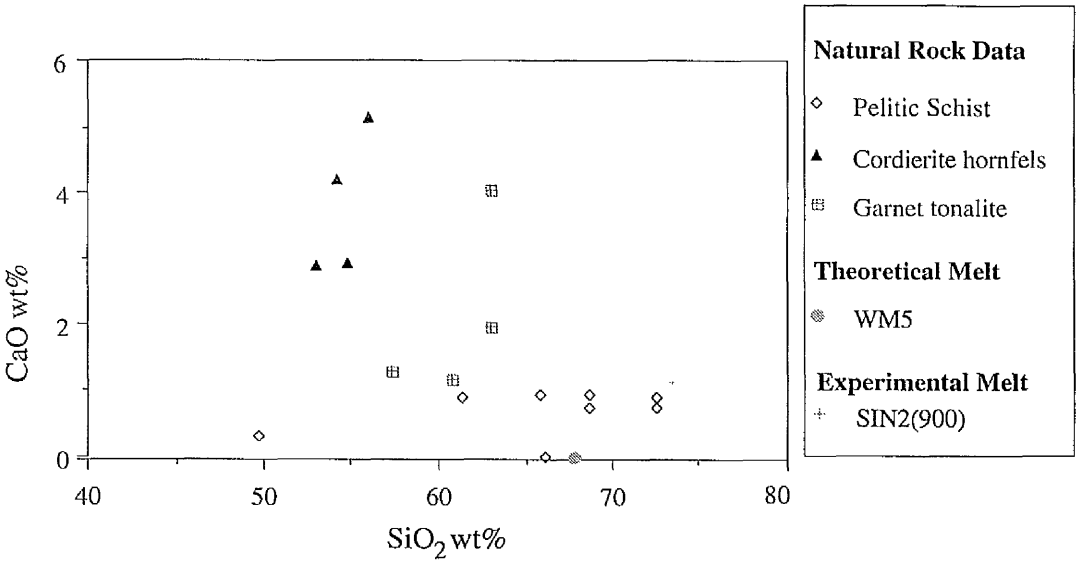

Figure 10.5.12 Graph plotting SiO_2-CaO contents of theoretical melt (Table 9.5.1) and experimentally derived melt (Table 10.6.1) against natural rock compositions from the pelitic schists, cordierite hornfelses and garnet tonalite from W margin of the Huntly Gabbro.

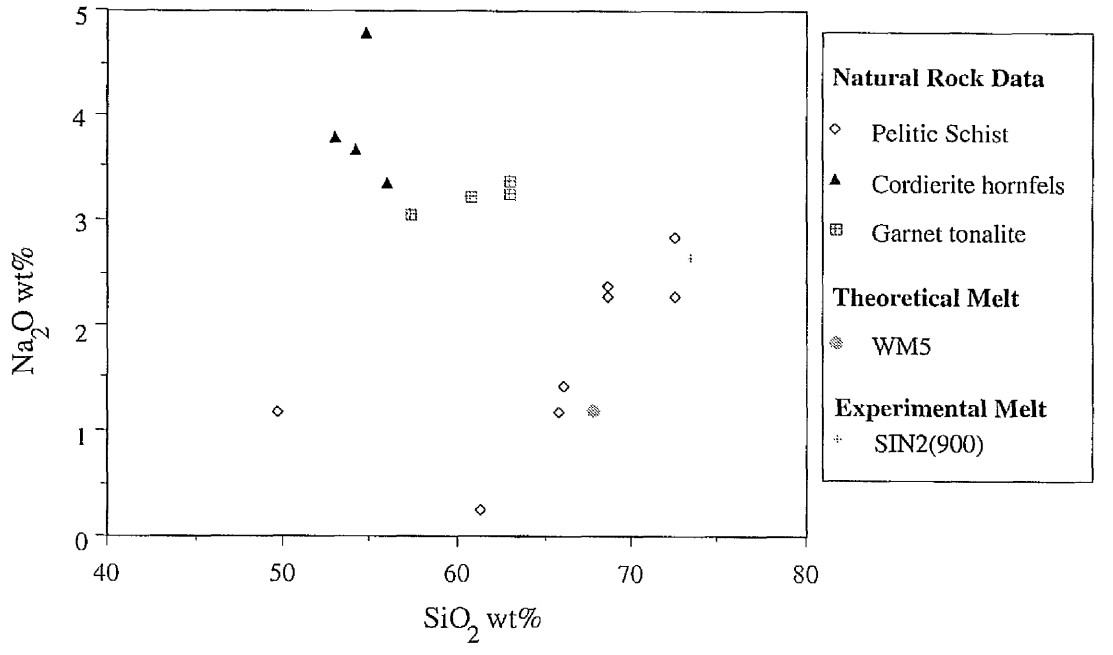

Figure 10.5.13 Graph plotting SiO_2-Na_2O contents of theoretical melt (Table 9.5.1) and experimentally derived melt (Table 10.6.1) against natural rock compositions from the pelitic schists, cordierite hornfelses and garnet tonalite from W margin of the Huntly Gabbro.

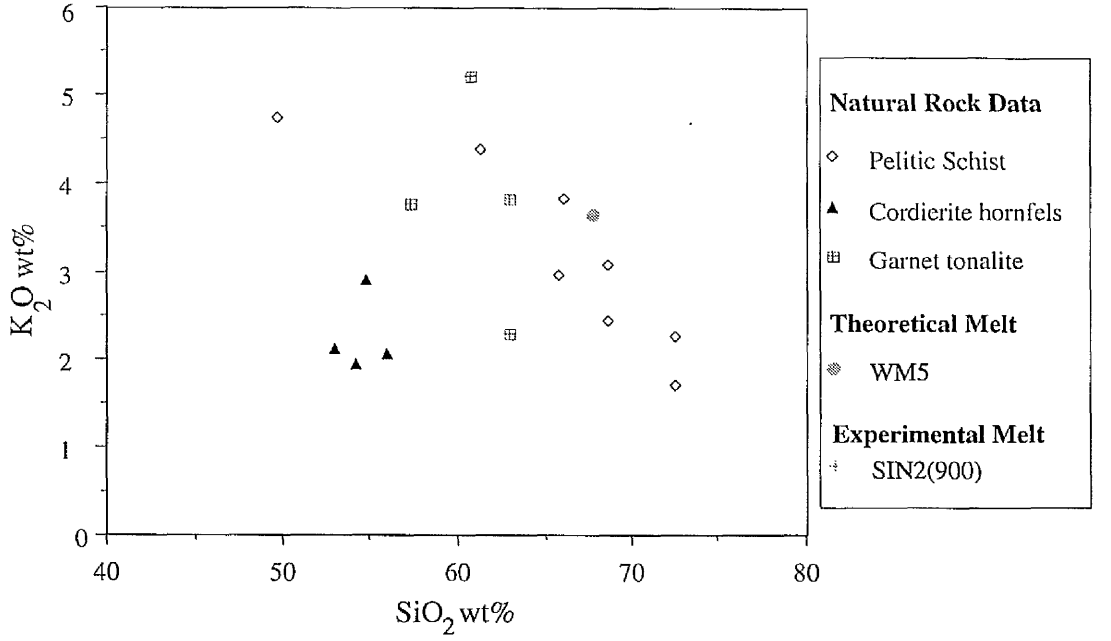

Figure 10.5.14 Graph plotting SiO_2-K_2O contents of theoretical melt (Table 9.5.1) and experimentally derived melt (Table 10.6.1) against natural rock compositions from the pelitic schists, cordierite hornfelses and garnet tonalite from W margin of the Huntly Gabbro.

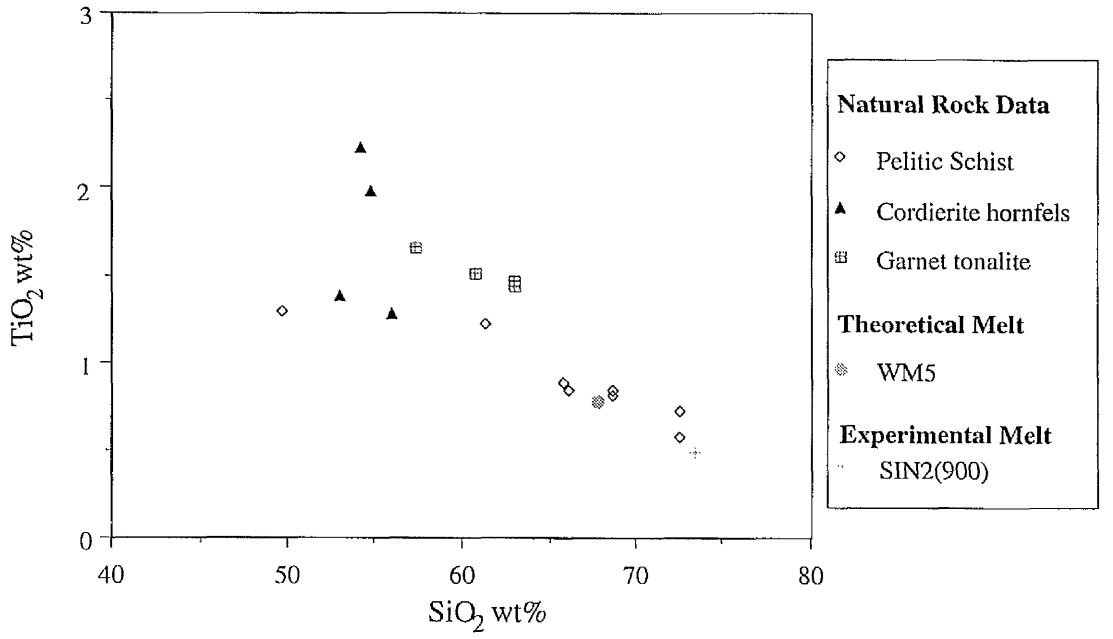

Figure 10.5.15 Graph plotting SiO_2-TiO_2 contents of theoretical melt (Table 9.5.1) and experimentally derived melt (Table 10.6.1) against natural rock compositions from the pelitic schists, cordierite hornfelses and garnet tonalite from W margin of the Huntly Gabbro.

Table 10.2.1 Whole rock chemistry and modal mineralogies of rock samples used for experimental work. All Fe is recalculated to FeO and H_2O contents were determined from weight losses on heating on the thermogravimetric balance.

Wt% Oxide	DD.CLAS112	DD.BOG1	DD.SIN2
	And-mica schist	**Mica schist**	**Grt-mica schist**
SiO_2	55.70	57.95	68.79
Al_2O_3	19.65	21.14	14.49
FeO	10.67	5.61	4.93
MnO	0.18	0.16	0.00
MgO	2.93	2.23	3.90
CaO	0.06	0.95	0.74
Na_2O	1.43	2.22	2.36
K_2O	5.31	5.30	3.08
TiO_2	1.45	1.47	0.84
H_2O	2.62	2.97	0.86
Total	**100.00**	**100.00**	**100.00**
Mg#	**0.33**	**0.42**	**0.59**
Modal Mineralogy			
muscovite	23	50	10
biotite	32	15	15
quartz	35	34	60
andalusite	10	0	0
plagioclase	0	0	2
garnet	0	0	3
staurolite	trace	trace	0
ilmenite	trace	trace	trace
rutile	0	0	trace

Table 10.3.1 Mean melt analyses from CLAS112(900). Mean compositions are given both from cold-stage analysis and from room-temperature analysis. The compositions are normalised to 100%, and 1σ standard deviations are given. The cold-stage analyses contain 40% more K, and 8% more Na and Ca than the room temperature analyses.

CLAS112(900)	COLD STAGE 14 analyses		ROOM TEMPERATURE 4 analyses	
Wt% Oxide	**Mean melt composition**	**Standard Deviation**	**Mean melt composition**	**Standard Deviation**
SiO_2	72.27	0.545	72.98	1.688
TiO_2	0.39	0.054	0.39	0.079
Al_2O_3	13.75	0.375	15.18	0.838
Cr_2O_3	0.00	0.000	0.00	0.000
FeO*	3.80	0.163	3.80	0.798
MnO	0.00	0.000	0.05	0.095
MgO	0.55	0.171	0.70	0.157
CaO	0.69	0.044	0.64	0.078
Na_2O	0.81	0.084	0.75	0.111
K_2O	7.73	0.118	5.51	0.323
TOTAL	**100.00**		**100.00**	

*total Fe as FeO.

Table 10.4.1 Representative analyses of mineral phases from CLAS112(900).

Wt% Oxide	Biotite	Orthopyroxene	Cordierite	Spinel
SiO_2	34.39	45.64	48.66	0.23
TiO_2	6.30	0.36	0.00	1.04
Al_2O_3	16.36	11.04	33.91	44.12
Cr_2O_3	0.00	0.00	0.00	0.00
Fe_2O_3	0.00	0.00	0.00	10.37
FeO	20.32	26.72	6.46	31.38
MnO	0.00	0.44	0.00	0.00
MgO	8.43	15.50	10.17	4.16
CaO	0.00	0.16	0.18	0.00
Na_2O	0.41	0.41	0.00	0.00
K_2O	9.68	0.18	0.67	0.14
TOTAL	**95.89**	**100.44**	**100.04**	**91.44**
Cations				
Si	5.268	1.734	4.901	0.015
Ti	0.726	0.010	0.000	0.050
Al	2.955	0.495	4.025	3.339
Cr	0.000	0.000	0.000	0.000
Fe^{3+}	0.000	0.000	0.000	0.501
Fe^{2+}	2.603	0.849	0.544	1.685
Mn	0.000	0.014	0.000	0.000
Mg	1.925	0.878	1.527	0.398
Ca	0.000	0.006	0.019	0.000
Na	0.122	0.030	0.000	0.000
K	1.892	0.009	0.085	0.012
(O)	22	6	18	8
Cation Total	**15.491**	**4.025**	**10.997**	**6.000**
Mg/(Mg+Fe)	**0.425**	**0.508**	**0.737**	**0.191**

Table 10.4.2 Representative analyses of mineral phases from BOG1(900).

Wt% Oxide	Cordierite	Wt% Oxide	Ilmenite
SiO_2	47.24	TiO_2	50.83
TiO_2	0.00	Al_2O_3	0.64
Al_2O_3	35.81	Fe_2O_3	5.11
Cr_2O_3	0.00	FeO	43.78
FeO	6.90	MnO	0.00
MnO	0.00	MgO	1.29
MgO	9.15		
CaO	0.24	**TOTAL**	**101.63**
Na_2O	0.00		
K_2O	0.44		
TOTAL	**99.77**		

Cations		Cations	
Si	4.770	Ti	1.879
Ti	0.000	Al	0.037
Al	4.262	Fe^{3+}	0.189
Cr	0.000	Fe^{2+}	1.800
Fe^{2+}	0.583	Mn	0.000
Mn	0.000	Mg	0.094
Mg	1.377	(O)	6
Ca	0.026	**Cation Total***	**4.000**
Na	0.000		
K	0.056		
(O)	18		
Cation Total	**10.992**		
Mg#	**0.703**		

Table 10.4.3 Representative analyses of mineral phases from SIN2(900).

Wt% Oxide	Cordierite	Orthopyroxene	Garnet (core)	Garnet (rim)	Plagioclase
SiO_2	49.22	47.65	36.90	40.79	61.19
TiO_2	0.00	0.50	0.00	0.58	-
Al_2O_3	30.72	12.22	20.75	20.36	23.69
Cr_2O_3	0.00	0.00	0.20	0.00	-
FeO	5.56	24.31	33.31	27.94	0.26
MnO	0.28	0.24	4.24	1.04	-
MgO	9.45	15.60	3.75	7.52	-
CaO	0.14	0.62	1.06	1.33	6.37
Na_2O	0.37	0.80	-	-	6.68
K_2O	0.39	-	-	-	1.05
TOTAL	**96.13**	**101.93**	**100.21**	**99.56**	**99.25**
Cations					
Si	5.135	1.754	5.948	6.296	2.743
Ti	0.000	0.014	0.000	0.068	-
Al	3.778	0.530	3.942	3.705	1.252
Cr	0.000	0.000	0.026	0.000	-
Fe^{2+}	0.486	0.748	4.491	3.607	0.010
Mn	0.024	0.007	0.578	0.136	-
Mg	1.469	0.856	0.900	1.731	-
Ca	0.015	0.024	0.183	0.219	0.306
Na	0.075	0.057	-	-	0.581
K	0.052	-	-	-	0.060
(O)	18	6	24	24	8
Cation Total	**10.907**	**3.990**	**16.068**	**15.762**	**4.952**
Mg#	**0.751**	**0.534**	**0.167**	**0.324**	**-**

Table 10.5.1 Mean experimental melt cold-stage analyses and CIPW norm calculations. All melt analyses are normalised to 100%. All Fe calculated as FeO for CIPW norm calculations.

Wt% Oxide	CLAS112(900)	BOG1(900)	SIN2(900)
SiO_2	72.27	72.33	73.59
TiO_2	0.39	0.56	0.49
Al_2O_3	13.75	14.51	14.35
Cr_2O_3	0.00	0.00	0.00
FeO	3.80	3.38	2.62
MnO	0.00	0.00	0.00
MgO	0.55	0.47	0.48
CaO	0.69	1.23	1.13
Na_2O	0.81	1.47	2.65
K_2O	7.73	6.03	4.69
Cl	0.00	0.02	0.00
TOTAL	**100.00**	**100.00**	**100.00**
CIPW norms			
quartz	32.77	34.95	35.42
corumdum	2.79	3.33	2.88
orthoclase	45.69	35.65	27.52
albite	6.87	12.47	22.31
anorthite	3.43	6.10	5.70
hypersphene	7.71	6.45	5.24
ilmenite	0.74	1.08	0.93

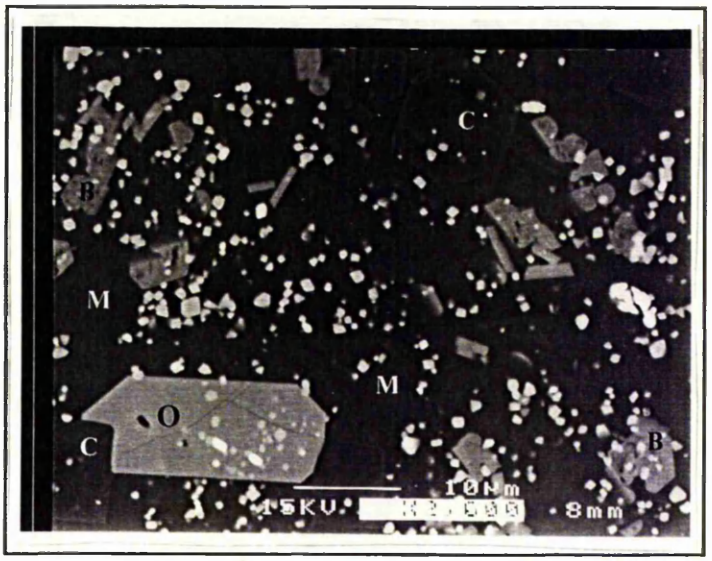

Plate 10.4.1 Backscattered electron image from run sample CLAS112(900). The mineral phases present are O-orthopyroxene, C-cordierite, B-biotite. The small bright phases are spinel and ilmenite. All of the mineral phases are suspended in a matrix of quenched melt (M). The cordierite and orthopyroxene both form euhedral crystals, while the biotite occurs mainly in clusters as small, ragged flakes.

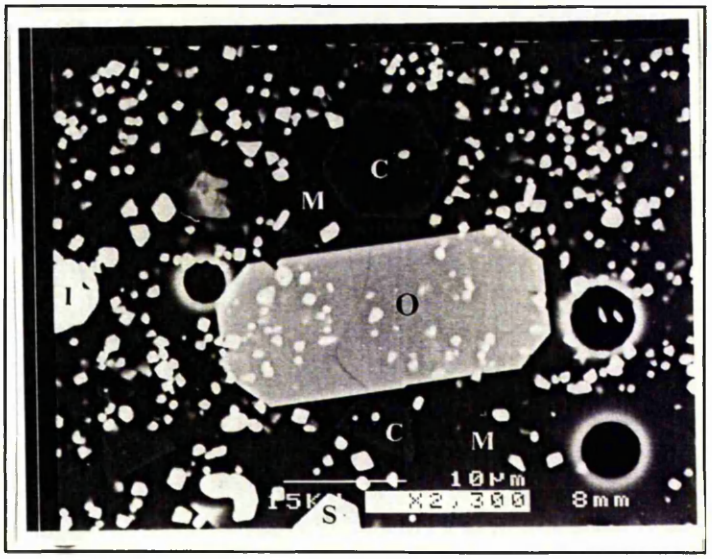

Plate 10.4.2 Backscattered electron image from run sample CLAS112(900). The large, bright phase is a euhedral orthopyroxene crystal. Above the orthopyroxene is a darker hexagonal cordierite. The small, very bright phases are a combination of I-ilmenite and S-spinel, with the ilmenite forming more rounded crystals All of the minerals are suspended in a matrix of quenched melt, which forms the modally most abundant phase.

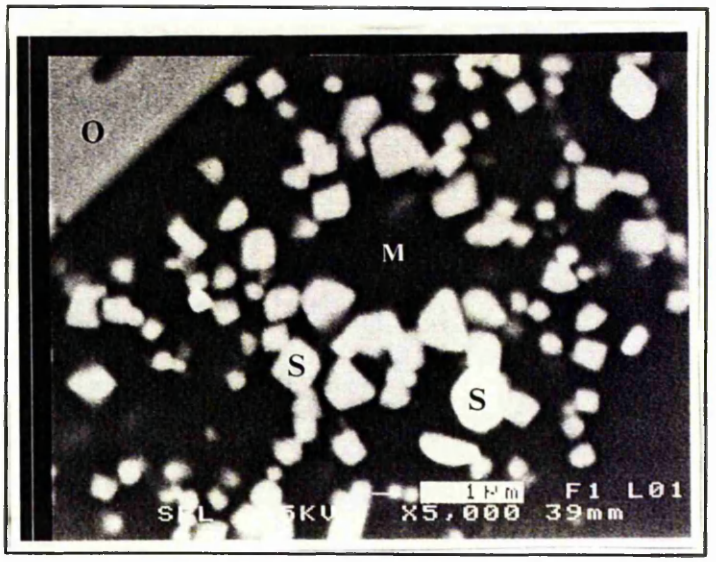

Plate 10.4.3 High magnification, backscattered electron image from run sample CLAS112(900), showing small, bright spinel crystals are suspended in the quenched melt. The grey phase at the top left of the image is part of an orthopyroxene crystal.

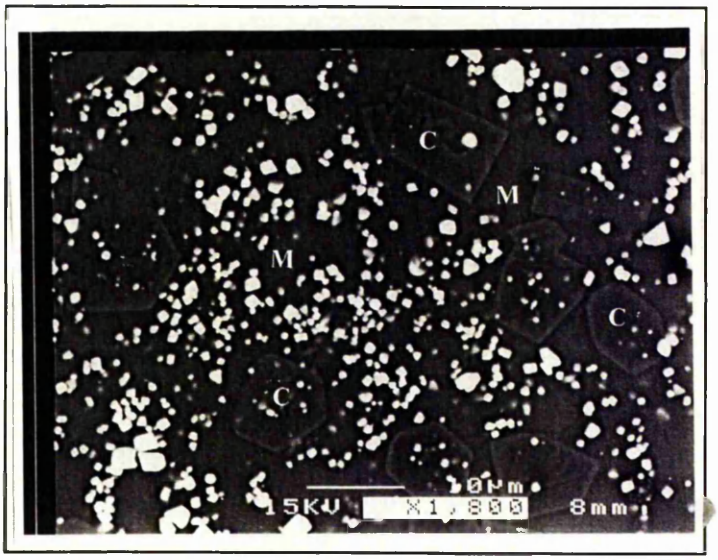

Plate 10.4.4 Backscattered electron image from run sample BOG1(900). The hexagonal cordierite crystals are suspended in the voluminous matrix of quenched melt. The bright phases are a mixture of both ilmenite and spinel.

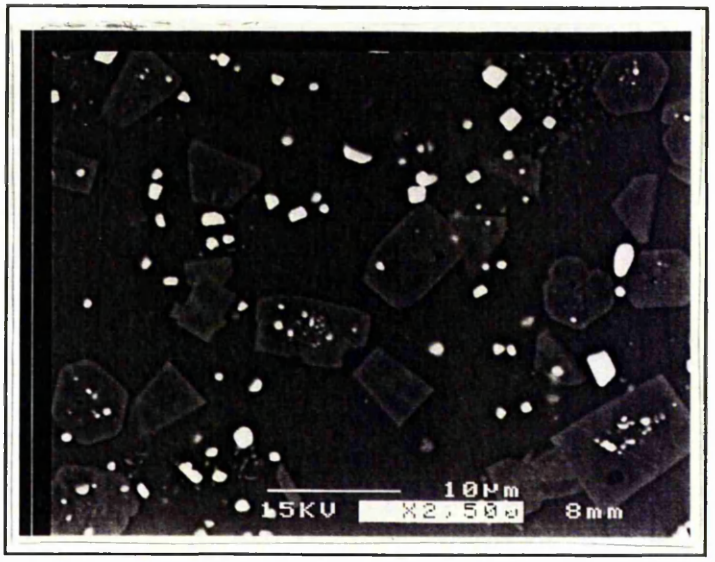

Plate 10.4.5 Backscattered electron image from run sample BOG1(900). Cordierite and bright ilmenite / spinel crystals occur are suspended in the voluminous quenched melt. The quenched melt covers over 70% of the area of the image.

Plate 10.4.6 Backscattered electron image from run sample SIN2(900). The mineral phases visible are orthopyroxene, cordierite, ilmenite, G-garnet, and Q-quartz. The plagioclase and melt have similar atomic contrast and cannot be distinguished separately. The orthopyroxene is smaller than in CLAS112(900), forming elongate crystals and needles. The cordierite is euhedral and hexagonal in cross section.

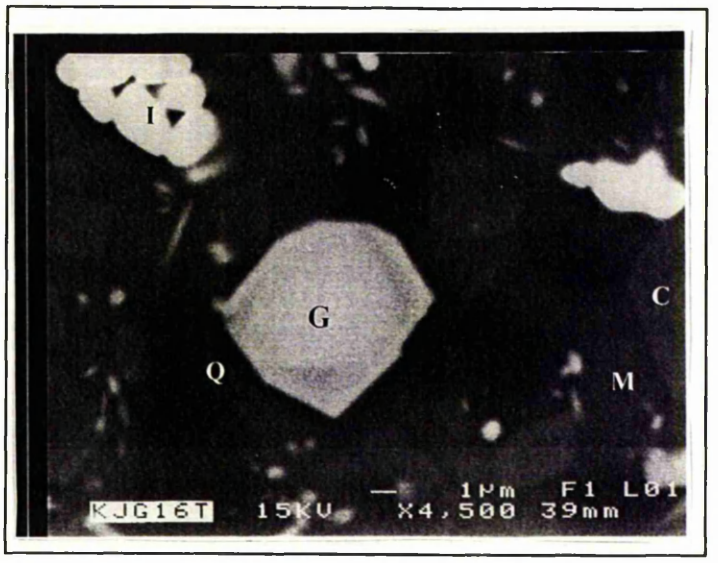

Plate 10.4.7 Backscattered electron image from run sample SIN2(900). Garnet crystal, with bright Fe-rich core, armoured by less bright (lower atomic contrast) more Mg-rich overgrowth rim. The other phases present are ilmenite, cordierite, quartz and melt. The image is taken from the non-garnet-seeded run.

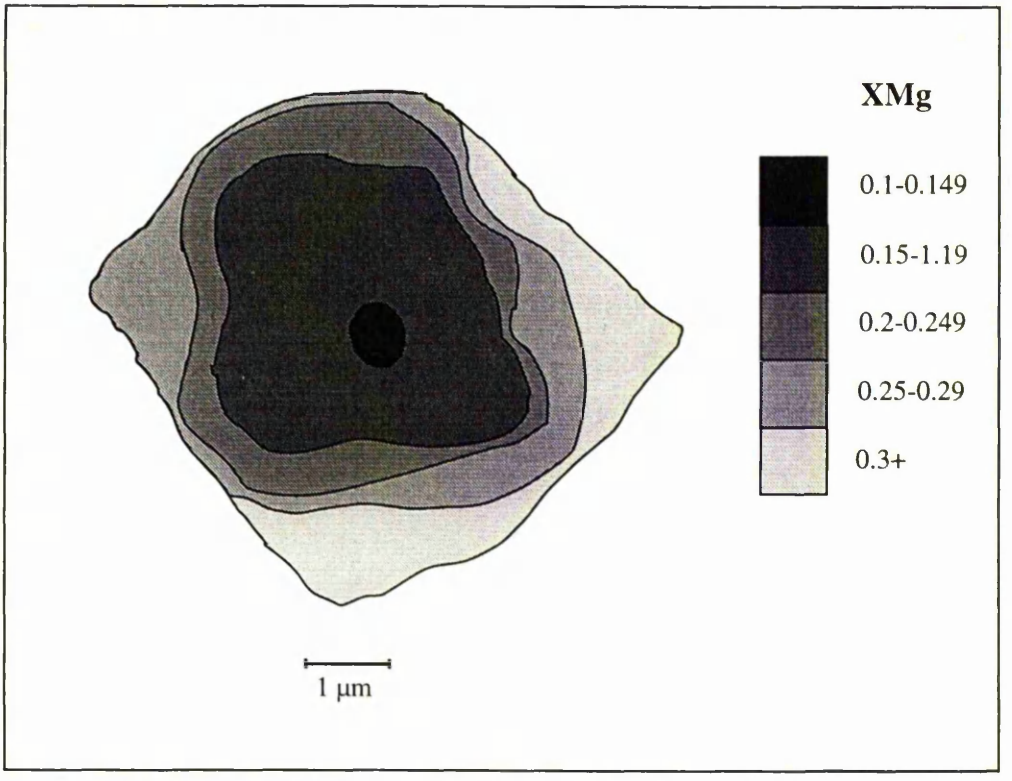

Figure 10.4.5 Zonation contour diagram from the garnet shown above, with contours of equal XMg (XMg = Mg/(Mg + Fe + Mn + Ca)). The inner zone of the garnet with low XMg values (0.1-0.19) is compositionally alike the original garnets from the starting sample DD.SIN2. The Mg-rich outer rim represents a new growth of higher-grade garnet, nucleating on an earlier grain. As the image comes from the non-seeded run, the garnet core therefore represents a relict grain from the starting sample DD.SIN2.

CHAPTER 11 DISCUSSIONS AND CONCLUSIONS

In this chapter the findings from the previous chapters are brought together and discussed. Then the implications of these findings for the processes involved in granitic genesis and crustal differentiation are addressed.

11.1 Regionally Metamorphosed Rocks

(i) Regionally metamorphosed rocks to the S and SW of the Huntly Gabbro

Field studies show that the regionally metamorphosed rocks from the S and SW margins of the Huntly Gabbro belong to Whitehills and Boyndie Bay 'Group' metasediments and amphibolites. The pelitic rocks closest to the intrusion, which crop-out on and around Clashmach Hill, consist of medium-grade andalusite-mica schists and mica schists. These lithologies trend towards, and are cut out by the S and SW margins of the Huntly Gabbro. To the S of the andalusite-bearing rocks, low-grade biotite-chlorite metasiltstones are exposed, though there is a gap in the succession between these two lithologies.

The metamorphic parageneses displayed by these rocks are typical of the classic low-pressure Buchan facies series as seen throughout NE Scotland (Harte & Hudson, 1979), with the biotite-chlorite metasiltstones belonging to the lowest-grade Biotite Zone assemblages, whilst the andalusite-bearing rocks contain higher-grade Staurolite Zone assemblages.

Using the aluminosilicate triple point of Holland & Powell (1990), the maximum pressure at which the andalusite-bearing schists could have crystallised would have been 4.7 kbars.

(ii) Regionally metamorphosed rocks to the W of the Huntly Gabbro

Immediately to the W of the Huntly intrusion, Portsoy 'Group' garnet-bearing metasediments are exposed. Although these lithologies could not be traced towards the W margin of the Huntly Gabbro, Read (1923b) showed that both Portsoy 'Group' rocks and amphibolites trended towards and were cut out by the Huntly Gabbro near Cormalet (locality 3e, Figure 4.1.1).

Closer to the Huntly intrusion garnet-mica schists are rapidly succeeded by muscovite-absent garnet-biotite gneisses, which also locally contain fibrolite. The lack of any K-feldspar in the gneisses and the relatively low temperatures given by geothermometry (630 to 640°C) both suggest that these rocks formed via the fluid-present melting reaction:

$$Ms + Bt + Qtz + H_2O = Sil + M. \qquad [11.1]$$

The high modal contents of quartz and plagioclase in the leucocratic layers in the gneisses and the low temperatures indicated by geothermometry is evidence of localised, closed-system partial melting, with no melt extraction.

(iii) Effects from the Huntly Gabbro

The metamorphic grade of the regionally metamorphosed rocks decreases away from both the S & SW and W margins of the Gabbro. However, none of these rocks show any obvious effects of thermal metamorphism (i.e. hornfelsing), although Ashworth (1976) showed that the sillimanite (fibrolite) overprint on the regionally metamorphic rocks was caused by the heating from the Huntly Gabbro. The decrease in metamorphic grade to the S of the intrusion is likely to be largely accidental, as similar metamorphic sequences (Biotite Zone rocks through to Staurolite Zone rocks) are seen in coastal sections near Banff, away from any Newer Gabbro intrusions (e.g. Hudson, 1980).

11.2 Silica-Poor Hornfelses

Three types of hornfels can be determined on petrological grounds: these are with increasing metamorphic grade, sillimanite-cordierite hornfelses, cordierite-K-feldspar hornfelses, and orthopyroxene-cordierite hornfelses. The hornfelses crystallised from a progressive series of melting reactions An early, muscovite-consuming reaction such as reaction 11.1 may have been fluid-present (i.e. the reaction that formed the K-feldspar-absent sillimanite-cordierite hornfels sample DD.DUN1). However, water activity calculations and low total volatile contents in cordierites indicate low aH_2O values for the hornfelses and most melting must therefore have taken place via mica-consuming, fluid-absent reactions (if a pervasive water-rich fluid was present then $aH_2O \approx 1.0$). These reactions are, with increasing temperature:

$$Ms + Qtz = Sil + Kfs + M \quad [11.2]$$

$$Bt + Qtz + Sil + Pl = Grt/Crd + Kfs + M \quad [11.3]$$

$$Bt + Sil + Qtz = Crd + Spl + M \quad [11.4]$$

$$Bt + Qtz = Opx \pm Kfs + M. \quad [11.5]$$

Geothermometry gives temperatures of up to 780°C for the sillimanite-cordierite hornfelses. These temperatures and the presence of abundant biotite in these rocks both imply that any extracted melt must have mostly formed from muscovite-consuming melting reactions (reactions 11.1 and 11.2). The quantity of melt produced would therefore be a function of the muscovite content of the protolith. Some of the lithologies shown to be the likely protoliths of the hornfelses contain up to 50% modal muscovite, and such lithologies would be capable of producing large melt volumes, even at relatively low temperatures (780 to 800°C).

The orthopyroxene-cordierite hornfelses give temperatures from 880 to 960°C from geothermometry. These rocks contain anhydrous mineral assemblages and biotite, when present is minor and Ti-rich. The mineralogy and whole-rock chemistry of the orthopyroxene-cordierite hornfelses show that these rocks are restitic and the temperatures given are in excess of those required for wholesale fluid-absent partial melting by muscovite and biotite-consuming reactions. Mixing calculations suggest that approximately 50% of melt was extracted from the protoliths of these hornfelses.

Experiments on the likely protoliths of the hornfelses from the S and SW margins of the Huntly mass were conducted at 900°C at 5 kbars under fluid-absent conditions. The experiments led to the formation of quenched melt volumes from 50 to 70%, with the solid run products consisting of combinations of cordierite, orthopyroxene, spinel, ilmenite and small amounts of Ti-saturated biotite. Compositionally, these minerals mimic the compositions and assemblages present in the orthopyroxene-cordierite hornfelses. Therefore, these experiments simulate the processes by which the orthopyroxene-cordierite hornfelses crystallised and the anhydrous nature of these hornfelses indicates that nearly all of the melt formed was efficiently extracted.

11.3 Cordierite Norites

The cordierite norites are igneous-textured rocks with similar mineral assemblages to the orthopyroxene-cordierite hornfelses. However, the cordierite norites always contain quartz and biotite. Textural and geochemical studies show that the cordierite norites do not represent the sole melt produced by partial melting, but instead are restite-rich rocks that crystallised in the presence of a relatively small fraction of melt. Petrographic and experimental work show that the cordierite, orthopyroxene, garnet and spinel form restitic crystals, whilst plagioclase, quartz and late, poikilitic biotites all crystallised from the melt. The low percentage of melt present in the cordierite norites suggests that these rocks may have crystallised in the presence of the last melt fraction produced, with this late melt not being sufficiently mobile to effectively segregate from its host, and instead crystallising *in-situ*.

The low total volatile content in the cordierite from sample DD.BQ38 and calculations on water activities from sample H.BHQ1 both indicate that the cordierite norites crystallised during low to medium aH_2O conditions. Therefore, as with the silica-poor hornfelses, the cordierite norites formed from fluid-absent melting reactions.

11.4 Garnet Tonalites

The garnet tonalites probably formed by similar processes to the cordierite norites and the garnet and cordierite, when present, both occur as entrained restitic crystals. However, textures displayed by plagioclase, quartz and biotite suggest that a large proportion of the tonailte probably represents material which crystallised from a melt.

A sequence is displayed in the field, with garnet tonalite starting as thin, garnetiferous, lithologically-controlled leucocratic bands, which then coalesce to form small 'melt pockets'. When the volume of tonalitic leucosome is large enough, the fine-grained hornfels forms xenoliths and in the most evolved rocks, hornfels only occurs as small, randomly oriented xenoliths. An inverse relationship occurs between melt volume and the abundance of garnets, with garnets modally most abundant in the thin leucocratic bands, but scarce or often absent in rocks where tonalite forms over 80% of total rock volume. This is evidence for the melt losing most of its restitic products over a relatively short distance, and any melt moving to higher structural levels would be relatively restite-free.

The garnet-hornblende tonalites are chemically distinct from the garnet tonalites and have a higher bulk Ca content than the latter rock type. These rocks have compositions which suggest that they were not formed from a pelitic protolith, but instead probably formed by partial melting of hornblende-plagioclase-quartz-bearing amphibolite. This is supported by the work of Rutter & Wyllie (1988), who showed that amphibolites were possible protoliths of such Ca-rich tonalitic melts.

11.5 Composition and Fate of the 'Extracted Melt'

Mixing calculations from whole-rock data show that the melt extracted from the restitic hornfelses was granitic and peraluminous. Experiments on the non-melted protoliths of the hornfelses formed melts of similar composition to the 'theoretical' melts. These melts all have compositions analogous to those displayed by 'S'-type granites.

Many of the restitic hornfelses occur as large xenoliths or rafts suspended in mafic igneous rock. Any melt extracted from these hornfelses would therefore have immediately passed into the surrounding mafic rock. The mafic rocks which surround such xenolithic rock are unlike the olivine-augite gabbros and norites from the centre of the Huntly-Knock intrusions, and instead contain hornblende, poikilitic biotite and often some minor quartz. The whole-rock chemical data from these hydrous mafic rocks shows trends, away from the non-xenolithic, anhydrous mafic rocks towards the compositions of pelitic-lithologies for some major and trace elements. The extracted granitic melt therefore, has probably at least partially mixed with the surrounding mafic melt, leading to the formation of hybrid melts, namely the biotite-hornblende dolerites and gabbros.

11.6 Implications for Granite Genesis and Crustal Differentiation

A number of implications for the processes involved in granite genesis and crustal differentiation can be drawn for the work in this thesis. These are as follows:

(i) Mica-rich pelitic schists, such as the Dalradian metasediments exposed in NE Scotland, are potentially fertile protoliths, from which large volumes (50 to 70%) of melt can be extracted via fluid-absent melting reactions.

(ii) Temperatures of approximately 800°C are required for the fluid-absent melting of muscovite-bearing assemblages in natural systems and if the muscovite is modally abundant then reasonably large quantities of melt may be formed. Temperatures in excess of 880°C will lead to the breakdown of virtually all the biotite present in natural systems via fluid-absent melting reactions. Although biotite can be stabilised to higher temperatures (950°C) by Ti and possibly some F, this biotite is likely to be scarce and such elevated temperatures are not required for the completion of fluid-absent melting in natural systems as suggested by Koberski (1995), unless unusually high F contents are present in the protoliths. The melts formed by these reactions will be strongly peraluminous and analogous to 'S'-type granites.

(iii) Melts formed from incongruent melting reactions can be extracted efficiently in hydrostatic conditions and will leave behind their complementary restite. The last fractions of melting may be unable to efficiently segregate, and will freeze *in-situ*, forming immobile igneous-textured rocks that contain a high proportion of entrained restite. Therefore almost all of the restite would remain *in-situ* and the extracted melts would be relatively restite-poor.

(iv) For major fluid-absent partial melting of metapelites to occur, temperatures in the range 850 to 950°C are required (e.g. Clemens, 1992 ; Stevens & Clemens, 1994 ; this study). Such temperatures can generally not be attained by large rock volumes without the introduction of large volumes of hot, mafic magma into the crust (e.g. England & Thompson, 1986 ; Huppert & Sparks, 1988). One mechanism by which such large volumes of mafic magma may be introduced into the lower crust would be by crustal intraplating and underplating (Huppert & Sparks, 1988).

Therefore, the rocks described in this thesis represent a smaller-scale analogue or snap-shot of the processes by which intrusion of large mafic igneous bodies, into the lower crust, could heat the crust to sufficient temperatures for major fluid-absent melting of large volumes of metapelitic rock to occur. This would lead to the formation of mobile 'S'-type granitic bodies, which would migrate upwards to higher structural levels and leave behind their complementary, depleted granulite-facies restitic residues. The restitic terrain would be depleted in Si and K, and relatively enriched in Al, Fe, Mg and Ca, whilst conversely, the intrusion of large volumes of 'S'-type granitoid into higher crustal levels would cause

enrichment in Si and K. This, therefore, represents a major process by which differentiation between the low-middle and upper crust can occur.

APPENDICES

APPENDIX I ELECTRON MICROPROBE

(i) Sample Preparation

Polished, uncovered thin sections were made from the samples selected for analysis. These sections were coated with a 20 nm carbon film before analysis.

(ii) Machines Used

(a) Geoscan Microprobe

Samples were analysed for major elements using the modified Cambridge Instrument Company Geoscan microprobe at the Dapartment of Geology in the University of Manchester. The machine uses energy dispersive spectrometer (E.D.S) analysis. The E.D.S. comprises a Kevex detector, a Harwell 2010 pulse processor and Link Systen electronics. Link Systems ZAF 4/FLS software is used to convert X-ray spectra obtained from the specimen into chemical analyses. The detection limit of the machine is approximately 0.2 wt%.

Operating Conditions

15 kV electron beam accelerating voltage,
75 degrees X-ray take-off angle,
a 40 second count time per analysis,
3 nA specimen current on cobalt metal,
2500 CPS output count rate from cobalt metal with 18% detection system dead time.

The Geoscan is calibrated for the following elements: Si, Ti, Al, Cr, Fe, Mn, Mg, Ca, Na, K, Cu, Ni, Zn and Ba.

(b) Cameca Microprobe

The Cameca microprobe was used for biotite analysis for two samples, to gain the F and Ba contents in this mineral. Wavelength-dispersive spectrometry (W.D.) was used for analysis of F, Ba and Ti, while other elements were analysed by E.D.S.

PROBE DATA FROM REGIONALLY METAMORPHOSED ROCKS

DD.SIN2																							
GARNET											PLAGIOCLASE												
%OXIDE	Grt1	Grt2	Grt3	Grt4	Grt5	Grt6	Grt7	Grt8	Grt9		%OXIDE	PLAG1	PLAG2	PLAG3	PLAG4	PLAG5	PLAG6							
SiO2	36.81	37.18	36.79	36.89	37.41	37.19	37.34	37.16	37.57		SiO2	62.98	62.62	61.23	61.66	61.43	62.18							
TiO2	0.05	0.01	0.00	0.00	0.00	0.02	0.00	0.00	0.00		Al2O3	23.53	23.60	23.26	23.26	23.08	23.50							
Cr2O3	0.06	0.09	0.00	0.03	0.00	0.04	0.00	0.00	0.00		CaO	4.66	4.71	4.71	4.67	4.61	4.31							
Al2O3	20.74	21.06	20.85	20.91	20.92	21.08	21.02	21.07	21.16		Na2O	8.93	8.96	8.86	9.08	8.88	9.05							
FeO	33.36	33.76	33.47	32.82	34.27	34.22	33.39	33.76	33.91		K2O	0.06	0.02	0.00	0.02	0.01	0.19							
MnO	3.99	3.87	3.79	3.98	3.65	3.74	4.11	3.85	3.59														
MgO	3.23	3.49	3.43	3.53	3.02	3.22	3.37	3.25	3.29		TOTAL	100.17	99.91	98.06	98.70	98.02	99.23							
CaO	1.11	0.99	1.12	1.01	1.09	1.06	1.00	1.12	1.13														
											CATIONS												
TOTAL	99.34	100.44	99.44	99.16	100.36	100.57	100.22	100.22	100.66		Si	2.78	2.772	2.764	2.767	2.773	2.773							
											Al	1.224	1.231	1.238	1.23	1.228	1.235							
CATIONS											Ca	0.221	0.223	0.228	0.225	0.223	0.206							
Si	5.981	5.969	5.968	5.984	6.016	5.973	6.001	5.981	6.008		Na	0.765	0.769	0.775	0.79	0.777	0.782							
Ti	0.006	0.001	0.000	0.000	0.000	0.003	0.000	0.000	0.001		K	0.003	0.001	0	0.001	0.001	0.011							
Cr	0.008	0.011	0.000	0.004	0.000	0.005	0.000	0.000	0.000		(O)	8	8	8	8	8	8							
Al	3.972	3.985	3.986	3.998	3.966	3.990	3.981	3.997			TOTAL	4.993	4.996	5.005	5.013	5.002	5.007							
Fe2+	4.533	4.533	4.541	4.453	4.609	4.597	4.487	4.544	4.535														
Mn	0.549	0.527	0.521	0.547	0.497	0.509	0.560	0.525	0.486		XAn	0.22	0.22	0.23	0.22	0.22	0.21							
Mg	0.782	0.835	0.829	0.853	0.724	0.770	0.807	0.780	0.783														
Ca	0.194	0.171	0.195	0.176	0.188	0.182	0.172	0.193	0.194														
(O)	24	24	24	24	24	24	24	24	24														
TOTAL	16.025	16.032	16.040	16.015	16.000	16.029	16.008	16.020	15.997														
Mg#	0.15	0.16	0.15	0.16	0.14	0.14	0.15	0.15	0.15														
PLAGIOCLASE					BIOTITE																		
%OXIDE	PLAG7	PLAG8	PLAG9		%OXIDE	BT1	BT2	BT3	BT4	BT5	BT6	BT7	BT8	BT9	BT10	BT11	BT12	BT13	BT14	BT15	BT16	BT17	BT18
SiO2	62.79	62.76	62.60		SiO2	36.56	35.54	36.37	35.46	36.37	36.18	35.89	35.43	35.65	35.65	35.69	35.66	35.86	35.86	35.74	35.69	35.77	36.57
Al2O3	23.68	23.50	23.80		TiO2	1.89	1.58	1.71	1.49	1.69	1.72	1.81	1.74	1.69	1.84	1.59	1.87	1.65	1.65	1.70	1.70	1.84	1.95
CaO	4.84	4.74	4.85		Cr2O3	0.00	0.03	0.11	0.14	0.06	0.20	0.06	0.11	0.10	0.00	0.12	0.00	0.00	0.00	0.00	0.00	0.00	0.00
Na2O	9.02	8.83	8.85		Al2O3	19.88	19.10	19.95	22.81	19.22	19.64	19.03	19.11	19.38	19.02	19.09	19.26	19.25	19.13	19.19	19.25	19.27	19.24
K2O	0.03	0.02	0.06		FeO	17.86	17.88	17.73	16.44	18.83	18.27	18.25	17.96	18.44	18.44	18.34	18.09	18.23	17.65	17.65	18.17	17.74	18.56
					MnO	0.09	0.00	0.00	0.00	0.00	0.00	0.00	0.00	0.00	0.00	0.00	0.00	0.00	0.00	0.00	0.00	0.00	0.00
TOTAL	100.37	99.84	100.16		MgO	10.95	10.32	10.14	9.22	10.33	10.80	10.30	10.60	10.59	10.48	10.37	10.37	10.73	10.30	10.77	10.42	10.61	10.81
					CaO	0.00	0.04	0.09	0.22	0.08	0.07	0.09	0.02	0.03	0.17	0.00	0.12	0.07	0.09	0.00	0.16	0.17	0.00
CATIONS					Na2O	0.70	0.73	0.69	0.65	0.75	0.72	0.58	0.55	0.79	0.74	0.70	0.68	0.68	0.74	0.80	0.80	0.71	0.84
Si	2.769	2.778	2.765		K2O	8.47	8.56	8.83	7.62	8.67	8.52	8.49	8.48	8.42	8.61	8.58	8.65	8.92	8.79	8.82	8.48	8.82	8.66
Al	1.531	1.526	1.539		Cl	0.06	-	-	-	-	-	-	-	-	-	-	-	-	-	-	-	-	-
Ca	0.229	0.225	0.23																				
Na	0.772	0.758	0.758		TOTAL	96.46	93.78	95.82	94.05	96.00	96.12	94.51	94.00	95.09	94.94	94.46	94.70	95.38	94.20	94.96	94.67	94.93	96.64
K	0.002	0.001	0.003																				
(O)	8	8	8		CATIONS																		
TOTAL	5.003	4.988	4.995		Si	5.415	5.436	5.456	5.312	5.450	5.397	5.449	5.406	5.386	5.405	5.430	5.407	5.407	5.458	5.398	5.413	5.408	5.434
					Ti	0.210	0.182	0.192	0.168	0.190	0.193	0.206	0.200	0.192	0.210	0.182	0.213	0.187	0.188	0.193	0.193	0.210	0.218
XAn	0.23	0.23	0.23		Cr	0.000	0.004	0.013	0.016	0.008	0.023	0.008	0.013	0.011	0.000	0.014	0.000	0.000	0.000	0.000	0.000	0.000	0.000
					Al	3.471	3.444	3.508	4.028	3.395	3.452	3.395	3.438	3.451	3.398	3.424	3.443	3.421	3.431	3.467	3.442	3.433	3.370
					Fe2+	2.213	2.267	2.313	2.060	2.359	2.279	2.317	2.291	2.331	2.339	2.334	2.295	2.299	2.247	2.228	2.305	2.243	2.300
					Mn	0.011	0.000	0.000	0.000	0.000	0.000	0.000	0.000	0.000	0.000	0.000	0.000	0.000	0.000	0.000	0.000	0.000	0.000
					Mg	2.418	2.354	2.254	2.058	2.308	2.402	2.332	2.411	2.356	2.369	2.351	2.344	2.413	2.336	2.422	2.355	2.396	2.393
					Ca	0.000	0.007	0.015	0.035	0.013	0.012	0.015	0.003	0.005	0.027	0.000	0.019	0.011	0.015	0.000	0.026	0.027	0.000
					Na	0.200	0.216	0.200	0.190	0.217	0.209	0.176	0.164	0.231	0.217	0.206	0.200	0.197	0.218	0.235	0.236	0.209	0.243
					K	1.601	1.671	1.650	1.456	1.657	1.620	1.645	1.650	1.623	1.664	1.665	1.674	1.717	1.706	1.698	1.641	1.702	1.642
					Cl	0.016	-	-	-	-	-	-	-	-	-	-	-	-	-	-	-	-	-
					(O)	22	22	22	22	22	22	22	22	22	22	22	22	22	22	22	22	22	22
					TOTAL	15.555	15.601	15.630	15.323	15.597	15.587	15.547	15.576	15.616	15.627	15.606	15.595	15.652	15.599	15.641	15.611	15.622	15.606
					Mg#	0.522	0.507	0.505	0.500	0.495	0.513	0.502	0.513	0.506	0.503	0.502	0.505	0.512	0.510	0.521	0.505	0.516	0.509
BIOTITE																							
%OXIDE	BT13	BT14	BT15	BT16	BT17	BT18																	
SiO2	35.86	35.86	35.74	35.69	35.77	36.57																	
TiO2	1.65	1.65	1.70	1.70	1.84	1.95																	
Cr2O3	0.00	0.00	0.00	0.00	0.00	0.00																	
Al2O3	19.25	19.13	19.19	19.25	19.27	19.24																	
FeO	18.23	17.65	17.65	18.17	17.74	18.56																	
MnO	0.00	0.00	0.00	0.00	0.00	0.00																	
MgO	10.73	10.30	10.77	10.42	10.61	10.81																	
CaO	0.07	0.09	0.00	0.16	0.17	0.00																	
Na2O	0.68	0.74	0.80	0.80	0.71	0.84																	
K2O	8.92	8.79	8.82	8.48	8.82	8.66																	
TOTAL	95.38	94.20	94.96	94.67	94.93	96.64																	
CATIONS																							
Si	5.407	5.458	5.398	5.413	5.408	5.434																	
Ti	0.187	0.188	0.193	0.193	0.210	0.218																	
Cr	0.000	0.000	0.000	0.000	0.000	0.000																	
Al	3.421	3.431	3.467	3.442	3.433	3.370																	
Fe2+	2.299	2.247	2.228	2.305	2.243	2.306																	
Mn	0.000	0.000	0.000	0.000	0.000	0.000																	
Mg	2.413	2.336	2.422	2.355	2.398	2.393																	
Ca	0.011	0.015	0.000	0.026	0.027	0.000																	
Na	0.197	0.218	0.235	0.236	0.209	0.243																	
K	1.717	1.706	1.698	1.641	1.702	1.642																	
(O)	22	22	22	22	22	22																	
TOTAL	15.652	15.599	15.641	15.611	15.622	15.606																	
Mg#	0.512	0.510	0.521	0.505	0.516	0.509																	

DD.CLAS66								
%OXIDE	Mu1	Mu2	Mu3	Mu4	Mu5	Mu6	Mu7	
SiO2	44.98	45.28	45.72	45.58	45.29	45.46	45.09	
TiO2	0.83	1.22	0.97	0.77	1.42	1.27	1.41	
Cr2O3	0.10	0.12	0.00	0.00	0.00	0.00	0.00	
Al2O3	34.01	34.44	34.63	34.59	34.66	34.21	34.42	
FeO	1.91	1.82	1.24	1.31	1.36	1.60	1.72	
MnO	0.00	0.00	0.00	0.00	0.00	0.00	0.00	
MgO	0.99	0.86	0.98	0.69	0.85	0.89	0.78	
CaO	0.00	0.00	0.11	0.11	0.00	0.10	0.07	
Na2O	0.47	0.52	0.49	0.44	0.56	0.49	0.45	
K2O	9.81	10.13	10.44	10.39	10.31	10.16	10.10	
TOTAL	93.11	94.38	94.58	93.86	94.44	94.17	94.04	
CATIONS								
Si	6.137	6.105	6.138	6.161	6.094	6.134	6.097	
Ti	0.085	0.123	0.098	0.078	0.144	0.129	0.143	
Cr	0.010	0.012	0.000	0.000	0.000	0.000	0.000	
Al	5.470	5.472	5.479	5.511	5.496	5.441	5.486	
Fe2+	0.218	0.205	0.139	0.148	0.153	0.180	0.194	
Mn	0.000	0.000	0.000	0.000	0.000	0.000	0.000	
Mg	0.202	0.173	0.196	0.138	0.170	0.178	0.157	
Ca	0.000	0.000	0.015	0.016	0.000	0.015	0.010	
Na	0.125	0.136	0.128	0.114	0.145	0.129	0.119	
K	1.708	1.742	1.788	1.791	1.770	1.750	1.742	
(O)	22	22	22	22	22	22	22	
TOTAL	13.955	13.968	13.981	13.957	13.972	13.956	13.948	

DD.BOG1 Probe Data									
%OXIDE	Tur1	Tur2	Tur3	Tur4	Tur5	Tur6	Tur7	Tur8	Tur9
SiO2	35.31	34.82	34.87	35.01	36.46	34.73	35.22	35.44	34.95
TiO2	1.27	0.98	0.95	1.06	0.41	0.98	1.01	0.69	1.14
Cr2O3	0.00	0.00	0.00	0.00	0.00	0.00	0.10	0.00	0.00
Al2O3	32.75	33.24	32.81	33.41	31.14	32.64	33.49	33.14	33.11
FeO	8.22	7.20	7.80	7.54	0.24	7.25	7.52	7.49	7.59
MnO	0.00	0.00	0.00	0.00	0.00	0.00	0.00	0.00	0.00
MgO	5.53	5.62	5.42	5.49	12.02	5.36	5.54	5.59	5.42
CaO	0.49	0.77	0.64	0.59	1.64	0.73	0.73	0.46	0.63
Na2O	2.06	1.98	1.72	1.77	2.37	1.63	1.88	1.97	1.86
K2O	0.07	0.04	0.06	0.06	0.00	0.00	0.08	0.08	0.04
TOTAL	85.69	84.66	84.27	84.94	84.28	83.31	85.57	84.87	84.73
Si	7.391	7.340	7.395	7.355	7.496	7.422	7.352	7.445	7.367
Ti	0.200	0.156	0.152	0.167	0.063	0.157	0.158	0.110	0.180
Cr	0.000	0.000	0.000	0.000	0.000	0.000	0.016	0.000	0.000
Al	8.079	8.259	8.202	8.273	7.548	8.222	8.241	8.205	8.225
Fe2+	1.438	1.269	1.384	1.324	0.041	1.295	1.313	1.316	1.338
Mn	0.000	0.000	0.000	0.000	0.000	0.000	0.000	0.000	0.000
Mg	1.724	1.767	1.715	1.720	3.685	1.709	1.725	1.751	1.703
Ca	0.109	0.174	0.144	0.134	0.361	0.166	0.164	0.103	0.143
Na	0.836	0.811	0.707	0.721	0.946	0.674	0.762	0.803	0.759
K	0.019	0.012	0.015	0.016	0.000	0.000	0.021	0.021	0.011
(O)	31	31	31	31	31	31	31	31	31
TOTAL	19.796	19.788	19.714	19.710	20.140	19.645	19.752	19.754	19.726

BIOTITE	DD.BOG1									
%OXIDE	Bt1	Bt2	Bt3	Bt4	Bt5	Bt6	Bt7	Bt8	Bt9	Bt10
SiO2	34.39	34.08	34.32	34.27	33.84	34.50	34.34	34.45	34.22	35.18
TiO2	2.91	2.58	2.52	2.57	2.47	2.45	3.05	2.67	2.27	2.86
Cr2O3	0.00	0.00	0.00	0.00	0.00	0.00	0.00	0.00	0.00	0.00
Al2O3	18.90	19.05	19.14	19.13	18.65	19.03	18.86	18.78	19.38	19.38
FeO	21.98	22.13	22.08	21.53	22.07	22.45	22.06	22.67	22.46	22.74
MnO	0.00	0.00	0.00	0.00	0.00	0.00	0.00	0.00	0.00	0.00
MgO	7.30	7.59	7.32	7.50	7.10	7.42	7.06	7.07	7.55	7.68
CaO	0.10	0.13	0.11	0.06	0.12	0.12	0.07	0.06	0.00	0.00
Na2O	0.62	0.61	0.45	0.48	0.66	0.50	0.48	0.40	0.74	0.70
K2O	8.60	8.71	8.83	8.69	8.25	8.76	8.64	8.62	8.32	9.02
TOTAL	94.78	94.88	94.76	94.22	93.15	95.22	94.56	94.71	94.93	97.57
CATIONS										
Si	5.328	5.287	5.324	5.328	5.339	5.332	5.334	5.353	5.295	5.307
Ti	0.339	0.301	0.294	0.300	0.293	0.284	0.356	0.312	0.265	0.325
Cr	0.000	0.000	0.000	0.000	0.000	0.000	0.000	0.000	0.000	0.000
Al	3.451	3.482	3.500	3.507	3.468	3.466	3.454	3.440	3.534	3.446
Fe2+	2.848	2.871	2.864	2.800	2.912	2.902	2.866	2.946	2.906	2.869
Mn	0.000	0.000	0.000	0.000	0.000	0.000	0.000	0.000	0.000	0.000
Mg	1.685	1.755	1.692	1.738	1.670	1.708	1.634	1.638	1.742	1.728
Ca	0.016	0.021	0.018	0.010	0.021	0.019	0.012	0.011	0.000	0.000
Na	0.187	0.184	0.135	0.143	0.201	0.151	0.144	0.119	0.222	0.205
K	1.699	1.723	1.747	1.724	1.661	1.726	1.713	1.709	1.642	1.736
(O)	22	22	22	22	22	22	22	22	22	22
TOTAL	15.553	15.624	15.574	15.550	15.565	15.588	15.513	15.528	15.606	15.616

MUSCOVITE									
%OXIDE	Mu1	Mu2	Mu3	Mu4	Mu5	Mu6	Mu7	Mu8	Mu9
SiO2	45.12	45.55	45.39	45.67	45.28	46.34	45.89	45.09	46.29
TiO2	1.25	1.36	1.61	1.37	1.35	0.48	0.80	0.95	0.89
Cr2O3	0.00	0.00	0.00	0.00	0.00	0.00	0.00	0.00	0.00
Al2O3	34.86	35.27	35.24	35.52	34.82	34.28	35.51	35.05	35.48
FeO	1.21	1.19	1.13	1.00	1.17	1.11	1.26	1.26	1.21
MnO	0.00	0.00	0.00	0.00	0.00	0.00	0.00	0.00	0.00
MgO	0.57	0.71	0.71	0.66	0.76	0.89	0.67	0.55	0.63
CaO	0.08	0.08	0.10	0.00	0.00	0.00	0.00	0.00	0.00
Na2O	1.10	0.96	0.97	1.20	1.03	0.76	0.87	0.94	1.16
K2O	9.51	9.48	9.54	9.71	9.62	9.63	9.23	9.51	9.63
TOTAL	93.70	94.59	94.69	95.13	94.03	93.48	94.22	93.36	95.30
CATIONS									
Si	6.096	6.087	6.065	6.075	6.096	6.249	6.136	6.107	6.139
Ti	0.127	0.137	0.162	0.137	0.137	0.049	0.080	0.097	0.089
Cr	0.000	0.000	0.000	0.000	0.000	0.000	0.000	0.000	0.000
Al	5.551	5.557	5.551	5.570	5.526	5.448	5.597	5.595	5.546
Fe2+	0.137	0.133	0.126	0.111	0.132	0.125	0.140	0.143	0.134
Mn	0.000	0.000	0.000	0.000	0.000	0.000	0.000	0.000	0.000
Mg	0.115	0.140	0.141	0.131	0.152	0.180	0.133	0.111	0.125
Ca	0.012	0.011	0.014	0.000	0.000	0.000	0.000	0.000	0.000
Na	0.288	0.249	0.252	0.309	0.268	0.198	0.225	0.247	0.298
K	1.639	1.616	1.627	1.647	1.653	1.656	1.574	1.644	1.63
(O)	22	22	22	22	22	22	22	22	22
TOTAL	13.965	13.930	13.938	13.980	13.964	13.905	13.885	13.944	13.961

DD.CLASS66

GARNET With Fe3+ Recalculations

%OXIDE	Grt1	Grt2	Grt2	Grt3	Grt3	Grt4	Grt4	Grt5	Grt5	Grt6	Grt6	Grt7	Grt7	Grt8	Grt8	Grt9	Grt9
SiO2	37.92	36.46	36.46	36.59	36.59	36.55	36.55	36.36	36.36	36.50	36.50	36.57	36.57	36.79	36.79	36.43	36.43
TiO2	0.00	0.00	0.00	0.00	0.00	0.00	0.00	0.00	0.00	0.11	0.11	0.00	0.00	0.00	0.00	0.00	0.00
Cr2O3	0.00	0.00	0.00	0.00	0.00	0.10	0.10	0.00	0.00	0.00	0.00	0.00	0.00	0.00	0.00	0.00	0.00
Al2O3	20.96	20.82	20.82	20.67	20.67	20.75	20.75	20.68	20.68	20.51	20.51	20.82	20.82	21.03	21.03	20.42	20.42
Fe2O3	-	-	1.37	-	0.78	-	0.95	-	1.59	-	1.22	-	1.45	-	0.84	-	1.36
FeO	23.90	25.71	24.48	25.44	24.73	25.92	25.06	26.28	24.85	25.32	24.22	25.70	24.40	25.40	24.65	26.02	24.79
MnO	15.19	13.56	13.56	13.28	13.28	13.32	13.32	13.28	13.28	14.11	14.11	13.73	13.73	13.62	13.62	13.57	13.57
MgO	1.41	2.02	2.02	2.11	2.11	2.06	2.06	1.94	1.94	1.96	1.96	1.96	1.96	1.95	1.95	1.90	1.90
CaO	1.99	1.38	1.38	1.43	1.43	1.16	1.16	1.34	1.34	1.35	1.35	1.51	1.51	1.60	1.60	1.26	1.26
TOTAL	101.37	99.96	100.10	99.51	99.59	99.86	99.96	99.88	100.03	99.85	99.97	100.28	100.42	100.39	100.48	99.60	99.74
CATIONS																	
Si	6.068	5.943	5.922	5.977	5.965	5.961	5.947	5.943	5.919	5.963	5.944	5.946	5.924	5.959	5.946	5.972	5.951
Ti	0.000	0.000	0.000	0.000	0.000	0.000	0.000	0.000	0.000	0.013	0.013	0.000	0.000	0.000	0.000	0.000	0.000
Cr	0.000	0.000	0.000	0.000	0.000	0.012	0.012	0.000	0.000	0.000	0.000	0.000	0.000	0.000	0.000	0.000	0.000
Al	3.953	4.001	3.987	3.979	3.971	3.988	3.978	3.985	3.969	3.950	3.938	3.990	3.975	4.016	4.007	3.946	3.932
Fe3+	-	-	0.167	-	0.096	-	0.117	-	0.194	-	0.150	-	0.176	-	0.102	-	0.167
Fe2+	3.199	3.505	3.325	3.475	3.372	3.535	3.410	3.592	3.383	3.459	3.299	3.495	3.306	3.441	3.332	3.567	3.387
Mn	2.058	1.873	1.866	1.838	1.834	1.840	1.836	1.839	1.832	1.953	1.947	1.891	1.884	1.869	1.865	1.885	1.878
Mg	0.336	0.492	0.490	0.513	0.512	0.500	0.499	0.472	0.470	0.477	0.476	0.475	0.473	0.472	0.471	0.464	0.462
Ca	0.341	0.242	0.241	0.250	0.250	0.203	0.203	0.234	0.233	0.235	0.234	0.262	0.261	0.277	0.276	0.222	0.221
(O)	24	24	24	24	24	24	24	24	24	24	24	24	24	24	24	24	24
TOTAL	15.955	16.056	16.000	16.032	16.000	16.039	16.000	16.065	16.000	16.050	16.000	16.059	16.000	16.034	16.000	16.056	16.000
Mg#	0.10	0.12	0.13	0.13	0.13	0.12	0.13	0.12	0.12	0.12	0.13	0.12	0.13	0.12	0.12	0.12	0.12

GARNET With Fe3+ Recalculations

%OXIDE	Grt10	Grt10	Grt11	Grt11	Grt12	Grt12	Grt13	Grt13	Grt14	Grt14	Grt15	Grt15
SiO2	36.05	36.05	36.98	36.98	36.73	36.73	36.84	36.84	36.89	36.89	36.54	36.54
TiO2	0.00	0.00	0.00	0.00	0.00	0.00	0.00	0.00	0.00	0.00	0.00	0.00
Cr2O3	0.00	0.00	0.00	0.00	0.00	0.00	0.00	0.00	0.00	0.00	0.00	0.00
Al2O3	20.41	20.41	20.71	20.71	20.63	20.63	20.66	20.66	20.59	20.59	20.66	20.66
Fe2O3	-	1.72	-	0.99	-	1.84	-	1.60	-	0.59	-	1.57
FeO	25.82	24.28	26.21	25.32	26.55	24.89	26.38	24.94	25.71	25.18	25.99	24.58
MnO	13.47	13.47	13.26	13.26	13.42	13.42	13.52	13.52	13.57	13.57	13.65	13.65
MgO	1.95	1.95	1.86	1.86	1.97	1.97	2.00	2.00	1.87	1.87	1.87	1.87
CaO	1.33	1.33	1.66	1.66	1.51	1.51	1.46	1.46	1.45	1.45	1.54	1.54
TOTAL	99.03	99.20	100.67	100.76	100.80	100.99	100.86	101.02	100.07	100.13	100.23	100.39
CATIONS												
Si	5.945	5.919	5.985	5.970	5.955	5.927	5.964	5.940	6.001	5.992	5.952	5.928
Ti	0.000	0.000	0.000	0.000	0.000	0.000	0.000	0.000	0.000	0.000	0.000	0.000
Cr	0.000	0.000	0.000	0.000	0.000	0.000	0.000	0.000	0.000	0.000	0.000	0.000
Al	3.968	3.950	3.950	3.940	3.941	3.923	3.941	3.925	3.947	3.941	3.967	3.951
Fe3+	-	0.212	-	0.120	-	0.224	-	0.194	-	0.072	-	0.191
Fe2+	3.562	3.334	3.546	3.417	3.599	3.358	3.571	3.362	3.498	3.421	3.540	3.335
Mn	1.882	1.874	1.817	1.812	1.843	1.834	1.853	1.846	1.870	1.867	1.883	1.875
Mg	0.479	0.477	0.455	0.454	0.475	0.473	0.482	0.480	0.455	0.454	0.454	0.452
Ca	0.235	0.234	0.287	0.286	0.262	0.261	0.254	0.253	0.253	0.253	0.268	0.267
(O)	24	24	24	24	24	24	24	24	24	24	24	24
TOTAL	16.071	16.000	16.040	16.000	16.075	16.000	16.065	16.000	16.024	16.000	16.064	16.000
Mg#	0.12	0.13	0.11	0.12	0.12	0.12	0.12	0.12	0.12	0.12	0.11	0.12

ILMENITE

%OXIDE	Ilm1
SiO2	2.07
TiO2	52.17
Cr2O3	0.00
Al2O3	1.45
FeO	37.93
MnO	5.62
MgO	0.13
CaO	0.00
Na2O	0.22
K2O	0.42
TOTAL	100.00
Si	0.051
Ti	0.962
Cr	0.000
Al	0.042
Fe2+	0.778
Mn	0.117
Mg	0.005
Ca	0.000
Na	0.011
K	0.013
(O)	22
TOTAL	1.979

BIOTITE

%OXIDE	Bt1	Bt2	Bt3	Bt4	Bt5	Bt6	Bt7	Bt8	Bt9	Bt10	Bt11	Bt12	Bt13	Bt14
SiO2	34.67	34.80	35.60	35.46	35.09	35.73	35.41	35.33	35.33	34.79	34.57	34.74	34.88	34.91
TiO2	2.80	3.11	2.94	3.04	2.66	2.53	3.15	3.48	3.11	2.47	3.18	3.77	3.06	3.18
Cr2O3	0.00	0.00	0.14	0.00	0.00	0.09	0.00	0.00	0.00	0.00	0.00	0.00	0.00	0.09
Al2O3	18.43	18.19	18.99	18.87	18.52	18.59	18.77	18.74	19.03	18.45	18.71	18.63	18.81	18.06
FeO	19.80	20.43	20.45	21.18	20.87	20.40	20.68	20.80	20.34	20.65	20.19	20.05	19.84	20.10
MnO	0.00	0.13	0.00	0.00	0.00	0.00	0.00	0.00	0.00	0.00	0.00	0.00	0.00	0.00
MgO	7.87	8.28	8.35	8.35	8.44	8.63	8.40	8.07	8.59	8.61	7.90	8.20	7.96	8.00
CaO	0.10	0.11	0.13	0.12	0.12	0.08	0.11	0.15	0.11	0.10	0.00	0.09	0.00	0.11
Na2O	0.47	0.45	0.49	0.49	0.38	0.50	0.70	0.50	0.48	0.43	0.52	0.56	0.46	0.47
K2O	9.06	8.97	9.28	9.22	9.09	9.16	8.24	9.02	9.47	8.57	9.15	9.09	9.13	9.04
TOTAL	93.20	94.49	96.35	96.74	95.16	95.70	95.46	96.08	96.45	94.07	94.21	95.12	94.13	93.96
CATIONS														
Si	5.411	5.382	5.385	5.361	5.389	5.437	5.364	5.367	5.346	5.390	5.358	5.382	5.391	5.430
Ti	0.328	0.362	0.335	0.346	0.307	0.289	0.359	0.397	0.354	0.288	0.370	0.322	0.356	0.371
Cr	0.000	0.000	0.016	0.000	0.000	0.011	0.000	0.000	0.000	0.000	0.000	0.000	0.000	0.011
Al	3.411	3.315	3.385	3.363	3.353	3.334	3.350	3.354	3.393	3.369	3.417	3.402	3.427	3.304
Fe2+	2.585	2.642	2.578	2.678	2.681	2.596	2.619	2.642	2.573	2.675	2.616	2.598	2.564	2.610
Mn	0.000	0.018	0.000	0.000	0.000	0.000	0.000	0.000	0.000	0.000	0.000	0.000	0.000	0.000
Mg	1.830	1.908	1.883	1.882	1.931	1.958	1.897	1.827	1.937	1.989	1.820	1.894	1.834	1.852
Ca	0.017	0.019	0.021	0.020	0.019	0.014	0.018	0.024	0.018	0.016	0.000	0.015	0.000	0.019
Na	0.141	0.136	0.143	0.143	0.112	0.146	0.206	0.146	0.139	0.129	0.156	0.168	0.137	0.140
K	1.803	1.770	1.791	1.779	1.780	1.778	1.785	1.748	1.828	1.693	1.809	1.796	1.800	1.790
(O)	22	22	22	22	22	22	22	22	22	22	22	22	22	22
TOTAL	15.526	15.552	15.537	15.572	15.572	15.563	15.598	15.505	15.588	15.549	15.546	15.577	15.509	15.527
Mg#	0.41	0.42	0.42	0.41	0.42	0.43	0.42	0.41	0.43	0.43	0.41	0.42	0.42	0.42

DD.CLAS112																		
BIOTITE											TOURMALINE			MUSCOVITE				
%OXIDE	Bt1	Bt2	Bt3	Bt4	Bt5	Bt6	Bt7	Bt8	Bt9		%OXIDE	Tur1		%OXIDE	Mu1	Mu2	Mu3	Mu4
SiO2	33.81	34.04	33.77	34.27	34.93	34.31	33.90	33.95	34.18		SiO2	35.24		SiO2	44.87	45.03	44.19	44.71
TiO2	2.41	2.45	2.65	2.42	2.35	2.36	2.55	2.70	2.67		TiO2	1.02		TiO2	0.82	0.74	0.97	0.55
Cr2O3	0.00	0.00	0.00	0.10	0.13	0.00	0.00	0.00	0.00		Cr2O3	0.10		Cr2O3	0.12	0.09	0.00	0.00
Al2O3	18.67	18.48	18.71	19.01	19.58	18.90	18.91	19.15	18.94		Al2O3	34.00		Al2O3	34.88	34.96	34.13	34.89
FeO	21.71	22.14	21.60	21.63	22.47	21.65	22.74	21.89	21.60		FeO	7.18		FeO	1.41	1.39	2.71	1.28
MnO	0.00	0.00	0.00	0.00	0.00	0.00	0.00	0.00	0.00		MnO	0.00		MnO	0.00	0.11	0.00	0.00
MgO	7.77	7.53	7.57	7.31	8.16	7.66	7.44	7.49	7.61		MgO	5.27		MgO	0.77	0.66	1.25	0.71
CaO	0.00	0.10	0.12	0.00	0.00	0.06	0.09	0.00	0.12		CaO	0.58		CaO	0.14	0.14	0.13	0.13
Na2O	0.56	0.51	0.57	0.45	0.58	0.39	0.53	0.57	0.55		Na2O	1.84		Na2O	0.97	0.91	0.89	1.01
K2O	8.45	8.60	8.67	8.61	8.95	8.71	8.04	8.88	8.71		K2O	0.00		K2O	9.64	9.85	9.39	9.86
TOTAL	93.37	93.84	93.65	93.80	97.14	94.05	94.20	94.63	94.38		TOTAL	85.23		TOTAL	93.61	93.88	93.66	93.13
CATIONS											CATIONS			CATIONS				
Si	5.317	5.339	5.300	5.354	5.286	5.349	5.292	5.278	5.314		Si	7.356		Si	6.081	6.091	6.028	6.092
Ti	0.284	0.289	0.313	0.285	0.267	0.277	0.299	0.316	0.312		Ti	0.159		Ti	0.084	0.075	0.099	0.056
Cr	0.000	0.000	0.000	0.012	0.016	0.000	0.000	0.000	0.000		Cr	0.016		Cr	0.013	0.009	0.000	0.000
Al	3.460	3.416	3.462	3.500	3.492	3.473	3.480	3.509	3.472		Al	8.366		Al	5.573	5.574	5.486	5.604
Fe	2.855	2.905	2.835	2.826	2.844	2.823	2.970	2.846	2.808		Fe	1.253		Fe	0.159	0.158	0.309	0.146
Mn	0.000	0.000	0.000	0.000	0.000	0.000	0.000	0.000	0.000		Mn	0.000		Mn	0.000	0.012	0.000	0.000
Mg	1.821	1.761	1.771	1.703	1.841	1.779	1.732	1.735	1.764		Mg	1.641		Mg	0.155	0.133	0.254	0.145
Ca	0.000	0.017	0.020	0.000	0.000	0.010	0.015	0.000	0.020		Ca	0.130		Ca	0.017	0.020	0.018	0.019
Na	0.170	0.155	0.173	0.137	0.169	0.119	0.160	0.172	0.167		Na	0.745		Na	0.255	0.238	0.236	0.266
K	1.695	1.720	1.735	1.715	1.727	1.733	1.602	1.762	1.729		K	0.000		K	1.666	1.700	1.634	1.714
(O)	22	22	22	22	22	22	22	22	22		(O)	31		(O)	22	22	22	22
TOTAL	15.602	15.602	15.609	15.532	15.642	15.563	15.550	15.618	15.586		TOTAL	19.666		TOTAL	14.003	14.010	14.064	14.042
GARNET With Fe3+ Recalculations						DD.SIN1 Probe Data												
%OXIDE	Grt1	Grt1	Grt2	Grt3	Grt3	Grt4	Grt4	Grt5	Grt5	Grt6	Grt6	Grt7	Grt7	Grt8	Grt8	Grt9	Grt9	Grt10	Grt10
SiO2	37.73	37.73	37.89	37.98	37.98	37.89	37.89	37.99	37.99	37.85	37.85	37.85	37.85	37.67	37.67	38.08	38.08	37.80	37.80
TiO2	0.00	0.00	0.03	0.00	0.00	0.04	0.04	0.00	0.00	0.09	0.09	0.09	0.09	0.01	0.01	0.05	0.05	0.05	0.05
Cr2O3	0.08	0.08	0.12	0.13	0.13	0.06	0.06	0.13	0.13	0.05	0.05	0.05	0.05	0.14	0.14	0.02	0.02	0.05	0.05
Al2O3	21.64	21.64	21.26	21.37	21.37	21.30	21.30	21.55	21.55	21.55	21.55	21.55	21.55	21.13	21.13	21.29	21.29	21.37	21.37
Fe2O3	-	1.29	-	-	0.30	-	1.09	-	1.14	-	1.45	-	1.45	-	1.33	-	0.33	-	1.21
FeO	33.42	32.26	32.94	33.21	32.94	33.04	32.06	33.34	32.31	33.70	32.40	33.70	32.40	33.76	32.56	33.13	32.83	33.45	32.36
MnO	2.47	2.47	2.29	2.93	2.93	2.25	2.25	2.13	2.13	2.86	2.86	2.86	2.86	2.85	2.85	2.41	2.41	2.65	2.65
MgO	5.18	5.18	5.20	4.83	4.83	5.68	5.68	5.61	5.61	5.09	5.09	5.09	5.09	4.91	4.91	5.30	5.30	5.14	5.14
CaO	0.70	0.70	0.62	0.70	0.70	0.71	0.71	0.75	0.75	0.77	0.77	0.77	0.77	0.66	0.66	0.67	0.67	0.82	0.82
TOTAL	101.21	101.34	100.34	101.14	101.17	100.97	101.08	101.49	101.61	101.95	102.10	101.95	102.10	101.14	101.27	100.95	100.98	101.33	101.45
CATIONS																			
Si	5.954	5.935	6.004	5.993	5.989	5.969	5.953	5.953	5.936	5.937	5.916	5.937	5.916	5.965	5.945	6.003	5.998	5.958	5.940
Ti	0.000	0.000	0.003	0.000	0.000	0.005	0.005	0.000	0.000	0.010	0.010	0.010	0.010	0.001	0.001	0.006	0.006	0.005	0.005
Cr	0.010	0.010	0.015	0.016	0.016	0.007	0.007	0.017	0.017	0.006	0.006	0.006	0.006	0.018	0.018	0.002	0.002	0.006	0.006
Al	4.018	4.005	3.971	3.974	3.971	3.955	3.944	3.987	3.976	3.985	3.971	3.985	3.971	3.944	3.931	3.955	3.952	3.970	3.958
Fe3+	-	0.153	-	-	0.036	-	0.129	-	0.135	-	0.170	-	0.170	-	0.158	-	0.039	-	0.144
Fe2+	4.404	4.237	4.366	4.383	4.344	4.353	4.213	4.369	4.222	4.421	4.235	4.421	4.235	4.471	4.298	4.367	4.324	4.410	4.253
Mn	0.329	0.328	0.307	0.392	0.392	0.301	0.300	0.282	0.281	0.380	0.379	0.380	0.379	0.382	0.381	0.322	0.322	0.353	0.352
Mg	1.217	1.213	1.228	1.135	1.134	1.333	1.329	1.310	1.306	1.189	1.185	1.189	1.185	1.159	1.155	1.245	1.244	1.208	1.204
Ca	0.119	0.119	0.106	0.119	0.119	0.120	0.120	0.127	0.127	0.129	0.129	0.129	0.129	0.113	0.113	0.113	0.113	0.138	0.138
(O)	24	24	24	24	24	24	24	24	24	24	24	24	24	24	24	24	24	24	24
TOTAL	16.051	16.000	16.000	16.012	16.000	16.043	16.000	16.045	16.000	16.057	16.000	16.057	16.000	16.053	16.000	16.013	16.000	16.048	16.000
Mg#	0.22	0.22	0.22	0.21	0.21	0.23	0.24	0.23	0.24	0.21	0.22	0.21	0.22	0.21	0.21	0.22	0.22	0.22	0.22
DD.SIN1						DD.SIN1													
GARNET With Fe3+ Recalculations						BIOTITE													
%OXIDE	Grt11	Grt11	Grt12	Grt12		%OXIDE	Bt1	Bt2	Bt3	Bt4	Bt5	Bt6	Bt7	Bt8	Bt9	Bt10	Bt11	Bt12	Bt13
SiO2	37.73	37.73	37.97	37.97		SiO2	36.49	36.34	36.75	36.59	36.77	36.56	36.38	35.97	35.71	36.11	35.81	36.03	36.00
TiO2	0.00	0.00	0.06	0.06		TiO2	1.82	1.59	2.05	1.66	1.82	1.84	2.20	1.87	1.74	1.96	1.75	1.91	1.77
Cr2O3	0.06	0.06	0.05	0.05		Cr2O3	0.11	0.03	0.14	0.10	0.25	0.12	0.07	0.17	0.00	0.00	0.00	0.00	0.00
Al2O3	21.75	21.75	21.42	21.42		Al2O3	19.57	19.27	19.18	19.53	19.23	19.60	19.35	19.33	19.19	18.30	18.79	19.12	19.20
Fe2O3	-	1.04	-	0.43		FeO	15.81	16.05	16.38	15.96	16.19	16.33	16.47	16.28	16.15	16.59	16.38	16.47	16.20
FeO	33.41	32.48	33.89	33.50		MnO	0.00	0.00	0.00	0.00	0.00	0.00	0.00	0.00	0.00	0.00	0.00	0.00	0.00
MnO	3.05	3.05	2.96	2.96		MgO	11.87	12.44	11.89	12.28	11.90	12.27	11.96	11.79	11.70	11.81	11.96	11.74	11.40
MgO	4.84	4.84	4.58	4.58		CaO	0.15	0.15	0.08	0.14	0.09	0.08	0.15	0.15	0.00	0.00	0.00	0.00	0.00
CaO	0.73	0.73	0.63	0.63		Na2O	0.78	0.93	0.79	0.86	0.84	0.81	0.93	0.73	0.71	0.69	0.84	0.67	0.77
						K2O	8.54	8.27	8.34	8.49	8.43	8.52	8.76	8.15	8.52	8.39	8.33	8.61	8.33
TOTAL	101.55	101.66	101.55	101.59															
						TOTAL	95.13	95.06	95.60	95.62	95.51	96.14	96.26	94.44	93.71	93.84	93.87	94.55	93.66
CATIONS																			
Si	5.938	5.923	5.984	5.978		CATIONS													
Ti	0.000	0.000	0.007	0.007		Si	5.435	5.421	5.454	5.425	5.460	5.400	5.386	5.406	5.417	5.478	5.428	5.423	5.455
Cr	0.007	0.007	0.006	0.006		Ti	0.203	0.178	0.228	0.185	0.203	0.205	0.245	0.211	0.198	0.223	0.200	0.216	0.202
Al	4.033	4.024	3.978	3.974		Cr	0.013	0.003	0.017	0.012	0.029	0.014	0.008	0.020	0.000	0.000	0.000	0.000	0.000
Fe3+	-	0.123	-	0.051		Al	3.436	3.388	3.355	3.413	3.367	3.413	3.376	3.425	3.431	3.272	3.358	3.393	3.428
Fe2+	4.398	4.264	4.466	4.410		Fe2+	1.969	2.003	2.033	1.979	2.010	2.018	2.039	2.046	2.050	2.104	2.077	2.073	2.052
Mn	0.406	0.405	0.395	0.395		Mn	0.000	0.000	0.000	0.000	0.000	0.000	0.000	0.000	0.000	0.000	0.000	0.000	0.000
Mg	1.136	1.133	1.076	1.075		Mg	2.636	2.766	2.630	2.714	2.635	2.701	2.640	2.642	2.646	2.672	2.703	2.634	2.575
Ca	0.122	0.122	0.105	0.105		Ca	0.023	0.024	0.013	0.022	0.015	0.012	0.023	0.024	0.000	0.000	0.000	0.000	0.000
(O)	24	24	24	24		Na	0.224	0.268	0.226	0.247	0.241	0.233	0.268	0.213	0.208	0.204	0.246	0.165	0.227
TOTAL	16.041	16.000	16.017	16.000		K	1.622	1.575	1.579	1.606	1.598	1.606	1.654	1.563	1.550	1.623	1.611	1.653	1.610
						(O)	22	22	22	22	22	22	22	22	22	22	22	22	22
Mg#	0.21	0.21	0.19	0.20		TOTAL	15.561	15.626	15.535	15.603	15.558	15.602	15.639	15.550	15.600	15.576	15.623	15.557	15.549
						Mg#	0.57	0.58	0.56	0.58	0.57	0.57	0.56	0.56	0.56	0.56	0.57	0.56	0.56

DD.SIN101

GARNET With Fe3+ Recalculations

%OXIDE	Grt1	Grt1	Grt2	Grt2	Grt3	Grt3	Grt4	Grt4	Grt5	Grt5	Grt6	Grt6	Grt7	Grt7	Grt8	Grt8	Grt9	Grt9
SiO2	37.96	37.96	37.80	37.80	37.59	37.59	38.07	38.07	38.22	38.22	37.75	37.75	37.99	37.99	38.38	38.38	37.90	37.90
TiO2	0.00	0.00	0.00	0.00	0.00	0.00	0.00	0.00	0.00	0.00	0.00	0.00	0.00	0.00	0.00	0.00	0.00	0.00
Cr2O3	0.00	0.00	0.00	0.00	0.00	0.00	0.00	0.00	0.00	0.00	0.18	0.18	0.00	0.00	0.00	0.00	0.00	0.00
Al2O3	21.15	21.15	20.98	20.98	21.01	21.01	21.62	21.62	21.44	21.44	21.00	21.00	21.22	21.22	21.36	21.36	21.06	21.06
Fe2O3	-	0.53	-	0.25	-	1.08	-	0.23	-	1.15	-	0.96	-	1.24	-	0.10	-	0.15
FeO	32.59	32.11	32.53	32.30	32.05	31.08	32.26	32.05	33.09	32.06	33.17	32.31	32.91	31.80	32.74	32.64	32.17	32.03
MnO	2.05	2.05	1.92	1.92	2.17	2.17	2.02	2.02	1.97	1.97	1.67	1.67	1.76	1.76	1.75	1.75	2.00	2.00
MgO	5.81	5.81	5.60	5.60	6.10	6.10	5.89	5.89	6.05	6.05	5.75	5.75	6.06	6.06	5.93	5.93	5.79	5.79
CaO	0.68	0.68	0.76	0.76	0.61	0.61	0.72	0.72	0.67	0.67	0.69	0.69	0.81	0.81	0.71	0.71	0.72	0.72
TOTAL	100.23	100.28	99.58	99.60	99.53	99.64	100.57	100.60	101.45	101.56	100.21	100.31	100.75	100.88	100.86	100.87	99.64	99.66
CATIONS																		
Si	6.006	5.998	6.021	6.017	5.985	5.969	5.988	5.985	5.979	5.962	5.988	5.974	5.982	5.964	6.021	6.019	6.023	6.021
Ti	0.000	0.000	0.000	0.000	0.000	0.000	0.000	0.000	0.000	0.000	0.000	0.000	0.000	0.000	0.000	0.000	0.000	0.000
Cr	0.000	0.000	0.000	0.000	0.000	0.000	0.000	0.000	0.000	0.000	0.023	0.023	0.000	0.000	0.000	0.000	0.000	0.000
Al	3.944	3.939	3.938	3.936	3.943	3.932	4.008	4.006	3.953	3.942	3.927	3.918	3.938	3.926	3.950	3.949	3.945	3.944
Fe3+	-	0.063	-	0.030	-	0.129	-	0.027	-	0.135	-	0.114	-	0.147	-	0.012	-	0.018
Fe2+	4.312	4.243	4.333	4.300	4.269	4.129	4.242	4.213	4.329	4.182	4.400	4.276	4.334	4.174	4.295	4.282	4.275	4.255
Mn	0.275	0.275	0.259	0.259	0.293	0.292	0.269	0.269	0.261	0.260	0.224	0.223	0.235	0.234	0.233	0.233	0.269	0.269
Mg	1.369	1.367	1.329	1.328	1.449	1.445	1.381	1.380	1.410	1.406	1.359	1.356	1.423	1.419	1.386	1.386	1.372	1.371
Ca	0.115	0.115	0.130	0.130	0.104	0.104	0.121	0.121	0.113	0.113	0.117	0.117	0.137	0.137	0.119	0.119	0.122	0.122
(O)	24	24	24	24	24	24	24	24	24	24	24	24	24	24	24	24	24	24
TOTAL	16.021	16.000	16.010	16.000	16.043	16.000	16.009	16.000	16.045	16.000	16.038	16.000	16.049	16.000	16.004	16.000	16.006	16.000
Mg#	0.24	0.24	0.23	0.24	0.25	0.26	0.25	0.25	0.25	0.25	0.24	0.24	0.25	0.25	0.24	0.24	0.24	0.24

GARNET With Fe3+ Recalculations

%OXIDE	Grt10	Grt10	Grt11	Grt11	Grt12	Grt12	Grt13	Grt13	Grt14	Grt14	Grt15	Grt16	Grt16	Grt17	Grt17	Grt18	Grt18	Grt19
SiO2	37.94	37.94	37.75	37.75	37.48	37.48	37.85	37.85	37.51	37.51	38.14	38.06	38.06	37.81	37.81	38.20	38.20	37.63
TiO2	0.00	0.00	0.00	0.00	0.00	0.00	0.00	0.00	0.00	0.00	0.00	0.00	0.00	0.00	0.00	0.00	0.00	0.00
Cr2O3	0.00	0.00	0.00	0.00	0.00	0.00	0.00	0.00	0.00	0.00	0.00	0.00	0.00	0.00	0.00	0.00	0.00	0.00
Al2O3	21.26	21.26	21.41	21.41	21.29	21.29	21.34	21.34	21.27	21.27	21.45	21.45	21.45	21.46	21.46	21.33	21.33	21.27
Fe2O3	-	0.73	-	0.53	-	1.03	-	1.14	-	1.43	-	-	1.07	-	0.45	-	1.09	-
FeO	32.69	32.03	32.89	32.42	32.97	32.05	32.74	31.71	32.61	31.33	32.09	32.53	31.57	31.94	31.53	32.73	31.75	31.69
MnO	1.83	1.83	1.94	1.94	1.90	1.90	2.20	2.20	2.18	2.18	2.07	2.12	2.12	2.20	2.20	2.21	2.21	2.28
MgO	5.88	5.88	5.54	5.54	5.60	5.60	5.87	5.87	5.82	5.82	5.81	6.09	6.09	5.92	5.92	6.05	6.05	5.97
CaO	0.79	0.79	0.69	0.69	0.70	0.70	0.66	0.66	0.72	0.72	0.72	0.74	0.74	0.69	0.69	0.70	0.70	0.76
TOTAL	100.38	100.45	100.23	100.28	99.94	100.04	100.66	100.77	100.11	100.26	100.26	100.99	101.10	100.02	100.06	101.22	101.33	99.60
CATIONS																		
Si	5.992	5.981	5.980	5.972	5.962	5.947	5.971	5.954	5.954	5.933	6.014	5.973	5.957	5.981	5.974	5.988	5.972	5.981
Ti	0.000	0.000	0.000	0.000	0.000	0.000	0.000	0.000	0.000	0.000	0.000	0.000	0.000	0.000	0.000	0.000	0.000	0.000
Cr	0.000	0.000	0.000	0.000	0.000	0.000	0.000	0.000	0.000	0.000	0.000	0.000	0.000	0.000	0.000	0.000	0.000	0.000
Al	3.957	3.950	3.998	3.993	3.991	3.981	3.969	3.958	3.980	3.966	3.986	3.968	3.958	4.002	3.998	3.941	3.930	3.985
Fe3+	-	0.087	-	0.063	-	0.123	-	0.135	-	0.170	-	-	0.126	-	0.054	-	0.129	-
Fe2+	4.318	4.223	4.357	4.288	4.386	4.252	4.319	4.172	4.330	4.144	4.232	4.270	4.133	4.226	4.167	4.290	4.150	4.212
Mn	0.245	0.245	0.260	0.260	0.256	0.255	0.295	0.294	0.293	0.292	0.276	0.282	0.281	0.295	0.295	0.294	0.293	0.307
Mg	1.384	1.381	1.308	1.306	1.327	1.324	1.380	1.376	1.378	1.373	1.365	1.425	1.421	1.397	1.395	1.413	1.409	1.414
Ca	0.133	0.133	0.118	0.118	0.119	0.119	0.111	0.111	0.122	0.122	0.121	0.124	0.124	0.117	0.117	0.117	0.117	0.129
(O)	24	24	24	24	24	24	24	24	24	24	24	24	24	24	24	24	24	24
TOTAL	16.029	16.000	16.021	16.000	16.041	16.000	16.045	16.000	16.057	16.000	15.994	16.042	16.000	16.018	16.000	16.043	16.000	16.028
Mg#	0.24	0.25	0.23	0.23	0.23	0.24	0.24	0.25	0.24	0.25	0.24	0.25	0.26	0.25	0.25	0.25	0.25	0.25

GARNET Analyses From Garnet Rims

%OXIDE	Grt19	Grt20	Grt20	GrtR1	GrtR1	GrtR2	GrtR2	GrtR3	GrtR3	GrtR4	GrtR4
SiO2	37.63	38.04	38.04	37.72	37.72	37.54	37.54	37.73	37.73	37.60	37.60
TiO2	0.00	0.00	0.00	0.00	0.00	0.00	0.00	0.00	0.00	0.00	0.00
Cr2O3	0.00	0.00	0.00	0.00	0.00	0.00	0.00	0.00	0.00	0.00	0.00
Al2O3	21.27	21.39	21.39	21.13	21.13	20.89	20.89	21.07	21.07	21.19	21.19
Fe2O3	0.70	-	0.05	-	0.70	-	0.85	-	0.10	-	1.31
FeO	31.06	31.48	31.43	33.21	32.58	33.34	32.57	32.71	32.62	33.37	32.19
MnO	2.28	2.30	2.30	2.36	2.36	2.32	2.32	2.34	2.34	2.58	2.58
MgO	5.97	6.12	6.12	5.07	5.07	4.99	4.99	5.17	5.17	5.05	5.05
CaO	0.76	0.66	0.66	0.85	0.85	0.83	0.83	0.71	0.71	0.91	0.91
TOTAL	99.67	99.99	100.00	100.34	100.41	99.91	100.00	99.73	99.74	100.69	100.82
CATIONS											
Si	5.971	6.006	6.005	5.993	5.983	5.999	5.986	6.016	6.014	5.966	5.947
Ti	0.000	0.000	0.000	0.000	0.000	0.000	0.000	0.000	0.000	0.000	0.000
Cr	0.000	0.000	0.000	0.000	0.000	0.000	0.000	0.000	0.000	0.000	0.000
Al	3.978	3.981	3.981	3.958	3.951	3.934	3.926	3.959	3.958	3.963	3.950
Fe3+	0.084	-	0.006	-	0.084	-	0.102	-	0.012	-	0.155
Fe2+	4.121	4.157	4.150	4.414	4.322	4.455	4.344	4.362	4.349	4.428	4.258
Mn	0.306	0.307	0.307	0.318	0.317	0.315	0.314	0.316	0.316	0.346	0.345
Mg	1.412	1.439	1.439	1.200	1.198	1.189	1.186	1.229	1.229	1.194	1.190
Ca	0.129	0.112	0.112	0.145	0.145	0.142	0.142	0.122	0.122	0.155	0.154
(O)	24	24	24	24	24	24	24	24	24	24	24
TOTAL	16.000	16.002	16.000	16.028	16.000	16.034	16.000	16.004	16.000	16.052	16.000
Mg#	0.26	0.26	0.26	0.21	0.22	0.21	0.21	0.22	0.22	0.21	0.22

PLAGIOCLASE

%OXIDE	Pl6	Pl7	Pl8	Pl9	Pl10	Pl11	Pl12	Pl13	Pl14	Pl15	Pl16	Pl17	Pl18	Pl19	Pl20
SiO2	63.09	62.97	63.19	62.60	63.42	62.69	63.62	62.86	62.85	62.60	62.84	63.40	62.53	63.98	61.92
Al2O3	22.56	22.67	23.63	22.91	23.07	23.14	22.76	23.00	23.02	22.97	22.66	22.81	23.04	23.26	23.04
CaO	3.77	3.72	4.50	4.04	4.16	4.36	3.60	4.34	4.24	4.33	4.02	3.91	4.20	4.20	4.15
Na2O	9.51	9.58	9.20	9.26	9.38	9.22	9.56	9.21	9.39	9.35	9.43	9.48	9.35	9.43	9.22
K2O	0.00	0.00	0.00	0.15	0.00	0.00	0.00	0.00	0.00	0.00	0.00	0.00	0.00	0.00	0.00
TOTAL	98.93	98.93	100.51	98.95	100.02	99.40	99.55	99.40	99.50	99.24	98.95	99.59	99.11	100.86	98.33
CATIONS															
Si	2.815	2.810	2.779	2.796	2.800	2.788	2.818	2.794	2.793	2.790	2.805	2.810	2.789	2.800	2.783
Al	1.186	1.192	1.225	1.206	1.201	1.213	1.188	1.205	1.206	1.207	1.192	1.192	1.211	1.200	1.221
Ca	0.180	0.178	0.212	0.193	0.197	0.208	0.171	0.207	0.202	0.207	0.192	0.186	0.201	0.197	0.200
Na	0.823	0.829	0.785	0.802	0.803	0.795	0.821	0.794	0.809	0.808	0.817	0.814	0.809	0.800	0.803
K	0.000	0.000	0.000	0.008	0.000	0.000	0.000	0.000	0.000	0.000	0.000	0.000	0.000	0.000	0.000
(O)	8	8	8	8	8	8	8	8	8	8	8	8	8	8	8
TOTAL	5.004	5.009	5.001	5.005	5.001	5.004	4.998	5.000	5.010	5.012	5.006	5.002	5.010	4.997	5.007

Analyses From Garnet Rims

%OXIDE	Pl1	Pl2	Pl3	Pl4	Pl5
SiO2	62.13	61.82	62.63	62.26	61.88
Al2O3	22.76	23.05	23.55	23.31	22.78
CaO	4.18	4.43	4.41	4.46	4.33
Na2O	9.18	9.11	9.14	9.13	9.22
K2O	0.00	0.00	0.00	0.09	0.00
TOTAL	98.25	98.42	99.74	99.25	98.21
CATIONS					
Si	2.794	2.779	2.776	2.776	2.787
Al	1.207	1.221	1.230	1.225	1.209
Ca	0.201	0.214	0.210	0.213	0.209
Na	0.800	0.794	0.786	0.790	0.805
K	0.000	0.000	0.000	0.005	0.000
(O)	8	8	8	8	8
TOTAL	5.002	5.008	5.002	5.009	5.010

DD.SIN101																		
BIOTITE																		
%OXIDE	Bt1	Bt2	Bt3	Bt4	Bt5	Bt6	Bt7	Bt8	Bt9	Bt10	Bt11	Bt12	BT13	Bt14	Bt15	Bt16	Bt17	Bt18
SiO2	36.79	36.50	36.91	36.75	36.87	36.72	36.82	37.29	36.94	36.69	37.10	36.72	37.25	36.60	36.87	36.67	36.96	37.09
TiO2	1.65	1.65	1.50	1.67	1.61	1.68	1.62	1.64	1.51	1.54	1.58	1.54	1.73	1.67	1.57	1.70	1.61	1.77
Cr2O3	0.00	0.00	0.00	0.00	0.21	0.00	0.00	0.00	0.00	0.00	0.00	0.00	0.19	0.00	0.00	0.00	0.00	0.00
Al2O3	19.18	19.02	19.32	19.11	19.01	19.20	19.03	19.33	19.11	19.06	19.26	18.97	19.53	19.45	18.99	19.05	18.99	19.02
FeO	14.40	15.08	15.04	15.13	15.01	14.43	14.56	14.57	15.18	14.67	14.72	15.20	14.59	14.76	14.86	14.91	15.45	15.47
MnO	0.00	0.00	0.00	0.00	0.00	0.00	0.00	0.00	0.00	0.00	0.00	0.00	0.00	0.00	0.00	0.00	0.00	0.00
MgO	13.31	13.23	13.10	13.21	12.92	13.13	13.26	13.05	12.93	13.26	13.12	13.04	12.83	12.64	12.97	12.68	13.01	13.12
CaO	0.00	0.00	0.00	0.00	0.00	0.00	0.14	0.00	0.00	0.00	0.00	0.00	0.00	0.00	0.00	0.00	0.00	0.00
Na2O	0.86	0.71	0.80	0.79	0.69	0.75	0.74	0.80	0.65	0.67	0.73	0.69	0.70	0.76	0.75	0.59	0.71	0.79
K2O	8.64	8.63	8.66	8.48	8.65	8.64	8.61	8.74	8.74	8.72	8.59	8.60	8.68	8.57	8.55	8.45	8.63	8.49
TOTAL	94.83	94.82	95.32	95.14	94.96	94.55	94.77	95.41	95.06	94.60	95.10	94.75	95.50	94.44	94.55	94.06	95.35	95.75
CATIONS																		
Si	5.461	5.439	5.463	5.451	5.480	5.466	5.473	5.498	5.487	5.468	5.489	5.474	5.485	5.460	5.495	5.491	5.478	5.471
Ti	0.185	0.185	0.167	0.186	0.180	0.188	0.181	0.181	0.169	0.172	0.176	0.172	0.191	0.187	0.176	0.192	0.180	0.197
Cr	0.000	0.000	0.000	0.000	0.024	0.000	0.000	0.000	0.000	0.000	0.000	0.000	0.023	0.000	0.000	0.000	0.000	0.000
Al	3.356	3.341	3.370	3.342	3.330	3.368	3.334	3.360	3.345	3.347	3.360	3.333	3.389	3.420	3.335	3.362	3.317	3.307
Fe2+	1.787	1.879	1.861	1.877	1.866	1.797	1.810	1.796	1.886	1.829	1.821	1.894	1.797	1.841	1.852	1.868	1.916	1.908
Mn	0.000	0.000	0.000	0.000	0.000	0.000	0.000	0.000	0.000	0.000	0.000	0.000	0.000	0.000	0.000	0.000	0.000	0.000
Mg	2.946	2.938	2.891	2.920	2.864	2.914	2.938	2.869	2.862	2.946	2.894	2.897	2.816	2.810	2.881	2.831	2.875	2.884
Ca	0.000	0.000	0.000	0.000	0.000	0.000	0.022	0.000	0.000	0.000	0.000	0.000	0.000	0.000	0.000	0.000	0.000	0.000
Na	0.249	0.205	0.230	0.228	0.198	0.216	0.213	0.229	0.187	0.192	0.209	0.199	0.201	0.220	0.217	0.172	0.203	0.226
K	1.637	1.641	1.635	1.604	1.640	1.640	1.632	1.643	1.657	1.658	1.621	1.634	1.631	1.631	1.626	1.615	1.631	1.598
(O)	22	22	22	22	22	22	22	22	22	22	22	22	22	22	22	22	22	22
TOTAL	15.621	15.628	15.617	15.608	15.582	15.589	15.603	15.576	15.593	15.612	15.570	15.603	15.533	15.569	15.582	15.531	15.600	15.591
Mg#	0.62	0.61	0.61	0.61	0.61	0.62	0.62	0.62	0.60	0.62	0.61	0.60	0.61	0.60	0.61	0.60	0.60	0.60
STAUROLITE																		
%OXIDE	St1	St2	St3	St4	St5	St6	St7	St8	St9	St10	St11	St12	St13	St14	St15	St16	St17	
SiO2	27.24	27.36	27.33	27.53	27.91	27.61	27.45	27.52	27.37	27.31	27.70	27.43	27.54	27.64	27.70	27.12	27.01	
TiO2	0.82	0.66	0.82	0.68	0.67	0.36	0.69	0.63	0.72	0.64	0.52	0.68	0.65	0.62	0.56	0.68	0.66	
Al2O3	52.81	52.89	52.78	53.41	53.67	53.23	53.28	53.41	52.88	52.52	53.46	53.08	52.86	52.90	52.91	52.43	52.98	
FeO	13.29	13.31	12.98	13.18	13.17	12.96	13.00	12.49	13.11	13.30	12.75	12.99	13.04	12.97	12.97	13.14	13.01	
MnO	0.00	0.00	0.00	0.00	0.00	0.00	0.00	0.00	0.00	0.00	0.00	0.00	0.00	0.00	0.00	0.00	0.00	
MgO	2.41	2.12	2.15	2.35	2.61	2.53	2.21	2.25	2.18	2.19	2.41	2.26	2.37	2.30	2.32	2.07	1.98	
CaO	0.00	0.00	0.00	0.00	0.00	0.00	0.12	0.00	0.00	0.00	0.00	0.00	0.00	0.00	0.00	0.00	0.00	
ZnO	0.73	0.64	0.51	0.62	0.52	0.77	0.70	0.65	0.89	0.77	0.58	0.48	0.53	0.74	0.81	0.84	0.56	
TOTAL	97.30	96.98	96.57	97.76	98.54	97.47	97.45	96.94	97.14	96.73	97.42	96.92	96.99	97.16	97.27	96.28	96.20	
CATIONS																		
Si	7.956	8.009	8.017	7.984	8.023	8.029	7.987	8.020	8.001	8.023	8.039	8.013	8.042	8.061	8.074	8.003	7.957	
Ti	0.180	0.145	0.180	0.148	0.144	0.079	0.152	0.137	0.157	0.141	0.114	0.150	0.143	0.136	0.123	0.152	0.147	
Al	18.183	18.248	18.249	18.261	18.182	18.246	18.275	18.350	18.224	18.185	18.290	18.276	18.199	18.188	18.175	18.237	18.398	
Fe2+	3.248	3.259	3.184	3.197	3.166	3.153	3.164	3.046	3.205	3.268	3.094	3.173	3.185	3.164	3.161	3.243	3.207	
Mn	0.000	0.000	0.000	0.000	0.000	0.000	0.000	0.000	0.000	0.000	0.000	0.000	0.000	0.000	0.000	0.000	0.000	
Mg	1.049	0.923	0.939	1.016	1.116	1.097	0.959	0.976	0.948	0.960	1.043	0.983	1.033	1.000	1.007	0.910	0.868	
Ca	0.000	0.000	0.000	0.000	0.000	0.000	0.038	0.000	0.000	0.000	0.000	0.000	0.000	0.000	0.000	0.000	0.000	
Zn	0.157	0.138	0.110	0.132	0.110	0.166	0.150	0.139	0.193	0.166	0.124	0.104	0.114	0.159	0.174	0.182	0.122	
(O)	48	48	48	48	48	48	48	48	48	48	48	48	48	48	48	48	48	
TOTAL	30.773	30.722	30.679	30.738	30.741	30.770	30.725	30.668	30.728	30.743	30.704	30.699	30.716	30.708	30.714	30.727	30.699	
Mg#	0.24	0.22	0.23	0.24	0.26	0.26	0.23	0.24	0.23	0.23	0.25	0.24	0.24	0.24	0.24	0.22	0.21	

PROBE DATA FROM PELITIC HORNFELSES

DD.BQ17

GARNET With Fe3+ Recalculations

%OXIDE	Grt1	Grt1	Grt2	Grt2	Grt3	Grt3	Grt4	Grt4	Grt5	Grt5	Grt6	Grt6	Grt7	Grt7	Grt8	Grt8	Grt9	Grt9
SiO2	37.84	37.84	37.91	37.91	37.71	37.71	37.74	37.74	38.01	38.01	38.00	38.00	37.75	37.75	37.82	37.82	37.85	37.85
TiO2	0.02	0.02	0.03	0.03	0.04	0.04	0.07	0.07	0.04	0.04	0.10	0.10	0.18	0.18	0.16	0.16	0.12	0.12
Cr2O3	0.16	0.16	0.06	0.06	0.00	0.00	0.06	0.06	0.07	0.07	0.14	0.14	0.21	0.21	0.06	0.06	0.16	0.16
Al2O3	21.21	21.21	21.36	21.36	21.33	21.33	21.33	21.33	21.74	21.74	21.53	21.53	21.33	21.33	21.61	21.61	21.45	21.45
Fe2O3	-	0.71	-	0.18	-	0.88	-	1.24	-	1.51	-	0.66	-	0.91	-	0.84	-	0.08
FeO	32.10	31.47	32.04	31.88	32.36	31.57	32.30	31.19	32.51	31.16	32.34	31.74	32.21	31.39	32.42	31.67	32.19	32.12
MnO	0.60	0.60	0.66	0.66	0.69	0.69	0.61	0.61	0.62	0.62	0.44	0.44	0.53	0.53	0.51	0.51	0.44	0.44
MgO	6.65	6.65	6.47	6.47	6.43	6.43	6.63	6.63	6.93	6.93	6.70	6.70	6.65	6.65	6.67	6.67	6.57	6.57
CaO	1.03	1.03	0.99	0.99	1.01	1.01	1.21	1.21	1.03	1.03	1.08	1.08	1.21	1.21	1.02	1.02	0.97	0.97
TOTAL	99.61	99.68	99.50	99.52	99.57	99.66	99.94	100.07	100.95	101.10	100.33	100.40	100.05	100.14	100.27	100.35	99.74	99.75
CATIONS																		
Si	5.984	5.974	5.996	5.993	5.975	5.962	5.955	5.937	5.934	5.912	5.963	5.953	5.949	5.936	5.943	5.931	5.972	5.968
Ti	0.003	0.003	0.003	0.003	0.005	0.005	0.008	0.008	0.005	0.005	0.012	0.012	0.021	0.021	0.019	0.019	0.014	0.014
Cr	0.020	0.020	0.007	0.007	0.000	0.000	0.007	0.007	0.008	0.008	0.017	0.017	0.026	0.026	0.007	0.007	0.019	0.019
Al	3.953	3.946	3.981	3.979	3.984	3.975	3.968	3.956	4.000	3.985	3.983	3.977	3.961	3.952	4.002	3.994	3.990	3.988
Fe3+	-	0.084	-	0.021	-	0.105	-	0.147	-	0.176	-	0.078	-	0.108	-	0.099	-	0.010
Fe2+	4.246	4.155	4.238	4.215	4.288	4.174	4.264	4.104	4.245	4.053	4.244	4.159	4.244	4.127	4.261	4.153	4.248	4.215
Mn	0.080	0.080	0.088	0.088	0.093	0.093	0.082	0.082	0.082	0.082	0.059	0.059	0.070	0.070	0.068	0.068	0.058	0.058
Mg	1.567	1.564	1.526	1.525	1.518	1.515	1.560	1.555	1.612	1.606	1.566	1.563	1.561	1.557	1.561	1.558	1.546	1.545
Ca	0.175	0.175	0.168	0.168	0.172	0.172	0.205	0.204	0.173	0.172	0.182	0.182	0.204	0.204	0.172	0.172	0.163	0.163
(O)	24	24	24	24	24	24	24	24	24	24	24	24	24	24	24	24	24	24
TOTAL	16.028	16.000	16.007	16.000	16.035	16.000	16.049	16.000	16.059	16.000	16.026	16.000	16.036	16.000	16.033	16.000	16.010	16.000
Mg#	0.27	0.27	0.26	0.27	0.26	0.27	0.27	0.27	0.28	0.28	0.27	0.27	0.27	0.27	0.27	0.27	0.27	0.27

GARNET With Fe3+ Recalculations

%OXIDE	Grt10	Grt10	Grt11	Grt11	Grt12	Grt12	Grt13	Grt13	Grt14	Grt14	Grt15	Grt16	Grt16
SiO2	37.69	37.69	37.67	37.67	37.92	37.92	37.81	37.81	38.14	38.14	37.98	37.43	37.43
TiO2	0.15	0.15	0.11	0.11	0.00	0.00	0.02	0.02	0.10	0.10	0.09	0.11	0.11
Cr2O3	0.11	0.11	0.06	0.06	0.06	0.06	0.15	0.15	0.19	0.19	0.02	0.14	0.14
Al2O3	21.35	21.35	21.42	21.42	21.61	21.61	21.55	21.55	21.60	21.60	21.26	21.46	21.46
Fe2O3	-	0.93	-	0.58	-	0.35	-	0.99	-	0.66	-	-	0.85
FeO	32.11	31.27	32.26	31.74	32.16	31.84	32.48	31.59	32.50	31.90	32.03	32.08	31.32
MnO	0.71	0.71	0.59	0.59	0.40	0.40	0.48	0.48	0.65	0.65	0.52	0.53	0.53
MgO	6.63	6.63	6.44	6.44	6.59	6.59	6.58	6.58	6.63	6.63	6.38	6.52	6.52
CaO	1.09	1.09	1.02	1.02	1.03	1.03	1.08	1.08	1.04	1.04	1.13	1.08	1.08
TOTAL	99.85	99.95	99.57	99.63	99.77	99.80	100.15	100.24	100.84	100.91	99.42	99.36	99.44
CATIONS													
Si	5.951	5.937	5.963	5.954	5.976	5.971	5.952	5.938	5.961	5.951	6.010	5.938	5.925
Ti	0.018	0.018	0.013	0.013	0.000	0.000	0.002	0.002	0.011	0.011	0.011	0.013	0.013
Cr	0.014	0.014	0.007	0.007	0.008	0.008	0.019	0.019	0.023	0.023	0.003	0.017	0.017
Al	3.973	3.964	3.996	3.990	4.015	4.011	3.998	3.988	3.979	3.973	3.965	4.012	4.003
Fe3+	-	0.111	-	0.069	-	0.042	-	0.117	-	0.078	-	-	0.102
Fe2+	4.240	4.119	4.271	4.196	4.239	4.193	4.276	4.149	4.247	4.162	4.239	4.257	4.146
Mn	0.095	0.095	0.079	0.079	0.054	0.054	0.064	0.064	0.086	0.086	0.069	0.072	0.072
Mg	1.561	1.557	1.520	1.518	1.548	1.547	1.545	1.541	1.545	1.542	1.505	1.541	1.538
Ca	0.185	0.185	0.174	0.174	0.174	0.174	0.183	0.183	0.174	0.174	0.192	0.184	0.184
(O)	24	24	24	24	24	24	24	24	24	24	24	24	24
TOTAL	16.037	16.000	16.023	16.000	16.014	16.000	16.039	16.000	16.026	16.000	15.994	16.034	16.000
Mg#	0.27	0.27	0.26	0.27	0.27	0.27	0.27	0.27	0.27	0.27	0.26	0.27	0.27

ILMENITE

%OXIDE	ILM1	ILM2	ILM3
SiO2	0.29	0.30	0.30
TiO2	50.56	50.24	51.39
MnO	0.00	0.00	0.00
MgO	0.66	0.49	0.59
CaO	0.05	0.04	0.03
FeO	46.48	47.40	47.37
TOTAL	98.05	98.47	99.68
CATIONS			
Si	0.007	0.008	0.008
Ti	0.979	0.972	0.979
Mn	0.000	0.000	0.000
Mg	0.025	0.019	0.022
Ca	0.002	0.001	0.001
Fe	1.001	1.020	1.004
(O)	3	3	3
TOTAL	2.014	2.02	2.014

%OXIDE	Crd1	Crd2	Crd3	Crd4	Crd5	Crd6	Crd7	Crd8	Crd9	Crd10	Crd11
SiO2	48.00	48.53	48.78	48.35	47.77	47.91	48.64	48.71	49.34	49.06	48.54
TiO2	0.00	0.07	0.06	0.02	0.00	0.00	0.00	0.00	0.00	0.00	0.09
Al2O3	32.39	32.90	32.66	32.61	32.37	32.75	32.57	33.21	33.37	33.01	32.79
Cr2O3	0.05	0.00	0.00	0.00	0.07	0.00	0.03	0.03	0.00	0.00	0.02
Fe2O3	-	-	-	-	-	-	-	-	-	-	-
FeO	8.49	8.68	8.70	8.28	8.76	8.70	8.45	7.21	7.04	9.14	8.93
MnO	0.00	0.00	0.13	0.03	0.00	0.00	0.00	0.00	0.00	0.00	0.00
MgO	8.33	8.56	8.28	8.59	8.45	8.54	8.53	9.59	10.01	8.32	8.28
TOTAL	97.25	98.76	98.61	97.87	97.41	97.90	98.21	98.75	99.76	99.52	98.65
CATIONS											
Si	4.999	4.981	5.014	4.998	4.977	4.964	5.013	4.968	4.975	5.004	4.991
Ti	0.000	0.006	0.005	0.001	0.000	0.000	0.000	0.000	0.000	0.000	0.007
Al	3.976	3.980	3.957	3.973	3.975	3.999	3.956	3.992	3.967	3.970	3.975
Cr	0.004	0.000	0.000	0.000	0.005	0.000	0.002	0.003	0.000	0.000	0.000
Fe3+	-	-	-	-	-	-	-	-	-	-	-
Fe2+	0.739	0.745	0.748	0.716	0.763	0.754	0.728	0.615	0.594	0.780	0.768
Mn	0.000	0.000	0.010	0.002	0.000	0.000	0.000	0.000	0.000	0.000	0.000
Mg	1.293	1.31	1.268	1.324	1.312	1.32	1.31	1.458	1.505	1.265	1.269
(O)	18	18	18	18	18	18	18	18	18	18	18
TOTAL	11.011	11.022	11.002	11.014	11.032	11.037	11.009	11.036	11.041	11.019	11.010
Mg#	0.64	0.64	0.63	0.65	0.63	0.64	0.64	0.70	0.72	0.62	0.62

K-FELDSPAR

%OXIDE	Kfs1	Kfs2	Kfs3
SiO2	64.20	62.37	62.78
Al2O3	19.15	18.88	19.01
CaO	0.47	0.38	0.41
Na2O	1.21	0.93	0.96
K2O	14.41	14.27	14.41
TOTAL	99.44	96.82	97.57
CATIONS			
Si	2.955	2.961	2.959
Al	1.039	1.056	1.056
Ca	0.023	0.019	0.021
Na	0.108	0.085	0.088
K	0.846	0.864	0.867
(O)	8	8	8
TOTAL	4.971	4.985	4.991

PLAGIOCLASE

%OXIDE	Pl1	Pl2	Pl3	Pl4	Pl5	Pl6	Pl7	Pl8	Pl9	Pl10	Pl11	Pl12	Pl13	Pl14	Pl15
SiO2	58.97	60.33	57.95	59.29	57.95	58.24	58.25	58.28	58.72	58.24	59.27	58.83	57.68	59.84	59.09
Al2O3	25.67	26.23	26.46	26.04	25.72	25.87	25.78	25.94	25.71	25.88	25.86	25.80	27.32	26.06	26.08
CaO	7.45	7.37	8.44	7.56	7.95	7.91	7.67	7.88	7.60	7.90	7.77	7.96	9.11	7.53	7.99
Na2O	7.07	7.16	6.58	6.99	6.71	6.81	6.85	6.88	6.94	6.74	6.78	6.77	6.10	7.10	6.88
K2O	0.59	0.71	0.40	0.55	0.41	0.31	0.37	0.38	0.50	0.48	0.62	0.53	0.47	0.53	0.41
TOTAL	99.76	101.79	99.82	100.42	98.73	99.14	98.92	99.36	99.46	99.23	100.31	99.89	100.68	101.05	100.44
CATIONS															
Si	2.642	2.647	2.599	2.637	2.624	2.625	2.630	2.623	2.638	2.624	2.641	2.634	2.569	2.644	2.629
Al	1.356	1.356	1.399	1.365	1.373	1.374	1.372	1.376	1.361	1.375	1.358	1.361	1.434	1.357	1.368
Ca	0.357	0.346	0.406	0.360	0.386	0.382	0.371	0.380	0.366	0.381	0.371	0.382	0.435	0.356	0.381
Na	0.615	0.609	0.572	0.603	0.589	0.595	0.600	0.600	0.604	0.589	0.586	0.587	0.527	0.609	0.594
K	0.034	0.040	0.023	0.031	0.023	0.018	0.021	0.022	0.029	0.027	0.035	0.030	0.027	0.030	0.023
(O)	8	8	8	8	8	8	8	8	8	8	8	8	8	8	8
TOTAL	5.004	4.998	4.999	4.996	4.995	4.994	4.994	5.001	4.998	4.996	4.991	4.994	4.992	4.996	4.995

DD.BQ17																		
ORTHOPYROXENE With Fe3+ Recalculations																		
OXIDE%	Opx1	Opx1	Opx2	Opx2	Opx3	Opx3	Opx4	Opx4	Opx5	Opx5	Opx6	Opx6	Opx7	Opx7	Opx8	Opx8	Opx9	Opx9
SiO2	46.74	46.74	47.04	47.04	48.49	48.49	47.85	47.85	46.74	46.74	48.02	48.02	47.05	47.05	46.69	46.69	47.48	47.48
TiO2	0.25	0.25	0.36	0.36	0.22	0.22	0.10	0.10	0.31	0.31	0.25	0.25	0.19	0.19	0.25	0.25	0.14	0.14
Cr2O3	0.07	0.07	0.08	0.08	0.00	0.00	0.21	0.21	0.22	0.22	0.09	0.09	0.17	0.17	0.18	0.18	0.11	0.11
Al2O3	5.62	5.62	6.00	6.00	3.57	3.57	4.59	4.59	5.96	5.96	6.28	6.28	5.32	5.32	6.03	6.03	5.74	5.74
Fe2O3	-	1.60	-	0.47	-	1.07	-	1.74	-	1.14	-	1.45	-	1.48	-	1.34	-	0.54
FeO	32.18	30.74	31.76	31.34	32.47	31.51	32.16	30.59	31.90	30.87	29.82	28.51	32.34	31.02	31.79	30.59	31.72	31.23
MnO	0.00	0.00	0.00	0.00	0.00	0.00	0.00	0.00	0.05	0.05	0.00	0.00	0.00	0.00	0.00	0.00	0.00	0.00
MgO	13.55	13.55	13.58	13.58	14.30	14.30	14.18	14.18	13.73	13.73	15.90	15.90	13.87	13.87	13.64	13.64	14.01	14.01
CaO	0.13	0.13	0.14	0.14	0.15	0.15	0.07	0.07	0.16	0.16	0.10	0.10	0.12	0.12	0.14	0.14	0.10	0.10
TOTAL	98.54	98.70	98.94	98.99	99.20	99.30	99.15	99.32	99.07	99.18	100.45	100.60	99.06	99.21	98.71	98.85	99.29	99.34
CATIONS																		
Si	1.865	1.854	1.859	1.856	1.921	1.913	1.896	1.884	1.849	1.841	1.849	1.839	1.865	1.855	1.855	1.846	1.867	1.863
Ti	0.008	0.008	0.011	0.011	0.006	0.006	0.003	0.003	0.009	0.009	0.007	0.007	0.006	0.006	0.007	0.007	0.004	0.004
Cr	0.002	0.002	0.002	0.002	0.000	0.000	0.006	0.006	0.007	0.007	0.003	0.003	0.005	0.005	0.006	0.006	0.003	0.003
Al	0.264	0.262	0.279	0.279	0.162	0.161	0.215	0.214	0.278	0.277	0.285	0.284	0.249	0.248	0.282	0.281	0.266	0.265
Fe3+	-	0.048	-	0.014	-	0.032	-	0.052	-	0.034	-	0.042	-	0.044	-	0.040	-	0.016
Fe2+	1.074	1.020	1.050	1.034	1.076	1.040	1.066	1.007	1.055	1.017	0.960	0.913	1.072	1.022	1.056	1.011	1.043	1.025
Mn	0.000	0.000	0.000	0.000	0.000	0.000	0.000	0.000	0.002	0.002	0.000	0.000	0.000	0.000	0.000	0.000	0.000	0.000
Mg	0.806	0.801	0.800	0.799	0.844	0.841	0.837	0.832	0.810	0.807	0.913	0.908	0.820	0.816	0.808	0.804	0.821	0.819
Ca	0.005	0.005	0.006	0.006	0.007	0.007	0.003	0.003	0.007	0.007	0.004	0.004	0.005	0.005	0.006	0.006	0.004	0.004
(O)	6	6	6	6	6	6	6	6	6	6	6	6	6	6	6	6	6	6
TOTAL	4.024	4.000	4.007	4.000	4.016	4.000	4.026	4.000	4.017	4.000	4.021	4.000	4.022	4.000	4.020	4.000	4.008	4.000

ORTHOPYROXENE With Fe3+ Recalculations						
OXIDE%	Opx10	Opx10	Opx11	Opx11	Opx12	Opx12
SiO2	47.10	47.10	47.21	47.21	46.65	46.65
TiO2	0.27	0.27	0.30	0.30	0.28	0.28
Cr2O3	0.09	0.09	0.21	0.21	0.18	0.18
Al2O3	5.97	5.97	5.58	5.58	6.05	6.05
Fe2O3	-	1.01	-	2.31	-	3.33
FeO	32.17	31.26	32.48	30.40	32.60	29.60
MnO	0.00	0.00	0.00	0.00	0.00	0.00
MgO	13.74	13.74	13.69	13.69	13.78	13.78
CaO	0.06	0.06	0.18	0.18	0.12	0.12
TOTAL	99.40	99.50	100.22	99.87	100.38	99.99
CATIONS						
Si	1.857	1.850	1.848	1.832	1.826	1.804
Ti	0.008	0.008	0.009	0.009	0.008	0.008
Cr	0.003	0.003	0.006	0.006	0.005	0.005
Al	0.277	0.276	0.257	0.255	0.279	0.276
Fe3+	-	0.030	-	0.067	-	0.097
Fe2+	1.061	1.027	1.063	0.987	1.067	0.957
Mn	0.000	0.000	0.000	0.000	0.000	0.000
Mg	0.807	0.804	0.799	0.792	0.804	0.794
Ca	0.002	0.002	0.008	0.008	0.005	0.005
(O)	6	6	6	6	6	6
TOTAL	4.015	4.000	4.034	3.956	4.049	3.946

SPINEL With Fe3+ Recalculations								
%OXIDE	Spl1	Spl1	Spl2	Spl2	Spl3	Spl3	Spl4	Spl4
SiO2	0.10	0.10	0.37	0.37	0.15	0.15	0.21	0.21
TiO2	0.12	0.12	0.10	0.10	0.00	0.00	0.12	0.12
Cr2O3	0.54	0.54	0.74	0.74	0.40	0.40	0.90	0.90
Al2O3	57.57	57.57	56.72	56.72	56.74	56.74	57.64	57.64
Fe2O3	-	3.62	-	3.11	-	4.47	-	4.01
FeO	32.90	29.63	32.16	29.36	33.89	29.87	33.41	29.80
MnO	0.00	0.00	0.00	0.00	0.00	0.00	0.00	0.00
MgO	5.93	5.93	6.17	6.17	6.00	6.00	5.81	5.81
ZnO	2.73	2.73	2.82	2.82	2.36	2.36	2.32	2.32
TOTAL	99.88	100.24	99.06	99.37	99.54	99.99	100.41	100.81
CATIONS								
Si	0.003	0.003	0.010	0.010	0.004	0.004	0.006	0.006
Ti	0.003	0.003	0.002	0.002	0.000	0.000	0.003	0.003
Cr	0.012	0.012	0.017	0.017	0.009	0.009	0.020	0.020
Al	1.923	1.905	1.907	1.891	1.909	1.886	1.920	1.900
Fe3+	-	0.077	-	0.066	-	0.095	-	0.084
Fe2+	0.780	0.696	0.767	0.695	0.809	0.705	0.790	0.697
Mn	0.000	0.000	0.000	0.000	0.000	0.000	0.000	0.000
Mg	0.251	0.249	0.263	0.261	0.255	0.252	0.245	0.242
Zn	0.057	0.056	0.059	0.059	0.050	0.049	0.048	0.047
(O)	4	4	4	4	4	4	4	4
TOTAL	3.029	3.000	3.025	3.000	3.036	3.000	3.032	3.000

DD.BQ41

GARNET

%OXIDE	Grt1	Grt2	Grt3	Grt4	Grt5	Grt6	Grt7	Grt8	Grt9	Grt10	Grt11	Grt12
SiO2	37.66	37.78	37.64	37.58	37.66	38.21	37.89	38.05	38.21	38.24	37.90	37.55
TiO2	0.11	0.10	0.15	0.12	0.20	0.09	0.14	0.14	0.06	0.18	0.18	0.15
Cr2O3	0.16	0.00	0.16	0.00	0.00	0.00	0.14	0.08	0.08	0.00	0.09	0.09
Al2O3	21.23	21.42	20.93	21.32	21.01	21.48	21.24	21.40	21.47	21.64	21.30	21.46
FeO	33.77	34.11	33.73	33.77	34.55	34.48	33.78	33.96	33.84	33.69	33.52	32.68
MnO	0.36	0.17	0.17	0.23	0.00	0.32	0.18	0.17	0.19	0.11	0.23	0.17
MgO	5.93	6.19	5.84	6.11	5.96	6.13	6.43	6.18	6.23	6.51	6.01	6.40
CaO	0.61	0.60	0.69	0.63	0.65	0.62	0.60	0.69	0.65	0.62	0.72	0.57
TOTAL	99.83	100.36	99.29	99.76	100.03	101.32	100.39	100.66	100.73	100.98	99.94	99.05
CATIONS												
Si	5.976	5.961	6.003	5.963	5.976	5.977	5.969	5.978	5.993	5.974	5.992	5.968
Ti	0.013	0.012	0.018	0.014	0.023	0.011	0.016	0.016	0.007	0.021	0.021	0.018
Cr	0.020	0.000	0.020	0.000	0.000	0.000	0.017	0.010	0.010	0.000	0.011	0.011
Al	3.970	3.984	3.934	3.987	3.930	3.961	3.944	3.964	3.969	3.984	3.970	4.020
Fe2+	4.481	4.500	4.499	4.482	4.585	4.511	4.452	4.463	4.439	4.401	4.433	4.344
Mn	0.049	0.022	0.022	0.031	0.000	0.042	0.025	0.022	0.025	0.014	0.031	0.023
Mg	1.403	1.455	1.388	1.446	1.410	1.428	1.509	1.448	1.457	1.515	1.416	1.516
Ca	0.104	0.101	0.118	0.106	0.111	0.103	0.101	0.117	0.110	0.104	0.122	0.097
(O)	24	24	24	24	24	24	24	24	24	24	24	24
TOTAL	16.016	16.035	16.002	16.029	16.035	16.033	16.033	16.018	16.010	16.013	15.996	15.997
Mg#	0.24	0.24	0.24	0.24	0.24	0.24	0.25	0.24	0.25	0.26	0.24	0.26

CORDIERITE

OXIDE%	Crd1	Crd2	Crd3	Crd4	Crd5
SiO2	49.24	49.60	48.48	48.69	48.86
TiO2	0.08	0.00	0.00	0.00	0.00
Cr2O3	0.00	0.00	0.00	0.00	0.00
Al2O3	33.15	33.43	33.06	32.55	32.96
FeO	9.29	8.94	9.45	8.98	8.68
MnO	0.00	0.00	0.00	0.00	0.00
MgO	8.22	8.83	8.24	8.04	8.26
TOTAL	99.97	100.80	99.23	98.26	98.76
CATIONS					
Si	5.001	4.989	4.970	5.024	5.009
Ti	0.006	0.000	0.000	0.000	0.000
Cr	0.000	0.000	0.000	0.000	0.000
Al	3.968	3.964	3.994	3.959	3.983
Fe	0.789	0.752	0.810	0.775	0.744
Mn	0.000	0.000	0.000	0.000	0.000
Mg	1.245	1.324	1.259	1.237	1.263
(O)	18	18	18	18	18
TOTAL	11.009	11.029	11.033	10.995	10.999
Mg#	0.61	0.64	0.61	0.61	0.63

ORTHOCLASE

%OXIDE	Opx1	Opx2	Opx3	Opx4	Opx5	Opx6	Opx7	Opx8	Opx9	Opx10	Opx11	Opx12	Opx13
SiO2	46.16	46.82	47.63	47.48	46.92	47.35	47.06	47.43	47.15	46.81	47.31	47.80	46.88
TiO2	0.33	0.41	0.25	0.19	0.24	0.24	0.26	0.27	0.24	0.18	0.18	0.30	0.22
Al2O2	6.94	6.53	5.51	5.71	6.15	5.71	5.68	5.67	5.15	6.04	5.43	5.48	5.73
Cr2O3	0.16	0.17	0.17	0.16	0.08	0.06	0.14	0.08	0.07	0.12	0.05	0.12	0.20
FeO	33.37	32.73	33.27	33.20	33.66	33.91	33.36	33.94	33.33	32.91	33.26	33.05	33.11
MnO	0.00	0.00	0.00	0.00	0.00	0.00	0.00	0.00	0.00	0.00	0.00	0.00	0.00
MgO	13.00	13.03	13.46	13.14	12.84	13.00	13.01	13.10	13.19	13.02	13.17	13.56	13.11
CaO	0.11	0.05	0.07	0.07	0.07	0.14	0.14	0.03	0.06	0.06	0.05	0.09	0.02
TOTAL	100.07	99.74	100.37	99.94	99.96	100.41	99.64	100.50	99.19	99.13	99.44	100.40	99.25
CATIONS													
Si	1.814	1.838	1.861	1.863	1.845	1.856	1.856	1.856	1.868	1.851	1.867	1.864	1.854
Ti	0.010	0.012	0.007	0.006	0.007	0.007	0.008	0.008	0.007	0.005	0.005	0.009	0.006
Al	0.321	0.302	0.254	0.264	0.285	0.264	0.264	0.261	0.241	0.282	0.252	0.252	0.267
Cr	0.005	0.005	0.005	0.005	0.002	0.002	0.004	0.002	0.002	0.003	0.001	0.004	0.006
Fe2+	1.097	1.075	1.087	1.089	1.107	1.111	1.100	1.111	1.104	1.088	1.098	1.078	1.095
Mn	0.000	0.000	0.000	0.000	0.000	0.000	0.000	0.000	0.000	0.000	0.000	0.000	0.000
Mg	0.761	0.762	0.784	0.768	0.753	0.759	0.765	0.764	0.779	0.768	0.775	0.788	0.773
Ca	0.005	0.002	0.003	0.003	0.003	0.006	0.006	0.001	0.003	0.003	0.002	0.004	0.001
(O)	6	6	6	6	6	6	6	6	6	6	6	6	6
TOTAL	4.013	3.996	4.001	3.998	4.002	4.005	4.003	4.003	4.004	4.001	4.000	3.999	4.002
Mg#	0.41	0.41	0.42	0.41	0.40	0.41	0.41	0.41	0.41	0.41	0.41	0.42	0.41

ANORTHOCLASE

%OXIDE	Anc1	Anc2	Anc3	Anc4	Anc5	Anc6	Anc7	Anc8
SiO2	64.27	64.74	64.53	64.89	64.86	64.55	64.20	65.23
Al2O3	20.91	21.11	20.78	19.99	21.29	20.41	20.03	20.90
CaO	2.02	2.12	2.17	1.41	2.40	1.76	1.39	2.07
Na2O	6.61	7.65	7.39	5.26	9.26	6.29	4.84	7.66
K2O	5.37	4.11	4.25	7.90	1.73	6.53	8.64	4.04
TOTAL	99.18	99.73	99.11	99.45	99.55	99.55	99.09	99.90
CATIONS								
Si	2.897	2.892	2.900	2.937	2.882	2.912	2.926	2.905
Al	1.111	1.111	1.101	1.066	1.115	1.085	1.076	1.097
Ca	0.098	0.102	0.104	0.069	0.114	0.085	0.068	0.099
Na	0.578	0.662	0.644	0.461	0.798	0.550	0.428	0.661
K	0.309	0.234	0.244	0.456	0.098	0.376	0.502	0.230
(O)	8	8	8	8	8	8	8	8
TOTAL	4.993	5.001	4.993	4.989	5.007	5.008	5.000	4.992

H.BHQ5

GARNET With Fe3+ Recalculations

%OXIDE	Grt1	Grt2	Grt2	Grt3	Grt3	Grt4	Grt4	Grt5	Grt5	Grt6	Grt6	Grt7	Grt7	Grt8	Grt8	Grt9	Grt9	Grt10	Grt10
SiO2	38.47	38.38	38.38	38.32	38.32	38.34	38.34	38.01	38.01	37.42	37.42	37.80	37.80	37.94	37.94	37.94	37.94	38.04	38.04
TiO2	0.00	0.03	0.03	0.00	0.00	0.06	0.06	0.02	0.02	0.02	0.02	0.11	0.11	0.13	0.13	0.05	0.05	0.07	0.07
Cr2O3	0.06	0.09	0.09	0.17	0.17	0.19	0.19	0.23	0.23	0.19	0.19	0.13	0.13	0.03	0.03	0.06	0.06	0.08	0.08
Al2O3	21.44	21.42	21.42	21.91	21.91	21.44	21.44	21.48	21.48	21.57	21.57	21.54	21.54	21.63	21.63	21.83	21.83	22.03	22.03
Fe2O3	0.00	-	0.23	-	1.00	-	0.69	-	0.61	-	1.28	-	0.38	-	0.58	-	0.38	-	0.82
FeO	32.43	32.39	32.18	32.63	31.73	33.10	32.48	32.50	31.96	31.80	30.65	31.93	31.59	31.42	30.90	31.67	31.33	32.24	31.50
MnO	0.76	0.84	0.84	0.64	0.64	0.67	0.67	0.70	0.70	0.86	0.86	0.60	0.60	0.86	0.86	0.75	0.75	0.66	0.66
MgO	6.16	6.22	6.22	6.48	6.48	6.21	6.21	6.40	6.40	6.51	6.51	6.51	6.51	6.74	6.74	6.53	6.53	6.48	6.48
CaO	1.40	1.40	1.40	1.47	1.47	1.31	1.31	1.09	1.09	1.28	1.28	1.17	1.17	1.31	1.31	1.32	1.32	1.40	1.40
TOTAL	100.71	100.75	100.77	101.62	101.72	101.31	101.38	100.42	100.48	99.65	99.78	99.80	99.84	100.07	100.12	100.15	100.19	100.99	101.07
CATIONS																			
Si	6.020	6.007	6.004	5.947	5.933	5.982	5.972	5.972	5.963	5.922	5.903	5.962	5.956	5.958	5.949	5.955	5.949	5.932	5.920
Ti	0.000	0.004	0.004	0.000	0.000	0.006	0.006	0.002	0.002	0.002	0.002	0.012	0.012	0.016	0.016	0.006	0.006	0.008	0.008
Cr	0.007	0.011	0.011	0.021	0.021	0.023	0.023	0.028	0.028	0.024	0.024	0.017	0.017	0.004	0.004	0.007	0.007	0.010	0.010
Al	3.955	3.951	3.949	4.009	3.999	3.943	3.936	3.977	3.971	4.024	4.011	4.003	3.999	4.004	3.998	4.039	4.035	4.050	4.042
Fe3+	0.000	-	0.027	-	0.117	-	0.081	-	0.072	-	0.153	-	0.045	-	0.069	-	0.045	-	0.096
Fe2+	4.245	4.240	4.211	4.235	4.108	4.320	4.232	4.270	4.192	4.210	4.044	4.211	4.162	4.127	4.052	4.158	4.109	4.205	4.101
Mn	0.100	0.111	0.111	0.084	0.084	0.089	0.089	0.093	0.093	0.116	0.116	0.081	0.081	0.115	0.115	0.100	0.100	0.087	0.087
Mg	1.437	1.451	1.450	1.499	1.495	1.445	1.443	1.499	1.497	1.536	1.531	1.531	1.530	1.579	1.577	1.528	1.527	1.507	1.504
Ca	0.234	0.234	0.234	0.244	0.243	0.219	0.219	0.183	0.183	0.217	0.216	0.198	0.198	0.220	0.220	0.222	0.222	0.233	0.233
(O)	24	24	24	24	24	24	24	24	24	24	24	24	24	24	24	24	24	24	24
TOTAL	15.998	16.009	16.000	16.039	16.000	16.027	16.000	16.024	16.000	16.051	16.000	16.015	16.000	16.023	16.000	16.015	16.000	16.032	16.000
Mg#	0.25	0.25	0.26	0.26	0.27	0.25	0.25	0.26	0.26	0.27	0.27	0.27	0.27	0.28	0.28	0.27	0.27	0.26	0.27

GARNET With Fe3+ Recalculations

%OXIDE	Grt11	Grt11	Grt12	Grt12	Grt13
SiO2	37.95	37.95	37.87	37.87	38.66
TiO2	0.08	0.06	0.07	0.07	0.19
Cr2O3	0.16	0.16	0.11	0.11	0.20
Al2O3	21.39	21.39	22.04	22.04	21.82
Fe2O3	-	1.30	-	1.66	0.00
FeO	31.92	30.75	32.08	30.58	32.00
MnO	0.66	0.66	0.86	0.86	0.77
MgO	6.91	6.91	6.89	6.89	6.68
CaO	1.31	1.31	1.23	1.23	1.28
TOTAL	100.36	100.49	101.15	101.31	101.60
CATIONS					
Si	5.954	5.935	5.898	5.874	5.980
Ti	0.007	0.007	0.008	0.008	0.021
Cr	0.020	0.020	0.014	0.014	0.024
Al	3.956	3.943	4.047	4.031	3.978
Fe3+	-	0.153	-	0.194	0.000
Fe2+	4.188	4.022	4.179	3.968	4.139
Mn	0.088	0.088	0.113	0.113	0.101
Mg	1.617	1.612	1.601	1.595	1.541
Ca	0.221	0.220	0.205	0.204	0.213
(O)	24	24	24	24	24
TOTAL	16.051	16.000	16.065	16.000	15.997
Mg#	0.28	0.29	0.28	0.29	0.27

ORTHOPYROXENE

%OXIDE	Opx1	Opx2	Opx3	Opx4	Opx5	Opx6	Opx7	Opx8	Opx9	Opx10	Opx11	Opx12
SiO2	48.77	48.68	47.98	49.40	47.82	47.21	47.57	47.12	48.34	49.27	48.86	46.99
TiO2	0.29	0.20	0.33	0.06	0.21	0.30	0.23	0.30	0.00	0.18	0.21	0.29
Cr2O3	0.09	0.00	0.00	0.14	0.15	0.10	0.13	0.04	0.18	0.15	0.19	0.13
Al2O3	6.14	4.84	5.33	4.43	4.61	6.17	5.03	5.90	5.00	4.78	4.90	5.94
FeO	30.39	30.57	30.78	31.70	30.80	31.63	32.23	31.42	32.32	31.21	30.34	31.84
MnO	0.47	0.40	0.56	0.31	0.60	0.00	0.03	0.00	0.00	0.00	0.00	0.00
MgO	14.61	14.58	14.19	14.41	14.93	14.16	13.76	14.11	13.97	14.99	15.64	13.92
CaO	0.12	0.18	0.15	0.08	0.09	0.23	0.15	0.67	0.17	0.11	0.18	0.22
TOTAL	100.87	99.45	99.32	100.54	99.21	99.80	99.12	99.55	99.99	100.69	100.32	99.33
CATIONS												
Si	1.868	1.896	1.877	1.909	1.877	1.843	1.876	1.845	1.886	1.895	1.882	1.847
Ti	0.008	0.006	0.010	0.002	0.006	0.009	0.007	0.009	0.000	0.005	0.006	0.009
Cr	0.003	0.000	0.000	0.004	0.005	0.003	0.004	0.001	0.006	0.004	0.006	0.004
Al	0.277	0.222	0.246	0.202	0.213	0.284	0.234	0.272	0.230	0.217	0.222	0.275
Fe2+	0.973	0.996	1.007	1.025	1.011	1.033	1.063	1.029	1.055	1.004	0.977	1.047
Mn	0.015	0.013	0.019	0.010	0.020	0.000	0.001	0.000	0.000	0.000	0.000	0.000
Mg	0.834	0.846	0.827	0.830	0.873	0.824	0.809	0.824	0.813	0.860	0.898	0.815
Ca	0.005	0.008	0.006	0.003	0.004	0.009	0.006	0.028	0.007	0.005	0.007	0.009
(O)	6	6	6	6	6	6	6	6	6	6	6	6
TOTAL	3.983	3.987	3.992	3.985	4.009	4.005	4.000	4.008	3.997	3.990	3.998	4.006
Mg#	0.46	0.46	0.45	0.45	0.46	0.44	0.43	0.44	0.44	0.46	0.48	0.44

CORDIERITE

%OXIDE	Crd1	Crd2	Crd3	Crd4	Crd5	Crd6	Crd7	Crd8	Crd9	Crd10	Crd11	Crd12	Crd13	Crd14	Crd15	Crd16	Crd17	Crd18
SiO2	48.97	48.87	48.89	48.34	47.89	48.73	47.77	48.57	48.61	48.38	48.44	48.34	48.53	48.57	49.11	49.13	48.87	49.38
TiO2	0.02	0.04	0.00	0.00	0.00	0.00	0.07	0.00	0.02	0.00	0.00	0.00	0.00	0.01	0.00	0.09	0.05	0.02
Al2O3	33.04	33.21	33.07	32.91	32.78	33.16	32.82	33.09	32.87	33.08	33.07	32.63	32.77	33.28	34.07	33.83	33.70	34.20
Cr2O3	0.03	0.00	0.00	0.07	0.04	0.01	0.00	0.00	0.06	0.00	0.04	0.00	0.00	0.09	0.00	0.00	0.01	0.00
FeO	9.08	8.21	8.71	8.28	8.50	8.75	9.04	8.66	8.40	8.80	8.75	8.49	8.53	9.49	8.25	8.82	8.54	8.65
MnO	0.00	0.00	0.10	0.00	0.07	0.00	0.00	0.00	0.05	0.00	0.00	0.03	0.00	0.00	0.08	0.01	0.19	0.09
MgO	8.36	8.77	8.50	8.77	8.36	8.68	8.45	8.88	8.63	8.71	8.81	8.53	8.60	8.40	8.13	8.04	7.96	7.91
TOTAL	99.49	99.10	99.27	98.36	97.64	99.33	98.15	99.20	98.63	98.98	99.11	98.02	98.44	99.83	99.64	99.91	99.31	100.25
CATIONS																		
Si	4.995	4.985	4.992	4.974	4.971	4.974	4.947	4.964	4.999	4.960	4.958	4.994	4.993	4.952	4.979	4.980	4.981	4.984
Ti	0.001	0.003	0.000	0.000	0.000	0.000	0.005	0.000	0.002	0.000	0.000	0.000	0.000	0.001	0.000	0.007	0.004	0.002
Al	3.973	3.992	3.980	3.992	4.011	3.989	4.006	3.986	3.977	3.996	3.990	3.974	3.973	4.000	4.072	4.042	4.050	4.068
Cr	0.002	0.000	0.000	0.005	0.003	0.001	0.000	0.000	0.005	0.000	0.003	0.000	0.000	0.007	0.000	0.000	0.001	0.000
Fe2+	0.774	0.701	0.744	0.712	0.738	0.747	0.783	0.740	0.721	0.755	0.749	0.734	0.734	0.809	0.700	0.748	0.728	0.730
Mn	0.000	0.000	0.009	0.000	0.006	0.000	0.000	0.000	0.004	0.000	0.000	0.003	0.000	0.000	0.007	0.000	0.016	0.007
Mg	1.271	1.334	1.293	1.345	1.294	1.321	1.305	1.353	1.320	1.332	1.344	1.314	1.319	1.276	1.228	1.214	1.210	1.191
(O)	18	18	18	18	18	18	18	18	18	18	18	18	18	18	18	18	18	18
TOTAL	11.016	11.015	11.018	11.028	11.023	11.032	11.046	11.043	11.019	11.043	11.044	11.019	11.020	11.045	10.986	10.991	10.990	10.982
Mg#	0.62	0.66	0.63	0.65	0.64	0.64	0.63	0.65	0.65	0.64	0.64	0.64	0.64	0.61	0.64	0.62	0.62	0.62

BIOTITE

%OXIDE	Bt1	Bt2	Bt3
SiO2	35.51	36.54	36.10
TiO2	5.33	6.42	6.63
Al2O3	16.14	16.35	15.77
Cr2O3	0.17	0.15	0.09
FeO	18.94	15.70	15.99
MnO	0.00	0.10	0.09
MgO	9.93	11.68	10.87
CaO	0.17	0.16	0.01
Na2O	0.47	0.30	0.22
K2O	9.28	9.18	9.18
TOTAL	95.939	96.577	94.949
CATIONS			
Si	5.389	5.398	5.444
Ti	0.609	0.714	0.752
Al	2.887	2.847	2.803
Cr	0.020	0.017	0.011
Fe2+	2.403	1.939	2.016
Mn	0.000	0.012	0.012
Mg	2.247	2.572	2.444
Ca	0.027	0.025	0.001
Na	0.138	0.129	0.065
K	1.796	1.734	1.765
(O)	22	22	22
TOTAL	15.516	15.387	15.313
Mg#	0.48	0.57	0.55

SPINEL With Fe3+ Recalculations

%OXIDE	Spl1	Spl2	Spl2	Spl3	Spl3	Spl4	Spl4
SiO2	0.13	0.21	0.21	0.03	0.03	0.07	0.07
TiO2	0.06	0.12	0.12	0.09	0.09	0.18	0.18
Al2O3	58.96	58.99	58.99	57.89	57.89	55.60	55.60
Cr2O3	1.37	2.14	2.14	0.96	0.96	0.98	0.98
Fe2O3	0.00	-	0.51	-	3.92	-	3.28
FeO	31.44	32.56	32.10	31.59	28.06	35.77	32.82
MnO	0.14	0.22	0.22	0.00	0.00	0.00	0.00
MgO	5.07	5.15	5.15	7.35	7.35	3.99	3.99
ZnO	2.30	2.15	2.15	2.39	2.39	2.01	2.01
CuO	0.00	0.26	0.00	0.00	-	0.00	-
TOTAL	99.461	101.788	101.8392	100.292	100.6847	98.594	98.92276
CATIONS							
Si	0.004	0.006	0.006	0.001	0.001	0.002	0.002
Ti	0.001	0.002	0.002	0.002	0.002	0.004	0.004
Al	1.959	1.927	1.924	1.911	1.891	1.910	1.893
Cr	0.030	0.047	0.047	0.021	0.021	0.023	0.023
Fe3+	0.000	-	0.011	-	0.082	-	0.071
Fe2+	0.741	0.755	0.743	0.740	0.651	0.872	0.793
Mn	0.003	0.005	0.000	0.000	0.000	0.000	0.000
Mg	0.213	0.213	0.213	0.307	0.304	0.173	0.171
Zn	0.048	0.044	0.044	0.049	0.048	0.043	0.043
Cu	0.000	0.005	0.005	0.000	0.000	-	0.000
(O)	4	4	4	4	4	4	4
TOTAL	2.999	3.004	2.995	3.031	3.000	3.027	3.000
Mg#	0.22	0.22	0.22	0.29	0.32	0.17	0.18

PLAGIOCLASE

%OXIDE	Pl1	Pl2	Pl3	Pl4	Pl5
SiO2	56.53	56.90	57.37	56.91	57.09
Al2O3	27.36	27.16	27.21	27.34	27.23
CaO	9.24	9.50	9.06	9.47	9.28
Na2O	5.79	5.96	6.12	5.94	5.95
K2O	0.54	0.47	0.45	0.43	0.49
TOTAL	99.46	99.98	100.21	100.09	100.03
CATIONS					
Si	2.551	2.556	2.567	2.553	2.561
Al	1.455	1.438	1.435	1.446	1.440
Ca	0.447	0.457	0.435	0.455	0.446
Na	0.507	0.519	0.531	0.517	0.517
K	0.031	0.027	0.026	0.024	0.028
(O)	8	8	8	8	8
TOTAL	4.991	4.997	4.994	4.995	4.992

PLAGIOCLASE

%OXIDE	Pl6	Pl7	Pl8	Pl9	Pl10
SiO2	57.51	56.78	58.24	57.23	57.42
Al2O3	27.17	27.36	27.10	27.61	27.25
CaO	9.22	9.61	8.98	9.54	9.09
Na2O	6.06	5.94	6.10	5.95	6.37
K2O	0.56	0.34	0.34	0.40	0.32
TOTAL	100.51	100.03	100.76	100.72	100.45
CATIONS					
Si	2.568	2.549	2.586	2.550	2.564
Al	1.430	1.448	1.418	1.450	1.434
Ca	0.441	0.462	0.427	0.455	0.435
Na	0.524	0.517	0.525	0.514	0.552
K	0.032	0.020	0.023	0.023	0.018
(O)	8	8	8	8	8
TOTAL	4.995	4.996	4.979	4.992	5.003

DD.PIR1

GARNET With Fe3+ Recalculations

%OXIDE	Grt1	Grt1	Grt2	Grt2	Grt3	Grt3	Grt4	Grt4	Grt5	Grt5	Grt6	Grt6	Grt7	Grt7	Grt8	Grt8	Grt9	Grt9
SiO2	37.70	37.70	37.37	37.37	38.66	38.66	38.16	38.16	37.73	37.73	37.52	37.52	38.65	38.65	38.24	38.24	37.79	37.79
TiO2	0.00	0.00	0.19	0.19	0.17	0.17	0.00	0.00	0.00	0.00	0.22	0.22	0.00	0.00	0.00	0.00	0.00	0.00
Cr2O3	0.00	0.00	0.00	0.00	0.00	0.00	0.00	0.00	0.00	0.00	0.00	0.00	0.00	0.00	0.00	0.00	0.00	0.00
Al2O3	21.24	21.24	21.20	21.20	21.78	21.78	21.31	21.31	21.63	21.63	21.06	21.06	21.99	21.99	21.29	21.29	21.54	21.54
Fe2O3	-	0.80	-	0.37	-	0.33	-	0.25	-	1.24	-	1.18	-	1.03	-	0.89	-	1.37
FeO	31.74	31.02	31.26	30.92	32.69	32.39	31.98	31.75	32.27	31.15	32.65	31.59	32.60	31.67	32.64	31.84	31.91	30.68
MnO	0.39	0.39	0.51	0.51	0.33	0.33	0.27	0.27	0.40	0.40	0.52	0.52	0.47	0.47	0.53	0.53	0.52	0.52
MgO	6.92	6.92	6.87	6.87	6.90	6.90	6.91	6.91	6.94	6.94	6.52	6.52	7.18	7.18	6.82	6.82	7.07	7.07
CaO	1.02	1.02	0.95	0.95	1.07	1.07	1.00	1.00	0.92	0.92	0.99	0.99	1.02	1.02	0.95	0.95	1.05	1.05
TOTAL	99.01	99.09	98.35	98.39	101.60	101.64	99.62	99.65	99.88	100.01	99.47	99.59	101.92	102.02	100.46	100.55	99.88	100.02
CATIONS																		
Si	5.982	5.970	5.965	5.959	5.980	5.975	6.011	6.007	5.944	5.926	5.959	5.942	5.959	5.944	5.996	5.983	5.949	5.929
Ti	0.000	0.000	0.023	0.023	0.019	0.019	0.000	0.000	0.000	0.000	0.026	0.026	0.000	0.000	0.000	0.000	0.000	0.000
Cr	0.000	0.000	0.000	0.000	0.000	0.000	0.000	0.000	0.000	0.000	0.000	0.000	0.000	0.000	0.000	0.000	0.000	0.000
Al	3.973	3.965	3.990	3.986	3.972	3.969	3.958	3.956	4.016	4.004	3.942	3.930	3.997	3.987	3.935	3.926	3.997	3.984
Fe3+	-	0.096	-	0.045	-	0.039	-	0.030	-	0.147	-	0.141	-	0.120	-	0.105	-	0.161
Fe2+	4.213	4.109	4.173	4.124	4.230	4.188	4.214	4.181	4.251	4.091	4.337	4.184	4.204	4.074	4.281	4.167	4.202	4.026
Mn	0.053	0.053	0.068	0.068	0.043	0.043	0.035	0.035	0.053	0.053	0.070	0.070	0.061	0.061	0.070	0.070	0.070	0.070
Mg	1.637	1.634	1.634	1.632	1.591	1.590	1.623	1.622	1.629	1.624	1.544	1.539	1.650	1.646	1.594	1.591	1.659	1.653
Ca	0.174	0.174	0.162	0.162	0.178	0.178	0.169	0.169	0.156	0.156	0.169	0.169	0.169	0.169	0.159	0.159	0.177	0.176
(O)	24	24	24	24	24	24	24	24	24	24	24	24	24	24	24	24	24	24
TOTAL	16.032	16.000	16.015	16.000	16.013	16.000	16.010	16.000	16.049	16.000	16.047	16.000	16.040	16.000	16.035	16.000	16.054	16.000
Mg#	0.28	0.28	0.28	0.28	0.27	0.28	0.28	0.28	0.28	0.28	0.26	0.27	0.28	0.29	0.27	0.28	0.28	0.29

GARNET With Fe3+ Recalculations

%OXIDE	Grt10	Grt10	Grt11	Grt11	Grt12	Grt12	Grt13	Grt13	Grt14	Grt14	Grt15	Grt15	Grt16	Grt16	Grt17	Grt17
SiO2	37.86	37.86	38.31	38.31	37.85	37.85	38.31	38.31	37.85	37.85	37.81	37.81	37.67	37.67	37.51	37.51
TiO2	0.00	0.00	0.00	0.00	0.00	0.00	0.00	0.00	0.00	0.00	0.23	0.23	0.00	0.00	0.00	0.00
Cr2O3	0.00	0.00	0.00	0.00	0.00	0.00	0.00	0.00	0.00	0.00	0.00	0.00	0.00	0.00	0.00	0.00
Al2O3	21.27	21.27	21.56	21.56	21.30	21.30	21.56	21.56	21.30	21.30	21.47	21.47	21.15	21.15	20.95	20.95
Fe2O3	-	0.68	-	0.66	-	0.50	-	0.66	-	0.50	-	1.19	-	1.05	-	0.80
FeO	31.92	31.30	32.42	31.82	32.33	31.88	32.42	31.82	32.33	31.88	32.29	31.22	31.95	31.00	32.10	31.38
MnO	0.48	0.48	0.37	0.37	0.00	0.00	0.37	0.37	0.00	0.00	0.45	0.45	0.38	0.38	0.30	0.30
MgO	6.88	6.88	6.98	6.98	6.85	6.85	6.98	6.98	6.85	6.85	7.01	7.01	6.95	6.95	6.69	6.69
CaO	0.94	0.94	0.92	0.92	0.90	0.90	0.92	0.92	0.90	0.90	0.96	0.96	0.99	0.99	0.99	0.99
TOTAL	99.34	99.40	100.55	100.62	99.24	99.29	100.55	100.62	99.25	99.30	100.22	100.34	99.08	99.19	98.54	98.61
CATIONS																
Si	5.990	5.980	5.988	5.978	5.993	5.986	5.988	5.978	5.993	5.986	5.939	5.922	5.979	5.963	5.993	5.981
Ti	0.000	0.000	0.000	0.000	0.000	0.000	0.000	0.000	0.000	0.000	0.027	0.027	0.000	0.000	0.000	0.000
Cr	0.000	0.000	0.000	0.000	0.000	0.000	0.000	0.000	0.000	0.000	0.000	0.000	0.000	0.000	0.000	0.000
Al	3.967	3.960	3.971	3.965	3.975	3.970	3.971	3.965	3.975	3.970	3.975	3.963	3.957	3.947	3.947	3.939
Fe3+	-	0.081	-	0.078	-	0.060	-	0.078	-	0.060	-	0.141	-	0.126	-	0.096
Fe2+	4.224	4.136	4.237	4.152	4.281	4.216	4.237	4.152	4.281	4.216	4.242	4.089	4.242	4.105	4.290	4.186
Mn	0.064	0.064	0.049	0.049	0.000	0.000	0.049	0.049	0.000	0.000	0.060	0.060	0.051	0.051	0.040	0.040
Mg	1.623	1.620	1.626	1.623	1.618	1.616	1.626	1.623	1.618	1.616	1.642	1.637	1.645	1.641	1.593	1.590
Ca	0.159	0.159	0.155	0.155	0.153	0.153	0.155	0.155	0.153	0.153	0.162	0.162	0.168	0.168	0.169	0.169
(O)	24	24	24	24	24	24	24	24	24	24	24	24	24	24	24	24
TOTAL	16.027	16.000	16.026	16.000	16.020	16.000	16.026	16.000	16.020	16.000	16.047	16.000	16.042	16.000	16.032	16.000
Mg#	0.28	0.28	0.28	0.28	0.27	0.28	0.28	0.28	0.27	0.28	0.28	0.29	0.28	0.29	0.27	0.28

CORDIERITE

OXIDE%	Crd1	Crd2	Crd3	Crd4	Crd5	Crd6	Crd7	Crd8	Crd9	Crd10	Crd11	Crd12	Crd13	Crd14	Crd15
SiO2	48.70	48.91	48.77	49.12	49.42	49.53	49.41	49.19	48.64	49.08	48.95	48.63	48.84	48.43	49.11
TiO2	0.00	0.00	0.00	0.00	0.00	0.00	0.00	0.00	0.00	0.00	0.00	0.00	0.00	0.16	0.00
Al2O3	32.80	32.62	32.85	33.09	33.25	33.23	33.25	33.32	33.01	33.11	32.95	32.58	32.71	32.80	32.87
Cr2O3	0.00	0.00	0.00	0.00	0.00	0.00	0.00	0.00	0.00	0.00	0.00	0.00	0.00	0.00	0.00
FeO	9.31	8.66	8.44	9.08	8.57	8.59	8.99	9.30	9.15	9.05	9.23	9.09	9.45	9.18	9.40
MnO	0.00	0.00	0.00	0.00	0.00	0.00	0.00	0.00	0.00	0.00	0.00	0.00	0.00	0.00	0.00
MgO	8.31	8.45	8.80	8.84	8.66	8.63	8.63	8.39	8.29	8.44	8.14	8.15	8.17	8.46	8.39
TOTAL	99.13	98.64	98.87	100.12	99.90	99.98	100.27	100.19	99.10	99.68	99.27	98.45	99.16	99.02	99.77
CATIONS															
Si	4.990	5.021	4.994	4.981	5.006	5.011	4.997	4.987	4.984	4.996	5.006	5.013	5.007	4.971	5.003
Ti	0.000	0.000	0.000	0.000	0.000	0.000	0.000	0.000	0.000	0.000	0.000	0.000	0.000	0.012	0.000
Al	3.964	3.947	3.965	3.955	3.970	3.966	3.963	3.981	3.987	3.972	3.972	3.958	3.953	3.968	3.946
Cr	0.000	0.000	0.000	0.000	0.000	0.000	0.000	0.000	0.000	0.000	0.000	0.000	0.000	0.000	0.000
Fe2+	0.798	0.744	0.723	0.770	0.726	0.727	0.761	0.788	0.784	0.771	0.789	0.783	0.810	0.788	0.801
Mn	0.000	0.000	0.000	0.000	0.000	0.000	0.000	0.000	0.000	0.000	0.000	0.000	0.000	0.000	0.000
Mg	1.270	1.293	1.343	1.336	1.307	1.302	1.301	1.267	1.267	1.280	1.241	1.252	1.248	1.295	1.275
(O)	18	18	18	18	18	18	18	18	18	18	18	18	18	18	18
TOTAL	11.022	11.005	11.025	11.042	11.009	11.006	11.022	11.023	11.022	11.019	11.008	11.006	11.018	11.034	11.025
Mg#	0.61	0.63	0.65	0.63	0.64	0.64	0.63	0.62	0.62	0.62	0.61	0.62	0.61	0.62	0.61

ILMENITE

%OXIDE	ILM1	ILM2	ILM3	ILM4	ILM5
SiO2	0.32	0.49	0.37	0.37	0.42
TiO2	51.84	51.67	51.33	51.96	51.16
Cr2O3	0.00	0.32	0.00	0.32	0.32
Al2O3	0.23	0.24	0.21	0.17	0.20
FeO	47.61	46.33	46.38	46.37	46.78
MnO	0.00	0.00	0.00	0.00	0.00
MgO	0.51	0.88	0.72	0.59	0.62
CaO	0.00	0.00	0.14	0.00	0.00
TOTAL	100.50	99.94	99.14	99.79	99.49
CATIONS					
Si	0.008	0.012	0.009	0.009	0.011
Ti	0.975	0.975	0.979	0.983	0.974
Cr	0.000	0.006	0.000	0.006	0.006
Al	0.007	0.007	0.006	0.005	0.006
Fe2+	1.004	0.972	0.984	0.976	0.990
Mn	0.000	0.000	0.000	0.000	0.000
Mg	0.019	0.033	0.027	0.022	0.023
Ca	0.000	0.000	0.004	0.000	0.000
(O)	3	3	3	3	3
TOTAL	2.013	2.005	2.009	2.001	2.010
Mg#	0.02	0.03	0.03	0.02	0.02

PLAGIOCLASE

%OXIDE	Pl1	Pl2	Pl3	Pl4	Pl5	Pl6	Pl7
SiO2	60.73	57.88	60.55	59.71	60.21	60.00	60.19
Al2O3	25.73	25.42	26.03	25.53	25.91	25.99	25.53
CaO	7.30	7.42	7.64	7.61	7.51	7.60	7.17
Na2O	7.11	6.57	6.98	6.73	7.01	6.83	6.96
K2O	0.78	0.75	0.78	0.69	0.64	0.65	0.85
BaO	0.00	0.00	0.00	0.00	0.00	0.00	0.00
FeO	0.32	0.29	0.00	0.00	0.27	0.00	0.33
TOTAL	101.97	98.32	101.98	100.27	101.56	101.06	101.03
CATIONS							
Si	2.663	2.635	2.653	2.659	2.651	2.650	2.664
Al	1.330	1.364	1.344	1.340	1.344	1.353	1.332
Ca	0.343	0.362	0.359	0.363	0.354	0.360	0.340
Na	0.604	0.580	0.593	0.581	0.599	0.584	0.597
K	0.043	0.043	0.043	0.039	0.036	0.037	0.048
Ba	0.000	0.000	0.000	0.000	0.000	0.000	0.000
Fe	0.012	0.011	0.000	0.000	0.010	0.000	0.012
(O)	8	8	8	8	8	8	8
TOTAL	4.995	4.995	4.992	4.982	4.994	4.984	4.993

DD.PIR1																
ORTHOPYROXENE																
%OXIDE	Opx1	Opx2	Opx3	Opx4	Opx5	Opx6	Opx7	Opx8	Opx9	Opx10	Opx11	Opx12				
SiO2	47.54	47.40	47.40	48.01	47.60	46.47	46.79	46.36	46.48	47.56	46.70	46.63				
TiO2	0.30	0.33	0.29	0.18	0.59	0.33	0.33	0.29	0.31	0.37	0.30	0.25				
Cr2O3	0.21	0.00	0.00	0.00	0.00	0.00	0.00	0.00	0.22	0.00	0.20	0.00				
Al2O3	6.23	6.05	6.45	5.30	5.84	7.05	7.03	7.10	6.09	5.66	6.07	6.21				
FeO	32.02	32.81	32.36	33.37	32.25	31.86	32.16	31.84	31.81	32.76	32.02	32.38				
MnO	0.00	0.00	0.00	0.00	0.00	0.00	0.00	0.00	0.00	0.00	0.00	0.00				
MgO	13.58	13.59	13.62	13.74	13.74	13.55	13.44	13.48	13.50	13.79	13.84	13.51				
CaO	0.11	0.17	0.00	0.11	0.17	0.15	0.15	0.14	0.21	0.18	0.13	0.16				
TOTAL	100.00	100.35	100.12	100.70	100.19	99.41	99.90	99.20	98.61	100.31	99.26	99.12				
CATIONS																
Si	1.853	1.848	1.847	1.869	1.854	1.824	1.828	1.823	1.842	1.855	1.839	1.841				
Ti	0.009	0.010	0.009	0.005	0.017	0.010	0.010	0.008	0.009	0.011	0.009	0.007				
Cr	0.006	0.000	0.000	0.000	0.000	0.000	0.000	0.000	0.007	0.000	0.006	0.000				
Al	0.286	0.278	0.296	0.243	0.268	0.326	0.324	0.329	0.285	0.260	0.282	0.289				
Fe	1.044	1.070	1.055	1.086	1.050	1.046	1.051	1.047	1.054	1.069	1.055	1.069				
Mn	0.000	0.000	0.000	0.000	0.000	0.000	0.000	0.000	0.000	0.000	0.000	0.000				
Mg	0.789	0.790	0.791	0.797	0.798	0.793	0.783	0.790	0.797	0.802	0.812	0.795				
Ca	0.005	0.007	0.000	0.004	0.007	0.006	0.006	0.006	0.009	0.008	0.005	0.007				
(O)	6	6	6	6	6	6	6	6	6	6	6	6				
Cat.Total	3.992	4.003	3.998	4.004	3.994	4.005	4.002	4.003	4.003	4.005	4.008	4.008				
Mg#	0.43	0.42	0.43	0.42	0.43	0.43	0.43	0.43	0.43	0.43	0.43	0.43				

DD.PIR4

GARNET With Fe3+ Recalculations																
%OXIDE	Grt1	Grt1	Grt2	Grt2	Grt3	Grt3	Grt4	Grt4	Grt5	Grt5	Grt6	Grt6	Grt7	Grt7		
SiO2	37.98	37.98	38.45	38.45	38.54	38.54	38.83	38.83	39.14	39.14	37.87	37.87	37.91	37.91		
TiO2	0.00	0.00	0.00	0.00	0.00	0.00	0.00	0.00	0.00	0.00	0.00	0.00	0.00	0.00		
Cr2O3	0.00	0.00	0.00	0.00	0.00	0.00	0.00	0.00	0.00	0.00	0.00	0.00	0.00	0.00		
Al2O3	21.69	21.69	21.41	21.41	21.60	21.60	22.06	22.06	21.95	21.95	21.51	21.51	21.48	21.48		
Fe2O3	-	2.04	-	0.69	-	0.72	-	1.14	-	1.44	-	0.76	-	1.51		
FeO	32.31	30.47	31.88	31.26	32.47	31.82	32.94	31.91	32.91	31.61	31.39	30.71	31.56	30.20		
MnO	0.43	0.43	0.51	0.51	0.48	0.48	0.37	0.37	0.58	0.58	0.36	0.36	0.52	0.52		
MgO	7.35	7.35	7.21	7.21	7.02	7.02	7.16	7.16	7.33	7.33	7.13	7.13	7.00	7.00		
CaO	1.12	1.12	1.06	1.06	0.99	0.99	1.09	1.09	1.20	1.20	1.17	1.17	1.20	1.20		
TOTAL	100.87	101.07	100.51	100.58	101.10	101.17	102.45	102.57	103.11	103.25	99.43	99.50	99.66	99.81		
CATIONS																
Si	5.926	5.897	6.003	5.993	5.992	5.982	5.960	5.944	5.971	5.951	5.971	5.960	5.972	5.950		
Ti	0.000	0.000	0.000	0.000	0.000	0.000	0.000	0.000	0.000	0.000	0.000	0.000	0.000	0.000		
Cr	0.000	0.000	0.000	0.000	0.000	0.000	0.000	0.000	0.000	0.000	0.000	0.000	0.000	0.000		
Al	3.988	3.968	3.939	3.932	3.958	3.951	3.991	3.980	3.946	3.932	3.998	3.991	3.989	3.974		
Fe3+	-	0.239	-	0.081	-	0.084	-	0.132	-	0.164	-	0.090	-	0.179		
Fe2+	4.215	3.955	4.163	4.075	4.222	4.131	4.228	4.085	4.199	4.020	4.139	4.041	4.185	3.990		
Mn	0.056	0.056	0.067	0.067	0.064	0.064	0.048	0.048	0.075	0.075	0.048	0.048	0.069	0.069		
Mg	1.708	1.700	1.677	1.674	1.627	1.624	1.637	1.633	1.667	1.661	1.676	1.673	1.643	1.637		
Ca	0.187	0.186	0.178	0.178	0.165	0.165	0.180	0.180	0.197	0.196	0.198	0.198	0.202	0.201		
(O)	24	24	24	24	24	24	24	24	24	24	24	24	24	24		
TOTAL	16.080	16.000	16.027	16.000	16.028	16.000	16.044	16.000	16.055	16.000	16.030	16.000	16.060	16.000		
Mg#	0.29	0.30	0.29	0.29	0.28	0.28	0.28	0.29	0.28	0.29	0.29	0.29	0.28	0.29		

ORTHOPYROXENE								
OXIDE%	Opx1	Opx2	Opx3	Opx4	Opx5	Opx6	Opx7	Opx8
SiO2	46.76	47.55	47.17	47.24	46.85	48.03	46.02	47.80
MgO	14.50	14.64	13.84	14.29	13.93	14.89	12.94	13.84
MnO	0.00	0.00	0.00	0.00	0.00	0.00	0.00	0.00
FeO	31.22	31.39	32.73	32.06	32.18	31.17	32.78	33.64
CaO	0.10	0.00	0.00	0.13	0.00	0.00	0.13	0.00
TiO2	0.24	0.19	0.26	0.23	0.22	0.00	0.00	0.22
Al2O3	6.45	6.48	6.28	6.45	6.03	5.96	7.69	5.29
Cr2O3	0.00	0.21	0.00	0.00	0.00	0.00	0.18	0.00
TOTAL	99.28	100.45	100.28	100.39	99.21	100.05	99.72	100.79
CATIONS								
Si	1.832	1.838	1.840	1.835	1.845	1.861	1.809	1.862
Mg	0.847	0.844	0.805	0.827	0.817	0.860	0.758	0.804
Mn	0.000	0.000	0.000	0.000	0.000	0.000	0.000	0.000
Fe	1.023	1.015	1.068	1.041	1.060	1.010	1.077	1.096
Ca	0.004	0.000	0.000	0.005	0.000	0.000	0.005	0.000
Ti	0.007	0.005	0.008	0.007	0.007	0.000	0.000	0.006
Al	0.298	0.296	0.289	0.295	0.280	0.272	0.356	0.243
Cr	0.000	0.006	0.000	0.000	0.000	0.000	0.005	0.000
(O)	6	6	6	6	6	6	6	6
TOTAL	4.011	4.004	4.010	4.010	4.009	4.003	4.010	4.011
Mg#	0.453	0.454	0.430	0.443	0.435	0.460	0.413	0.423

PLAGIOCLASE						
%OXIDE	Pl1	Pl2	Pl3	Pl4	Pl5	Pl6
SiO2	59.18	59.64	59.86	59.61	59.27	59.48
Al2O3	25.41	25.73	26.03	25.63	26.15	26.17
CaO	7.31	7.38	7.67	7.45	7.54	7.58
Na2O	7.25	7.36	7.20	7.09	7.00	7.03
K2O	0.35	0.31	0.33	0.31	0.41	0.52
TOTAL	99.50	100.41	101.10	100.09	100.37	100.78
CATIONS						
Si	2.654	2.651	2.644	2.655	2.636	2.636
Al	1.343	1.348	1.355	1.346	1.371	1.367
Ca	0.351	0.351	0.363	0.356	0.359	0.360
Na	0.631	0.634	0.615	0.612	0.603	0.604
K	0.020	0.017	0.019	0.018	0.023	0.030
(O)	8	8	8	8	8	8
TOTAL	4.999	5.001	4.996	4.987	4.992	4.997

PROBE DATA FROM IGNEOUS-TEXTURED ROCKS

H.BHQ1

GARNET

% OXIDE	Grt1	Grt2	Grt3	Grt4	Grt5	Grt6	Grt7	Grt8	Grt9	Grt10
SiO2	39.28	38.55	38.61	38.44	38.71	38.73	39.23	38.92	38.71	38.83
TiO2	0.09	0.22	0.05	0.18	0.00	0.00	0.13	0.22	0.00	0.00
Al2O3	22.20	21.92	22.27	22.10	22.23	22.17	22.27	22.54	22.31	22.61
Cr2O3	0.17	0.17	0.36	0.15	0.12	0.00	0.04	0.00	0.00	0.13
FeO	32.47	30.90	30.46	29.82	31.91	30.71	30.18	30.60	30.74	30.45
MnO	1.25	0.64	0.95	0.73	0.86	0.78	0.95	0.79	0.84	0.93
MgO	5.44	6.64	7.01	7.34	6.06	6.76	6.92	7.03	6.70	7.45
CaO	1.05	1.16	0.98	1.07	1.01	1.19	1.09	1.21	1.26	0.97
TOTAL	**101.95**	**100.20**	**100.69**	**99.82**	**100.90**	**100.34**	**100.80**	**101.31**	**100.55**	**101.36**
Si	6.057	5.979	5.982	5.958	5.998	6.022	6.051	5.973	5.988	5.956
Ti	0.010	0.026	0.006	0.021	0.000	0.000	0.015	0.026	0.000	0.000
Al	4.035	4.009	4.068	4.036	4.060	4.062	4.048	4.078	4.068	4.088
Cr	0.021	0.021	0.044	0.019	0.014	0.000	0.005	0.000	0.000	0.016
Fe2+	4.187	4.009	3.947	3.864	4.136	3.994	3.893	3.927	3.978	3.906
Mn	0.164	0.085	0.125	0.095	0.113	0.103	0.124	0.102	0.110	0.120
Mg	1.250	1.535	1.619	1.696	1.400	1.567	1.590	1.608	1.546	1.703
Ca	0.174	0.192	0.163	0.177	0.168	0.198	0.180	0.199	0.208	0.159
(O)	24	24	24	24	24	24	24	24	24	24
TOTAL	15.898	15.856	15.954	15.866	15.889	15.946	15.906	15.913	15.898	15.948
Mg#	**0.23**	**0.28**	**0.29**	**0.31**	**0.25**	**0.28**	**0.29**	**0.29**	**0.28**	**0.30**

ORTHOPYROXENE

% OXIDE	Opx1	Opx2	Opx3	Opx4	Opx5	Opx6	Opx7	Opx8	Opx9	Opx10	Opx11
SiO2	48.17	47.99	49.82	47.82	48.66	49.29	49.12	50.13	49.40	48.32	49.66
TiO2	0.21	0.20	0.08	0.37	0.29	0.40	0.23	0.16	0.00	0.13	0.02
Al2O3	6.22	5.66	4.88	6.55	4.99	5.14	3.83	3.58	4.21	5.84	3.31
Cr2O3	0.00	0.18	0.16	0.16	0.03	0.07	0.00	0.01	0.06	0.22	0.00
FeO	29.71	29.79	29.75	29.63	30.16	29.65	30.49	30.15	30.18	30.15	29.99
MnO	0.25	0.25	0.24	0.29	0.05	0.25	0.24	0.19	0.41	0.24	0.33
MgO	14.67	14.80	15.84	14.59	15.09	15.52	15.54	15.43	15.55	14.98	15.28
CaO	0.06	0.09	0.14	0.11	0.06	0.17	0.14	0.10	0.11	0.14	0.03
Na2O	0.01	0.38	0.54	0.00	0.36	0.61	0.00	0.21	0.00	0.05	0.88
TOTAL	**99.31**	**99.34**	**101.45**	**99.52**	**99.68**	**101.08**	**99.59**	**99.95**	**99.91**	**100.06**	**99.50**
CATIONS											
Si	1.869	1.868	1.893	1.848	1.886	1.878	1.908	1.932	1.908	1.866	1.932
Ti	0.006	0.006	0.002	0.010	0.008	0.012	0.006	0.004	0.000	0.004	0.000
Al	0.285	0.260	0.219	0.298	0.228	0.230	0.176	0.162	0.192	0.266	0.152
Cr	0.000	0.006	0.005	0.004	0.000	0.002	0.000	0.000	0.000	0.006	0.000
Fe2+	0.964	0.970	0.945	0.958	0.978	0.946	0.990	0.972	0.974	0.974	0.976
Mn	0.008	0.008	0.008	0.010	0.002	0.008	0.008	0.006	0.014	0.008	0.010
Mg	0.848	0.859	0.897	0.842	0.872	0.882	0.900	0.886	0.896	0.862	0.886
Ca	0.003	0.004	0.004	0.004	0.002	0.008	0.006	0.004	0.004	0.006	0.002
Na	0.001	0.029	0.040	0.000	0.026	0.044	0.000	0.016	0.000	0.004	0.066
(O)	6	6	6	6	6	6	6	6	6	6	6
TOTAL	3.984	4.010	4.013	3.974	4.002	4.010	3.994	3.982	3.988	3.996	4.024
Mg#	**0.47**	**0.47**	**0.49**	**0.47**	**0.47**	**0.48**	**0.48**	**0.48**	**0.48**	**0.47**	**0.48**

CORDIERITE

% OXIDE	Crd1	Crd2	Crd3	Crd4	Crd5	Crd6	Crd7	Crd8
SiO2	50.13	48.25	49.66	48.92	49.38	49.84	49.55	50.31
TiO2	0.00	0.00	0.00	0.00	0.00	0.00	0.00	0.00
Al2O3	33.97	33.79	33.48	32.81	33.40	33.52	33.41	34.04
Cr2O3	0.00	0.00	0.07	0.00	0.00	0.00	0.00	0.00
FeO	8.70	7.96	8.30	8.67	8.58	8.38	7.89	8.48
MnO	0.29	0.34	0.25	0.00	0.00	0.00	0.00	0.00
MgO	7.83	8.16	8.29	8.51	8.83	8.82	9.19	9.07
TOTAL	**100.91**	**98.51**	**100.05**	**98.91**	**100.19**	**100.57**	**100.04**	**101.90**
FORMULA								
Si	5.027	4.953	5.019	5.010	4.989	5.009	4.997	4.992
Ti	0.000	0.000	0.000	0.000	0.000	0.000	0.000	0.000
Al	4.015	4.088	3.988	3.960	3.978	3.971	3.972	3.981
Cr	0.000	0.000	0.006	0.000	0.000	0.000	0.000	0.000
Fe2+	0.729	0.683	0.701	0.742	0.725	0.704	0.666	0.701
Mn	0.025	0.030	0.021	0.000	0.000	0.000	0.000	0.000
Mg	1.170	1.249	1.250	1.298	1.330	1.322	1.382	1.342
(O)	18	18	18	18	18	18	18	18
TOTAL	10.966	11.003	10.985	11.010	11.022	11.006	11.017	11.016
Mg#	**0.62**	**0.65**	**0.64**	**0.64**	**0.65**	**0.65**	**0.67**	**0.66**

H.BHQ1									
BIOTITE									
% OXIDE	Bt1	Bt2	Bt3	Bt4	Bt5	Bt6	Bt7	Bt8	Bt9
SiO2	35.80	35.90	36.33	35.70	36.25	35.98	35.85	35.91	36.16
Al2O3	16.82	16.99	17.46	16.77	17.49	17.17	17.33	17.34	17.70
FeO	17.45	16.82	18.31	18.46	19.31	18.85	19.10	18.64	18.37
MnO	0.00	0.00	0.00	0.10	0.00	0.00	0.06	0.00	0.00
MgO	10.51	10.04	9.92	9.70	9.79	9.53	9.56	9.68	10.09
CaO	0.06	0.13	0.02	0.07	0.01	0.08	0.03	0.00	0.02
Na2O	0.05	0.00	0.00	0.01	0.00	0.00	0.05	0.05	0.30
K2O	9.24	9.47	9.53	9.42	9.54	9.25	9.32	9.24	9.62
Cl	0.14	0.06	0.05	0.04	0.07	0.10	0.10	0.03	0.13
FO	0.31	0.32	0.29	0.14	0.35	0.51	0.38	0.34	0.46
TiO2	5.32	5.57	6.32	5.65	5.59	5.55	5.61	5.65	5.30
BaO	0.48	0.52	0.50	0.45	0.37	0.36	0.39	0.28	0.42
P2O5	0.00	0.00	0.00	0.00	0.00	0.00	0.00	0.00	0.00
Cr2O3	0.00	0.19	0.20	0.16	0.10	0.12	0.05	0.00	0.05
NiO	0.04	0.00	0.00	0.04	0.00	0.00	0.00	0.01	0.06
ZnO	0.36	0.04	0.00	0.11	0.00	0.01	0.21	0.30	0.00
TOTAL	**96.59**	**96.03**	**98.92**	**96.82**	**98.86**	**97.51**	**98.03**	**97.45**	**98.70**
CATIONS									
Si	5.391	5.415	5.340	5.376	5.355	5.388	5.350	5.365	5.349
Al	2.985	3.020	3.025	2.976	3.045	3.031	3.048	3.053	3.086
Fe	2.197	2.122	2.251	2.325	2.385	2.361	2.383	2.329	2.272
Mn	0.000	0.000	0.000	0.013	0.000	0.000	0.008	0.000	0.000
Mg	2.360	2.256	2.173	2.176	2.156	2.126	2.126	2.156	2.225
Ca	0.010	0.020	0.003	0.012	0.001	0.012	0.005	0.000	0.003
Na	0.014	0.000	0.000	0.002	0.000	0.000	0.014	0.013	0.087
K	1.775	1.821	1.791	1.809	1.798	1.768	1.774	1.761	1.816
Cl	0.037	0.016	0.013	0.009	0.018	0.025	0.025	0.008	0.033
F	0.147	0.151	0.134	0.067	0.163	0.243	0.177	0.161	0.216
Ti	0.603	0.631	0.699	0.640	0.621	0.625	0.629	0.634	0.590
Ba	0.028	0.030	0.029	0.027	0.022	0.021	0.023	0.016	0.024
P	0.000	0.000	0.000	0.000	0.000	0.000	0.000	0.000	0.000
Cr	0.000	0.023	0.023	0.019	0.011	0.014	0.006	0.000	0.006
Ni	0.005	0.000	0.000	0.005	0.000	0.000	0.000	0.001	0.007
Zn	0.040	0.004	0.000	0.012	0.000	0.001	0.023	0.033	0.000
(O)	22	22	22	22	22	22	22	22	22
TOTAL	**15.592**	**15.509**	**15.481**	**15.468**	**15.575**	**15.615**	**15.591**	**15.53**	**15.714**
Mg#	**0.52**	**0.52**	**0.49**	**0.48**	**0.47**	**0.47**	**0.47**	**0.48**	**0.49**

DD.CASB2i

GARNET

%OXIDE	Grt1	Grt2	Grt3	Grt4	Grt5	Grt6
SiO2	38.55	38.60	38.12	38.40	38.71	38.24
TiO2	0.10	0.14	0.00	0.00	0.00	0.14
Cr2O3	0.00	0.00	0.00	0.00	0.20	0.00
Al2O3	21.76	21.77	21.52	21.23	21.78	21.41
FeO	28.77	28.97	28.92	28.46	28.08	29.39
MnO	1.89	1.76	1.81	1.82	1.84	1.62
MgO	7.66	7.92	7.85	7.57	7.89	7.59
CaO	1.71	1.81	1.79	1.66	1.83	1.84
TOTAL	100.43	100.96	100.01	99.14	100.33	100.23
CATIONS						
Si	5.983	5.963	5.955	6.034	5.996	5.968
Ti	0.012	0.016	0.000	0.000	0.000	0.017
Cr	0.000	0.000	0.000	0.000	0.024	0.000
Al	3.981	3.964	3.962	3.931	3.977	3.939
Fe2+	3.734	3.743	3.778	3.740	3.638	3.835
Mn	0.248	0.230	0.239	0.243	0.242	0.214
Mg	1.771	1.824	1.828	1.773	1.822	1.765
Ca	0.284	0.300	0.300	0.279	0.304	0.308
(O)	24	24	24	24	24	24
TOTALS	16.013	16.040	16.062	16.000	16.003	16.046
Mg#	0.32	0.33	0.33	0.32	0.33	0.32

ORTHOPYROXENE

%OXIDE	Opx1	Opx2	Opx3	Opx4	Opx5	Opx6	Opx7	Opx8	Opx9	Opx10
SiO2	48.64	49.71	49.97	48.51	49.80	49.96	50.10	50.65	50.16	49.39
TiO2	0.21	0.30	0.22	0.21	0.10	0.17	0.26	0.22	0.00	0.31
Cr2O3	0.10	0.00	0.00	0.17	0.10	0.00	0.10	0.00	0.00	0.13
Al2O3	4.35	4.36	4.00	4.58	4.16	3.94	4.43	3.56	4.29	4.49
FeO	27.76	27.75	27.83	27.30	28.22	27.43	26.67	27.09	26.52	27.34
MnO	0.36	0.48	0.52	0.39	0.42	0.36	0.21	0.44	0.24	0.31
MgO	16.86	17.11	17.16	17.09	17.50	17.73	18.09	18.19	18.27	17.72
CaO	0.19	0.23	0.24	0.20	0.16	0.23	0.21	0.22	0.23	0.20
TOTAL	98.45	99.93	99.94	98.44	100.45	99.82	100.07	100.36	99.70	99.88
CATIONS										
Si	1.892	1.900	1.911	1.884	1.898	1.908	1.900	1.920	1.908	1.886
Ti	0.006	0.009	0.006	0.006	0.003	0.005	0.007	0.006	0.000	0.009
Cr	0.003	0.000	0.000	0.005	0.003	0.000	0.003	0.000	0.000	0.004
Al	0.199	0.197	0.180	0.209	0.187	0.177	0.198	0.159	0.192	0.202
Fe2+	0.903	0.887	0.890	0.887	0.899	0.876	0.846	0.859	0.844	0.873
Mn	0.012	0.016	0.017	0.013	0.013	0.012	0.007	0.014	0.008	0.010
Mg	0.978	0.975	0.978	0.990	0.994	1.010	1.023	1.028	1.036	1.009
Ca	0.008	0.010	0.010	0.008	0.006	0.009	0.009	0.009	0.009	0.008
(O)	6	6	6	6	6	6	6	6	6	6
TOTAL	4.001	3.994	3.992	4.002	4.003	3.997	3.993	3.995	3.997	4.001
Mg#	0.52	0.52	0.52	0.53	0.53	0.54	0.55	0.54	0.55	0.54

ORTHOPYROXENE

%OXIDE	Opx11	Opx12	OPx13	Opx14	Opx15	Opx16
SiO2	49.60	49.52	49.62	49.43	49.48	49.81
TiO2	0.28	0.31	0.24	0.19	0.26	0.28
Cr2O3	0.13	0.12	0.14	0.09	0.19	0.00
Al2O3	4.65	4.08	3.49	4.23	4.12	4.09
FeO	27.37	26.67	27.60	27.95	27.49	27.15
MnO	0.36	0.44	0.43	0.49	0.39	0.62
MgO	17.54	17.72	17.29	17.18	17.35	17.38
CaO	0.20	0.21	0.20	0.23	0.24	0.18
TOTAL	100.12	99.05	99.01	99.79	99.52	99.51
CATIONS						
Si	1.889	1.903	1.916	1.897	1.900	1.908
Ti	0.008	0.009	0.007	0.006	0.008	0.008
Cr	0.004	0.004	0.004	0.003	0.006	0.000
Al	0.209	0.185	0.159	0.191	0.186	0.185
Fe2+	0.872	0.857	0.891	0.897	0.882	0.870
Mn	0.012	0.014	0.014	0.016	0.013	0.020
Mg	0.996	1.015	0.996	0.983	0.993	0.993
Ca	0.008	0.008	0.008	0.009	0.010	0.007
(O)	6	6	6	6	6	6
TOTALS	3.998	3.995	3.995	4.002	3.998	3.991
Mg#	0.53	0.54	0.53	0.52	0.53	0.53

PLAGIOCLASE

%OXIDE	Pl1	Pl2	Pl3	Pl4	Pl5	Pl6	Pl7	Pl8
SiO2	54.44	53.46	53.63	49.86	50.02	48.23	47.96	54.66
Al2O3	29.52	28.86	28.53	32.10	31.73	32.43	33.56	29.06
CaO	11.70	11.47	11.19	15.13	14.74	15.53	16.87	11.21
Na2O	5.15	5.02	5.14	3.09	3.25	2.60	2.03	5.11
K2O	0.07	0.07	0.00	0.00	0.00	0.00	0.00	0.00
BaO	0.00	0.13	0.00	0.00	0.00	0.00	0.00	0.00
FeO	0.12	0.12	0.14	0.13	0.14	0.26	0.00	0.00
TOTAL	101.01	99.11	98.63	100.31	99.88	99.05	100.41	100.03
CATIONS								
Si	2.436	2.440	2.455	2.269	2.284	2.228	2.189	2.461
Al	1.557	1.552	1.539	1.722	1.708	1.766	1.805	1.542
Ca	0.561	0.561	0.549	0.738	0.721	0.769	0.825	0.541
Na	0.447	0.444	0.456	0.272	0.288	0.233	0.180	0.446
K	0.004	0.004	0.000	0.000	0.000	0.000	0.000	0.000
Ba	0.000	0.002	0.000	0.000	0.000	0.000	0.000	0.000
Fe	0.005	0.005	0.005	0.005	0.005	0.010	0.000	0.000
(O)	8	8	8	8	8	8	8	8
TOTAL	5.010	5.008	5.004	5.006	5.006	5.006	4.999	4.990

CORDIERITE

OXIDE%	Crd1	Crd2	Crd3	Crd4	Crd5	Crd6	Crd7	Crd8	Crd9	Crd10	Crd11	Crd12	Crd13	Crd14	Crd15
SiO2	49.19	48.80	49.46	49.05	49.53	49.20	49.56	49.33	49.32	48.76	49.11	49.94	49.93	49.64	49.82
TiO2	0.00	0.00	0.00	0.00	0.00	0.00	0.00	0.00	0.00	0.11	0.09	0.00	0.00	0.00	0.00
Al2O3	33.48	33.07	33.36	33.46	33.56	33.06	33.36	33.19	33.14	32.98	32.84	33.66	33.17	33.42	33.39
Cr2O3	0.00	0.00	0.00	0.00	0.00	0.00	0.00	0.00	0.00	0.00	0.00	0.00	0.00	0.00	0.00
FeO	6.66	6.75	6.54	6.81	6.87	6.86	6.99	6.70	6.66	6.46	6.60	6.76	6.45	6.82	6.78
MnO	0.10	0.00	0.00	0.00	0.00	0.12	0.12	0.00	0.14	0.11	0.00	0.11	0.00	0.09	0.00
MgO	9.93	9.58	9.64	9.62	9.75	9.72	9.84	9.53	9.65	9.71	9.42	10.00	9.99	9.95	9.89
TOTAL	99.36	98.21	98.99	98.94	99.72	98.96	99.87	98.74	98.90	98.12	98.05	100.47	99.54	99.92	99.87
CATIONS															
Si	4.973	4.991	5.009	4.980	4.989	4.998	4.991	5.012	5.007	4.988	5.024	4.993	5.027	4.992	5.007
Ti	0.000	0.000	0.000	0.000	0.000	0.000	0.000	0.000	0.000	0.009	0.007	0.000	0.000	0.000	0.000
Al	3.990	3.987	3.982	4.004	3.985	3.959	3.961	3.975	3.966	3.976	3.959	3.967	3.936	3.962	3.956
Cr	0.000	0.000	0.000	0.000	0.000	0.000	0.000	0.000	0.000	0.000	0.000	0.000	0.000	0.000	0.000
Fe	0.563	0.578	0.554	0.578	0.579	0.583	0.588	0.569	0.565	0.553	0.564	0.566	0.543	0.574	0.570
Mn	0.009	0.000	0.000	0.000	0.000	0.010	0.011	0.000	0.012	0.009	0.000	0.009	0.000	0.008	0.000
Mg	1.497	1.460	1.455	1.456	1.465	1.472	1.477	1.443	1.460	1.480	1.436	1.490	1.499	1.491	1.482
(O)	18	18	18	18	18	18	18	18	18	18	18	18	18	18	18
TOTAL	11.032	11.016	11.000	11.018	11.018	11.022	11.028	10.999	11.010	11.015	10.990	11.025	11.005	11.027	11.015
Mg#	0.73	0.72	0.72	0.72	0.72	0.72	0.72	0.72	0.72	0.73	0.72	0.72	0.73	0.72	0.72

BIOTITE

%OXIDE	Bt1	Bt1	Bt3	Bt4	Bt5	Bt6	Bt7	Bt8	Bt9	Bt10	Bt11	Brt12	Bt13	Bt14
SiO2	36.35	36.10	35.69	35.28	36.64	35.96	36.20	36.28	36.11	36.45	36.38	36.95	37.01	35.46
TiO2	4.23	4.22	4.82	4.81	4.28	4.14	4.00	3.36	4.84	4.84	4.23	4.40	4.63	4.19
Cr2O3	0.10	0.10	0.15	0.13	0.14	0.20	0.19	0.27	0.15	0.00	0.16	0.18	0.14	0.14
Al2O3	16.23	16.15	15.74	15.76	16.14	15.83	15.97	16.30	16.05	16.02	16.27	16.31	16.44	16.03
FeO	16.64	16.27	15.19	15.10	14.84	14.39	13.83	13.74	15.05	15.22	15.16	15.44	15.00	15.74
MnO	0.00	0.00	0.00	0.00	0.00	0.00	0.00	0.00	0.00	0.00	0.00	0.00	0.00	0.00
MgO	12.57	12.73	12.86	12.99	13.51	13.93	14.24	14.77	13.32	13.51	13.64	14.17	13.46	12.99
CaO	0.08	0.11	0.10	0.00	0.00	0.00	0.13	0.09	0.13	0.11	0.00	0.11	0.06	0.00
Na2O	0.47	0.67	0.66	0.52	0.56	0.58	0.56	0.67	0.60	0.80	0.58	0.52	0.63	0.62
K2O	8.79	8.80	8.66	8.63	9.10	8.83	8.76	8.76	8.66	8.69	8.77	8.72	8.80	8.48
Cl2O	0.00	0.00	0.00	0.06	0.00	0.09	0.04	0.00	0.00	0.11	0.04	0.00	0.00	0.00
TOTAL	95.46	95.14	93.87	93.29	95.20	93.94	93.92	94.24	94.92	95.75	95.21	96.81	96.17	93.65
FORMULA														
Si	5.452	5.433	5.423	5.395	5.472	5.440	5.456	5.445	5.414	5.422	4.435	5.427	5.460	5.407
Ti	0.477	0.478	0.551	0.553	0.480	0.471	0.453	0.379	0.545	0.542	0.475	0.486	0.513	0.481
Cr	0.012	0.012	0.018	0.016	0.017	0.024	0.023	0.031	0.018	0.000	0.018	0.021	0.017	0.017
Al	2.870	2.865	2.819	2.842	2.842	2.822	2.838	2.883	2.836	2.809	2.865	2.823	2.859	2.882
Fe2+	2.087	2.048	1.930	1.932	1.853	1.821	1.743	1.724	1.887	1.894	1.894	1.896	1.851	2.007
Mn	0.000	0.000	0.000	0.000	0.000	0.000	0.000	0.000	0.000	0.000	0.000	0.000	0.000	0.000
Mg	2.810	2.856	2.913	2.960	3.007	3.142	3.199	3.305	2.977	2.997	3.038	3.102	2.960	2.953
Ca	0.013	0.017	0.017	0.000	0.000	0.000	0.020	0.015	0.021	0.018	0.000	0.018	0.010	0.000
Na	0.137	0.194	0.193	0.155	0.161	0.170	0.164	0.196	0.176	0.231	0.167	0.148	0.181	0.184
K	1.683	1.689	1.679	1.685	1.734	1.704	1.684	1.677	1.657	1.649	1.671	1.634	1.657	1.649
Cl	0.000	0.000	0.000	0.013	0.000	0.018	0.009	0.000	0.000	0.022	0.008	0.000	0.000	0.000
(O)	22	22	22	22	22	22	22	22	22	22	22	22	22	22
TOTAL	15.541	15.592	15.543	15.551	15.566	15.612	15.589	15.655	15.531	15.584	14.571	15.555	15.508	15.580
Mg#	0.57	0.58	0.60	0.61	0.62	0.63	0.65	0.66	0.61	0.61	0.62	0.62	0.62	0.60

DD.BQ38

GARNET With Fe3+ Recalculations

%OXIDE	Grt1	Grt1	Grt2	Grt2	GRt3	Grt3	Grt4	Grt4	Grt5	Grt5	Grt6	Grt6	Grt7	Grt7	Grt8	Grt8	Grt9	Grt9
SiO2	38.25	38.25	38.44	38.44	38.16	38.16	38.60	38.60	38.19	38.19	37.56	37.56	38.29	38.29	37.88	37.88	37.75	37.75
TiO2	0.00	0.00	0.00	0.00	0.00	0.00	0.00	0.00	0.00	0.00	0.00	0.00	0.00	0.00	0.00	0.00	0.00	0.00
Cr2O3	0.00	0.00	0.00	0.00	0.00	0.00	0.00	0.00	0.00	0.00	0.00	0.00	0.00	0.00	0.00	0.00	0.00	0.00
Al2O3	21.52	21.52	21.74	21.74	21.31	21.31	21.79	21.79	21.44	21.44	21.10	21.10	21.74	21.74	21.40	21.40	21.39	21.39
Fe2O3	-	0.89	-	1.16	-	0.89	-	0.13	-	1.79	-	1.08	-	1.64	-	1.32	-	1.31
FeO	32.02	31.22	32.44	31.40	32.20	31.40	31.83	31.72	32.69	31.08	31.48	30.51	32.12	30.64	31.86	30.68	31.87	30.69
MnO	0.83	0.83	0.86	0.86	0.82	0.82	0.79	0.79	0.85	0.85	0.88	0.88	0.85	0.85	0.92	0.92	0.83	0.83
MgO	6.68	6.68	6.68	6.68	6.49	6.49	6.66	6.66	6.63	6.63	6.49	6.49	6.92	6.92	6.63	6.63	6.63	6.63
CaO	1.40	1.40	1.42	1.42	1.45	1.45	1.36	1.36	1.50	1.50	1.52	1.52	1.51	1.51	1.43	1.43	1.40	1.40
TOTAL	100.70	100.78	101.58	101.69	100.42	100.51	101.03	101.04	101.29	101.46	99.02	99.13	101.44	101.60	100.11	100.25	99.87	100.00
CATIONS																		
Si	5.981	5.968	5.966	5.949	5.992	5.979	6.000	5.998	5.958	5.932	5.978	5.962	5.946	5.922	5.964	5.945	5.958	5.939
Ti	0.000	0.000	0.000	0.000	0.000	0.000	0.000	0.000	0.000	0.000	0.000	0.000	0.000	0.000	0.000	0.000	0.000	0.000
Cr	0.000	0.000	0.000	0.000	0.000	0.000	0.000	0.000	0.000	0.000	0.000	0.000	0.000	0.000	0.000	0.000	0.000	0.000
Al	3.966	3.957	3.976	3.965	3.944	3.935	3.992	3.991	3.942	3.925	3.958	3.947	3.980	3.964	3.971	3.958	3.98	3.967
Fe3+	-	0.105	-	0.135	-	0.105	-	0.015	-	0.209	-	0.129	-	0.191	-	0.155	-	0.155
Fe2+	4.187	4.073	4.210	4.064	4.229	4.115	4.139	4.123	4.266	4.038	4.191	4.051	4.172	3.964	4.196	4.027	4.207	4.038
Mn	0.109	0.109	0.113	0.113	0.109	0.109	0.104	0.104	0.112	0.112	0.119	0.119	0.112	0.112	0.123	0.123	0.11	0.110
Mg	1.557	1.554	1.545	1.541	1.518	1.515	1.543	1.543	1.542	1.535	1.539	1.535	1.602	1.596	1.557	1.552	1.56	1.555
Ca	0.235	0.234	0.235	0.234	0.243	0.242	0.227	0.227	0.250	0.249	0.258	0.257	0.252	0.251	0.241	0.240	0.237	0.236
(O)	24	24	24	24	24	24	24	24	24	24	24	24	24	24	24	24	24	24
TOTAL	16.035	16.000	16.045	16.000	16.035	16.000	16.005	16.000	16.070	16.000	16.043	16.000	16.064	16.000	16.052	16.000	16.052	16.000
Mg#	0.27	0.28	0.27	0.27	0.26	0.27	0.27	0.27	0.27	0.28	0.27	0.27	0.28	0.29	0.27	0.28	0.27	0.28

GARNET With Fe3+ Recalculations

%OXIDE	Grt10	Grt10	Grt11	Grt11	Grt12	Grt12	Grt13	Grt13	Grt14	Grt14	Grt15	Grt15
SiO2	37.62	37.62	37.70	37.70	38.36	38.36	38.05	38.05	37.94	37.94	37.83	37.83
TiO2	0.00	0.00	0.00	0.00	0.00	0.00	0.00	0.00	0.00	0.00	0.00	0.00
Cr2O3	0.00	0.00	0.00	0.00	0.00	0.00	0.00	0.00	0.00	0.00	0.00	0.00
Al2O3	21.52	21.52	21.37	21.37	21.54	21.54	21.75	21.75	21.23	21.23	21.61	21.61
Fe2O3	-	1.11	-	0.81	-	1.05	-	2.00	-	0.81	-	0.96
FeO	31.52	30.52	31.72	30.99	32.23	31.28	32.10	30.30	32.65	31.92	32.33	31.47
MnO	0.86	0.86	0.76	0.76	0.87	0.87	0.82	0.82	0.72	0.72	0.92	0.92
MgO	6.64	6.64	6.50	6.50	6.64	6.64	7.01	7.01	6.00	6.00	6.34	6.34
CaO	1.39	1.39	1.35	1.35	1.45	1.45	1.44	1.44	1.58	1.58	1.49	1.49
TOTAL	99.54	99.65	99.39	99.47	101.08	101.19	101.17	101.37	100.12	100.20	100.52	100.62
CATIONS												
Si	5.950	5.934	5.974	5.962	5.980	5.965	5.926	5.897	5.992	5.980	5.945	5.931
Ti	0.000	0.000	0.000	0.000	0.000	0.000	0.000	0.000	0.000	0.000	0.000	0.000
Cr	0.000	0.000	0.000	0.000	0.000	0.000	0.000	0.000	0.000	0.000	0.000	0.000
Al	4.011	4.000	3.990	3.982	3.958	3.948	3.993	3.974	3.952	3.944	4.002	3.993
Fe3+	-	0.132	-	0.096	-	0.123	-	0.233	-	0.096	-	0.114
Fe2+	4.169	4.026	4.203	4.099	4.202	4.069	4.182	3.929	4.312	4.208	4.249	4.125
Mn	0.115	0.115	0.102	0.102	0.115	0.115	0.108	0.107	0.097	0.097	0.123	0.123
Mg	1.564	1.560	1.534	1.531	1.543	1.539	1.628	1.620	1.412	1.409	1.468	1.465
Ca	0.235	0.234	0.229	0.229	0.243	0.242	0.241	0.240	0.267	0.266	0.251	0.250
(O)	24	24	24	24	24	24	24	24	24	24	24	24
TOTAL	16.044	16.000	16.032	16.000	16.041	16.000	16.078	16.000	16.032	16.000	16.038	16.000
Mg#	0.27	0.28	0.27	0.27	0.27	0.27	0.28	0.29	0.25	0.25	0.26	0.26

ORTHOPYROXENE

OXIDE%	Opx1	Opx2	Opx3	Opx4	Opx5	Opx6	Opx7	Opx8	Opx9	Opx10	Opx11	Opx12	Opx13	Opx14
SiO2	49.70	48.68	48.18	48.11	49.12	47.89	48.81	47.66	48.06	48.30	48.41	47.48	47.87	47.49
TiO2	0.20	0.00	0.31	0.25	0.00	0.27	0.25	0.23	0.00	0.27	0.24	0.40	0.28	0.23
Al2O3	3.66	4.83	5.44	5.86	3.44	5.26	5.21	5.07	5.16	5.40	5.52	6.97	5.43	5.83
Cr2O3	0.00	0.19	0.00	0.18	0.00	0.00	0.00	0.00	0.00	0.00	0.00	0.00	0.20	0.00
FeO	31.68	32.17	31.81	30.88	31.46	30.64	31.25	30.52	31.30	31.27	31.28	31.64	31.30	31.21
MnO	0.00	0.00	0.00	0.00	0.00	0.00	0.00	0.00	0.00	0.00	0.00	0.00	0.00	0.00
MgO	15.26	14.88	15.03	15.23	15.17	15.02	14.87	14.72	14.89	14.98	14.90	14.40	14.91	14.67
CaO	0.19	0.00	0.19	0.17	0.15	0.26	0.13	0.17	0.16	0.23	0.19	0.19	0.14	0.19
TOTAL	100.68	100.74	100.96	100.67	99.35	99.33	100.52	98.36	99.57	100.45	100.53	101.07	100.12	99.61
CATIONS														
Si	1.916	1.882	1.857	1.852	1.921	1.869	1.881	1.878	1.875	1.866	1.868	1.826	1.858	1.853
Ti	0.006	0.000	0.009	0.007	0.000	0.008	0.007	0.007	0.000	0.008	0.007	0.011	0.008	0.007
Al	0.166	0.220	0.247	0.266	0.159	0.242	0.237	0.235	0.237	0.246	0.251	0.316	0.248	0.268
Cr	0.000	0.006	0.000	0.005	0.000	0.000	0.000	0.000	0.000	0.000	0.000	0.000	0.006	0.000
Fe	1.022	1.040	1.025	0.994	1.090	1.000	1.007	1.006	1.021	1.011	1.009	1.018	1.016	1.018
Mn	0.000	0.000	0.000	0.000	0.000	0.000	0.000	0.000	0.000	0.000	0.000	0.000	0.000	0.000
Mg	0.877	0.858	0.864	0.874	0.885	0.874	0.855	0.865	0.866	0.863	0.857	0.826	0.863	0.853
Ca	0.008	0.000	0.008	0.007	0.006	0.011	0.005	0.007	0.007	0.009	0.008	0.008	0.006	0.008
(O)	6	6	6	6	6	6	6	6	6	6	6	6	6	6
TOTAL	3.995	4.006	4.010	4.005	4.061	4.004	3.992	3.998	4.006	4.003	4.000	4.005	4.005	4.007
Mg#	0.46	0.45	0.46	0.47	0.45	0.47	0.46	0.46	0.46	0.46	0.46	0.45	0.46	0.46

PLAGIOCLASE

%OXIDE	Pl1	Pl2	Pl3	Pl4	Pl5	Pl6	Pl7	Pl8	Pl9	Pl10
SiO2	57.95	55.50	53.51	53.75	53.35	53.51	53.26	53.77	54.45	53.51
Al2O3	26.86	29.18	29.74	29.56	29.63	30.16	30.12	30.03	29.74	29.97
CaO	8.63	11.26	12.40	11.96	12.23	12.47	12.71	12.36	12.26	12.41
Na2O	6.35	5.32	4.41	4.63	4.63	4.58	4.47	4.54	4.42	4.49
K2O	0.49	0.16	0.18	0.00	0.15	0.15	0.13	0.14	0.18	0.21
TOTAL	100.27	101.42	100.25	99.90	99.98	100.86	100.69	100.84	101.04	100.59
CATIONS										
Si	2.588	2.468	2.415	2.428	2.414	2.402	2.396	2.412	2.433	2.408
Al	1.414	1.529	1.582	1.574	1.580	1.596	1.597	1.588	1.576	1.590
Ca	0.413	0.536	0.600	0.579	0.593	0.600	0.613	0.594	0.587	0.598
Na	0.550	0.458	0.386	0.406	0.406	0.398	0.390	0.395	0.383	0.392
K	0.028	0.009	0.011	0.000	0.008	0.009	0.007	0.008	0.010	0.012
(O)	8	8	8	8	8	8	8	8	8	8
TOTAL	4.993	5.000	4.994	4.987	5.001	5.005	5.003	4.997	4.989	5.000

DD.BQ38

CORDIERITE

OXIDE%	Crd1	Crd2	Crd3	Crd4	Crd5	Crd6	Crd7	Crd8	Crd9	Crd10	Crd11	Crd12	Crd13	Crd14	Crd15	Crd16	Crd17	Crd18
SiO2	49.46	48.94	49.42	49.76	49.34	49.14	48.94	48.87	48.77	49.27	49.29	48.37	48.36	49.42	48.94	48.71	48.96	49.06
TiO2	0.00	0.00	0.00	0.00	0.00	0.00	0.00	0.00	0.00	0.00	0.00	0.00	0.00	0.00	0.00	0.00	0.00	0.00
Al2O3	33.53	32.84	33.52	33.57	32.92	32.98	33.11	32.58	32.92	33.36	33.44	32.74	32.66	33.15	33.35	32.96	33.01	33.04
Cr2O3	0.00	0.00	0.00	0.00	0.00	0.00	0.00	0.00	0.00	0.00	0.00	0.00	0.00	0.00	0.00	0.00	0.00	0.00
FeO	8.31	8.05	8.46	8.34	8.25	8.43	8.63	8.64	8.36	8.13	8.39	8.16	8.34	8.25	8.21	8.14	8.38	8.18
MnO	0.00	0.00	0.00	0.00	0.00	0.00	0.00	0.00	0.00	0.00	0.00	0.00	0.00	0.00	0.00	0.00	0.00	0.00
MgO	8.93	8.73	8.99	9.17	8.62	8.77	9.02	8.35	8.72	9.10	9.00	8.85	8.71	9.00	8.91	8.80	8.85	8.98
TOTAL	100.22	98.56	100.40	100.83	99.13	99.33	99.70	98.45	98.76	99.85	100.13	98.13	98.06	99.82	99.42	98.60	99.20	99.26
CATIONS																		
Si	4.989	5.014	4.981	4.989	5.028	5.005	4.975	5.026	4.995	4.985	4.980	4.985	4.991	5.004	4.977	4.992	4.993	4.996
Ti	0.000	0.000	0.000	0.000	0.000	0.000	0.000	0.000	0.000	0.000	0.000	0.000	0.000	0.000	0.000	0.000	0.000	0.000
Al	3.987	3.966	3.983	3.967	3.954	3.959	3.967	3.949	3.975	3.979	3.983	3.977	3.973	3.957	3.998	3.982	3.969	3.966
Cr	0.000	0.000	0.000	0.000	0.000	0.000	0.000	0.000	0.000	0.000	0.000	0.000	0.000	0.000	0.000	0.000	0.000	0.000
Fe2+	0.701	0.690	0.713	0.699	0.704	0.718	0.733	0.743	0.716	0.688	0.709	0.704	0.720	0.699	0.698	0.697	0.715	0.697
Mn	0.000	0.000	0.000	0.000	0.000	0.000	0.000	0.000	0.000	0.000	0.000	0.000	0.000	0.000	0.000	0.000	0.000	0.000
Mg	1.342	1.334	1.351	1.371	1.309	1.332	1.367	1.281	1.332	1.373	1.355	1.360	1.339	1.358	1.351	1.344	1.346	1.363
(O)	18	18	18	18	18	18	18	18	18	18	18	18	18	18	18	18	18	18
TOTAL	11.019	11.004	11.028	11.026	10.995	11.014	11.042	10.999	11.018	11.025	11.027	11.026	11.023	11.018	11.024	11.015	11.023	11.022
Mg#	0.66	0.66	0.65	0.66	0.65	0.65	0.65	0.63	0.65	0.67	0.66	0.66	0.65	0.66	0.66	0.66	0.65	0.66

BIOTITE With W.D. Analysis for Ti, Ba and F

%OXIDE	Bt1	Bt2	Bt3	Bt4	Bt5	Bt6	Bt7	Bt8	Bt9	Bt10	Bt11	Bt12	Bt13	Bt14	Bt15
SiO2	36.53	36.37	36.37	36.11	36.55	36.03	36.72	36.27	36.00	35.96	36.11	36.23	36.18	36.50	36.64
Al2O3	17.66	17.24	17.32	17.29	17.12	16.95	17.75	17.24	17.48	17.26	17.44	17.18	17.23	17.26	17.84
FeO	18.31	18.36	18.45	18.48	18.60	18.88	18.54	18.48	18.73	18.56	18.14	18.24	18.52	18.09	18.46
MnO	0.08	0.14	0.07	0.14	0.00	0.00	0.00	0.04	0.00	0.00	0.03	0.10	0.00	0.02	0.00
MgO	10.54	10.45	10.13	10.16	10.68	10.27	10.89	10.40	10.68	10.63	10.91	10.97	11.08	11.37	11.47
CaO	0.06	0.00	0.00	0.00	0.00	0.06	0.00	0.11	0.13	0.01	0.06	0.13	0.00	0.05	0.09
Na2O	0.07	0.03	0.27	0.37	0.41	0.33	0.43	0.58	0.00	0.11	0.00	0.34	0.62	0.36	0.42
K2O	9.46	9.47	9.06	9.28	9.41	9.43	9.12	9.24	9.50	9.37	9.46	9.46	9.23	9.39	9.45
Cl	0.04	0.04	0.73	0.07	0.13	0.00	0.13	0.06	0.07	0.04	0.02	0.14	0.07	0.08	0.00
F	0.12	0.16	0.18	0.15	0.38	0.27	0.24	0.27	0.16	0.24	0.24	0.36	0.28	0.44	0.41
TiO2	5.28	5.44	5.33	5.13	5.10	5.05	4.23	4.71	4.76	4.73	4.12	4.41	4.42	4.43	4.33
BaO	0.36	0.34	0.98	0.48	0.39	0.29	0.30	0.39	0.34	0.35	0.27	0.30	0.42	0.27	0.29
Cr2O3	0.06	0.07	0.19	0.13	0.10	0.03	0.20	0.01	0.17	0.14	0.25	0.11	0.30	0.00	0.225
TOTAL	98.58	98.11	99.06	97.79	98.86	97.59	98.55	97.79	98.02	97.40	97.03	97.97	98.34	98.27	99.62
CATIONS															
Si	5.368	5.380	5.384	5.373	5.391	5.382	5.404	5.398	5.345	5.370	5.397	5.389	5.361	5.398	5.345
Al	3.059	3.005	3.022	3.033	2.975	2.984	3.078	3.024	3.059	3.038	3.073	3.012	3.010	3.009	3.068
Fe	2.251	2.271	2.284	2.300	2.295	2.358	2.282	2.300	2.326	2.318	2.267	2.269	2.294	2.237	2.253
Mn	0.010	0.017	0.008	0.018	0.000	0.000	0.000	0.005	0.000	0.000	0.003	0.012	0.000	0.003	0.000
Mg	2.309	2.303	2.235	2.254	2.347	2.287	2.389	2.306	2.364	2.367	2.431	2.432	2.446	2.505	2.495
Ca	0.010	0.000	0.000	0.000	0.000	0.010	0.000	0.017	0.020	0.002	0.009	0.020	0.000	0.009	0.014
Na	0.019	0.009	0.077	0.108	0.118	0.096	0.123	0.166	0.000	0.032	0.000	0.098	0.178	0.102	0.119
K	1.775	1.788	1.711	1.762	1.771	1.797	1.713	1.754	1.799	1.786	1.804	1.796	1.744	1.770	1.759
Cl	0.011	0.010	0.018	0.018	0.033	0.000	0.033	0.014	0.019	0.009	0.005	0.034	0.017	0.020	0.000
F	0.057	0.076	0.086	0.068	0.178	0.126	0.110	0.127	0.073	0.115	0.115	0.169	0.132	0.206	0.188
Ti	0.584	0.605	0.593	0.574	0.565	0.568	0.467	0.527	0.532	0.531	0.463	0.493	0.492	0.493	0.475
Ba	0.021	0.020	0.057	0.028	0.022	0.017	0.017	0.023	0.020	0.020	0.016	0.018	0.024	0.016	0.016
Cr	0.006	0.008	0.022	0.015	0.011	0.004	0.023	0.002	0.019	0.016	0.029	0.012	0.035	0.000	0.026
(O)	22	22	22	22	22	22	22	22	22	22	22	22	22	22	22
TOTAL	15.480	15.492	15.497	15.551	15.706	15.629	15.639	15.663	15.576	15.604	15.612	15.754	15.733	15.768	15.758

SPINEL With Fe3+ Recalculations

%OXIDE	Spl1	Spl1	Spl2	Spl2	Spl3	Spl3	Spl4	Spl4	Spl5	Spl5
SiO2	0.00	0.00	0.00	0.00	0.00	0.00	0.00	0.00	0.00	0.00
TiO2	0.00	0.00	0.00	0.00	0.22	0.22	0.00	0.00	0.00	0.00
Al2O3	56.81	56.81	56.88	56.88	56.19	56.19	56.32	56.32	54.11	54.11
Cr2O3	0.75	0.75	0.38	0.38	1.21	1.21	0.00	0.00	1.96	1.96
Fe2O3	-	4.08	-	4.71	-	4.34	-	4.91	-	5.97
FeO	34.70	31.03	35.03	30.80	35.32	31.42	34.81	30.39	36.03	30.66
MnO	0.00	0.00	0.00	0.00	0.00	0.00	0.00	0.00	0.00	0.00
MgO	5.54	5.54	5.29	5.29	4.85	4.85	5.86	5.86	5.42	5.42
CaO	0.00	0.00	0.00	0.00	0.00	0.00	0.00	0.00	0.00	0.00
ZnO	1.42	1.42	2.28	2.28	2.81	2.81	1.34	1.34	1.66	1.66
TOTAL	99.23	99.64	99.87	100.34	100.60	101.03	98.33	98.82	99.18	99.77
CATIONS										
Si	0.000	0.000	0.000	0.000	0.000	0.000	0.000	0.000	0.000	0.000
Ti	0.000	0.000	0.000	0.000	0.005	0.005	0.000	0.000	0.000	0.000
Al	1.918	1.897	1.917	1.893	1.893	1.871	1.918	1.893	1.856	1.826
Cr	0.017	0.017	0.009	0.009	0.027	0.027	0.000	0.000	0.045	0.044
Fe3+	-	0.087	-	0.100	-	0.092	-	0.105	-	0.129
Fe2+	0.831	0.735	0.838	0.727	0.844	0.742	0.841	0.725	0.877	0.734
Mn	0.000	0.000	0.000	0.000	0.000	0.000	0.000	0.000	0.000	0.000
Mg	0.237	0.234	0.226	0.223	0.207	0.205	0.252	0.249	0.235	0.231
Ca	0.000	0.000	0.000	0.000	0.000	0.000	0.000	0.000	0.000	0.000
Zn	0.030	0.030	0.048	0.047	0.059	0.058	0.029	0.029	0.036	0.035
(O)	4	4	4	4	4	4	4	4	4	4
TOTAL	3.033	3.000	3.038	3.000	3.035	3.000	3.040	3.000	3.049	3.000
Mg#	0.22	0.24	0.21	0.23	0.20	0.22	0.23	0.26	0.21	0.24

DD.CASB5																
GARNET																
%OXIDE	Grt1	Grt1	Grt2	Grt2	Grt3	Grt3	Grt4	Grt4	Grt5	Grt5	GrtR6	GrtR6	GrtR7	GrtR7	GrtR8	GrtR8
SiO2	38.69	38.69	38.56	38.56	38.44	38.44	38.39	38.39	38.74	38.74	38.46	38.46	37.07	37.07	38.31	38.31
TiO2	0.00	0.00	0.17	0.17	0.00	0.00	0.00	0.00	0.00	0.00	0.00	0.00	0.00	0.00	0.00	0.00
Cr2O3	0.00	0.00	0.00	0.00	0.00	0.00	0.00	0.00	0.00	0.00	0.00	0.00	0.00	0.00	0.00	0.00
Al2O3	22.02	22.02	21.71	21.71	21.76	21.76	21.89	21.89	22.10	22.10	21.79	21.79	21.02	21.02	21.77	21.77
Fe2O3	-	1.22	-	0.75	-	1.52	-	1.47	-	0.88	-	0.85	-	0.84	-	0.95
FeO	29.81	28.71	29.14	28.47	29.30	27.93	29.30	27.98	29.62	28.83	29.01	28.25	31.12	30.36	31.34	30.48
MnO	1.21	1.21	1.76	1.76	1.81	1.81	1.76	1.76	1.70	1.70	1.89	1.89	1.39	1.39	1.33	1.33
MgO	7.70	7.70	7.64	7.64	7.75	7.75	7.74	7.74	7.53	7.53	7.66	7.66	5.47	5.47	6.08	6.08
CaO	2.01	2.01	1.88	1.88	1.86	1.86	1.84	1.84	1.83	1.83	1.70	1.70	2.19	2.19	2.44	2.44
TOTAL	101.43	101.55	100.85	100.93	100.91	101.07	100.92	101.06	101.52	101.61	100.50	100.58	98.26	98.34	101.26	101.35
CATIONS																
Si	5.957	5.940	5.969	5.958	5.954	5.932	5.945	5.924	5.961	5.948	5.972	5.960	5.971	5.958	5.966	5.952
Ti	0.000	0.000	0.020	0.020	0.000	0.000	0.000	0.000	0.000	0.000	0.000	0.000	0.000	0.000	0.000	0.000
Cr	0.000	0.000	0.000	0.000	0.000	0.000	0.000	0.000	0.000	0.000	0.000	0.000	0.000	0.000	0.000	0.000
Al	3.995	3.983	3.961	3.954	3.972	3.957	3.995	3.981	4.010	4.001	3.989	3.981	3.991	3.983	3.996	3.987
Fe3+	-	0.141	-	0.087	-	0.176	-	0.170	-	0.102	-	0.099	-	0.102	-	0.111
Fe2+	3.838	3.686	3.774	3.680	3.795	3.605	3.794	3.610	3.813	3.703	3.768	3.661	4.192	4.081	4.081	3.961
Mn	0.158	0.158	0.230	0.230	0.238	0.237	0.231	0.230	0.221	0.221	0.248	0.247	0.189	0.189	0.175	0.175
Mg	1.767	1.762	1.764	1.761	1.791	1.784	1.786	1.780	1.728	1.724	1.774	1.770	1.313	1.310	1.412	1.409
Ca	0.332	0.331	0.311	0.310	0.309	0.308	0.306	0.305	0.301	0.300	0.282	0.281	0.378	0.377	0.407	0.406
(O)	24	24	24	24	24	24	24	24	24	24	24	24	24	24	24	24
TOTAL	16.047	16.000	16.029	16.000	16.059	16.000	16.057	16.000	16.034	16.000	16.033	16.000	16.034	16.000	16.037	16.000
Mg#	0.32	0.32	0.32	0.32	0.32	0.33	0.32	0.33	0.31	0.32	0.32	0.33	0.24	0.24	0.26	0.26
ORTHOPYROXENE																
%OXIDE	Opx1	Opx2	Opx3	Opx4	Opx5	Opx6	Opx7	Opx8	Opx9	Opx10						
SiO2	49.67	50.62	49.83	50.72	49.63	50.01	50.25	50.18	50.05	49.02						
TiO2	0.00	0.12	0.12	0.24	0.14	0.30	0.24	0.13	0.13	0.23						
Al2O3	4.20	4.71	4.42	4.12	4.22	4.62	4.78	3.98	4.28	3.91						
Cr2O3	0.00	0.00	0.00	0.00	0.00	0.18	0.17	0.00	0.00	0.09						
FeO	27.31	27.29	27.24	27.80	27.28	27.12	27.61	28.01	28.20	27.77						
MnO	0.41	0.42	0.40	0.44	0.44	0.24	0.36	0.62	0.58	0.41						
MgO	17.54	17.93	17.47	17.65	17.74	17.88	17.91	17.38	17.47	16.97						
CaO	0.17	0.21	0.16	0.21	0.26	0.23	0.16	0.20	0.12	0.29						
TOTAL	99.31	101.31	99.64	101.17	99.70	100.57	101.47	100.49	100.83	98.69						
CATIONS																
Si	1.907	1.900	1.904	1.911	1.899	1.891	1.887	1.910	1.899	1.903						
Ti	0.000	0.004	0.004	0.007	0.004	0.008	0.007	0.004	0.004	0.007						
Al	0.190	0.208	0.199	0.183	0.190	0.206	0.212	0.179	0.192	0.179						
Cr	0.000	0.000	0.000	0.000	0.000	0.005	0.005	0.000	0.000	0.003						
Fe2+	0.877	0.856	0.871	0.876	0.873	0.858	0.867	0.891	0.895	0.901						
Mn	0.013	0.013	0.013	0.014	0.014	0.008	0.011	0.020	0.019	0.013						
Mg	1.004	1.003	0.995	0.991	1.012	1.008	1.003	0.986	0.988	0.982						
Ca	0.007	0.009	0.007	0.008	0.010	0.009	0.006	0.008	0.005	0.012						
(O)	6	6	6	6	6	6	6	6	6	6						
TOTAL	3.998	3.993	3.993	3.990	4.002	3.993	3.998	3.998	4.002	4.000						
Mg#	0.53	0.54	0.53	0.53	0.54	0.54	0.54	0.53	0.52	0.52						
BIOTITE																
%OXIDE	Bt1	Bt2	Bt3	Bt4	Bt5	Bt6	Bt7	Bt8	Bt9	Bt10	Bt11	Bt12	Bt13			
SiO2	36.38	36.50	36.63	36.18	36.93	36.11	36.56	37.00	36.73	36.80	36.33	36.61	37.11			
TiO2	4.22	4.24	4.36	5.02	5.01	4.98	5.21	5.25	3.96	4.38	3.33	4.53	3.72			
Cr2O3	0.00	0.00	0.00	0.00	0.19	0.00	0.22	0.00	0.00	0.00	0.00	0.00	0.00			
Al2O3	16.70	16.82	16.42	16.47	16.42	16.12	16.31	16.63	16.40	16.51	17.20	16.59	16.76			
FeO	16.88	16.05	16.78	16.43	16.53	15.74	15.94	16.06	16.29	16.68	16.95	16.54	16.43			
MnO	0.00	0.00	0.00	0.00	0.00	0.00	0.00	0.00	0.00	0.00	0.00	0.00	0.00			
MgO	12.96	12.94	12.84	12.64	12.74	13.04	12.83	13.04	13.06	12.66	13.72	12.81	13.12			
CaO	0.12	0.00	0.00	0.14	0.15	0.00	0.00	0.00	0.00	0.00	0.15	0.00	0.13			
Na2O	0.51	0.58	0.67	0.70	0.64	0.55	0.57	0.69	0.69	0.57	0.77	0.53	0.56			
K2O	8.89	8.82	8.64	8.81	8.99	8.91	8.99	9.10	8.69	8.96	8.01	8.98	9.02			
TOTAL	96.65	95.95	96.32	96.38	97.60	95.44	96.63	97.76	95.82	96.56	96.46	96.57	96.85			
CATIONS																
Si	5.395	5.425	5.439	5.376	5.418	5.404	5.406	5.404	5.471	5.453	5.374	5.423	5.473			
Ti	0.470	0.474	0.486	0.561	0.553	0.560	0.580	0.576	0.443	0.489	0.370	0.504	0.413			
Cr	0.000	0.000	0.000	0.000	0.021	0.000	0.025	0.000	0.000	0.000	0.000	0.000	0.000			
Al	2.919	2.947	2.874	2.885	2.839	2.843	2.842	2.864	2.878	2.884	2.998	2.896	2.913			
Fe2+	2.093	1.996	2.084	2.042	2.028	1.969	1.971	1.961	2.028	2.066	2.097	2.049	2.027			
Mn	0.000	0.000	0.000	0.000	0.000	0.000	0.000	0.000	0.000	0.000	0.000	0.000	0.000			
Mg	2.865	2.868	2.842	2.800	2.785	2.909	2.827	2.838	2.900	2.796	3.026	2.828	2.884			
Ca	0.019	0.000	0.000	0.023	0.024	0.000	0.000	0.000	0.000	0.000	0.024	0.000	0.020			
Na	0.146	0.166	0.192	0.202	0.181	0.158	0.163	0.195	0.200	0.163	0.220	0.152	0.159			
K	1.682	1.672	1.637	1.670	1.683	1.701	1.696	1.695	1.651	1.693	1.511	1.697	1.697			
(O)	22	22	22	22	22	22	22	22	22	22	22	22	22			
TOTAL	15.589	15.548	15.554	15.559	15.532	15.544	15.510	15.533	15.571	15.544	15.620	15.549	15.586			
Mg#	0.58	0.59	0.58	0.58	0.58	0.60	0.59	0.59	0.59	0.58	0.59	0.58	0.59			

DD.CASB5

SPINEL With Fe3+ Recalculations

%OXIDE	Spl1	Spl1	Spl2	Spl2	Spl3	Spl3	Spl4	Spl4	Spl5	Spl5	Spl6	Spl6	SPl7	Spl7	Spl8	Spl8	SPl9	SPl9
SiO2	0.00	0.00	0.00	0.00	0.00	0.00	0.00	0.00	0.00	0.00	0.00	0.00	0.00	0.00	0.00	0.00	0.00	0.00
TiO2	0.00	0.00	0.00	0.00	0.00	0.00	0.00	0.00	0.00	0.00	0.00	0.00	0.00	0.00	0.00	0.00	0.00	0.00
Al2O3	60.28	60.28	60.28	60.28	59.97	59.97	59.88	59.88	59.24	59.24	59.16	59.16	59.05	59.05	58.87	58.87	59.04	59.04
Cr2O3	0.00	0.00	0.00	0.00	0.00	0.00	0.00	0.00	0.00	0.00	0.00	0.00	0.00	0.00	0.00	0.00	0.00	0.00
Fe2O3	-	2.85	-	2.59	-	2.97	-	2.57	-	2.80	-	2.28	-	2.14	-	2.27	-	2.53
FeO	32.33	29.76	32.50	30.17	32.53	29.86	32.45	30.13	32.12	29.60	31.94	29.89	30.82	28.89	32.03	29.99	31.74	29.46
MnO	0.00	0.00	0.00	0.00	0.00	0.00	0.00	0.00	0.00	0.00	0.00	0.00	0.00	0.00	0.00	0.00	0.00	0.00
MgO	6.79	6.79	6.72	6.72	6.42	6.42	6.43	6.43	6.55	6.55	6.48	6.48	6.68	6.68	6.09	6.09	6.47	6.47
CaO	0.00	0.00	0.00	0.00	0.00	0.00	0.00	0.00	0.00	0.00	0.00	0.00	0.00	0.00	0.00	0.00	0.00	0.00
ZnO	2.03	2.03	1.83	1.83	2.39	2.39	2.04	2.04	2.10	2.10	1.66	1.66	2.05	2.05	1.86	1.86	1.93	1.93
TOTAL	101.42	101.71	101.32	101.58	101.31	101.61	100.79	101.04	100.00	100.28	99.24	99.47	98.61	98.82	98.85	99.08	99.17	99.43
CATIONS																		
Si	0.000	0.000	0.000	0.000	0.000	0.000	0.000	0.000	0.000	0.000	0.000	0.000	0.000	0.000	0.000	0.000	0.000	0.000
Ti	0.000	0.000	0.000	0.000	0.000	0.000	0.000	0.000	0.000	0.000	0.000	0.000	0.000	0.000	0.000	0.000	0.000	0.000
Al	1.957	1.943	1.958	1.945	1.956	1.941	1.959	1.946	1.954	1.940	1.961	1.949	1.965	1.954	1.964	1.952	1.960	1.947
Cr	0.000	0.000	0.000	0.000	0.000	0.000	0.000	0.000	0.000	0.000	0.000	0.000	0.000	0.000	0.000	0.000	0.000	0.000
Fe3+	-	0.059	-	0.053	-	0.061	-	0.053	-	0.059	-	0.048	-	0.045	-	0.048	-	0.053
Fe	0.745	0.681	0.749	0.691	0.753	0.686	0.753	0.695	0.752	0.688	0.751	0.699	0.728	0.679	0.758	0.706	0.748	0.690
Mn	0.000	0.000	0.000	0.000	0.000	0.000	0.000	0.000	0.000	0.000	0.000	0.000	0.000	0.000	0.000	0.000	0.000	0.000
Mg	0.279	0.277	0.276	0.274	0.265	0.263	0.266	0.264	0.273	0.271	0.272	0.270	0.281	0.279	0.257	0.255	0.272	0.270
Ca	0.000	0.000	0.000	0.000	0.000	0.000	0.000	0.000	0.000	0.000	0.000	0.000	0.000	0.000	0.000	0.000	0.000	0.000
Zn	0.041	0.041	0.037	0.037	0.049	0.049	0.042	0.042	0.043	0.043	0.034	0.034	0.043	0.043	0.039	0.039	0.040	0.040
(O)	4	4	4	4	4	4	4	4	4	4	4	4	4	4	4	4	4	4
TOTAL	3.022	3.000	3.020	3.000	3.023	3.000	3.020	3.000	3.022	3.000	3.018	3.000	3.017	3.000	3.018	3.000	3.020	3.000
Mg#	0.27	0.29	0.27	0.28	0.26	0.28	0.26	0.28	0.27	0.28	0.27	0.28	0.28	0.29	0.25	0.27	0.27	0.28

CORDIERITE

OXIDE%	Crd1	Crd2	Crd3	Crd4	Crd5	Crd6	Crd7	Crd8	Crd9	Crd10	Crd11	Crd12	Crd13	Crd14
SiO2	49.07	48.68	49.86	49.36	49.20	49.23	48.82	49.04	48.99	48.97	48.85	48.57	49.35	49.23
TiO2	0.00	0.00	0.00	0.00	0.00	0.00	0.00	0.00	0.00	0.00	0.00	0.00	0.00	0.00
Al2O3	32.99	32.99	33.54	33.37	33.23	33.08	32.92	33.51	33.14	32.86	32.97	33.05	33.22	33.10
Cr2O3	0.00	0.00	0.00	0.00	0.00	0.00	0.00	0.00	0.00	0.00	0.00	0.00	0.00	0.00
FeO	6.61	6.61	7.00	6.85	6.90	6.66	6.67	6.67	6.35	6.82	6.48	6.52	6.85	6.49
MnO	0.00	0.19	0.00	0.00	0.00	0.00	0.00	0.00	0.00	0.00	0.00	0.00	0.00	0.00
MgO	9.74	9.89	9.81	9.78	9.84	9.83	9.90	9.88	9.91	9.66	9.79	9.95	9.70	9.67
TOTAL	98.40	98.35	100.21	99.36	99.16	98.80	98.31	99.11	98.38	98.30	98.10	98.09	99.12	98.48
CATIONS														
Si	5.004	4.975	5.000	4.991	4.987	5.002	4.987	4.969	4.992	5.004	4.996	4.971	5.001	5.012
Ti	0.000	0.000	0.000	0.000	0.000	0.000	0.000	0.000	0.000	0.000	0.000	0.000	0.000	0.000
Al	3.965	3.974	3.965	3.977	3.970	3.962	3.965	4.002	3.981	3.958	3.974	3.987	3.968	3.971
Cr	0.000	0.000	0.000	0.000	0.000	0.000	0.000	0.000	0.000	0.000	0.000	0.000	0.000	0.000
Fe2+	0.564	0.565	0.587	0.579	0.585	0.566	0.570	0.565	0.541	0.583	0.555	0.558	0.580	0.552
Mn	0.000	0.016	0.000	0.000	0.000	0.000	0.000	0.000	0.000	0.000	0.000	0.000	0.000	0.000
Mg	1.480	1.507	1.466	1.474	1.487	1.489	1.508	1.492	1.505	1.472	1.492	1.519	1.466	1.467
(O)	18	18	18	18	18	18	18	18	18	18	18	18	18	18
TOTAL	11.013	11.037	11.018	11.021	11.029	11.019	11.030	11.028	11.019	11.017	11.017	11.035	11.015	11.002

PLAGIOCLASE

%OXIDE	Pl1
SiO2	54.44
Al2O3	29.52
CaO	11.70
Na2O	5.15
K2O	0.07
BaO	0.00
FeO	0.12
TOTAL	101.01
CATIONS	
Si	2.436
Al	1.557
Ca	0.561
Na	0.447
K	0.004
Ba	0.000
Fe	0.005
(O)	8
TOTAL	5.010

APPENDIX II

CORDIERITE WEIGHT LOSS RUNS ON THE THEROMOGRAVIMETRIC BALANCE

STA 1500H

Polymer Laboratories

SMPL ID : 10035
RUN ID : 1 for DD
SIZE : 16.800 MG
OPERATOR: CD

DATE RUN: Mar/17/1994
GAS 1 : Ar 30ml/min
GAS 2 :
COMMENT : coarse

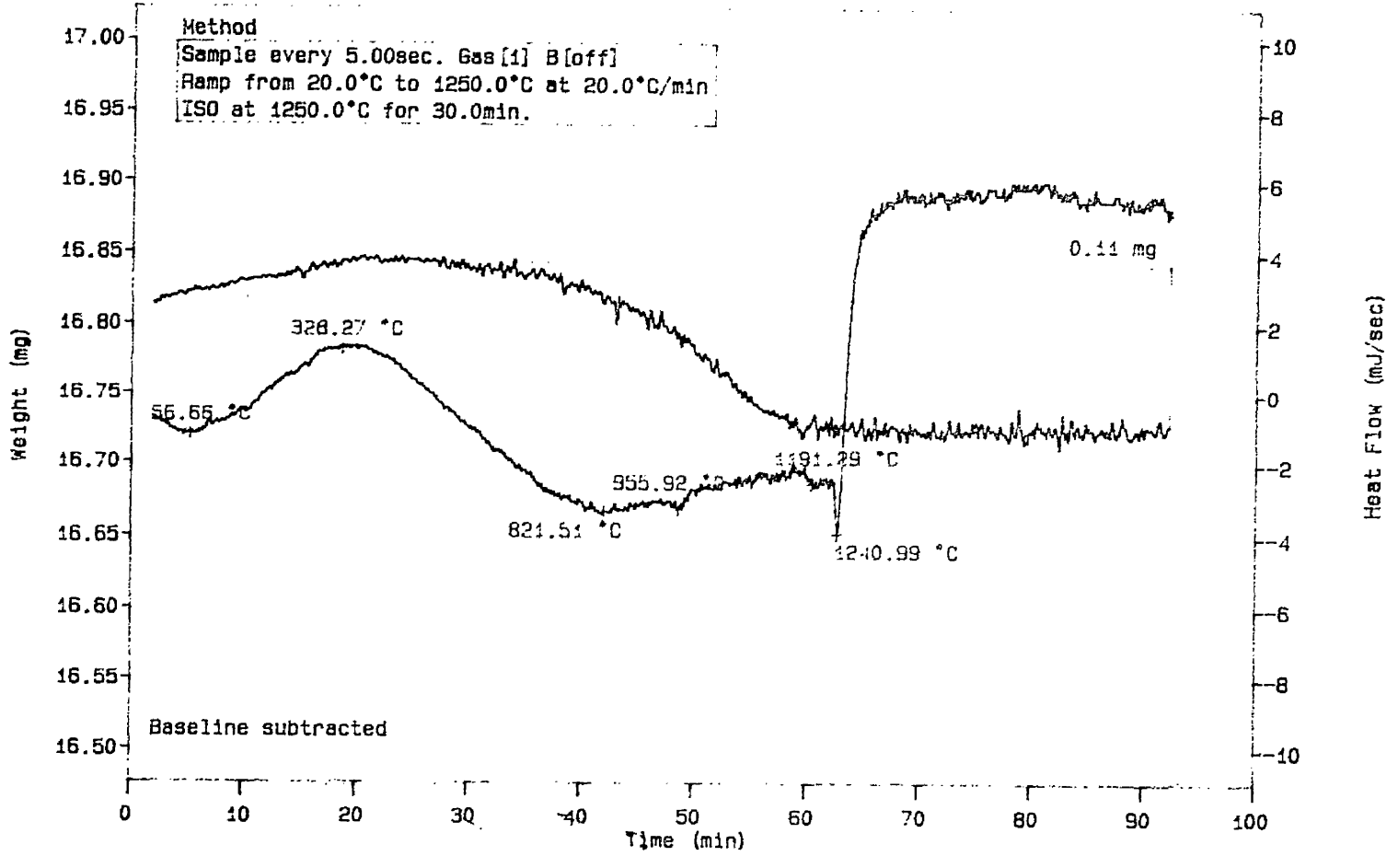

VERSION: V5.40

STA 1500H

Polymer Laboratories

SMPL ID : BQ38
RUN ID : 3
SIZE : 14.770 MG
OPERATOR: JC

DATE RUN: Oct/19/1993
GAS 1 : Ar 30 ml/min
GAS 2 :
COMMENT : holding at 900

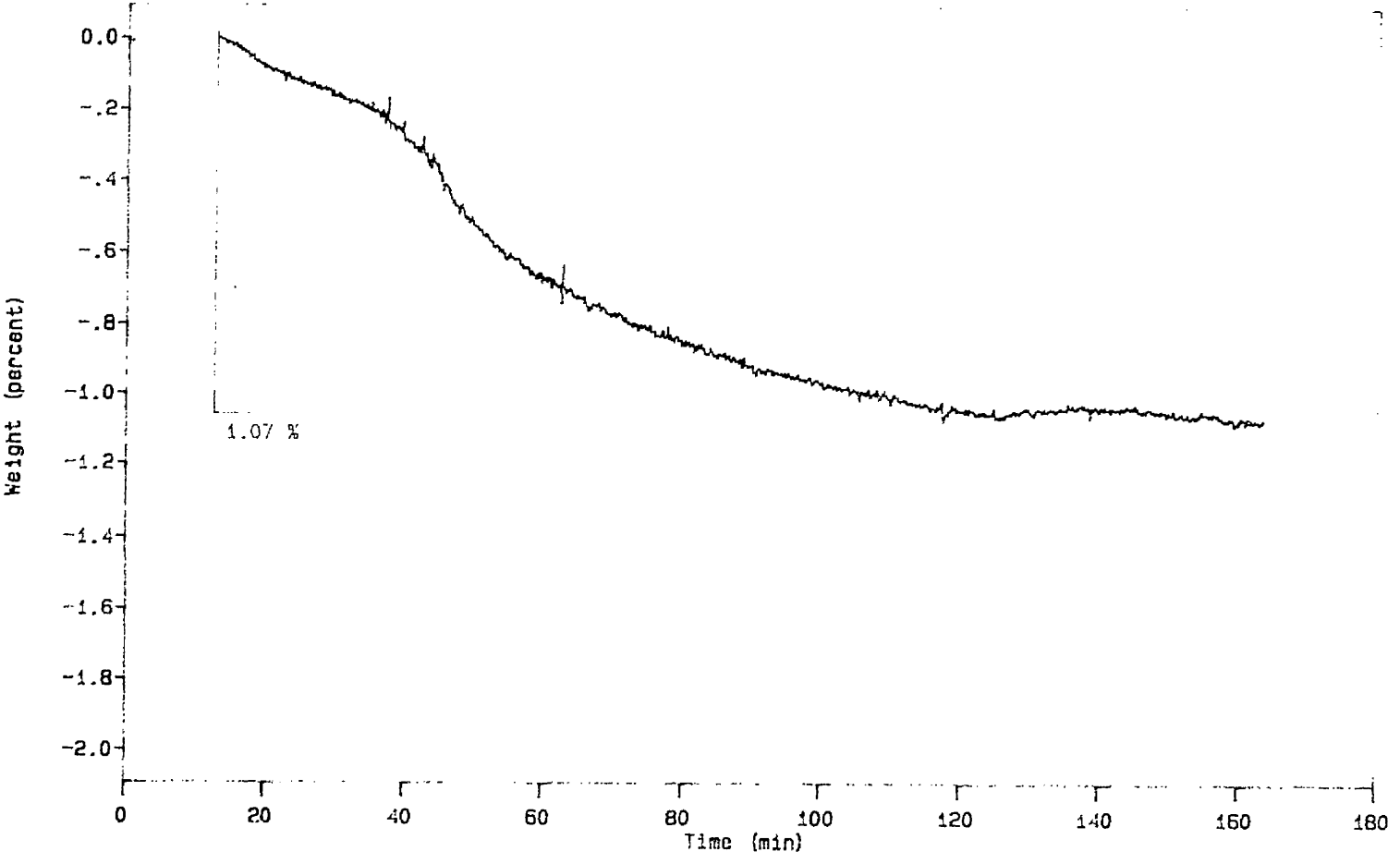

VERSION: V5.40

APPENDIX III

ACTIVITY MODELS FOR BIOTITE, GARNETS AND PLAGIOCLASE

Activity models for biotites used in this study, from Patino Douce et al. (1993) are:

$$a_{phlogopite} = 9.481 X^2_{M2_{Mg}} X_{M1_{Mg}} X_{IV_{Al}} X^3_{Si} X_K X^2_{OH}$$

$$a_{annite} = 9.481 X^2_{M2_{Fe}} X_{M1_{Fe}} X_{IV_{Al}} X^3_{Si} X_K X^2_{OH}$$

Activity models for garnets used in this study, from Berman (1990) are:

$$a_{Gr} = (X_{Gr} \cdot \gamma_{Gr})^3$$
$$a_{Py} = (X_{Py} \cdot \gamma_{Py})^3$$
$$a_{Alm} = (X_{Alm} \cdot \gamma_{Alm})^3$$

where Gr = grossular, Py = pyrope and Alm = almandine. The activity coefficient (γ) is given by:

$$\begin{aligned}
3RT \ln \gamma_{Gr} &= W_{112}(2X_1X_2 - 2X_1^2X_2) + W_{122}(X_1^2 - 2X_1X_2^2) \\
&+ W_{113}(2X_1X_3 - 2X_1^2X_3) + W_{133}(X_1^2 - 2X_1X_3^2) \\
&+ W_{114}(2X_1X_4 - 2X_1^2X_4) + W_{144}(X_1^2 - 2X_1X_4^2) \\
&+ W_{223}(-2X_1^2X_3) + W_{233}(-2X_2X_3^2) \\
&- W_{224}(-2X_1^2X_4) + W_{244}(-2X_2X_4^2) \\
&+ W_{334}(-2X_3^2X_4) + W_{344}(-2X_3X_4^2) \\
&+ W_{123}(X_2X_3 - 2X_1X_2X_3) - W_{124}(X_2X_4 - 2X_1X_2X_4) \\
&+ W_{134}(X_3X_4 - 2X_1X_3X_4) + W_{234}(-2X_1X_3X_4)
\end{aligned}$$

$$\begin{aligned}
3RT \ln \gamma_{Py} &= W_{112}(X_1^2 - 2X_1^2X_2) + W_{122}(2X_1X_2 - 2X_1X_2^2) \\
&- W_{113}(-2X_1^2X_3) + W_{133}(-2X_1X_3^2) \\
&+ W_{114}(-2X_1^2X_4) - W_{144}(-2X_1X_4^2) \\
&+ W_{223}(2X_2X_3 - 2X_1^2X_3) + W_{233}(X_2^2 - 2X_2X_3^2) \\
&- W_{224}(2X_2X_4 - 2X_1^2X_4) + W_{244}(X_2^2 - 2X_2X_4^2) \\
&+ W_{334}(-2X_3^2X_4) + W_{344}(-2X_3X_4^2) \\
&+ W_{123}(X_1X_3 - 2X_1X_2X_3) + W_{124}(X_1X_4 - 2X_1X_2X_4) \\
&+ W_{134}(-2X_1X_3X_4) + W_{234}(X_3X_4 - 2X_2X_3X_4)
\end{aligned}$$

$$\begin{aligned}
3RT \ln \gamma_{Alm} &= W_{112}(-2X_1^2X_2) + W_{122}(-2X_1X_2^2) \\
&+ W_{113}(X_1^2 - 2X_1^2X_3) + W_{133}(2X_1X_3 - 2X_1X_3^2) \\
&+ W_{114}(-2X_1^2X_4) + W_{144}(-2X_1X_4^2) \\
&+ W_{223}(X_2^2 - 2X_1^2X_3) + W_{233}(2X_2X_3 - 2X_2X_3^2) \\
&+ W_{224}(-2X_1^2X_4) + W_{244}(-2X_2X_4^2) \\
&+ W_{334}(2X_3X_4 - 2X_3^2X_4) + W_{344}(X_4^2 - 2X_3X_4^2) \\
&+ W_{123}(X_1X_2 - 2X_1X_2X_3) + W_{124}(-2X_1X_2X_4) \\
&+ W_{134}(X_1X_4 - 2X_1X_3X_4) + W_{234}(X_2X_4 - 2X_2X_3X_4)
\end{aligned}$$

where 1 = grossular, 2 = pyrope, 3 = almandine and 4 = spessartine.
R = gas constant and the interaction parameters (e.g. W_{123}) are:

Parameter	W_n (J/mol)
112	21 560
122	69 200
113	20 320
133	2620
223	230
233	3720
123	58 825
124	45 424
134	11 470
234	1975

The activity model for plagioclase used in this study, from Elkins and Grove (1990) is:

$$
\begin{aligned}
a_{An} = X_{An} \cdot \exp\{(&W_{OrAb}[X_{Ab}X_{Or}(1/2 - X_{An} - 2X_{Ab})] \\
&+ W_{AbOr}[X_{Ab}X_{Or}(1/2 - X_{An} - 2X_{Or})] \\
&+ W_{AbAn}[2X_{Ab}X_{An}(1 - X_{An}) \\
&\quad + X_{Ab}X_{Or}(1/2 - X_{An})] \\
&+ W_{AnAb}[X_{Ab}^2(1 - 2X_{An}) \\
&\quad + X_{Ab}X_{Or}(1/2 - X_{An})] \\
&+ W_{OrAn}[2X_{Or}X_{An}(1 - X_{An}) \\
&\quad + X_{Ab}X_{Or}(1/2 - X_{An})] \\
&+ W_{AnOr}[X_{Or}^2(1 - 2X_{An}) \\
&\quad + X_{Ab}X_{Or}(1/2 - X_{An})] \\
&+ W_{OrAbAn}[X_{Or}X_{Ab}(1 - 2X_{An})]\}/RT\}
\end{aligned}
$$

Where An = anorthite, Ab = albite and Or = orthoclase and the interaction parameters are:

	W_1	W_2
W_{AbOr}	18810	18810
W_{OrAn}	27320	27320
W_{AbAn}	28226	7924
		(525)
W_{AnAb}	8471	0.0
W_{OrAn}	47396	40317
		(460)
W_{AnOr}	52468	38974
		(292)
W_{AbOrAn}	8700	12545
		(965)

APPENDIX IV XRF WHOLE ROCK ANALYSIS

Pressed boric acid pellets were made from each sample, these pellets contained 2 ± 0.05 grams of sample powder. The pellets were analysed by X-ray Fluorescence (XRF) using a Phillps PW 1450 X-ray spectrometer in the Department of Geology of Manchester University. Each sample was analysed for major elements and selected trace elements. Details of the technique used and the correction procedures involved are described by Brown et al. (1973).

The probable maximum errors are given below.

Content of element in sample (wt% or ppm)	80%	40%	30%	20%	10%-5%	1%-50ppm	10ppm
Relative error (%)	1	2	3	4	5	10	20

APPENDIX V

S.E.M. ANALYSIS OF RUN PRODUCTS

APPENDIX V

The S.E.M. used in this study is a JEOL JSM 6400.

Beam current for analysis 1.5 nA.

Count time 40 seconds.

Data acqusition and processing as with Geoscan Microprobe, Appendix I.

SIN2(900)				RUN PRODUCT MINERAL ANALYSES								
ORTHOPYROXENE							PLAGIOCLASE					
%OXIDE	Opx1	Opx2	Opx3	Opx4	Opx5		%OXIDE	Pl1	Pl2			
SiO2	47.65	45.76	44.88	46.40	47.30		SiO2	61.19	61.26			
TiO2	0.50	0.83	0.85	0.48	0.62		Al2O3	23.69	23.91			
Al2O3	12.22	14.26	13.92	10.87	10.76		FeO	0.26	0.28			
Cr2O3	0.00	0.00	0.00	0.00	0.00		CaO	6.37	6.20			
FeO	24.31	23.16	23.51	23.36	23.39		Na2O	6.68	6.50			
MnO	0.24	0.20	0.20	0.00	0.32		K2O	1.05	1.19			
MgO	15.60	14.77	14.69	17.66	18.10							
CaO	0.62	0.20	0.27	0.00	0.19		TOTAL	99.25	99.34			
Na2O	0.80	0.73	0.43	0.00	0.56							
							CATIONS					
TOTAL	101.93	99.90	98.76	98.76	101.25		Si	2.743	2.742			
							Al	1.252	1.262			
CATIONS							Fe	0.010	0.010			
Si	1.754	1.710	1.702	1.750	1.750		Ca	0.306	0.297			
Ti	0.014	0.023	0.024	0.014	0.017		Na	0.581	0.564			
Al	0.530	0.628	0.622	0.483	0.469		K	0.060	0.068			
Cr	0.000	0.000	0.000	0.000	0.000		(O)	8	8			
Fe	0.748	0.724	0.745	0.737	0.724		TOTAL	4.952	4.943			
Mn	0.007	0.006	0.006	0.000	0.010							
Mg	0.856	0.823	0.830	0.993	0.998		XAn	0.32	0.32			
Ca	0.024	0.008	0.011	0.000	0.008							
Na	0.057	0.053	0.032	0.000	0.040							
(O)	6	6	6	6	6							
TOTAL	3.990	3.975	3.972	3.977	4.016							
Mg#	0.534	0.532	0.527	0.574	0.580							

CORDIERITE											
%OXIDE	Crd1	Crd2	Crd3	Crd4	Crd5	Crd6	Crd7	Crd8	Crd9	Crd10	Crd11
SiO2	49.22	48.39	48.91	54.83	51.55	53.29	48.68	50.26	47.11	47.18	48.11
TiO2	0.00	0.00	0.00	0.00	0.00	0.00	0.00	0.00	0.00	0.00	0.00
Al2O3	30.72	31.96	32.12	29.65	30.96	30.96	33.05	32.26	32.48	31.49	32.47
Cr2O3	0.00	0.00	0.00	0.00	0.00	0.00	0.00	0.00	0.00	0.00	0.00
FeO	5.56	5.46	6.50	5.72	5.87	7.16	7.13	5.89	6.71	6.66	6.62
MnO	0.28	0.22	0.00	0.00	0.00	0.23	0.00	0.00	0.21	0.00	0.00
MgO	9.45	9.93	9.50	8.52	8.86	8.68	9.64	9.64	9.50	8.88	9.34
CaO	0.14	0.17	0.20	0.17	0.19	0.13	0.00	0.20	0.00	0.22	0.20
Na2O	0.37	0.60	0.53	0.30	0.55	0.71	0.62	0.48	0.37	0.37	0.60
K2O	0.39	0.46	0.45	0.46	0.78	0.66	0.43	0.76	0.44	0.58	0.53
TOTAL	96.13	97.20	98.21	99.66	98.75	101.80	99.55	99.49	96.82	95.37	97.87
CATIONS											
Si	5.135	5.003	5.023	5.467	5.231	5.273	4.940	5.078	4.919	4.996	4.964
Ti	0.000	0.000	0.000	0.000	0.000	0.000	0.000	0.000	0.000	0.000	0.000
Al	3.778	3.896	3.888	3.474	3.703	3.611	3.953	3.842	3.997	3.931	3.950
Cr	0.000	0.000	0.000	0.000	0.000	0.000	0.000	0.000	0.000	0.000	0.000
Fe	0.486	0.472	0.559	0.477	0.498	0.592	0.605	0.498	0.585	0.590	0.571
Mn	0.024	0.020	0.000	0.000	0.000	0.019	0.000	0.000	0.019	0.000	0.000
Mg	1.469	1.531	1.454	1.266	1.340	1.280	1.458	1.452	1.479	1.403	1.437
Ca	0.015	0.018	0.022	0.018	0.021	0.014	0.000	0.022	0.000	0.024	0.023
Na	0.075	0.121	0.106	0.058	0.108	0.137	0.122	0.094	0.074	0.075	0.120
K	0.052	0.061	0.058	0.059	0.101	0.083	0.055	0.099	0.058	0.078	0.070
(O)	18	18	18	18	18	18	18	18	18	18	18
TOTAL	10.907	10.940	10.946	10.702	10.793	10.789	10.956	10.892	10.999	10.944	10.945
Mg#	0.751	0.764	0.722	0.726	0.729	0.684	0.707	0.745	0.717	0.704	0.716

GARNET	core	core	core	core	core	rim	rim	rim
%OXIDE	Grt1	Grt2	Grt3	Grt4	Grt5	Grt6	Grt7	Grt8
SiO2	38.09	37.74	36.90	37.12	38.01	38.22	38.41	40.79
TiO2	0.00	0.00	0.00	0.00	0.00	0.30	0.38	0.58
Al2O3	21.55	21.11	20.75	20.80	21.40	21.31	20.69	20.36
Cr2O3	0.00	0.00	0.20	0.00	0.00	0.00	0.00	0.00
FeO	31.77	31.40	33.31	32.11	30.41	27.61	28.88	27.94
MnO	3.28	3.51	4.24	3.99	3.50	1.26	1.16	1.04
MgO	5.41	5.13	3.75	4.12	5.65	8.54	7.93	7.52
CaO	1.83	1.68	1.06	1.05	1.15	1.41	1.44	1.33
TOTAL	101.93	100.56	100.21	99.18	100.11	98.65	98.89	99.56
CATIONS								
Si	5.942	5.971	5.948	5.992	5.999	5.996	6.042	6.296
Ti	0.000	0.000	0.000	0.000	0.000	0.036	0.045	0.068
Al	3.961	3.937	3.942	3.958	3.981	3.941	3.835	3.705
Cr	0.000	0.000	0.026	0.000	0.000	0.000	0.000	0.000
Fe	4.144	4.155	4.491	4.336	4.014	3.623	3.800	3.607
Mn	0.434	0.470	0.578	0.545	0.467	0.167	0.155	0.136
Mg	1.259	1.209	0.900	0.992	1.329	1.998	1.859	1.731
Ca	0.306	0.284	0.183	0.181	0.195	0.237	0.243	0.219
(O)	24	24	24	24	24	24	24	24
TOTAL	16.046	16.026	16.068	16.004	15.985	15.998	15.979	15.762
Mg#	0.233	0.225	0.167	0.186	0.249	0.355	0.329	0.324

BOG1(900)			RUN PRODUCT MINERAL ANALYSES													
CORDIERITE																
%OXIDE	Crd1	Crd2	CRd3	Crd4	Crd5	Crd6	Crd7	Crd8	Crd9	Crd10	Crd11	Crd12	Crd13	Crd14	Crd15	Crd16
SiO2	47.24	47.71	49.02	48.13	48.14	48.16	48.73	52.44	47.94	49.17	46.69	45.38	46.11	46.85	46.00	46.61
TiO2	0.00	0.00	0.00	0.00	0.00	0.00	0.00	0.00	0.17	0.00	0.00	0.53	0.52	0.00	0.00	0.00
Al2O3	35.81	35.25	33.53	34.37	34.14	33.89	32.00	30.22	33.47	32.15	32.47	31.95	32.51	32.22	32.47	33.11
Cr2O3	0.00	0.00	0.00	0.00	0.00	0.00	0.00	0.00	0.00	0.00	0.00	0.00	0.00	0.00	0.00	0.00
FeO	6.90	7.31	7.70	7.05	7.75	6.84	8.21	7.55	7.54	8.02	6.72	7.41	7.54	7.58	7.20	6.29
MnO	0.00	0.00	0.00	0.00	0.00	0.00	0.00	0.00	0.00	0.00	0.00	0.00	0.00	0.00	0.00	0.00
MgO	9.15	9.29	9.11	9.52	9.19	9.66	8.16	7.69	9.41	8.04	8.78	8.67	8.60	8.66	8.82	9.48
CaO	0.24	0.24	0.20	0.21	0.26	0.00	0.29	0.33	0.29	0.25	0.29	0.15	0.23	0.18	0.31	0.28
Na2O	0.00	0.45	0.30	0.47	0.57	0.40	0.39	0.51	0.39	0.30	0.45	0.45	0.50	0.35	0.37	0.48
K2O	0.44	0.45	0.53	0.61	0.54	0.51	0.84	1.29	0.49	0.73	0.57	0.52	0.50	0.54	0.58	0.57
TOTAL	99.77	100.71	100.41	100.35	100.58	99.45	98.63	100.03	99.69	98.67	95.95	95.05	96.51	96.38	95.75	96.83
CATIONS																
Si	4.770	4.802	4.950	4.857	4.866	4.885	5.024	5.303	4.884	5.056	4.917	4.856	4.861	4.932	4.877	4.868
Ti	0.000	0.000	0.000	0.000	0.000	0.000	0.000	0.000	0.013	0.000	0.000	0.042	0.041	0.000	0.000	0.000
Al	4.262	4.182	3.991	4.088	4.067	4.052	3.889	3.602	4.019	3.897	4.030	4.031	4.040	3.998	4.058	4.076
Cr	0.000	0.000	0.000	0.000	0.000	0.000	0.000	0.000	0.000	0.000	0.000	0.000	0.000	0.000	0.000	0.000
Fe	0.583	0.615	0.651	0.595	0.655	0.580	0.708	0.638	0.642	0.690	0.592	0.663	0.665	0.668	0.638	0.549
Mn	0.000	0.000	0.000	0.000	0.000	0.000	0.000	0.000	0.000	0.000	0.000	0.000	0.000	0.000	0.000	0.000
Mg	1.377	1.394	1.371	1.433	1.385	1.460	1.254	1.159	1.429	1.232	1.378	1.383	1.352	1.359	1.393	1.476
Ca	0.026	0.026	0.022	0.023	0.028	0.000	0.032	0.036	0.032	0.028	0.032	0.018	0.026	0.020	0.035	0.032
Na	0.000	0.088	0.059	0.092	0.111	0.078	0.079	0.100	0.077	0.060	0.091	0.093	0.101	0.071	0.076	0.097
K	0.056	0.058	0.069	0.078	0.069	0.066	0.110	0.167	0.063	0.096	0.076	0.071	0.067	0.073	0.079	0.075
(O)	18	18	18	18	18	18	18	18	18	18	18	18	18	18	18	18
TOTAL	10.992	10.993	10.963	10.973	10.973	10.977	10.875	10.702	10.987	10.875	10.917	10.975	10.959	10.957	10.966	10.969
Mg#	0.703	0.694	0.678	0.707	0.679	0.716	0.639	0.645	0.690	0.641	0.699	0.676	0.670	0.670	0.686	0.729

ILMENITE						
%OXIDE	Ilm1	Ilm2	Ilm3	Ilm4	Ilm5	Ilm6
TiO2	50.86	49.17	50.35	49.37	50.83	50.23
Al2O3	0.61	0.85	0.70	0.48	0.64	0.65
FeO	48.63	46.61	48.01	47.05	48.37	47.52
MnO	0.36	0.28	0.00	0.44	0.00	0.00
MgO	1.29	1.50	1.33	1.37	1.29	1.51
TOTAL	101.76	98.42	100.40	98.71	101.12	99.91
CATIONS						
Ti	1.905	1.898	1.905	1.906	1.909	1.908
Al	0.036	0.051	0.042	0.029	0.038	0.039
Fe	2.025	2.000	2.020	2.020	2.021	2.007
Mn	0.015	0.012	0.000	0.019	0.000	0.000
Mg	0.096	0.115	0.100	0.105	0.096	0.114
(O)	6	6	6	6	6	6
TOTAL	4.077	4.076	4.067	4.079	4.064	4.068

CLAS112(900)			RUN PRODUCT MINERAL ANALYSES		
SPINEL					
%OXIDE	Spl1	Sp1*	Spl2	Spl2*	
SiO2	0.23	0.23	2.04	2.04	
Al2O3	44.12	44.12	44.03	44.03	
TiO2	1.04	1.04	0.85	0.85	
MgO	4.16	4.16	4.55	4.55	
Fe2O3	-	10.37	-	9.87	
FeO	40.72	31.38	40.41	31.53	
MnO	0.00	0.00	0.00	0.00	
Cr2O3	0.00	0.00	0.00	0.00	
CaO	0.00	0.00	0.00	0.00	
Na2O	0.00	0.00	0.34	0.34	
K2O	0.14	0.14	0.25	0.25	
Cl	0.00	0.00	0.00	0.00	
TOTAL	90.40	91.44	92.45	93.44	
CATIONS					
Si	0.015	0.015	0.131	0.127	
Al	3.447	3.339	3.336	3.239	
Ti	0.052	0.050	0.041	0.040	
Mg	0.411	0.398	0.436	0.423	
Fe 3+	-	0.501	-	0.464	
Fe 2+	2.257	1.685	2.172	1.646	
Mn	0.000	0.000	0.000	0.000	
Cr	0.000	0.000	0.000	0.000	
Ca	0.000	0.000	0.000	0.000	
Na	0.000	0.000	0.042	0.041	
K	0.012	0.012	0.021	0.020	
Cl	0.000	0.000	0.000	0.000	
(O)	8	8	8	8	
TOTAL	6.194	6.000	6.179	6.000	
* normalised for Fe3+					

ORTHOPYROXENE											
%OXIDE	Opx1	Opx2	Opx3	Opx4	Opx5	Opx6	Opx7	Opx8	Opx9	Opx10	Opx11
SiO2	45.36	45.62	45.64	45.47	46.41	45.77	46.02	45.99	46.93	46.61	45.80
TiO2	0.40	0.51	0.36	0.36	0.50	0.47	0.49	0.46	0.46	0.37	0.40
Al2O3	9.54	10.16	11.04	9.75	9.26	10.04	8.54	9.67	7.97	10.47	9.83
Cr2O3	0.00	0.00	0.00	0.00	0.00	0.00	0.00	0.00	0.00	0.00	0.00
FeO	27.00	26.21	26.72	28.17	27.75	26.51	27.37	27.15	29.28	27.19	27.81
MnO	0.44	0.50	0.44	0.50	0.52	0.37	0.48	0.48	0.41	0.37	0.36
MgO	16.02	16.69	15.50	15.61	16.35	16.59	16.64	16.98	15.81	15.73	16.30
CaO	0.00	0.11	0.16	0.00	0.00	0.11	0.00	0.13	0.18	0.16	0.00
TOTAL	98.75	99.81	99.85	99.86	100.79	99.87	99.54	100.86	101.04	100.90	100.51
CATIONS											
Si	1.751	1.736	1.734	1.743	1.756	1.739	1.764	1.738	1.786	1.754	1.736
Ti	0.012	0.014	0.010	0.010	0.014	0.013	0.014	0.013	0.013	0.011	0.01
Al	0.434	0.456	0.495	0.440	0.413	0.449	0.386	0.431	0.358	0.465	0.439
Cr	0.000	0.000	0.000	0.000	0.000	0.000	0.000	0.000	0.000	0.000	0.00
Fe	0.872	0.834	0.849	0.903	0.878	0.842	0.878	0.858	0.932	0.856	0.881
Mn	0.014	0.016	0.014	0.016	0.017	0.012	0.016	0.062	0.013	0.012	0.01
Mg	0.922	0.947	0.878	0.892	0.922	0.940	0.951	0.956	0.897	0.882	0.921
Ca	0.000	0.005	0.006	0.000	0.000	0.005	0.000	0.005	0.007	0.006	0.00
(O)	6	6	6	6	6	6	6	6	6	6	6
TOTAL	4.005	4.008	3.986	4.004	4.000	4.000	4.009	4.063	4.006	3.986	4.000
Mg#	*0.514*	*0.532*	*0.508*	*0.497*	*0.512*	*0.527*	*0.520*	*0.527*	*0.490*	*0.507*	*0.511*

CORDIERITE																	
%OXIDE	Crd1	Crd2	Crd3	Crd4	Crd5	Crd6	Crd7	Crd8	Crd9	Crd10	Crd11	Crd12	Crd13	Crd14	Crd15	Crd16	Crd17
SiO2	48.48	49.79	48.54	47.71	48.66	48.02	48.53	47.21	47.22	47.61	46.47	46.39	50.92	46.28	47.84	46.64	47.71
TiO2	0.00	0.00	0.17	1.11	0.00	0.00	0.24	0.00	0.00	0.18	0.00	0.00	0.16	0.00	0.00	0.00	0.00
Al2O3	33.56	33.42	34.19	32.78	33.91	33.61	33.44	33.22	32.67	32.36	32.55	32.06	29.66	32.21	32.99	32.97	32.69
Cr2O3	0.00	0.00	0.00	0.00	0.00	0.00	0.00	0.00	0.00	0.00	0.00	0.00	0.00	0.00	0.00	0.00	0.00
FeO	6.87	7.21	7.81	8.92	6.46	7.17	6.87	6.27	6.77	7.13	6.97	7.25	7.79	6.74	7.48	5.22	6.89
MnO	0.00	0.00	0.00	0.00	0.00	0.00	0.24	0.00	0.00	0.00	0.21	0.00	0.23	0.00	0.25	0.00	0.00
MgO	10.00	9.52	9.91	9.09	10.17	9.82	9.70	10.14	9.58	9.41	9.58	8.89	7.47	9.47	9.38	10.43	9.54
CaO	0.14	0.00	0.00	0.00	0.18	0.12	0.00	0.13	0.11	0.00	0.11	0.00	0.13	0.13	0.13	0.17	0.11
Na2O	0.49	0.00	0.32	0.28	0.00	0.40	0.29	0.37	0.34	0.00	0.31	0.00	0.00	0.29	0.25	0.40	0.33
K2O	0.80	0.82	0.58	0.50	0.67	0.62	0.69	0.78	0.68	0.55	0.65	0.58	1.26	0.68	0.55	0.86	0.54
TOTAL	100.33	100.75	101.52	100.39	100.04	99.75	100.00	98.12	97.38	97.23	96.85	95.18	97.62	95.81	98.85	96.68	97.80
CATIONS																	
Si	4.897	4.979	4.851	4.858	4.901	4.877	4.914	4.866	4.907	4.941	4.871	4.922	5.282	4.885	4.916	4.857	4.929
Ti	0.000	0.000	0.000	0.085	0.000	0.000	0.018	0.000	0.000	0.014	0.000	0.000	0.013	0.000	0.000	0.000	0.000
Al	3.995	3.939	4.028	3.934	4.025	4.023	3.992	4.037	4.001	3.958	4.021	4.009	3.627	4.008	3.996	4.046	3.980
Cr	0.000	0.000	0.000	0.000	0.000	0.000	0.000	0.000	0.000	0.000	0.000	0.000	0.000	0.000	0.000	0.000	0.000
Fe	0.581	0.603	0.653	0.760	0.544	0.609	0.582	0.541	0.589	0.619	0.611	0.644	0.675	0.595	0.642	0.454	0.595
Mn	0.000	0.000	0.000	0.000	0.000	0.000	0.021	0.000	0.000	0.000	0.019	0.000	0.020	0.000	0.021	0.000	0.000
Mg	1.506	1.418	1.476	1.379	1.527	1.487	1.464	1.558	1.483	1.455	1.497	1.406	1.156	1.490	1.437	1.618	1.469
Ca	0.015	0.000	0.000	0.000	0.019	0.013	0.000	0.015	0.012	0.000	0.012	0.000	0.014	0.015	0.014	0.019	0.013
Na	0.095	0.000	0.062	0.056	0.000	0.079	0.057	0.074	0.069	0.000	0.063	0.000	0.000	0.059	0.049	0.080	0.067
K	0.103	0.104	0.074	0.065	0.085	0.080	0.089	0.102	0.090	0.072	0.087	0.079	0.167	0.092	0.072	0.115	0.070
(O)	18	18	18	18	18	18	18	18	18	18	18	18	18	18	18	18	18
TOTAL	10.979	10.939	11.008	11.016	10.997	10.996	10.991	11.002	10.980	10.987	11.019	10.981	10.773	10.978	11.012	10.975	10.973
Mg#	*0.722*	*0.702*	*0.693*	*0.645*	*0.737*	*0.709*	*0.716*	*0.742*	*0.716*	*0.702*	*0.710*	*0.686*	*0.631*	*0.715*	*0.691*	*0.781*	*0.712*

BIOTITE																	
%OXIDE	Bt1	Bt2	Bt3	Bt4	Bt5	Bt6	Bt7	Bt8	Bt9	Bt10	Bt11	Bt12	Bt13	Bt14	Bt15		
SiO2	36.55	35.21	36.11	35.72	36.57	35.03	38.20	36.84	35.85	37.75	34.39	33.69	34.77	36.58	34.02		
TiO2	6.27	6.29	6.40	5.97	5.90	6.13	6.00	6.59	6.78	6.52	6.30	5.50	6.58	5.97	4.74		
Al2O3	17.48	17.98	16.76	17.07	19.06	16.02	15.90	16.82	16.42	16.54	16.36	17.27	16.43	16.11	16.41		
Cr2O3	0.00	0.00	0.00	0.00	0.00	0.00	0.00	0.00	0.00	0.00	0.00	0.00	0.00	0.00	0.00		
FeO	20.18	20.89	20.66	20.70	20.69	18.88	18.66	20.64	20.55	20.38	20.32	20.46	20.88	20.25	20.63		
MnO	0.00	0.00	0.00	0.00	0.24	0.00	0.00	0.00	0.00	0.00	0.00	0.00	0.00	0.00	0.00		
MgO	8.04	8.35	9.48	9.25	8.15	9.02	7.99	9.44	9.08	8.71	8.43	8.31	8.26	8.58	8.76		
CaO	0.17	0.13	0.00	0.00	0.00	0.00	0.14	0.16	0.20	0.13	0.00	0.00	0.14	0.00	0.17		
Na2O	0.48	0.30	0.37	0.46	0.52	0.59	0.00	0.48	0.61	0.40	0.41	0.40	0.37	0.37	0.33		
K2O	9.14	9.21	9.29	9.40	8.45	9.05	9.09	9.57	9.41	9.23	9.68	9.53	9.55	9.40	9.58		
TOTAL	98.30	98.35	99.07	98.57	99.58	94.73	95.98	100.54	98.89	99.66	95.89	95.15	96.97	97.25	94.63		
CATIONS																	
Si	5.397	5.238	5.319	5.298	5.306	5.370	5.708	5.350	5.307	5.491	5.268	5.207	5.275	5.472	5.304		
Ti	0.696	0.704	0.709	0.666	0.644	0.706	0.675	0.720	0.754	0.714	0.726	0.640	0.751	0.671	0.555		
Al	3.043	3.152	2.910	2.985	3.261	2.894	2.801	2.878	2.864	2.837	2.955	3.147	2.939	2.840	3.016		
Cr	0.000	0.000	0.000	0.000	0.000	0.000	0.000	0.000	0.000	0.000	0.000	0.000	0.000	0.000	0.000		
Fe	2.492	2.598	2.546	2.568	2.510	2.421	2.332	2.507	2.543	2.480	2.603	2.644	2.649	2.533	2.690		
Mn	0.000	0.000	0.000	0.000	0.029	0.000	0.000	0.000	0.000	0.000	0.000	0.000	0.000	0.000	0.000		
Mg	1.770	1.852	2.083	2.046	1.762	2.062	1.781	2.045	2.003	1.888	1.925	1.915	1.869	1.917	2.036		
Ca	0.027	0.020	0.000	0.000	0.000	0.000	0.022	0.026	0.032	0.021	0.000	0.000	0.022	0.000	0.028		
Na	0.137	0.085	0.106	0.132	0.147	0.176	0.000	0.134	0.174	0.114	0.122	0.188	0.108	0.108	0.098		
K	1.722	1.747	1.747	1.778	1.564	1.771	1.733	1.772	1.776	1.712	1.892	1.879	1.848	1.793	1.905		
(O)	22	22	22	22	22	22	22	22	22	22	22	22	22	22	22		
TOTAL	15.284	15.396	15.420	15.473	15.223	15.400	15.052	15.432	15.453	15.257	15.491	15.620	15.461	15.334	15.632		
Mg#	*0.415*	*0.416*	*0.450*	*0.443*	*0.412*	*0.460*	*0.433*	*0.449*	*0.441*	*0.432*	*0.425*	*0.420*	*0.414*	*0.431*	*0.431*		

COLD STAGE MELT ANALYSES AND CIPW norm Calculations

CLAS112(900)		Melt Cold Stage Analyses										
%OXIDE	CL1	CL2	CL3	CL4	CL5	CL6	CL7	CL8	CL9	CL10	CL11	CL12
SiO2	70.52	72.56	72.54	72.60	72.23	72.16	72.27	72.09	72.47	72.79	72.33	72.59
TiO2	0.38	0.39	0.42	0.32	0.34	0.32	0.38	0.41	0.42	0.32	0.45	0.49
Al2O3	15.01	13.71	13.84	13.60	13.61	13.58	13.64	13.76	13.62	13.44	13.70	13.63
Cr2O3	0.00	0.00	0.00	0.00	0.00	0.00	0.00	0.00	0.00	0.00	0.00	0.00
FeO	4.05	3.68	3.49	3.81	3.97	4.00	3.81	3.97	3.85	3.74	3.86	3.57
MnO	0.00	0.00	0.00	0.00	0.00	0.00	0.00	0.00	0.00	0.00	0.00	0.00
MgO	1.12	0.47	0.45	0.54	0.51	0.54	0.52	0.48	0.48	0.47	0.44	0.52
CaO	0.72	0.65	0.74	0.73	0.69	0.69	0.70	0.64	0.61	0.76	0.64	0.68
Na2O	0.77	0.71	0.74	0.72	0.95	0.93	0.72	0.85	0.76	0.76	0.91	0.79
K2O	7.43	7.82	7.78	7.68	7.69	7.79	7.96	7.80	7.78	7.73	7.68	7.73
Cl	0.00	0.00	0.00	0.00	0.00	0.00	0.00	0.00	0.00	0.00	0.00	0.00
TOTAL	100.00	100.00	100.00	100.00	100.00	100.00	100.00	100.00	100.00	100.00	100.00	100.00
Mg#	0.33	0.18	0.19	0.20	0.19	0.19	0.19	0.18	0.18	0.18	0.17	0.21

BOG1(900)		Melt Cold Stage Analyses								
%OXIDE	BG1	BG2	BG3	BG4	BG5	BG6	BG7	BG8	BG9	BG10
SiO2	72.85	73.02	72.82	71.99	72.29	70.22	72.66	73.05	71.30	73.08
TiO2	0.41	0.46	0.64	0.98	0.69	0.47	0.51	0.53	0.46	0.51
Al2O3	14.50	14.24	14.23	13.90	14.41	16.15	14.37	13.89	15.12	14.27
Cr2O3	0.00	0.00	0.00	0.00	0.00	0.00	0.00	0.00	0.00	0.00
FeO	3.08	3.12	3.20	3.72	3.26	3.73	3.07	3.43	4.09	3.07
MnO	0.00	0.00	0.00	0.00	0.00	0.00	0.00	0.00	0.00	0.00
MgO	0.41	0.31	0.34	0.45	0.55	1.12	0.39	0.34	0.47	0.37
CaO	1.19	1.22	1.21	1.27	1.17	1.26	1.17	1.17	1.32	1.31
Na2O	1.52	1.66	1.51	1.55	1.51	1.30	1.63	1.43	1.30	1.32
K2O	6.05	5.97	5.98	6.05	6.13	5.75	6.20	6.17	5.94	6.06
Cl	0.00	0.00	0.08	0.09	0.00	0.00	0.00	0.00	0.00	0.00
TOTAL	100.00	100.00	100.00	100.00	100.00	100.00	100.00	100.00	100.00	100.00
Mg#	0.19	0.15	0.16	0.18	0.23	0.35	0.18	0.15	0.17	0.18

SIN2(900)		Melt Cold Stage Analyses								
%OXIDE	SN1	SN2	SN3	SN4	SN5	SN6	SN7	SN8	SN9	SN10
SiO2	72.63	72.48	74.27	72.74	73.86	73.61	74.19	74.19	73.99	73.92
TiO2	0.97	0.46	0.36	0.40	0.34	0.28	0.48	0.48	0.66	0.48
Al2O3	13.54	15.06	14.12	15.01	14.40	14.83	14.01	14.01	14.15	14.38
Cr2O3	0.00	0.00	0.00	0.00	0.00	0.00	0.00	0.00	0.00	0.00
FeO	3.71	3.01	2.54	2.28	2.49	2.30	2.49	2.49	2.55	2.34
MnO	0.00	0.00	0.00	0.00	0.00	0.00	0.00	0.00	0.00	0.00
MgO	0.98	0.46	0.33	0.52	0.45	0.48	0.38	0.38	0.32	0.54
CaO	1.02	1.16	1.03	1.89	0.99	1.38	0.93	0.93	0.99	0.98
Na2O	2.38	2.69	2.68	2.84	2.67	2.67	2.65	2.65	2.62	2.61
K2O	4.76	4.68	4.68	4.32	4.81	4.45	4.85	4.85	4.73	4.76
Cl	0.00	0.00	0.00	0.00	0.00	0.00	0.00	0.00	0.00	0.00
TOTAL	100.00	100.00	100.00	100.00	100.00	100.00	100.00	100.00	100.00	100.00
Mg#	0.32	0.22	0.19	0.29	0.24	0.27	0.21	0.21	0.18	0.29

CIPW norms

CLAS112	C1	C2	C3	C4	C5	C6	C7	C8	C9	C10	C11	C12
quartz	31.29	33.61	33.60	33.70	31.97	31.54	32.44	32.19	33.35	33.56	32.72	33.56
corundum	4.35	2.93	2.86	2.78	2.47	2.36	2.57	2.76	2.84	2.44	2.73	2.73
orthoclase	43.91	46.21	45.98	45.39	45.45	46.03	47.04	46.10	45.98	45.68	45.38	45.68
albite	6.52	6.01	6.26	6.09	8.04	7.87	6.09	7.19	6.43	6.43	7.70	6.68
anorthite	3.57	3.22	3.67	3.62	3.42	3.42	3.47	3.18	3.03	3.77	3.17	3.37
hypersthene	9.60	7.28	6.84	7.81	8.00	8.16	7.66	7.81	7.57	7.51	7.44	7.04
ilmenite	0.72	0.74	0.80	0.61	0.65	0.61	0.72	0.78	0.80	0.61	0.85	0.93
TOTAL	*100.00*	*100.00*	*100.00*	*100.00*	*100.00*	*100.00*	*100.00*	*100.00*	*100.00*	*100.00*	*100.00*	*100.00*

BOG1	BG1	BG2	BG3	BG4	BG5	BG6	BG7	BG8	BG9	BG10
quartz	35.42	35.17	35.88	34.08	34.51	33.51	34.18	35.63	34.40	36.67
corundum	3.29	2.83	3.08	2.50	3.16	5.50	2.85	2.73	4.15	3.16
orthoclase	35.79	35.28	35.37	35.79	36.22	33.98	36.64	36.46	35.10	35.82
albite	12.86	14.05	12.79	13.13	12.78	11.00	13.79	12.10	11.00	11.17
anorthite	5.90	6.05	6.01	6.31	5.80	6.25	5.80	5.80	6.55	6.50
hypersthene	6.00	5.74	5.67	6.34	6.22	8.86	5.77	6.27	7.92	5.72
ilmenite	0.78	0.87	1.22	1.86	1.31	0.89	0.97	1.01	0.87	0.97
TOTAL	*100.00*	*100.00*	*100.00*	*100.00*	*100.00*	*100.00*	*100.00*	*100.00*	*100.00*	*100.00*

SIN2	SN1	SN2	SN3	SN4	SN5	SN6	SN7	SN8	SN9	SN10
quartz	34.55	33.58	36.21	33.25	37.18	35.66	35.94	36.41	36.01	35.97
corundum	2.62	3.46	2.77	2.23	2.91	3.11	2.71	2.92	3.15	3.21
orthoclase	28.13	27.66	27.65	25.53	27.60	26.30	28.67	27.95	28.15	28.03
albite	20.14	22.76	22.68	24.03	21.93	22.59	22.43	22.17	22.08	22.17
anorthite	5.06	5.75	5.11	9.38	4.77	6.85	4.61	4.91	4.86	4.89
hypersthene	7.65	5.91	4.89	4.82	4.98	4.96	4.73	4.39	4.85	4.93
ilmenite	1.84	0.87	0.68	0.76	0.63	0.53	0.91	1.25	0.91	0.80
TOTAL	*100.00*	*100.00*	*100.00*	*100.00*	*100.00*	*100.00*	*100.00*	*100.00*	*100.00*	*100.00*

DD.CUM19

GARNET With Fe3+ Corrections

%OXIDE	Grt1	Grt1	Grt2	Grt2	Grt3	Grt3	Grt4	Grt4	Grt5	Grt5	Grt6	Grt6	Grt7	Grt7	Grt8	Grt8
SiO2	36.76	36.76	37.00	37.00	37.06	37.06	36.74	36.74	36.83	36.82	37.00	37.00	36.71	36.71	36.90	36.90
TiO2	0.00	0.00	0.00	0.00	0.00	0.00	0.00	0.00	0.00	0.00	0.00	0.00	0.00	0.00	0.00	0.00
Cr2O3	0.00	0.00	0.00	0.00	0.00	0.00	0.00	0.00	0.00	0.00	0.00	0.00	0.00	0.00	0.00	0.00
Al2O3	20.53	20.53	20.80	20.80	20.72	20.72	20.43	20.43	20.66	20.66	20.72	20.72	20.43	20.43	20.54	20.54
Fe2O3	-	0.59	-	0.52	-	0.87	-	1.08	-	1.18	-	1.46	-	2.14	-	1.38
FeO	32.27	31.74	32.73	32.26	32.52	31.74	33.04	32.07	33.11	32.03	33.51	32.20	33.79	31.87	33.16	31.92
MnO	1.27	1.27	1.10	1.10	1.16	1.16	0.30	0.30	0.69	0.69	0.80	0.80	0.63	0.63	0.89	0.89
MgO	2.02	2.02	1.92	1.92	1.97	1.97	1.87	1.87	1.91	1.91	1.96	1.96	1.88	1.88	1.57	1.57
CaO	6.12	6.12	6.47	6.47	6.55	6.55	6.43	6.43	6.14	6.14	6.02	6.02	6.26	6.26	6.64	6.64
TOTAL	98.96	99.01	100.02	100.07	99.97	100.06	98.81	98.92	99.33	99.45	100.01	100.15	99.70	99.91	99.68	99.82
CATIONS																
Si	5.975	5.966	5.950	5.942	5.965	5.952	5.991	5.975	5.976	5.958	5.971	5.949	5.959	5.927	5.982	5.961
Ti	0.000	0.000	0.000	0.000	0.000	0.000	0.000	0.000	0.000	0.000	0.000	0.000	0.000	0.000	0.000	0.000
Cr	0.000	0.000	0.000	0.000	0.000	0.000	0.000	0.000	0.000	0.000	0.000	0.000	0.000	0.000	0.000	0.000
Al	3.933	3.927	3.943	3.938	3.932	3.923	3.928	3.917	3.953	3.941	3.941	3.927	3.910	3.889	3.925	3.911
Fe3+	-	0.072	-	0.063	-	0.105	-	0.132	-	0.144	-	0.176	-	0.260	-	0.167
Fe2+	4.387	4.309	4.403	4.334	4.378	4.264	4.505	4.361	4.494	4.337	4.523	4.330	4.588	4.304	4.496	4.313
Mn	0.175	0.175	0.150	0.150	0.158	0.158	0.042	0.042	0.095	0.095	0.110	0.110	0.087	0.087	0.122	0.122
Mg	0.489	0.488	0.461	0.460	0.472	0.471	0.454	0.453	0.462	0.461	0.472	0.470	0.454	0.452	0.378	0.377
Ca	1.065	1.063	1.114	1.113	1.130	1.128	1.124	1.121	1.068	1.065	1.042	1.038	1.089	1.083	1.153	1.149
(O)	24	24	24	24	24	24	24	24	24	24	24	24	24	24	24	24
TOTAL	16.024	16.000	16.021	16.000	16.035	16.000	16.044	16.000	16.048	16.000	16.059	16.000	16.087	16.000	16.056	16.000
Mg#	0.10	0.10	0.09	0.10	0.10	0.10	0.09	0.09	0.09	0.10	0.09	0.10	0.09	0.09	0.08	0.08

ORTHOPYROXENE

%OXIDE	Opx1	Opx2	Opx3	Opx4	Opx5	Opx6	Opx7
SiO2	48.34	47.64	48.09	47.83	46.91	47.13	47.04
TiO2	0.00	0.00	0.18	0.19	0.26	0.17	0.30
Cr2O3	0.00	0.00	0.00	0.00	0.00	0.00	0.00
Al2O3	0.70	0.69	0.66	1.01	0.91	0.90	0.98
FeO	40.84	42.26	42.56	42.53	41.72	41.69	41.66
MnO	0.00	0.00	0.00	0.00	0.00	0.00	0.00
MgO	8.94	7.83	7.64	8.05	7.57	7.63	7.42
CaO	0.94	0.95	0.66	0.96	1.00	0.97	0.90
TOTAL	99.77	99.36	99.80	100.58	98.37	98.49	98.29
CATIONS							
Si	1.981	1.978	1.986	1.961	1.967	1.972	1.972
Ti	0.000	0.000	0.006	0.006	0.008	0.005	0.009
Cr	0.000	0.000	0.000	0.000	0.000	0.000	0.000
Al	0.034	0.034	0.032	0.049	0.045	0.045	0.048
Fe2+	1.400	1.467	1.469	1.458	1.463	1.459	1.461
Mn	0.000	0.000	0.000	0.000	0.000	0.000	0.000
Mg	0.546	0.484	0.470	0.492	0.473	0.476	0.464
Ca	0.041	0.042	0.029	0.042	0.045	0.043	0.040
(O)	6	6	6	6	6	6	6
TOTAL	4.002	4.005	3.992	4.008	4.001	4.000	3.994
Mg#	0.28	0.25	0.24	0.25	0.24	0.25	0.24

HORNBLENDE

%OXIDE	Hbl1	Hbl2	Hbl3	Hbl4	Hbl5	Hbl6	Hbl7	Hbl8	Hbl9	Hbl10
SiO2	39.45	40.67	41.11	41.38	39.16	39.49	40.89	39.68	39.85	40.21
TiO2	1.46	1.45	1.30	1.28	1.34	0.00	1.45	1.42	1.49	1.81
Al2O3	13.28	12.99	12.81	12.18	13.03	16.22	12.87	13.38	13.45	13.46
FeO	26.04	25.61	24.73	26.13	26.64	27.06	25.79	25.26	25.32	25.69
MnO	0.00	0.00	0.00	0.00	0.00	0.00	0.00	0.00	0.00	0.00
MgO	4.53	4.44	5.48	5.28	5.66	2.94	4.54	4.22	4.49	4.36
CaO	9.88	10.39	10.87	10.20	9.20	10.32	10.36	10.48	10.61	10.43
Na2O	1.86	1.79	1.83	1.58	1.63	1.36	1.51	1.99	1.70	1.95
K2O	0.87	0.92	0.90	0.80	0.78	0.95	0.87	0.91	0.96	0.93
TOTAL	97.36	98.25	99.03	98.83	97.43	98.33	98.27	97.36	97.86	98.82
CATIONS										
Si	6.213	6.322	6.317	6.391	6.168	6.152	6.347	6.238	6.226	6.225
Ti	0.173	0.169	0.151	0.149	0.158	0.000	0.169	0.168	0.176	0.211
Al	2.465	2.380	2.321	2.218	2.419	2.978	2.354	2.479	2.477	2.455
Fe2+	3.430	3.329	3.179	3.375	3.510	3.526	3.349	3.321	3.308	3.326
Mn	0.000	0.000	0.000	0.000	0.000	0.000	0.000	0.000	0.000	0.000
Mg	1.063	1.029	1.254	1.215	1.330	0.682	1.050	0.989	1.016	1.006
Ca	1.666	1.730	1.789	1.688	1.552	1.722	1.723	1.766	1.776	1.729
Na	0.567	0.540	0.545	0.475	0.498	0.411	0.455	0.608	0.513	0.585
K	0.175	0.183	0.177	0.158	0.157	0.189	0.172	0.183	0.180	0.184
(O)	23	23	23	23	23	23	23	23	23	23
TOTAL	15.752	15.682	15.733	15.669	15.792	15.660	15.619	15.752	15.702	15.721
Mg#	0.24	0.24	0.28	0.26	0.27	0.16	0.24	0.23	0.24	0.23

HORNBLENDE

%OXIDE	Hbl11	Hbl12	Hbl13
SiO2	39.75	40.81	38.17
TiO2	1.35	1.44	1.36
Al2O3	14.26	13.09	13.34
FeO	26.47	24.94	27.84
MnO	0.00	0.00	0.00
MgO	4.29	4.87	5.69
CaO	9.80	10.93	8.32
Na2O	1.46	1.34	1.66
K2O	1.08	0.87	0.88
TOTAL	98.35	98.29	97.27
CATIONS			
Si	6.184	6.316	6.062
Ti	0.147	0.168	0.162
Al	2.615	2.387	2.497
Fe2+	3.444	3.228	3.698
Mn	0.000	0.000	0.000
Mg	0.995	1.123	1.348
Ca	1.650	1.813	1.416
Na	0.440	0.402	0.512
K	0.214	0.172	0.178
(O)	23	23	23
TOTAL	15.689	15.609	15.873
Mg#	0.22	0.26	0.27

BIOTITE

%OXIDE	Bt1	Bt2	Bt3	Bt4	Bt5	Bt6	Bt7	Bt8	Bt9	Bt10	Bt11
SiO2	34.50	35.04	34.92	35.03	33.92	32.95	34.68	34.09	34.69	34.45	34.74
TiO2	4.60	4.68	4.78	4.56	5.02	3.85	4.86	4.66	5.08	4.91	5.49
Cr2O3	0.00	0.00	0.00	0.00	0.00	0.00	0.00	0.00	0.00	0.00	0.00
Al2O3	14.92	15.39	15.14	15.35	15.25	14.99	14.95	15.37	15.28	15.04	15.00
FeO	27.91	27.37	27.61	27.42	28.84	30.56	28.83	28.43	28.45	28.79	27.57
MnO	0.00	0.00	0.00	0.00	0.00	0.00	0.00	0.00	0.00	0.00	0.00
MgO	5.40	6.13	6.16	5.95	5.99	5.45	5.53	5.47	5.30	5.39	5.62
CaO	0.21	0.18	0.15	0.00	0.13	0.60	0.00	0.00	0.00	0.15	0.21
Na2O	0.42	0.33	0.27	0.32	0.46	0.30	0.61	0.30	0.33	0.39	0.33
K2O	8.68	9.16	9.13	8.97	8.42	8.05	8.91	8.93	9.06	9.03	9.02
TOTAL	96.63	98.26	98.69	97.59	98.02	96.84	98.38	97.24	98.19	98.15	97.96
CATIONS											
Si	5.427	5.402	5.379	5.431	5.279	5.252	5.383	5.347	5.381	5.364	5.383
Ti	0.544	0.542	0.554	0.531	0.588	0.462	0.568	0.550	0.592	0.575	0.639
Cr	0.000	0.000	0.000	0.000	0.000	0.000	0.000	0.000	0.000	0.000	0.000
Al	2.766	2.797	2.748	2.805	2.797	2.816	2.735	2.840	2.794	2.761	2.739
Fe2+	3.672	3.529	3.560	3.556	3.754	4.073	3.743	3.728	3.691	3.749	3.573
Mn	0.000	0.000	0.000	0.000	0.000	0.000	0.000	0.000	0.000	0.000	0.000
Mg	1.266	1.409	1.414	1.376	1.390	1.293	1.279	1.278	1.225	1.251	1.298
Ca	0.036	0.029	0.025	0.000	0.025	0.103	0.000	0.000	0.000	0.025	0.035
Na	0.127	0.098	0.230	0.095	0.139	0.122	0.184	0.091	0.101	0.117	0.098
K	1.743	1.801	1.795	1.775	1.671	1.637	1.765	1.786	1.792	1.793	1.783
(O)	22	22	22	22	22	22	22	22	22	22	22
TOTAL	15.580	15.607	15.705	15.569	15.640	15.759	15.657	15.620	15.576	15.635	15.548
Mg#	0.256	0.285	0.284	0.279	0.270	0.241	0.255	0.255	0.249	0.250	0.266

CUMMINGTONITE

%OXIDE	Cum1
SiO2	50.76
TiO2	0.00
Al2O3	0.47
FeO	38.24
MnO	0.00
MgO	7.27
CaO	0.33
Na2O	0.41
K2O	0.00
TOTAL	97.48
CATIONS	
Si	8.001
Ti	0.000
Al	0.087
Fe2+	5.041
Mn	0.000
Mg	1.708
Ca	0.056
Na	0.126
K	0.000
(O)	23
TOTAL	15.019

DD.CUM22

GARNET With Fe3+ Corrections

%OXIDE	Grt 1	Grt 1	Grt 2	Grt 2	Grt 3	Grt 3	Grt 4	Grt 5	Grt 5	Grt 6	Grt 6	Grt 7	Grt 7	Grt 8	Grt 8
SiO2	37.25	37.25	37.39	37.39	37.50	37.50	37.86	37.57	37.57	37.17	37.17	37.04	37.04	37.41	37.41
TiO2	0.00	0.00	0.02	0.02	0.00	0.00	0.00	0.00	0.00	0.07	0.07	0.11	0.11	0.09	0.09
Cr2O3	0.00	0.00	0.00	0.00	0.14	0.14	0.04	0.00	0.00	0.07	0.07	0.07	0.07	0.01	0.01
Al2O3	20.64	20.64	20.84	20.84	21.13	21.13	21.47	20.96	20.96	20.77	20.77	21.00	21.00	21.19	21.19
Fe2O3	-	0.89	-	0.80	-	0.55	0.00	-	0.97	-	0.30	-	1.17	-	0.45
FeO	36.79	35.99	37.76	37.05	37.04	36.55	36.65	36.86	35.98	36.71	36.44	36.82	35.77	37.36	36.95
MnO	0.20	0.20	0.19	0.19	0.34	0.34	0.00	0.15	0.15	0.19	0.19	1.22	1.22	0.15	0.15
MgO	3.05	3.05	2.69	2.69	2.83	2.83	3.13	3.14	3.14	2.74	2.74	2.63	2.63	2.77	2.77
CaO	2.29	2.29	2.09	2.09	2.25	2.25	2.25	2.47	2.47	2.33	2.33	2.11	2.11	2.17	2.17
TOTAL	100.22	100.31	100.99	101.06	101.23	101.29	101.38	101.15	101.25	100.06	100.08	100.99	101.11	101.14	101.19
CATIONS															
Si	6.003	5.98952	5.997	5.98503	5.984	5.97578	5.999	5.993	5.97843	5.999	5.9945	5.948	5.93058	5.975	5.96829
Ti	0	0	0.002	0.002	0	0	0	0	0	0.009	0.00899	0.013	0.01296	0.011	0.01099
Cr	0	0	0	0	0.017	0.01698	0.004	0	0	0.008	0.00799	0.009	0.00897	0.002	0.002
Al	3.92	3.9112	3.939	3.93114	3.974	3.96854	4.01	3.94	3.93042	3.952	3.94904	3.975	3.96336	3.989	3.98452
Fe3+	-	0.10776	-	0.09581	-	0.06591	0	-	0.11672	-	0.03597	-	0.14059	-	0.05394
Fe2+	4.958	4.83911	5.065	4.95908	4.943	4.8703	4.857	4.917	4.78833	4.955	4.91531	4.945	4.78993	4.99	4.93045
Mn	0.027	0.02694	0.026	0.02595	0.046	0.04594	0	0.02	0.01995	0.026	0.02598	0.165	0.16452	0.02	0.01998
Mg	0.733	0.73135	0.644	0.64271	0.673	0.67208	0.74	0.746	0.74419	0.66	0.65951	0.63	0.62815	0.66	0.65926
Ca	0.395	0.39411	0.359	0.35828	0.385	0.38447	0.382	0.423	0.42197	0.403	0.4027	0.362	0.36094	0.371	0.37058
(O)	24	24	24	24	24	24	24	24	24	24	24	24	24	24	24
TOTAL	16.036	16	16.032	16	16.022	16	15.992	16.039	16	16.012	16	16.047	16	16.018	16
Mg#	0.13	0.13	0.11	0.11	0.12	0.12	0.13	0.13	0.13	0.12	0.12	0.11	0.12	0.12	0.12

%OXIDE	Bt1	Bt2	Bt3	Bt4	Bt5	Bt6	Bt7	Bt8
SiO2	34.61	34.10	33.76	33.98	34.24	33.88	33.87	34.23
TiO2	5.17	4.74	4.26	4.22	4.22	5.14	5.02	5.09
Cr2O3	0.04	0.05	0.00	0.00	0.00	0.07	0.00	0.04
Al2O3	18.67	18.03	17.46	18.13	18.04	17.58	17.72	17.70
FeO	24.10	24.69	25.77	24.99	25.24	24.56	24.58	24.95
MnO	0.00	0.00	0.00	0.00	0.00	0.00	0.00	0.00
MgO	5.17	5.43	5.03	5.25	5.39	4.70	5.00	5.31
CaO	0.04	0.03	0.12	0.14	0.10	0.14	0.09	0.09
Na2O	0.47	0.38	0.45	0.46	0.47	0.38	0.50	0.37
K2O	9.32	9.14	8.52	9.11	8.96	9.07	9.14	9.09
TOTAL	97.59	96.58	95.37	96.29	96.66	95.51	95.92	96.86
CATIONS								
Si	5.275	5.274	5.311	5.283	5.299	5.305	5.283	5.285
Ti	0.592	0.551	0.504	0.494	0.491	0.605	0.589	0.591
Cr	0.004	0.009	0.000	0.000	0.000	0.009	0.000	0.004
Al	3.353	3.286	3.237	3.323	3.291	3.244	3.257	3.221
Fe2+	3.072	3.193	3.391	3.249	3.267	3.216	3.206	3.222
Mn	0.000	0.000	0.000	0.000	0.000	0.000	0.000	0.000
Mg	1.176	1.251	1.180	1.217	1.243	1.097	1.163	1.222
Ca	0.007	0.004	0.021	0.024	0.017	0.023	0.015	0.014
Na	0.138	0.113	0.137	0.138	0.142	0.118	0.152	0.111
K	1.812	1.804	1.710	1.807	1.769	1.812	1.819	1.900
(O)	22	22	22	22	22	22	22	22
TOTAL	15.429	15.485	15.491	15.535	15.519	15.429	15.484	15.570
Mg#	0.28	0.28	0.26	0.27	0.28	0.25	0.27	0.27

K-FELDSPAR

%OXIDE	Kfs 1	Kfs 2	Kfs 3	Kfs 4	Kfs 5	Kfs 6	Kfs 7
SiO2	64.26	63.73	64.04	65.25	64.84	63.85	64.31
TiO2	0.67	1.03	0.74	-	-	-	-
Al2O3	19.00	19.58	19.24	19.66	19.55	18.95	18.93
CaO	0.23	0.23	0.20	0.34	0.24	0.17	0.12
Na2O	1.18	1.68	1.87	1.39	1.41	1.51	1.41
K2O	14.08	13.77	13.71	14.05	14.17	13.89	13.96
TOTAL	99.42	100.02	99.80	100.69	100.21	98.37	98.72
CATIONS							
Si	2.963	2.925	2.944	2.967	2.965	2.975	2.983
Ti	0.023	0.035	0.026	-	-	-	-
Al	1.033	1.059	1.043	1.054	1.054	1.041	1.035
Ca	0.012	0.011	0.010	0.017	0.012	0.008	0.006
Na	0.105	0.150	0.166	0.122	0.125	0.137	0.126
K	0.829	0.806	0.804	0.815	0.827	0.825	0.826
(O)	8	8	8	8	8	8	8
TOTAL	4.965	4.986	4.993	4.975	4.983	4.986	4.976

PLAGIOCLASE

%OXIDE	Pl1	Pl2	Pl3	Pl4	Pl5	Pl6	Pl7	Pl8	Pl9	Pl10	Pl11
SiO2	58.78	59.01	59.80	59.88	58.35	59.18	58.90	59.53	59.34	59.07	61.21
Al2O3	25.29	25.25	25.40	25.39	25.75	25.86	25.65	25.70	25.33	26.23	24.25
CaO	7.27	6.87	6.96	6.93	7.42	7.33	7.35	7.20	6.80	7.62	4.80
Na2O	7.47	7.63	7.63	7.63	7.24	7.32	7.39	7.43	7.73	7.30	8.40
K2O	0.10	0.16	0.16	0.16	0.22	0.22	0.31	0.21	0.14	0.16	0.69
TOTAL	98.90	98.92	99.94	99.99	98.99	99.91	99.61	100.06	99.34	100.38	99.35
CATION											
Si	2.651	2.659	2.666	2.667	2.632	2.642	2.641	2.653	2.662	2.627	2.735
Al	1.345	1.341	1.334	1.333	1.369	1.361	1.356	1.350	1.339	1.375	1.277
Ca	0.351	0.332	0.333	0.331	0.359	0.351	0.353	0.344	0.327	0.363	0.230
Na	0.653	0.667	0.660	0.659	0.633	0.634	0.643	0.641	0.672	0.629	0.728
K	0.006	0.009	0.009	0.009	0.012	0.012	0.018	0.012	0.008	0.009	0.040
(O)	8	8	8	8	8	8	8	8	8	8	8
TOTAL	5.006	5.008	5.002	4.999	5.005	5.000	5.011	5.000	5.008	5.003	5.010

DD.TYQ5

GARNET With Fe3+ Corrections

%OXIDE	Grt1	Grt1	Grt2	Grt2	Grt3	Grt3	Grt4	Grt4	Grt5	Grt5	Grt6	Grt6	Grt7	Grt7	Grt8	Grt8	Grt9	Grt9
SiO2	36.94	36.94	37.28	37.28	37.02	37.02	37.58	37.58	37.42	37.42	37.35	37.35	37.70	37.70	37.63	37.63	37.75	37.75
TiO2	0.12	0.12	0.02	0.02	0.00	0.00	0.03	0.03	0.03	0.03	0.00	0.00	0.07	0.07	0.02	0.02	0.13	0.13
Cr2O3	0.00	0.00	0.00	0.00	0.06	0.06	0.03	0.03	0.00	0.00	0.07	0.07	0.00	0.00	0.06	0.06	0.00	0.00
Al2O3	20.93	20.93	21.12	21.12	21.40	21.40	21.43	21.43	21.40	21.40	21.29	21.29	21.40	21.40	21.01	21.01	21.19	21.19
Fe2O3	-	1.79	-	1.02	-	1.35	-	0.80	-	1.31	-	0.92	-	1.03	-	1.13	-	0.18
FeO	32.58	30.98	32.06	31.14	32.77	31.55	31.88	31.15	31.98	30.81	31.88	31.05	32.19	31.25	32.28	31.26	31.75	31.59
MnO	2.24	2.24	2.44	2.44	2.91	2.91	2.41	2.41	2.71	2.71	2.57	2.57	2.48	2.48	2.56	2.56	2.71	2.71
MgO	4.33	4.33	4.35	4.35	3.90	3.90	4.57	4.57	4.47	4.47	4.40	4.40	4.55	4.55	4.40	4.40	4.31	4.31
CaO	2.61	2.61	2.53	2.53	2.21	2.21	2.53	2.53	2.55	2.55	2.46	2.46	2.56	2.56	2.60	2.60	2.53	2.53
TOTAL	99.75	99.93	99.80	99.90	100.25	100.38	100.45	100.53	100.56	100.69	100.02	100.11	100.94	101.04	100.56	100.67	100.37	100.39
CATIONS																		
Si	5.931	5.904	5.965	5.950	5.924	5.904	5.959	5.947	5.942	5.923	5.957	5.943	5.957	5.942	5.980	5.963	5.995	5.992
Ti	0.015	0.015	0.002	0.002	0.000	0.000	0.004	0.004	0.004	0.004	0.000	0.000	0.009	0.009	0.002	0.002	0.015	0.015
Cr	0.000	0.000	0.000	0.000	0.007	0.007	0.003	0.003	0.000	0.000	0.009	0.009	0.000	0.000	0.008	0.008	0.000	0.000
Al	3.962	3.944	3.982	3.972	4.036	4.022	4.005	3.997	4.004	3.991	4.004	3.995	3.986	3.976	3.936	3.925	3.966	3.964
Fe3+	-	0.215	-	0.123	-	0.161	-	0.096	-	0.155	-	0.111	-	0.123	-	0.135	-	0.021
Fe2+	4.376	4.141	4.290	4.156	4.385	4.209	4.227	4.123	4.247	4.078	4.253	4.132	4.253	4.119	4.290	4.143	4.217	4.194
Mn	0.304	0.303	0.331	0.330	0.394	0.393	0.324	0.323	0.364	0.363	0.347	0.346	0.331	0.330	0.344	0.343	0.365	0.365
Mg	1.036	1.031	1.038	1.035	0.930	0.927	1.080	1.078	1.058	1.055	1.046	1.044	1.072	1.069	1.043	1.040	1.019	1.019
Ca	0.448	0.446	0.433	0.432	0.378	0.377	0.430	0.429	0.433	0.432	0.421	0.420	0.433	0.432	0.442	0.441	0.430	0.430
(O)	24	24	24	24	24	24	24	24	24	24	24	24	24	24	24	24	24	24
TOTAL	16.072	16.000	16.041	16.000	16.054	16.000	16.032	16.000	16.052	16.000	16.037	16.000	16.041	16.000	16.045	16.000	16.007	16.000
Mg#	0.19	0.20	0.19	0.20	0.17	0.18	0.20	0.21	0.20	0.21	0.20	0.20	0.20	0.21	0.20	0.20	0.19	0.20

BIOTITE

%OXIDE	Bt1	Bt2	Bt3	Bt4	Bt5	Bt6	Bt7	Bt8	Bt9	Bt10
SiO2	35.34	35.13	35.26	35.49	35.43	35.10	35.56	35.36	35.48	34.47
TiO2	4.65	4.86	4.69	4.79	5.29	5.02	5.02	4.93	4.88	5.15
Cr2O3	0.17	0.10	0.02	0.03	0.00	0.12	0.12	0.04	0.00	0.08
Al2O3	16.21	16.14	16.38	16.35	16.24	16.18	16.31	16.23	16.34	16.19
FeO	21.51	21.44	20.85	20.95	20.87	21.12	21.45	20.88	21.41	19.78
MnO	0.00	0.00	0.00	0.00	0.00	0.00	0.00	0.00	0.00	0.00
MgO	9.36	9.29	9.38	9.05	8.97	9.10	9.18	9.12	9.41	8.67
CaO	0.14	0.10	0.09	0.11	0.15	0.13	0.08	0.09	0.19	0.17
Na2O	0.50	0.47	0.45	0.24	0.57	0.24	0.47	0.40	0.35	0.43
K2O	9.28	9.37	9.18	9.16	9.34	9.50	9.44	9.33	9.10	9.12
TOTAL	97.17	96.90	96.29	96.16	96.86	96.49	97.64	96.38	97.17	94.04
CATIONS										
Si	5.361	5.347	5.374	5.410	5.375	5.357	5.364	5.388	5.366	5.368
Ti	0.531	0.556	0.537	0.549	0.603	0.576	0.570	0.565	0.555	0.603
Cr	0.021	0.012	0.002	0.004	0.000	0.015	0.014	0.005	0.000	0.010
Al	2.898	2.896	2.942	2.937	2.904	2.910	2.900	2.915	2.913	2.971
Fe	2.728	2.729	2.657	2.671	2.647	2.696	2.706	2.661	2.708	2.576
Mn	0.000	0.000	0.000	0.000	0.000	0.000	0.000	0.000	0.000	0.000
Mg	2.117	2.108	2.130	2.057	2.028	2.070	2.065	2.072	2.122	2.013
Ca	0.023	0.017	0.015	0.018	0.024	0.021	0.013	0.014	0.031	0.028
Na	0.145	0.138	0.132	0.069	0.167	0.070	0.139	0.117	0.102	0.131
K	1.796	1.819	1.785	1.781	1.807	1.850	1.816	1.813	1.756	1.811
(O)	22	22	22	22	22	22	22	22	22	22
TOTAL	15.620	15.622	15.574	15.496	15.555	15.565	15.587	15.550	15.553	15.511
Mg#	0.44	0.44	0.44	0.44	0.43	0.43	0.43	0.44	0.44	0.44

PLAGIOCLASE

%OXIDE	Pl1	Pl2	Pl3	Pl4	Pl5
SiO2	58.20	58.04	58.01	58.27	58.52
Al2O3	26.50	26.41	26.89	26.58	26.74
CaO	8.33	8.29	8.68	8.30	8.32
Na2O	6.76	6.80	6.51	6.63	6.78
K2O	0.32	0.33	0.24	0.40	0.34
TOTAL	100.11	99.87	100.34	100.18	100.70
CATIONS					
Si	2.602	2.602	2.588	2.603	2.600
Al	1.396	1.396	1.414	1.399	1.401
Ca	0.399	0.398	0.415	0.397	0.396
Na	0.586	0.591	0.563	0.574	0.584
K	0.018	0.019	0.013	0.023	0.019
(O)	8	8	8	8	8
TOTAL	5.001	5.006	4.993	4.996	5.000

REFERENCES

ADDITIONAL REFERENCES ON BACK OF PAGE 405

Allan, W.C., 1970. The Morven-Cabrach intrusion. *Scottish Journal of Geology,* **6,** 53-72.

Anderton, R. 1980. Did Iapetus start to open during the Cambrian? *Nature, London,* **286,** 706-708.

Armbruster, Th., 1986. The role of Na in the structure of low cordierite: A single crystal X-ray study. *American Mineralogist,* **71,** 746-757.

Armbruster, Th. and Bloss, F.D., 1980. Channel H_2O and CO_2 in cordierites. *Nature, London,* **286,** 140-141.

Ashcroft, W.A., 1970. Note on the contacts of the Belhelvie igneous intrusion. *Scottish Journal of Geology,* **6,** 73-74.

Ashcroft, W.A., and Munro, M., 1978. The structure of the eastern part of the Insch mafic intrusion Aberdeenshire. *Scottish Journal of Geology,* **14** 55-79.

Ashcroft, W.A., Kneller, B.C., Leslie, A.G. and Munro, M., 1984. Major shear zones and autochthonous Dalradian in the north-east Scottish Caledonides. *Nature, London,* **310,** 760-762.

Ashworth, J.R., 1972. Migmatites of the Huntly-Portsoy area, north-east Scotland. *Ph.D. thesis. Unpublished.*

Ashworth, J.R., 1975. The sillimanite zones of the Huntly-Portsoy area, North East Scotland. *Geological Magazine,* **112,** 113.136.

Ashworth, J.R., 1976. Petrogenesis of migmatites in the Huntly-Portsoy area, north-east Scotland. *Mineralogical Magazine,* **40,** 661-682.

Baker, A.J., 1987. Models for the tectonothermal evolution of the eastern Dalradian of Scotland. *Journal of Metamorphic Geology,* **5,** 101-118.

Bamford, D., Nunn, K., Prodehl,C. and Jacob, B., 1977. LISPB-III. Upper crustal structure of northern Britain. *Journal of the Geological Society, London,* **133,** 481-488.

Barrow, G., 1893. On an intrusion of muscovite biotite gneiss in the southeast Highlands of Scotland and its accompanying metamorphism. *Journal of the Geological Society, London,* **49,** 330-358.

Barrow, G., 1912. On the geology of lower Deeside and the southern Highland Border. *Proceedings of the Geology Association , London,* **23,** 268-273.

Beddoe-Stephens, B., 1990. Pressures and temperatures of Dalradian metamorphism and the andalusite-kyanite transformation in the northeast Grampians. *Scottish Journal of Geology,* **26,** 3-14.

Berman, R.G., 1990. A general method for thermodynamic calculations, with a revised garnet solution model and geologic applications. *Geological Society of America Abstracts with Programs,* **20,** A98.

Berman, R.G., 1990. Mixing properties of Ca-Mg-Fe-Mn garnets. *American Mineralogist,* **75,** 328-344.

Bhattacharya, A., 1986. Some geobarometers involving cordierite in the FeO-Al_2O_3-$SiO_2(\pm H_2O)$ system: Refinements, thermodynamic calibration, and applicability in granulite facies rocks. *Contributions to Mineralogy and Petrology,* **94,** 387-304.

Bhattacharya, A., Mazumdar, A.C. and Sen, S.K., 1988. Fe-Mg mixing in cordierite: constraints from natural data and implications for cordierite-garnet geothermometry in granulites. *American Mineralogist,* **73,** 338-344.

Bhattacharya, A., Krishnakumar, K., Raith, M. and Sen, S.K., 1991. An improved set of a-X parameters for pyrope-almandine binary and refinement of orthopyroxene-garnet thermometer and orthopyroxene-garnet-plagioclase-quartz barometer. *Journal of Petrology,* **32,** 629-656.

Bhattacharya, A., Mohanty, L., Maji, A., Sen, S.K. and Raith, M., 1992. Non-ideal mixing in the phlogopite-annite binary: constraints from experimental data on Mg-Fe partitioning and a reformulation of the biotite-garnet geothermometer. C.M.P 109 p107-111.

Bohlen, S.R., Boettcher, A.L., Wall, V.J. and Clemens, J.D., 1983. Stability of phlogopite-quartz and sanadine-quartz: A model for melting in the lower crust. *Contributions to Mineralogy and Petrology,* **83,** 270-277.

Bohlen, S.R., Wall, V.J. and Boettcher, A.L., 1983. Experimental investigation and application of garnet granulite equilibria. *Contributions to Mineralogy and Petrology,* **83,** 52-61.

Boyd, R. and Munro, M., 1978. Deformation of the Belhelvie Mass, Aberdeenshire. *Scottish Journal of Geology,* **14** 29-44.

Brown, G.C. and Fyfe, W.S., 1970. The production of granitic melts during ultrametamorphism. *Contributions to Mineralogy and Petrology,* **28,** 310-318.

Brown, G.C., Hughes, D.J. and Esson, J., 1973. New XRF data retrieval techniques and their application to U.S.G.S. standard rocks. *Chemical Geology,* **11,** 223-229.

Chinner, G.A., 1966. The distribution of pressure and temperature during Dalradian metamorphism. *Journal of the Geological Society, London,* **122,** 159-186.

Chinner, G.A. and Schrairer, J.F., 1962. The join $Ca_3Al_2Si_3O_{12}$-$Mg_3Al_2Si_3O_{12}$ and its bearing on the system CaO-MgO-Al_2O_3-SiO_2 at atmospheric pressure. *American Journal of Science,* **260,** 611-634.

Clark, P.D. and Wadworth, W.J., 1970. The Insch layered intrusion. *Scottish Journal of Geology,* **6,** 7-25.

Clemens, J.D., 1990. The granulite - granite connexion. In: *Granulites and Crustal Evolution.* (eds. Vielzeuf, D. and Vidal, Ph.), NATO ASI Series, Kluwer Academic Publishers, Dordrecht, 25-36.

Clemens, J.D., 1992. Partial melting and granulite genesis: a partisan overview. *Precambrian Research,* **55,** 297-301.

Clemens, J.D. and Vielzeuf, D., 1987. Constraints on melting and magma production in the crust. *Earth and Planetry Science Letters,* **86,** 287-306.

Clemens, J.D. and Wall, V.J., 1981. Origin and crystallisation of some peraluminous (S-type) granitic magmas. *Canadian Mineralogist,* **19,** 111-131.

Dempster, T.J., Hudson, N.F.C. and Rogers, G., 1995. Metamorphism and cooling of the NE Dalradian. *Journal of the Geological Society, London,* **152,** 431-437.

Droop, G.T.R., 1987. A general equation for estimating Fe3+ concentrations in ferromagnesian silicates and oxides from microprobe analyses, using stoichiometric criteria. *Mineralogical Magazine,* **51,** 431-437.

Droop, G.T.R. and Charnley, N.R., 1985. Comparative geobarometry of pelitic hornfelses associated with the Newer Gabbros: a preliminary study. *Journal of the Geological Society, London,* **142,** 53-62.

Edgar, A.D., 1973. Experimental petrology: basic principles and technology. *Clarendon press, Oxford.*

Elkins, L.T. and Grove, T.L., 1990. Ternary feldspar experiments and thermodynamic models. *American Mineralogist,* **75,** 544-559.

Elles, G.L. and Tilley, C.E., 1930. Metamorphism in relation to structure in the Scottish Highlands. *Transactions of the Royal Society, Edinburgh,* **56,** 621-646.

England, P.C. and Thompson, A.B., 1986. Some thermal and tectonic models for crustal melting in continental collision zones. In: *Collision Tectonics* (Eds: Coward, M.P. and Ries, A.C.), Geological Society of London Special Publication, **19,** 83-94.

Essene, E.J., 1989. The current status of thermobarometry in metamorphic rocks. In: *Evolution of Metamorphic Belts* (eds. Daly, J.S., Cliff, R.A. and Yardley, B.W.D.), *Special Publication, Geological Society of London,* **43,** 1-44.

Ferry, J.M., and Spear, F.S., 1978. Experimental calibration of the partitioning of Fe and Mg between biotite and garnet. *Contributions on Mineralogy and Petrology,* **66,** 113-117.

Fettes, D.J., 1970. The structural and metamorphic state of the Dalradian ricks and their bearing on the age of emplacement of the basic sheet. *Scottish Journal of Geology,* **6,** 108-118.

Fitzsimons, I.C.W., 1994. Cordierite migmatites from East Antartica: geochemical constraints on volatile distribution during crustal anatexis. *Mineralogical Magazine,* **58A,** 274-275.

Frost, M.J., 1962. Metamorphic grade and iron-magnesium distribution between coexisting garnet-biotite and garnet-hornblende. *Geological Magazine,* **99,** 427-438.

Ganguly, J. and Saxena, S.K., 1984. Mixing properties of aluminosilicate garnets: constraints from natural and experimental data, and application to geothermo-barometry. *American Minerlogist,* **69,** 88-97.

Ghent, E.D., 1976. Plagioclase-garnet-Al_2SiO_5-quartz: a potential geobarometer-geothermometer. *American Minerlogist,* **61,** 710-714

Ghent, E.D. and Stout, M.Z., 1981..Geobarometry and geothermometry of plagioclase-biotite-garnet-muscovite assemblages. *Contributions to Mineralogy and Petrology,* **76,** 92-97.

Goldman, D.S. and Albee, A.L., 1977. Correlation of Mg/Fe partitioning between garnet and biotite with 18O/16O partitioning between quartz and magnetite. *American Journal of Science,* **277,** 750-767.

Goldman, D.S., Rossman, G.R. and Dollase, W.A., 1977. Channel constituents in cordierite. *American Mineralogist* , **62,** 1144-1157.

Goldsmith, J.R., 1980. The melting and breakdown of anorthite at high pressures and temperatures. *American Mineralogist* , **65,** 272-284.

Gordillo, C.E., Schreyer, W., Werding, G. and Abraham, K., 1985. Lithium in Na, Be-vordierites from El Peñón, Sierre de Córdoba, Argentina. *Contributions to Mineralogy and Petrology,* **90,** 93-101.

Graham, C.M. 1986. The role of the Cuachan Lineament during Dalradian evolution. *Scottish Journal of Geology,* **22,** 257-270.

Graham, C.M. and Powell, R., 1984. A garnet-hornblende goethermometer and application to the Peloma Schists, southern California. *Journal of Metamorphic Geology,* **2,** 13-32.

Grant, J.A., 1985. Phase equilibria in partial melting of pelitic rocks. In: *Migmatites* (eds: Ashworth, J.R.), Blackie and Son, Glasgow, 86-144.

Grant, J.A., 1986. Quartz-phlogopite-liquid equilibria and origins of charnokites. *American Mineralogist,* **71,** 1071-1075.

Gribble, C.D., 1966. The thermal aureole of the Haddo House norite in Aberdeenshire. *Scottish Journal of Geology,* **2,** 306-313.

Gribble, C.D., 1968. The cordierite-bearing rocks of the Haddo House and Arnage Districts, Aberdeeenshire. *Contributions on Mineralogy and Petrology,* **17,** 315-330.

Gribble, C.D., 1970. The role of partial fusion in the genesis of cerrtain cordierite-bearing rocks. *Scottish Journal of Geology,* **6,** 75-82.

Gribble, C.D., and O'Hara, M.J., 1967. Interaction of basic magma and pelitic materials. *Nature, London,* **214,** 1198-1201.

Harley, S.L., 1984a. An experimental study of partitioning of Fe and Mg between garnet and orthopyroxene. *Contributions on Mineralogy and Petrology,* **86,** 359-373.

Harley, S.L., 1984b. The solubility of alumina in orthopyroxene coexisting with garnet in FeO-MgO-Al_2O_3-SiO_2 and CaO-FeO-MgO-Al_2O_3-SiO_2.

Harley, S.L. and Green, D.H., 1982. Garnet-orthopyroxene barometry for granulites and peridotites. *Nature, London,* **300,** 697-701.

Harris, A.L., and Pitcher, W.S., 1975. The Dalradian Supergroup. *In* Harris,A.L. *et al* (Eds.) A correlation of Precambrian rocks of the British Isles. *Special reproduction of the geological Society, London.* **6,** 52-75.

Harte, B. and Hudson, N.F.C., 1979. In: *The Caledonides of the British Isles - reviewed* (eds. Harris, A.L., Holland, C.H. and Leake, B.E.), *Special Publication, Geological Society of London,* **8,** 323-337. Scottish academic press.

Haselton, H.T. and Newton, R.C., 1980. Calorimetry of synthetic pyrope-grossular garnets and their stabilities at high temperatures and high pressures. *Journal of Geophysical Research,* **85,** 6973-6982.

Helgeson, H.C., Delany, J.M., Nesbitt, H.W. and Bird, D.K., 1978. Summary and critique of the thermodynamic properites of rock forming minerals. *American Journal of Science,* **278-A.**

Hodges, K.V. and Spear, F.S., 1982. Geothermometry, geobarometry and the Al_2SiO_5 triple point at Mt. Moosilauke, New Hampshire. *American Mineralogist,* **67,** 1118-1134.

Holdaway, M.J. and Lee, S.M., 1977. Fe-Mg cordierite stability in high grade pelitic rocks bases on experimental, theoretical and natural observations. *Contributions to Mineralogy and Petrology,* **63,** 175-198.

Holland, T.J.B. and Powell, R., 1985. An internally consistant thermodynamic dataset with uncertanties and correlations: 2. Data and results. *Journal of Metamorphic Geology,* **3,** 343-370.

Holland, T.J.B. and Powell, R., 1990. An enlarged and updated internally consistant thermodynamic dataset: the system K_2O-Na_2O-CaO-MgO-MnO-FeO-Fe_2O_3-Al_2O_3-TiO_2-SiO_2-C-H_2-O_2. *Journal of Metamorphic Geology,* **8,** 89-124.

Hudson, N.F.C,, 1985. Conditions of Dalradian metamorphism in the Buchan area, NE Scotland. *Journal of the Geological Society, London,* **142,** 63-76.

Huppert, H.E. and Sparks, R.S.J., 1988. The generation of granitic magmas by intrusion of basalt into continental crust. *Journal of Petrology,* **29,** 599-624.

Indares, A. and Martingnole, J., 1985. Biotite-garnet geothermometry in the granulite facies: the influence of Al and Ti in biotite. *American Mineralogist,* **70,** 272-278.

Johannes, W., 1985. The significance of experimental studies for the formation of migmatites. In: *Migmatites* (ed Ashworth, J.R.), 36-85. Blackie. U.K.

Johannes, W. and Holtz, F., 1990. Formation and composition of H_2O-undersaturated granitic melts. In: *High-temperature Metamorphism and Crustal Anatexis* (eds Ashworth, J.R. & Brown, M.), *Mineralogical Society Series,* **2,** 87-104.

Johannes, W.A. and Shreyer, W., 1981. Experimental introduction of CO_2 and H_2O into Mg-cordierite. *American Journal of Science,* **281,** 299-317.

Johnson, M.R.W., 1962. Relations of movement and metamorphism in the Dalradians of Banffshire. *Transactions of the Edinburgh geological Society,* **19,** 29-64.

Johnson, M.R.W., 1983. Dalradian In: *Geology of Scotland* (ed. Craig, G.Y.), pp 77-104. Scottish Academic Press.

Kneller, B.C. and Leslie, A.G., 1984. Amphibolite facies metamorphism on shear zones in the Buchan area of NE Scotland. *Journal of Metamorphic Geology,* **2,** 83-94.

Koberski, U., 1995. The effect of fluorine and titanium on the vapout-absent melting of phlogopite and quartz. *Mineralogical Magazine,* **59,** 566-570.

Kretz, R., 1983. Symbols for rock-forming minerals. *American Mineralogist,* **68,** 277-279.

Lamb, W. and Valley, J.W., 1984. Metamorphism of reduced granulites in low-CO2 vapiur-free environment, *Nature, London,* **312,** 56-58.

Lambert, R.St.J. and McKerrow, W.S., 1976. The Grampian Orogeny. *Scottish Journal of Geology,* **12,** 293-300.

Le Breton, N. and Thompson, A.B., 1988, Fluid-absent (dehydration) melting of biotite in metapelites in the early stages of crustal anatexis. *Contributions to Mineralogy and Petrology,* **99,** 226-237.

Lee, H.Y. and Ganguly, J., 1988. Equilibrium compositions of coexisting garnet and orthopyroxene: Experimental determinations in the system FeO-MgO-Al_2O_3-SiO_2, and applications. *Journal of Petrology,* **29,** 93-113.

Leslie, A.G., 1984. Field relations in thre north-eatsern part of the Insch mafic mass, Aberdeenshire. *Scottish Journal of Geology,* **20,** 215-235.

Lonker, S.W., 1981. The P-T-X relations of the cordierite-garnet-sillimanite-quartz equilibrium. *American Journal of Science,* **281,** 1056-1090.

Luth, W.D., Jahns, R.H. and Tuttle, O.F., 1964. The granit system at pressres of 4 to 10 kilobars. *Journal of Geophysical Research,* **69,** 659-773.

McGregor, D.M. and Wilson, C.D.V., 1967. Gravity and magnetic surveys of the younger gabbros of Aberdeenshire. *Journal of the Geological Society, London,* **123,** 99-123.

Munro, M., 1970. A re-assessment of the 'younger' basic rocks between Huntly and Portsoy based on new borehole evidence. *Scottish Journal of Geology,* **6,** 41-52.

Munro, M., 1984. Cumulate relations in the 'Younger Basic' masses of the Huntly-Portsoy area, Grampian Region. *Scottish Journal of Geology,* **20,** 343-359.

Munro, M. and Gallagher, J.W., 1984. Disruption of the 'Younger Basic' masses in the Huntly-Portsoy area, Grampian Region. *Scottish Journal of Geology,* **20,** 361-382.

Newton, R.C. and Haselton, H.T., 1981. Thermodynamics of the garnet-plagioclase-Al_2SiO_5-quartz geobarometer. In: *Thermodynamics of minerals and melts* (eds. Newton, R.C., Navrotsky, A. and Wood, B.J.), *New York, Springer-Verlag,* 129-145.

Newton, R.C. and Perkins, D., 1982. Thermodynamic calibration of geobarometers based on the assemblages garnet-plagioclase-orthopyroxene (clinopyroxene-quartz. *American Mineralogist,* **67,** 203-222.

Nichols, G.T., Berry, R.F. and Green, D.H., 1992. Internally consistent gahnitic spinel-cordierite-garnet equilibria in the FMASHZn system: geothermometry and applications. *Contributions to Mineralogy and Petrology,* **111,** 362-377.

O'Hara, M.J. and Yarwood, G. 1978. High P-T point on an Archaean geotherm, implied magma genesis by crustal anatexis and consequences for garnet-pyroxene barometry. *Philosophycal Transactions of the Royal Society, London,* **288,** 441-456.

O'Neill, H-StC and Wood, B.J., 1979. An experimental study on Fe-Mg partitioning between garnet and olivine and it's calibration as a geothemometer. *Contributions to Mineralogy and Petrology,* **70,** 59-70.

Pankhurst, R.J., 1969. Strontium isotope studies applied to petrogenesis in the basic igneous province of North-East Scotland. *Journal of Petrology,* **10,** 116-145.

Pankhurst, R.J., 1970. Geochronology of the basic igneous complexes. *Scottish Jourtnal of Geology,* **6,** 83-107.

Patiño Douce, A.E., 1993. Titanium substitution in biotite: an empirical model with applications to thermometry, O2 and H2O barometries, and consequences for biotite stability. *Chemical Geology,* **108,** 133-162.

Patiño Douce, A.E. and Johnston, A.D., 1993. Octahedral excess mixing properties in biotite: a working model with applications to geothermometry and geobarometry. *American Mineralogist,* **78,** 113-131.

Perkins, D.and Newton, R.C., 1981. Charnokite geobarometers based on coexisting garnet-plagioclase-pyroxene-quartz. *Nature, London,* **292,** 144-146.

Perkins, D. and Chipera, 1985. Garnet-orthopyroxene-plagioclase-quartz barometry: refinement and application to the English River subprovince and the Minnesota River valley. *Contributions to Mineralogy and Petrology,* **89,** 69-80.

Phillips, G.N., (1980). Water activity changes across an amphibolite-granulite facies transition, Broken Hill, Australia. *Contributions to Minerlogy and Petrology,* **75,** 377-386.

Phillips, W.E.A., Stillman, C.J. and Murphy, T., 1976. A Caledonian plate tectonic model. *Journal of the Geological Society, London,* **132,** 579-609.

Pigage, R.T. and Greenwood, H.J., 1982. *American Journal of Science,* **282,** 943-969.

Powell, R., 1988. An internally consistent thermodynamic dataset with uncertainties and correlations: 3. Applications to geobarometry, worked examples and a computer program. *Journal of Metamorphic Geology,* **6,** 173-204.

Powell, R. and Downes, J. 1990. Garnet porphyroblast-bearing leucosomes in metapelites: mechanisms, phase diagrams, and an example from Broken Hill, Australia. In: *High-temperature Metamorphism and Crustal Anatexis* (eds Ashworth, J.R. and Brown, M.), *Mineralogical Society Series,* **2,** 105-123..

Powell, R. and Holland, T., 1990. Calculated mineral equilibria in the pelite system, KFMASH (K_2O-FeO-$MgOAl_2O_3$-SiO_2-H_2O), Journal of Metamorphic Geology, 6.

Ramsay, D.M. and Sturt, B.A., 1979. The status of the Banff Nappe. In: *The Caledonides of the British Isles - reviewed* (eds. Harris, A.L., Holland, C.H. & Leake, B.E.), *Special Publication, Geological Society of London,* **8,** 105-123.

Read, H.H., 1919. The two magmas of Strathbogie and Lower Banffshire. *Geological Magazine,* **56,** 177-183.

Read, H.H., 1923a. The petrology of the Arnage district in Aberdeenshire; a study of assimilation. *Journal of the Geological Society, London,* **79,** 446-484.

Read, H.H., 1923b. The Geology of Banff, Huntly, Turriff. *Memoir of the geological Survey of Scotland.*

Read, H.H., 1955. The Banff Nappe: an interpretation of the structure of the Dalradian rocks of north-east Scotland. *Proceedings of the Geological Association,* **66,** 1-29.

Read, H.H. and Farquhar, O.S., 1956. The Buchan Anticline of the Banff nappe of Dalradian rocks in north-east Scotland. *Journal of the Geological Society, London,* **112,** 131-154.

Richardson, S.W., 1968. Staurolite stability in part of the system Fe-Al-Si-O-H. *Journal of Petrology,* **9,** 467-488.

Robertson, S., 1988. Relationships between 'younger' and 'older basics' in the Glen Gairn area, North Deeside. *Scottish Journal of Geology,* **24,** 89-92.

Rodgers, G., Dempster, T.J., Bluck, B.J. and Tanner, P.W.G., 1989. A high precision U-Pb age for the Ben Vurich granite: implications for the evolution of the Scottish Dalradian Supergroup. *Journal of the Geological Society, London,* **146,** 789-798.

Rumble, D., 1988. Fluid flow during regional metamorphism (abstract). EOS, **69,** 464.

Rutter, E.H. and Brodie, K.H., 1985. The permeation of water into hydrating shear zones. In: *Metamorphic Reactions, Kinetics, Textures and Deformation* (eds: Thompson, A.B. and Rubie, D.C.). Springer, New York, 242-250.

Rutter, M.J. and Wyllie, P.J., 1988. Melting of vapour-absent tonalite at 10 kbar to simulate dehydration-melting in the deep crust. *Nature, London,* **331,** 159-160.

Saxena, S.K., 1969. Silicate solid-solution and geothermometry. 3-Distribution of Fe and Mg between coexisting garnet and biotie. *Contributions to Mineralogy and Petrology,* **22,** 259-267.

Sen, S.K. and Bhattacharya, A., 1984. An orthopyroxene-garnet thermometer and its application to the Madras charnokites. *Contributions to Mineralogy and Petrology,* **88,** 64-71.

Shackleton, R.M., 1948. Overturned rhythmic banding in the Huntly gabbro of Aberdeenshire. *Geological Magazine,* **85,** 358-360.

Smith, J.V. and Schreyer, W., 1962. Location of argon and water in cordierite. *Mineralogical Magazine,* **27,** 225-238.

Spear, F.S. and Cheney, J.T., 1989. A petrogenetic grid for pelitic schists in the system SiO_2-Al_2O_3-FeO-MgO-K_2O-H_2O. *Contributions to Mineralogy and Petrology,* **101,** 149-164.

Stevens, G., 1995. Compositional controls on partial melting in high-grade metapelites, a petrological and experimental study. *Ph.D. thesis. Unpublished.*

Stevens, G. and Clemens, J.D., 1994. Fuid-absent melting and the role of fluids in the lithosphere: a slanted summary? *Chemical Geology,* **108,** 1-17.

Stevens, G. and Van Reenan, D., 1992. Partial melting and the origin of metapelitic granulites in the Southern Marginal Zone of the Limpopo Belt, South Africa, *Precambrian Research,* **55,** 303-319.

Stewart, F.H., 1942. Chemical data on a silica-poor argillaceous hornfels and its constituent minerals. *Mineralogical Magazine,* **26,** 260-266.

Stewart, F.H., 1946. The gabbroic complex of Belhelvie in Aberdeenshire. *ournal of the Geological Society, London,* **102,** 465-498.

Stewart, F.H. and Johnson, M.R.W., 1960. The structural problem of the younger gabbros of north-east Scotland. *Transactions of the Edinburgh geological Society,* **18,** 104-112.

Storre, B. 1977. Dry melting of muscovite + quartz in the range Ps = 7 kb to Ps = 20 kb. *Contributions to Mineralogy and Petrology,* **37,** 87-89.

Sturt, B.A., Ramsay, D.M., Pringle, I.R. and Teggin, D.E., 1977. Precambrian gneisses in the Dalradian sequence of northeast Scotland. *Journal of the Geological Society, London,* **134,** 41-44.

Sutton, J. and Watson, J., 1955. The Boyndie Syncline of the Dalradian of the Banffshire coast, *Journal of the Geological Society, London,* **112,** 103-130.

Tanner, P.W.G. and Leslie, A.G., 1994. A pre-D2 age for the 590 Ma Ben Vuirich Granite in the Dalradian of Scotland. *Journal of the Geological Society, London,* **151,** 209-212.

Thompson, A.B., 1976. Mineral reactions in pelitic rocks. I. Prediction of P-T-X(Fe-Mg) phase relations. II. Calculations of some P-T-X(Mg-Fe) phase relations. *American Journal of Science,* **276,** 401-454.

Thompson, A.B., 1982. Dehydration melting of pelitic rocks and the generation of H_2O-undersaturated granitic liquids. *American Journal of Science,* **282,** 1567-1595.

Thompson, A.B., 1983. Fluid-absent metamorphism. *Journal of the Geological Society, London,* **140,** 533-547.

Thomson, A.B., 1990. Heat, fluids, and melting in the granulite facies. In: *Granulites and Crustal Evolution* (eds Vielzeuf, D. & Vidal, Ph.), 37-57, Kluwer Academic Publishers. Netherlands.

Treagus, J.E. and Roberts, J.L., 1981. The Boyndie Syncline, a D1 structure in the Dalradian of Scotland. *Geological Journal,* **16,** 125-135.

Tuttle, O.F. and Bowen, N.L., 1958. Origin of granite in the light of experimental studies in the system $NaAlSi_3O_8$-$KAlSi_3O_8$-SiO_2-H_2O. *Geological Society of America, Memoir* , **74.**

Ulmer, G.C., 1971 (ed) Research techniques for high pressure and high temperature. Springer, New York.

Vernon, R.H., Clarke, G.L. and Collins, W.J., 1990. Local, mid-crustal granulite facies metamorphism and melting: an example in the Mount Stafford area, central Australia. In: High-Temperature Metamorphism and Crustal Anatexis (eds: Ashwoth, J.R. and Brown, M.)., Unwin Hyman, London, 272-319.

Vielzeuf, D. and Holloway, J.R., 1988. Experimental determination of the fluid-absent reactions in the pelitic system. Cosequences for crustal differentiation. *Contributions to Minerlogy and Petrology,* **98,** 257-276.

Vry, J.K., Brown, P.E. and Valley, J.W., 1990. Cordierite volatile content and the role of CO_2 in high-grade metamorphism. *American Mineralogist,* **75,** 71-88.

Wadsworth, W.J., Stewart, F.H. and Rothstein, A.T.V., 1966. Cryptic layering in the Belhelvie intrusion, Aberdeenshire. *Scottish Journal of Geology,* **2,** 54-66.

Waters, D.J., 1988. Partial melting and the formation of granulite facies assemblages in Namaqualand, South Africa. *Journal of Metamorphic Geology,* **6,** 387-404.

Watson, E.B. and Brenan, J.M., 1987. Fluids in the lithosphere, 1. Experimentally determined wetting characteristics of CO_2 - H_2O fluids and there implications for fluid transport, host-rock physical properties, and fluid inclusion formation. *Earth Planetry Science Letters,* **85,** 497-515.

Watt, W.R., 1914. The geology of the country around Huntly (Aberdeenshire). *Journal of the Geological Society, London,* **70,** 266-293.

Weedon, D.S., 1970. The ultrabasic/basic rocks of the Huntly region. *Scottish Journal of Geology,* **6,** 26-40.

White, A.J.R. and Chappell, B.W., 1977. Ultrametamorphism and granitoid genesis. *Tectonophysics,* **43,** 7-22.

Wood, B.J., 1975. The influence of pressure, temperature and bulk composition on the appearance of garnet in orthgneisses - an example from South Harris, Scotland. *Earth and Planetry Science Letters,* **26,** 299-311.

Wood, B.J. and Banno, S., 1973. Garnet-orthopyroxene and orthopyroxene-clinopyroxene equilibria in the system CaO-MgO-Al_2O_3-SiO_2. *Geochimica et Cosmochmica Acta,* **48,** 299-311.

Wood, B.J. and Fraser, D.G., 1977. Elementary thermodynamics for geologists. *Oxford University press.*

Wood, B.J. and Holloway, J.R., 1988. Simulating the Earth. *Unwin Hyman, Boston.*

Wood, D.L. and Nassau, K., 1967. Infrared spectra of foreign molecules in beryl. *Journal of Chemical Physics,* **47,** 2220-2228.

Yardley, B.W.D. and Senior, A., 1982. Basic magmatism in Connemara, Ireland: evidence for a volcanic arc? *Journal of the Geological Society, London,* **139,** 67-70.

Applegate, J.D.R. and Hodges, K.V., 1994. Empirical evaluation of solution models for pelitic minerals and their application to thermobarometry. *Contributions to Mineralogy and Petrology,* **117,** 56-65.

Harley, S.L., 1984b. The solubility of alumina in orthopyroxene coexisting with garnet in $FeO-MgO-Al_2O_3-SiO_2$ and $CaO-FeO-MgO-Al_2O_3-SiO_2$. *Journal of Petrology,* **25,** 665-696.

Hudson, N.F.C., 1980. Regional metamorphism of some Dalradian pelites in the Buchan area, N.E. Scotland. *Contributions to Mineralogy and Petrology,* **73,** 39-51.

Miller, R.R., 1985. Geology of the Strange Lake alkalic complex and the associated Zr-Y--Nb-Be-REE mineralization. (In: Granite related mineral deposits Eds: Taylor, R.P. and Strong, D.F.), Halifax.

Peterson, J.W. and Newton, R.C., 1990. Experimental biotite-quartz melting in the $KMASH-CO_2$ system and the role of CO_2 in the petrogenesis of granites and related rocks. *American Mineralogist,* **75,** 1029-1042.

Rutter, M.J. and Wyllie, P.J., 1988. Crustal differentiation, granitoid segregatio and migmatite genesis; an experimental approach. *Chemical Geology,* **70,** 73.

Sengupta, P., Dasgupta, S., Bhattacharya, P.K. and Hariya, Y., 1990. Mixing behavior in quaternary garnet solid-solution and extended Ellis and Green garnet-clinopyroxene geothermometer. *Contributions to Mineralogy and Petrology,* **103,** 220-227.

JOHN RYLANDS
TY
RY